



TESIS DOCTORAL

Desarrollo de membranas compuestas de paladio mediante electroless pore-plating para la producción de hidrógeno de alta pureza.

Autor:

David Martínez Díaz

Directores:

José Antonio Calles Martín

Alicia Carrero Fernández

Programa de Doctorado en Tecnologías Industriales: Química, Ambiental, Energética, Electrónica, Mecánica y de los Materiales

Escuela Internacional de Doctorado

2021

Resumen

Summary

Resumen

Las emisiones de dióxido de carbono de carácter antropogénico, generado principalmente por el uso masivo de combustibles fósiles en los sectores industrial, energético y de transporte, son una de las principales causas responsables del deterioro progresivo del medio ambiente generado por el calentamiento global. En este contexto, resultan críticas la promoción del uso de energías renovables y la mejora de la eficiencia energética de multitud de procesos químicos e industriales para lograr reducir los actuales niveles de emisiones de CO₂. El uso de hidrógeno como vector energético limpio se presenta como una de las alternativas más prometedoras para facilitar esta transición energética, ya que puede obtenerse mediante diversas tecnologías a partir de materias primas, como gran parte de los residuos orgánicos y el agua. Sin embargo, en la mayoría de los casos este gas no se obtiene con la pureza requerida en ciertas aplicaciones, como por ejemplo las pilas de combustible tipo PEM para generación de energía eléctrica, dado que típicamente se encuentra mezclado con elementos como nitrógeno, vapor de agua u óxidos de carbono, entre otros. Por consiguiente, siempre es necesaria una etapa adicional de purificación aguas abajo del reactor o del equipo de producción general. Esta separación puede llevarse a cabo mediante una etapa independiente a través de diversas tecnologías, principalmente, destilación criogénica, absorción por cambio de presión o mediante el uso de membranas selectivas. Estas últimas permiten su acoplamiento en la propia etapa de reacción, conocida como reactor de membrana, de forma que las etapas de reacción química y separación se llevan a cabo de manera simultánea en una misma unidad. El uso de este tipo de dispositivos puede proporcionar importantes ventajas competitivas en comparación con los esquemas tradicionales de proceso, pudiendo destacar el posible desplazamiento del equilibrio químico en reacciones reversibles para la mejora del rendimiento y conversión, una buena escalabilidad para diferentes niveles de producción, la posibilidad de operar a condiciones de operación más suaves, o la propia intensificación del proceso al requerir un menor número de equipos. Todo ello permitiría reducir tanto los costes de operación, asociados a las menores necesidades energéticas del proceso, como los costes fijos por el menor número de equipos necesarios en comparación con un proceso en dos etapas.

En este contexto, el objetivo principal de la presente Tesis Doctoral es el desarrollo de nuevas membranas compuestas de base paladio que permitan

Resumen

mejorar su capacidad de permeación y mantener una adecuada resistencia mecánica y selectividad al hidrógeno. Para ello, se ha actuado principalmente en dos etapas claves del proceso de fabricación de las membranas, a) la modificación de la morfología original de los soportes porosos de acero 316L empleados para la fabricación de las membranas y b) la propia técnica de deposición del paladio mediante *Electroless Pore-Plating* (ELP-PP). En primer lugar, se estudió el efecto de incorporar diferentes capas intermedias entre el soporte de la membrana y la capa selectiva de Pd. En concreto se usaron interfases de grafito, óxido de cerio denso y óxido de cerio mesoporoso sobre los propios soportes de acero poroso para modificar sus propiedades superficiales y facilitar la posterior deposición de una capa de paladio con mejores propiedades en términos de espesor y homogeneidad. Posteriormente también se analizó la influencia del dopado con núcleos de Pd finamente distribuidos de algunas de las partículas que conformaban estas capas intermedias antes de su propia incorporación sobre el soporte poroso de acero, en sustitución de la habitual etapa de activación superficial previa requerida para la etapa ELP-PP. Sobre todas estas membranas compuestas se realizaron una serie de ensayos de permeación tanto con gases puros como mezclas de diferente composición y concentración para varias condiciones de operación, principalmente temperatura, presión y dirección del flujo de permeado. Por otro lado, también se realizó un análisis económico sobre las diferentes alternativas planteadas, así como su escalado a una mayor longitud y la demostración de las propiedades exhibidas por las membranas seleccionadas mediante su integración en un reactor de membrana para la producción de H₂ mediante reformado con vapor de ácido acético.

Con la primera modificación, basada en el uso de grafito como capa intermedia, se intentó demostrar el efecto beneficioso que puede generar la presencia de un material adicional sobre la superficie de soportes porosos de acero inoxidables. Éste fue seleccionado debido a la simplicidad del proceso de incorporación, consistente en su aplicación directa mediante su roce con la mina de un lápiz de tipo 2B. Con este tipo de membranas compuestas se consiguió un espesor final de la capa de paladio cercano a 17 µm y una permeanza de H₂ de $4,01 \cdot 10^{-4}$ mol m⁻² s⁻¹ Pa^{-0.5} a 400 °C. Estos valores suponen una reducción del espesor de la capa selectiva al H₂ del 43% y una mejora de la capacidad de permeación en torno al 250%, manteniendo una elevada selectividad, respecto a otras membranas compuestas desarrolladas previamente mediante ELP-PP sobre soportes porosos de acero inoxidables sin la capa intermedia de grafito, tomado como referencia.

Una vez evidenciado de forma genérica el beneficio de incorporar una capa intermedia para el desarrollo de membranas compuestas de paladio, se llevó a cabo un estudio más exhaustivo para la selección de los materiales potencialmente más atractivos para preparar este tipo de capas intermedias. Para ello, se seleccionó el óxido de cerio como uno de los más adecuados debido a su elevada resistencia química y mecánica en las típicas condiciones de operación de una membrana de paladio, y su similar coeficiente térmico de expansión al resto de materiales que conforman la propia membrana (acero 316L y paladio). El uso del óxido de cerio como capa intermedia implicó el desarrollo completo del método de deposición, esta vez mediante la técnica de recubrimiento por inmersión, incluyendo tanto el dispositivo necesario para ello como la optimización de los parámetros del propio proceso. Con este tipo de membranas con partículas de óxido de cerio densas como capa intermedia se consiguió un espesor final de la capa de paladio cercano a 15 µm, algo inferior al logrado de forma preliminar con el grafito, y una permeanza de H₂ de $5,37 \cdot 10^{-4}$ mol m⁻² s⁻¹ Pa^{-0,5} a 400 °C. Estos valores suponen una reducción del espesor de la capa selectiva del 50% y una mejora de la capacidad de permeación en torno al 350% respecto a otras membranas ELP-PP sin ningún tipo de capa intermedia de tipo cerámico, tomado como referencia.

Además de la optimización del método de deposición de las capas intermedias de óxido de cerio denso, también se propuso modificar el propio proceso de activación superficial de los soportes requerido para llevar a cabo la posterior deposición de paladio mediante ELP-PP. Éste consiste en la generación de pequeños núcleos de paladio homogéneamente distribuidos sobre la superficie de los soportes para facilitar una posterior deposición homogénea del paladio. Típicamente, esto se lleva a cabo justo antes de la propia deposición del paladio, es decir, una vez se ha finalizado la modificación del soporte mediante la incorporación de la/s capas intermedias. Sin embargo, en la presente Tesis Doctoral se propuso la realización de esta etapa de activación directamente sobre las partículas de óxido de cerio antes de ser incorporadas al propio soporte de acero poroso, de forma que pudiera mejorar la dispersión de estos núcleos de paladio generados sobre las partículas y centrarse éstos únicamente en la zona que ocupa la capa intermedia. Esta nueva distribución de los núcleos de paladio permitió obtener membranas con menores espesores de la capa de paladio (inferior a 10 µm), lo que supuso una disminución del 70% en comparación con otras membranas compuestas desarrolladas mediante ELP-PP sin capa

Resumen

intermedia. Respecto a la capacidad de permeación, este nuevo tipo de membranas exhibieron permeanzas de hidrógeno en torno a los $6,26 \cdot 10^{-4}$ mol m⁻² s⁻¹ Pa^{-0,5} a 400 °C, lo que implica un aumento de la capacidad de permeación superior al 400%.

El último tipo de interfase desarrollada en el presente trabajo se basa en el uso de partículas de cerio mesoporoso, que manteniendo la misma naturaleza del material con el que se prepara este tipo de capas introduce una cierta porosidad intraparticular, en contraste con las partículas densas comerciales empleadas hasta este momento. Estas nuevas partículas se sintetizaron mediante un proceso de nanoreplicación empleando SBA-15 como plantilla, que se elimina posteriormente para dar lugar a partículas mesoporosas de óxido de cerio con la estructura inversa. Con este tipo de membranas se consiguieron espesores de la capa de paladio en torno a 12 µm y una permeanza de H₂ de $1,03 \cdot 10^{-3}$ mol m⁻² s⁻¹ Pa^{-0,5} a 400 °C. Estos valores suponen una reducción del espesor de la capa selectiva del 60% además de una mejora de la capacidad de permeación notablemente superior, situándose en torno al 680% respecto a membranas ELP-PP sin capa intermedia.

Por otro lado, de manera adicional a los ensayos de permeación llevados a cabo con H₂ puro sobre los diferentes tipos de membranas compuestas incluidos en la presente Tesis Doctoral, también se realizaron una serie de experimentos con mezclas de H₂/N₂. En estos ensayos se mantuvo una alta selectividad H₂/N₂ para todas las membranas, independientemente del material empleado como capa intermedia, obteniendo valores superiores a 10.000. Sin embargo, se observaron claros fenómenos de polarización por concentración durante el proceso de permeación, con caídas en los flujos de permeado en el intervalo 10-50% en función de las condiciones de operación empleadas. En general, este efecto tiende a estabilizarse para altos grados de dilución, es similar independientemente de la temperatura de operación considerada y es más acusado para las membranas que presentan una mayor capacidad de permeación inicial o cuando los ensayos se llevan a cabo recogiendo el permeado por la parte externa de la capa de paladio de las membranas. Pese a ello, debe destacarse que todas las membranas mantuvieron una excelente resistencia mecánica independientemente de la dirección del flujo de permeado considerado para los ensayos que se llevaron a cabo a diferentes presiones y temperaturas (1-4 bar y 350-450 °C).

Con todos estos datos se realizó una estimación preliminar de los costes asociados al proceso de fabricación a escala de laboratorio para cada una de las membranas compuestas que incluían capas intermedias basadas en el uso de óxidos de cerio. En este análisis se tuvieron en cuenta todas las etapas necesarias para preparar cada tipo de membrana, el número de ciclos necesario de cada una de ellas, la cantidad de reactivos químicos empleados y las necesidades energéticas del proceso. Además, el coste estimado para cada tipo de membrana se relacionó con su capacidad de permeación mediante un parámetro denominado como factor M, cuyas unidades son $\text{€}/10^4 \text{ mol m}^{-2} \text{ s}^{-1} \text{ Pa}^{-0.5}$. De este modo, las membranas que proporcionaron la mejor relación entre coste y capacidad de permeación fueron las desarrolladas con una capa intermedia de óxido de cerio denso dopado con paladio. Por tanto, estas fueron seleccionadas como las más adecuadas para su escalado e implementación en un reactor de membrana. Respecto al escalado, no se detectaron diferencias significativas en la morfología o la permeabilidad en comparación con las membranas más cortas. Así, este tipo de membranas se empleó para la producción de H₂ mediante reformado con vapor de ácido acético en este tipo de dispositivos. Gracias a la implementación de la membrana en el propio sistema de reacción se obtuvo un aumento tanto de la conversión de ácido acético (10%) como del rendimiento a H₂ (9%), en comparación con los resultados obtenidos al realizar los mismos experimentos sin la incorporación de la membrana selectiva, pese a no haber optimizado de forma rigurosa las condiciones de operación consideradas en estos ensayos.

De manera general, puede concluirse que el uso de capas intermedias afecta positivamente al rendimiento de las membranas compuestas que las contienen, permitiendo tanto la disminución del espesor de la capa selectiva incorporada mediante ELP-PP como el asociado aumento de la capacidad de permeación de H₂. El óxido de cerio se presenta como uno de los materiales más adecuados para la preparación de este tipo de capas intermedias debido a la buena integración de sus propiedades mecánico-físicas con las del resto de materiales que componen la membrana (principalmente, acero y paladio). Además, la activación de las partículas cerámicas con núcleos de paladio de manera previa a su incorporación como capa intermedia es capaz de lograr una disminución del espesor final de la capa selectiva de paladio (inferior a 10 μm) y un consiguiente aumento de la capacidad de permeación de H₂. Algo similar puede lograrse mediante la sustitución de partículas de ceria densas por otras con una cierta porosidad intraparticular, aunque su mayor

Resumen

coste de fabricación compromete la ventaja competitiva lograda por la mejora de sus propiedades. Así, tras analizar técnico-económicamente todas las alternativas planteadas, las membranas compuestas de paladio con una capa intermedia de óxido de cerio denso dopado con paladio fueron seleccionadas como las más adecuadas para su escalado y posterior integración en un reactor de membrana. Estas membranas exhibieron una adecuada resistencia mecánica frente a las condiciones de operación empleadas en un proceso de reformado con vapor de ácido acético para la producción de hidrógeno.

Esta tesis doctoral se presenta como compendio de los siguientes artículos científicos, todos ellos publicados en revistas internacionales de alto impacto:

- I. D. Martinez-Diaz, R. Sanz, A. Carrero, J.A. Calles, D. Alique. **Effective H₂ separation through Electroless Pore-Plated Pd-membranes containing Graphite lead barriers.** *Membranes* 10 (2020) 410.
- II. D. Martinez-Diaz, R. Sanz, J.A. Calles, D. Alique. **H₂ permeation increase of electroless pore-plated Pd/PSS membranes with CeO₂ intermediate barriers.** *Separation and Purification Technology* 216 (2019) 16-24.
- III. D. Martinez-Diaz, D. Alique, J.A. Calles, R. Sanz. **Pd-thickness reduction in electroless pore-plated membranes by using doped-ceria as interlayer.** *International Journal of Hydrogen Energy* 45 (2020) 7278-7289.
- IV. D. Martinez-Diaz, D. Martínez del Monte, E. García-Rojas, D. Alique, J.A. Calles, R. Sanz. **Comprehensive permeation analysis and mechanical resistance of electroless pore-plated pd-membranes with ordered mesoporous ceria as intermediate layer.** *Separation and Purification Technology* 258 (2021) 118066.
- V. D. Martinez-Diaz, P. Leo, A. Carrero, J.A. Calles, D. Alique. **Life cycle assessment of H₂-selective Pd membranes fabricated by ELP-PP.** *Journal of cleaner production* (under revision).
- VI. G. Adduci, D. Martinez-Diaz, D. Sanz-Villanueva, A. Caravella, J.A. Calles, R. Sanz, D. Alique. **Stability of electroless pore-plated Pd-membranes in acetic acid steam membrane-reformers for ultra-pure hydrogen production.** *Fuel Processing Technology* 212 (2021) 106619.

Summary

The current emissions of anthropogenic carbon dioxide are mainly generated by the use of fossil fuels in the industrial, energy, and transport sectors, being the main responsible for global warming and progressive deterioration of the environment. In this context, the promotion of clean renewable energies as well as the adoption of efficient energy strategies to reduce CO₂ emissions are critical issues. The use of hydrogen as a clean energy vector is one of the most promising alternatives to facilitate a progressive transition towards this situation since it could be obtained from a wide variety of feedstock by multiple techniques. However, in most cases it is not directly produced with the minimum required purity for certain applications, i.e. PEM-type fuel cells for power generation, being mixed with other compounds such as nitrogen, steam, or carbon oxides, among others. Therefore, it will be always necessary an additional down-stream separation step after the main production unit. In a first approach, this purification is usually carried out by an independent step that can be achieved through diverse technologies such as cryogenic distillation, pressure swing adsorption, or membrane separation. The last alternative allows an additional possibility by coupling the separation with the chemical reaction itself in a same unit denoted as membrane reactor. The use of this alternative can provide important competitive advantages compared to traditional process schemes in which both reaction and separation steps are carried out independently. In this manner, it could be possible to overcome possible equilibrium restrictions of chemical reactions by selective separation of a product according to the Le Châtelier's principle. It could be used to improve the process performance and productivity, work at milder operating conditions and intensify the process itself due to the reduction of required equipment. Moreover, it could be easily scaled for different production levels. All these advantages make possible to reduce both operating costs, associated with a lower energy demand and fixed costs due to the limited number of equipment.

In this context, the main objective of this Ph.D. Thesis is the development of new palladium-composite membranes that allow improving their permeation capacity while maintaining enough hydrogen selectivity and mechanical resistance against diverse operation conditions. In this regard, great efforts have focused on two key stages of the membrane manufacturing process related to the modification of the original morphology

Summary

of porous stainless steel (PSS) supports and the palladium deposition by Electroless Pore-Plating (ELP-PP). First, the effect of incorporating different intermediate layers formed by graphite, dense cerium oxide, or mesoporous cerium oxide onto the PSS supports was addressed. The main objective of this strategy is based on the modification of the original surface properties, thus facilitating the subsequent incorporation of the Pd film with good homogeneity and lower thickness. Subsequently, the generation of first palladium nuclei onto the ceramic particles, before their incorporation onto the PSS support as intermediate layer, was also analyzed. This strategy replaces the traditional surface sensitization/activation step required for any metal incorporation by electroless techniques. A series of permeation tests with both pure gases and mixtures of diverse concentrations were carried out at diverse main operating conditions (including temperature, pressure, and permeate flux direction) for all the samples. Additionally, detailed economic analysis about the fabrication costs was also performed for each proposed alternative with aim to select the most suitable one for an eventual scale-up and future commercialization. In this context, the selected fabrication strategy was scaled-up to longer dimensions, while the previously exhibited main properties of the membranes were tested again after its integration in a membrane reactor for H₂ production through acetic acid steam reforming (AASR-MR).

The first modification of PSS supports, based on the use of graphite as intermediate layer, was performed to demonstrate the potential beneficial effect of including additional layers onto the surface of raw supports. This material was selected due to the simple incorporation process, based on a direct application by rubbing with the lead of a 2B-type pencil. Following this preparation strategy, a final Pd-thickness of 17 µm and H₂ permeance of $4.01 \cdot 10^{-4} \text{ mol m}^{-2} \text{ s}^{-1} \text{ Pa}^{-0.5}$ at 400 °C were reached. These values imply a 43% reduction of the Pd-thickness and an improvement of around 250% in the permeation capacity but maintaining a really high H₂-selectivity, in comparison to other similar PSS/Pd composite-membranes prepared by ELP-PP without any intermediate layer.

After demonstrating the potential benefit of considering the use of intermediate layers to improve the development of Pd-membranes, the most adequate material to prepare these interlayers was further analyzed in depth. In this way, cerium oxide was selected as one of the most suitable ceramic materials due to its high chemical and mechanical resistances under typical operating conditions of most Pd-membranes. Moreover, its thermal

expansion coefficient is very close to that of other membrane constituents (mainly stainless steel and palladium), thus ensuring an eventual better mechanical resistance against successive heating-cooling cycles during operation. In this work, the use of this material, commercial dense cerium oxide, as intermediate layer implied the complete development of the incorporation method, by means of vacuum-assisted dip-coating (VA-DC), including both device design and optimization of the operating process conditions (1-4 bar y 350-450 °C).

This composite-membrane, including dense cerium oxide particles as intermediate layer, exhibited a final Pd-thickness of around 15 µm, slightly lower than the previously achieved when using graphite as intermediate layer. This lower thickness represents a reduction of around 50% compared to other ELP-PP membranes without any type of intermediate layer. As a consequence of this reduction in the Pd-film, H₂ permeance was increased up to $5.37 \cdot 10^{-4}$ mol m⁻² s⁻¹ Pa^{-0.5} at 400 °C, representing an improvement of around 350% in the permeation capacity.

On the other hand, it was also proposed a modification of the conventional PSS surface activation performed to facilitate the subsequent Pd-deposition by ELP-PP. Typically, this step is carried out just before the Pd-deposition step; in other words, once the incorporation of eventual intermediate layers has been completed. However, this work proposes to carry out this activation step directly on the CeO₂ particles before being incorporated as intermediate layer, being possible to improve in this way the palladium nuclei dispersion around the new surface of modified supports, including the new porous-structure.

The new distribution of the Pd nuclei reached by this strategy allowed to decrease the Pd thickness below 10 µm, which represented a decrease of 70% compared to other composite membranes developed by ELP-PP without any intermediate layer. Therefore, these membranes exhibited higher H₂ permeances of around $6.26 \cdot 10^{-4}$ mol m⁻² s⁻¹ Pa^{-0.5} at 400 °C, which implies an increase of the permeation capacity greater than 400%.

The last type of intermediate layer developed in the present work is based on the use of mesoporous CeO₂ particles, which introduces a certain intra-particular porosity against the commercial dense particles previously described but maintains the main advantages provided by the ceramic material. The new porosity could be used to minimize possible resistances of the supports against the gas transport through the porous media as well as

Summary

being functionalized for particular applications of interest. These new particles were synthesized through nano-casting using SBA-15 as a template, which is subsequently removed to obtain mesoporous cerium oxide particles with a reverse structure. Following this strategy, Pd-thicknesses of around 12 µm and H₂ permeance of $10.3 \cdot 10^{-4}$ mol m⁻² s⁻¹ Pa^{-0.5} at 400 °C were achieved. These values represent a reduction in the selective layer thickness of 60% but an improvement in the permeation capacity around 680% compared to other ELP-PP membranes without any intermediate layer.

In addition to the permeation tests carried out with pure gases (H₂ and N₂) on the different composite-membranes included in this study, a series of experiments with binary H₂/N₂ mixtures were also carried out. In these tests, a high H₂/N₂ selectivity above 10,000 was maintained for all the membranes, independently of the considered material to prepare the intermediate layers. However, a clear concentration-polarization effect was observed during permeation, decreasing the permeate fluxes in the range 10-50% in function of the considered operating conditions. In general, this effect tends to stabilize for high dilution grade being certainly similar for any operating temperature, thus suggesting a certain independency of this parameter. However, the above-mentioned effect on the permeation capacity of the composite-membranes becomes more pronounced for membranes presenting a higher initial permeation capacity or while permeating from the inner to the outer surface of the composite-membranes. Nevertheless, it should be noted that all the membranes maintained excellent mechanical resistance independently of the permeation direction considered for these tests, as well as against the different pressures and temperatures analyzed.

With all these results, a preliminary cost estimation associated with the laboratory-scale manufacturing process was made for each alternative including intermediate layers based on CeO₂. For this analysis, all required steps to prepare each membrane type, as well as, chemical reagents and energy demands were taken into account. Moreover, the estimated cost of each membrane type was related with their permeation capacity using a parameter denoted as M-factor, whose units are €/10⁻⁴ mol m⁻² s⁻¹ Pa^{-0.5}. In this way, the best result was obtained with the Pd membranes that contain dense CeO₂ particles with Pd nuclei. Thus, this membrane type was selected as the most suitable one for their scale-up and implementation in a membrane reactor. No significant differences related to both morphology or membrane performance were detected during the fabrication of longer composite ELP-PP membranes, almost tripling the length of the original ones. Therefore, the

new longer membranes were mounted in a membrane reactor to perform the acetic acid steam reforming for ultra-pure H₂ production. Due to the membrane implementation in the reaction system, and despite not performing a rigorous optimization of the operating conditions, a slight increase of acetic acid conversion (10%) and H₂ yield (9%) were obtained in comparison to similar experiments performed in a traditional fixed-bed reactor.

To sum up, it can be concluded that the use of intermediate layers has a clear positive effect on the performance of composite membranes prepared onto PSS supports, allowing a decrease in the Pd- thickness and the consequent increase of H₂ permeation capacity. Cerium oxide is proposed as one of the most suitable materials for the preparation of this type of intermediate layers due to the good integration of its mechanical-physical properties with the other membrane materials (stainless steel and palladium). Moreover, the activation of ceramic particles with Pd-nuclei before their incorporation as intermediate layer is able to decrease the required final Pd-thickness below 10 µm for reaching fully dense membranes. Consequently, an increase of the H₂ permeation capacity was also reached. A certainly similar effect can be achieved by replacing the dense ceria particles by mesoporous ones, although their higher manufacturing costs compromise the competitive advantage achieved by improving their performance. Thus, after a techno-economic analysis of different alternatives, the composite membranes including dense CeO₂ particles doped with Pd-nuclei as intermediate layer were selected as the most suitable alternative. These membranes were scaled-up to longer dimensions of the supports and integrated in a real membrane reactor to perform AASR. The good mechanical stability of this type of membranes was demonstrated at these conditions.

Finally, it should be highlighted that the present Ph.D. Thesis is presented by compendium of scientific articles published international journals with high impact as a result of the promising reached insights. The most relevant ones are listed below:

- I. D. Martinez-Diaz, R. Sanz, A. Carrero, J.A. Calles, D. Alique. **Effective H₂ separation through Electroless Pore-Plated Pd-membranes containing Graphite lead barriers.** *Membranes* 10 (2020) 410.
- II. D. Martinez-Diaz, R. Sanz, J.A. Calles, D. Alique. **H₂ permeation increase of electroless pore-plated Pd/PSS membranes with CeO₂ intermediate barriers.** *Separation and Purification Technology* 216 (2019) 16-24.
- III. D. Martinez-Diaz, D. Alique, J.A. Calles, R. Sanz. **Pd-thickness reduction in electroless pore-plated membranes by using doped-ceria as interlayer.** *International Journal of Hydrogen Energy* 45 (2020) 7278-7289.
- IV. D. Martinez-Diaz, D. Martínez del Monte, E. García-Rojas, D. Alique, J.A. Calles, R. Sanz. **Comprehensive permeation analysis and mechanical resistance of electroless pore-plated pd-membranes with ordered mesoporous ceria as intermediate layer.** *Separation and Purification Technology* 258 (2021) 118066.
- V. D. Martinez-Diaz, P. Leo, A. Carrero, J.A. Calles, D. Alique. **Life cycle assessment of H₂-selective Pd membranes fabricated by ELP-PP.** *Journal of cleaner production* (under revision).
- VI. G. Adduci, D. Martinez-Diaz, D. Sanz-Villanueva, A. Caravella, J.A. Calles, R. Sanz, D. Alique. **Stability of electroless pore-plated Pd-membranes in acetic acid steam membrane-reformers for ultra-pure hydrogen production.** *Fuel Processing Technology* 212 (2021) 106619.

1	Introducción y objetivos	1
1.1	<i>Generalidades</i>	1
1.2	<i>El hidrógeno</i>	5
1.3	<i>Producción de hidrógeno</i>	7
1.3.1	Fuentes no renovables	9
1.3.2	Fuentes renovables	12
1.3.3	Etapa de purificación	15
1.4	<i>Tecnología de membranas.....</i>	16
1.5	<i>Membranas de paladio</i>	21
1.5.1	Tratamientos químicos.....	25
1.5.2	Tratamientos mecánicos	26
1.5.3	Incorporación de capas intermedias	27
1.5.4	Preparación de la capa selectiva de Pd	33
1.5.5	Preparación de aleaciones	42
1.6	<i>Objetivos.....</i>	51
2	Metodología	53
2.1	<i>Preparación de membranas.....</i>	55
2.1.1	Acondicionamiento del soporte comercial	55
2.1.2	Modificación superficial de los soportes.....	56
2.1.3	Deposición de la capa selectiva.....	58
2.2	<i>Técnicas de caracterización.....</i>	60
2.2.1	Microscopía electrónica de barrido (SEM).....	60
2.2.2	Microscopía electrónica de transición (TEM).....	60
2.2.3	Perfilometría óptica 3D	61
2.2.4	Difracción de rayos X (DRX).....	61
2.2.5	Difracción láser	61
2.2.6	Espectroscopía de emisión atómica (ICP-AES)	61
2.2.7	Gravimetría.....	62
2.2.8	Ensayos de permeación de gases	62
3	Discusión general	67
3.1	<i>Incorporación de capas intermedias</i>	69
3.2	<i>Modificación de soportes con partículas de CeO₂ comercial</i>	74

Índice

3.3	<i>Modificación del proceso de activación, capas intermedias de óxido de cerio dopadas con paladio.....</i>	84
3.4	<i>Modificación de soportes con partículas de CeO₂ mesoporoso ...</i>	93
3.5	<i>Análisis económico</i>	102
3.6	<i>Escalado e integración en sistemas de reacción</i>	109
4	Conclusiones	113
5	Referencias	123
6	Anexos.....	155

1

Introducción y objetivos

1.1 Generalidades

El continuo crecimiento de la población y la intensificación de la economía ha implicado un aumento de la demanda energética mundial. Hasta la actualidad, este incremento ha sido cubierto por el uso masivo de combustibles fósiles, causando efectos perjudiciales sobre el calentamiento global debido a la gran emisión de gases de efecto invernadero, así como otros contaminantes asociados a la combustión [1]. Esta situación es aún más problemática debido al agotamiento de estos recursos fósiles a nivel mundial y, por lo tanto, representa un escenario claramente insostenible para el futuro. En los últimos años, se ha sugerido un amplio conjunto de alternativas para el reemplazo progresivo de los combustibles fósiles como recurso energético primario [2,3]. En esta situación, la implementación de la llamada economía del hidrógeno se considera una opción real y está recibiendo gran atención en los últimos años [4–8].

El hidrógeno es presentado como un vector energético muy prometedor debido a su viabilidad a largo plazo, alta densidad de energía ($14 \text{ J}\cdot\text{kg}^{-1}\cdot^{\circ}\text{C}^{-1}$), bajas emisiones de combustión y elevada presencia de este como recurso. De hecho, el hidrógeno es el elemento más abundante en la Tierra, aunque generalmente se encuentra combinado con otros elementos, principalmente en moléculas de agua e hidrocarburos. La idea es transferir la energía obtenida de diferentes fuentes de energía primaria, preferentemente renovables (es decir, eólica, solar o biomasa, entre otras), al hidrógeno, el cual puede almacenarse, transportarse y eventualmente utilizarse en diferentes aplicaciones energéticas. Idealmente, el hidrógeno puede obtenerse del agua mediante el uso de estas energías renovables, minimizando así el impacto ambiental mientras se cubre la demanda de energía [9,10]. Sin embargo, la generación de hidrógeno por procesos termoquímicos parece ser una opción más realista en el futuro cercano para reducir costes [11–14]. El hidrógeno puede generarse a partir de una amplia variedad de materias primas que contienen hidrocarburos, tanto para sistemas de producción centralizados como descentralizados, mediante el uso de tecnologías relativamente maduras [14], siendo especialmente atractivo el uso de biomasa y materiales residuales [15–19]. En estos casos, habitualmente se produce una mezcla de compuestos gaseosos, siendo necesario purificar el hidrógeno hasta los niveles requeridos de acuerdo con la aplicación final, es decir, principalmente celdas de combustible PEM, turbinas o motores de combustión [20]. De hecho, la etapa de purificación del hidrógeno es un proceso crucial en la implementación exitosa de la

1. Introducción

economía del hidrógeno, tanto desde el punto de vista técnico como el económico.

Entre las alternativas disponibles para la purificación de hidrógeno, se ha propuesto y utilizado en la práctica el uso de membranas para aplicaciones de separación / producción de hidrógeno. Esta tecnología muestra ventajas relevantes tales como bajo consumo de energía, buenas propiedades medioambientales y potencial para combinarse con una unidad de reacción en un reactor de membrana multifuncional [21,22]. La combinación simultánea de la reacción química y la separación de hidrógeno en un único paso da como resultado beneficios adicionales en términos de aumento de conversión al cambiar el equilibrio de la reacción a medida que uno de los productos, el hidrógeno, se separa selectivamente del medio de reacción [23,24]. En particular, las membranas densas metálicas se han propuesto durante años debido a su posibilidad de proporcionar una selectividad hacia el hidrógeno completa [25,26]. Por lo tanto, la estructura de los metales que pertenecen a los grupos III-V, como Pd, Ni y Pt (puros y aleados), tiene la capacidad de permitir la difusión de hidrógeno a través de su red metálica, evitando la penetración de otras moléculas [27,28]. De esta manera, el mecanismo de solución-difusión, representado en la Figura 1.1.1, se usa para describir el proceso de permeación de hidrógeno en estas membranas selectivas al H₂.

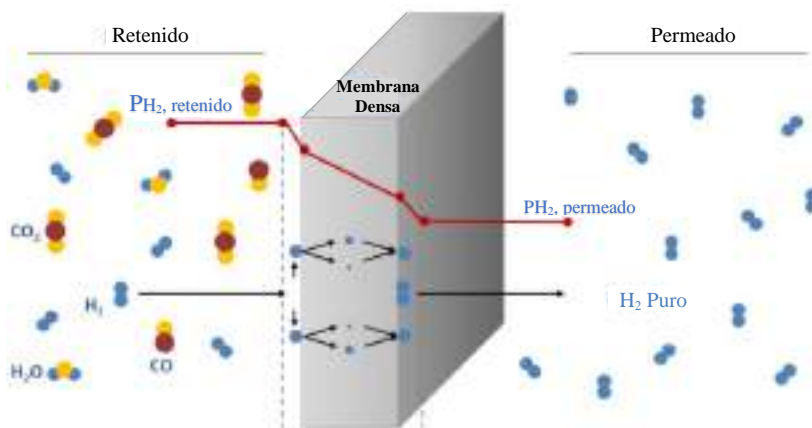


Figura 1.1.1. Mecanismo de solución-difusión para la permeación de hidrógeno a través de una membrana metálica densa [29].

Hasta la fecha, el paladio es el metal más estudiado para la preparación de membranas selectivas al H₂. Los primeros estudios datan del siglo XIX, cuando Deville y Troost descubrieron la capacidad del hidrógeno de penetrar

en el paladio [30,31] y Graham determinó que este metal podía absorber cien veces su propio volumen en hidrógeno [32]. Sin embargo, el uso de membranas de paladio para aplicaciones de separación / producción de hidrógeno no aparece hasta los años cincuenta. A partir de esta década, como lo demuestra el número de publicaciones científicas relacionadas con el tema, estas membranas han ganado un interés creciente. Esta tendencia se puede observar en la Figura 1.1.2, donde se muestra el número de documentos científicos publicados por año y región, considerando como palabras clave: hidrógeno, paladio y membrana o reactor de membrana. Debe señalarse el aumento de publicaciones realizado durante los últimos años, principalmente debido a una mayor conciencia sobre la protección del medio ambiente y el desarrollo de energías renovables, donde el hidrógeno emerge como un vector de energía limpia muy prometedor que, como se mencionó anteriormente, debe ser previamente purificado [20,25]. Analizando el número de publicaciones por región, es evidente que este tema se investiga ampliamente en todo el mundo, encabezando la lista se encuentran los Estados Unidos de América con políticas muy ambiciosas, pero seguido de cerca por diferentes países de Asia (Japón y China) y Europa (principalmente Italia, Alemania, los Países Bajos y España).

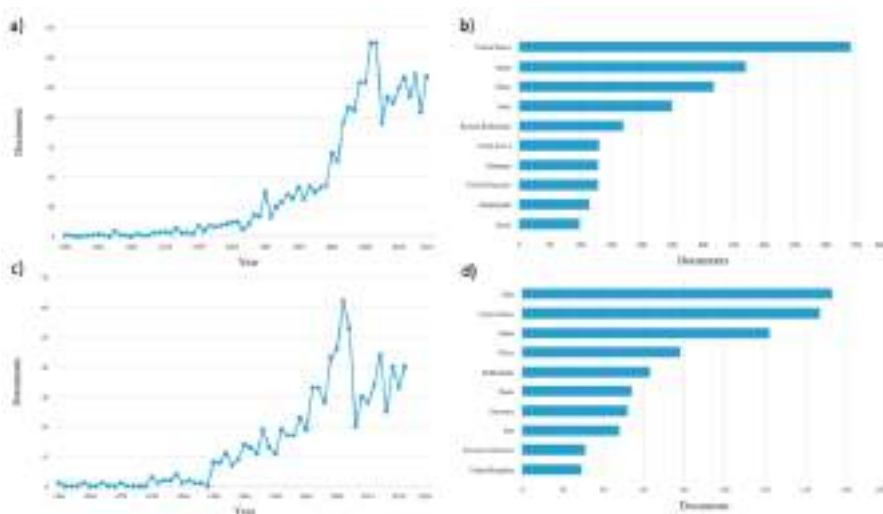


Figura 1.1.2. Análisis de citas usando como palabras claves: paladio+ membrana+ hidrógeno (a, b) y paladio+ reactor de membrana+ hidrógeno (c, d). (fuente: Scopus)

Actualmente, los principales esfuerzos se centran en reducir el coste de estas membranas y aumentar su resistencia mecánica, vida útil y reproducibilidad de fabricación [33,34]. El paladio es un elemento caro y

1. Introducción

escaso, del cual se espera que la creciente demanda de su uso en aplicaciones a gran escala siga aumentando su precio [35]. Dos de las estrategias más estudiadas para reducir el coste de las membranas son: (a) minimizar la cantidad de paladio requerida para lograr una capa completamente densa [36–39] y (b) aumentar la vida útil del uso, ya que estas membranas pueden sufrir desactivación por envenenamiento y agrietamiento por estrés térmico o mecánico [40–44]. Teniendo en cuenta la ecuación utilizada típicamente para describir el flujo de permeación de hidrógeno (J_{H_2}) a través de una membrana de base Pd (ecuación de Richardson, ecuación (1)) en función de la permeabilidad al hidrógeno (k), el espesor del metal (t) y fuerza impulsora ($P_{H_2,ret}^n - P_{H_2,per}^n$) es obvio que una disminución en el espesor del metal provoca un aumento de la capacidad de permeación [28,45].

$$J_{H_2} = \frac{k}{t} (P_{H_2,ret}^n - P_{H_2,per}^n) \quad \text{Ec.1}$$

En el caso de una membrana base Pd totalmente libre de defectos, la permeación de hidrógeno está determinada por la solución-difusión en el metal y el factor exponencial toma el valor $n = 0,5$, esta ecuación se conoce como ley de Sievert.

Sin embargo, la preparación de capas de paladio ultradelgadas conlleva dos problemas principales: (i) limitación de la resistencia mecánica de la membrana y (ii) dificultad para obtener películas libres de defectos. La fabricación de membranas compuestas, haciendo uso de soportes porosos intenta superar estos problemas y, por lo tanto, mantener propiedades mecánicas adecuadas que ahorren paladio [46–50]. Por otro lado, muchos autores centran sus esfuerzos en desarrollar nuevos procesos de fabricación para garantizar una mejor reproducibilidad y reducir el número de membranas rechazadas [50–52] o modificar la capa selectiva (aleaciones base Pd) para mejorar algunas propiedades particulares, como la resistencia a la fragilización por hidrógeno o la desactivación por compuestos de azufre [53–57].

Se pueden usar diversas tecnologías para incorporar una película delgada del metal selectivo, preferiblemente Pd o aleaciones base Pd, sobre un soporte poroso. Se puede mencionar el arrollamiento mecánico [58–60], la deposición física en fase vapor [61–64], la deposición química en fase vapor [65–67], la deposición electroquímica [68–70] y la deposición no electroquímica [34,63,71,72]. Esta última opción (*electroless plating*, o su acrónimo ELP) proporciona importantes ventajas en términos de adherencia

y uniformidad de la capa depositada, tanto en superficies no conductoras como conductoras, incluso con geometrías complejas. Además, debido al bajo coste del equipamiento necesario este proceso es utilizado para la mayoría de los estudios realizados en este campo [73–76].

1.2 El hidrógeno

El hidrógeno no se encuentra libre en nuestro planeta, sino que está enlazado a otros átomos debido a su elevada reactividad. Es por esto por lo que no es considerado como una fuente de energía primaria, sino un portador o vector de energía, como la electricidad. El concepto de utilización del hidrógeno como un vector energético se fortaleció notablemente tras la crisis energética global de 1974. A pesar de que el potencial del hidrógeno es conocido desde hace más de dos siglos, fue primero el carbón y más tarde el petróleo los combustibles que han impulsado el desarrollo social e industrial hasta la fecha. Esto es lo que se conoce como economía de los combustibles fósiles donde la mayoría de los medios de transporte (aviones, trenes, barcos y automóviles) están alimentados prácticamente de manera exclusiva por derivados del petróleo como gasolina, diésel o queroseno. Además, un amplio porcentaje de las centrales eléctricas actuales usa también este tipo de combustibles fósiles como materia prima, ya sea petróleo, gas natural o carbón. Debido al aumento constante del consumo de estos recursos, los cuales no son ilimitados, es necesario el desarrollo de nuevas tecnologías que puedan abastecer esta creciente demanda del consumo energético global. Unido al pensamiento de evitar el agotamiento completo de estos recursos naturales aparece la mayor concienciación de la sociedad sobre las consecuencias negativas de la emisión de gases de efecto invernadero, lo que ha desembocado en la búsqueda de mejoras tecnológicas que conduzcan al cumplimiento de ambos objetivos, todo ello amparado bajo acuerdos y tratados de carácter político y económico.

Es en esta situación donde la economía del hidrógeno aparece, teniendo como promesa la eliminación de la dependencia e inconvenientes asociados al uso masivo de los combustibles fósiles [77]. El uso del H₂ tiene como intención utilizar este gas como vector en los sectores energéticos, transporte, industriales, residenciales y comerciales. Una vez separado, el H₂ puede convertirse en electricidad o utilizarse directamente como combustible o reactivo en ciertas industrias (Figura 1.2.1). En particular, el H₂ es compatible con pilas de combustible, motores de combustión interna o turbinas de combustión para generación de energía con cero emisiones de

1. Introducción

gases de efecto invernadero. La economía del H₂ podría ayudar a reducir significativamente las emisiones de gases de efecto invernadero especialmente si este se produce a partir de fuentes de energía renovables o energía nuclear, además de en sistemas basados en combustibles fósiles con captura de carbono [78]. El hidrógeno puede ser almacenado, transportado en camión o por tuberías para usarse posteriormente bajo demanda. A pesar de ello, la baja densidad de este producto hace necesario el transporte y almacenamiento de este producto a elevada presión o combinado con otros elementos (como el transporte de amoniaco).

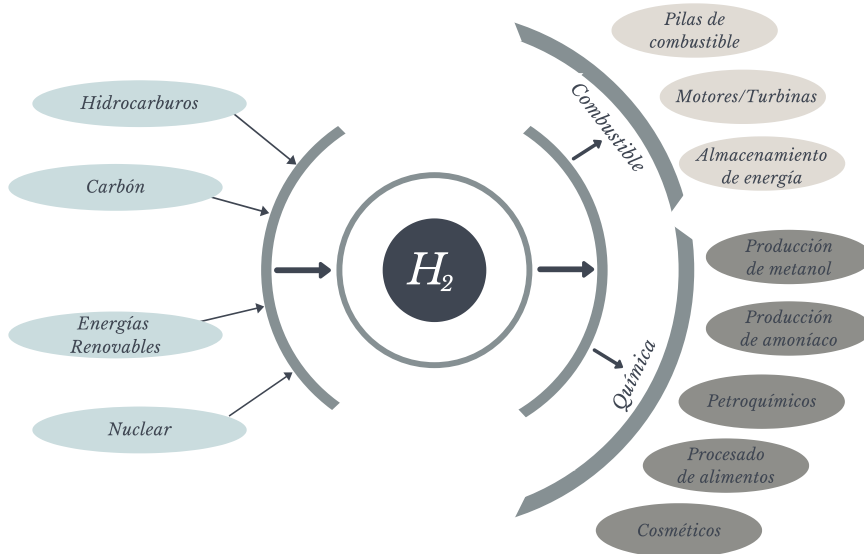


Figura 1.2.1. Visión del hidrógeno como vector energético.

En términos globales, distintas iniciativas aparecen en torno a la economía del H₂. Vale la pena mencionar el ejemplo de la *International Partnership for H₂ and Fuel Cells in the Economy* (IPHE) [79], cuya misión es facilitar y acelerar la transición a sistemas de energía y movilidad limpios y eficientes que utilizan H₂ y tecnologías de pilas de combustible tanto en aplicaciones a nivel usuario como a nivel industrial. Está formada por países como Estados Unidos de América, Canadá, Brasil, Rusia, Sudáfrica, República de Corea, Japón, India, China, además de la Comisión Europea. Las principales iniciativas se centran en regulaciones, códigos, estándares y seguridad.

A nivel europeo, los proyectos de I+D fueron financiados inicialmente por la Comisión Europea (CE) y desde 2008 por la *Fuel Cells and Hydrogen*

Joint Undertaking (FCH JU) [80] con el objetivo de desarrollar tecnologías H₂ listas para su comercialización en 2020. La FCH JU juega un papel importante en reunir recursos bajo una asociación pública / privada garantizando así el enfoque comercial, para hacer coincidir las actividades de I + D con las necesidades y expectativas de la industria, permitiendo escalar e intensificar los vínculos entre la industria y la comunidad de investigación. En los últimos 10 años, la FCH JU ha apoyado fuertemente estas tecnologías con un total de 893 millones de euros y asegurando otra inversión de capital similar de otras fuentes. Estas inversiones se realizan con el objetivo de desarrollar pilas de combustible e infraestructuras para el H₂ (producción, almacenamiento y distribución), tanto para aplicaciones de transporte como producción eléctrica, además de financiar proyectos transversales sobre seguridad, educación o regulaciones.

1.3 Producción de hidrógeno

A pesar de que el hidrógeno está siendo producido para diversas aplicaciones [81], está ganando popularidad para su uso como portador de energía para mercados estacionarios y de transporte con tecnología de pilas de combustible [82]. La Figura 1.3.1a muestra la capacidad de producción de hidrógeno a nivel mundial de los diferentes países agrupados según su localización geográfica. Este valor global se estima en aproximadamente 400 millones de metros cúbicos por día. Puede observarse como la mayor capacidad de producción se encuentra en Asia, seguido de América y Europa [83]. Hay que destacar que, de cada región, el país con una mayor capacidad de producción es Estados Unidos de América (28%), Japón (10%) y República de Corea (10%), Alemania (5%) y Egipto (0,1%) [83]. Dentro del continente europeo los países con una mayor capacidad de producción son Alemania, Países Bajos, España, Italia y Rusia. Para puntualizar el caso de España, a este país se le atribuye en torno al 2% de la capacidad de producción de hidrógeno global. La Figura 1.3.1b muestra la capacidad productiva de H₂ de los países del continente europeo [83].

1. Introducción

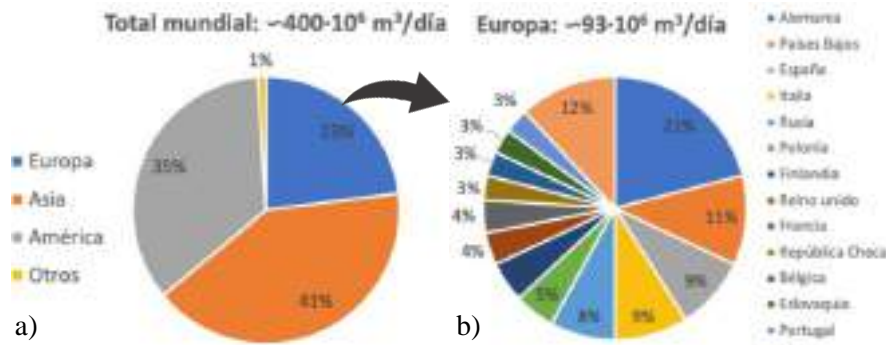


Figura 1.3.1. Capacidad de producción de hidrógeno en 2020 a nivel mundial (a) y a nivel europeo (b) [83].

Actualmente, procesos como el reformado de metano con vapor [84] y la electrólisis [85,86] son los principales métodos de producción de H₂. Además de la utilización de estos métodos, es importante el desarrollo de nuevas tecnologías tanto a partir de combustibles fósiles como de energías renovables, siendo especialmente necesario enfocar la producción desde los recursos de energías renovables [87]. En el siguiente apartado se resumen los procesos de producción de hidrógeno más utilizados, mostrando un esquema visual de los principales en la Figura 1.3.2.

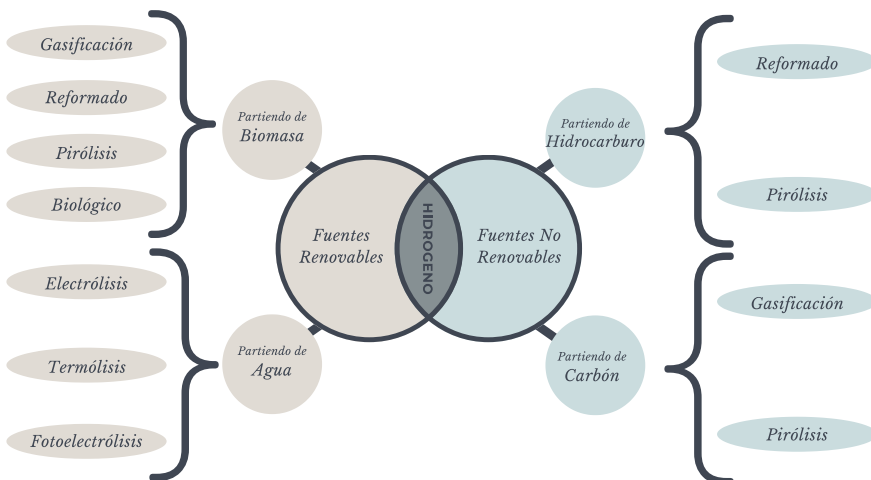


Figura 1.3.2. Principales métodos de producción de hidrógeno basados en combustibles fósiles y fuentes de energía renovables.

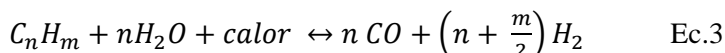
1.3.1 Fuentes no renovables

Actualmente, los combustibles fósiles son el principal recurso para la producción de hidrógeno, debido a su precio ya que éste se usa en su mayor parte como materia prima para procesos de refino o en la industria petroquímica [88]. Se estima que aproximadamente el 48% de esta producción de hidrógeno a partir de combustibles fósiles se realiza a partir de gas natural, seguido de un 30% producido a partir de aceites pesados y nafta y un 18% utilizando carbón [89]. Las dos alternativas tecnológicas más utilizadas con este tipo de materia prima son el reformado y la pirolisis.

El reformado se define como un proceso químico a partir del cual el combustible fósil es convertido en H₂ [12,90]. Esta técnica suele implicar varias etapas consecutivas: generación de gas de reformado o síntesis, reacción de desplazamiento de gas de agua (en inglés *Water Gas Shift*, WGS) y purificación de gas. Además del hidrocarburo, se deben añadir otros reactivos como puede ser vapor (reformado con vapor), oxígeno (reformado oxidativo) o ambos (reformado autotérmico) [91]. Por lo general, a pesar de los distintos reactivos que pueden añadirse junto al hidrocarburo, la reacción de desplazamiento de gas de agua suele aplicarse sobre el gas de síntesis para disminuir de esta manera la presencia de monóxido de carbono, a la vez que se incrementa la producción de H₂, tal y como se describe en la siguiente ecuación:

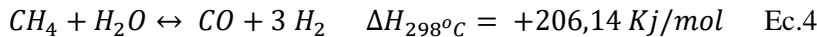


Uno de los procesos más desarrollados es el reformado con vapor, obteniendo eficiencias superiores al 85%, y usado ampliamente en producción de hidrógeno a gran escala [92]. Las materias primas involucradas en este proceso consisten en metano, gas natural y otros gases que contienen metano a través de varias combinaciones de hidrocarburos ligeros, incluyendo etano, propano, butano, pentano, nafta ligera o pesada [12]. La etapa de reformado de vapor con agua se basa en la siguiente reacción endotérmica:



El combustible más comúnmente utilizado es el metano (CH₄), siendo en este caso la reacción claramente endotérmica requiriendo 206,14 kJ por mol de metano para que la reacción tenga lugar. En este caso la reacción es la siguiente:

1. Introducción



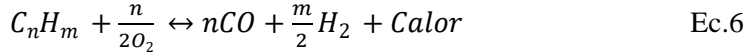
Este tipo de procesos tienen lugar a temperaturas en torno a 800-1000 °C y presiones moderadas, comprendidas entre 13 y 30 bar [90,91]. Es habitual utilizar una relación de 2,8-3,2 partes de vapor por cada parte de carbono, mientras que, respecto al catalizador son ampliamente utilizados los de base Ni, Co, Rh, Pd y Pt [90]. El coste de producción de H₂ para una planta con una capacidad de diseño de 380,000 kg/día, con un factor de capacidad del 90% y un coste de gas natural de 34 US\$/MWh, se estima en 2,27 y 2,08 US\$/kg con y sin captura de carbono, respectivamente [93].

Una alternativa este proceso es el reformado oxidativo. En este proceso, similar al anterior, el hidrocarburo reacciona con vapor para transformarse en H₂ y CO₂, destacando el uso de la oxidación parcial al realizar el proceso con una presencia de O₂ en el medio de reacción en una cantidad por debajo de la estequiométrica [90]. El agente oxidante puede ser tanto oxígeno puro como aire. Como materia prima puede utilizarse desde metano hasta nafta utilizando catalizadores de las mismas familias a los mencionados anteriormente. La reacción del proceso en caso de partir de metano sería la siguiente:



En este proceso generalmente la reacción tiene lugar a temperaturas superiores a 700 °C, utilizando presiones comprendidas entre 1 y 30 bares [90]. Hay que destacar que esta reacción es muy rápida y exotérmica. Este proceso es altamente beneficioso en el caso de trabajar con aceites pesados residuales, debido a que, durante la desulfuración (posterior al reformado), se obtiene O₂ el cual es recirculado para continuar con el propio proceso. En un estudio de un caso típico utilizando carbón como materia prima, se reportó el coste del kg de H₂ como 1,63 y 1,34 US\$ con y sin captura de carbono, respectivamente [93,94].

Otra alternativa a es el reformado autotérmico, donde la oxidación exotérmica parcial proporciona el calor durante el reformado con vapor endotérmico, lo que conduce a una mayor producción de H₂. Es decir, se utilizan como reactivos el combustible, vapor y oxígeno o aire [91]. Las reacciones principales de este proceso para un hidrocarburo genérico son las siguientes:



Típicamente, el vapor es inyectado, junto con O₂ o aire, en la cámara de reformado para que tengan lugar de manera simultánea las reacciones de reformado y oxidación [95]. A pesar de la alta temperatura de operación necesaria (1100-1500 °C) [90], este proceso implica menores costes de inversión, dando lugar a que las plantas avanzadas de reformado autotérmico a gran escala con ~ 90% de captura de CO₂ y una eficiencia de ~ 73% permiten un coste de producción de H₂ aproximado de 1,48 US\$ por kg [96].

Los procesos de pirolisis implican la descomposición térmica bajo condiciones específicas para la producción de H₂. Dentro del campo de los combustibles fósiles, este proceso puede realizarse utilizando como materia prima tanto carbón como hidrocarburos pesados, siendo más eficiente el uso de estos últimos por su mayor contenido en hidrógeno. La descomposición termocatalítica de hidrocarburos líquidos más ligeros produce H₂ y carbono elemental, mientras que las fracciones de hidrocarburos más pesadas necesitan la realización de dos etapas, una primera hidrogasificación seguida de un posterior craqueo de metano para la obtención de H₂ [97,98]. Estos procesos no requieren la posterior captura de CO₂ u otros gases residuales, lo que puede llegar a suponer una disminución del coste final del H₂ en aproximadamente un 30% respecto a los procesos de reformado [98,99]. El mayor inconveniente de esta tecnología está relacionado con la etapa de separación de H₂ debido a la baja presión parcial de H₂ en la mezcla de reacción. Las reacciones principales asociadas a un proceso de pirolisis son las siguientes [100,101]:



Este tipo de procesos tiene lugar a temperaturas entre los 300 y 650 °C [100], destacando el uso de catalizadores metálicos del grupo VIIIB como Ni, Co, Fe, Ru, Rh, Pt, Pd [102] soportados generalmente sobre SiO₂ o Al₂O₃ [103]. Igual que en el caso del reformado, puede aplicarse una etapa de reacción de desplazamiento de gas de agua para incrementar la producción de H₂ a la vez que se reducen las emisiones CO (Ec. 2).

1. Introducción

La gasificación desde combustibles fósiles se basa principalmente en la transformación de carbón o compuestos sólidos de tipo carbonoso desde su estado sólido a un gas de síntesis compuesto fundamentalmente por CO e H₂. Este proceso se desarrolla a elevada temperatura (700-1400 °C) [100], con un rango de presiones entre 1 y 30 bares, lo que conlleva un elevado consumo energético. Unido a esto, los bajos rendimientos asociados a este proceso junto a la emisión de CO₂ a la atmósfera, son los principales inconvenientes de este proceso. Para este proceso destaca el uso de catalizadores base Ni, aunque también se utilizan otros con base Pt, Ru, Zr y Rh [104]. De manera análoga a lo comentado para el caso del reformado y la pirólisis, la reacción de desplazamiento de gas de agua para reducir las emisiones de CO e incrementar la producción de H₂ al mismo tiempo (Ec. 2).

1.3.2 Fuentes renovables

Como se comentó previamente, las alarmantes cifras sobre el continuo aumento de emisiones de CO₂ antropogénico requiere la necesidad de un cambio tecnológico hacia alternativas fuera del ciclo de carbono. Ante esta disyuntiva, y previendo un cada vez más próximo agotamiento de los combustibles fósiles tradicionales y el aumento la conciencia sobre el respeto al medio ambiente, se prevé que se produzca una importante transición y el uso de recursos renovables domine el sector energético en las próximas décadas. Las siguientes secciones resumen algunos de los principales métodos para la producción de H₂ a partir de materias primas de carácter renovable.

La biomasa es una materia prima de carácter renovable y puede ser obtenida a partir de una gran variedad de fuentes tales como madera y restos de poda, pastos o cultivos específicos y residuos de éstos. También pueden englobarse en esta categoría los residuos orgánicos, tanto de carácter doméstico como industrial, y los desechos de ganadería producidos por la cría de animales, lo que puede tener un especial atractivo en términos de valorización energética [105]. La producción de hidrógeno a partir de los diferentes tipos de biomasa se puede llevar a cabo, de manera general, mediante procesos termoquímicos y/o biológicos.

El hidrógeno, entre otras alternativas, puede ser producido a partir de biomasa mediante procesos como la gasificación o pirólisis [106]. El primero de estos procesos se realiza a elevada temperatura (800-1.200 °C) [107], donde el CH₄ y CO generados junto con otros productos gaseosos pueden ser

post-procesados para un mayor rendimiento a H₂ mediante reformado con vapor y reacciones WGS, como ya se comentó en apartados anteriores [108–110]. La eficiencia de este proceso varía en función del tipo de materia prima, el catalizador empleado y la temperatura, el número de etapas [111]. En un proceso típico de gasificación- vaporización- reformado- compresión- WGS de biomasa se requieren de entrada 2,4 TJ de energía de materia prima por cada TJ de H₂ producido [112]. Se estima que para una planta con una producción de 139.700 kgH₂/día que utiliza biomasa, con un coste de 46-80 \$ por tonelada, el coste de producción de H₂ sea de 1,77 a 2,05 \$ por kg [93]. Por otro lado, la pirólisis de biomasa generalmente se lleva a cabo a ~ 550 °C en atmósfera inerte [113]. Las variables que afectan en mayor medida al proceso de pirólisis son las mismas que se han comentado previamente para el proceso de gasificación [111]. El coste de la producción de H₂ estimado está en el rango de 1,25 a 2,20 US\$/kgH₂, dependiendo del tipo de biomasa y el tamaño del lote [113].

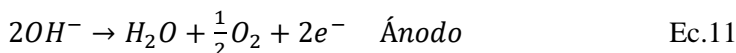
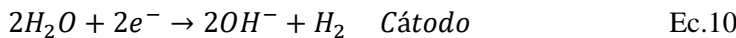
Como alternativa a estos procesos existen los procesos biológicos. Los más empleados para la producción de H₂ son la bio-fotólisis directa e indirecta, la fotofermentación y la fermentación oscura. Estos procesos destacan entre otros debido a su bajo consumo de energía y al uso de condiciones de operación sencillas, 30-40 °C y presión atmosférica [100,114]. El proceso biológico de producción de H₂ involucra la fotólisis de agua asistida por bacterias o algas a través de sistemas de enzimas hidrogenasa o nitrogenasa, y el uso de biomasa para procesos fermentativos donde las materias que contienen carbohidratos se convierten en ácidos orgánicos y posteriormente en H₂ gaseoso mediante tecnologías de bioprocесamiento [115,116]. En caso de la utilización de la bio-fotólisis directa para la producción de hidrógeno, con un foto-biorreactor con una eficiencia de conversión solar del 10% y un coste de 50 US\$/m², podrían alcanzarse precios de 2,13 US\$/kgH₂ [117]. En el caso de la biofotólisis indirecta los precios podrían alcanzar valores de 1,42 US\$/kgH₂, aunque este proceso se encuentra todavía en una etapa conceptual [118]. Por otro lado, la producción de H₂ basada en algas es un proceso prometedor ya que utiliza fuentes de combustible renovables y CO₂ [119]. Sin embargo, el proceso está limitado debido a ciertos inconvenientes, como el bajo potencial de producción de H₂ y el requisito de una gran superficie para recoger la luz. Otro proceso de biofotólisis es la fermentación, la cual implica la conversión microbiana de materia prima orgánica en presencia o ausencia de oxígeno en alcoholos, acetona, etc [116,120]. Estos procesos son prometedores para la

1. Introducción

producción de H₂, ya que utilizan materiales de desecho y proporcionan una generación de energía económica de manera simultánea al tratamiento de desechos. Sin embargo, la baja eficiencia de conversión de energía solar y la demanda de foto-biorreactores anaeróbicos, son algunas de las principales barreras que restringen estos procesos [121–123]. De hecho, el proceso termoquímico es superior en comparación con el proceso biológico debido a una cinética más rápida.

Otra alternativa ampliamente utilizada es la producción de H₂ mediante la división de la molécula de agua. Esta es una de las rutas más ambiciosas y que tendría grandes beneficios medioambientales al encontrarse totalmente fuera del ciclo del carbono. Dentro de las diferentes posibilidades existentes, las técnicas de electrólisis, termólisis y fotoelectrólisis son algunas de las más prometedoras, detallándose a continuación sus características más relevantes [85,124,125].

La producción de H₂ mediante la electrólisis del agua consiste en descomponer la molécula de H₂O en sus elementos constituyentes, hidrógeno y oxígeno, mediante la aplicación de una corriente eléctrica. Este proceso endotérmico es ampliamente conocido, basado en dos reacciones redox complementarias (Ec. 10 y 11), aunque aún no resulta competitivo al compararlo con otras alternativas termoquímicas [86].



Una de las alternativas más atractivas es emplear el excedente de electricidad generado a partir de recursos de energía renovable, como la eólica y la solar, para llevar a cabo la electrólisis, produciendo H₂ verde, pudiendo además ayudar a minimizar las fluctuaciones en los sistemas de energía renovable mediante el almacenamiento de H₂ [126] en sistemas de producción centralizados o descentralizados. En los procesos de electrólisis, se produce H₂ puro en el cátodo y éste es separado del agua y el O₂, que se genera en el ánodo. El proceso de electrólisis para la producción de H₂ a gran escala a partir de agua no puede competir en la actualidad con las otras técnicas debido a la gran necesidad de energía eléctrica (~ 40 kWh/kgH₂). Actualmente, los electrolizadores alcalinos comerciales, con una eficiencia aproximada del 73%, pueden alcanzar tasas de producción anual de 380.000 kgH₂ con un consumo de energía del sistema de 53,4 kWh/kgH₂, lo que supone un coste de 3,2 US\$/ kgH₂ [127]. A pesar de esto hay que destacar

que los electrolizadores jugarán un papel importante en la transición hacia la economía H₂ con electricidad generada a partir de fuentes renovables. Esto implica la integración de las energías renovables en la red, donde el H₂ se considera el único vector energético. Los electrolizadores pueden convertir la electricidad renovable en H₂ que puede almacenarse, transportarse y distribuirse a los usuarios finales para diversas aplicaciones.

El proceso de termólisis implica la división de la molécula de agua a alta temperatura, ~ 2.500 °C, debido a su alta energía libre de Gibbs. Para hacer que este proceso sea más sostenible, se han propuesto varios ciclos termoquímicos de división del agua utilizando catalizadores basados en Cu-Cl o SnO₂ que utilizan flujo solar o energía nuclear, con el interés futuro de centrar su aplicación en acumuladores solares [128]. En este caso el coste de producción del kg de H₂ dependerá principalmente del coste del equipamiento utilizado y de los problemas de corrosión asociados a este, además de la eficiencia general del sistema [129].

El proceso de foto-electrólisis implica la división del agua por la carga generada en un electrodo semiconductor mediante la absorción de luz visible [130]. Se utilizan materiales semiconductores que generan pares de electrones a partir de la absorción de fotones, al mismo tiempo es aplicado un potencial de polarización el cual hace que los electrones separados fluyan a través de un circuito externo hacia el cátodo para acoplarse con H⁺ para la producción de H₂. Mientras tanto en el ánodo tiene lugar la división de la molécula de agua para generar H⁺ y O₂. Este proceso está limitado principalmente por el transporte de carga y la eficiencia de absorción de la luz visible del electrodo semiconductor [131]. Un estudio reciente sobre este proceso de producción de hidrógeno estimo un coste aproximado de 10,36 US\$/kgH₂ [132].

1.3.3 Etapa de purificación

Una vez producido el hidrógeno, su purificación es una etapa crucial, para adaptarlo de esta manera a los requisitos de calidad que la posterior aplicación necesite. Hay que destacar que las tecnologías de purificación son muy relevantes a la hora de implantar el hidrógeno como vector energético de una manera eficiente. Como se comentó previamente, de manera general el hidrógeno es obtenido junto a otros subproductos, siendo necesaria la separación de este del resto de compuestos. Actualmente destaca el uso de la adsorción por cambios de presión (PSA), la destilación criogénica o la tecnología de membranas.

1. Introducción

La adsorción por cambios de presión está basada en la diferencia de afinidades de los diferentes compuestos de una corriente gaseosa por un determinado material adsorbente. Con este proceso pueden alcanzarse valores de pureza muy elevados (99,99%) con factores de recuperación en torno al 70-85%. A pesar de ser la tecnología más extendida universalmente para este proceso presenta un elevado gasto energético, lo que repercute en su rentabilidad económica especialmente para pequeñas producciones.

La destilación criogénica aprovecha las diferencias entre las temperaturas de los puntos de ebullición de los componentes de la corriente gaseosa para realizar la separación. Este proceso se realiza a baja temperatura, lo cual supone también un elevado gasto energético y económico. Los factores de recuperación de hidrógeno de este proceso son superiores a los mencionados previamente para la adsorción por cambios de presión (>85%), pero no se alcanza niveles de pureza superiores al 95%.

Por otro lado, la tecnología de membranas apareció como una alternativa a estos procesos de purificación de hidrógeno. Esta tecnología puede alcanzar valores de pureza muy elevados (99,99%) y permite combinarse con los procesos de reacción en una unidad denominada reactor de membrana. Este concepto se propuso por primera vez a finales de la década de los 60, pero la mayor parte del desarrollo se ha logrado tan solo en los últimos 20 años, momento en donde se encuentran la mayoría de las publicaciones y patentes sobre el tema. El uso de un reactor de membrana puede proporcionar algunas ventajas en comparación con un proceso tradicional de reacción y separación, como la mejora de la productividad, la obtención del producto purificado en un solo paso o el desarrollo de un proceso simple con un menor coste de capital al necesitar menos equipos. Además, a diferencia de los procesos anteriores este método permite la realización de la etapa de separación en continuo sin añadir aditivos al medio y puede ser económicamente viable para bajos volúmenes de producción. Debido a que esta tecnología es la que se desarrolla en este trabajo, en el siguiente apartado se ampliaran los fundamentos de este método de separación.

1.4 Tecnología de membranas

Las membranas son básicamente barreras que permiten el flujo selectivo de algunos componentes de una corriente de mezcla de gases. De manera general las membranas deben tener las siguientes características: alta selectividad al producto deseado, alto flujo, bajo coste y alta estabilidad

mecánica y química. Las membranas pueden clasificarse siguiendo diferentes criterios, los más utilizados son su naturaleza, su estructura y el régimen de separación en el que trabajan. Según su naturaleza se pueden encontrar dos tipos distintos, naturales y sintéticas. Dentro del primero pueden encontrarse membranas inorgánicas y biológicas, mientras que el segundo grupo puede dividirse a su vez en orgánicas (poliméricas) e inorgánicas (cerámicas, vítreas y metálicas). Según su estructura las membranas pueden organizarse en dos grandes grupos, macroscópicas y microscópicas. Las membranas con una estructura macroscópica pueden a su vez subdividirse en laminares, tubulares y fibras huecas. Por otro lado, las membranas con una estructura microscópica pueden organizarse según su configuración, simétricas y asimétricas, y según su porosidad, distinguiendo entre densas y porosas. Dentro de las membranas con una configuración microscópica porosa se distinguen tres categorías atendiendo al criterio de tamaño de poro: microporosas (tamaños de poro < 2 nm), mesoporosas (2-50 nm) y macroporosas (> 50 nm) [120]. Finalmente, atendiendo al criterio del régimen de separación pueden encontrarse tres tipos de membranas: porosas, densas y de intercambio iónico. La Figura 1.4.1 muestra un esquema general de las distintas clasificaciones de las membranas, atendiendo a los distintos criterios previamente descritos.



Figura 1.4.1. Clasificación de membranas según su estructura, régimen de separación y naturaleza.

En concreto, para la separación de hidrógeno se han utilizado distintos tipos de membranas entre las que destaca el uso de membranas poliméricas [133], de carbono [134], cerámicas microporosas [79], cerámicas densas [135] y metálicas densas [136,137]. Como comportamiento general las membranas que presentan un alto flujo de permeado suelen presentar bajos valores de selectividad. Por ejemplo, las membranas poliméricas, de carbono o cerámicas microporosas suelen obtener altos flujos, debido principalmente a las bajas selectividades. Por el contrario, las membranas densas cerámicas y metálicas están asociadas a valores de selectividad muy elevados, generando en ocasiones flujos de permeado bajos. A pesar de esto, no hay una única membrana válida para la separación de hidrógeno ya que habrá que seleccionar en cada caso la membrana más adecuada para las condiciones de operación del proceso y la pureza del H₂ deseada, sin olvidarse del coste.

Las membranas poliméricas presentan la principal ventaja de su bajo coste, además de poder fabricarse de una manera relativamente sencilla. Destaca el uso de Nafion® a pesar de presentar problemas de absorción de agua y su baja temperatura de uso (< 100 °C), aunque en la actualidad se han

presentado modificaciones de este permitiendo aumentar poco a poco la temperatura de trabajo [138]. También se han desarrollado otro tipo de materiales que se han podido utilizar para la fabricación de membranas como es el caso de la polisulfona sulfonada (S-PSU), el polibenzimidazol sulfonado (S-PBI), el polietersulfona sulfonado (S-PES) o el poli (éter-éter-cetona) sulfonado (S-PEEK) [139]. Por otro lado, también destaca el desarrollo de los polímeros de microporosidad intrínseca, conocidos como PIMs (*polymers of intrinsic microporosity*). Estos se definen como polímeros macromoleculares con un alto volumen de poros interconectados de menos de 2 nm de diámetro [140]. Dentro de esta categoría el material conocido como TPIM-1 destaca por presentar uno de los valores de selectividad H₂/N₂ más elevados, a pesar de que este valor es solamente 156 [133].

Respecto a las membranas de carbono, estas presentan un coste de fabricación superior al de las poliméricas. Como ventaja presenta una elevada temperatura de trabajo de hasta 900 °C. los principales inconveniente son el bajo flujo de permeado y selectividad (< 200), además de su fragilidad [28,134].

Las membranas cerámicas microporosas se caracterizan por ser inertes a cualquier tipo de gas y operar en un amplio rango de temperaturas (200-600 °C). Igual que en el caso de las membranas comentadas previamente, presenten una baja selectividad al hidrógeno (< 300). Pueden ser fabricadas a partir de numerosos materiales como alúmina, zirconia, sílice o zeolitas, siendo los dos últimos los más relevantes [28,134].

El uso de cerámicas densas para la fabricación de membranas para la separación de hidrógeno está asociado a una selectividad muy elevada (> 1000) y unos flujos de permeado bajo. En este caso la temperatura de trabajo permitida para esta membrana es la más elevada, llegando al valor de 900 °C. Estas membranas se basan en el uso de perovskitas, material que se compone de mezclas de óxidos alcalineoterreos con la estructura cristalina ideal ABO₃ [141]. La composición de estos materiales va desde formulaciones simples como BaCe_{0,80}Y_{0,20}O_{3-δ}, BaZr_{0,9}Fe_{0,1}O_{3-δ} o SrCe_{0,95}Tb_{0,05}O_{3-δ}, hasta fórmulas más complejas que añaden aleantes para mejorar sus propiedades de permeación o estabilidad como Ni-BaZr_{0,10}Ce_{0,70}Y_{0,10}Yb_{0,10}O_{3-δ}, Pd-BaCe_{0,40}Zr_{0,40}Gd_{0,10}Dy_{0,10}O_{3-δ} o La_{5,5}WO_{11,25-δ}-La_{0,87}Sr_{0,13}CrO_{3-δ} [135].

Las membranas metálicas densas se presentan como una buena alternativa para la obtención de hidrógeno de elevada pureza. Presentan

1. Introducción

selectividades ideales (> 1000) y elevados flujos de permeado. No están compuestas por materiales frágiles y permiten trabajar a elevada temperatura (< 700 °C). Dentro de los metales permeables al hidrógeno destacan el niobio, vanadio, tántalo y paladio. Por otro lado, también se han desarrollado membranas metálicas amorfas, como $Zr_{36}Ni_{64}$, $Nb_{20}Ti_{40}Ni_{40}$, o $(Ti_{45}Zr_{16}Be_{20}Cu_{10}Ni_9)_{100-x}Nb_x$ [142]. La Figura 1.4.2, muestra una representación gráfica de la permeabilidad al hidrógeno frente a la selectividad H_2/N_2 para los diferentes tipos de membranas utilizadas. Puede observarse como las membranas metálicas densas presentan una alta permeabilidad, además de una alta selectividad. A pesar de la amplia variedad de membranas metálicas [143], la tecnología de membranas basadas en Pd es la más desarrollada actualmente debido a que presentan una alta permeabilidad y selectividad al hidrógeno, una estabilidad térmica razonable y una resistencia mecánica adecuada [136,137].

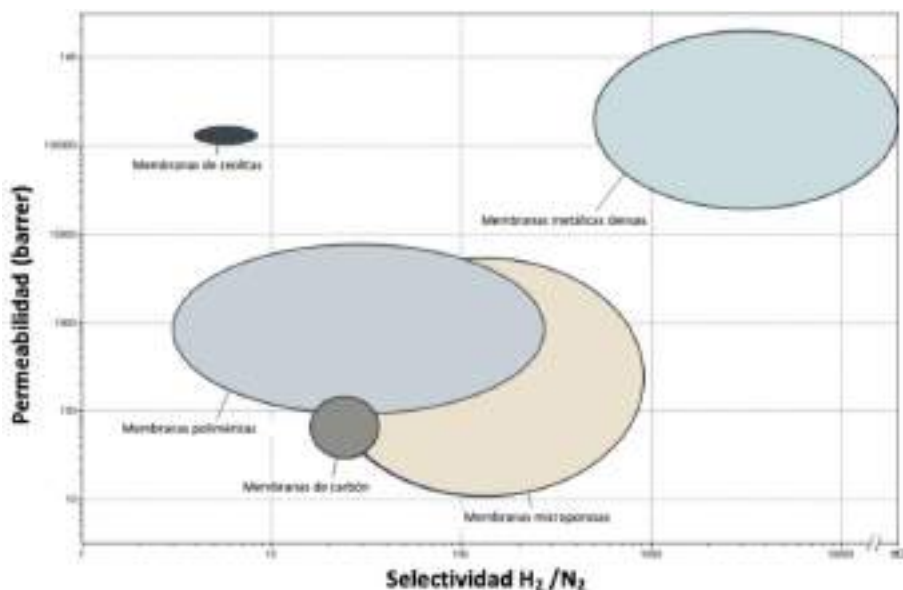


Figura 1.4.2. Visión general de la permeabilidad y selectividad al H_2 para diversos tipos de membranas [136]

1.5 Membranas de paladio

Las membranas densas de base Pd pueden clasificarse en dos grupos principales, autosoportadas y soportadas. Respecto al primer tipo, generalmente se preparan a partir de láminas de paladio relativamente gruesas (o aleaciones base Pd) que, como Tosti y col. Indican, en caso de buscar geometrías tubulares, son laminadas en frío y posteriormente soldadas [17,144]. Los espesores típicos varían de 50 a 150 µm. Sin embargo, como se mencionó anteriormente, una capa gruesa de Pd disminuye la velocidad de permeación del hidrógeno y aumenta el coste de la membrana. Por lo tanto, el desarrollo de nuevas membranas delgadas sin poner en peligro la resistencia mecánica y la presencia de defectos es el objetivo principal de muchos investigadores en este campo [60,61,145]. Este objetivo puede lograrse mediante la fabricación de membranas soportadas, en las que se incorpora una delgada capa de Pd en la superficie de un material poroso que proporciona la resistencia mecánica requerida a la membrana soportada [72,146–148]. Esta compleja tarea es objeto de numerosos estudios, ya que se deben considerar muchos factores, por ejemplo, la compatibilidad entre el soporte y la capa selectiva, la cual determina la resistencia mecánica de la membrana debido a grietas que se pueden formar a altas temperaturas como consecuencia de la diferencia en los coeficientes de expansión.

Se pueden utilizar como soporte para la capa selectiva al H₂ numerosos materiales porosos como, por ejemplo, el vidrio Vycor [149,150], metales sinterizados [72,146,151], una amplia variedad de cerámicas [54,72,152,153] e incluso polímeros [154–156]. Las características más relevantes para la selección de los soportes incluyen propiedades de porosidad (principalmente porosidad media y distribución de tamaños de poro), rugosidad de la superficie y estabilidad mecánica, química y térmica [157]. En este contexto, se consideran factores positivos una gran porosidad con una distribución de tamaños de poro estrecha, alta resistencia mecánica y resistencia química, además de un coeficiente de expansión térmica similar al de la capa selectiva [158]. En cuanto a las propiedades texturales, la porosidad del soporte debe estar lo suficiente abierta e interconectada para no ser una limitación al transporte del gas a través del soporte, además los tamaños boca y garganta de los poros son considerados críticos [159]. Se acepta que generalmente tanto el tamaño de poro como la rugosidad determinan fuertemente la morfología y la continuidad de la capa selectiva.

1. Introducción

En este sentido, Mardilovich y col. [160] indicaron que el espesor mínimo de una capa de Pd preparada mediante deposición no electroquímica sobre un soporte poroso es aproximadamente tres veces el tamaño de poro medio de los poros más grandes. A pesar de que el vidrio Vycor fue uno de los primeros soportes porosos utilizados para incorporar Pd mediante ELP [149,150], actualmente es más frecuente el uso de metales porosos sinterizados [72,146,161,162] o materiales cerámicos [54,72,152,163].

Actualmente, el uso de soportes porosos polímeros en reactores de membrana, que generalmente operan a alta temperatura, es escaso debido a la baja resistencia térmica de estos materiales [164]. Para esta aplicación en particular, los soportes metálicos son los preferidos, como el acero inoxidable 316L [72,151], Hastelloy [165,166], Inconel [162], níquel [167] o, en algunos casos particulares, aleaciones base Ti como Ti-Al [168] o Ti-Ni [169]. Por lo general, estos garantizan buenas propiedades mecánicas, dureza y un coeficiente de expansión térmico similar al del paladio, en el rango de $10,5\text{--}12,5 \cdot 10^{-6} \text{ }^{\circ}\text{C}^{-1}$. Además, estos materiales se sellan y se acoplan fácilmente a los módulos de un reactor de membrana, normalmente fabricados en acero inoxidable [164]. Sin embargo, estos soportes presentan poros relativamente grandes con una amplia distribución de tamaños de poro, lo cual dificulta la generación de una capa de Pd delgada y sin defectos. De hecho, es habitual que los fabricantes no proporcionen el valor concreto de los tamaños de poro en estos soportes, dando un valor promedio relativo, conocido como grado medio, que representa el tamaño de partícula que es rechazado en un 95% en un proceso de filtración [63]. Además, también es posible que aparezca la interdifusión metálica entre el soporte y la capa selectiva base Pd después de operar a altas temperaturas durante largos períodos de tiempo. Este fenómeno causa una acusada disminución en la capacidad de permeación [157]. Para superar ambos inconvenientes, el soporte original puede modificarse antes de la incorporación de la capa selectiva al H₂ [157,161,167].

Por otro lado, los soportes cerámicos proporcionan una superficie más lisa con un control preciso de la porosidad y distribuciones estrechas de tamaños de poros, de hasta unos pocos nanómetros [39]. Estas propiedades facilitan la deposición de capas selectivas sin defectos y con un grosor realmente bajo, es por eso que muchos investigadores optan por usar las cerámicas como soportes para membranas [42,54,152]. Entre algunas posibilidades, predomina el uso de alúmina, Al₂O₃ [170,171], que generalmente combina las partículas α - Al₂O₃ y γ - Al₂O₃ para preparar

soportes asimétricos. Esta asimetría es generada mediante la formación de poros grandes en el núcleo, para garantizar mayores permeabilidades, y pequeños en la parte exterior, para facilitar la incorporación de una capa selectiva delgada [72]. Sin embargo, estos materiales presentan un coeficiente de expansión térmica notablemente diferente al de los materiales utilizados para la capa selectiva. Además, tienen una resistencia mecánica baja, lo cual pone en peligro la integridad de la membrana soportada, factor determinante en los reactores de membrana [159]. Otra alternativa menos frecuente para preparar soportes cerámicos es el uso de zirconia estabilizada con itria ($\text{ZrO}_2\text{-YSZ}$), con un coeficiente de expansión térmica de $10,0 \cdot 10^{-6} \text{ }^{\circ}\text{C}^{-1}$, valor más cercano al de los metales utilizados para la capa selectiva [153,164].

De cualquier modo, tanto soportes metálicos como cerámicos pueden ser usados para la preparación de membranas soportadas totalmente densas de base Pd, aunque en la actualidad todavía no se ha alcanzado una solución prevalente. Las ventajas proporcionadas por los soportes cerámicos son problemas cuando se utilizan soportes metálicos y viceversa, por lo que se pueden observar diferentes tendencias de uso en la literatura. Algunos autores se inclinan hacia soportes cerámicos, formados principalmente por alúmina, para garantizar la incorporación de una capa selectiva delgada sin defectos, centrándose principalmente en la preparación de la membrana, mientras que otros prefieren el uso de soportes metálicos pensando en la aplicación e integración real de las membranas en dispositivos industriales de acero inoxidable.

Independientemente del material constituyente de los soportes, la geometría de este también es importante, pudiéndose encontrar distintas configuraciones en la literatura, principalmente geometrías planas [168,169], tubulares [72,146] y de fibra hueca [172,173]. En general, el uso de materiales cerámicos y metálicos en geometrías tubulares son lo más frecuente en caso de considerar su uso en un reactor de membrana, mientras que los soportes metálicos con geometría plana son más frecuentes en el caso de estudiar la preparación de la membrana solo con fines de purificación [174–176]. Sin embargo, esta situación ha cambiado en los últimos años con la aparición de geometrías de tipo disco y fibras huecas en el diseño de sistemas de reactores con microcanales [177].

La Tabla 1.5.1 resume los soportes inorgánicos más frecuentes presentes en la literatura para la preparación de membranas base Pd,

1. Introducción

indicando parámetros importantes tales como material, geometría, porosidad media y tamaños de poros. Se han considerado varios fabricantes relevantes en todo el mundo, como Mott Metallurgical Corporation (Estados Unidos de América), Pall Corporation (Estados Unidos de América), GKN Sinter Metal (Reino Unido), Inopor GmbH (Alemania), TAMI industries (Francia) o NGK Insulators (Japón). Actualmente, se pueden lograr precios más bajos para los soportes cerámicos, a pesar de que presentan tamaños de poro más pequeños que los metálicos, aunque su reutilización no es fácil debido a la frecuente rotura durante la operación.

Tabla 1.5.1 Soportes inorgánicos comerciales más comúnmente utilizados para la preparación de membranas de paladio.

Compañía	Material	Geometría	Espesor (mm)	Porosidad (%)	Tamaño poro (nm)
Mott	Ac.Inox: 304L,316L,310, 347,430 Hastelloy: C-22, C-276, X, N, B Inconel: 600, 625, 690	Disco, placa, copa, tubo	1-3		0,1-100·10 ³
GKN	Ac. Inox: 304L 316L, 904L, 310 Hastelloy: C-22, C-276, X Inconel: 600, 625 Monel: 400 Bronce Titanio	Disco, tubo	1,5-3		0,1-200·10 ³
Pall	Ac. Inox: 304L 316L, 310 SC Hastelloy: X Inconel: 600 Monel: 400 SiC/Al ₂ O ₃ Mullita	Copa, tubo	- ^(a)		>0,1·10 ^{3(a)}
Inopor	α -Al ₂ O ₃ TiO ₂ ZrO ₂ γ -Al ₂ O ₃ SiO ₂	Tubo, tubo multicanal	40-55 30-55 30-40 40-55 30-55 30-40	70-800 100-800 5-30 1 110 3 5-10 1	
Tami	TiO ₂ /ZrO ₂	Tubo, tubo multicanal	2		4,5·10 ³

^(a) bajo pedido

Como se mencionó anteriormente, no es común el uso directo de soportes comerciales para preparar membranas soportadas, especialmente en el caso de sustratos metálicos. Por el contrario, es habitual realizar pretratamientos y modificaciones superficiales del soporte para mejorar la calidad final de la membrana. Además de los procedimientos convencionales de limpieza inicial, la mayoría de estas modificaciones se centran en la mejora de la adherencia de las capas y / o la reducción de los tamaños medios de poro y la rugosidad de la superficie del soporte para lograr capas selectivas más delgadas. Estos tratamientos se pueden clasificar en tres categorías generales: (i) tratamiento químico, (ii) tratamiento físico e (iii) incorporación de una capa intermedia. Considerando la gran importancia de estas modificaciones en las propiedades finales de la membrana y sus costes, algunos de los avances más relevantes y prácticas extendidas se resumirán en los siguientes apartados. Se ha prestado especial atención a los soportes metálicos ya que, como se mencionó anteriormente, pueden ser más adecuados para su integración en reactores de membrana para la producción de hidrógeno. Además, debe tenerse en cuenta que la superficie externa de los soportes cerámicos no suele modificarse antes de depositar la capa selectiva debido a las buenas propiedades originales en términos de diámetro medio de poros y rugosidad de la superficie.

1.5.1 Tratamientos químicos

El uso de productos químicos para modificar la superficie de los soportes porosos se conoce comúnmente como grabado. Se aplica generalmente en materiales poliméricos, pero también se puede usar para modificar algunas propiedades superficiales de materiales inorgánicos. Estos tratamientos consisten en sumergir el soporte en una solución corrosiva, tradicionalmente un ácido fuerte y mantenerlo a temperatura controlada durante un corto período de tiempo. El efecto principal de estos tratamientos es disolver películas finas de óxidos formadas en la parte superior de los soportes, pudiendo también eliminar parte del propio material del soporte. El efecto de este tratamiento está determinado principalmente por la composición del soporte, la concentración de ácido, la temperatura y el tiempo del tratamiento. Mardilovich y col. [178] utilizaron una solución de ácido clorhídrico para tratar un soporte comercial de acero inoxidable, logrando un aumento notable de la rugosidad en la superficie, con un tratamiento de tan solo 5 minutos de inmersión. Además, la nueva superficie generada mostró mejores propiedades para la posterior incorporación de paladio, aumentando la velocidad de recubrimiento y mejorando su

1. Introducción

adherencia. Un tratamiento similar fue reportado por Li y col. [179] mezclando en este caso el ácido clorhídrico con cierta cantidad de ácido nítrico. Por otro lado, Kim y col. [169] lo hicieron también para preparar una membrana de Pd soportada, en este caso sobre un soporte de níquel poroso. De esta manera, el pretratamiento de grabado de un soporte inorgánico puede proporcionar beneficios para la posterior deposición de la capa selectiva a un coste relativamente bajo, independientemente del uso posterior de cualquier otro tratamiento adicional como la modificación mecánica o la incorporación de una capa adicional.

1.5.2 Tratamientos mecánicos

El desbaste de la superficie externa puede llevarse a cabo como una alternativa diferente para modificar los soportes comerciales, principalmente los metálicos. La plasticidad de las partículas metálicas que forman el soporte es utilizada para reducir tanto el tamaño externo de los poros como la rugosidad, mediante un tratamiento mecánico con un material abrasivo. Una de las primeras referencias sobre el uso de esta alternativa, para la preparación de membranas soportadas de base Pd, fue publicada por Jayaraman y col. En los años noventa, utilizaron lijas comerciales con diferentes números de grano para desbastar la superficie original del soporte [180]. En particular, utilizaron lijas comerciales con grados # 320, # 500 y # 800. Más tarde, Mardilovich y col. [178] utilizaron un proceso de pulido similar para modificar la superficie de los soportes porosos de acero inoxidable. Indicaron que era posible reducir el tamaño de poro externo medio, aunque también se pierde porosidad, disminuyendo la capacidad de permeación del soporte modificado hasta un 20%, respecto al soporte no tratado. Más recientemente, el trabajo de técnicas similares basadas en el uso de papel de lija abrasivo ha seguido siendo utilizado y reportado en la literatura, como evidencia de los trabajos publicados por Li y col. [179], Ryi y col. [181] o Pinacci y col. [182]. Estas técnicas de desbaste no solo se han propuesto para modificar las propiedades superficiales de los soportes, sino que también es posible la reparación de algunos defectos superficiales en capas selectivas [183]. A pesar de que este tipo de tratamientos mecánicos de desbaste son los predominantes, también es posible encontrar algún trabajo en el que se utiliza el granallado de alta velocidad con partículas iónicas para lograr la deformación plástica de las partículas metálicas del soporte. Sin embargo, el alto coste de esta alternativa hace que los abrasivos tradicionales prevalezcan [184].

Sin embargo, algunos investigadores tienen opiniones críticas sobre estos tratamientos mecánicos debido a la reducción de la capacidad de permeación del soporte y la disminución de la adhesión de la capa selectiva. En este contexto, está ampliamente aceptado que la adhesión entre el soporte y la capa selectiva depende de la unión mecánica y el anclaje. En consecuencia, es recomendable cierta rugosidad en el soporte para garantizar una buena adhesión de los recubrimientos [185,186]. Esto se indica claramente en trabajos publicados por Collins [187] y Huang [188], donde los poros más grandes y una cierta aspereza externa en los soportes mejoran la adhesión del recubrimiento. De esta manera, se puede afirmar que es necesario lograr una solución de compromiso entre la modificación de la superficie original y mantener ciertos puntos de anclaje para garantizar una adherencia adecuada de la capa selectiva.

1.5.3 Incorporación de capas intermedias

A pesar de usar tratamientos químicos y / o mecánicos, la incorporación de una capa interfase entre el soporte comercial y la capa selectiva es la alternativa más utilizada para mejorar la superficie externa del soporte original. Esta opción puede ser utilizada simultáneamente para diferentes objetivos, como la modificación de la morfología original, la mitigación de la interdifusión metálica entre soporte y Pd, la mejora de la adhesión de la capa selectiva, la prevención de la corrosión del soporte o incluso la incorporación de los primeros núcleos metálicos como superficie activada. Esta última suele ser la razón principal para incorporar una capa interfases en soportes cerámicos, debido a que estos soportes comerciales ya presentan una superficie lisa con una distribución de tamaños de poro muy estrecha, hasta 3 nm [72,189], por lo que generalmente no hay necesidad de realizar otras modificaciones adicionales. Sin embargo, los soportes metálicos muestran típicamente una superficie rugosa y tamaños de poros anchos [63,72], siendo la incorporación de una capa intermedia una etapa crítica para lograr la deposición de una capa selectiva realmente delgada. Considerando como objetivo final la obtención de una membrana compuesta, la composición y grosor de la capa interfase deben ajustarse a un coste razonable, no habiendo alcanzado en la actualidad una solución única.

De cualquier modo, uno de los factores más importantes a considerar es la compatibilidad entre los diferentes componentes de la membrana soportada. La Figura 1.5.1 muestra el coeficiente de expansión térmico para algunos de los materiales más utilizados como capa interfase, además de los

1. Introducción

principales materiales utilizados como soporte (acero inoxidable 316L, Alúmina o Hastelloy X) y los componentes de la capa selectiva (principalmente paladio, plata, cobre y oro).

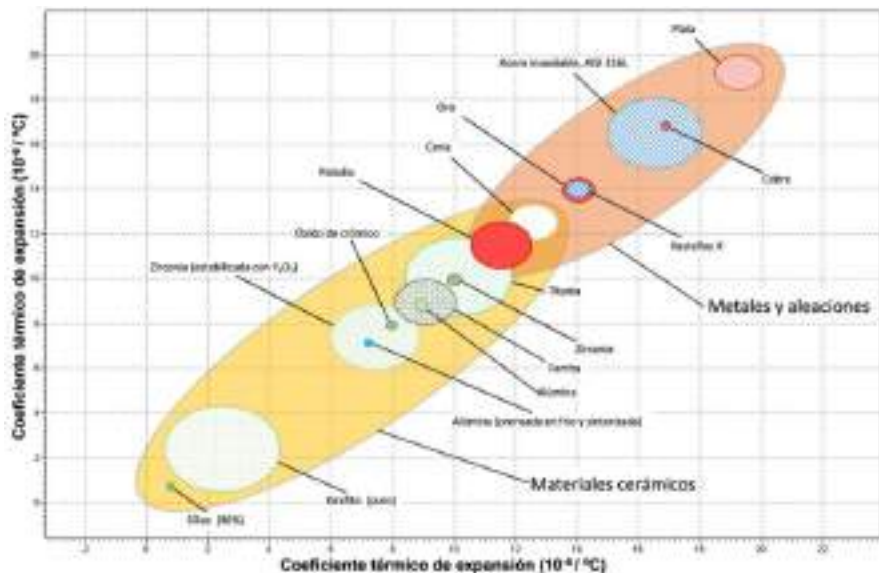


Figura 1.5.1. Coeficientes de expansión térmica de los principales materiales utilizados para la fabricación de membranas de base paladio selectivas al hidrógeno [29].

En general, se considera que cuanto más parecidos sean los coeficientes de expansión térmico de los elementos de membrana soportados mejor puede ser la resistencia mecánica en condiciones de funcionamiento, generalmente a temperaturas moderadas o altas. Según los datos que se muestran en la Figura 1.5.1, el óxido de cerio aparece como una alternativa muy atractiva, con un coeficiente de expansión térmica entre el paladio y los soportes metálicos más habituales. Este material fue empleado por Tong y col. [190] para modificar un soporte tubular de acero inoxidable macro poroso para la preparación de membranas de Pd soportadas con una capa selectiva de alrededor de 13 μm de espesor. Pusieron de manifiesto una muy buena estabilidad del sistema después de experimentos a largo plazo, obteniendo una permeabilidad al hidrógeno casi igual al valor teórico para una membrana de Pd puro. Una capa interfase de CeO₂ similar fue preparada por Qiao y col. [191] para evitar la difusión intermetálica entre un soporte poroso de acero y una capa selectiva de aleación PdCu. Esta capa intermedia fue preparada mediante el método sol-gel y la modificación del soporte original también mejoró la adherencia de la capa selectiva.

Además de CeO₂, también otros materiales se han incorporado con éxito como capa interfase, a pesar de que presenten un coeficiente de expansión térmico diferente a los de la capa selectiva o el soporte. Un primer grupo relevante está formado por el óxido de zirconio y materiales relacionados. Algunos autores, como Wang y col. [192] o Gao y col. [193], modificaron soportes comerciales de acero inoxidable mediante la incorporación de partículas de ZrO₂ para reducir el grosor de la capa selectiva de hidrógeno hasta valores cercanos a 10 µm. Otro ejemplo sería el realizado por Tarditi y col. logrando también un espesor similar [161] mediante la incorporación de las partículas de ZrO₂ a través de un método asistido por vacío, mientras que Lee y col. [194] redujeron todavía más el espesor, hasta 3,5 µm obteniendo una mayor permeabilidad. Otros investigadores utilizaron partículas de zirconia estabilizada con itria (YSZ) con el fin de aumentar la estabilidad de la estructura del material [51,185]. Las referencias en la literatura presentan el uso de YSZ como capa interfase con el doble objetivo de reducir el espesor del paladio y prevenir la difusión intermetálica entre el soporte y la capa selectiva, indicando los métodos de sol-gel o la pulverización de plasma atmosférico como técnicas adecuadas para la incorporación de material [71,146,195].

Considerando las propiedades superficiales relativamente buenas de la alúmina como material para la fabricación de soportes, el uso de este material como capa interfase para la modificación de soportes metálicos también ha sido propuesto por diferentes autores. De esta manera, Yepes y col. [196] y Li y col. [197] consiguieron disminuir el tamaño de poro original del soporte metálico al incorporar una capa interfase de alúmina, evitando además posibles procesos de interdifusión entre el soporte original y la capa selectiva. Broglia y col. [198] desarrollaron un proceso de incorporación de partículas de γ -Al₂O₃ mediante la aplicación de un recubrimiento por inmersión del soporte para lograr una capa de Pd totalmente libre de defectos de alrededor de 11 µm. Chi y col. [199] detallaron el uso de partículas de alúmina con diferentes tamaños para una mejor modificación de los soportes de acero comerciales. Utilizaron partículas de un tamaño cercano a 10 µm para llenar los poros más anchos y partículas más pequeñas (tamaño aproximado de 1 µm) para obtener una superficie lisa final. Por lo tanto, finalmente lograron una delgada capa de Pd libre de defectos con menos de 5 µm de espesor y buena estabilidad térmica. Lee y col. [194] compararon el efecto del uso de Al₂O₃ y ZrO₂ demostrando que ambos materiales actúan

1. Introducción

efectivamente como barrera de difusión, aunque el uso de alúmina produce una menor permeabilidad de la membrana.

Otro material utilizado como capa interfase es el SiO₂, siendo posible realizar diferentes funciones con esta capa como modificar la superficie del soporte, limitar la difusión intermetálica o incluso ser el catalizador para algunos procesos químicos. Por ejemplo, Nam y col. [200] modificaron un sustrato comercial de acero inoxidable 316L mediante la incorporación de sílice amorfa. De esta forma, redujeron el espesor de la capa selectiva, constituida por una aleación de PdCu, hasta 2 μm y manteniendo una permeabilidad de hidrógeno de $8,37 \cdot 10^{-7} \text{ mol} \cdot \text{m}^{-2} \cdot \text{s}^{-1} \cdot \text{Pa}^{-1}$ y una selectividad H₂/N₂ de alrededor de 70.000 a 450 °C. Por otro lado, Calles y col. [63] publicaron el uso de tres diferentes materiales silíceos como capa interfase para preparar membranas de Pd soportadas en acero inoxidable: sílice amorfa desordenada, sílice amorfa ordenada (HMS) y sílice cristalina (silicalita-1). En todos los casos, se redujo tanto la rugosidad como el tamaño de poro de los soportes originales y, en consecuencia, el espesor de Pd mínimo requerido para obtener una capa selectiva libre de defectos. Los mejores resultados se obtuvieron con el uso de silicalita-1, reduciendo el espesor de Pd hasta 5 μm y obteniendo una permeabilidad de hidrógeno de $1,42 \cdot 10^{-4} \text{ mol} \cdot \text{m}^{-2} \cdot \text{s}^{-1} \cdot \text{Pa}^{-0,5}$ con una selectividad de hidrógeno completa a 400 °C. Se pueden encontrar modificaciones similares de soportes metálicos con capas de sílice microporosas para aumentar la permeabilidad de H₂ de la membrana compuesta sin la utilización de ninguna otra capa adicional [201] o incluso combinarse con paladio en estructuras de matriz mixta [202]. Recientemente, estos materiales también se han aplicado en la parte externa de las membranas de Pd soportadas una vez finalizadas para reparar pequeños defectos y poros, aumentando significativamente la selectividad al H₂ con un coste muy bajo [203].

Otros materiales que también se han utilizado son aluminosilicatos, como las zeolitas, materiales cristalinos con distribución controlada de tamaños de poro y propiedades catalíticas adicionales. Entre la gran variedad de estructuras posibles, reportadas en la literatura se encuentra el uso de zeolitas NaA [204], NaX [205], Z-21 [206], tipo FAU [207] y TS-1 [208,209]. En general, el mayor coste de estos materiales limita su uso a procesos muy específicos, principalmente a reactores de membrana en los que la zeolita pueda desempeñar el papel tanto de modificador del soporte como de catalizador.

Otro método bastante simple para modificar el soporte, con alta reproducibilidad y coste razonable, es la oxidación directa de los soportes de acero 316L en atmósfera de aire a altas temperaturas. Este proceso produce un recubrimiento exterior de Fe_2O_3 - Cr_2O_3 , que puede disminuir el proceso de interdifusión metálica [146]. Ma y col. [210] patentaron un método controlado de oxidación in-situ para preparar membranas compuestas de Pd sobre soportes porosos de acero inoxidable y, por lo tanto, lograr barreras efectivas de interdifusión con tratamientos térmicos superiores a 600 °C. Después de este trabajo pionero, otros investigadores como Guazzone y col. [211] o Mateos-Pedrero y col. [212] han trabajado sobre la modificación de soportes metálicos mediante la incorporación de óxidos metálicos derivados de un proceso de oxidación a temperaturas superiores a 400 °C. Principalmente, solo se pueden observar ligeras modificaciones en la superficie de soporte con los tratamientos térmicos debido al espesor muy limitado de la nueva capa de óxido y, en consecuencia, el espesor de Pd no se reduce tanto como cuando se usan otras alternativas. En caso de utilizar temperaturas realmente altas para el tratamiento (> 700 °C), se genera una mayor cantidad de óxidos, y como consecuencia la porosidad del soporte disminuye drásticamente.

En los últimos años, se han investigado otros materiales para desarrollar nuevas capas intermedias y lograr mejores membranas soportadas. Algunas de estas novedades son el uso de capas finas de TiN obtenidas por pulverización catódica [213], una combinación de plata, como barrera de difusión, y gel de hidróxido de aluminio, para llenar los poros más grandes del soporte [214], multicapas bimetálicas de Pd y Ag [215], níquel [216] o incluso polvos de wolframio [48]. Sin embargo, a pesar de estos resultados prometedores, aún no se ha encontrado una solución definitiva [217,218].

Finalmente, a pesar de que la presencia de una capa intermedia en sustratos cerámicos es menos común, también se pueden encontrar algunos casos en la literatura. Por ejemplo, el trabajo publicado por Hu y col. [219], en el que un soporte macroporoso de Al_2O_3 se modificó con grafito de un lápiz 2B convencional. Con este método, lograron una membrana soportada totalmente libre de defectos con un espesor de paladio de 5 μm . A pesar de que la incorporación de capas intermedias en los soportes cerámicos antes de incorporar el recubrimiento selectivo final es escasa, es posible encontrar algunos trabajos que utilizan esta alternativa para mejorar la etapa de activación de la superficie, según lo publicado por Zhao y col. [220]

1. Introducción

utilizaron una disolución de bohemia modificada con Pd (II) para mejorar la superficie original, obteniendo un espesor de la capa selectiva de solo 1 μm . Una aplicación muy particular de esta metodología es la síntesis de membranas en las cuales las partículas YSZ se utilizan para modificar la superficie original de los soportes cerámicos en una doble capa [221].

En la Tabla 1.5.2. se resumen las alternativas más relevantes, incluidas en esta sección, para modificar los soportes comerciales. En la tabla se indican datos sobre la naturaleza del soporte y las alternativas de modificación se recopilan, así como otros parámetros relevantes como la composición, el espesor de la capa selectiva y la permeación de H_2 de la membrana final.

Tabla 1.5.2 Alternativas de modificación de soportes comerciales inorgánicos para la preparación de membranas de base Pd.

Soporte	Modificación	Detalles	Capa selectiva	Espesor	Temperatura T (°C)	Permeación $A^{\text{Pd}} (\text{kPa})$	Capacidad Permeación	Selectividad al H ₂	MFP
PSS	Química	HCl, T min	Pd	20,0	350	100	$3,11 \cdot 10^{-10}$	n.d.	[179]
PSS	Química	HCl- SnO_2	Pd	3,8	493-593	100	$3,24 \cdot 10^{-4} \cdot 3,34 \cdot 10^{-10}$	n.d.	[179]
Ni	Química	HCl	Pd	6,3	450	100	$3,81 \cdot 10^{-10}$	>1000	[181]
Al_2O_3	Modificada	Líquido	Pd	6,5	n.d.	n.d.	n.d.	n.d.	[180]
Ni	Modificada	Líquido	Pd/Cu/Ni	12,0	289-500	134-278	$1,16 \cdot 10^{-3} \cdot 3,00 \cdot 10^{-10}$	n.d.	[181]
PSS	Modificada	Ion Shot Peening	Pd	6,8	490	100	$5,80 \cdot 10^{-10}$	n.d.	[184]
PSS	Capa intermedia	CeO_2 partículas	Pd	11,0	396	200	$2,75 \cdot 10^{-10}$	n.d.	[190]
PSS	Capa intermedia	CeO_2 sol-gel	Pd/Cu	8,8	450	100	74,000*	23449	[181]
PSS	Capa intermedia	ZrO_2 sol-gel	Pd	10,0	590	100	$8,30 \cdot 10^{-10}$	n.d.	[182]
PSS	Capa intermedia	ZrO_2 sol-gel	Pd/Cu	10,0	486	100	$1,00 \cdot 10^{-10}$	n.d.	[185]
PSS	Capa intermedia	ZrO_2 sol-gel	Pd/Al ₂ O ₃	10,0	490	100	$1,19 \cdot 10^{-10}$	>1000*	[181]
PSS	Capa intermedia	YSZ partículas	Pd	27,7	493-498	30-300*	$4,39 \cdot 10^{-10}$	n.d.	[171]
PSS	Capa intermedia	YSZ partículas	Pd	11,8	350-393	0,258	$4,16 \cdot 10^{-4} \cdot 4,10 \cdot 10^{-10}$	n.d.	[146]
Base X	Capa intermedia	YSZ-Al ₂ O ₃ -YSZ	PdAg	4,5	460-500	100	$1,00 \cdot 10^{-10}$	>20000*	[163]
PSS	Capa intermedia	Al_2O_3 sol-gel	Pd	11,0	n.d.	n.d.	n.d.	n.d.	[198]
PSS	Capa intermedia	Al_2O_3 partículas	Pd	>3,0	390	n.d.	$2,94 \cdot 10^{-10}$	1124	[199]
PSS	Capa intermedia	SiO_2 partículas	Pd/Cu	2,8	450	n.d.	$9,37 \cdot 10^{-10}$	70,600	[200]
PSS	Capa intermedia	Silicato-1 sol-gel	Pd	3,8	393-498	39-238	$1,42 \cdot 10^{-10}$	n.d.	[161]
PSS	Capa intermedia	Zirconia StAB	Pd	19,0	450	50	$1,10 \cdot 10^{-10}$	800	[204]
PSS	Capa intermedia	Zirconia PAU	Pd	1,8	290	100	$1,29 \cdot 10^{-10}$	n.d.	[207]
Al_2O_3	Capa intermedia	Zirconia TS-1	Pd	2,8	393-498	30-300	$1,48 \cdot 10^{-10}$	148	[209]
PSS	Capa intermedia	$\text{Fe}_{0,9}\text{Cr}_{0,1}\text{O}_2$	Pd	31,0	390	n.d.	$2,06 \cdot 10^{-10}$	n.d.	[211]
PSS	Capa intermedia	$\text{Fe}_{0,9}\text{Cr}_{0,1}\text{O}_2$	Pd	19,0	n.d.	n.d.	n.d.	n.d.	[212]
PSS	Capa intermedia	Valladolid	Pd/Cu	5,0-20,8	n.d.	n.d.	n.d.	n.d.	[48]
PSS	Capa intermedia	Al_2O_3 /gel	Pd	5,8	690	200	$1,50 \cdot 10^{-10}$	n.d.	[217]
Al_2O_3	Capa intermedia	Holonost	Pd	1,8	410	n.d.	$2,23 \cdot 10^{-4} \cdot 1,37^{+0}$	26,136	[218]
Al_2O_3	Capa intermedia	YSZ partículas	Pd	1,8	460-500	158-486	$0,10 \cdot 0,00^{+0}$	n.d.	[11]

Capacidad de permeación: * Permeación [mol $\text{m}^{-2} \cdot \text{s}^{-1} \cdot \text{Pa}^{-1}$]; ** Permeación [mol $\text{m}^{-2} \cdot \text{s}^{-1} \cdot \text{Pa}^{-1}$]; *** Flujo de permeación [mol $\text{m}^{-2} \cdot \text{s}^{-1}$]

1.5.4 Preparación de la capa selectiva de Pd

Actualmente, existe una gran variedad de técnicas para realizar la deposición de paladio o sus aleaciones sobre soportes porosos con el fin de obtener membranas permeoselectivas al hidrógeno. Entre ellas, destacan el arrollamiento mecánico, la deposición química en fase vapor (CVD), la deposición física en fase vapor (PVD), la deposición electroquímica (EDP) y la deposición no electroquímica (ELP). A continuación, se resumen brevemente las principales características de cada una de ellas.

1.5.4.1 Arrollamiento mecánico

A pesar de no ser una técnica de deposición como tal, esta técnica es también utilizada para la obtención de capas selectivas al hidrógeno que se disponen en membranas compuestas [17]. Se basa en la preparación de láminas de paladio, en general relativamente gruesas (50-200 μm) mediante un proceso mecánico de laminación [60]. Posteriormente, se enrollan con la ayuda de un soporte metálico y se sueldan los extremos de la lámina con el objetivo de conseguir la continuidad y resistencia mecánica. El principal inconveniente de este proceso es la necesidad de utilizar láminas gruesas para garantizar la calidad de la soldadura, lo que repercute negativamente tanto en el coste final de la membrana como en el flujo de permeado obtenido [223]. Para mejorar ambos inconvenientes, actualmente, la fabricación de membranas mediante este proceso se basa principalmente en la aleación PdAg [60,222].

1.5.4.2 Deposición química en fase vapor (CVD)

En este proceso se parte de reactivos gaseosos para buscar una reacción en la superficie del sustrato a recubrir, formando una especie sólida junto a otros productos gaseosos [224,225]. Generalmente estos procesos tienen una cinética de reacción lenta, por lo que es necesario una etapa de activación para agilizar la deposición [226]. Esta activación puede ser térmica, con plasma o con láser, permitiendo estos últimos disminuir la temperatura del proceso y aumentando ampliamente el coste del equipamiento necesario [225,227]. Como principales ventajas presenta una gran facilidad para depositar recubrimientos multicapa con una alta adherencia, además de permitir trabajar a gran escala y ser un proceso industrializable. A pesar de esto, el elevado coste y temperatura del proceso limita las posibilidades de uso de esta tecnología, además de los problemas medioambientales por el uso de gases muy tóxicos y reactivos [224,225,227].

1.5.4.3 Deposición física en fase vapor (PVD)

La deposición física en fase vapor consiste en la evaporación de un metal que se deposita y se condensa sobre una superficie determinada sin que tenga lugar ninguna reacción química. Para evaporar los materiales cuyo punto de fusión es muy elevado se procede al calentamiento hasta su evaporación directamente con un haz de electrones [225]. El proceso de evaporación tiene lugar a todas las temperaturas, pero la presión de vapor tiene una variación exponencial con la temperatura y que sólo depende del calor latente de vaporización. Debido a esto, este proceso se realiza a vacío para aumentar la velocidad del proceso, lo que además permite que los átomos viajen hacia el sustrato en línea recta sin pérdidas de energía cinética. Como consecuencia de este desplazamiento lineal, es necesario utilizar múltiples fuentes y sistemas planetarios para obtener recubrimientos con cierta homogeneidad en superficies complejas [225]. Otra tecnología de evaporación es el *sputtering*, la cual consiste en el bombardeo del blanco a evaporar con iones altamente energéticos. Para ello se utiliza un gas inerte como el Ar que se encarga de iniciar y mantener el plasma, debido a la colisión de los iones de Ar excitados por el plasma la fuente metálica es evaporada y posteriormente depositada sobre la superficie deseada con ayuda de campos magnéticos para confinar el plasma [228].

La deposición física de vapor es un proceso menos laborioso que la deposición química en fase vapor descrita previamente, que proporciona una tasa de deposición más rápida, permitiendo además un mejor control sobre el espesor depositado al no depender de una etapa de reacción [226]. Esta técnica además permite la deposición de la capa a temperaturas relativamente bajas y, por lo tanto, permite no degradar las propiedades mecánicas de los sustratos [229]. Con esta técnica se pueden depositar múltiples materiales manteniendo un control muy preciso de la composición de la capa depositada. A pesar de suponer un menor coste que los procesos de deposición en fase vapor, el precio de esta tecnología sigue siendo elevado [230].

1.5.4.4 Deposición electroquímica (EPD)

La deposición electroquímica o electrodeposición tiene lugar sobre una superficie conductora que actúa como electrodo [225]. Debido al campo eléctrico generado entre los dos electrodos del sistema por la aplicación de una corriente externa, los iones metálicos en disolución migran hacia el cátodo, donde son neutralizados e incluidos en la matriz metálica,

producíendose por tanto la deposición. Esta tecnología presenta unos costes de proceso inferiores a las de CVD o PVD, siendo la necesidad de aplicar corriente eléctrica uno de los gastos principales [225]. Con esta técnica se pueden depositar todos los materiales metálicos menos electronegativos que el zinc, con la ventaja de poder realizarlo a baja temperatura [231]. Como principal desventaja presenta la falta de homogeneidad en los recubrimientos en geometrías complejas y la elevada porosidad de los recubrimientos. Para intentar mejorar en cierta medida la homogeneidad del recubrimiento se puede recurrir a la agitación, tanto de las piezas a recubrir como del baño electrolítico [226]. Por otro lado, para obtener una película totalmente densa suele ser necesario aumentar el espesor del recubrimiento, además de la optimización de la cuba electrolítica, el baño electrolito, los electrodos y la temperatura del proceso [226]. La Figura 1.5.2, muestra una comparativa entre los distintos métodos de obtención de la capa selectiva en términos de temperaturas del proceso y espesores obtenidos, incluyendo además de las técnicas descritas con anterioridad la deposición no electroquímica (ELP) que se describirá con una mayor profundidad en el siguiente apartado. Puede observarse cómo tanto la deposición electroquímica como la no electroquímica, pueden utilizarse a temperaturas inferiores a las requeridas por los procesos de PVD, CVD o incluso el enrollamiento mecánico, debido a la necesidad de la etapa de soldadura. Además, espesores delgados como en el caso del PVD o CVD también pueden obtenerse con las técnicas basadas en reacciones químicas sin cambio de fase.

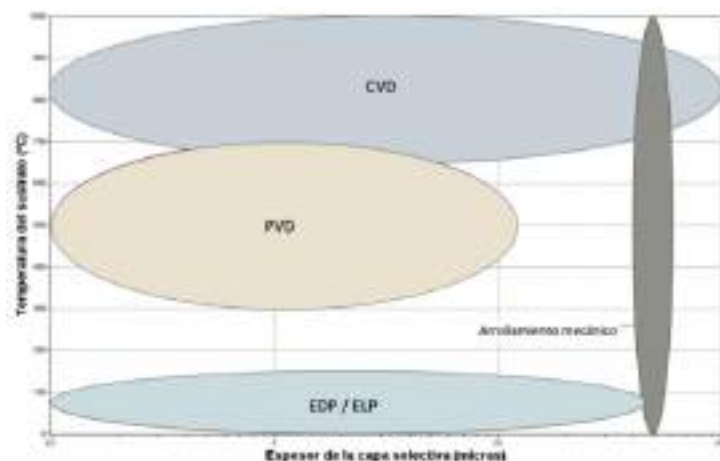


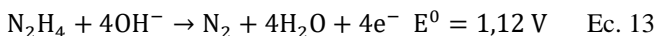
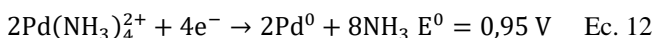
Figura 1.5.2. Valores de temperatura y espesor de la capa selectiva asociados a los principales procesos de fabricación utilizados.

1. Introducción

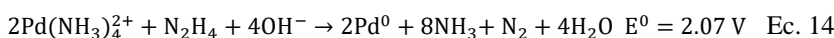
1.5.4.5 Deposición no electroquímica (ELP)

El término deposición no electroquímica (ELP) fue acuñado por primera vez a mediados de los años cuarenta por Brenner y Riddell para definir la deposición de metal en ausencia de una fuente externa de corriente eléctrica [232]. La aplicación de la tecnología ELP a la incorporación de paladio sobre soportes porosos se ha utilizado ampliamente para preparar membranas selectivas de hidrógeno durante años. Esta técnica no requiere un equipo costoso y tampoco supone altos costes operativos, debido principalmente a que se realiza a baja temperatura y no presenta la necesidad de electrodos o fuentes de electricidad externas. Además, el ELP permite la deposición de películas delgadas y homogéneas en geometrías complejas e incluso en materiales no conductores [111,155–157], siendo la opción más ampliamente utilizada sobre el resto de métodos.

El uso del ELP para la preparación de membranas selectivas de H₂ se basa en la deposición de paladio (o materiales de aleación relacionados, como se comentará posteriormente) sobre una superficie, como un soporte poroso, desde una disolución acuosa que contiene el precursor metálico. Por lo general, este precursor se disuelve y se estabiliza para formar un complejo antes de ser reducido a través de una reacción química autocatalítica controlada [236,237]. En los últimos años, la mayoría de los trabajos publicados utilizan hidróxido de amonio y ácido etilendiaminotetraacético para formar complejos con el precursor del paladio. Por otro lado, se utiliza hidracina como agente reductor debido a que se genera nitrógeno como único subproducto de la reacción química, evitando de este modo la deposición de otros compuestos no beneficiosos en la capa selectiva, como por ejemplo, cuando se usa fósforo [235,237,238]. La hidrazina es un agente reductor fuerte tanto en medios ácidos como alcalinos, permitiendo la reducción de los iones metálicos dependiendo de las condiciones de reacción [239–241]. A continuación, se presentan las principales reacciones químicas involucradas en el proceso de deposición de paladio:



Siendo la reacción global del proceso la siguiente:



Para lograr una deposición homogénea de Pd, una buena adherencia y tiempos de inicio de reacción reducidos, los soportes deben primero ser

activados o sensibilizados. Este proceso consiste en la deposición de pequeños núcleos de paladio antes de la deposición de la capa selectiva de paladio [242]. Convencionalmente, este paso se ha llevado a cabo mediante inmersiones repetitivas en soluciones ácidas de estaño y paladio [243]. Sin embargo, algunos estudios sugieren problemas en la estabilidad de la membrana a temperaturas de operación altas causadas por residuos de estaño, que conducen a la formación de defectos y poros en la capa de Pd, como Paglieri y col. indicaron por primera vez [244]. Este comportamiento fue respaldado más recientemente por otros autores como Wei y col. publicando recientemente un estudio detallado sobre la correlación entre la presencia de residuos de estaño y la estabilidad de la membrana [245]. Teniendo en cuenta estos efectos negativos de los tratamientos clásicos de sensibilización-activación, se han propuesto métodos alternativos para evitar el uso de soluciones de estaño. Se han usado diferentes enfoques, tales como el uso de partículas activadas con núcleos de Pd para la preparación de capas intermedias [105,193,195,246]; superficies de alúmina anódica catalizada para facilitar el ELP de Pd [247]; el aumento de la tasa de deposición de núcleos de Pd y la ruptura de conglomerados mediante ultrasonidos [248]; la incorporación, descomposición y reducción de una solución de acetato de paladio en cloroformo en la superficie [249]; o, directamente, la generación de partículas de Pd de tamaño nanométrico por reducción directa de una solución altamente diluida con una mezcla de amoníaco-hidrazina [52,72]. Sin embargo, hasta la fecha no se ha encontrado una solución mejor y el método clásico sigue siendo ampliamente utilizado por muchos investigadores [28,47,239].

En los últimos años, se han realizado grandes esfuerzos para reducir el coste general de la fabricación de membranas base Pd, centrándose principalmente en la reducción del espesor de la capa de paladio, pero asegurando la ausencia de defectos en el recubrimiento [36,38,39,250]. Como se comentó previamente, una estrategia se basa en la preparación de membranas soportadas, que generalmente implica la modificación de soportes originales para facilitar la incorporación de una capa de paladio delgada libre de defectos [21,63]. Otras estrategias se centran para mejorar el proceso de deposición de metales, particularmente la deposición no electrolítica, para lograr una mejor adherencia, homogeneidad, una mayor cobertura de poros o, en general, una mejor estabilidad de la capa selectiva de H₂ base Pd con un espesor reducido.

1. Introducción

De este modo, Uemiya y col. [251] consiguieron aumentar la velocidad de incorporación del metal al sumergir el soporte poroso en una solución que contiene hidrazina antes de cada etapa de recubrimiento electrolítico. Otros autores intentaron mejorar la incorporación de paladio en las zonas profundas de la rugosidad superficial, donde las partículas de metal depositadas cierran con eficacia las bocas de los poros del soporte completando una capa totalmente densa y continua mediante el mecanismo del puente [252]. Zhao y col. [220] y Zhang y col. [253] informaron el uso de vacío en el interior de los soportes para lograr una microestructura uniforme de la capa de Pd con un espesor inferior a las depositadas de manera convencional. Otros investigadores obtuvieron resultados similares, como Yeung [254], Souleimanova [255] o Li [256] cuando se genera un efecto osmótico entre la solución con la fuente metálica y una solución acuosa de sacarosa.

Pacheco Tanaka y col. [51,53,257] desarrollaron membranas soportadas en las que la incorporación de Pd o aleaciones base Pd mediante un proceso de deposición no electroquímico asistido por vacío entre dos capas cerámicas de óxido de circonio, una de ellas activada con núcleos de Pd previamente y depositado sobre un soporte tubular de alúmina. Este tipo particular de membranas, en las que la capa selectiva se coloca en una estructura de tipo sándwich se denominaron membranas de tipo *pore-filled*. Las principales ventajas descritas por los autores incluyen la capacidad de operar la membrana por debajo de la temperatura crítica y mejorar la estabilidad mecánica, respecto a otras membranas soportadas basadas en un recubrimiento externo convencional. Además, la estructura sandwich también proporciona a la capa selectiva una protección adicional contra el envenenamiento [158].

Siguiendo también este concepto de estructuras tipo sándwich, Goldbach y col. [258] desarrollaron membranas soportadas de aleación base Pd, denominadas como *duplex*, en las cuales el soporte queda colocado entre dos capas selectivas. Hay que destacar que las capas selectivas no estaban totalmente libres de defectos, pero debido a la casuística de la distribución de los defectos en cada una de las capas se obtuvieron membranas con una alta selectividad. Este fenómeno puede explicarse debido a que el H₂ puede atravesar libremente las capas de Pd, pero por el contrario el N₂ debe pasar a través de un defecto de la primera capa y recorrer la porosidad interconectada del soporte hasta encontrar otro defecto a través del cual poder sobrepasar la segunda capa selectiva. De este modo el recorrido del N₂ para atravesar la

membrana es más largo, conllevando un tiempo mayor, que el realizado por el H₂, lo cual da lugar a un aumento en la selectividad H₂/N₂. Una representación esquemática de este concepto se representa en la Figura 1.5.3, donde se pueden observar los recorridos que deben realizar los diferentes gases para atravesar la membrana.

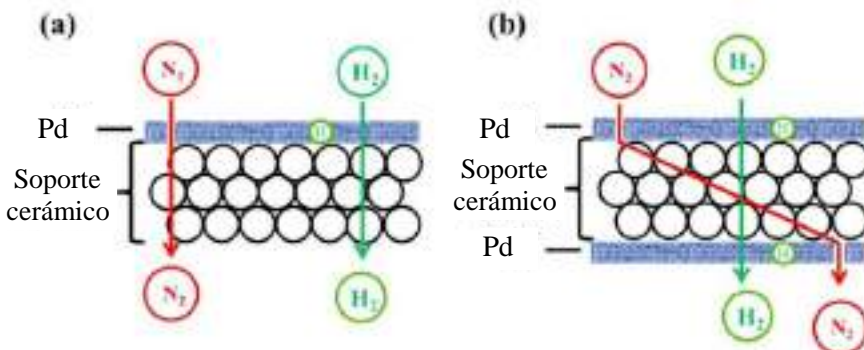


Figura 1.5.3. Representación esquemática de la distancia mínima de difusión del H₂ y N₂ con una capa selectiva (a) y dos capas selectivas (b) [258].

Por otro lado, diferentes estudios se centran en modificar la composición de los baños necesarios para formar el recubrimiento, con el objetivo de mejorar las propiedades finales de la capa selectiva. En este contexto, se ha demostrado que los baños que contienen ácido etilendiaminotetraacético (EDTA) presentan buena estabilidad a diferentes temperaturas, aunque da como resultado una pureza limitada de la capa de paladio debido a la incorporación de depósitos de partículas de carbono del complejo EDTA dentro del metal [165,259,260]. Estos depósitos de carbono podrían disminuir el rendimiento de la membrana por la formación de CO₂ en algunas condiciones de funcionamiento. Por lo tanto, también se ha investigado la preparación de baños libres de EDTA, logrando rendimientos de deposición de paladio aceptables con buena estabilidad de los baños de deposición en ausencia de este estabilizador [165,259,260].

Otros autores han estudiado la influencia de la fluidodinámica entre el soporte y el líquido del baño. Llegando a la conclusión de que la rotación del soporte durante el proceso de deposición aumenta la velocidad de recubrimiento y la homogeneidad de la capa de Pd, como observaron Chi y col. [261]. En comparación con el ELP estático, el uso de la rotación del soporte durante el proceso repercutió en la obtención de superficies más

1. Introducción

uniformes y lisas de las membranas de Pd, lo que a su vez mejora su estabilidad.

A pesar del esfuerzo realizado en la investigación para mejorar la calidad y la rentabilidad de las membranas de Pd, muchos otros estudios se centran en disminuir el número de membranas rechazadas debido a la presencia de defectos o grietas durante los procesos de fabricación. En este sentido, han aparecido nuevas alternativas para la reparación de posibles defectos generados en la superficie de Pd. Por ejemplo, Li y col. [256] utilizaron los fundamentos del efecto osmótico para la incorporación de Pd de manera preferentemente en los defectos de la capa de Pd a reparar. Siguiendo este procedimiento, aseguraron la desaparición de los defectos con el consiguiente aumento significativo en el factor de separación de hidrógeno ideal, sin una reducción notable del flujo de permeación ni incremento significativo del espesor. Con fundamentos similares, Zeng y col. [262] repararon defectos localizados en membranas soportadas de base Pd. En este caso, el método fuerza la reacción química para la reducción del paladio alrededor de los defectos al alimentar la fuente de metal y el agente reductor desde lados opuestos de la membrana soportada.

Sobre la base de estos procedimientos de reparación, otros investigadores reportaron la adición por separado de la fuente de Pd y el baño reductor para la preparación membranas de Pd directamente sobre soportes comerciales de acero [50,52,72,146–148]. Este nuevo procedimiento, denominado Electroless Pore-Plating (ELP-PP), la pared del soporte es utilizada para mantener separadas la fuente de Pd y la disolución de hidrazina. En estas condiciones, la hidrazina difunde preferentemente a través de los poros del soporte, reaccionando con el complejo amino-paladio cerca del área de los poros. Idealmente, en caso de una activación adecuada de la superficie interna del poro, esta reducción se inicia desde la porosidad interna del soporte de una manera similar al método de reparación [50,52,263]. Destacaron que es posible disminuir el consumo de la fuente de paladio y minimizar el número de membranas rechazadas siguiendo esta metodología, reduciendo consecuentemente el coste total de la preparación de membranas. Esto es posible debido a que el contacto entre los reactivos se vuelve progresivamente más difícil durante la incorporación de Pd, hasta la obtención del bloqueo completo de los poros del soporte, momento en el que se detiene el proceso de reacción. Un esquema sobre la alternativa ELP-PP se muestra en la Figura 1.5.4. Este proceso dificulta el aumento de la incorporación de paladio después de bloquear los poros, en contraste con el

incremento de espesor constante alcanzado por ELP convencional, lo que resulta en una película completamente densa con un espesor más reducido.

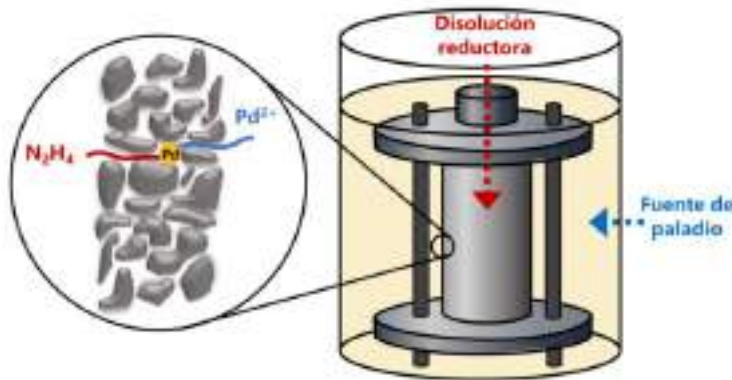


Figura 1.5.4. Esquema del proceso de deposición de paladio no electrolítico mediante la alternativa ELP-PP.

A pesar de la incorporación preferente de Pd en los poros del soporte, los autores observaron la generación de una película externa en el soporte de acero, comercial o modificado, causada por la gran variedad de diámetros de poro existente en los soportes [50,52,263]. La hidrazina no puede pasar a través de los poros más pequeños ya que estos quedan completamente cerrados por paladio en un tiempo relativamente corto, mientras que el agente reductor si puede difundir fácilmente a través de los más anchos, parcialmente cerrados, hasta la superficie externa en contacto con el baño de paladio, donde se forma la capa exterior. De esta manera, se reportó que varios parámetros afectan fuertemente al proceso de ELP-PP: (i) características de los poros del soporte (diámetro promedio de poros y porosidad), (ii) formulación de los baños utilizados, reductor y fuente metálica y (iii) relación entre la longitud de la membrana y volumen de soluciones.

Finalmente, algunos investigadores proponen la mejora de las propiedades de las membranas, centrándose principalmente en un aumento de la permeación y la estabilidad térmica de manera simultánea a la diminución de la presencia de defectos, al usar un tratamiento térmico adicional ($> 640^{\circ}\text{C}$) después de la deposición del recubrimiento de paladio [43]. Aunque esta alternativa no es estrictamente una mejora del proceso de deposición, puede usarse para mejorar la membrana preparada previamente. Los avances más relevantes para la incorporación de Pd por deposición no

1. Introducción

electroquímica se presentan en la Tabla 1.5.3. Donde las mejoras clave y los detalles experimentales se resumen junto a la información sobre el material de soporte, las modificaciones del soporte, el espesor de la capa selectiva y las propiedades de permeación.

Tabla 1.5.3 Modificaciones al proceso de deposición ELP para la preparación de membranas base en Pd.

Modificación ELP	Beneficio	Soporte	Modificación Soporte	Espesor	Formación Tiempo s(h:min)	Capacidad Permeación mol m ⁻² s ⁻¹	Selectividad al H ₂	REF
Aleación pura	Vacio	Al ₂ O ₃	—	4,0	100 100	8,78 10 ⁻¹⁴	1000	[207]
Aleación pura	Vacio	Al ₂ O ₃	Triturado	1,0	400 100	2,25 10 ⁻¹¹ -1,07 10 ⁻¹⁰	20-100	[226]
Aleación pura	Efecto estratificado	Vysot glass	—	1,6	4,0 4,0	—	n.d.	[254]
Aleación pura	Efecto estratificado	Vysot glass	—	2,1	4,0 4,0	—	n.d.	[223]
Capa promoción	Pura-efecto	Al ₂ O ₃	YSZ-porosidad	0,6	100-1000 100-1000	6,18 10 ⁻¹⁰ -10 ⁻⁹	n.d.	[211]
Reducción-deposición C	Sin ESDA	Al ₂ O ₃	ZrO ₂	1,2	740 118	300 10 ⁻¹⁰	n.d.	[229]
Reducción-deposición C	Sin ESDA	PtS	Al ₂ O ₃	5,0	400 100	1,05 10 ⁻¹⁰	500	[208]
Método interpenetrado	Susurro reacción	Al ₂ O ₃	ZrO ₃	3,0	150-180 100-400	5,00 10 ⁻¹⁰	>1000	[261]
Reparación	Efecto estratificado	PtS	—	10,0	425-477 64-116	2,09 10 ⁻⁹	400-1000	[295]
Reparación	Degradación puntual	α-Al ₂ O ₃ , γ-Al ₂ O ₃	γ-Al ₂ O ₃	8,0	580 300	7,20 10 ⁻¹⁰ -4,56 10 ⁻¹⁰	n.d.	[262]
Densificación-metano	ELP-PP	PtS	Pt _{0.5} Co _{0.5} O ₂	10-200	350-420 300-700	1,09 10 ⁻¹⁰ -4,08 10 ⁻¹⁰	—	[271]
Mutacionamiento Pd	Tratamiento	PtS	YSZ	4,9	400 82	1,48 10 ⁻¹⁰	200-2000	[471]
				2740°C				

Capacidad de permeación = Permeación (mol m⁻² s⁻¹ Pa⁻¹); Permeación (mol m⁻² s⁻¹ Pa⁻¹); Flujo de permeación (mol m⁻² s⁻¹)

1.5.5 Preparación de aleaciones

Independientemente del uso de un proceso de deposición no electroquímica convencional o mejorado, muchos investigadores respaldan la preparación de aleaciones en las que el paladio se combina con algunas cantidades de otros metales para mejorar el comportamiento de permeación, la estabilidad térmica y mecánica y la tolerancia al envenenamiento de la membrana [57,264–266]. Por lo tanto, en esta sección se presenta una descripción general de las aleaciones base Pd más frecuentes, detallando los procedimientos y principales beneficios obtenidos, así como las tendencias recientes y las perspectivas futuras.

El Pd puro puede sufrir el llamado fenómeno de fragilización por hidrógeno debido a la expansión de la red cristalina provocada por la transición de la fase α a la β . Este fenómeno ocurre cuando el metal está expuesto a una atmósfera de hidrógeno a temperaturas y presiones inferiores a 298 °C y 2 MPa, respectivamente. Esta transición de fase genera tensiones, especialmente en el caso de geometrías tubulares, lo que a menudo conduce a la ruptura de la capa de Pd y, por lo tanto, a la consiguiente pérdida de selectividad al hidrógeno de la membrana. Este inconveniente puede evitarse trabajando en condiciones de funcionamiento por encima del punto crítico mencionado cuando la membrana está expuesta al hidrógeno o variando el punto de trabajo dentro del diagrama de fases del Pd [267]. La última opción puede realizarse mediante la aleación de Pd puro con otros metales, como por ejemplo, plata [53,174,268–270], cobre [167,170], rutenio [265,271] u oro [272,273]. Está demostrado que las aleaciones basadas en Pd con

concentraciones específicas de estos metales modifican la fase del hidruro metálico dentro del diagrama, evitando los fenómenos de fragilización mencionados [28].

Otro problema que afecta negativamente a la permeabilidad de las membranas densas de base Pd es el envenenamiento irreversible por contaminantes químicos, como el monóxido de carbono o el azufre. Estas moléculas son quimisorbidas sobre la capa metálica, siendo también posible una reacción química con hidrógeno para formar especies que bloquean los sitios activos para la disociación en la superficie y dificultan la penetración del hidrógeno. Algunas aleaciones ayudan a evitar este efecto de envenenamiento mientras mantienen un factor de separación de hidrógeno completo ideal [158], incluso en presencia de compuestos de azufre que tradicionalmente causan el envenenamiento irreversible en películas de Pd puro [28,170,264,274].

La preparación de aleaciones eficientes con base de Pd mediante un proceso de deposición no electroquímica, con una composición precisa es actualmente uno de los hitos más importantes para la implementación de membranas industriales. Como se comentó previamente, la deposición física en fase vapor ofrece múltiples posibilidades para incorporar diferentes metales a la membrana con un control realmente bueno de la composición de la aleación [62,275–277]. Sin embargo, esta técnica tiene cierta dificultad para generar capas libres de defectos en superficies rugosas y altos costes de inversión [61]. Por lo tanto, en la fecha actual, la incorporación de metal por deposición no electroquímica está ampliamente adoptada [260].

En general, la incorporación de metales mediante la deposición no electroquímica para la preparación de aleaciones puede realizarse de diferentes maneras después de una activación previa del soporte, como se ilustra en la Figura 1.5.5. Primero, puede utilizarse un baño único que contenga todos los componentes de la aleación, es decir, materiales A y B, depositando de este modo de manera simultánea todos ellos, denominándose esta variante como codeposición (Figura 1.5.5a). En este caso, los componentes de la aleación se distribuyen aleatoriamente en la capa selectiva con una composición similar en ambas direcciones, longitudinal y transversal. Por lo tanto, se favorece la consecución de una capa homogénea en composición en el siguiente tratamiento térmico para formar la aleación. Sin embargo, esta opción solo es posible en el caso de utilizar metales con propiedades análogas que puedan reducirse en condiciones similares, como

1. Introducción

por ejemplo el paladio y la plata. Sin embargo, la cinética del proceso de reducción suele ser diferente para otros componentes y, en consecuencia, no es fácil definir las condiciones del baño para lograr la composición de aleación deseada [28,75,278,279]. Otra posibilidad para preparar membranas de aleaciones de Pd se basa en deposiciones secuenciales de cada constituyente, incorporando toda la cantidad requerida de material B sobre una capa formada previamente por el material A (Figura 1.5.5b) o viceversa (Figura 1.5.5c), ambas alternativas se conocen como deposiciones secuenciales consecutivas. Otra alternativa de deposiciones secuenciales es la alternancia de diferentes capas formadas por cada constituyente hasta lograr la composición y grosor deseado (Figura 1.5.5d, e, métodos alternos). En estos casos, es posible incorporar metales de diferentes baños utilizando los mismos o diferentes agentes reductores con la condición de que no ocurra desplazamiento galvánico. La cinética de los procesos de deposición se puede controlar, al igual que la composición final de la aleación. El inconveniente más relevante de las deposiciones secuenciales es la dificultad de lograr una buena homogeneidad de la aleación a través del espesor total de la capa [280].

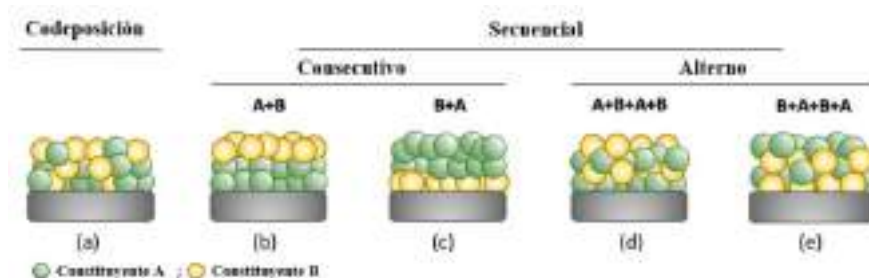


Figura 1.5.5. Diferentes alternativas al proceso de deposición de aleaciones binarias mediante la deposición no electroquímica: codeposición (a), deposición secuencial consecutiva (b, c) y deposición secuencial alterna (d, e)[29].

En cualquier caso, siempre se requiere un tratamiento térmico adicional para lograr la difusión de átomos dentro del material sólido para formar la aleación, independientemente del uso de alternativas secuenciales o la codeposición para la incorporación de los metales. Este proceso, también conocido como aleado, puede llevarse a cabo bajo atmósfera inerte (generalmente utilizando Ar, He o N₂) [167,214,281] o en presencia de hidrógeno [53,162,265,278,282]. Los procesos de aleación tradicionales para membranas de base Pd utilizan una atmósfera inerte a presión ambiental y

requieren tiempos bastante largos [54]. Sin embargo, desarrollos recientes prefieren procesos más rápidos en atmósfera de hidrógeno a presión. En este caso, se observó que el hidrógeno disuelto forma vacantes en la red cristalina de paladio, favoreciendo la movilidad de otros componentes de la aleación y, en consecuencia, reduciendo el tiempo requerido para obtener la aleación [273]. Como se mencionó anteriormente, las capas preparadas por codeposición necesitan tratamientos térmicos más suaves (tiempos más cortos o temperaturas más bajas) para el aleado completo, en comparación con las capas generadas por deposición secuencial (consecutiva o alternativa) [163,280]. Teniendo en cuenta que la preparación de aleaciones con un control preciso es un desafío decisivo para la aplicación a gran escala de membranas basadas en Pd [283,284], las continuación se resumen algunos de los avances más relevantes en este campo, distinguiendo entre la preparación de aleaciones binarias y ternarias. Entre la gran cantidad de aleaciones posibles de diferentes pares de metales, las aleaciones binarias base Pd son las más frecuentemente estudiadas y utilizadas para la producción de hidrógeno.

Como se mencionó anteriormente, la aleación de paladio con otro componente puede evitar la fragilización por hidrógeno y mejorar las propiedades mecánicas y químicas. En algunos casos específicos, la permeabilidad al hidrógeno puede incluso aumentar, dependiendo de la composición de la aleación. La Figura 1.5.6 muestra el valor de la permeabilidad del paladio puro y algunas de sus aleaciones. Puede observarse como en algún caso pueden superar este valor solo en una ventana de composición estrecha, mientras que otras también funcionan en una amplia gama de composiciones. Las desviaciones respecto a la composición objetivo o la diferencia de composición dentro de la propia capa selectiva metálica pueden deteriorar notablemente el comportamiento de permeación con respecto al paladio puro. Por ejemplo, esto ocurre cuando excede el 36% o el 21% en peso para el caso de aleaciones con plata u oro, respectivamente. Para las aleaciones de paladio y cobre, las pequeñas desviaciones del valor objetivo de $Pd_{60}Cu_{40}$ implican una disminución drástica en la permeabilidad al hidrógeno.

1. Introducción

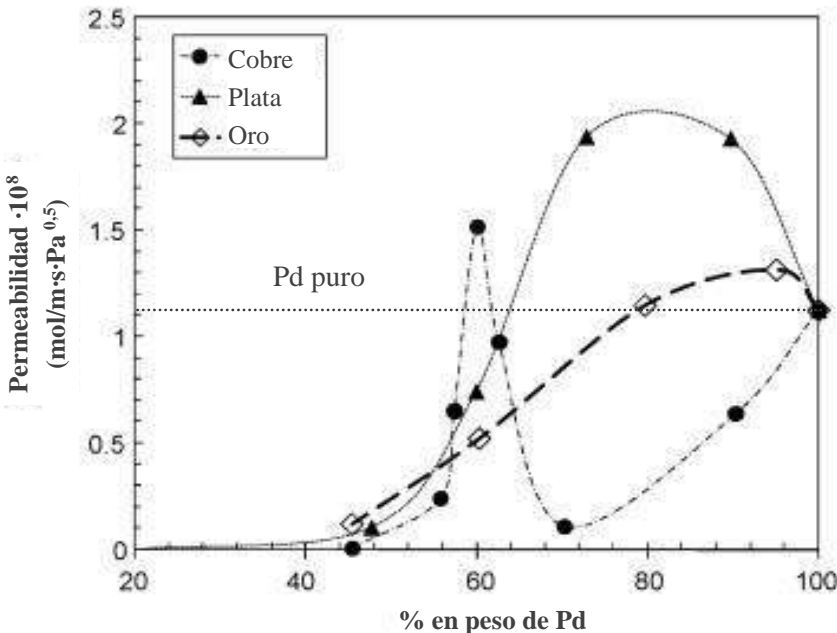


Figura 1.5.6. Permeabilidad de H_2 en función de la composición de la aleación de Pd con Cu, Ag y Au a $350^\circ C$ [284].

Una de las primeras alternativas para la preparación de aleaciones binarias de base Pd consiste en la incorporación de plata, utilizada desde los años ochenta para la separación de isótopos de hidrógeno [285,286]. La resistencia a la fragilización por hidrógeno mejora significativamente después de la incorporación de plata en la capa de paladio [279], así como la permeabilidad al hidrógeno original también puede aumentarse para algunas condiciones particulares [287]. Como se mostró previamente en la Figura 1.5.6, la adición de plata sobre paladio para preparar una aleación binaria de PdAg aumenta la permeabilidad de la membrana, respecto al Pd puro, en una amplia gama de composiciones, desde porcentajes de Ag muy bajos hasta alrededor del 36% en peso [284]. Particularmente, se demuestra que usando una composición de $Pd_{77}Ag_{23}$, la permeación de hidrógeno alcanza un máximo y, por lo tanto, muchos investigadores de todo el mundo han adoptado esta composición como objetivo principal de la composición de la capa selectiva. Con respecto al procedimiento de preparación para obtener esta aleación mediante una deposición no electroquímica, se pueden encontrar ampliamente en la bibliografía las alternativas de codeposición [163] y deposición secuencial [280].

El uso de cobre como elemento de aleación para la preparación de membranas basadas en Pd no solo mejora la resistencia contra la fragilización por hidrógeno, sino que también aumenta ligeramente la permeación en comparación con las membranas de paladio puro al mismo tiempo que conserva la capacidad de permeación en presencia de mezclas de gases que contienen compuestos de azufre [55,191,283]. Además, el cobre es bastante más barato que el paladio y, por lo tanto, la reducción porcentual de Pd en la capa selectiva (composición óptima alrededor de $Pd_{60}Cu_{40}$) reduce su coste final. La preparación de las membranas de PdCu mediante deposición no electroquímica generalmente se lleva a cabo de manera secuencial incorporando paladio en primer lugar, seguido de cobre, con un tratamiento de aleado posterior a alta temperatura. En este caso, la codeposición estable es realmente difícil debido a la diferente naturaleza de cada metal y el desplazamiento galvánico del cobre por el paladio debido al menor potencial de reducción del primero [288]. Sin embargo, el uso de aleaciones de PdCu está restringido a un rango de composición muy estrecho y preciso, debido a la caída drástica del permeado de H_2 cuando se producen pequeñas variaciones en el 40% de contenido de Cu [170,259,289,290].

La adición de oro en una capa selectiva de paladio aporta beneficios similares a los obtenidos con el cobre en las aleaciones de base Pd. Principalmente mejoran la tolerancia al azufre [159], aunque el coste de las membranas resultantes es mayor debido al elevado precio del oro con respecto al del cobre y la necesidad de un mayor contenido en paladio para este tipo de aleaciones, generalmente superior al 80% [284]. Sin embargo, consta de un amplio rango de composiciones en los que la aleación PdAu exhibe una estructura cúbica centrada en las caras, lo que asegura una mayor permeabilidad respecto a las membranas de Pd puro [283]. Este hecho es muy beneficioso para la preparación de la membrana, ya que es posible aumentar la permeación con todos los contenidos de Au inferiores al 21%, mientras se mantiene la tolerancia al azufre. Entre estas posibilidades, una composición de $Pd_{90}Au_{10}$ podría presentarse como objetivo, ofreciendo las mejores propiedades en la membrana resultante [284]. Respecto a la preparación de este tipo membranas, el procedimiento ampliamente descrito en la mayoría de los trabajos publicados es la combinación de la deposición no electroquímica del Pd y la consecutiva incorporación de Au por desplazamiento galvánico [161,162,279].

Las aleaciones binarias mencionadas anteriormente basadas en paladio, plata, cobre y oro son las alternativas más comúnmente utilizadas

1. Introducción

por los investigadores para la separación selectiva de H₂. Sin embargo, también es posible encontrar la combinación de paladio con otros metales para lograr ventajas adicionales en la reducción de costes o el aumento de la capacidad de permeación. En este contexto, la principal limitación para explorar nuevas aleaciones es la posibilidad de incorporar los metales mediante la deposición no electroquímica, prefiriéndose utilizar la deposición física en fase vapor [62,277]. Sin embargo, como se detalló anteriormente, el uso de la deposición no electroquímica para la preparación de membranas selectivas al H₂ es recomendado en términos de rentabilidad económica [34]. En este contexto, se ha explorado el uso de níquel [216,291] o platino [153,265] para preparar aleaciones base Pd mediante procesos no electroquímicos. Las membranas soportadas de aleación Pd-Ni muestran estabilidad térmica a largo plazo a 300 °C bajo permeación constante de hidrógeno [291]. A diferencia de la aleación PdNi, las aleaciones PdRu y PdPt [265] mostraron estabilidad térmica a largo plazo a mayores temperaturas. Las membranas basadas en una película delgada de PdRu fueron preparadas por codeposición con contenidos realmente bajos en rutenio (< 2% en peso) [271], mientras que las membranas de PdPt se forman alternando capas de Pd y Pt [153] con una carga final de platino de alrededor del 25% en peso.

También se ha considerado que la formulación de aleaciones ternarias para combinar simultáneamente las mejoras asociadas a cada componente [75]. Sin embargo, las investigaciones publicadas sobre la preparación de estas aleaciones mediante deposición no electroquímica aún son escasas, y se iniciaron hace solamente unos años. Los primeros trabajos sugieren que ciertas composiciones particulares parecen alcanzar mejoras adicionales en las propiedades de la membrana en comparación con las aleaciones binarias, en términos de aumento de permeabilidad al hidrógeno y / o la resistencia química [57]. Aleando Pd simultáneamente con otros dos o más metales (por ejemplo, Ag, Cu o Au), es posible mejorar no solo la permeabilidad de la membrana sino también las resistencias mecánicas y químicas al envenenamiento por azufre al mismo tiempo [42,279]. Además, el uso de materiales más baratos, como Ag o Cu, en estas formulaciones reduce el coste final de la membrana [292–295]. Por otro lado, el cobre y el oro presentan puntos de fusión más altos que la plata, aunque ligeramente una menor permeabilidad de sus aleaciones binarias con paladio. Por lo tanto, agregar estos metales en aleaciones de PdAg para conformar una aleación ternaria podría aumentar la estabilidad térmica de la membrana [42,57,296].

como por ejemplo: PdAgCu [297], PdAgAu [42] o incluso la combinación de ambos sin la adición de plata (PdCuAu) [278].

Objetivos

Desde un punto de vista ambiental, la utilización masiva de combustibles fósiles en los sectores industrial y de transporte constituye la principal fuente de emisión de gases de efecto invernadero responsables del calentamiento global del planeta, principalmente metano y dióxido de carbono. El uso de hidrógeno se postula como una alternativa atractiva para paliar esta problemática, lo que previsiblemente incrementaría su demanda como vector energético durante las próximas décadas. El departamento de Tecnología Química, Energética y Mecánica de la Universidad Rey Juan Carlos ha establecido una serie de líneas de investigación cuyo objetivo es el estudio y desarrollo de diferentes tecnologías para la producción, purificación y almacenamiento de hidrógeno con el fin de poder implementarlas de forma satisfactoria en los sectores industrial y de transporte.

La presente Tesis Doctoral se enmarca dentro de una de estas líneas de investigación, y presenta como objetivo principal el desarrollo de nuevas membranas compuestas de base paladio que permitan mejorar su capacidad de permeación y mantener una adecuada selectividad al hidrógeno y resistencia mecánica frente a diversas condiciones de operación.

Para alcanzar este objetivo principal, se han establecido los siguientes objetivos parciales o específicos:

- Modificación superficial de soportes porosos de acero inoxidable mediante la incorporación de capas intermedias con el fin de reducir su rugosidad y tamaño medio de poros originales, para facilitar la posterior deposición de una capa de paladio de reducido espesor mediante la técnica de Electroless Pore-Plating.
- Modificación del proceso de activación superficial de los soportes necesario para la posterior incorporación del paladio con objeto de lograr una mejor distribución de los centros de nucleación en las zonas de interés.
- Evaluación de la morfología, capacidad de permeación, selectividad hacia el hidrógeno y resistencia de las membranas preparadas frente a diversas condiciones de operación que incluyen presión, temperatura y dirección del flujo de permeado.

1. Objetivos

- Análisis de los posibles fenómenos de polarización por concentración que afectan a la capacidad de permeación de membranas de paladio mediante la realización de ensayos con, mezclas de gases en distintas concentraciones a diferentes condiciones de operación.
- Estudio tecno-económico de los diferentes tipos de membranas desarrollados para la selección de la alternativa más prometedora.
- Integración del tipo de membrana de paladio seleccionada en un reactor de membrana para la producción y purificación simultánea de hidrógeno mediante reformado con vapor de ácido acético. Análisis de la resistencia mecánica exhibida por la membrana en estas condiciones y los resultados alcanzados en comparación con los obtenidos en un reactor de tipo convencional.

2

Metodología

2.1 Preparación de membranas

En el presente trabajo de investigación se han preparado membranas selectivas al hidrógeno. Estás membranas están compuestas por un tubo de acero poroso, que hace la función de soporte, y una capa metálica de base paladio, que funciona como membrana selectiva al hidrógeno. Los soportes de acero utilizados son adquiridos a la empresa “Mott Metallurgical Steel”, mientras que la capa metálica es generada mediante deposición no electroquímica (ELP).

Respecto al soporte de acero poroso comercial, está fabricado mediante pulvimetallurgia a partir de partículas de acero 316L. Estos soportes tienen una geometría cilíndrica con un diámetro exterior de 12,9 mm, un espesor de pared de 1,9 mm y una longitud de 150,0 mm. Además, el soporte presenta una porosidad del 20% y un grado de 0,1 μm . Este último valor indica el tamaño mínimo de partícula que no puede atravesar el soporte, siendo rechazadas el 95% de las partículas de este tamaño.

Antes de proceder a la deposición de la capa selectiva se realizan una serie de etapas, como son el acondicionamiento inicial del soporte comercial, la modificación superficial del soporte mediante la incorporación de capas intermedias y el proceso de activación con núcleos de paladio sobre el soporte modificado. En el presente trabajo se ha analizado el efecto del orden de realización de esta última, habiéndose realizado membranas siguiendo la secuencia descrita previamente o realizando la activación directamente sobre las partículas de manera previa a su incorporación como capa intermedia. Una vez realizadas estas etapas, independientemente del orden seguido, se continua con la deposición de la capa selectiva mediante deposición no electroquímica, concretamente mediante el proceso *Electroless pore-plating (ELP-PP)*.

2.1.1 Acondicionamiento del soporte comercial

Para comenzar con la preparación de una membrana lo primero que se ha realizado es un corte sobre los soportes originales, para adecuar la longitud del soporte poroso a las dimensiones del reactor. Este corte se realiza mediante una microcortadora Buehler modelo Isomet 4000, dejando la longitud final de los soportes en 30 mm.

Una vez realizado el corte, para evitar que la presencia de contaminantes afecte a la preparación o uso de la membrana se realiza una

2. Metodología

etapa de limpieza en tres pasos. Primero se sumerge el soporte en una disolución de ácido clorhídrico 0,1 M durante 5 minutos. Seguidamente se introduce durante el mismo tiempo en una disolución 0,1 M de hidróxido sódico. Para finalizar, se introduce el soporte en una disolución de etanol comercial 96% v/v durante 15 minutos. Estas etapas se llevan a cabo en un baño de ultrasonidos a una temperatura de 60 °C, realizando un aclarado con agua desionizada entre etapas.

2.1.2 Modificación superficial de los soportes

Con el objetivo de disminuir los problemas generales del uso de un soporte metálico para la fabricación de la membrana, se realiza la modificación de la superficie mediante la incorporación de una capa intermedia de óxidos mixtos hierro-cromo y posteriormente otra de grafito o óxido de cerio. Dichos problemas pueden resumirse, principalmente, en un tamaño medio de poro elevado y con una amplia distribución de tamaños, además de la posible aparición de interdifusión metálica entre el soporte y la capa selectiva durante el uso de la membrana. El uso de interfases también está normalmente ligado a la obtención de una membrana más delgada, lo cual implica una mejora en la capacidad de permeación de la misma.

2.1.2.1 Capa intermedia de óxidos mixtos hierro-cromo

La realización de esta interfase se lleva a cabo a partir de los propios componentes del soporte de acero 316L, mediante un tratamiento térmico. Para este proceso se introduce el soporte en una mufla tubular, con una atmósfera oxidante de aire a 600 °C durante 12 horas. Además, se ha utilizado una velocidad de calentamiento y enfriamiento de 1,8 °C/min [298].

2.1.2.2 Capa intermedia de grafito

De manera posterior a la generación de la capa de óxidos mixtos Fe-Cr, la incorporación de la capa intermedia de grafito se aplicó directamente mediante el pintado de la superficie del soporte poroso con una mina de grafito extraída de un lapicero 2B. Para ello se recubrió completamente toda la superficie del soporte, repitiendo este proceso dos veces de manera previa a la retira del exceso superficial mediante un lavado con agua. Finalizar, el soporte modificado es calcinado a 500 °C durante 5 h en aire, para garantizar la eliminación de los compuestos orgánicos que formaban parte de la mina. De manera análoga a lo realizado en la etapa de generación de la capa intermedia de óxidos mixtos Fe-Cr, la velocidad de calentamiento y enfriamiento es de 1,8 °C/min.

2.1.2.3 Capa intermedia de óxido de cerio

Tras la generación de la capa intermedia de óxidos mixtos Fe-Cr, la incorporación de la intermedia de CeO₂ se lleva a cabo mediante un proceso de recubrimiento por inmersión asistida por vacío (*Vacum-assisted Dip-Coating method*). Para ello se prepara una suspensión acuosa con un 10 y un 2% en volumen de partículas de óxido de cerio y alcohol polivinílico, respectivamente. El soporte se coloca en un dispositivo, similar al representado en la Figura 2.1.1, el cual sella el soporte mediante el uso de unas juntas de silicona, permitiendo al mismo tiempo aplicar vacío en el interior. Una vez realizado dicho montaje, se introduce el conjunto en la suspensión de partículas, aplicando una fuerte agitación, durante 5 minutos. Este ciclo de inmersión del soporte en la suspensión de partículas de CeO₂ se realiza dos veces, dejando un tiempo de secado entre ciclos de 2 horas. Respecto al vacío, este se realiza únicamente en la segunda mitad del último ciclo, lo que ayuda a la deposición de las partículas en el interior de los poros del soporte. Una vez realizados ambos ciclos, se elimina el exceso de material mediante un lavado con agua desionizada. Para finalizar, se calcina el soporte modificado a 500 °C durante 5 h en aire, para garantizar la estabilidad de la interfase eliminando los compuestos orgánicos que formaban parte de la suspensión. En este caso, la velocidad de calentamiento y enfriamiento también es de 1,8 °C/min.

En el presente trabajo de investigación se han realizado interfases de óxido de cerio con partículas densas y mesoporosas. Las primeras son adquiridas a la empresa “Alfa Aesar”, por el contrario, las segundas son sintetizadas mediante nano replicación usando como plantilla SBA-15.

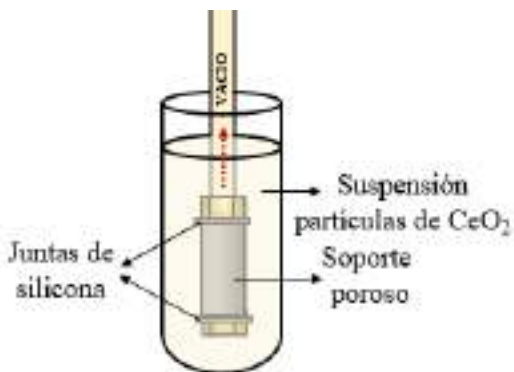


Figura 2.1.1 Esquema del proceso de deposición de la capa intermedia.

2. Metodología

2.1.3 Deposición de la capa selectiva

2.1.3.1 Proceso de activación

Para poder obtener una capa selectiva delgada, homogénea y libre de defectos, es necesario realizar la activación de la superficie a recubrir de manera previa a la generación del recubrimiento. Esta activación consiste en la deposición de pequeños núcleos de paladio homogéneamente distribuidos. En este proceso se utilizan dos disoluciones, cuya composición se recoge en la Tabla 2.1.1. Los núcleos de paladio se generan mediante la reducción directa del paladio metálico contenido en la sal de cloruro de paladio al reaccionar con una disolución reductora que contiene hidracina.

Tabla 2.1.1 Composición de las disoluciones utilizadas en la activación.

Componentes	Baño de Pd	Baño reductor
HCl 35% (ml/l)	1,0	-
PdCl ₂ (g/l)	0,1	-
N ₂ H ₄ (ml/l)	-	10,0
NH ₄ OH 32% (ml/l)	-	119,6

En este trabajo, se ha evaluado el efecto de realizar esta activación en dos superficies distintas. En el primer caso, la activación se realiza sobre la superficie del soporte metálico, modificado previamente con las capas intermedias. Para ello se coloca el soporte modificado en un dispositivo de Teflón, similar al esquematizado en la Figura 2.1.2, el cual permite asegurar la estanqueidad de la zona interior mediante el uso de juntas de silicona. Este montaje se introduce en el baño de paladio, al mismo tiempo que se añade el baño reductor en el interior. Debido al diferente valor de mojabilidad de ambas disoluciones con la superficie del soporte modificado, la disolución interior empieza a difundir a través de los poros hasta entrar en contacto con la disolución exterior, dando lugar a la deposición de los núcleos de paladio. Como consecuencia de este proceso de difusión a través de los poros, los núcleos se generan tanto en la zona interior de los poros como la superficie externa del soporte. Esta activación se lleva a cabo a temperatura ambiente durante 2 horas, utilizando una relación volumétrica de baño interior/exterior

de 1/16. Una vez finalizado este proceso, los soportes se introducen en una estufa durante 8 horas a 100 °C para su secado completo.

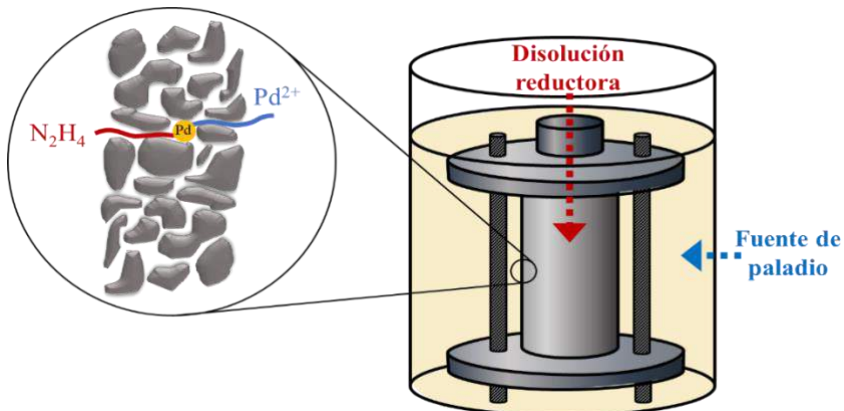


Figura 2.1.2 Esquema del proceso de deposición de paladio no electrolítico mediante la alternativa ELP-PP.

El segundo proceso consiste en la activación superficial de las partículas de CeO₂, de manera previa a su incorporación como interfase en el soporte metálico. Para ello se añaden las partículas al baño de paladio y, aplicando una fuerte agitación, se dosifica gota a gota el baño reductor. La agitación se mantiene durante 2 horas a temperatura ambiente, posteriormente las partículas se filtran y secan durante 8 horas a 100 °C en una estufa. La relación de cantidades entre partículas, baño de Pd y baño reductor es una de las variables que se analizará en detalle posteriormente en el apartado resultados.

2.1.3.2 Deposición de paladio

La deposición de paladio se realiza mediante un proceso no electroquímico conocido como *Electroless Pore-Plating* (ELP-PP), el cual fue desarrollado previamente en la Universidad Rey Juan Carlos [52]. Esto método se diferencia de los convencionales por la adición de la fuente de paladio y el agente reductor por lados opuestos del soporte. Las disoluciones utilizadas se recogen en la Tabla 2.1.2. Al igual que en el primer método de activación, el soporte se monta en un dispositivo (Figura 2.1.2) donde la disolución reductora añadida en el interior del soporte difunde a través de los poros, hasta ponerse en contacto y reaccionar con la fuente de paladio situada en la zona exterior. La deposición de paladio se lleva a cabo a 60 °C, en ciclos de 2 o 7 horas hasta conseguir una membrana libre de defectos. Entre ciclos se realiza la extracción de la membrana del dispositivo, seguida de un lavado

2. Metodología

en agua desionizada y un secado a 110 °C durante 8 horas. La relación de volúmenes entre baño interior/exterior es también de 1/16.

Tabla 2.1.2 Composición de las disoluciones utilizadas para la deposición.

Componentes	Baño de Pd	Baño reductor
NH ₄ OH 32% (ml/l)	390,0	-
PdCl ₂ (g/l)	5,4	-
EDTA (g/l)	70,0	-
N ₂ H ₄ (ml/l)	-	10,0

2.2 Técnicas de caracterización

En este apartado se describen las técnicas de caracterización empleadas durante el presente trabajo, tanto para el análisis de la membrana obtenida como para los componentes de la misma.

2.2.1 Microscopía electrónica de barrido (SEM)

El microscopio electrónico de barrido (SEM) utilizado para la caracterización de los materiales ha sido un equipo Hitachi modelo S-2400N equipado con detectores de electrones secundarios (SE) y retrodispersados (BSE). Los primeros, son utilizados principalmente para obtener información topográfica, mientras que los segundos se usan para obtener información composicional. Además, para poder realizar un análisis composicional semicuantitativo, se utilizó la técnica dispersiva de rayos X acoplada al SEM. En el presente trabajo de investigación se ha utilizado la microscopía electrónica de barrido no solo para analizar la superficie final de la membrana, sino también el soporte comercial y la incorporación de las capas interfases, así como cortes transversales de las muestras tras los ensayos a alta temperatura.

2.2.2 Microscopía electrónica de transición (TEM)

Un microscopio electrónico de transición (TEM) de la compañía JEOL modelo JEM-2100 fue utilizado para la caracterización inicial de partículas que posteriormente se incorporarían como capa interfase al soporte metálico.

2.2.3 Perfilometría óptica 3D

La perfilometría óptica añade un escáner vertical de la muestra (eje z) a la microscopía óptica convencional. Permitiendo crear una imagen 3D a partir de la combinación de las partes de la muestra en foco del plano xy, para las distintas distancias focales del eje z. El modelo utilizado es el Zeta-20 de la compañía ZETA Instruments, el cual permite tomar imágenes a diferentes magnificaciones, llegando a resoluciones inferiores a 0,2 μm a 500 aumentos. En este trabajo la perfilometría óptica se utilizó para caracterizar la rugosidad superficial del soporte inicial, así como después de cada una de las modificaciones realizadas sobre el mismo, incorporación de capas intermedias y capas selectivas.

2.2.4 Difracción de rayos X (DRX)

Los espectros de difracción rayos X proporcionan información cualitativa y cuantitativa de las fases cristalinas presentes en la muestra. Para este análisis se empleó un difractómetro Philips modelo X'PERT PRO MPD/MRD con K_{α} del Cu (1,54 Å) y un monocromador secundario. Estos resultados se han utilizado para identificar la presencia de fases cristalinas en el soporte de la membrana, antes y después de cada una de las capas depositadas, así como el ordenamiento estructural de algunos de los compuestos utilizados como capa interfase de la membrana.

2.2.5 Difracción láser

Esta tecnología es aplicada mediante un analizador de tamaño de partícula Mastersizer 2000, el cual puede evaluar tanto el tamaño como la distribución de tamaño de las partículas. En este trabajo se ha utilizado dicha técnica para evaluar estos dos parámetros comentados previamente, sobre las partículas de óxido de cerio que se incorporan como capa interfase en la membrana.

2.2.6 Espectroscopía de emisión atómica (ICP-AES)

La técnica de espectroscopía de emisión atómica de plasma acoplado por inducción (ICP-AES) permite evaluar la concentración de un elemento en disolución, realizando previamente medidas de calibrado con patrones certificados. Antes de realizar el análisis, se somete a las muestras sólidas a un tratamiento de digestión, para favorecer la disolución de todos los componentes. En el presente trabajo se ha utilizado un aparato VARIAN,

2. Metodología

modelo Varian Vista AX Pro. Este equipo se ha usado para analizar la carga de paladio incorporada a las partículas de ceria durante la etapa de activación.

2.2.7 Gravimetría

Los ensayos gravimétricos se basan en la medida de la ganancia o pérdida de masa, por diferencia de pesada, que se han producido en una muestra después de haberlo sometido a un determinado proceso. En este trabajo se ha utilizado una balanza analítica de alta precisión Kern & Sohn ABS-4, con una precisión de $\pm 0,0001$ g. En el presente trabajo de investigación se ha utilizado el análisis gravimétrico para evaluar la ganancia de peso adquirida tras cada incorporación de capa interfase o ciclo de deposición de la capa selectiva. Teniendo en cuenta las dimensiones del soporte comercial y la densidad del componente a evaluar puede calcularse un espesor de capa aparente, considerando que todo el material se deposita sobre la cara externa del diámetro exterior.

2.2.8 Ensayos de permeación de gases

Las membranas realizadas se han caracterizado en términos de capacidad de permeación realizando una serie de ensayos de permeación con gases. Estos ensayos consisten en hacer pasar un gas o mezclas de gases a través de la membrana, en distintas condiciones de presión y temperatura, analizando el caudal (Q_{perm}) y la composición (C_i) del gas permeado. De este modo y teniendo el valor del área superficial de la membrana (A), se puede obtener mediante la siguiente ecuación el flujo de permeado (J_i):

$$J_i = \frac{Q_{perm} \cdot C_i}{A} \quad (Ec. 2.1)$$

Otro factor que determina la calidad de la membrana es la selectividad de esta hacia un producto, en este caso el hidrógeno. Este factor de separación (α) se define como la relación entre el flujo de hidrógeno permeado obtenido ($J_{H_2}^{perm}$) y el flujo del resto de gases presentes en el permeado (J_i^{perm}). Cuando esta medida se realiza alimentando gases puros de manera independiente (H_2 y N_2 , habitualmente) recibe el nombre de factor de separación ideal y se expresa como:

$$\alpha_{H_2/i} = \frac{J_{H_2}^{perm}}{J_i^{perm}} \quad (Ec. 2.2)$$

Por otro lado, también puede realizar esta medida alimentando una mezcla de gases. De este modo se obtiene el factor de separación real, para

el cual es necesario analizar la composición de las corrientes. Además de la selectividad, estos ensayos permiten determinar cómo afecta la presencia de otros gases en el alimento a la permeación de hidrógeno, los cuales pueden producir fenómenos de polarización, inhibición o contaminación de la capa selectiva.

2.2.8.1 Ensayo preliminar: detección de fugas

Con el objetivo de poder determinar cuándo una membrana está finalizada y lista para ser utilizada en ensayos de permeación a alta temperatura, se realiza una prueba preliminar de detección de fugas a temperatura ambiente. Para ello se coloca la membrana en un dispositivo similar al representado en la Figura 2.1.2, el cual permite presurizar el interior con un gas inerte. Una vez finalizado el montaje de la membrana en el dispositivo, el conjunto se introduce en un recipiente con etanol y se presuriza el interior de la membrana con helio (< 3 bar). En estas condiciones, si la capa metálica depositada presenta alguna discontinuidad, como poros o grietas, el gas interior podrá salir a través del defecto dando lugar a la formación de burbujas en la superficie. En caso de detectar la presencia de burbujas se realizan ciclos de deposición ELP-PP adicionales, hasta obtener una membrana libre de defectos. A pesar de ser una prueba sencilla, esta es de gran utilidad a la hora de la seleccionar membranas de buena calidad.

2.2.8.2 Ensayo de permeación de gases

Una vez obtenida una membrana con una capa selectiva aparentemente libre de defectos, se procede al montaje de ésta en el sistema experimental de permeación representado en la Figura 2.2.1. Esta instalación cuenta con tres líneas de entrada que permiten trabajar con hidrógeno, nitrógeno y dióxido de carbono, de manera independiente o simultánea. Cada línea dispone de un controlador de caudal másico de gas de la empresa Bronkhorst Hi-tec, modelo F-201CV-AGD-11-V, con una capacidad de 400 mL/min ($\pm 1\%$). Estos controladores, FIC-01 para el H₂, 02 para el N₂ y 03 para el CO₂, actúan sobre sus correspondientes válvulas, CV-01, 02 y 03, uniéndose como una única corriente de alimentación al reactor. Por otro lado, se dispone de una cuarta línea de entrada la cual se utiliza para introducir N₂ como gas de arrastre en la zona de permeado. En este caso el controlador utilizado, FIC-04, es el mismo modelo a los anteriores, pero con una capacidad máxima 200 mL/min ($\pm 1\%$), el cual actúa sobre la válvula CV-04 para regular el caudal. A la salida del módulo de permeación se obtienen dos

2. Metodología

corrientes, permeado y retenido. El permeado está formado por la cantidad de gas que ha conseguido atravesar la membrana, mientras que el retenido se compone del gas que no lo ha hecho. La instalación cuenta con un medidor de caudal másico de gas (FI-01) Bronkhorst Hi-tec modelo F-111B-AGD-11-V que posee una capacidad máxima de 200 mL/min ($\pm 1\%$), el cual puede medir la corriente de permeado o retenido, En función de la posición de las válvulas manuales V-03, V-04, V-05 y V-06. La composición de ambas salidas, permeado y retenido, pueden ser determinadas mediante análisis cromatográfico mediante un MicroGC Varian CP-4900. Debido a la necesidad de una fuerza impulsora para que se produzca la permeación, en este caso una diferencia de presión parcial de hidrógeno entre ambos lados de la membrana, la instalación cuenta con un controlador de presión backpressure Bronkhorst (PIC-01) modelo P-702CV-AGD-11-V, cuyo máximo son 10 barg. Este controlador actúa sobre la corriente de retenido, mientras que la de permeado se mantiene a presión atmosférica.

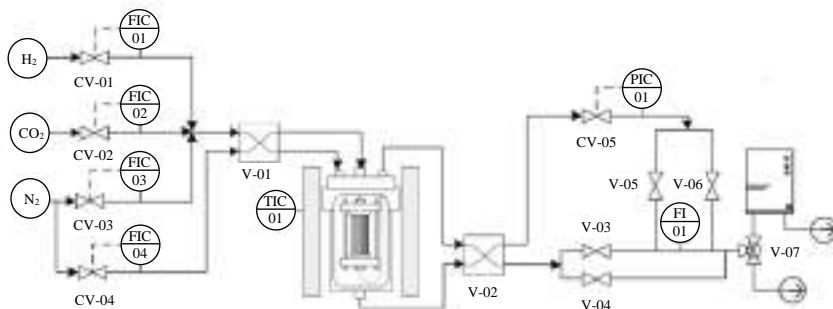


Figura 2.2.1 Esquema de la instalación experimental para la permeación de gases.

Respecto al módulo de permeación, éste consiste en un recipiente cilíndrico de acero, el cual se sella mediante el uso de una junta de grafito. Alrededor de este se coloca una camisa calefactora que permite alcanzar la temperatura de operación, controlada mediante un controlador de temperatura (TIC-01), modelo Eurotherm 2216e, y un termopar tipo K situado en una zona próxima a la superficie exterior de la membrana. En el interior de este cilindro metálico se encuentra la membrana, de 30 mm de longitud, colocada en una celda metálica, similar a las utilizadas para la deposición de la capa selectiva. En este caso las juntas utilizadas para sellar el área de contacto entre membrana y celda son de grafito, debido a la imposibilidad de usar juntas de silicona a la temperatura de trabajo. Las líneas de gases del módulo de permeación están unidas a dos válvulas

manuales, V-01 y V-02, las cuales controlan la dirección del fluido. De este modo se obtiene la posibilidad de realizar ensayos con dos direcciones de permeación en la membrana, dando lugar a dos modos de operación, denominados como in-out y out-in. En el modo in-out, la corriente de alimento se introduce en el interior de la membrana, dando lugar a que la permeación se produzca desde el interior al exterior. Por el contrario, en el modo out-in el alimento se introduce por el exterior de la membrana, teniendo que permear el gas hacia la zona interna. Una representación esquemática de los modos de operación se presenta en la Figura 2.2.2.

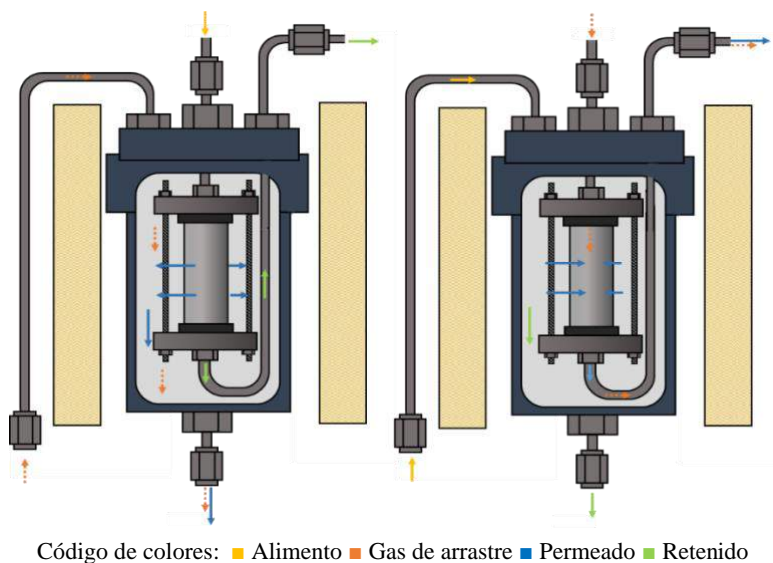


Figura 2.2.2 Esquema de la celda de permeación de la instalación experimental describiendo los dos modos de operación posibles: modo in-out (a) y out-in (b).

Utilizando la instalación experimental previamente descrita se han realizado ensayos de permeación a distintas temperaturas (350-450 °C), incrementos de presión (0,2-3 bar), utilizando los dos modos de operación posibles (in-out, out-in). Para ello se han alimentado gases puros (H_2 , N_2) y mezclas de estos. Hay que destacar que en las etapas de calentamiento y enfriamiento se han realizado introduciendo N_2 por la corriente de alimento y de gas de arrastre, con una diferencia de presión entre corrientes de 0,2 bar y utilizando el modo de operación out-in. De esta manera se pretende proteger a la membrana del fenómeno de fragilización por hidrógeno, el cual puede darse en membranas de paladio a temperaturas inferiores a 293 °C en

2. Metodología

presencia de este gas. Una vez alcanzada la temperatura deseada y manteniendo el N₂ como único gas de alimento, se comprueba el caudal de la corriente de permeado a diferentes presiones. En caso de haber obtenido una capa selectiva densa, libre de defectos, no se observará caudal en la corriente permeado, saliendo todo el caudal alimentado por la corriente retenido. Posteriormente, se cambia la alimentación de N₂ a H₂ y se espera a realizar las mediciones de caudal hasta obtener un valor de permeado estable. Para comprobar la estabilidad de las membranas este proceso de calentamiento, estabilización con H₂ y enfriamiento se repite un mínimo de 5 veces antes de evaluar cómo afectan el resto de variables a la permeación.

3

Discusión general

3.1 Incorporación de capas intermedias

La modificación superficial de los soportes comerciales utilizados para la preparación de membranas soportadas de base paladio, con objeto de mejorar sus propiedades originales, ha despertado un gran interés en los últimos años. Existe la posibilidad de emplear para tal fin tratamientos de diversa naturaleza, incluyendo procesos químicos, mecánicos o incorporación de capas intermedias, y todos ellos persiguen mejorar las propiedades superficiales de los soportes en términos de tamaño medio de poro y rugosidad para así favorecer la posterior incorporación de una capa de paladio de reducido espesor con una buena homogeneidad. En primer lugar, se busca mantener una porosidad elevada, pero con una distribución de tamaño medio de poro lo más estrecha y reducida posible para que puedan ser cubiertos en su totalidad más fácilmente por partículas de paladio. Además, la disminución de la rugosidad superficial original de los soportes asociadas a este tipo de modificaciones también puede favorecer la posterior formación de capas de paladio con menores espesores. Así, globalmente este tipo de modificaciones persiguen la adecuación de la superficie original de los soportes porosos empleados en la preparación de las membranas soportadas para así facilitar la posterior deposición de la capa selectiva de paladio con un menor espesor, pero firmemente adheridas al propio soporte. De este modo, puede obtenerse un importante beneficio económico ligado tanto a la reducción de la cantidad de paladio, de alto coste, requerido en cada una de las membranas como a la disminución del número de membranas rechazadas debido a problemas de roturas o delaminación, en servicio o durante su fabricación.

En este trabajo de investigación se ha estudiado cómo afecta la incorporación de distintas capas intermedias a las propiedades superficiales de soportes porosos comerciales de acero inoxidable 316L (PSS), así como a la posterior incorporación de la capa selectiva de paladio necesaria para la obtención de membranas selectivas al H₂ mediante la técnica ELP-PP, desarrollada con anterioridad por el propio grupo de investigación. Debe destacarse que estas capas intermedias no se incorporaron directamente sobre la superficie del soporte comercial, si no que estos fueron previamente oxidados en aire a 600 °C durante 12 horas, como ya se detalló previamente en el apartado de metodología, con objeto de que posibles etapas de calcinación requeridas para la incorporación de estas nuevas capas

3. Discusión general

intermedias no afectaran de forma diferente a los propios soportes en función del material empleado.

En este contexto, inicialmente se analizó de forma global los posibles efectos beneficiosos que podría tener la incorporación de una capa intermedia adicional en el desarrollo y uso de membranas de paladio sintetizadas sobre soportes PSS mediante ELP-PP. Para ello, se seleccionó el grafito como material de partida debido principalmente a la simplicidad del proceso de modificación. Estas capas se incorporaron pintando directamente la superficie del soporte PSS previamente oxidado con un lápiz 2B, de forma que el grafito contenido en la mina de este cubriera fácilmente la totalidad de la superficie del soporte. De este modo, no fue necesario el diseño y uso de ningún dispositivo específico. La morfología de superficie externa del soporte obtenida tras este tipo de modificación se analizó mediante microscopía electrónica de barrido, recogiéndose una imagen de la misma en la Figura 3.1.1. En ella puede observarse cómo las partículas de grafito se depositaron preferencialmente en las partes más profundas de la porosidad externa del soporte, pudiéndose distinguir los granos de acero pertenecientes al soporte original del grafito añadido debido a la eliminación del exceso de material llevada a cabo en la superficie del soporte. Esto implica una disminución considerable del tamaño medio de las bocas de los poros, que previsiblemente pueden ser cubiertos por paladio con una mayor facilidad que los originales, de mayor diámetro. Esto conduciría no sólo a un menor coste de fabricación de este tipo de membranas (por la menor cantidad de paladio necesaria para formar una capa continua) sino también por la mayor capacidad de permeación de hidrógeno que esta reducción del espesor de paladio conllevaría.

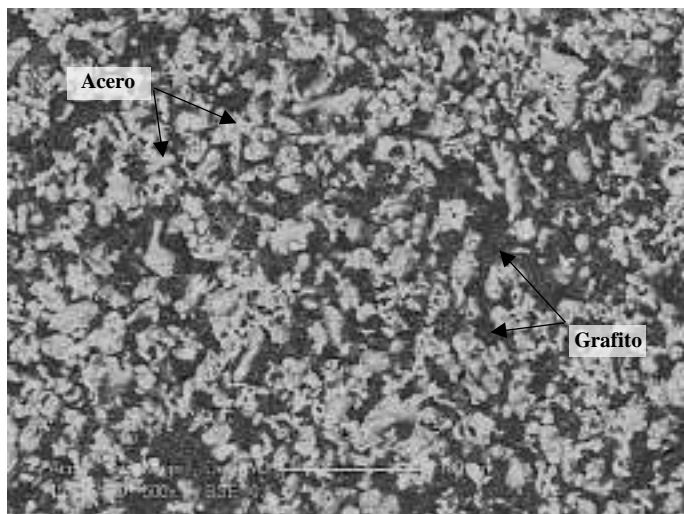


Figura 3.1.1 Imagen SEM de vista superior de soporte de PSS oxidado tras la incorporación de la capa intermedia de grafito.

Para demostrar esta hipótesis, una vez generada la capa intermedia de grafito se llevó a cabo incorporación de la capa de Pd selectiva al H₂ mediante ELP-PP. En este caso, se consiguió reducir el espesor medio de la capa selectiva de Pd, estimado mediante análisis gravimétrico, hasta 17 µm, en contraste con el valor de 30 µm necesario cuando el soporte carece de este tipo de capa intermedia. Analizando el corte transversal de la membrana (Figura 3.1.2) puede observarse que el espesor real de la capa externa se mantiene en el intervalo 8-12 µm. La diferencia obtenida entre el espesor real de la capa externa y el anteriormente estimado mediante gravimetría puede explicarse debido a la presencia de paladio no solo en la superficie externa del soporte, sino que también en el interior de algunos de sus poros (hasta una profundidad cercana a las 35 µm desde la superficie externa). Esto se debe a la propia naturaleza del proceso de deposición empleado para la incorporación del paladio, ELP-PP, en el que las disoluciones que contienen la fuente de paladio y el agente reductor se alimentan desde lados opuestos del soporte, encontrándose ambas en los poros del mismo, que es donde se inicia la reacción de deposición del Pd.

3. Discusión general

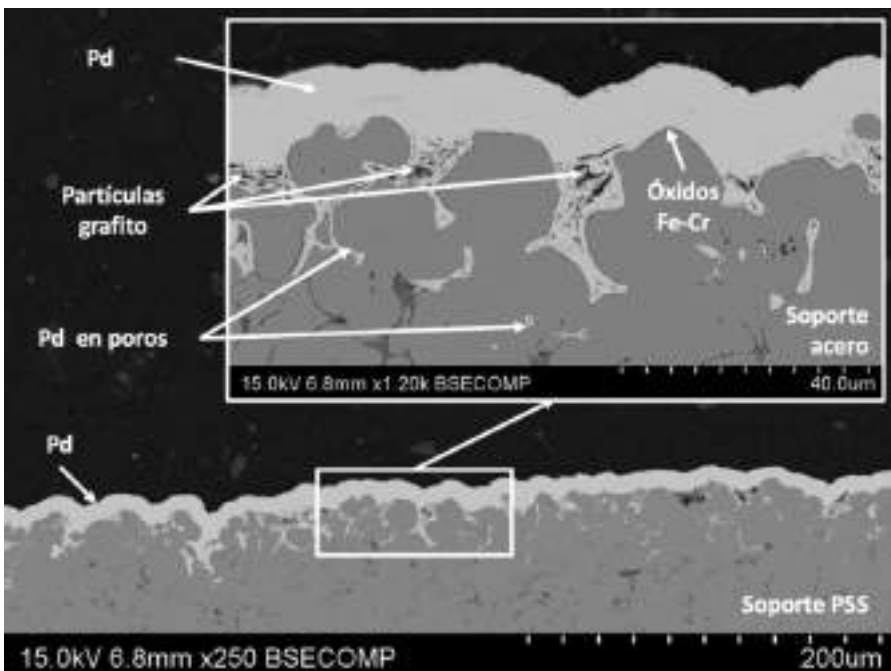


Figura 3.1.2 Micrografía SEM del corte transversal de la membrana compuesta de Pd con capa intermedia de grafito a varios aumentos.

Con este tipo de membranas se realizaron ensayos de permeación de H₂ a alta temperatura (350-450 °C) y diferentes presiones transmembrana (0,5-2,5 bar). La Figura 3.1.3 recoge los principales resultados alcanzados en estos ensayos, pudiendo observar de forma general el efecto que ambos parámetros ejercen sobre los flujos de permeado. En este punto, es necesario indicar que los valores de flujo presentados hacen referencia a ensayos llevados a cabo con hidrógeno puro. Sin embargo, también se realizaron ensayos con nitrógeno para evaluar la selectividad de la membrana, no siendo detectado este gas en la corriente de permeado para ninguna de las condiciones de operación analizadas. De este modo, teniendo en cuenta los flujos de permeado obtenidos y el límite de detección del caudalímetro empleado para estos experimentos (1 NmL / h), se puede garantizar una selectividad ideal de la membrana H₂/N₂ ≥10.000.

También es importante destacar que pese a que, de forma general, un aumento de presión provoca un aumento en el flujo de permeado obtenido, tal y como predice la ley de Sieverts que rige el comportamiento de este tipo de membranas, la intersección con el origen no es del todo clara Figura

3.1.3a. Este ajuste lineal puede mejorarse significativamente si se considera la presencia de una resistencia adicional al proceso de permeación típico basado en un mecanismo de solución-difusión que se da en membranas densas, lo que implica la presencia de una mínima diferencia de presión transmembrana para conseguir un flujo de permeado, como se observa en la Figura 3.1.3b. Esta particularidad, asociada al propio proceso de incorporación del paladio mediante ELP-PP y encontrada con anterioridad para otras membranas, se abordará de forma más extensa con posterioridad. En cualquier caso, bajo estas premisas, se alcanzaron valores de permeanza entre $3,24 \cdot 10^{-4}$ y $4,33 \cdot 10^{-4} \text{ mol m}^{-2} \text{ s}^{-1} \text{ Pa}^{-0,5}$ ($350\text{-}450^\circ\text{C}$), lo que supuso una significativa mejora respecto a los resultados obtenidos previamente con membranas que carecían de una capa intermedia ($k_{H_2}=1,00 \cdot 10^{-4}$ - $2,00 \cdot 10^{-4} \text{ mol m}^{-2} \text{ s}^{-1} \text{ Pa}^{-0,5}$) [52]. Esto se debe principalmente a la reducción del 43% alcanzada sobre el espesor de la capa de paladio necesario para la obtención de una membrana compuesta totalmente densa con la nueva estrategia de síntesis planteada.

Finalmente, el efecto de la temperatura sobre la operación de la membrana se traduce en una energía de activación de $10,6 \text{ kJ mol}^{-1}$, valor situado dentro del intervalo típico que exhiben otras membranas de paladio recogidas en literatura especializada [71].

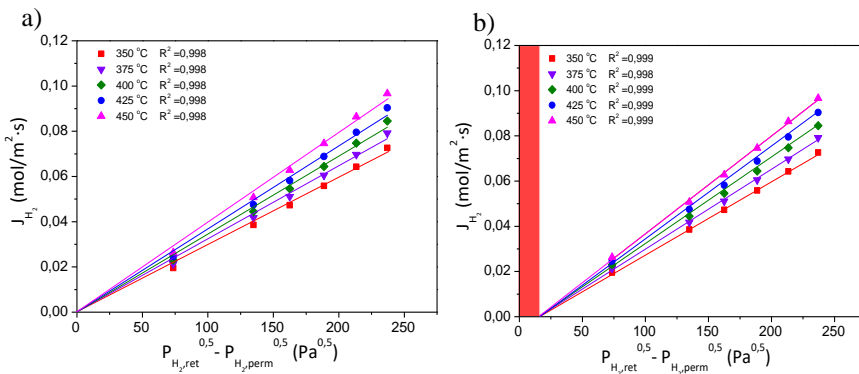


Figura 3.1.3 Ensayos de permeación de hidrógeno de una membrana con capa intermedia de grafito después de la deposición de Pd por ELP-PP: a) ajustando a la ley de Sieverts mediante (0,0) y b) considerando la presencia de una resistencia adicional al proceso de permeación de H_2 .

3.2 Modificación de soportes con partículas de CeO₂ comercial

Una vez comprobado el efecto beneficioso de la incorporación de una capa intermedia en el desarrollo de membranas de paladio compuestas el siguiente paso que se realizó fue la selección de un material más adecuado para la fabricación de dichas interfases. Teniendo en cuenta las condiciones de operación a las que se utilizan las membranas de paladio es importante encontrar un material que tenga estabilidad química y mecánica a temperaturas superiores a los 350 °C, debido a esto se optó por trabajar con materiales cerámicos. En concreto se seleccionó el óxido de cerio (CeO₂) debido a su coeficiente térmico de expansión, cuyo valor ($12,0\text{-}13,0 \cdot 10^{-6} \text{ }^{\circ}\text{C}^{-1}$) se encuentra entre los otros materiales que conforman la membrana compuesta, acero inoxidable 316L y paladio ($15,0\text{-}18,0 \cdot 10^{-6} \text{ }^{\circ}\text{C}^{-1}$ and $10,0\text{-}13,0 \cdot 10^{-6} \text{ }^{\circ}\text{C}^{-1}$, respectivamente). Esto posiciona al óxido de cerio como un material a tener en cuenta debido a que el conjunto de la membrana compuesta sufrirá menos con los ciclos de calentamiento y enfriamiento, evitando así posibles roturas y/o delaminaciones asociadas a los diferentes coeficientes de expansión. A diferencia del resto de materiales que se han incorporado habitualmente como capa interfase, ZrO₂-Y₂O₃, Al₂O₃, SiO₂, el CeO₂ es el único que presenta un coeficiente de expansión térmico superior al del paladio, siendo por tanto el más cercano al acero inoxidable 316L, utilizado como soporte poroso. La Figura 3.2.1, muestra los coeficientes de expansión térmicos más comúnmente utilizados para la preparación de membranas compuestas de base paladio, mostrando los valores tanto de los materiales que forman la capa selectiva (en rojo) como los de los soportes y capas interfases (en azul y verde, respectivamente).

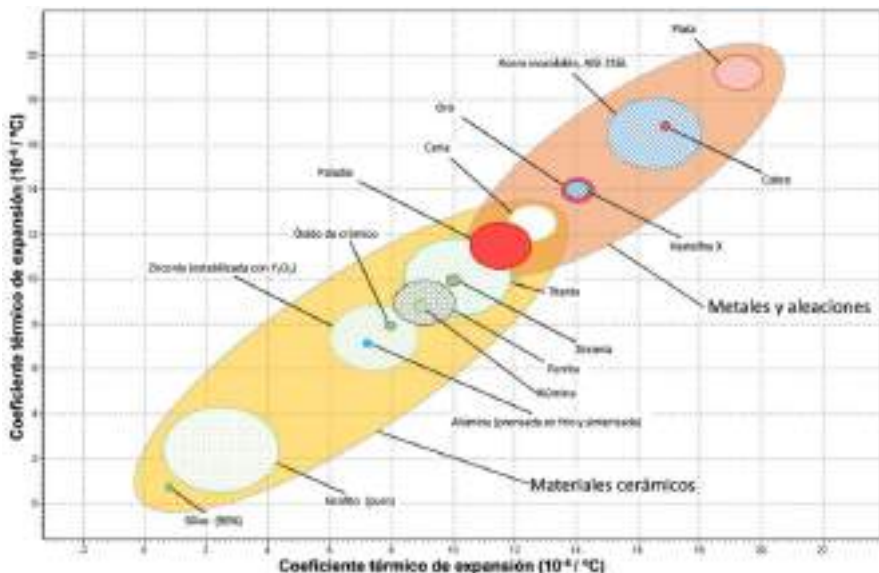


Figura 3.2.1 Coeficientes de expansión térmicos de los principales materiales utilizados para la fabricación de membranas de base paladio selectivas al hidrógeno H₂ [29].

Una vez seleccionado el óxido de cerio como material para la capa intermedia, el siguiente paso fue la selección y optimización del método de preparación de las capas. En este trabajo se seleccionó el método de recubrimiento por inmersión (*dip-coating*), debido principalmente a su sencillez y bajo requerimiento del equipamiento necesario para aplicar método. Con el objetivo de anclar en mayor medida la capa intermedia al soporte poroso se realizó este proceso aplicando vacío al mismo tiempo, lo que promueve la deposición de las partículas de ceria en el interior de la porosidad del soporte. Para eso se sellaron ambos lados del soporte tubular, permitiendo la conexión de la línea de vacío por uno de los extremos (Figura 2.1.1). Una vez montado el soporte poroso en este dispositivo que permite la aplicación de vacío, el conjunto se introduce en una suspensión de partículas de CeO₂ densas durante 5 minutos, dos veces, aplicando vacío únicamente durante la segunda mitad del último ciclo. La suspensión utilizada es de base acuosa y contiene un 10 y un 2% en volumen de partículas de óxido de cerio y alcohol polivinílico, respectivamente. Siguiendo este método primero se obtiene una capa interfase gruesa, la cual colapsa la porosidad del soporte de acero inoxidable lo que impediría la posterior deposición de la capa de paladio por ELP-PP, debido a que la hidracina del interior del soporte no podría difundir hacia el exterior a través de los poros debido al bloqueo de las partículas. De este modo, para determinar la cantidad de partículas

3. Discusión general

óptimas para la capa intermedia se pusieron 3 grados de retirada del exceso de material mediante lavados con agua MiliQ. La Figura 3.2.2 recoge las superficies analizadas con un perfilómetro óptico de los soportes de acero poroso oxidados sin modificar y modificados con partículas de ceria después de eliminar el exceso de ceria en distintos grados. Como puede observarse, el soporte oxidado, identificado como OXI (Figura 3.2.2.a), presenta una superficie muy rugosa, con un valor de rugosidad media de $R_a = 4,579 \pm 0,3 \mu\text{m}$. La morfología observada en esta superficie mantiene la morfología original de un soporte típico de acero poroso, como se publicó previamente [263,298]. La primera muestra analizada que contiene una capa intermedia de ceria, OXI-CeO₂-01, ha sido preparada con el grado de retirada de ceria más bajo después del paso de recubrimiento por inmersión asistido con vacío. Como consecuencia se alcanzó un aumento de peso de 0,0373 g respecto al propio peso de ese mismo soporte oxidado antes de la incorporación de la interfase (Figura 3.2.2.b). Este valor del incremento de masa asociado a las partículas de ceria es lo que se considerará como referencia para evaluar y comparar con los otros grados de retirada del exceso de CeO₂. En estas condiciones, la ceria remanente cubre completamente toda la superficie del soporte oxidado, ocultando por completo todos los poros originales. Como resultado, se obtuvo la rugosidad superficial media más baja de todas las analizadas con un valor de $R_a = 1,137 \pm 0,2 \mu\text{m}$. La segunda alternativa, grado de retirada medio (OXI-CeO₂-02), genera una mayor retirada de material, obteniendo un incremento de masa de 0,0219 g de CeO₂ en la capa intermedia (Figura 3.2.2.c). En este caso, parte de la superficie del soporte oxidado puede observarse ya que las partículas de ceria remanentes se sitúan en el interior de los poros, debido a la retirada de las más superficiales en la etapa de lavado. Como consecuencia se obtiene un aumentando de la rugosidad media, respecto a la alternativa anterior, con un valor de R_a de $2,343 \pm 0,2 \mu\text{m}$. La última modificación implica el mayor grado de retirada de partículas de ceria del soporte modificado, (OXI-CeO₂-03), quedando únicamente las partículas cerámicas colocadas dentro de la porosidad del soporte metálico ancladas con fuerte adherencia. El peso total de la ceria remanente se situó en torno a los 0,0165 g, alcanzando un alto valor de rugosidad cercano al del soporte PSS oxidado, $R_a = 3,794 \pm 0,4 \mu\text{m}$ (Figura 3.2.2.d).

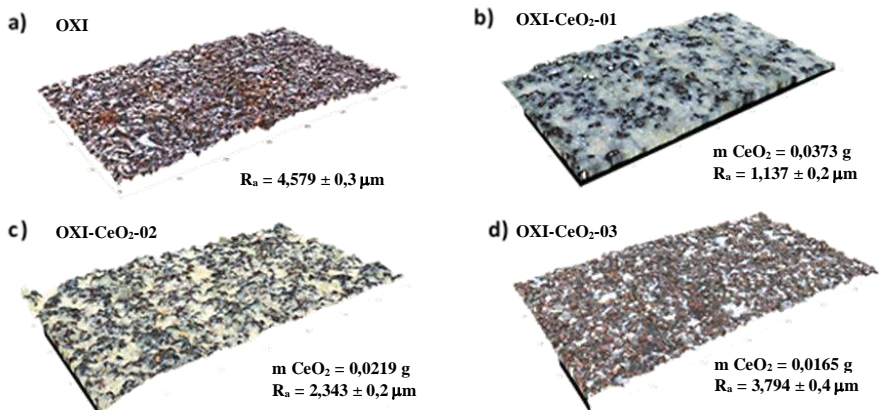


Figura 3.2.2 Morfología superficial obtenida mediante perfilometría óptica ($\times 500$) para el soporte PPS oxidado antes (a) y después de la incorporación de las capas intermedias de CeO₂ con distintos grados de retirada de exceso: OXI-CeO₂-01 (b), OXI-CeO₂-02 (c) y OXI-CeO₂-03 (d).

Como se ha explicado previamente, las modificaciones de los soportes comerciales mediante la incorporación de capas intermedias cerámicas facilitan la deposición de una capa delgada de Pd libre de defectos, pero también pueden afectar tanto a la resistencia mecánica como a la permeabilidad del sustrato original, comprometiendo la futura permeabilidad de la membrana compuesta. Debido a esto, para completar la caracterización de los soportes modificados se debe analizar la permeación de los mismos, con el fin de seleccionar la estrategia más adecuada para la preparación de membranas compuestas selectivas de H₂. La Figura 3.2.3 muestra los flujos de permeado obtenidos como resultados de estos experimentos. Se realizaron experimentos con nitrógeno puro con diferencias de presión en el intervalo de 0,5 a 1,0 bar a temperatura ambiente. El soporte oxidado sin capa interfase de ceria, es tomado como referencia para este estudio, presentando un flujo en el rango de 0,551-1,233 mol m⁻² s⁻¹ para las presiones analizadas.

3. Discusión general

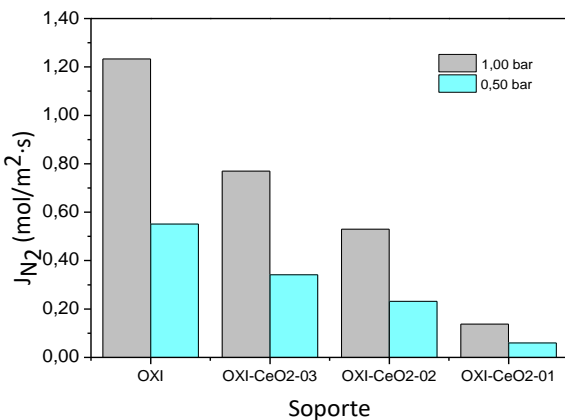


Figura 3.2.3 Flujo de N₂ de los soportes de PSS oxidados y modificados con CeO₂ a temperatura ambiente.

Como puede observarse, el caudal de N₂ permeado disminuye progresivamente a medida que aumenta la cantidad de ceria de la capa intermedia. Así, el soporte modificado con la mayor cantidad de ceria (muestra OXI-CeO₂-01) presenta el menor caudal para ambas presiones evaluadas, obteniendo 0,059 y 0,137 mol m⁻² s⁻¹ para 0,5 y 1,0 bar, respectivamente. Este hecho se explica debido al bloqueo casi completo de los poros originales del soporte metálico con las partículas densas de CeO₂, reduciendo de este modo la porosidad abierta original. Además, el uso de vacío durante la preparación de la capa intermedia junto al elevado espesor de la capa intermedia provoca un alto grado de compactación de las partículas cerámicas y, en consecuencia, una marcada disminución de la permeación del sustrato. Por otro lado, en caso de aplicar el grado de retirada de CeO₂ más alto (OXI-CeO₂-03), la caída del permeado disminuyó solamente hasta un 30% (0,341 y 0,769 mol m⁻² s⁻¹ para 0,5 y 1,0 bar, respectivamente) respecto al soporte oxidado (OXI). Este resultado evidencia la baja modificación de la superficie de soporte lograda siguiendo este procedimiento experimental, como ya se discutió anteriormente en términos de rugosidad externa. Finalmente, también se analizó la situación intermedia (OXI-CeO₂-02), retirando parcialmente el exceso de partículas de CeO₂, pero manteniendo una buena cobertura de la mayor parte de los poros y asegurando una adecuada modificación del soporte para facilitar la posterior incorporación de la capa de paladio. En estas condiciones, se observaron datos de permeación congruentes entre las anteriores muestras, con valores de 0,231 y 0,529 mol m⁻² s⁻¹ para 0,5 y 1,0 bar, respectivamente.

En resumen, la incorporación de una capa intermedia de CeO₂ sobre un soporte de PSS oxidado afecta significativamente a la morfología superficial resultante y a las propiedades de permeación (

Tabla 3.2.1), siendo de esperar también cierta influencia sobre la posterior deposición de paladio mediante ELP-PP. Debido a la naturaleza de este proceso de deposición, donde la disolución reductora atraviesa la porosidad del soporte, cualquier modificación del soporte puede afectar al método de deposición del Pd. Para evaluar este efecto, se llevaron a cabo algunos experimentos preliminares para depositar la capa de Pd en las condiciones experimentales óptimas determinadas previamente. Durante estos experimentos la disolución reductora de hidracina (con una concentración 0,2 M) encontró una fuerte resistencia a pasar a través de la porosidad el soporte OXI-CeO₂-01, modificado con la mayor cantidad de partículas de CeO₂, debido al colapso de la mayoría de los poros con las partículas cerámicas. Por otro lado, en el soporte modificado con la menor cantidad de CeO₂ (OXI-CeO₂-03), la mayoría de los poros externos originales solo se han reducido ligeramente, lo que dificulta la generación de una capa de paladio densa total con un espesor limitado. Por lo tanto, se eligió utilizar la situación intermedia que posibilita simultáneamente la reducción de la rugosidad superficial y el tamaño de los poros, pero manteniendo un gran número de poros interconectados con un diámetro suficiente para facilitar la difusión de la hidracina a través del soporte desde el interior hacia el exterior. La reproducibilidad de este proceso se confirmó mediante la preparación de 10 soportes modificados con ceria en condiciones experimentales análogas, obteniendo en todos los casos una cantidad incorporada de ceria en torno a $0,0201 \pm 0,0020$ g.

Tabla 3.2.1 Propiedades de los soportes modificados con capas intermedias de CeO₂.

Capa intermedia	m_{CeO_2} (g)	Ra (μm)	J_{N_2} (mol/m ² ·s)	
			$\Delta P=0,50\text{bar}$	$\Delta P=1,00\text{ bar}$
OXI	-	$4,579 \pm 0,3$	0,550	1,233
OXI-CeO ₂ -01	0,0373	$1,137 \pm 0,2$	0,059	0,137
OXI-CeO ₂ -02	0,0219	$2,343 \pm 0,2$	0,231	0,529
OXI-CeO ₂ -03	0,0165	$3,794 \pm 0,4$	0,341	0,769

La superficie externa obtenida para la muestra seleccionada (OXI-CeO₂-02) se analizó adicionalmente mediante microscopía electrónica de barrido. La Figura 3.2.4 muestra las imágenes de SEM, incluyendo la superficie del soporte oxidado sin capa intermedia de CeO₂ (OXI) para poder

3. Discusión general

realizar una comparación. Como se puede observar, con el soporte oxidado se obtiene una superficie más rugosa con una amplia distribución de diámetros de boca de poros (Figura 3.2.4a), mientras que muchos de estos poros más grandes quedan cubiertos con partículas de CeO₂ tras la incorporación de la capa intermedia (Figura 3.2.4b). Observando con más detalle en la imagen ampliada, estas partículas cerámicas permanecen preferentemente en la parte más profunda de los poros externos del soporte metálico una vez eliminado el exceso de material, pero manteniendo una estructura porosa con tamaños de boca de poro más pequeños. Estos poros más pequeños pueden ser cerrados con paladio con mayor facilidad que los originales, más grandes, lo que promueve la generación de una capa selectiva delgada con una alta capacidad de permeación al H₂.

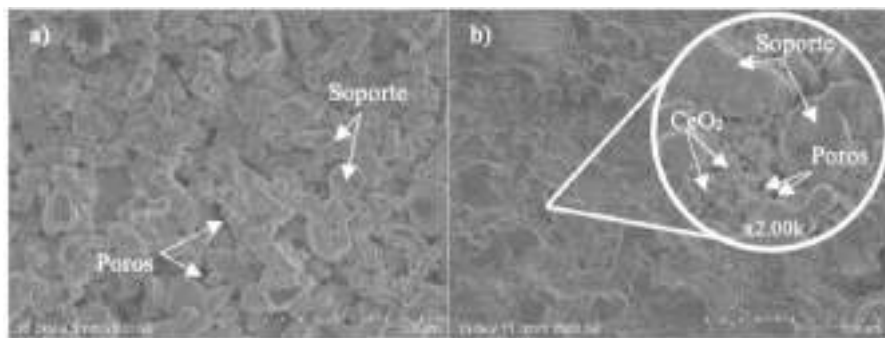


Figura 3.2.4 Imágenes SEM de la superficie externa para: (a) soporte PSS oxidado y (b) modificación seleccionada mediante la incorporación de una capa intermedia de CeO₂, OXI-CeO₂-02.

Una vez seleccionado el grado intermedio de retirada del exceso de partículas de ceria como el más adecuado (OXI-CeO₂-02), el siguiente objetivo es obtener una capa de paladio continua y sin defectos, lo que asegura una elevada selectividad. Además, es necesario que ésta tenga la suficiente resistencia mecánica para soportar las condiciones de operación a las que será sometida. Por otro lado, también se busca un elevado valor de permeación de H₂, por lo que será necesario obtener una capa selectiva delgada sin que se vean comprometidas las premisas anteriores. Con este tipo de capa interfase el espesor medio de la capa selectiva de Pd, estimado a partir de análisis gravimétricos, fue de 15 μm . La Figura 3.2.5 muestra las imágenes SEM obtenidas de una membrana compuesta de este tipo después de depositar la capa paladio, incluyendo tanto la superficie externa (Figura 3.2.5a) como la vista del corte transversal (Figura 3.2.5b).

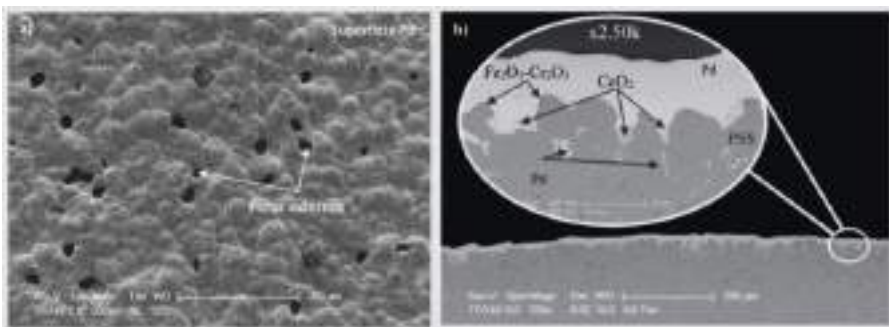


Figura 3.2.5 Imágenes SEM después de la deposición de Pd por ELP-PP sobre el soporte modificado OXI-CeO₂-02: a) vista superior (antes de los experimentos de permeación) y b) sección transversal (después de los experimentos de permeación).

Como se puede observar en la Figura 3.2.5a, la superficie externa de la capa de paladio depositada por ELP-PP presentó una superficie relativamente lisa con la aparición de algunas cavidades superficiales. Sin embargo, estos poros no se pudieron encontrar analizando el corte transversal (Figura 3.2.5b), por lo que se estableció que estas cavidades superficiales no están interconectadas debido a la incorporación de paladio dentro de estas. Teniendo en cuenta la naturaleza y características del ELP-PP utilizado en este trabajo, la presencia de poros externos no implica una baja calidad (en términos de selectividad de H₂) de la membrana. De hecho, se llevó a cabo una prueba de fugas preliminar a temperatura ambiente, en la que no se detectó flujo de gas (helio) en el lado del permeado para todo el rango de diferencias de presión (hasta 3 bar). Analizando el corte transversal (Figura 3.2.5b), tanto las partículas de ceria como la capa de paladio pueden distinguirse fácilmente del soporte PSS. Las primeras se incorporaron cubriendo parcialmente las bocas de los poros más grandes del soporte poroso de acero inoxidable, mientras que el paladio se depositó simultáneamente en el interior de los poros y en la superficie externa debido al paso de la hidracina a través de los poros más grandes, solo parcialmente cubiertos. Esta morfología particular, es inherente al proceso ELP-PP si el soporte presenta una cierta distribución de tamaños de poro, ya reportado en trabajos previos [50,52,72,147]. En este contexto, se espera que la deposición de paladio dentro de los poros proporcione un buen anclaje para la capa selectiva al H₂ y, en consecuencia, aumentar la resistencia mecánica de la membrana compuesta. Finalmente, atendiendo al espesor real de la capa externa de paladio, se puede concluir que en la imagen SEM se observó un valor muy cercano (alrededor de 15 μm) al estimado a partir de los análisis gravimétricos. Lo que supuso una reducción del 50% respecto al valor de 30

3. Discusión general

um tomado como referencia, obtenido con membranas desarrolladas siguiendo el mismo procedimiento experimental, pero sin capa intermedia.

Como se detalló en el apartado experimental, se realizaron experimentos de permeación con gases puros (nitrógeno e hidrógeno) para determinar las propiedades de este tipo de membranas compuestas a altas temperaturas, en un rango de 350 a 475 °C, para evitar la posible fragilización por hidrógeno de la película de paladio. Hay que destacar que, para todo el conjunto de experimentos realizados no se detectó nitrógeno en el lado del permeado, demostrando de este modo una buena calidad de la membrana. Después de las pruebas de permeación con nitrógeno puro, se realizaron 5 ciclos térmicos con hidrógeno puro para analizar la estabilidad de la membrana y de las medidas de permeado. Para cada ciclo, la celda de membrana se calentó hasta 400 °C en una atmósfera de nitrógeno, cambiando la alimentación de gas a hidrógeno puro para determinar el flujo de permeación después de un período de estabilización de 2 h. Finalmente, se enfriaba el sistema en atmósfera de nitrógeno para volver a temperatura ambiente. En general, hay que destacar que los flujos obtenidos para cada ciclo térmico variaron levemente con una desviación que osciló entre el 1-2% con respecto al valor promedio determinado de todos los experimentos. De este modo, el comportamiento de permeación de esta membrana OXI-CeO₂-02, formada por un soporte de PSS oxidado, una capa intermedia de ceria y una capa selectiva de paladio, puede considerarse estable. La Figura 3.2.6 resume todos los resultados obtenidos en los ensayos de permeación con H₂ puro, donde se muestra el flujo de permeado de H₂ a distintas presiones y diferentes temperaturas. La Figura 3.2.6a muestra el ajuste matemático de los datos medidos, evidenciando una tendencia lineal entre el flujo y la fuerza impulsora que se mantiene independientemente de la temperatura experimental. A pesar de que un aumento de presión provoca un aumento del flujo, como sugiere la ley de Sieverts, la intersección con el origen (que implica que no hay permeación cuando no se aplica una fuerza impulsora) no es claro. Este ajuste lineal puede mejorarse significativamente considerando la presencia de una resistencia adicional al proceso de permeación (Figura 3.2.6b), como ya se sugirió previamente en otros trabajos en los que se analizaron membranas compuestas preparadas mediante ELP-PP [50,72]. Esta resistencia adicional al fenómeno de permeación implica la presencia de un valor de presión mínimo por debajo del cual no se produce la permeación de hidrógeno a través de la membrana de paladio. La contribución del soporte a este efecto es considerada como insignificante,

como ya se publicó previamente [50,72]. Sin embargo, es necesario señalar que la resistencia adicional al fenómeno de permeación determinada para la membrana OXI-CeO₂-02 es significativamente menor, en torno al 30%, del valor previamente determinado para una membrana similar, también preparada por ELP-PP, pero sin la presencia de una capa intermedia de CeO₂ [50,72]. Este nuevo comportamiento podría derivarse de la reducción de tamaño de los poros más grandes del soporte metálico como consecuencia de la incorporación de las partículas de ceria, reduciéndose también parcialmente el espesor de la capa externa de Pd y su penetración en los poros del soporte. En resumen, se alcanzó un aumento del flujo de hidrógeno obteniendo una permeanza en el rango de $4,74 \cdot 10^{-4} - 6,35 \cdot 10^{-4}$ mol m⁻² s⁻¹ Pa^{-0.5} (respecto a los valores tomados como referencia de $1,00 \cdot 10^{-4} - 2,00 \cdot 10^{-4}$ mol m⁻² s⁻¹ Pa^{-0.5} obtenido para una membrana ELP-PP similar sin capa intermedia de ceria [52]). De este modo, se puede garantizar una selectividad ideal de H₂ / N₂ ≥ 10.000, teniendo en cuenta el límite de detección del caudalímetro de gas utilizado en estos experimentos (1 NmL / h). Además, se calculó una energía de activación de 8,9 kJ mol⁻¹, valor que está situado dentro del rango de otras membranas de paladio reportadas en la literatura [71]. Como última observación, también es necesario mencionar que la membrana exhibió un rendimiento y una estabilidad realmente buenos durante tiempos prolongados (> 400 h) a alta temperatura (≥ 350 °C).

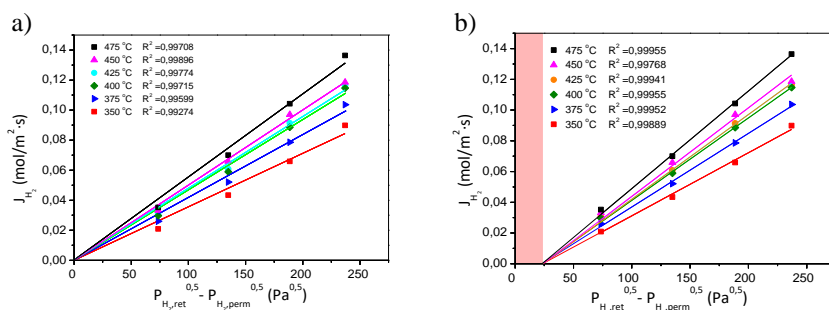


Figura 3.2.6 Ensayos de permeación de la membrana OXI-CeO₂-02 después de la deposición de Pd por ELP-PP: a) ajustando a la ley de Sieverts mediante (0,0) y b) considerando la presencia de una resistencia adicional al proceso de permeación de H₂.

3.3 Modificación del proceso de activación, capas intermedias de óxido de cerio dopadas con paladio.

Una vez analizados todos los beneficios obtenidos con el uso de partículas de CeO₂ comerciales y optimizadas las condiciones del proceso de generación de capas interfases, se propone seguir trabajando con este material para el desarrollo de capas intermedias. Para seguir mejorando el rendimiento de este tipo de membranas compuestas se propone la modificación del método de activación previo a la deposición de paladio mediante ELP-PP. Como ya se ha comentado anteriormente, la activación del soporte es un proceso necesario mediante el cual se generan una serie de centros de nucleación de paladio homogéneamente distribuidos. Con este proceso se consigue favorecer el posterior crecimiento de la capa selectiva de paladio continua y sin defectos. De modo general este proceso se realiza sobre el soporte una vez ha sido acondicionado para la deposición de Pd. En este trabajo se ha analizado el efecto de la generación de estos centros de nucleación de paladio directamente sobre las partículas de óxido de cerio de manera previa a su incorporación sobre el soporte de acero inoxidable como capa intermedia. En este apartado se recoge el estudio de optimización del proceso de activación directamente sobre las partículas de CeO₂ y sus efectos sobre el posterior desarrollo de la deposición de la capa selectiva de paladio, esperando mejorar los resultados ya obtenidos con las capas intermedias de óxido de cerio comercial tanto en términos de disminución del espesor de la capa selectiva como en el aumento de la permeación de H₂.

Por tanto, de manera previa a su incorporación como capa interfase las partículas de CeO₂ se doparon con núcleos de paladio. Para el procedimiento de dopado, la composición de ambos baños (fuente metálica y reductor) es idéntica a las utilizadas anteriormente para la activación del soporte. Se consideraron diversas relaciones entre la cantidad de partículas de CeO₂ y el precursor de Pd, desde 1:6 a 1:36 (vol.). Respecto a la relación entre el agente reductor y fuente metálica, esta se mantuvo constante con una relación 1:30 (vol.) para todos los experimentos, garantizando de esta manera que se ha aportado la suficiente cantidad de agente reductor para reducir todos los iones metálicos. Es importante destacar que las partículas utilizadas para este tipo de interfases dopadas con núcleos de paladio son las mismas a las usadas previamente en el apartado 3.2. La Tabla 3.3.1 recoge la carga de Pd alcanzada en las partículas de CeO₂ después de la etapa de dopado realizada en las diferentes condiciones experimentales utilizadas (analizada mediante

espectroscopía de emisión atómica de plasma acoplado por inducción), así como la eficiencia del proceso (η_{dopado}), expresada como la relación entre los núcleos de Pd depositados sobre las partículas de CeO₂ y la cantidad de metal disponible en la disolución para el dopado.

Tabla 3.3.1 Cargas de paladio obtenidas en las partículas de CeO₂ después de los procesos de dopado.

Ratio CeO ₂ /Fuente metálica (vol.)	Carga Pd (ppm)	$\eta_{\text{dopado}} (\%)$
1:6	92,31	26,21
1:9	186,30	34,91
1:18	569,36	52,40
1:36	1077,95	52,00

Una relación menor entre la cantidad de partículas de CeO₂ y la disolución que contiene la carga metálica implica una mayor cantidad de paladio disponible para la generación de núcleos de Pd durante el proceso de dopado. De hecho, se alcanza un aumento de la carga de Pd depositado en las partículas de CeO₂ cuando se usa un mayor volumen de disolución. Una tendencia similar se obtiene al analizar la eficiencia del proceso de dopaje, lo que conlleva a un rendimiento máximo de dopaje (η_{dopado}) en torno al 52%. Además, todas las muestras exhibieron una buena distribución de los núcleos de Pd alrededor de las partículas de ceria, independientemente de la carga de Pd alcanzada, aunque se pudo observar un color gris más oscuro a medida que la carga de Pd aumentaba. Por lo tanto, el color amarillo original de las partículas de CeO₂ comerciales se convierte progresivamente en un gris oscuro cuando hay una mayor cantidad de paladio disponible en el medio. Finalmente, con el fin de evaluar el efecto de cada tipo de partícula en la posterior deposición de paladio por ELP-PP, se utilizaron todas las muestras resumidas en la Tabla 3.3.1 para preparar una capa intermedia siguiendo el procedimiento experimental seleccionado anteriormente como el más adecuado. Como resultado, se observó que las partículas dopadas con una relación igual o menor a 1:18 (vol.) provocaron una ganancia de peso de Pd en la membrana después del primer ciclo de ELP-PP similar al obtenido en caso de utilizar el proceso de activación convencional sobre una capa intermedia previamente incorporada. Por el contrario, en el caso de utilizar las partículas con las relaciones de 1:6 y 1:9 se obtuvo una ganancia de peso inferior a la mitad que con las partículas anteriormente mencionadas, mostrando la poca eficacia de ambas alternativas como proceso de

3. Discusión general

activación. De este modo, teniendo en cuenta la ganancia de masa de paladio durante el primer ciclo y considerando que la eficiencia del proceso de dopado parece no aumentar al aumentar la relación partículas / disolución, se han seleccionado las partículas de CeO₂ dopado con Pd preparado con la relación 1:18 (vol.) como las más adecuadas para continuar el estudio. Estas partículas cuentan con una carga de paladio de 569,36 ppm.

Igual que en las membranas preparadas anteriormente, antes de la incorporación de capa intermedia mediante un recubrimiento por inmersión asistido con vacío, los soportes porosos de acero inoxidable (PSS) 316L son calcinados durante 12h a 600 °C en atmósfera de aire. Estos soportes mantienen la morfología externa después del proceso de calcinación, presentando una superficie relativamente rugosa con valores de R_a en torno a los $4,579 \pm 0,3 \mu\text{m}$. Esta rugosidad presenta un valor muy cercano a los obtenidos para los soportes PSS sin modificación alguna ($R_a = 5,082 \pm 0,4 \mu\text{m}$). Esta rugosidad externa del soporte PSS calcinado se redujo a la mitad al incorporar las partículas de CeO₂ dopadas como capa intermedia, alcanzando la rugosidad un valor promedio de $R_a = 2,726 \pm 0,4 \mu\text{m}$. La Figura 3.3.1 muestra la morfología externa obtenida mediante perfilometría óptica de soportes PSS calcinados antes (Figura 3.3.1a) y después de incorporar la capa intermedia de CeO₂ dopado con una relación de partículas / disolución metálica de 1:18 vol. (Figura 3.3.1b). Como puede observarse, las partículas de CeO₂ dopadas (de color blanco) se colocaron preferentemente alrededor de las áreas más profundas cubriendo los poros más grandes del soporte de PSS calcinado (de tonos pardos).

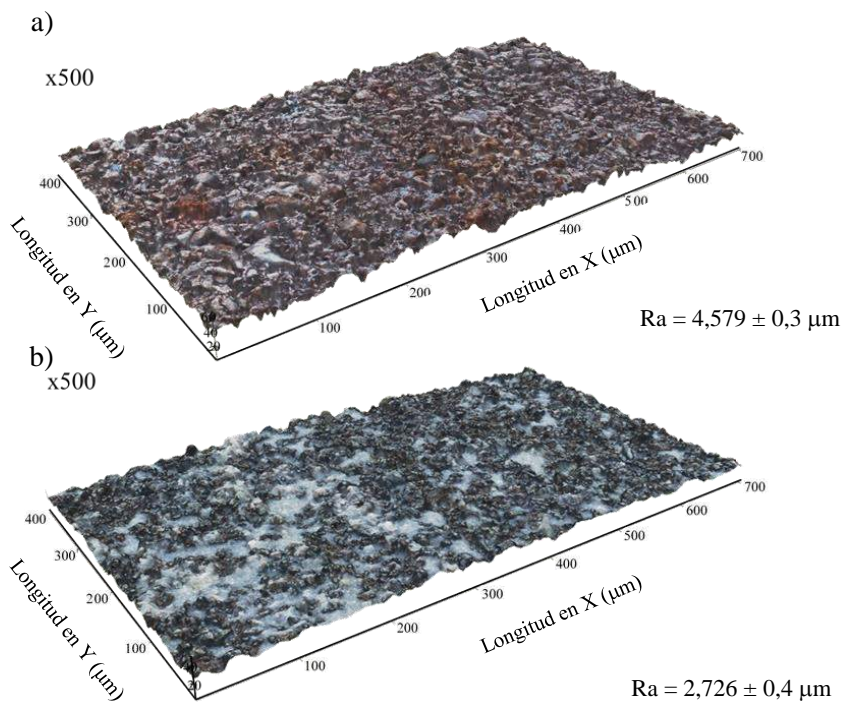


Figura 3.3.1 Morfología superficial obtenida mediante perfilometría óptica del soporte PSS calcinado antes (a) y después (b) de la incorporación de la capa intermedia.

Para analizar la variación morfológica de la superficie externa del soporte, se adquirieron imágenes SEM tras la incorporación de partículas de CeO₂ dopadas como capa intermedia (Figura 3.3.2). Como se comentó previamente la imagen SEM del soporte de PSS calcinado (Figura 3.2.4a) reveló una superficie rugosa con una amplia variedad de diámetros de boca de poros de hasta unas pocas micras. Esta morfología cambió notablemente después de la incorporación de partículas de CeO₂ dopadas (Figura 3.3.2), debido a que estas partículas se depositaron principalmente dentro de los poros más grandes de la superficie externa del soporte de PSS calcinado. Además, se generan nuevos poros entre las partículas cerámicas de la capa intermedia con un tamaño de boca significativamente menor que los poros originales del soporte, lo que puede promover la generación de una capa de paladio delgada. Analizando esta comparación, esta nueva superficie es bastante similar a la obtenida previamente cuando se utilizan partículas de CeO₂ sin dopar como capa intermedia (Figura 3.2.4b). De hecho, sobre el soporte calcinado se incorporaron 0,0184 g de CeO₂ dopado, obteniendo así una variación por debajo del 8% con respecto a la ganancia media de peso

3. Discusión general

obtenida al utilizar partículas de CeO₂ comerciales directamente como capa intermedia. Esta similitud entre ambas modificaciones se evidenció también con pruebas de permeación con N₂ sobre el soporte modificado, obteniendo con las partículas dopadas valores muy similares a los ya publicados para el uso de partículas comerciales. Para las nuevas interfaces dopadas se obtuvieron valores de flujo de N₂ de 0,299 y 0,784 mol m⁻² s⁻¹ a temperatura ambiente para incrementos de presión de 0,5 y 1,0 bar, respectivamente. Con ambas interfaces tanto el diámetro medio de los poros, como la rugosidad externa, se reducen notablemente mientras se mantuvo una permeabilidad adecuada. Por lo que puede concluirse que el proceso de dopado de las partículas no afectó significativamente a las propiedades morfológicas de las capas intermedias generadas.

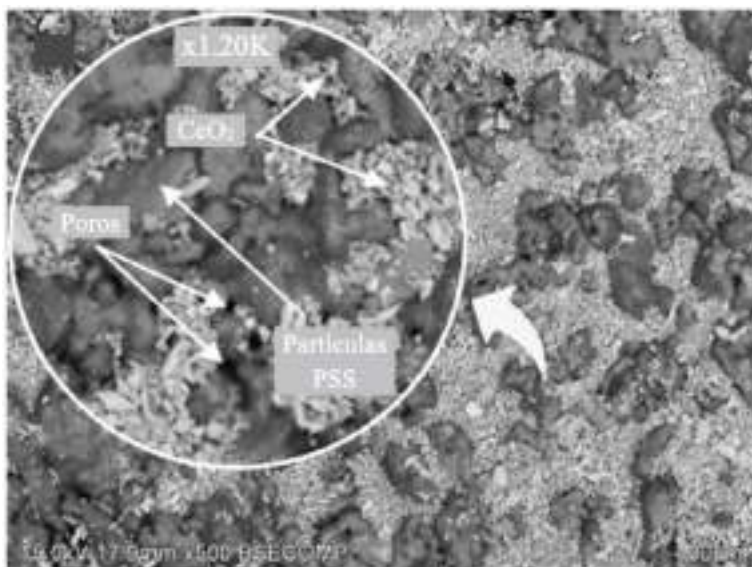


Figura 3.3.2 Imagen SEM de la superficie externa del soporte de PSS calcinado después de la incorporación de partículas de CeO₂ dopadas como capa intermedia.

Respecto a la incorporación de la capa selectiva, esta se depositó mediante ELP-PP siguiendo el mismo procedimiento detallado previamente. La Figura 3.3.3 recoge dos micrografías de la superficie externa obtenidas tras la incorporación de Pd por ELP-PP sobre soportes PSS modificados con una capa intermedia formada por partículas de CeO₂ dopadas. Como puede observarse, se formó una capa superior de paladio aparentemente homogénea y continua sobre la superficie externa del soporte. Esta capa superior presenta algunas cavidades residuales, como ya pudo observarse también en otras membranas fabricadas mediante ELP-PP (Figura 3.2.5a). Sin embargo, la

presencia de estas cavidades en la capa superficial de Pd no perjudicó a la calidad de la membrana en términos selectividad al H₂. Este hecho fue confirmado mediante una prueba de fugas con He a temperatura ambiente, lo que evidenció un buen sellado de todos los poros del soporte con paladio al no presenciarse flujo de He. Como resultado del uso de una capa intermedia de óxido de cerio dopado con núcleos de paladio se logró una capa selectiva de tan solo 9 μm de espesor, estimado mediante análisis gravimétrico, en contraste con la capa de Pd de 15 μm de espesor que se obtuvo como resultado de la generación de una capa interfase generada de manera análoga con partículas de CeO₂ comerciales sin dopar. Por lo tanto, se alcanzó una reducción del espesor de la capa Pd estimado mediante gravimetría de un 40% cuando se reemplaza el uso de partículas de CeO₂ comerciales sin dopar por partículas de CeO₂ dopadas con núcleos de Pd como capa intermedia.

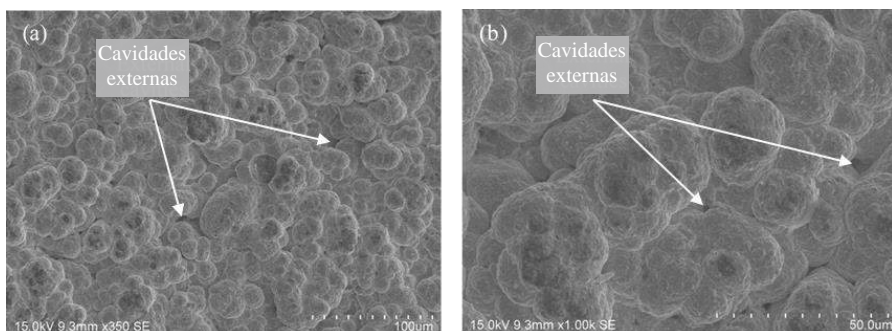


Figura 3.3.3 Imágenes SEM de la superficie de Pd incorporado por ELP-PP sobre un soporte modificado con CeO₂ dopado a un aumento: (a) x350 y (b) x1000.

La Figura 3.3.4 muestra la vista del corte transversal de una membrana preparada usando partículas de CeO₂ comercial sin dopar como capa intermedia (Figura 3.3.4a) y otra usando las mismas partículas de CeO₂ pero dopadas con Pd (Figura 3.3.4b) para su comparación directa. En ambos casos, la mayoría de los poros externos de los soportes PSS se llenan con paladio, como es habitual en las membranas preparadas mediante ELP-PP. La presencia de Pd dentro de los poros puede explicarse debido a que ambos reactivos se encuentran dentro de los propios poros, mientras que la mayor velocidad de difusión de la disolución reductora de hidracina desde el lado interior del sustrato hacia el exterior puede explicar el bloqueo preferencial de los poros en la zona más cercana a la superficie externa del sustrato tubular. Por otro lado, la distribución de los poros del soporte PSS modificado hace que este proceso de difusión a través del soporte sea

3. Discusión general

ciertamente heterogéneo, por lo que la hidracina puede llegar hasta la superficie externa del PSS con mayor facilidad a través de los poros más grandes, lo que hace posible la formación de una capa en la superficie externa continua de Pd. Sin embargo, se pueden apreciar diferencias significativas en esta capa externa de Pd en caso de utilizar partículas de CeO₂ comerciales o dopadas como capa intermedia. Las membranas de Pd que contienen una capa intermedia formada por CeO₂ comercial sin dopar (Figura 3.3.4a), presentan un espesor de Pd externo real muy cercano al estimado por análisis gravimétrico, en el rango de 13-17 µm. Esta capa de Pd cubre casi por completo la morfología original del soporte de PSS calcinado, proporcionando una superficie externa muy plana. Por el contrario, el uso de una capa intermedia formada por partículas de CeO₂ dopadas con Pd deriva en una película externa de Pd notablemente más delgada (Figura 3.3.4b) con alrededor de 5 µm, a pesar de la estimación antes mencionada del análisis gravimétrico de 9 µm. Además, esta capa externa de Pd, al ser más delgada, replica mejor la morfología superficial original del soporte de PSS, sin recubrir por completo con sobre espesores las bocas de los poros más anchos. La nueva distribución de núcleos de Pd alrededor de cada partícula de CeO₂ facilita el crecimiento homogéneo de la capa de paladio sobre la superficie del soporte, evitando los crecimientos heterogéneos en la dirección del espesor de la propia capa, lo que ayuda a obtener una membrana completamente densa con menores espesores de la capa selectiva de Pd. Además, el uso de las partículas dopadas también aumenta la cantidad de paladio que se deposita en el interior de los poros, haciendo que la membrana quede completamente densa con mayor facilidad. De hecho, esto puede observarse analizando como el espesor externo real de 5 µm obtenido mediante SEM (Figura 3.3.4b), es significativamente menor al estimado mediante análisis gravimétrico ($t_{e, Pd} = 9 \mu m$). Esta diferencia, no se observó en el caso de utilizar partículas de CeO₂ sin dopar como capa intermedia, donde la cantidad de Pd depositado dentro de los poros del soporte poroso tiene una menor influencia respecto a la cantidad total del Pd incorporado en la membrana. Cabe señalar que ambas membranas, preparadas con capas intermedias de partículas de CeO₂ comercial dopadas o sin dopar, se obtuvieron siguiendo el mismo procedimiento experimental, tanto para la incorporación de la capa intermedia como para la capa de Pd, ambos descritos previamente en la sección metodología. Por tanto, puede concluirse que el nuevo procedimiento experimental aquí propuesto parece ciertamente atractivo en términos de reducción del espesor de capa de Pd.

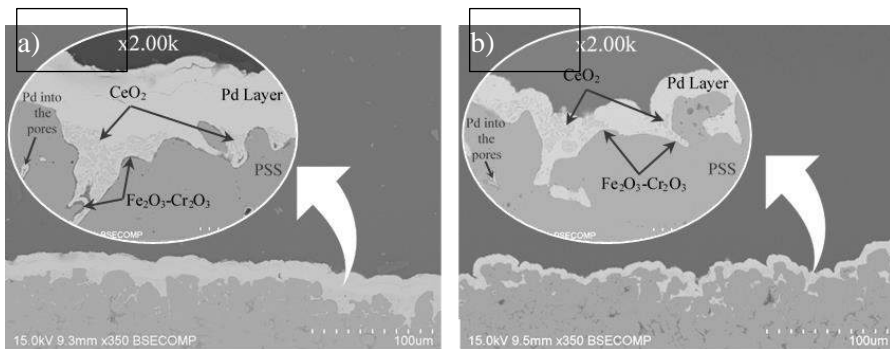


Figura 3.3.4 Imágenes SEM del corte transversal de las membranas preparadas sobre soportes PSS modificados con capas intermedias formadas por: (a) CeO₂ comercial o (b) dopado con Pd.

Respecto a los ensayos de permeación, se han realizado experimentos con gases puros (N₂ y H₂) y mezclas a diferentes temperaturas (350-450 °C) y diferencias de presión (0,5-2,0 bar). De manera previa a la realización de estos experimentos, se realizaron pruebas de fugas con He a temperatura ambiente para asegurar la continuidad de la capa de Pd, donde no se observó flujo de gas. Posteriormente, durante los ensayos a alta temperatura tampoco se detectó flujo (de N₂ en este caso) en la corriente de permeado para ninguna de las temperaturas probadas, considerando que el límite mínimo de detección del caudalímetro de gas utilizado es 1 NmL h⁻¹. Además, igual que en los ensayos realizados previamente para las membranas con capas interfases de óxido de cerio comercial sin dopar se realizaron 5 ciclos térmicos secuenciales con un tiempo de operación promedio de alrededor de 5 h por ciclo antes de considerar estos datos de permeado de H₂ como estables. Los resultados obtenidos se resumen en la Figura 3.3.5, donde el flujo de H₂ se representa frente a la presión parcial de H₂ a diferentes temperaturas. Estos resultados muestran que el flujo de H₂ permeado aumenta al mismo tiempo que lo hace la fuerza impulsora o la temperatura. Además, se obtuvo una tendencia lineal entre el flujo y la fuerza impulsora, independientemente de la temperatura de funcionamiento. Sin embargo, como se mencionó en las secciones anteriores, puede observarse como estas tendencias no se observa el punto de corte con el punto (0,0), en contraste con el comportamiento esperado para las membranas base Pd según la ley de Sieverts ($n = 0,5$). Este comportamiento particular, ya descrito previamente, puede explicarse considerando la presencia de una resistencia adicional al proceso de permeación, cuando se utiliza el método ELP-PP. La

3. Discusión general

resistencia adicional obtenida en este caso para las membranas preparada usando CeO₂ dopado como capa intermedia es muy cercana a los valores obtenidos previamente usando partículas de CeO₂ comerciales sin dopar. Siendo el valor de esta resistencia alrededor de un 35% inferior al determinado para membranas ELP-PP sin capa intermedia, donde el Pd se depositó siguiendo el mismo procedimiento [38,49]. Teniendo en cuenta este comportamiento, los valores de permeancia oscilaron entre 4,50·10⁻⁴ y 6,39·10⁻⁴ mol m⁻² s⁻¹ Pa^{-0,5} a temperaturas entre 350 y 450 °C. Estos valores representan un aumento del 30% con respecto al uso de ceria comercial como capa intermedia. De esta manera, se ha conseguido un aumento en la permeancia de H₂ de 4,46·10⁻⁴ a 5,73·10⁻⁴ mol m⁻² s⁻¹ Pa^{-0,5} a 400 °C. Esta mejora se debe principalmente a la disminución del espesor de la capa selectiva de paladio en un 40%, así como a la nueva morfología de la película selectiva H₂ alcanzada debido al uso del CeO₂ dopado, como se analizó previamente en la Figura 3.3.4.

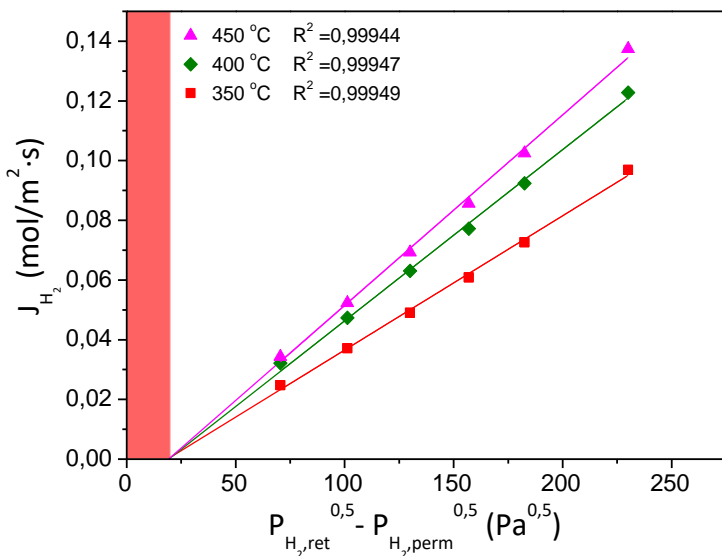


Figura 3.3.5 Flujo de permeado de la membrana preparada con partículas de ceria dopada como capa intermedia, considerando la presencia de una resistencia adicional al proceso de permeación de H₂.

Después de todos estos experimentos a alta temperatura, llevados a cabo durante más de 120 h, la membrana mostró una integridad mecánica completa. Esta resistencia mecánica se confirmó en una prueba de estabilidad

a largo plazo con H₂ puro a 400 °C y ΔP = 1 bar, recuperando el flujo de H₂ inicial y manteniendo una permeación y una selectividad estable (selectividad H₂/N₂ ideal ≥ 10.000) a pesar de prolongar el tiempo de operación de la membrana hasta 720 h. Como resultado, la membrana compuesta estuvo funcionando durante más de 30 días (aproximadamente 850 h) sin ningún problema mecánico.

3.4 Modificación de soportes con partículas de CeO₂ mesoporoso

Una vez analizados los beneficios obtenidos en caso de realizar un proceso de dopado con núcleos de paladio directamente sobre las partículas de ceria, de manera previa a su incorporación como capa intermedia, se planteó otra posible vía de mejora respecto al uso de las partículas densas de óxido de cerio comercial sin dopar. En este caso en lugar de realizar una modificación química sobre la partícula comercial, añadiendo núcleos de paladio, se propuso modificar la morfología de las propias partículas. Se planteó la posibilidad de usar partículas porosas en lugar de partículas densas, como se habían utilizado hasta el momento. La idea inicial de este concepto es conseguir un aumento de la permeabilidad inicial del soporte modificado con la capa intermedia de partículas, debido a que estas partículas porosas restringirán en menor medida el flujo de gas a través del soporte.

Estás nuevas partículas se sintetizaron mediante un proceso de nanoreplicación usando como plantilla SBA-15, dando lugar a partículas mesoporosas de óxido de cerio. Respecto a las propiedades texturales este material presentó una superficie BET de 135 m²/g, con un tamaño medio de poro de 10-12 nm. Estas partículas de ceria mesoporosa presentaron un diámetro medio de 100 nm, valor similar al tamaño de las partículas densas utilizadas previamente para la preparación de capas intermedias. La figura Figura 3.4.1a muestra una imagen TEM de una de estas partículas mesoporosas, donde puede observarse la presencia de nanopartículas de ceria (7-12 nm de diámetro) que se unen ordenadamente formando cadenas, que a su vez se aglomeran dando lugar a las partículas de ceria mesoporosa. Una vez sintetizadas estas partículas de ceria mesoporosa, se incorporaron sobre soportes porosos de acero inoxidables, previamente oxidados, mediante el mismo proceso de recubrimiento por inmersión asistido con vacío descrito anteriormente para la preparación de membranas con partículas densas de óxido de cerio. Por tanto, el tipo de partícula utilizada para la generación de

3. Discusión general

la capa intermedia es la única variable respecto a las membranas preparadas usando óxido de cerio comercial sin dopar, ya que estas partículas no se activaron con núcleos de paladio de manera previa a su incorporación y la capa de paladio se depositó también mediante ELP-PP. La superficie final del soporte modificado puede observarse en la Figura 3.4.1b donde, al igual que en los casos anteriores, la mayor parte de los poros más grandes están llenos de partículas, reduciendo por tanto el tamaño medio de las bocas de los poros, promoviendo de este modo la posterior generación de una capa selectiva de paladio delgada. En términos de permeación con este tipo de interfases se obtuvo un flujo N₂ de 1,233 mol m⁻² s⁻¹ a temperatura ambiente con una presión transmembrana de 1,0 bar. Este valor supone solamente una disminución del 30% respecto al flujo de N₂ obtenido por un soporte sin capa intermedia, lo que supone una menor reducción del flujo de N₂ respecto al uso de partículas densas (52%). Por tanto, puede concluirse que el uso de las partículas de ceria mesoporosas implica un mayor flujo de permeado del soporte modificado, ya que ambos tipos de capas intermedias se prepararon siguiendo el mismo procedimiento y ambos materiales presentan un tamaño de partícula similar (100 nm).

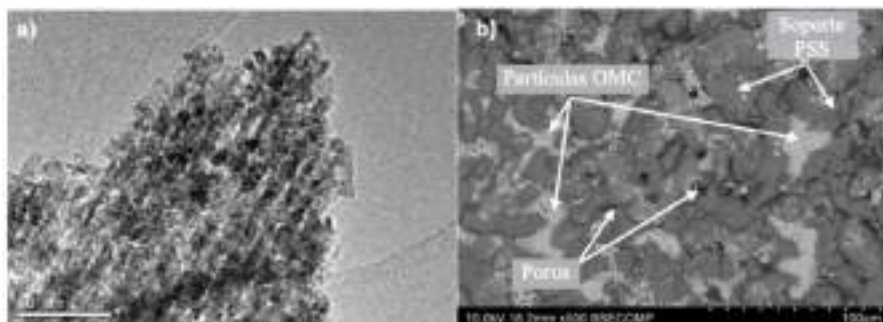


Figura 3.4.1 Micrografías TEM de una partícula de óxido de cerio mesoporoso (a) y SEM de la superficie externa del soporte PSS calcinado después de la deposición de partículas.

Respecto a la capa selectiva de paladio, la Figura 3.4.2a muestra la superficie obtenida, donde se observa una morfología similar a las previamente analizadas depositadas también mediante ELP-PP. El espesor de esta capa selectiva se estimó en 9 μm mediante análisis gravimétricos. La Figura 3.4.2b muestra el corte transversal de una de estas membranas, donde puede observarse como el espesor real de la capa externa de paladio se encuentra entre 7-12 μm, en concordancia con el espesor estimado mediante gravimetría. De manera análoga a lo que sucedía en el caso de utilizar

partículas densas, las partículas porosas se depositaron también en el interior de los poros más grandes.

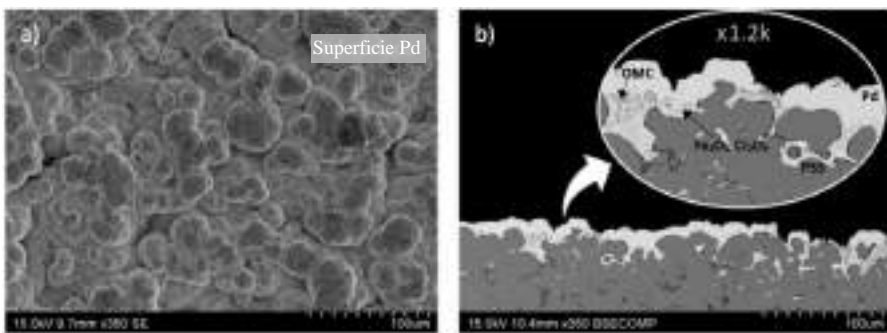


Figura 3.4.2 Micrografías SEM de la membrana compuesta de Pd preparada sobre un soporte de PSS con una capa intermedia de OMC: a) Superficie externa y b) Vista del corte transversal.

En los ensayos de permeación con H₂ (Figura 3.4.3) estas membranas mostraron una capacidad de permeación superior a las previamente utilizadas con interfases de óxido de cerio denso, tanto comercial como dopado. En este contexto, se obtuvieron permeanzas de $7,81 \cdot 10^{-4}$ a $9,91 \cdot 10^{-4}$ mol m⁻² s⁻¹ Pa^{-0.5} para temperaturas entre 350 y 450 °C, respectivamente, lo que implica una selectividad ideal $\alpha_{H_2/N_2} \geq 24.000$, teniendo en cuenta el límite mínimo de detección del caudalímetro de gas utilizado para la corriente de permeado.

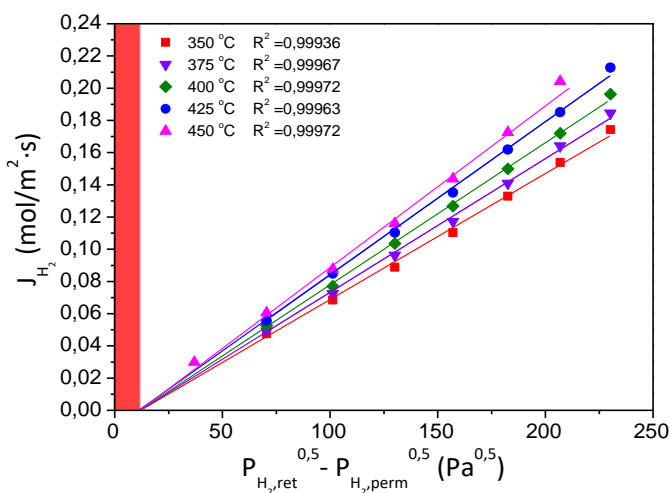
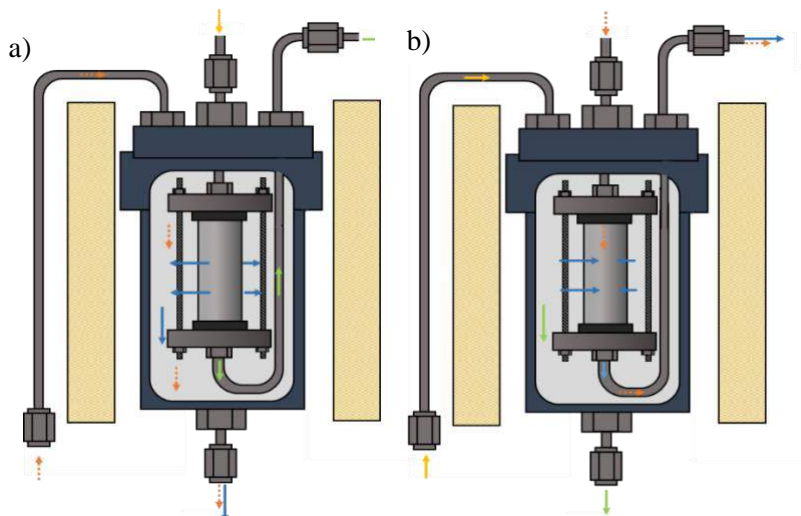


Figura 3.4.3 Flujo de permeado de la membrana preparada con partículas de ceria mesoporosa como capa intermedia, considerando la presencia de una resistencia adicional al proceso de permeación de H₂.

3. Discusión general

Llegado este punto es importante destacar que también se analizó el efecto del modo de operación variando la dirección del flujo de hidrógeno utilizando los dos modos de operación que permite la instalación experimental: in-out (Figura 3.4.4a) y out-in (Figura 3.4.4b) a temperaturas y diferencias de presión transmembrana en el rango 350-450 °C y 0,5-2,0 bar, respectivamente. Estos experimentos se realizaron con todos los tipos de membranas con CeO₂, es decir, con interfases de óxido de cerio denso (comercial y dopado con paladio) y con óxido de cerio mesoporoso.



Código de colores: ■ Alimento ■ Gas de arrastre ■ Permeado ■ Retenido

Figura 3.4.4 Esquema de la celda de permeación de la instalación experimental describiendo los dos modos de operación posibles: modo in-out (a) y out-in (b).

Los datos de permeancia obtenidos a 400 °C para todos tipos de membranas analizados y ambos modos de operación se recogen en la Tabla 3.4.1. Puede observarse como al utilizar el modo de funcionamiento in-out los valores de permeancia obtenidos son superiores a los valores alcanzados en caso de operar usando el modo opuesto, permeando desde el exterior hacia el interior (modo out-in).

Tabla 3.4.1 Resumen de las permeanzas obtenidas a 400°C con los diferentes tipos de membranas para ambos modos de operación.

Tipo de membrana	Permeanza de H ₂ 400 °C (mol/s m ² Pa ^{0.5})	
	In-Out	Out-in
CeO ₂ denso	5,37·10 ⁻⁴	4,46·10 ⁻⁴
CeO ₂ denso dopado	6,39·10 ⁻⁴	5,73·10 ⁻⁴
CeO ₂ mesoporoso	1,03·10 ⁻³	8,82·10 ⁻⁴

Esta variación podría deberse a la incorporación de Pd en el interior de los poros del sustrato asociada al proceso de deposición ELP-PP. Este hecho provoca que las superficies internas y externas de las películas de Pd se vuelvan significativamente diferentes y, por lo tanto, también los procesos involucrados en la permeación global del hidrógeno a través de la membrana. Para entender mejor esta hipótesis, la Figura 3.4.5 representa una vista esquemática de una sección transversal típica de una membrana ELP-PP, marcando en diferentes colores las superficies de la película de Pd tanto externa como interna (rojo y azul, respectivamente). Como se puede observar, la superficie exterior del paladio es relativamente más lisa en comparación con la interior, que presenta una mayor tortuosidad provocada por la infiltración de paladio en el interior de los poros del soporte. De este modo, la superficie de paladio disponible para la disociación de H₂ es significativamente mayor en el lado interno que en el externo. Por tanto, se puede adsorber más H₂ sobre el lado del retenido de la película de Pd cuando se trabaja en el modo de operación de in-out y, como consecuencia, se alcanza una mayor permeabilidad. Por otro lado, al realizar estos ensayos se puede destacar la resistencia mecánica de las membranas preparadas, principalmente al trabajar en el modo in-out en el que la presión genera tensiones de tracción sobre la capa de paladio que podría dar lugar a la aparición de delaminaciones de la capa de paladio. Al no producirse este hecho, queda comprobado el buen anclaje de la capa selectiva al soporte debido a la deposición parcial de paladio dentro de los poros que proporciona el método de deposición ELP-PP.

3. Discusión general

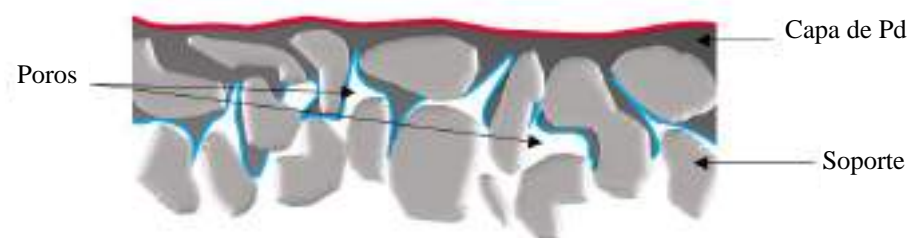


Figura 3.4.5 Vista esquemática de una membrana ELP-PP, distinguiendo la superficie externa (marcada en rojo, ●) y la interna (marcada en azul, ●) de la película de Pd generada sobre el soporte poroso.

Además de estos ensayos con H₂ puro en ambos modos de operación, se realizaron experimentos con mezclas binarias de H₂-N₂ para analizar la influencia del uso mezclas y los posibles efectos de concentración-polarización. Los resultados obtenidos para estos experimentos, realizados a 400 °C en los dos modos de funcionamiento posibles (out-in e in-out, Figura 3.4.4), se muestran en la Figura 3.4.6, donde se comparan los resultados obtenidos para membranas con capas intermedias de CeO₂ denso comercial (dopado y sin dopar) y mesoporoso. En general, un aumento del contenido de N₂ en la corriente de alimentación siempre promueve una reducción en la permeabilidad al H₂, independientemente del modo de permeación, a pesar de tener en cuenta el efecto de dilución inherente en la mezcla para cálculo de datos. Este comportamiento sugiere la influencia de posibles efectos de concentración-polarización en la capa de Pd como principal responsable de la pérdida de permeabilidad. Este efecto es claramente más pronunciado en el caso de trabajar con el modo de funcionamiento in-out. Hay que recordar que las permeanzas alcanzadas en esta configuración (in-out) fueron mayores que las obtenidas en caso de operar en sentido contrario (out-in), manteniéndose esta tendencia para todo el conjunto de experimentos (Tabla 3.4.1). Sin embargo, a pesar de estos valores mayores, la caída en la permeanza relativa fue más relevante en la configuración in-out. Este resultado particular puede explicarse debido a los diferentes caminos que el H₂ necesita seguir para atravesar la membrana compuesta en caso de utilizar un modo de permeación u otro.

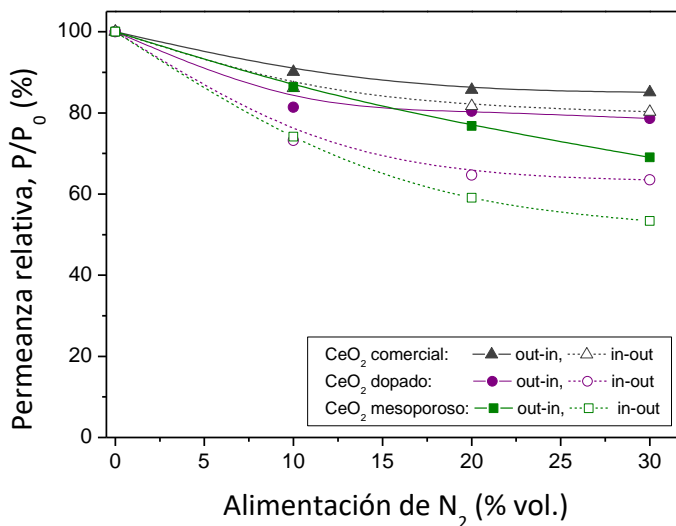


Figura 3.4.6 Efecto de la dilución de la corriente de alimentación con mezclas binarias de H₂-N₂ a 400 °C para membranas con capas intermedias de CeO₂ comercial (triángulos) o dopado (círculos) y mesoporoso (cuadrados) para ambos modos de permeación: in-out (símbolos rellenos) y out-in (símbolos vacíos).

Con el fin de realizar esta explicación de una manera más clara, se han diseñado dos esquemas simples para el proceso de permeación al alimentar mezclas binarias de H₂-N₂ y operar en los modos antes mencionados (Figura 3.4.7). Como puede verse en el esquema, al considerar el modo de operación out-in (Figura 3.4.7a), el H₂ puede alcanzar fácilmente la superficie externa de la capa de Pd, penetrando a través de esta capa mientras el N₂ es rechazado. Aunque puede producirse un efecto de polarización-concentración debido a los movimientos contrarios de las nuevas moléculas de H₂ que intentan alcanzar la capa de Pd y las moléculas de N₂ rechazadas que regresan a la fase de volumen retenido, la alta velocidad de la corriente de alimentación a lo largo de la dirección axial elimina fácilmente las moléculas de la superficie de Pd, relativamente lisa. Por el contrario, considerando el modo de operación de in-out, la corriente de alimentación debe primero atravesar el medio poroso, formado por el soporte acero poroso y la capa intermedia de ceria, antes de llegar a la capa de Pd (Figura 3.4.7b). Entonces, las moléculas de N₂ rechazadas tienen mayor dificultad para abandonar el medio poroso, permaneciendo durante algún tiempo y, por lo tanto, dificultando el transporte de nuevas moléculas de H₂ hacia la capa de Pd. Como resultado de estos diferentes procesos, se

3. Discusión general

obtuvo una caída más alta en la permeanza relativa en caso de operar con el modo in-out. Por otro lado, para resumir el efecto de las mezclas binarias H₂-N₂ sobre las distintas membranas que contienen CeO₂ como capa intermedia, se puede afirmar que las capas de Pd con mayor capacidad de permeación se ven más afectadas por la polarización por concentración producida el alimento de corrientes de H₂ diluidas, a pesar de alcanzar siempre valores de flujo H₂ permeado superiores en todas las condiciones. Este efecto se observa independientemente de permear desde el interior hacia el lado exterior o viceversa (in-out o out-in, respectivamente).

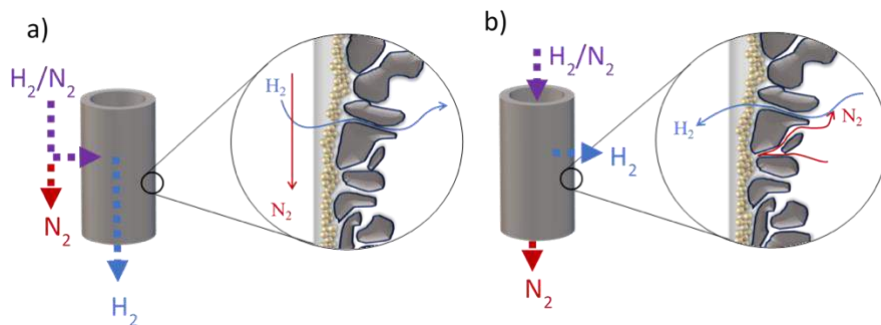


Figura 3.4.7 Mecanismo de permeación alimentando una mezcla de hidrógeno y nitrógeno en el modo de operación a) in-out y b) out-in

Para terminar con los análisis sobre la alimentación de mezclas binarias de H₂-N₂, se completaron los ensayos analizando el efecto de la temperatura. Estos resultados experimentales se han recopilado en la Figura 3.4.8, donde también se representa la variación relativa de la permeanza alcanzada en cada temperatura y modo de operación, para una membrana con partículas de ceria mesoporoso como capa intermedia. Cabe señalar que las caídas de permeanza fueron similares para todas las pruebas realizadas a diferentes temperaturas y concentraciones de N₂ en el rango de 350-450 °C y 0-50% vol., Respectivamente. Además, también se mantuvo la influencia del uso de los modos de funcionamiento in-out o out-in, obteniendo un mayor efecto para la primera configuración. Por ejemplo, la caída de permeanza relativa observada en el caso de alimentar la mezcla más diluida (50% en volumen de N₂) fue de alrededor del 40% para el modo de operación de out-in, mientras que esta caída se produjo hasta un 50% con el modo in-out. Analizando globalmente todo el conjunto de experimentos, se puede apreciar que la desviación entre todos los resultados experimentales fue menor al 5% para cada concentración de N₂ en la mezcla con ambos modos de operación,

siendo posible concluir que el efecto concentración-polarización no se vio afectado sensiblemente por temperatura.

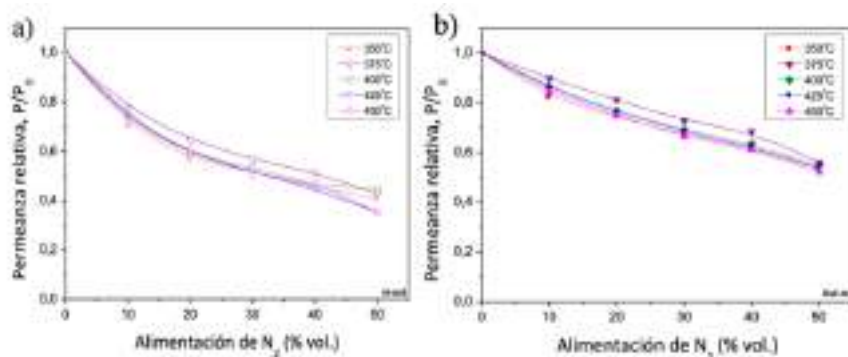


Figura 3.4.8. Variación de la permeancia al alimentar mezclas binarias de H_2-N_2 en distintas proporciones a diferentes temperaturas y modos de operación: in-out (a) o out-in (b).

A modo de resumen en la Figura 3.4.9 se pueden comparar algunos de los parámetros más relevantes de los distintos tipos de membranas preparadas como el espesor de la capa selectiva de paladio estimado mediante gravimetría (Figura 3.4.9a) y la permeanza de los distintos tipos de membranas compuestas (Figura 3.4.9b). Respecto al espesor de la capa selectiva (Figura 3.4.9a), con el uso de partículas de óxido de cerio denso comercial, se consiguió disminuir el espesor de la capa selectiva en un 50%, respecto al tipo de membranas tomadas como referencia (sin capa intermedia de CeO_2) pasando de valores de 30 a tan solo 15 μm . Como consecuencia de esta modificación también se consiguió aumentar la capacidad de permeación en un 350% obteniendo una permeanza de $4,46 \cdot 10^{-4} \text{ mol m}^{-2} s^{-1} Pa^{-0.5}$ a 400 °C (Figura 3.4.9b), manteniendo una elevada selectividad H_2/N_2 . Desde este punto se consiguió mejorar el comportamiento de permeación de dos maneras distintas: (a) modificando el proceso de activación del ciclo ELP-PP, usando partículas de CeO_2 dopadas con núcleos de Pd y (b) modificando la morfología de las partículas de CeO_2 de la capa intermedia, utilizando partículas de óxido de cerio mesoporoso. Con la modificación (a) se consiguió aumentar la permeanza al H_2 en un 400%, respecto a membranas sin capa intermedia de ceria, obteniendo valores de permeanza de $5,73 \cdot 10^{-4} \text{ mol m}^{-2} s^{-1} Pa^{-0.5}$ (Figura 3.4.9b). En términos de espesor de la capa de paladio, se disminuyó el espesor hasta valores inferiores a las 10 μm (Figura 3.4.9a), estimadas mediante análisis gravimétricos. Esta disminución en el espesor de la capa selectiva pudo conseguirse debido a la nueva distribución de los núcleos de paladio generados en las partículas de manera

3. Discusión general

previa a su incorporación como capa intermedia y como consecuencia se obtuvo el correspondiente aumento de la permeanza.

Por otro lado, sustituyendo las partículas comerciales densas por partículas mesoporosas, el espesor final de las membranas de este tipo se estimó en 12 µm (Figura 3.4.9a). A pesar de tener un espesor superior a las previamente mencionadas, la permeanza al H₂ aumentó en mayor medida, un 680% respecto a membranas sin capa intermedia de ceria, obteniendo valores de permeanza de $1,03 \cdot 10^{-3}$ mol m⁻² s⁻¹ Pa^{-0,5} a 400 °C (Figura 3.4.9b). La porosidad de las partículas permite un mejor crecimiento de la capa de paladio en dirección horizontal (desde la vista del corte transversal), permitiendo así reducir el espesor respecto a las partículas densas. Por otro lado, esta porosidad limita en menor medida el flujo de H₂ a través de la membrana, como ya se observó previamente con el N₂ en el caso del soporte.

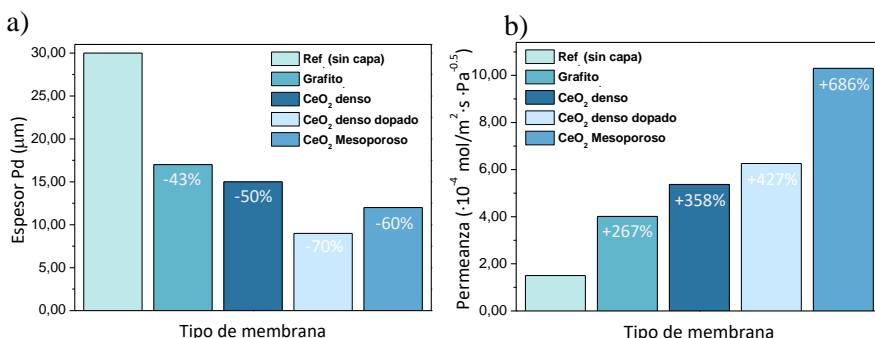


Figura 3.4.9 Comparación de los valores de espesores de la capa de paladio y permeanza para los distintos tipos de membranas desarrolladas.

3.5 Análisis económico

Una vez analizada tanto la morfología obtenida como el comportamiento de las membranas compuestas que han sido preparadas mediante el uso de diversas capas intermedias, se ha llevado a cabo un análisis económico sobre los costes asociados a la preparación a escala de laboratorio, de cada uno de los tipos de membrana planteados con el objeto de seleccionar la estrategia de síntesis más adecuada para un posible escalado y aplicación industrial. Hay que recordar que todas estas membranas están realizadas sobre un soporte de acero poroso de geometría tubular con una longitud de 30 mm y un diámetro exterior de 12,7 mm. Además, en todos los casos el método de deposición de paladio utilizado fue el ELP-PP.

La Figura 3.5.1 muestra un esquema de las distintas etapas necesarias para la fabricación de membranas compuestas que contienen una capa intermedia basada en CeO₂, ya sea en forma de partículas densas (dopadas o no) o de partículas con una cierta porosidad interna. A modo de referencia se han añadido también las etapas necesarias para la obtención de una membrana compuesta de paladio sin que se incluya ningún tipo de capa cerámica intermedia adicional. En general, estas etapas se dividen en 2 categorías: modificación superficial de los soportes (MS) y deposición de paladio (DP). Las etapas asociadas a la modificación superficial de los soportes engloban su lavado inicial (MS-1), oxidación (MS-2), deposición de la capa intermedia (MS-3), posible necesidad de calcinación de las mismas (MS-4) o etapas adicionales para lograr un material con cierta porosidad intraparticular (síntesis de SBA-15 o proceso de nanoreplicación, denominadas como, MS-5 y MS-6, respectivamente). Por otro lado, dentro del conjunto de etapas asociadas a la deposición de paladio se encuentran la activación del soporte modificado (DP-1), el proceso de ELP-PP para la formación de la capa densa de paladio (DP-2) junto con el posterior lavado y secado tras cada ciclo de deposición (DP-3). Debe destacarse que el proceso de activación realizado directamente sobre las partículas que forman la capa intermedia (“DP-1”), y no sobre el soporte modificado, se ha incluido dentro de la categoría de modificación superficial a pesar de estar asociado al proceso de deposición. También debe destacarse que no es necesario la realización de todas y cada una de las etapas descritas para la síntesis de los distintos tipos de membrana analizados.

Las características particulares de cada una de las disoluciones utilizadas en las diferentes etapas descritas con anterioridad se recogen en la Tabla 3.5.1, donde se identifican los reactivos químicos y materiales necesarios en cada una de ellas, junto con la cantidad requerida de los mismos.

3. Discusión general

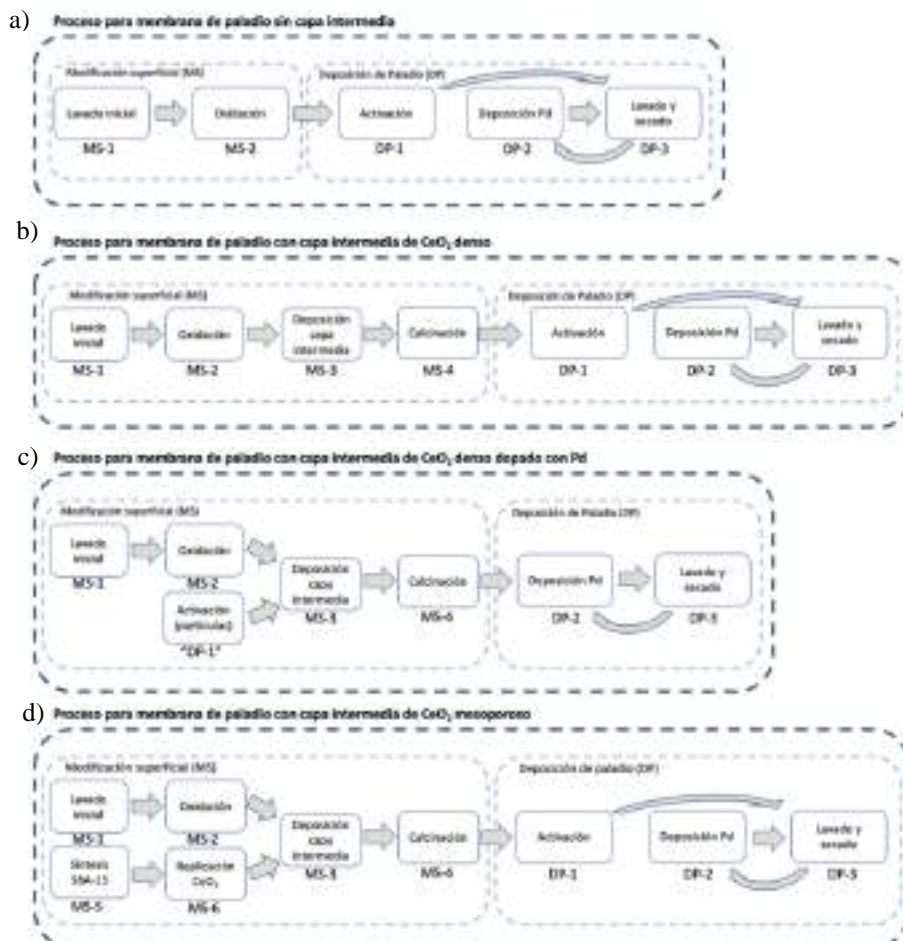


Figura 3.5.1 Esquema de los distintos procesos de síntesis de membranas analizados.

Tabla 3.5.1 Disoluciones utilizadas en la síntesis de los distintos tipos de membranas.

MS-1 (Levado inicial)	MS-2 (Dep. capa intermedia)	MS-3 (interior VBN-13)	MS-4 (depósito CeO_2)
Disolución MS-1.1	Disolución MS-1.1	Disolución MS-3.1	Disolución MS-4.1
NaOH (g/l)	CeO_2 (g/l)	HNO_3 (g/l)	PdCl_2 (g/l)
H_2O_2 (molar)	PVA (g/l)	H_2O_2 (molar)	52,5
Disolución MS-1.2	H_2O_2 (molar)	TEOS (g/l)	$\text{Ce}(\text{NO}_3)_3 \cdot 6\text{H}_2\text{O}$ (g/l)
KCl 20% (molar)	2	H_2O_2 (molar)	33,3
H_2O_2 (molar)	-	EDTA (g/l)	Ethanol (molar)
Disolución MS-1.3	-	-	1000
Etileno 96% (molar)	1000	-	-
MS-5 (Levado final)	DP-1 (Activación)	DP-2 (Depósito Pd)	DP-3 (Lavado y secado)
Disolución DP-1.1	Disolución DP-1.1	Disolución DP-1.1	Disolución DP-1.1
PdCl_2 (g/l)	PdCl_2 (g/l)	PdCl_2 (g/l)	PdCl_2 (g/l)
HCl 35% (molar)	0,1	1	2,4
H_2O_2 (molar)	1	1	330
H_2O_2 (molar)	-	H_2O_2 (molar)	76
Disolución DP-1.2	CeO_2 (g/l)	186,6	H_2O_2 (molar)
NH_4OH 32% (molar)	120	120	H_2O_2 (molar)
N_2H_4 (molar)	20	N_2H_4 (molar)	10
H_2O_2 (molar)	-	H_2O_2 (molar)	-
	H_2O_2 (molar)		

Además de todos los productos químicos y materiales descritos hasta el momento, el consumo eléctrico asociado a cada una de las etapas necesarias para la fabricación de cada tipo de membrana también se ha tenido en cuenta en este estudio. Por todo ello es importante recordar la escala de laboratorio considerada para analizar desde el punto de vista económico los procedimientos de síntesis desarrollados para las diferentes membranas. En este contexto, para cada una de las etapas consideradas como necesarias para preparar una membrana según las diferentes estrategias planteadas es posible gestionar de forma simultánea un número diferente de membranas. Así, en las etapas MS-1, DP-1, DP-2 y DP-3 es posible manipular cuatro membranas simultáneamente, mientras que solo se pueden procesar al mismo tiempo dos unidades en los pasos MS-2 y MS-4. Por otro lado, los pasos MS-3 y DP-1 se realizan de manera individual para cada membrana. Esta información es relevante ya que los costes eléctricos asociados a cada una de las etapas por unidad funcional (en este caso, una membrana con longitud de 30 mm) dependerán del número de membranas que puede procesarse al mismo tiempo. Teniendo en cuenta todas estas consideraciones, la

Tabla 3.5.2 recoge el desglose de número de etapas necesarias, cantidad de cada una de las disoluciones y el consumo eléctrico requerido en cada caso para la fabricación de cada tipo de membrana incluido en este estudio. Este tipo de requerimientos se ha traducido en costes monetarios para un análisis más claro. Para ello se tomó como referencia el coste medio del kilovatio hora en España en 2020, el cual se fijó en 0,14 €/kWh.

De forma general, puede concluirse que el coste global de preparación de una membrana sobre un soporte PSS mediante ELP-PP (95,10 €) puede reducirse notablemente mediante el uso de capas intermedias de ceria. De este modo según el tipo de material empleado para este tipo de capas intermedias, mayor o menor es el nivel de ahorro, alcanzando un coste total de 65,41 € cuando se emplea una capa intermedia formada por partículas de CeO₂ denso, 66,03 € cuando estas partículas son porosas o 50,05 € cuando las partículas de CeO₂ denso son previamente dopadas con núcleos de paladio. Teniendo en cuenta que el coste del soporte de acero poroso se mantiene constante para las diferentes alternativas planteadas (32,50 €), se ha descartado su influencia para proceder a un análisis más detallado de los costes asociados a la propia modificación de éste, incluyendo en este punto tanto su modificación superficial como la posterior incorporación de la capa de paladio mediante ELP-PP. Como resultado, los costes de estas etapas de fabricación, ordenados de mayor a menor son: 62,60 € para una membrana sin capa intermedia, 33,53 € cuando se incluye una capa intermedia de CeO₂ mesoporoso, 32,91 € cuando las partículas de CeO₂ empleadas en esta capa

3. Discusión general

son completamente densas o 17,55 € cuando estas partículas de CeO₂ densas se dopan con núcleos de paladio antes de llevar a cabo la deposición de paladio mediante ELP-PP.

Tabla 3.5.2 Costes de las distintas etapas para cada tipo de membrana.

Etapa	Tipo de interfase						
	Sin capa intermedia	CeO ₂ directo	CeO ₂ directo depósito	CeO ₂ in-suspension			
Lavado inicial (MS-1)^(a)							
Nº ciclos	1	1	1	1	1		
Consumo eléctrico	0,3357 kW	0,0047 €	0,3357 kW	0,0047 €	0,3357 kW	0,0047 €	
Dissolución MS-1.1	50 ml	0,0010 €	50 ml	0,0010 €	50 ml	0,0010 €	
Dissolución MS-1.2	50 ml	0,0020 €	50 ml	0,0020 €	50 ml	0,0020 €	
Dissolución MS-1.3	50 ml	0,3750 €	50 ml	0,3750 €	50 ml	0,3750 €	
Oxidación (MS-2)^(b)							
Nº ciclos	1	1	1	1	1		
Consumo eléctrico	0,8429 kW	0,8488 €	0,8429 kW	0,8488 €	0,8429 kW	0,8488 €	
Deposición capa inter. (MS-3)^(c)							
Nº ciclos	-	1	1	1	1		
Consumo eléctrico							
Suspensión MS-3.1		12,5 ml	0,5045 €	12,5 ml	0,5045 €	12,5 ml	0,5045 €
Calefacción (MS-4)^(d)							
Nº ciclos	1	1	1	1	1		
Consumo eléctrico		1,2893 kW	0,4605 €	1,2893 kW	0,4605 €	1,2893 kW	0,4605 €
Sistema RRA-15 (MS-5)^(e)							
Nº ciclos	-	-	-	-	-		
Consumo eléctrico							
Dissolución MS-5.1					19,4934 kW	2,7162 €	
					50 ml	3,6449 €	
Replicación CeO₂ (MS-6)^(f)							
Nº ciclos	-	-	-	-	-	-	
Consumo eléctrico							
Dissolución MS-6.1					23,9771 kW	3,3568 €	
					450 ml	3,9984 €	
Atracción (DP-1)^(g)							
Nº ciclos	1	1	1	1	1		
Consumo eléctrico							
Dissolución DP-1.1	50 ml	0,2450 €	50 ml	0,2450 €	50 ml	0,2450 €	
Dissolución DP-1.2	50 ml	0,0010 €	50 ml	0,0010 €	50 ml	0,0010 €	
Activación partículas (DP-2)^(h)							
Nº ciclos	-	-	-	1	-		
Consumo eléctrico							
Dissolución "DP-2.1"				30 ml	0,5368 €		
Dissolución "DP-2.2"				30 ml	0,0066 €		
Lavado y secado (DP-3)⁽ⁱ⁾							
Nº ciclos	28 ± 3	13 ± 2	7 ± 1	9 ± 2			
Consumo eléctrico	20,6400 kW	3,4498 €	11,4400 kW	1,6016 €	6,1600 kW	0,8624 €	
H ₂ O MSQ	1400 ml	450 ml	-	350 ml	-	400 ml	
Deposición PA (DP-4)^(j)							
Nº ciclos	27 ± 3	12 ± 2	7 ± 1	8 ± 2			
Consumo eléctrico	2,3246 kW	0,3257 €	1,1500 kW	0,1617 €	0,6936 kW	0,0937 €	
Dissolución DP-4.1	200 ml	57,2800 €	100 ml	28,6400 €	50 ml	14,3200 €	
Dissolución DP-4.2	81 ml	0,0659 €	46 ml	0,0350 €	21 ml	0,0178 €	
Costes							
Consumo eléctrico	-4,8289 €	3,0773 €	2,2721 €	8,4934 €			
PaCl ₂	32,5140 €	26,3780 €	13,2112 €	13,3106 €			
Otros reactivos	5,4530 €	3,4333 €	2,0646 €	11,7281 €			
Modificación del soporte	62,5978 €	32,9108 €	17,5499 €	33,5263 €			
Separación 316L	30 mm 32,5000 €	30 mm 32,5000 €	30 mm 32,5000 €	30 mm 32,5000 €			
Total	92,0978 €	65,4108 €	38,0459 €	66,0265 €			

n: Número de piezas que pueden realizarse al mismo tiempo en una etapa.

3. Discusión general

Para analizar de una forma más clara estos resultados, la Figura 3.5.2 muestra la distribución de costes asociados al consumo de la fuente de paladio y otros reactivos, junto al consumo eléctrico para los distintos tipos de membranas sintetizadas. En general, puede observarse que con ambos tipos de interfaces de CeO_2 denso se ha conseguido una reducción en todos los gastos asociados tanto al consumo de reactivos como de electricidad. Sin embargo, con el uso de interfaces de CeO_2 mesoporoso se obtuvo una clara reducción del coste asociado a la fuente de paladio, pero no al consumo eléctrico y al de otros reactivos, necesarios para la obtención del propio material empleado. Esto incluye la síntesis del material SBA-15 empleado como agente director de la estructura porosa buscada y el proceso de nanoreplicación para la obtención del material final, lo que eleva su coste. En líneas generales, el uso de CeO_2 supuso una reducción del coste total para la modificación del soporte en un 47,21 y un 46,44% para partículas densas y mesoporosas, respectivamente. Por otro lado, la realización de la etapa de activación directamente sobre las partículas de CeO_2 denso supuso la mayor reducción de costes, un 71,96%.

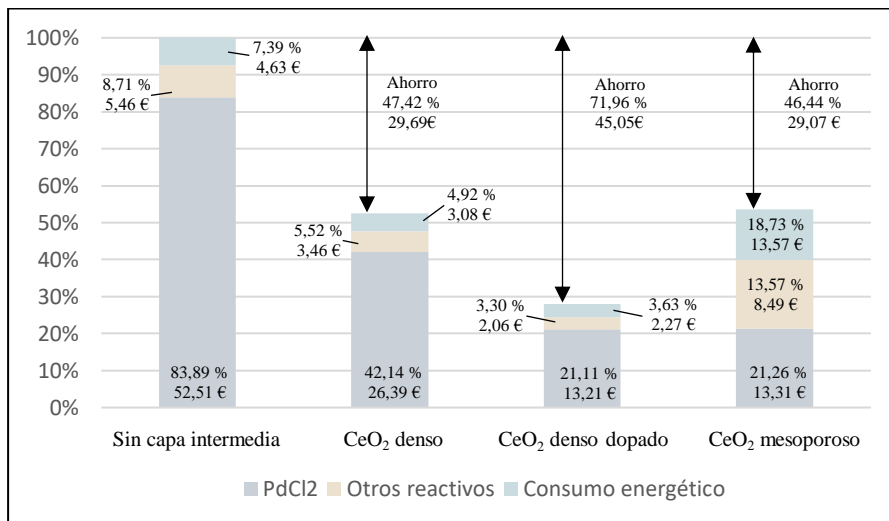


Figura 3.5.2 Distribución de costes de los distintos procesos de fabricación.

Para finalizar este estudio, se han evaluado los resultados experimentales obtenidos mediante ensayos de permeación de manera conjunta con los obtenidos en el análisis económico. Para ello, se ha tenido en cuenta la capacidad de permeación de cada uno de los tipos de membranas junto a los costes estimados para su fabricación definiendo un nuevo parámetro denominado “factor M”, cuyas unidades son $\text{€}/10^4 \text{ mol m}^{-2} \text{ s}^{-1} \text{ Pa}^{-1}$.

^{0,5}. De este modo, el tipo de membrana que minimice este factor será seleccionado como más adecuado, ya que ofrecerá una mayor capacidad de permeación por unidad monetaria. Como resultado, la membrana que ofrece un menor factor M es la que contiene CeO₂ denso dopado como capa intermedia, con un valor M=2,80. A continuación, se sitúa el uso de partículas mesoporosas como capa intermedia, con un valor M= 3,26. Estas últimas, a pesar de ofrecer una mayor permeanza que las anteriores ($10,3 \cdot 10^{-4}$ mol m⁻² s⁻¹ Pa^{-0,5}, frente a $6,26 \cdot 10^{-4}$ mol m⁻² s⁻¹ Pa^{-0,5} a 400 °C), pierden esta ventaja competitiva debido al incremento en su coste de fabricación (un 191% superior). Respecto al uso de partículas de CeO₂ densas, el coste final obtenido es más del doble de los mencionados anteriormente, obteniéndose un factor M=6,13. Por último, la membrana usada como referencia, es decir, sin capa intermedia obtuvo el peor resultado con factor M de 41,73 €/10⁻⁴ mol m⁻² s⁻¹ Pa^{-0,5}. La Tabla 3.5.3 recoge a modo de resumen todos estos resultados. En conclusión, puede afirmarse que las membranas que contienen una capa intermedia de CeO₂ denso dopado parecen ser la alternativa más prometedora para su escalado a mayores longitudes y su integración en reactores de membrana reales.

Tabla 3.5.3 Coste, permeanza y factor M de los distintos tipos de membranas.

	Sin capa intermedia	CeO ₂ densa	CeO ₂ denso dopado	CeO ₂ mesoporosa
Coste (€)	62,60	32,91	17,55	33,53
Permeanza (10^{-4} mol m ⁻² s ⁻¹ Pa ^{-0,5})	1,5	5,37	6,26	10,3
Factor M (€ / 10^{-4} mol m ⁻² s ⁻¹ Pa ^{-0,5})	41,73	6,13	2,80	3,26

3.6 Escalado e integración en sistemas de reacción

Teniendo en cuenta las propiedades de los distintos tipos de membranas preparados junto a los resultados del análisis económico realizado previamente, se seleccionaron las membranas compuestas de paladio con una capa intermedia de óxido de cerio denso dopado con paladio como las más adecuadas para su escalado y posterior integración en un reactor de membrana. Así, la preparación de este tipo de membranas se escaló a mayores longitudes de los soportes porosos (7 cm). Con estas nuevas dimensiones se pudo observar como el aumento de peso asociado a la incorporación de la capa intermedia de CeO₂ se mantuvo proporcional a la longitud de la pieza. Respecto a la capa selectiva de paladio, se observó una buena homogeneidad también en la dirección longitudinal, además de valores de permeanza y espesores similares a los previamente obtenidos con las membranas de menor longitud. Con respecto a la economía del proceso de fabricación, la preparación de membranas de mayor longitud resultó beneficiosa en términos de costes, reduciéndose éste de 5,85 a 3,27 €/cm cuando la longitud de los soportes porosos pasó de 3 a 7 cm. Esto se debe principalmente a que el escalado a una mayor longitud de las membranas no es proporcional a la evolución de las necesidades en reactivos o consumo eléctrico debido a ligeros cambios en el equipamiento experimental y el factor de economía de escala. De esta forma, el escalado de la membrana en las condiciones realizadas supuso una reducción del 44 % por cada cm de membrana.

Los buenos resultados alcanzados durante el escalado de las membranas permitieron el análisis de su comportamiento junto al catalizador de Ni/SBA-15 en forma de pellets en un reactor de membrana real para producir hidrógeno de alta pureza mediante reformado con vapor de ácido acético. Este particular proceso de obtención de hidrógeno se seleccionó por su relación con algunos de los proyectos de investigación desarrollados en el propio departamento, en los que se tratan de valorizar algunos de los subproductos de la producción de bioaceites mediante licuefacción hidrotérmica de microalgas. Uno de ellos es la fracción acuosa generada durante el propio proceso de licuefacción de las microalgas, cuya composición puede simularse mediante el uso de ácido acético como compuesto modelo. Así, el desarrollo de este tipo de reacciones en un reactor de membrana que permita la separación continua del hidrógeno generado durante la reacción química permitiría no sólo analizar su viabilidad técnica sino también comprobar la estabilidad mecánica y de comportamiento de las

membranas preparadas en diferentes casos. La Figura 3.6.1 recoge todos los resultados alcanzados tras una hora en las diferentes reacciones químicas llevadas a cabo a $T=450\text{ }^{\circ}\text{C}$, $\text{GHSV}=4500\text{ h}^{-1}$ y $P=1,0\text{-}3,0\text{ bar}$. Todos estos resultados obtenidos en el reactor de membrana, denotado como PBMR (packed bed membrane-reactor) fueron comparados con los resultados obtenidos en condiciones de operación equivalente en un sistema de reacción tradicional, denotado como PBR (packed bed reactor) en los que no se producía la separación in situ del hidrógeno generado en la misma.

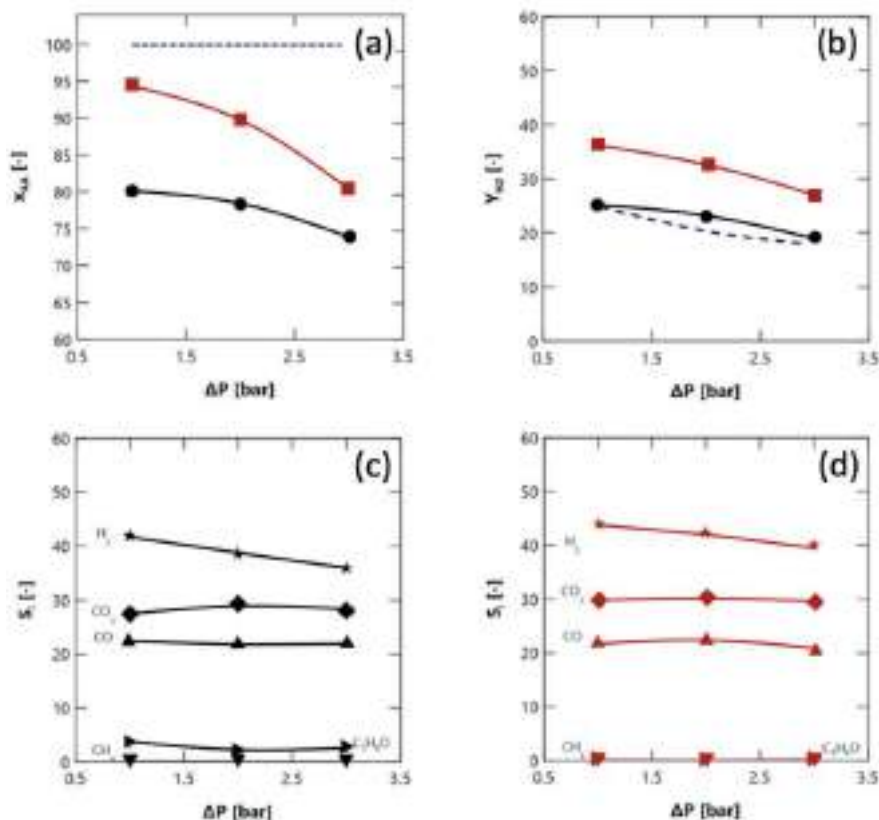


Figura 3.6.1 Efecto de presión en experimentos de reformado con vapor de ácido acético ($T = 450\text{ }^{\circ}\text{C}$, $\text{GHSV} = 4500\text{ h}^{-1}$) en configuraciones PBR (negro, ●) y PBMR (rojo, ●): conversión de ácido acético (a), rendimiento de hidrógeno (b), selectividad de productos en PBR (c) y PBMR (d). Referencia de equilibrio termodinámico: ---.

Tal y como puede observarse, en términos generales se obtiene un efecto beneficioso con la incorporación de la membrana selectiva al hidrógeno en el medio de reacción para todas las condiciones analizadas, tanto en términos de conversión de ácido acético como de rendimiento a hidrógeno, principal producto de interés. En este punto debe destacarse que

3. Discusión general

la integridad mecánica de la membrana se mantuvo durante el transcurso de la totalidad de los experimentos aquí recogidos, no observándose ningún tipo de deterioro en la capa de paladio ni un descenso en su selectividad al hidrógeno.

Analizando con un mayor grado de detalle los resultados obtenidos en este estudio, resulta evidente la disminución obtenida en el avance de la reacción de reformado a medida que aumenta la presión cuando se emplea una configuración de tipo PBR sin ningún tipo de separación simultánea del hidrógeno generado. Esto se debe al efecto negativo que tiene la presión del sistema sobre las principales reacciones involucradas en el proceso. De hecho, las reacciones de reformado con vapor propiamente dicha y a la de descomposición térmica son las más afectadas por un aumento en la presión debido al mayor aumento del número de moles entre productos y reactivos ($\Delta n = +3$). Comparando los resultados alcanzados en esta configuración con la implementación de un sistema de tipo PBMR es evidente el desplazamiento del equilibrio químico debido a la permeación simultánea de hidrógeno a través de la membrana introducida en el sistema, lo que supuso un aumento de hasta un 15% en la conversión de ácido acético (Figura 3.6.1a). Es sabido que la velocidad de reacción directa puede favorecerse eliminando selectivamente uno de los productos del medio de reacción, reduciendo consecuentemente la velocidad de la reacción inversa [299,300]. Ésta es una de las principales ventajas de trabajar con reactores de membrana a través de las cuales el hidrógeno pueda extraerse de manera simultánea a la propia reacción química en una única operación [28,301,302]. De este modo, se podría alcanzar una conversión más alta manteniendo una temperatura de funcionamiento constante, tal como ocurre en el presente caso, o mantener un cierto grado de producción trabajando a unas condiciones de operación menos exigentes (menor temperatura). Esto es lo que se conoce como intensificación de procesos. Sin embargo, también se observa que este desplazamiento del equilibrio químico producido por la permeación de H₂ a través de la membrana no pudo compensar las restricciones termodinámicas derivadas de las condiciones experimentales utilizadas. De esta manera, el impacto negativo del aumento de presión sobre la termodinámica del proceso general de reformado con vapor de ácido acético, ya mencionado con anterioridad, prevalece al efecto beneficioso de incluir una membrana en el sistema pese a que mayores presiones favorecen una mayor permeación de hidrógeno, lo que a su vez provocaría un mayor desplazamiento del equilibrio químico. En cualquier caso, el efecto

beneficioso de la incorporación de una membrana al sistema de reacción también se evidencia en la Figura 3.6.1 b, donde se puede observar una mejora significativa en el rendimiento a hidrógeno al reemplazar la configuración PBR convencional por la PBMR, superando incluso los valores del equilibrio. Este hecho sugiere que se generan diferencias en la selectividad del producto cuando se combina una extracción continua de hidrógeno a través de una membrana altamente selectiva con un catalizador en un PBMR. Por otro lado, es necesario un análisis más detallado para explicar los resultados alcanzados en la selectividad de los productos en la corriente de retenido para los sistemas PBR y PBMR en las diferentes condiciones analizadas (Figura 3.6.1c y 3.6.1d). En este contexto, en todos los casos se alcanzó una marcada selectividad hacia el hidrógeno, siendo el valor de esta superior en el caso de utilizar la configuración PBMR. De hecho, el hidrógeno fue el principal producto de las reacciones químicas involucradas en el proceso catalítico en términos de selectividad, con valores que oscilaron entre el 35 y el 45%, seguido del dióxido de carbono y del monóxido de carbono, oscilando ambos entre el 20 y 30%. Hay que destacar, que debido al uso de la configuración PBMR una parte del H₂ producido (~9%) se obtiene totalmente separado del resto de productos, con una elevada pureza, ya que este se recoge de la corriente de permeado.

En cualquier caso, en lo relativo al objetivo de este trabajo, debe destacarse que todos estos ensayos del comportamiento de la membrana en sistemas PBMR se han llevado a cabo en unas condiciones de operación no optimizadas con el objetivo principal de analizar el comportamiento de las propias membranas foco de la presente Tesis Doctoral, no tanto el ajuste de las mismas para maximizar los procesos de generación de hidrógeno y su recuperación. Con tal fin, este tipo de ensayos se consideran suficientes para demostrar la robustez mecánica de las membranas seleccionadas y la posibilidad de su integración satisfactoria en sistemas reales para la intensificación de procesos químicos mediante el uso de reactores de membrana, pudiendo ser el punto inicial de futuros desarrollos e investigaciones.

4

Conclusiones Conclusions

Conclusiones

Tras analizar todos los resultados experimentales generados a lo largo de la presente investigación, se puede concluir que se logró sintetizar nuevas membranas compuestas de Pd con alta capacidad de permeación y elevada selectividad al H₂ utilizando diversos tipos de capas intermedias entre el soporte de acero poroso y capa selectiva de Pd. Esta conclusión principal se puede dividir en los siguientes ítems parciales de acuerdo con los objetivos específicos considerados para esta Tesis Doctoral:

- El uso de los diferentes tipos de capas intermedias analizadas, basadas tanto en grafito como óxido de cerio, permitió reducir el espesor necesario para lograr una capa de paladio totalmente densa entre un 40-70% en comparación con el uso directo. de soportes calcinados para la preparación de membranas. Esto permitió un aumento de la permeanza de hidrógeno en un 250-680% con α_{H_2/N_2} mayor a 10.000.
- En particular, la incorporación de grafito como capa intermedia permitió la preparación de membranas con alrededor de 17 μm de espesor de paladio y permeanzas $4,01 \cdot 10^{-4} \text{ mol m}^{-2} \text{ s}^{-1} \text{ Pa}^{-0.5}$ a 400 °C. Estos valores representan una mejora significativa de estos parámetros, aumentando un 43% y 250%, respectivamente, en comparación con el tipo de membranas de referencia (Pd sobre soportes PSS calcinado).
- Este material preliminar fue sustituido por óxido de cerio debido a su elevada resistencia química y mecánica en las típicas condiciones de operación de una membrana de paladio, además de su coeficiente térmico de expansión, más cercano al del resto de materiales que conforman la propia membrana (acero 316L y paladio).
- La sustitución del grafito de la capa intermedia por partículas de CeO₂ densas redujo ligeramente el espesor de Pd hasta 15 μm (reducción del 50% respecto a las membranas de referencia) y consecuentemente aumentó la permeanza a 400 °C en un 350% hasta $5,37 \cdot 10^{-4} \text{ mol m}^{-2} \text{ s}^{-1} \text{ Pa}^{-0.5}$.
- La modificación del proceso de activación, realizándose directamente sobre las propias partículas de la capa interfase antes de su incorporación al soporte, generó una mejor distribución de los núcleos de paladio. Esto permitió obtener membranas con espesores de la capa de paladio inferiores a 10 μm , lo que supone una reducción del 70% con respecto a las membranas de referencia. Este nuevo tipo de

4. Conclusiones

membranas exhibió permeanzas de hidrógeno a 400 °C en torno a los $6,26 \cdot 10^{-4}$ mol m⁻² s⁻¹ Pa^{-0,5}, lo que supone un aumento del 400% sobre los valores iniciales de referencia.

- Por otro lado, el uso de partículas de CeO₂ mesoporosas en lugar de densas presentó importantes mejoras en términos de permeación. De este modo se alcanzaron espesores de Pd similares (alrededor de 12 µm) pero la permeanza a 400 °C aumento en un 680% (respecto a las membranas de referencia) alcanzando un valor de $1,03 \cdot 10^{-3}$ mol m⁻² s⁻¹ Pa^{-0,5}.
- En todas las membranas preparadas, a pesar de mantener una alta selectividad H₂/N₂ (superior a 10,000), se observaron efectos de polarización por concentración que disminuyeron los flujos de permeado en el rango de 10-50%, dependiendo de las condiciones particulares de funcionamiento.
- En este contexto, se realizó un análisis tecnoeconómico preliminar de las estrategias de preparación de membranas mencionadas anteriormente, calculando un nuevo factor M valorar tanto el coste de fabricación de la membrana como su capacidad de permeación. El resultado se obtuvo con las membranas que contienen partículas de CeO₂ densas dopadas como capa intermedia, obteniendo un valor de 2,80 €/10⁻⁴ mol m⁻² s⁻¹ Pa^{-0,5}, lo que representa una reducción del 93,3% respecto a las membranas de referencia (Pd sobre soportes PSS calcinados).
- Por lo tanto, la estrategia de fabricación de membranas seleccionada se aplicó a mayores longitudes de los soportes tubulares, sin detectar diferencias significativas en la morfología o la permeabilidad en comparación con las membranas más cortas. Esta membrana más larga se integró en un reactor de membrana para la producción de H₂ mediante reformado con vapor de ácido acético, manteniendo su integridad mecánica y aumentando tanto la conversión de ácido acético como el rendimiento a H₂ en un 10% y 9%, respectivamente, respecto a los valores obtenidos al utilizar un reactor tradicional.

Recomendaciones para trabajo futuro

A partir de los resultados y conclusiones extraídos de la presente investigación, se proponen las siguientes recomendaciones:

- Por Evaluar el efecto de la incorporación de los tipos de capas intermedias desarrolladas en el presente trabajo sobre soportes de acero poroso con un grado de porosidad medio mayor al utilizado actualmente ($0,1 \mu\text{m}$), mucho más económicos, con el objetivo de obtener una mejor relación entre el coste y la capacidad de permeación.
- Desarrollar un proceso de deposición en continuo de paladio mediante ELP-PP, lo que supondría un primer paso en la industrialización del proceso.
- Sustituir la actual capa selectiva por una aleación de base Pd que permitan tanto elevar la capacidad de permeación como disminuir los costes de la propia capa, como es el caso de la aleación PdAg.
- Modificar el proceso de fabricación para obtener la capa selectiva en la superficie interna de los soportes tubulares. Esto puede reducir los efectos de polarización por concentración observados en el reactor de membrana utilizado, debido a su modo de operación (in-out), mejorando la capacidad de permeación durante el proceso de reacción.
- Adaptar el método de deposición ELP-PP para la deposición de capas selectivas de Pd sobre soportes con geometrías planas, lo que permitiría la integración de estas en otro tipo de dispositivos.

Conclusions

In general, after analyzing all the experimental results generated throughout the present research, it can be concluded that new composite Pd-membranes with high permeation capacity and almost complete H₂-selectivity were reached by using diverse intermediate layers between the porous stainless-steel support and the top Pd-film. This main conclusion can be divided into the following partial items accordingly to the specific objectives considered for this Ph.D. Thesis:

- Different materials based on graphite or cerium oxide were used as intermediate layers providing a significant reduction in the range of 40-70% the required thickness to obtain a fully dense membrane in the subsequent ELP-PP Pd-film in comparison to the direct use of calcined supports for the membrane preparation. It was traduced into an increase of the hydrogen permeance by 250-680% while maintaining α_{H_2/N_2} greater than 10,000 in all cases.
- Particularly, the incorporation of a graphite barrier allowed the preparation of composite-membranes with around 17 µm of palladium thickness and H₂ permeance of $4.01 \cdot 10^{-4}$ mol m⁻² s⁻¹ Pa^{-0.5} at 400 °C. These values represent a significant improvement of these parameters, increasing by 43% and 250%, respectively, in comparison to the reference membrane (Pd onto calcined PSS supports, taken as reference).
- This preliminary material was replaced by cerium oxide due to its high chemical and mechanical resistance under the typical operating conditions for a palladium membrane, in addition to its thermal expansion coefficient, closer to the other membrane materials (316L steel and palladium).
- The substitution of graphite by dense CeO₂ particles reduced slightly the Pd-thickness up to 15 µm (overall reduction of 50% respect the reference membrane) and consequently increased the H₂ permeance at 400 °C around 350% up to $5.37 \cdot 10^{-4}$ mol m⁻² s⁻¹ Pa^{-0.5}.
- The activation process with Pd nuclei onto the last membranes containing dense CeO₂ particles as intermediate barrier was modified, directly incorporating the metal sites over the surface of the ceramic particles before their incorporation onto the support. It generated a better distribution of these Pd nuclei, making possible to reduce the Pd-thickness below 10 µm, which represents a reduction of 70% regarding

4. Conclusions

the reference membrane. This type of membranes exhibited H₂-permeances at 400 °C of around $6.26 \cdot 10^{-4}$ mol m⁻² s⁻¹ Pa^{-0.5}, representing an increase of 400% over the initial reference values.

- On the other hand, the use of mesoporous CeO₂ particles instead of dense ones generated noticeable improvements in terms of permeation performance. In this way, similar Pd thicknesses were reached (around 12 µm) but the H₂ permeance at 400 °C increased in 680% to reach the value of $1.03 \cdot 10^{-3}$ mol m⁻² s⁻¹ Pa^{-0.5}.
- In all the membranes, despite maintaining a high H₂/N₂ selectivity (greater than 10,000) even while testing binary gas mixtures with diverse concentration formed by H₂ and N₂, clear concentration-polarization effects were observed, decreasing the permeate fluxes in the range of 10-50% depending on the particular operating conditions.
- In this context, a preliminary techno-economic analysis of the above-mentioned membrane preparation strategies was performed, calculating a new M-factor to relate the membrane fabrication cost and its permeation capacity. The lower value was reached for ELP-PP membranes containing doped dense CeO₂ particles as intermediate layer, obtaining $2.80 \cdot 10^{-4}$ mol m⁻² s⁻¹ Pa^{-0.5}, which represents a reduction of 93.3% compared to other ELP-PP membranes directly prepared onto calcined PSS supports.
- Therefore, the selected membrane fabrication strategy was scaled-up to longer lengths of the tubular PSS supports, not detecting an appreciable difference in either morphology or permeance in comparison to the previous membranes. This longer membrane was integrated into a membrane reactor for H₂ production by acetic acid steam reforming, maintaining its mechanical integrity while increasing both the conversion of acetic acid and the H₂ yield by 10% and 9%, respectively, concerning the obtained values when using a traditional packed-bed reactor.

Recommendations for future works

Taking into account the results and conclusions included in the present Doctoral Thesis, the next recommendations are enounced for future works:

- Incorporating the developed intermediate layers onto porous steel supports with an average pore size greater than the currently used (0.1 μm), cheaper, with the aim of obtaining a better relationship between cost and capacity permeation.
- The development of a continuous Pd deposition process by ELP-PP, which would be a first step in the process industrialization.
- Replace the current selective layer with a Pd-based alloy that allows to increase the permeation capacity and to reduce the costs of the layer itself, such as the PdAg alloy.
- Modify the manufacturing process to obtain the selective layer on the inner surface of the tubular supports. This fact can reduce the observed concentration polarization effects in the used membrane reactor, due to its operation mode (in-out), improving the permeation capacity during the reaction process.
- Adapt the ELP-PP deposition method for the Pd deposition onto flat supports, which would allow their integration in other types of devices.

5

Referencias

- [1] N. Grunewald, S. Klasen, I. Martínez-Zarzoso, C. Muris, The Trade-off Between Income Inequality and Carbon Dioxide Emissions, *Ecol. Econ.* 142 (2017) 249–256. doi:10.1016/j.ecolecon.2017.06.034.
- [2] I. Henriques, P. Sadorsky, Investor implications of divesting from fossil fuels, *Glob. Financ. J.* (2017). doi:<https://doi.org/10.1016/j.gfj.2017.10.004>.
- [3] C. Furlan, C. Mortarino, Forecasting the impact of renewable energies in competition with non-renewable sources, *Renew. Sustain. Energy Rev.* 81 (2018) 1879–1886. doi:<https://doi.org/10.1016/j.rser.2017.05.284>.
- [4] E.S. Hanley, J.P. Deane, B.P.Ó. Gallachóir, The role of hydrogen in low carbon energy futures—A review of existing perspectives, *Renew. Sustain. Energy Rev.* (2017). doi:<https://doi.org/10.1016/j.rser.2017.10.034>.
- [5] N. Muradov, Low to near-zero CO₂ production of hydrogen from fossil fuels: Status and perspectives, *Int. J. Hydrogen Energy.* 42 (2017) 14058–14088. doi:<https://doi.org/10.1016/j.ijhydene.2017.04.101>.
- [6] T. Abbasi, S.A. Abbasi, ‘Renewable’ hydrogen: Prospects and challenges, *Renew. Sustain. Energy Rev.* 15 (2011) 3034–3040. doi:<https://doi.org/10.1016/j.rser.2011.02.026>.
- [7] F.J. Vivas, A. De las Heras, F. Segura, J.M. Andújar, A review of energy management strategies for renewable hybrid energy systems with hydrogen backup, *Renew. Sustain. Energy Rev.* 82 (2018) 126–155. doi:<https://doi.org/10.1016/j.rser.2017.09.014>.
- [8] A. Valente, D. Iribarren, J. Dufour, Harmonised life-cycle global warming impact of renewable hydrogen, *J. Clean. Prod.* 149 (2017) 762–772. doi:<https://doi.org/10.1016/j.jclepro.2017.02.163>.
- [9] R. Li, Latest progress in hydrogen production from solar water splitting via photocatalysis, photoelectrochemical, and photovoltaic-photoelectrochemical solutions, *Chinese J. Catal.* 38 (2017) 5–12. doi:[https://doi.org/10.1016/S1872-2067\(16\)62552-4](https://doi.org/10.1016/S1872-2067(16)62552-4).
- [10] M. Moniruddin, B. Ilyassov, X. Zhao, E. Smith, T. Serikov, N. Ibrayev, R. Asmatulu, N. Nuraje, Recent progress on perovskite materials in photovoltaic and water splitting applications, *Mater. Today Energy.* (2017). doi:<https://doi.org/10.1016/j.mtener.2017.10.005>.
- [11] F. Rau, A. Herrmann, H. Krause, D. Fino, D. Trimis, Production of hydrogen by autothermal reforming of biogas, *Energy Procedia.* 120 (2017) 294–301. doi:<https://doi.org/10.1016/j.egypro.2017.07.218>.
- [12] S. Sengodan, R. Lan, J. Humphreys, D. Du, W. Xu, H. Wang, S. Tao, Advances in reforming and partial oxidation of hydrocarbons for hydrogen production and fuel cell applications, *Renew. Sustain. Energy Rev.* 82 (2018) 761–780. doi:<https://doi.org/10.1016/j.rser.2017.09.071>.
- [13] X. Li, A. Li, C.J. Lim, J.R. Grace, Hydrogen permeation through Pd-based composite membranes: Effects of porous substrate, diffusion barrier and sweep gas, *J. Memb. Sci.* 499 (2016) 143–155. doi:10.1016/j.memsci.2015.10.037.
- [14] C. Coutanceau, S. Baranton, T. Audichon, Chapter 2 - Hydrogen Production From Thermal Reforming BT - Hydrogen Electrochemical Production, in: *Hydrog. Energy Fuel Cells Prim.*, Academic Press, 2018: pp. 7–15. doi:<https://doi.org/10.1016/B978-0-12-811250-2.00002-9>.

Bibliografía

- [15] M.A. Hossain, J. Jewaratnam, P. Ganesan, Prospect of hydrogen production from oil palm biomass by thermochemical process – A review, *Int. J. Hydrogen Energy.* 41 (2016) 16637–16655. doi:<https://doi.org/10.1016/j.ijhydene.2016.07.104>.
- [16] S. Devasahayam, V. Strezov, Thermal Decomposition of Magnesium Carbonate with Biomass and Plastic Wastes for Simultaneous Production of Hydrogen and Carbon Avoidance, *J. Clean. Prod.* (2017). doi:<https://doi.org/10.1016/j.jclepro.2017.11.017>.
- [17] S. Tosti, C. Cavezza, M. Fabbricino, L. Pontoni, V. Palma, C. Ruocco, Production of hydrogen in a Pd-membrane reactor via catalytic reforming of olive mill wastewater, *Chem. Eng. J.* 275 (2015) 366–373. doi:[10.1016/j.cej.2015.04.001](https://doi.org/10.1016/j.cej.2015.04.001).
- [18] T. Tian, Q. Li, R. He, Z. Tan, Y. Zhang, Effects of biochemical composition on hydrogen production by biomass gasification, *Int. J. Hydrogen Energy.* 42 (2017) 19723–19732. doi:<https://doi.org/10.1016/j.ijhydene.2017.06.174>.
- [19] S. Zahedi, R. Solera, J.L. García-Morales, D. Sales, Effect of the addition of glycerol on hydrogen production from industrial municipal solid waste, *Fuel.* 180 (2016) 343–347. doi:<https://doi.org/10.1016/j.fuel.2016.04.063>.
- [20] A. Murugan, A.S. Brown, Review of purity analysis methods for performing quality assurance of fuel cell hydrogen, *Int. J. Hydrogen Energy.* 40 (2015) 4219–4233. doi:<https://doi.org/10.1016/j.ijhydene.2015.01.041>.
- [21] P. Pinacci, A. Basile, 3 – Palladium-based composite membranes for hydrogen separation in membrane reactors, in: *Handb. Membr. React.*, 2013: pp. 149–182. doi:[10.1533/9780857097330.1.149](https://doi.org/10.1533/9780857097330.1.149).
- [22] G. Di Marcoberardino, M. Binotti, G. Manzolini, J.L. Viviente, A. Arratibel, L. Roses, F. Gallucci, Achievements of European projects on membrane reactor for hydrogen production, *J. Clean. Prod.* 161 (2017) 1442–1450. doi:<https://doi.org/10.1016/j.jclepro.2017.05.122>.
- [23] H. Yin, A.C.K. Yip, A Review on the Production and Purification of Biomass-Derived Hydrogen Using Emerging Membrane Technologies, *Catal.* . 7 (2017). doi:[10.3390/catal7100297](https://doi.org/10.3390/catal7100297).
- [24] R. Dittmeyer, T. Boeltken, P. Piermartini, M. Selinsek, M. Loewert, F. Dallmann, H. Kreuder, M. Cholewa, A. Wunsch, M. Belimov, S. Farsi, P. Pfeifer, Micro and micro membrane reactors for advanced applications in chemical energy conversion, *Curr. Opin. Chem. Eng.* 17 (2017) 108–125. doi:<https://doi.org/10.1016/j.coche.2017.08.001>.
- [25] N.A. Al-Mufachi, N. V Rees, R. Steinberger-Wilkens, Hydrogen selective membranes: A review of palladium-based dense metal membranes, *Renew. Sustain. Energy Rev.* 47 (2015) 540–551. doi:<http://dx.doi.org/10.1016/j.rser.2015.03.026>.
- [26] N.D. Deveau, Y.H. Ma, R. Datta, Beyond Sieverts' law: A comprehensive microkinetic model of hydrogen permeation in dense metal membranes, *J. Memb. Sci.* 437 (2013) 298–311. doi:<http://dx.doi.org/10.1016/j.memsci.2013.02.047>.
- [27] S. Adhikari, S. Fernando, Hydrogen Membrane Separation Techniques, *Ind. Eng. Chem. Res.* 45 (2006) 875–881. doi:[10.1021/ie050644l](https://doi.org/10.1021/ie050644l).
- [28] M.R. Rahimpour, F. Samimi, A. Babapoor, T. Tohidian, S. Mohebi, Palladium membranes applications in reaction systems for hydrogen separation and purification: A review, *Chem. Eng. Process. Process Intensif.* 121 (2017) 24–49. doi:[10.1016/J.CEP.2017.07.021](https://doi.org/10.1016/J.CEP.2017.07.021).
- [29] D. Alique, D. Martinez-Díaz, R. Sanz, J.A. Calles, Review of supported pd-based

- membranes preparation by electroless plating for ultra-pure hydrogen production, *Membranes (Basel)*. 8 (2018) 1–39. doi:10.3390/membranes8010005.
- [30] H. Deville, L. Troost, Sur la permeabilité du fer à haute température, *Comptes Rendus*. 57 (1863) 965–967.
- [31] H. Deville, Note sur le passage des gaz au travers des corps solides homogènes, *Comptes Rendus*. 59 (1864) 102.
- [32] G. T, On the absorption and dialytic separation of gases by colloid septa, *Phil. Trans. Roy. Soc.* 156 (1866) 399–439.
- [33] Z.W. Dunbar, I.C. Lee, Effects of elevated temperatures and contaminated hydrogen gas mixtures on novel ultrathin palladium composite membranes, *Int. J. Hydrogen Energy*. 42 (2017) 29310–29319. doi:<https://doi.org/10.1016/j.ijhydene.2017.10.032>.
- [34] S. Yun, S. Ted Oyama, Correlations in palladium membranes for hydrogen separation: A review, *J. Memb. Sci.* 375 (2011) 28–45. doi:10.1016/j.memsci.2011.03.057.
- [35] A. Helmi, F. Gallucci, M. van Sint Annaland, Resource scarcity in palladium membrane applications for carbon capture in integrated gasification combined cycle units, *Int. J. Hydrogen Energy*. 39 (2014) 10498–10506. doi:<https://doi.org/10.1016/j.ijhydene.2014.05.009>.
- [36] V. Jayaraman, Y.S. Lin, Synthesis and hydrogen permeation properties of ultrathin palladium-silver alloy membranes, *J. Memb. Sci.* 104 (1995) 251–262. doi:[https://doi.org/10.1016/0376-7388\(95\)00040-J](https://doi.org/10.1016/0376-7388(95)00040-J).
- [37] S. Yun, J.H. Ko, S.T. Oyama, Ultrathin palladium membranes prepared by a novel electric field assisted activation, *J. Memb. Sci.* 369 (2011) 482–489. doi:<https://doi.org/10.1016/j.memsci.2010.12.015>.
- [38] T. Maneerung, K. Hidajat, S. Kawi, Ultra-thin (<1 μm) internally-coated Pd–Ag alloy hollow fiber membrane with superior thermal stability and durability for high temperature H₂ separation, *J. Memb. Sci.* 452 (2014) 127–142. doi:10.1016/j.memsci.2013.10.040.
- [39] J. Melendez, E. Fernandez, F. Gallucci, M. van Sint Annaland, P.L. Arias, D.A. Pacheco Tanaka, Preparation and characterization of ceramic supported ultra-thin (~1 μm) Pd–Ag membranes, *J. Memb. Sci.* 528 (2017) 12–23. doi:10.1016/j.memsci.2017.01.011.
- [40] J.L.C.S. Feitosa, A.G.B. da Cruz, A.C. Souza, F.P. Duda, Stress effects on hydrogen permeation through tubular multilayer membranes: Modeling and simulation, *Int. J. Hydrogen Energy*. 40 (2015) 17031–17037. doi:<https://doi.org/10.1016/j.ijhydene.2015.07.107>.
- [41] B. Dittmar, A. Behrens, N. Schödel, M. Rüttinger, T. Franco, G. Straczewski, R. Dittmeyer, Methane steam reforming operation and thermal stability of new porous metal supported tubular palladium composite membranes, *Int. J. Hydrogen Energy*. 38 (2013) 8759–8771. doi:<https://doi.org/10.1016/j.ijhydene.2013.05.030>.
- [42] J. Melendez, N. de Nooijer, K. Coenen, E. Fernandez, J.L. Viviente, M. van Sint Annaland, P.L. Arias, D.A.P. Tanaka, F. Gallucci, Effect of Au addition on hydrogen permeation and the resistance to H₂S on Pd–Ag alloy membranes, *J. Memb. Sci.* 542 (2017) 329–341. doi:10.1016/J.MEMSCI.2017.08.029.
- [43] H.W. Abu El Hawa, S.-T.B. Lundin, S.N. Paglieri, A. Harale, J. Douglas Way, The

Bibliografía

- influence of heat treatment on the thermal stability of Pd composite membranes, *J. Memb. Sci.* 494 (2015) 113–120. doi:10.1016/J.MEMSCI.2015.07.021.
- [44] S.-T.B. Lundin, N.S. Patki, T.F. Fuerst, C.A. Wolden, J.D. Way, Inhibition of hydrogen flux in palladium membranes by pressure-induced restructuring of the membrane surface, *J. Memb. Sci.* 535 (2017) 70–78. doi:10.1016/J.MEMSCI.2017.04.025.
- [45] A.I. Livshits, The hydrogen transport through the metal alloy membranes with a spatial variation of the alloy composition: Potential diffusion and enhanced permeation, *Int. J. Hydrogen Energy.* 42 (2017) 13111–13119. doi:<https://doi.org/10.1016/j.ijhydene.2017.04.016>.
- [46] E. Fernandez, A. Helmi, J.A. Medrano, K. Coenen, A. Arratibel, J. Melendez, N.C.A. de Nooijer, V. Spallina, J.L. Viviente, J. Zuñiga, M. van Sint Annaland, D.A. Pacheco Tanaka, F. Gallucci, Palladium based membranes and membrane reactors for hydrogen production and purification: An overview of research activities at Tecnalia and TU/e, *Int. J. Hydrogen Energy.* 42 (2017) 13763–13776. doi:10.1016/j.ijhydene.2017.03.067.
- [47] Y. Guo, H. Wu, X. Fan, L. Zhou, Q. Chen, Palladium composite membrane fabricated on rough porous alumina tube without intermediate layer for hydrogen separation, *Int. J. Hydrogen Energy.* 42 (2017) 9958–9965. doi:<https://doi.org/10.1016/j.ijhydene.2017.01.226>.
- [48] S. Nayebossadri, S. Fletcher, J.D. Speight, D. Book, Hydrogen permeation through porous stainless steel for palladium-based composite porous membranes, *J. Memb. Sci.* 515 (2016) 22–28. doi:10.1016/j.memsci.2016.05.036.
- [49] N. Itoh, E. Suga, T. Sato, Composite palladium membrane prepared by introducing metallic glue and its high durability below the critical temperature, *Sep. Purif. Technol.* 121 (2014) 46–53. doi:10.1016/J.SEPPUR.2013.05.055.
- [50] J.A. Calles, R. Sanz, D. Alique, L. Furones, P. Marín, S. Ordoñez, Influence of the selective layer morphology on the permeation properties for Pd-PSS composite membranes prepared by electroless pore-plating: Experimental and modeling study, *Sep. Purif. Technol.* 194 (2018) 10–18. doi:10.1016/J.SEPPUR.2017.11.014.
- [51] D.A.P. Tanaka, M.A.L. Tanco, J. Okazaki, Y. Wakui, F. Mizukami, T.M. Suzuki, Preparation of “pore-fill” type Pd–YSZ– γ -Al₂O₃ composite membrane supported on α -Al₂O₃ tube for hydrogen separation, *J. Memb. Sci.* 320 (2008) 436–441. doi:<http://dx.doi.org/10.1016/j.memsci.2008.04.044>.
- [52] R. Sanz, J.A. Calles, D. Alique, L. Furones, New synthesis method of Pd membranes over tubular {PSS} supports via “pore-plating” for hydrogen separation processes, *Int. J. Hydrogen Energy.* 37 (2012) 18476–18485. doi:<http://dx.doi.org/10.1016/j.ijhydene.2012.09.084>.
- [53] D.A. Pacheco, M.A. Llosa, S. Niwa, Y. Wakui, F. Mizukami, T. Namba, T.M. Suzuki, Preparation of palladium and silver alloy membrane on a porous α -alumina tube via simultaneous electroless plating, 247 (2005) 21–27. doi:10.1016/j.memsci.2004.06.002.
- [54] G. Zeng, A. Goldbach, L. Shi, H. Xu, On alloying and low-temperature stability of thin, supported PdAg membranes, *Int. J. Hydrogen Energy.* 37 (2012) 6012–6019. doi:10.1016/j.ijhydene.2011.12.126.
- [55] L. Zhao, A. Goldbach, C. Bao, H. Xu, Sulfur inhibition of PdCu membranes in the presence of external mass flow resistance, *J. Memb. Sci.* 496 (2015) 301–309.

- doi:10.1016/j.memsci.2015.08.046.
- [56] A.M. Tarditi, F. Braun, L.M. Cornaglia, Novel PdAgCu ternary alloy: Hydrogen permeation and surface properties, *Appl. Surf. Sci.* 257 (2011) 6626–6635. doi:10.1016/j.apsusc.2011.02.089.
- [57] H. Jia, P. Wu, G. Zeng, E. Salas-Colera, A. Serrano, G.R. Castro, H. Xu, C. Sun, A. Goldbach, High-temperature stability of Pd alloy membranes containing Cu and Au, *J. Memb. Sci.* 544 (2017) 151–160. doi:10.1016/j.memsci.2017.09.012.
- [58] S. Tosti, Supported and laminated Pd-based metallic membranes, *Int. J. Hydrogen Energy.* 28 (2003) 1445–1454. doi:10.1016/S0360-3199(03)00028-4.
- [59] K. Zhang, S.K. Gade, Ø. Hatlevik, J.D. Way, A sorption rate hypothesis for the increase in {H₂} permeability of palladium-silver (Pd–Ag) membranes caused by air oxidation, *Int. J. Hydrogen Energy.* 37 (2012) 583–593. doi:<http://dx.doi.org/10.1016/j.ijhydene.2011.09.078>.
- [60] S. Tosti, L. Bettinali, V. Violante, Rolled thin Pd and Pd–Ag membranes for hydrogen separation and production, *Int. J. Hydrogen Energy.* 25 (2000) 319–325. doi:10.1016/S0360-3199(99)00044-0.
- [61] S. Tosti, L. Bettinali, S. Castelli, F. Sarto, S. Scaglione, V. Violante, Sputtered, electroless, and rolled palladium-ceramic membranes, *J. Memb. Sci.* 196 (2002) 241–249. doi:10.1016/S0376-7388(01)00597-X.
- [62] T.A. Peters, T. Kaleta, M. Stange, R. Bredesen, Development of thin binary and ternary Pd-based alloy membranes for use in hydrogen production, *J. Memb. Sci.* 383 (2011) 124–134. doi:10.1016/j.memsci.2011.08.050.
- [63] J.A. Calles, R. Sanz, D. Alique, Influence of the type of siliceous material used as intermediate layer in the preparation of hydrogen selective palladium composite membranes over a porous stainless steel support, *Int. J. Hydrogen Energy.* 37 (2012) 6030–6042. doi:10.1016/j.ijhydene.2011.12.164.
- [64] T.A. Peters, M. Stange, R. Bredesen, 2 - Fabrication of palladium-based membranes by magnetron sputtering, in: A. Doukelis, K. Panopoulos, A. Koumanakos, E. Kakaras (Eds.), *Palladium Membr. Technol. Hydrol. Prod. Carbon Capture Other Appl.*, Woodhead Publishing, 2015: pp. 25–41. doi:<http://dx.doi.org/10.1533/9781782422419.1.25>.
- [65] L. Huang, C.S. Chen, Z.D. He, D.K. Peng, G.Y. Meng, Palladium membranes supported on porous ceramics prepared by chemical vapor deposition, *Thin Solid Films.* 302 (1997) 98–101. doi:[https://doi.org/10.1016/S0040-6090\(97\)00035-7](https://doi.org/10.1016/S0040-6090(97)00035-7).
- [66] C.-S. Jun, K.-H. Lee, Palladium and palladium alloy composite membranes prepared by metal-organic chemical vapor deposition method (cold-wall), *J. Memb. Sci.* 176 (2000) 121–130. doi:[https://doi.org/10.1016/S0376-7388\(00\)00438-5](https://doi.org/10.1016/S0376-7388(00)00438-5).
- [67] S.M. Lee, N. Xu, S.S. Kim, A. Li, J.R. Grace, C.J. Lim, T. Boyd, S.-K. Ryi, A. Susdorf, A. Schaad, Palladium/ruthenium composite membrane for hydrogen separation from the off-gas of solar cell production via chemical vapor deposition, *J. Memb. Sci.* 541 (2017) 1–8. doi:<https://doi.org/10.1016/j.memsci.2017.06.093>.
- [68] S.C. Chen, G.C. Tu, C.C.Y. Hung, C.A. Huang, M.H. Rei, Preparation of palladium membrane by electroplating on AISI 316L porous stainless steel supports and its use for methanol steam reformer, *J. Memb. Sci.* 314 (2008) 5–14. doi:<https://doi.org/10.1016/j.memsci.2007.12.066>.
- [69] C.-H. Chen, Y.-R. Huang, C.-W. Liu, K.-W. Wang, Preparation and modification of

Bibliografía

- PdAg membranes by electroless and electroplating process for hydrogen separation, *Thin Solid Films.* 618 (2016) 189–194. doi:<https://doi.org/10.1016/j.tsf.2016.04.049>.
- [70] K. Yoshii, Y. Oshino, N. Tachikawa, K. Toshima, Y. Katayama, Electrodeposition of palladium from palladium(II) acetylacetone in an amide-type ionic liquid, *Electrochim. Commun.* 52 (2015) 21–24. doi:<https://doi.org/10.1016/j.elecom.2015.01.003>.
- [71] R. Sanz, J.A. Calles, D. Alique, L. Furones, S. Ordóñez, P. Marín, P. Corengia, E. Fernandez, Preparation, testing and modelling of a hydrogen selective Pd/YSZ/SS composite membrane, *Int. J. Hydrogen Energy.* 36 (2011) 15783–15793. doi:[10.1016/j.ijhydene.2011.08.102](https://doi.org/10.1016/j.ijhydene.2011.08.102).
- [72] D. Alique, M. Imperatore, R. Sanz, J.A. Calles, M. Giacinti Baschetti, Hydrogen permeation in composite Pd-membranes prepared by conventional electroless plating and electroless pore-plating alternatives over ceramic and metallic supports, *Int. J. Hydrogen Energy.* 41 (2016) 19430–19438. doi:[10.1016/j.ijhydene.2016.06.128](https://doi.org/10.1016/j.ijhydene.2016.06.128).
- [73] S.-K. Ryi, S.-W. Lee, D.-K. Oh, B.-S. Seo, J.-W. Park, J.-S. Park, D.-W. Lee, S.S. Kim, Electroless plating of Pd after shielding the bottom of planar porous stainless steel for a highly stable hydrogen selective membrane, *J. Memb. Sci.* 467 (2014) 93–99. doi:[10.1016/j.memsci.2014.04.058](https://doi.org/10.1016/j.memsci.2014.04.058).
- [74] R. Sari, Z. Yaakob, M. Ismail, W.R.W. Daud, L. Hakim, Palladium–alumina composite membrane for hydrogen separator fabricated by combined sol–gel, and electroless plating technique, *Ceram. Int.* 39 (2013) 3211–3219. doi:<https://doi.org/10.1016/j.ceramint.2012.10.006>.
- [75] A.M. Tarditi, M.L. Bosko, L.M. Cornaglia, Electroless Plating of Pd Binary and Ternary Alloys and Surface Characteristics for Application in Hydrogen Separation, in: Elsevier, Oxford, 2017: pp. 1–24. doi:<https://doi.org/10.1016/B978-0-12-803581-8.09166-9>.
- [76] B. Zhang, Chapter 1 - History—From the Discovery of Electroless Plating to the Present BT - Amorphous and Nano Alloys Electroless Depositions, in: Elsevier, Oxford, 2016: pp. 3–48. doi:<https://doi.org/10.1016/B978-0-12-802685-4.00001-7>.
- [77] Z. Abdin, A. Zafaranloo, A. Rafiee, W. Mérida, W. Lipiński, K.R. Khalilpour, Hydrogen as an energy vector, *Renew. Sustain. Energy Rev.* 120 (2020) 109620. doi:<https://doi.org/10.1016/j.rser.2019.109620>.
- [78] F. Dawood, M. Anda, G.M. Shafiullah, Hydrogen production for energy: An overview, *Int. J. Hydrogen Energy.* 45 (2020) 3847–3869. doi:<https://doi.org/10.1016/j.ijhydene.2019.12.059>.
- [79] International partnership for hydrogen and fuel cells in the economy., (n.d.). <https://www.iphe.net/>.
- [80] Fuel Cells and Hydrogen Joint Undertaking, (n.d.). <https://www.fch.europa.eu>.
- [81] P. Hoffman, Hydrogen—the optimum chemical fuel, *Appl. Energy.* 47 (1994) 183–199. doi:[10.1016/0306-2619\(94\)90078-7](https://doi.org/10.1016/0306-2619(94)90078-7).
- [82] I. Staffell, D. Scamman, A. Velazquez Abad, P. Balcombe, P.E. Dodds, P. Ekins, N. Shah, K.R. Ward, The role of hydrogen and fuel cells in the global energy system, *Energy Environ. Sci.* 12 (2019) 463–491. doi:[10.1039/c8ee01157e](https://doi.org/10.1039/c8ee01157e).
- [83] A.M.K. Hassan Nazir, Cindrella Luis, Sujin Jose, Jyoti Prakash, Navaneethan Muthuswamy, Marthe Buan, Cristina Flox, Sai Chavan, Xuan Shi, Pertti Kauranen, Tanja Kallio, Gilberto Maia, Kaido Tammeveski, Nikolaos Lympertopoulos, Elena

- Carcadea, Emre Veziroglu, Alfr, Is the H₂ Economy realizable in the foreseeable future? Part I: H₂ Production Methods, *Int. J. Hydrogen Energy.* (2020) (in-press). doi:10.1016/j.ijhydene.2020.
- [84] A. Kumar, R. Singh, A.S.K. Sinha, Catalyst modification strategies to enhance the catalyst activity and stability during steam reforming of acetic acid for hydrogen production, *Int. J. Hydrogen Energy.* 44 (2019) 12983–13010. doi:10.1016/J.IJHYDENE.2019.03.136.
- [85] S. Shiva Kumar, V. Himabindu, Hydrogen production by PEM water electrolysis – A review, *Mater. Sci. Energy Technol.* 2 (2019) 442–454. doi:10.1016/J.MSET.2019.03.002.
- [86] J. Chi, H. Yu, Water electrolysis based on renewable energy for hydrogen production, *Chinese J. Catal.* 39 (2018) 390–394. doi:10.1016/S1872-2067(17)62949-8.
- [87] L. Barelli, G. Bidini, F. Gallorini, S. Servili, Hydrogen production through sorption-enhanced steam methane reforming and membrane technology: A review, *Energy.* 33 (2008) 554–570. doi:10.1016/J.ENERGY.2007.10.018.
- [88] T. da Silva Veras, T.S. Mozer, D. da Costa Rubim Messeder dos Santos, A. da Silva César, Hydrogen: Trends, production and characterization of the main process worldwide, *Int. J. Hydrogen Energy.* (2017). doi:10.1016/j.ijhydene.2016.08.219.
- [89] P. Nikolaidis, A. Poullikkas, A comparative overview of hydrogen production processes, *Renew. Sustain. Energy Rev.* 67 (2017) 597–611. doi:10.1016/J.RSER.2016.09.044.
- [90] Ram B. Gupta, *Hydrogen Fuel: Production, Transport, and Storage*, CRC Press, 2009.
- [91] R. Carapellucci, L. Giordano, Steam, dry and autothermal methane reforming for hydrogen production: A thermodynamic equilibrium analysis, *J. Power Sources.* 469 (2020) 228391. doi:10.1016/j.jpowsour.2020.228391.
- [92] V. Stenberg, M. Rydén, T. Mattisson, A. Lyngfelt, Exploring novel hydrogen production processes by integration of steam methane reforming with chemical-looping combustion (CLC-SMR) and oxygen carrier aided combustion (OCAC-SMR), *Int. J. Greenh. Gas Control.* 74 (2018) 28–39. doi:10.1016/J.IJGGC.2018.01.008.
- [93] J.R. Bartels, M.B. Pate, N.K. Olson, An economic survey of hydrogen production from conventional and alternative energy sources, *Int. J. Hydrogen Energy.* 35 (2010) 8371–8384. doi:10.1016/J.IJHYDENE.2010.04.035.
- [94] J. Chen, W. Xu, F. Zhang, H. Zuo, J. E, K. Wei, G. Liao, Y. Fan, Thermodynamic and environmental analysis of integrated supercritical water gasification of coal for power and hydrogen production, *Energy Convers. Manag.* 198 (2019) 111927. doi:10.1016/J.ENCONMAN.2019.111927.
- [95] Y. Yan, Y. Cui, L. Zhang, L. Li, J. Zhang, Y. Chen, Q. Tang, C. Lin, Experimental investigation of methane auto-thermal reforming in hydrogen-permeable membrane reactor for pure hydrogen production, *Int. J. Hydrogen Energy.* 41 (2016) 13069–13076. doi:10.1016/J.IJHYDENE.2016.06.076.
- [96] K. Damen, M. van Troost, A. Faaij, W. Turkenburg, A comparison of electricity and hydrogen production systems with CO₂ capture and storage. Part A: Review and selection of promising conversion and capture technologies, *Prog. Energy Combust. Sci.* 32 (2006) 215–246. doi:10.1016/J.PECS.2005.11.005.

Bibliografía

- [97] S. Thangalazhy-Gopakumar, S. Adhikari, R.B. Gupta, M. Tu, S. Taylor, Production of hydrocarbon fuels from biomass using catalytic pyrolysis under helium and hydrogen environments, *Bioresour. Technol.* 102 (2011) 6742–6749. doi:10.1016/J.BIORTech.2011.03.104.
- [98] N. Muradov, Hydrogen via methane decomposition: an application for decarbonization of fossil fuels, *Int. J. Hydrogen Energy.* 26 (2001) 1165–1175. doi:10.1016/S0360-3199(01)00073-8.
- [99] N. Muradov, Catalysis of methane decomposition over elemental carbon, *Catal. Commun.* 2 (2001) 89–94. doi:10.1016/S1566-7367(01)00013-9.
- [100] M. Nasir Uddin, W.M.A.W. Daud, H.F. Abbas, Potential hydrogen and non-condensable gases production from biomass pyrolysis: Insights into the process variables, *Renew. Sustain. Energy Rev.* 27 (2013) 204–224. doi:10.1016/j.rser.2013.06.031.
- [101] G.W. Huber, S. Iborra, A. Corma, Synthesis of Transportation Fuels from Biomass: Chemistry, Catalysts, and Engineering, *Chem. Rev.* 106 (2006) 4044–4098. doi:10.1021/cr068360d.
- [102] M. Mihet, M.D. Lazar, Methanation of CO₂ on Ni/γ-Al₂O₃: Influence of Pt, Pd or Rh promotion, *Catal. Today.* 306 (2018) 294–299. doi:10.1016/j.cattod.2016.12.001.
- [103] M.M. Jaffar, M.A. Nahil, P.T. Williams, Methane Production from the Pyrolysis–Catalytic Hydrogenation of Waste Biomass: Influence of Process Conditions and Catalyst Type, *Energy & Fuels.* 33 (2019) 7443–7457. doi:10.1021/acs.energyfuels.9b01524.
- [104] J. Ren, J.P. Cao, X.Y. Zhao, F.L. Yang, X.Y. Wei, Recent advances in syngas production from biomass catalytic gasification: A critical review on reactors, catalysts, catalytic mechanisms and mathematical models, *Renew. Sustain. Energy Rev.* 116 (2019) 109426. doi:10.1016/j.rser.2019.109426.
- [105] Y. Guo, Y. Jin, H. Wu, L. Zhou, Q. Chen, X. Zhang, X. Li, Preparation of palladium membrane on Pd/silicalite-1 zeolite particles modified macroporous alumina substrate for hydrogen separation, *Int. J. Hydrogen Energy.* 39 (2014) 21044–21052. doi:10.1016/j.ijhydene.2014.10.089.
- [106] A. Arregi, M. Amutio, G. Lopez, J. Bilbao, M. Olazar, Evaluation of thermochemical routes for hydrogen production from biomass: A review, *Energy Convers. Manag.* 165 (2018) 696–719. doi:10.1016/J.ENCONMAN.2018.03.089.
- [107] M. Shahabuddin, M.T. Alam, B.B. Krishna, T. Bhaskar, G. Perkins, A review on the production of renewable aviation fuels from the gasification of biomass and residual wastes, *Bioresour. Technol.* 312 (2020) 123596. doi:10.1016/j.biortech.2020.123596.
- [108] H.I. Villafán-Vidales, C.A. Arancibia-Bulnes, D. Riveros-Rosas, H. Romero-Paredes, C.A. Estrada, An overview of the solar thermochemical processes for hydrogen and syngas production: Reactors, and facilities, *Renew. Sustain. Energy Rev.* 75 (2017) 894–908. doi:10.1016/J.RSER.2016.11.070.
- [109] Y. Liu, R. Lin, Y. Man, J. Ren, Recent developments of hydrogen production from sewage sludge by biological and thermochemical process, *Int. J. Hydrogen Energy.* 44 (2019) 19676–19697. doi:10.1016/J.IJHYDENE.2019.06.044.
- [110] D. Alique, B. Giacomo, R. Sanz, J.A. Calles, S. Tosti, Ultra-Pure Hydrogen via Co-Valorization of Olive Mill Wastewater and Bioethanol in Pd-Membrane Reactors, *Processes.* 8 (2020) 219.

- [111] D. Iribarren, A. Susmozas, F. Petrakopoulou, J. Dufour, Environmental and exergetic evaluation of hydrogen production via lignocellulosic biomass gasification, *J. Clean. Prod.* 69 (2014) 165–175. doi:10.1016/J.JCLEPRO.2014.01.068.
- [112] C. Koroneos, A. Dompros, G. Roumbas, Hydrogen production via biomass gasification—A life cycle assessment approach, *Chem. Eng. Process. Process Intensif.* 47 (2008) 1261–1268. doi:10.1016/J.CEP.2007.04.003.
- [113] A. Demirbaş, Biomass resource facilities and biomass conversion processing for fuels and chemicals, *Energy Convers. Manag.* 42 (2001) 1357–1378. doi:10.1016/S0196-8904(00)00137-0.
- [114] P. Mishra, S. Krishnan, S. Rana, L. Singh, M. Sakinah, Z. Ab Wahid, Outlook of fermentative hydrogen production techniques: An overview of dark, photo and integrated dark-photo fermentative approach to biomass, *Energy Strateg. Rev.* 24 (2019) 27–37. doi:10.1016/J.ESR.2019.01.001.
- [115] H. Argun, F. Kargi, Bio-hydrogen production by different operational modes of dark and photo-fermentation: An overview, *Int. J. Hydrogen Energy.* 36 (2011) 7443–7459. doi:10.1016/J.IJHYDENE.2011.03.116.
- [116] K. Bolatkhan, B.D. Kossalbayev, B.K. Zayadan, T. Tomo, T.N. Veziroglu, S.I. Allakhverdiev, Hydrogen production from phototrophic microorganisms: Reality and perspectives, *Int. J. Hydrogen Energy.* 44 (2019) 5799–5811. doi:10.1016/J.IJHYDENE.2019.01.092.
- [117] M. Ni, D.Y.C. Leung, M.K.H. Leung, K. Sumathy, An overview of hydrogen production from biomass, *Fuel Process. Technol.* 87 (2006) 461–472. doi:10.1016/J.FUPROC.2005.11.003.
- [118] P.C. Hallenbeck, J.R. Benemann, Biological hydrogen production; fundamentals and limiting processes, *Int. J. Hydrogen Energy.* 27 (2002) 1185–1193. doi:10.1016/S0360-3199(02)00131-3.
- [119] A. Sánchez-Bayo, D. López-Chicharro, V. Morales, J.J. Espada, D. Puyol, F. Martínez, S. Astals, G. Vicente, L.F. Bautista, R. Rodríguez, Biodiesel and biogas production from Isochrysis galbana using dry and wet lipid extraction: A biorefinery approach, *Renew. Energy.* 146 (2020) 188–195. doi:<https://doi.org/10.1016/j.renene.2019.06.148>.
- [120] B.N. Lukyanov, D. V Andreev, V.N. Parmon, Catalytic reactors with hydrogen membrane separation, *Chem. Eng. J.* 154 (2009) 258–266. doi:<https://doi.org/10.1016/j.cej.2009.04.023>.
- [121] N. Ren, W. Guo, B. Liu, G. Cao, J. Ding, Biological hydrogen production by dark fermentation: challenges and prospects towards scaled-up production, *Curr. Opin. Biotechnol.* 22 (2011) 365–370. doi:10.1016/J.COPBIO.2011.04.022.
- [122] G. Kumar, S. Shobana, D. Nagarajan, D.-J. Lee, K.-S. Lee, C.-Y. Lin, C.-Y. Chen, J.-S. Chang, Biomass based hydrogen production by dark fermentation — recent trends and opportunities for greener processes, *Curr. Opin. Biotechnol.* 50 (2018) 136–145. doi:10.1016/J.COPBIO.2017.12.024.
- [123] D. Nagarajan, D.-J. Lee, A. Kondo, J.-S. Chang, Recent insights into biohydrogen production by microalgae – From biophotolysis to dark fermentation, *Bioresour. Technol.* 227 (2017) 373–387. doi:10.1016/J.BIORTECH.2016.12.104.
- [124] J. Jia, L.C. Seitz, J.D. Benck, Y. Huo, Y. Chen, J.W.D. Ng, T. Bilir, J.S. Harris, T.F. Jaramillo, Solar water splitting by photovoltaic-electrolysis with a solar-to-hydrogen efficiency over 30%, *Nat. Commun.* 7 (2016) 1–6. doi:10.1038/ncomms13237.

Bibliografía

- [125] G. Liu, Y. Sheng, J.W. Ager, M. Kraft, R. Xu, Research advances towards large-scale solar hydrogen production from water, *EnergyChem.* 1 (2019) 100014. doi:10.1016/J.ENCHEM.2019.100014.
- [126] Y. Zhang, L. Wang, N. Wang, L. Duan, Y. Zong, S. You, F. Maréchal, J. Van herle, Y. Yang, Balancing wind-power fluctuation via onsite storage under uncertainty: Power-to-hydrogen-to-power versus lithium battery, *Renew. Sustain. Energy Rev.* 116 (2019) 109465. doi:10.1016/J.RSER.2019.109465.
- [127] P.M. Diéguez, A. Ursúa, P. Sanchis, C. Sopena, E. Guelbenzu, L.M. Gandía, Thermal performance of a commercial alkaline water electrolyzer: Experimental study and mathematical modeling, *Int. J. Hydrogen Energy.* 33 (2008) 7338–7354. doi:10.1016/J.IJHYDENE.2008.09.051.
- [128] T. Wajda, K. Gabriel, Thermolysis reactor scale-up for pilot scale CuCl hybrid hydrogen production, *Int. J. Hydrogen Energy.* 44 (2019) 9779–9790. doi:10.1016/J.IJHYDENE.2018.11.187.
- [129] S.Z. Baykara, Experimental solar water thermolysis, *Int. J. Hydrogen Energy.* 29 (2004) 1459–1469. doi:10.1016/J.IJHYDENE.2004.02.011.
- [130] K.S. Joya, Y.F. Joya, K. Ocakoglu, R. van de Krol, Water-Splitting Catalysis and Solar Fuel Devices: Artificial Leaves on the Move, *Angew. Chemie Int. Ed.* 52 (2013) 10426–10437. doi:10.1002/anie.201300136.
- [131] S. Yu, X.B. Fan, X. Wang, J. Li, Q. Zhang, A. Xia, S. Wei, L.Z. Wu, Y. Zhou, G.R. Patzke, Efficient photocatalytic hydrogen evolution with ligand engineered all-inorganic InP and InP/ZnS colloidal quantum dots, *Nat. Commun.* 9 (2018) 1–10. doi:10.1038/s41467-018-06294-y.
- [132] I. Dincer, C. Acar, Review and evaluation of hydrogen production methods for better sustainability, *Int. J. Hydrogen Energy.* 40 (2015) 11094–11111. doi:10.1016/J.IJHYDENE.2014.12.035.
- [133] Y. Wang, X. Ma, B.S. Ghanem, F. Alghunaimi, I. Pinna, Y. Han, Polymers of intrinsic microporosity for energy-intensive membrane-based gas separations, *Mater. Today Nano.* 3 (2018) 69–95. doi:10.1016/j.mtnano.2018.11.003.
- [134] F. Gallucci, E. Fernandez, P. Corengia, M. van Sint Annaland, Recent advances on membranes and membrane reactors for hydrogen production, *Chem. Eng. Sci.* 92 (2013) 40–66. doi:10.1016/j.ces.2013.01.008.
- [135] S.S. Hashim, M.R. Somalu, K.S. Loh, S. Liu, W. Zhou, J. Sunarso, Perovskite-based proton conducting membranes for hydrogen separation: A review, *Int. J. Hydrogen Energy.* 43 (2018) 15281–15305. doi:10.1016/j.ijhydene.2018.06.045.
- [136] D. Alique, R. Sanz, J.A. Calles, 2 - Pd membranes by electroless pore-plating: synthesis and permeation behavior, in: A. Basile, F. Gallucci (Eds.), *Curr. Trends Futur. Dev. Membr.*, Elsevier, 2020: pp. 31–62. doi:<https://doi.org/10.1016/B978-0-12-818332-8.00002-8>.
- [137] S. Yolcular, Hydrogen recovery from methylcyclohexane as a chemical hydrogen carrier using a palladium membrane reactor, *Energy Sources, Part A Recover. Util. Environ. Eff.* 38 (2016) 2148–2152. doi:10.1080/15567036.2015.1030476.
- [138] M.B. Karimi, F. Mohammadi, K. Hooshyari, Recent approaches to improve Nafion performance for fuel cell applications: A review, *Int. J. Hydrogen Energy.* 44 (2019) 28919–28938. doi:10.1016/j.ijhydene.2019.09.096.
- [139] A. Iulianelli, I. Gatto, F. Trotta, M. Biasizzo, E. Passalacqua, A. Carbone, A.

- Bevilacqua, G. Clarizia, A. Gugliuzza, A. Basile, Electrochemical characterization of sulfonated PEEK-WC membranes for PEM fuel cells, *Int. J. Hydrogen Energy.* 38 (2013) 551–557. doi:10.1016/j.ijhydene.2012.07.115.
- [140] M. Usman, A. Ahmed, B. Yu, Q. Peng, Y. Shen, H. Cong, A review of different synthetic approaches of amorphous intrinsic microporous polymers and their potential applications in membrane-based gases separation, *Eur. Polym. J.* 120 (2019) 109262. doi:10.1016/j.eurpolymj.2019.109262.
- [141] T. Wang, Z. Liu, X. Xu, J. Zhu, G. Zhang, W. Jin, Insights into the design of nineteen-channel perovskite hollow fiber membrane and its oxygen transport behaviour, *J. Memb. Sci.* 595 (2020) 117600. doi:10.1016/j.memsci.2019.117600.
- [142] A. Paolone, D. Chandra, 9 - Amorphous metal membranes, in: A. Basile, F. Gallucci (Eds.), *Curr. Trends Futur. Dev. Membr.*, Elsevier, 2020: pp. 209–233. doi:<https://doi.org/10.1016/B978-0-12-818332-8.00009-0>.
- [143] D.A. [Pacheco Tanaka], J.A. Medrano, J.L. [Viviente Sole], F. Gallucci, 1 - Metallic membranes for hydrogen separation, in: A. Basile, F. Gallucci (Eds.), *Curr. Trends Futur. Dev. Membr.*, Elsevier, 2020: pp. 1–29. doi:<https://doi.org/10.1016/B978-0-12-818332-8.00001-6>.
- [144] S. Tosti, M. Fabbricino, L. Pontoni, V. Palma, C. Ruocco, Catalytic reforming of olive mill wastewater and methane in a Pd-membrane reactor, *Int. J. Hydrogen Energy.* 41 (2016) 5465–5474. doi:10.1016/j.ijhydene.2016.02.014.
- [145] S.Tosti, A.Adrover, A.Basile, V.Camilli, G.Chiappetta, V.Violante, Characterization of thin wall Pd–Ag rolled membranes, *Int. J. Hydrogen Energy.* 28 (2003) 105–112. doi:10.1016/S0360-3199(02)00034-4.
- [146] J.A. Calles, R. Sanz, D. Alique, L. Furones, Thermal stability and effect of typical water gas shift reactant composition on H₂ permeability through a Pd-YSZ-PSS composite membrane, *Int. J. Hydrogen Energy.* 39 (2014) 1398–1409. doi:10.1016/j.ijhydene.2013.10.168.
- [147] R. Sanz, J.A. Calles, D. Alique, L. Furones, H₂ production via water gas shift in a composite Pd membrane reactor prepared by the pore-plating method, *Int. J. Hydrogen Energy.* 39 (2014) 4739–4748. doi:10.1016/j.ijhydene.2013.12.145.
- [148] R. Sanz, J.A. Calles, D. Alique, L. Furones, S. Ordóñez, P. Marín, Hydrogen production in a Pore-Plated Pd-membrane reactor: Experimental analysis and model validation for the Water Gas Shift reaction, *Int. J. Hydrogen Energy.* 40 (2015) 3472–3484. doi:10.1016/j.ijhydene.2014.11.120.
- [149] H. Masuda, K. Nishio, N. Baba, Preparation of microporous metal membrane using two-step replication of interconnected structure of porous glass, *J. Mater. Sci. Lett.* 13 (1994) 0–1.
- [150] Y.S. Cheng, K.L. Yeung, Palladium-silver composite membranes by electroless plating technique, *J. Memb. Sci.* 158 (1999) 127–141. doi:10.1016/S0376-7388(99)00009-5.
- [151] A.S. Augustine, I.P. Mardilovich, N.K. Kazantzis, Y. Hua Ma, Durability of PSS-supported Pd-membranes under mixed gas and water-gas shift conditions, *J. Memb. Sci.* 415–416 (2012) 213–220. doi:10.1016/j.memsci.2012.05.001.
- [152] F. Roa, J. Douglas Way, R.L. McCormick, S.N. Paglieri, Preparation and characterization of Pd-Cu composite membranes for hydrogen separation, *Chem. Eng. J.* 93 (2003) 11–22. doi:10.1016/S1385-8947(02)00106-7.

Bibliografía

- [153] A.E. Lewis, D.C. Kershner, S.N. Paglieri, M.J. Slepicka, J.D. Way, Pd-Pt/YSZ composite membranes for hydrogen separation from synthetic water-gas shift streams, *J. Memb. Sci.* 437 (2013) 257–264. doi:10.1016/j.memsci.2013.02.056.
- [154] Seong Young Kong, Da Hye Kim, Dirk Henkensmeier, Hyoung-Juhn Kim, Hyung Chul Ham, Jonghee Han, Sung Pil Yoon, Chang Won Yoon, Sun Hee Choi, Ultrathin layered Pd/PBI-HFA composite membranes for hydrogen separation, *Sep. Purif. Technol.* 179 (2017) 486–493. doi:10.1016/J.SEPPUR.2017.02.033.
- [155] Da Hye Kim, Seong Young Kong, Geun-Hyuk Lee, Chang Won Yoon, Hyung Chul Ham, Jonghee Han, Kwang Ho Song, Dirk Henkensmeier, Sun Hee Choi, Effect of PBI-HFA surface treatments on Pd/PBI-HFA composite gas separation membranes, *Int. J. Hydrogen Energy.* 42 (2017) 22915–22924. doi:10.1016/J.IJHYDENE.2017.07.140.
- [156] Rajesh Kumar, Kamakshi, Manoj Kumar, Kamlendra Awasthi, Selective deposition of Pd nanoparticles in porous PET membrane for hydrogen separation, *Int. J. Hydrogen Energy.* 42 (2017) 15203–15210. doi:10.1016/J.IJHYDENE.2017.03.202.
- [157] D. Alique, Processing and Characterization of Coating and Thin Film Materials, in: J. Zhang, Y. Jung (Eds.), *Adv. Ceram. Met. Coat. Thin Film Mater. Energy Environ.*, 2018. doi:10.1007/978-3-319-59906-9.
- [158] A. Arratibel Plazaola, D. Pacheco Tanaka, M. Van Sint Annaland, F. Gallucci, Recent Advances in Pd-Based Membranes for Membrane Reactors, *Molecules.* 22 (2017) 51. doi:10.3390/molecules22010051.
- [159] H. Li, A. Caravella, H.Y. Xu, Recent progress in Pd-based composite membranes, *J. Mater. Chem. A.* 4 (2016) 14069–14094. doi:10.1039/C6TA05380G.
- [160] I.P. Mardilovich, E. Engwall, Y.H. Ma, Dependence of hydrogen flux on the pore size and plating surface topology of asymmetric Pd-porous stainless steel membranes, *Desalination.* 144 (2002) 85–89. doi:10.1016/S0011-9164(02)00293-X.
- [161] A. Tarditi, C. Gerboni, L. Cornaglia, PdAu membranes supported on top of vacuum-assisted ZrO₂-modified porous stainless steel substrates, *J. Memb. Sci.* 428 (2013) 1–10. doi:10.1016/j.memsci.2012.10.029.
- [162] C. Chen, Y.H. Ma, The effect of H₂S on the performance of Pd and Pd / Au composite membrane, *J. Memb. Sci.* 362 (2010) 535–544. doi:10.1016/j.memsci.2010.07.002.
- [163] E. Fernandez, A. Helmi, K. Coenen, J. Melendez, J.L. Viviente, D.A. Pacheco Tanaka, M. van Sint Annaland, F. Gallucci, Development of thin Pd–Ag supported membranes for fluidized bed membrane reactors including WGS related gases, *Int. J. Hydrogen Energy.* 40 (2015) 3506–3519. doi:10.1016/J.IJHYDENE.2014.08.074.
- [164] S. James F, A. William, Materials Science Engineering Hand Book, Third edit, Boca Raton, 2001.
- [165] S.K. Ryi, N. Xu, A. Li, C.J. Lim, J.R. Grace, Electroless Pd membrane deposition on alumina modified porous Hastelloy substrate with EDTA-free bath, *Int. J. Hydrogen Energy.* 35 (2010) 2328–2335. doi:10.1016/j.ijhydene.2010.01.054.
- [166] E. Fernandez, J.A. Medrano, J. Melendez, M. Parco, J.L. Viviente, M. van Sint Annaland, D.A. Pacheco Tanaka, Preparation and characterization of metallic supported thin Pd–Ag membranes for hydrogen separation, *Chem. Eng. J.* 305 (2016) 182–190. doi:10.1016/J.CEJ.2015.09.119.
- [167] S.K. Ryi, H.S. Ahn, J.S. Park, D.W. Kim, Pd-Cu alloy membrane deposited on CeO₂

- modified porous nickel support for hydrogen separation, *Int. J. Hydrogen Energy.* 39 (2014) 4698–4703. doi:10.1016/j.ijhydene.2013.11.031.
- [168] D. Zhang, S. Zhou, Y. Fan, N. Xu, Y. He, Preparation of dense Pd composite membranes on porous Ti-Al alloy supports by electroless plating, *J. Memb. Sci.* 387–388 (2012) 24–29. doi:10.1016/j.memsci.2011.10.004.
- [169] S.S. Kim, N. Xu, A. Li, J.R. Grace, C.J. Lim, S.K. Ryi, Development of a new porous metal support based on nickel and its application for Pd based composite membranes, *Int. J. Hydrogen Energy.* 40 (2015) 3520–3527. doi:10.1016/j.ijhydene.2014.08.075.
- [170] A. Kulprathipanja, G.O. Alptekin, J.L. Falconer, J.D. Way, Pd and Pd-Cu membranes: Inhibition of H₂ permeation by H₂S, *J. Memb. Sci.* 254 (2005) 49–62. doi:10.1016/j.memsci.2004.11.031.
- [171] J. Okazaki, D.A. Pacheco Tanaka, M.A. Llosa Tanco, Y. Wakui, T. Ikeda, F. Mizukami, T.M. Suzuki, Preparation and Hydrogen Permeation Properties of Thin Pd-Au Alloy Membranes Supported on Porous α -Alumina Tube, *Mater. Trans.* 49 (2008) 449–452. doi:10.2320/matertrans.MBW200720.
- [172] W.P. Wang, S. Thomas, X.L. Zhang, X.L. Pan, W.S. Yang, G.X. Xiong, H₂/N₂ gaseous mixture separation in dense Pd/ α -Al₂O₃ hollow fiber membranes: Experimental and simulation studies, *Sep. Purif. Technol.* 52 (2006) 177–185. doi:10.1016/j.seppur.2006.04.007.
- [173] B.K.R. Nair, J. Choi, M.P. Harold, Electroless plating and permeation features of Pd and Pd/Ag hollow fiber composite membranes, *J. Memb. Sci.* 288 (2007) 67–84. doi:10.1016/j.memsci.2006.11.006.
- [174] M. Incelli, A. Santucci, S. Tosti, M. Sansovini, M. Carlini, Heavy water decontamination tests through a Pd-Ag membrane reactor: Water Gas Shift and Isotopic Swamping performances, *Fusion Eng. Des.* 124 (2016) 692–695. doi:10.1016/j.fusengdes.2017.06.021.
- [175] C. Yu, H. Xu, An efficient palladium membrane reactor to increase the yield of styrene in ethylbenzene dehydrogenation, *Sep. Purif. Technol.* 78 (2011) 249–252. doi:10.1016/j.seppur.2011.01.040.
- [176] A. Brunetti, A. Caravella, E. Fernandez, D.A. Pacheco Tanaka, F. Gallucci, E. Drioli, E. Curcio, J.L. Viviente, G. Barbieri, Syngas upgrading in a membrane reactor with thin Pd-alloy supported membrane, *Int. J. Hydrogen Energy.* 40 (2015) 10883–10893. doi:10.1016/j.ijhydene.2015.07.002.
- [177] M.A. Rahman, F.R. García-García, K. Li, Development of a catalytic hollow fibre membrane microreactor as a microreformer unit for automotive application, *J. Memb. Sci.* 390–391 (2012) 68–75. doi:10.1016/j.memsci.2011.11.009.
- [178] P.P. Mardilovich, Y. She, Y.H. Ma, M.-H. Rei, Defect-free palladium membranes on porous stainless-steel support, *AIChE J.* 44 (1998) 310–322. doi:10.1002/aic.690440209.
- [179] A. Li, J. R. Grace, C.J. Lim, Preparation of thin Pd-based composite membrane on planar metallic substrate: Part I: Pre-treatment of porous stainless steel substrate, *J. Memb. Sci.* 298 (2007) 175–181. doi:10.1016/j.memsci.2007.04.016.
- [180] V. Jayaraman, Y.S. Lin, M. Pakala, R.Y. Lin, Fabrication of ultrathin metallic membranes on ceramic supports by sputter deposition, *J. Memb. Sci.* 99 (1995) 89–100. doi:10.1016/0376-7388(94)00212-H.
- [181] S.-K. Ryi, J.-S. Park, S.-H. Kim, D.-W. Kim, K.-I. Cho, Formation of a defect-free

Bibliografía

- Pd–Cu–Ni ternary alloy membrane on a polished porous nickel support (PNS), *J. Memb. Sci.* 318 (2008) 346–354. doi:10.1016/j.memsci.2008.02.055.
- [182] P. Pinacci, F. Drago, Influence of the support on permeation of palladium composite membranes in presence of sweep gas, *Catal. Today.* 193 (2012) 186–193. doi:10.1016/j.cattod.2012.02.041.
- [183] S.-K. Ryu, J.-S. Park, K.-R. Hwang, C.-B. Lee, S.-W. Lee, Repair of Pd-based composite membrane by polishing treatment, 2011. doi:10.1016/j.ijhydene.2011.07.120.
- [184] N. Jemaa, J. Shu, S. Kaliaguine, B.P.A. Grandjean, Thin Palladium Film Formation on Shot Peening Modified Porous Stainless Steel Substrates, *Ind. Eng. Chem. Res.* 35 (1996) 973–977. doi:10.1021/ie950437t.
- [185] Y. Huang, R. Dittmeyer, Preparation of thin palladium membranes on a porous support with rough surface, *J. Memb. Sci.* 302 (2007) 160–170. doi:10.1016/j.memsci.2007.06.040.
- [186] Huang Y., Li X., Fan Y., Xu N., Palladium-based composite membranes: principle, preparation and characterization, *Prog. Chem.* 18 (2006) 230–238.
- [187] J.P. Collins, J.D. Way, Catalytic decomposition of ammonia in a membrane reactor, *J. Memb. Sci.* 96 (1994) 259–274. doi:[http://dx.doi.org/10.1016/0376-7388\(94\)00138-3](http://dx.doi.org/10.1016/0376-7388(94)00138-3).
- [188] Y. Huang, S. Shu, Z. Lu, Y. Fan, Characterization of the adhesion of thin palladium membranes supported on tubular porous ceramics, *Thin Solid Films.* 515 (2007) 5233–5240. doi:<http://dx.doi.org/10.1016/j.tsf.2006.12.182>.
- [189] J. Coronas, J. Santamaría, Catalytic reactors based on porous ceramic membranes, *Catal. Today.* 51 (1999) 377–389. doi:10.1016/S0920-5861(99)00090-5.
- [190] J. Tong, Y. Matsumura, H. Suda, K. Haraya, Thin and dense Pd/CeO₂/MPSS composite membrane for hydrogen separation and steam reforming of methane, *Sep. Purif. Technol.* 46 (2005) 1–10. doi:10.1016/J.SEPPUR.2005.03.011.
- [191] A. Qiao, K. Zhang, Y. Tian, L. Xie, H. Luo, Y.S. Lin, Y. Li, Hydrogen separation through palladium–copper membranes on porous stainless steel with sol–gel derived ceria as diffusion barrier, *Fuel.* 89 (2010) 1274–1279. doi:10.1016/J.FUEL.2009.12.006.
- [192] D. Wang, J. Tong, H. Xu, Y. Matsumura, Preparation of palladium membrane over porous stainless steel tube modified with zirconium oxide, *Catal. Today.* 93–95 (2004) 689–693. doi:<http://dx.doi.org/10.1016/j.cattod.2004.06.060>.
- [193] H. Gao, J.Y. S. Lin, Y. Li, B. Zhang, Electroless plating synthesis, characterization and permeation properties of Pd–Cu membranes supported on ZrO₂ modified porous stainless steel, *J. Memb. Sci.* 265 (2005) 142–152. doi:10.1016/j.memsci.2005.04.050.
- [194] C.-B. Lee, S.-W. Lee, J.-S. Park, S.-K. Ryu, D.-W. Lee, K.-R. Hwang, S.-H. Kim, Ceramics used as intermetallic diffusion barriers in Pd-based composite membranes sputtered on porous nickel supports, *J. Alloys Compd.* 578 (2013) 425–430. doi:10.1016/j.jallcom.2013.06.007.
- [195] K. Zhang, H. Gao, Z. Rui, P. Liu, Y. Li, Y.S. Lin, High-Temperature Stability of Palladium Membranes on Porous Metal Supports with Different Intermediate Layers, *Ind. Eng. Chem. Res.* 48 (2009) 1880–1886. doi:10.1021/ie801417w.
- [196] D. Yepes, L.M. Cornaglia, S. Irusta, E.A. Lombardo, Different oxides used as

- diffusion barriers in composite hydrogen permeable membranes, *J. Memb. Sci.* 274 (2006) 92–101. doi:<http://dx.doi.org/10.1016/j.memsci.2005.08.003>.
- [197] A. Li, J.R. Grace, C.J. Lim, Preparation of thin Pd-based composite membrane on planar metallic substrate: Part II. Preparation of membranes by electroless plating and characterization, *J. Memb. Sci.* 306 (2007) 159–165. doi:<http://dx.doi.org/10.1016/j.memsci.2007.08.042>.
- [198] M. Broglia, P. Pinacci, M. Radaelli, A. Bottino, G. Capannelli, A. Comite, G. Vanacore, M. Zani, Synthesis and characterization of Pd membranes on alumina-modified porous stainless steel supports, *Desalination*. 245 (2009) 508–515. doi:[10.1016/j.desal.2009.01.004](https://doi.org/10.1016/j.desal.2009.01.004).
- [199] Y.-H. Chi, P.-S. Yen, M.-S. Jeng, S.-T. Ko, T.-C. Lee, Preparation of thin Pd membrane on porous stainless steel tubes modified by a two-step method, *Int. J. Hydrogen Energy*. 35 (2010) 6303–6310. doi:[10.1016/j.ijhydene.2010.03.066](https://doi.org/10.1016/j.ijhydene.2010.03.066).
- [200] S.-E. Nam, K.-H. Lee, Hydrogen separation by Pd alloy composite membranes: introduction of diffusion barrier, *J. Memb. Sci.* 192 (2001) 177–185. doi:[10.1016/S0376-7388\(01\)00499-9](https://doi.org/10.1016/S0376-7388(01)00499-9).
- [201] T. Van Gestel, F. Hauler, M. Bram, W.A. Meulenberg, H.P. Buchkremer, T. Van Gestel, F. Hauler, M. Bram, W.A. Meulenberg, H.P. Buchkremer, Synthesis and characterization of hydrogen-selective sol-gel SiO₂ membranes supported on ceramic and stainless steel supports, *Sep. Purif. Technol.* 121 (2014) 20–29. doi:<http://dx.doi.org/10.1016/j.seppur.2013.10.035>.
- [202] M. Kanezashi, D. Fuchigami, T. Yoshioka, T. Tsuru, Control of Pd dispersion in sol-gel-derived amorphous silica membranes for hydrogen separation at high temperatures, *J. Memb. Sci.* 439 (2013) 78–86. doi:<http://dx.doi.org/10.1016/j.memsci.2013.03.037>.
- [203] L. Zheng, H. Li, T. Xu, F. Bao, H. Xu, Defect size analysis approach combined with silicate gel/ceramic particles for defect repair of Pd composite membranes, *Int. J. Hydrogen Energy*. 41 (2016) 18522–18532. doi:[10.1016/j.ijhydene.2016.08.169](https://doi.org/10.1016/j.ijhydene.2016.08.169).
- [204] M.L. Bosko, F.Ojeda, E.A. Lombardo, L.M. Cornaglia, NaA zeolite as an effective diffusion barrier in composite Pd/PSS membranes, *J. Memb. Sci.* 331 (2009) 57–65. doi:[10.1016/j.memsci.2009.01.005](https://doi.org/10.1016/j.memsci.2009.01.005).
- [205] M. Dehghani Mobarake, P. Jafari, M. Irani, Preparation of Pd-based membranes on Pd/TiO₂ modified NaX/PSS substrate for hydrogen separation: Design and optimization, *Microporous Mesoporous Mater.* 226 (2016) 369–377. doi:[10.1016/j.micromeso.2016.02.022](https://doi.org/10.1016/j.micromeso.2016.02.022).
- [206] J. Yu, C. Qi, J. Zhang, C. Bao, H. Xu, Synthesis of a zeolite membrane as a protective layer on a metallic Pd composite membrane for hydrogen purification, *J. Mater. Chem. A*. 3 (2015) 5000–5006. doi:[10.1039/C4TA06463A](https://doi.org/10.1039/C4TA06463A).
- [207] K. Sato, M. Natsui, Y. Hasegawa, Preparation of Double Layer Membrane Combined with Palladium Metal and FAU Zeolite for Catalytic Membrane Reactor, *Mater. Trans.* 56 (2015) 473–478. doi:[10.2320/matertrans.MF201402](https://doi.org/10.2320/matertrans.MF201402).
- [208] X. Wang, X. Tan, B. Meng, X. Zhang, Q. Liang, H. Pan, S. Liu, TS-1 zeolite as an effective diffusion barrier for highly stable Pd membrane supported on macroporous [small alpha]-Al₂O₃ tube, *RSC Adv.* 3 (2013) 4821–4834. doi:[10.1039/C3RA23086D](https://doi.org/10.1039/C3RA23086D).
- [209] S. Abate, U. Díaz, A. Prieto, S. Gentiluomo, M. Palomino, S. Perathoner, A. Corma, G. Centi, Influence of Zeolite Protective Overlayer on the Performances of Pd Thin

Bibliografía

- Film Membrane on Tubular Asymmetric Alumina Supports, *Ind. Eng. Chem. Res.* 55 (2016) 4948–4959. doi:10.1021/acs.iecr.6b00690.
- [210] Y.H. Ma, P.P. Mardilovich, Y. She, Hydrogen gas-extraction module and method of fabrication, (2000).
- [211] F. Guazzone, E.E. Engwall, Y.H. Ma, Effects of surface activity, defects and mass transfer on hydrogen permeance and n-value in composite palladium-porous stainless steel membranes, *Catal. Today.* 118 (2006) 24–31. doi:<http://dx.doi.org/10.1016/j.cattod.2005.12.010>.
- [212] C. Mateos-Pedrero, M.A. Soria, I. Rodríguez-Ramos, A. Guerrero-Ruiz, Modifications of porous stainless steel previous to the synthesis of Pd membranes, in: *Stud. Surf. Sci. Catal.*, 2010: pp. 779–783. doi:10.1016/S0167-2991(10)75159-4.
- [213] S.-E. Nam, K.-H. Lee, Preparation and Characterization of Palladium Alloy Composite Membranes with a Diffusion Barrier for Hydrogen Separation, *Ind. Eng. Chem. Res.* 44 (2005) 100–105. doi:10.1021/ie040025x.
- [214] M.E. Ayturk, I.P. Mardilovich, E.E. Engwall, Y.H. Ma, Synthesis of composite Pd-porous stainless steel (PSS) membranes with a Pd/Ag intermetallic diffusion barrier, *J. Memb. Sci.* 285 (2006) 385–394. doi:10.1016/j.memsci.2006.09.008.
- [215] J.-H. Lee, J.-Y. Han, K.-M. Kim, S.-K. Ryi, D.-W. Kim, Development of homogeneous Pd–Ag alloy membrane formed on porous stainless steel by multi-layered films and Ag-upfilling heat treatment, *J. Memb. Sci.* 492 (2015) 242–248. doi:10.1016/j.memsci.2015.04.029.
- [216] M. Pujari, A. Agarwal, R. Uppaluri, A. Verma, Role of electroless nickel diffusion barrier on the combinatorial plating characteristics of dense Pd/Ni/PSS composite membranes, *Appl. Surf. Sci.* 305 (2014) 658–664. doi:10.1016/j.apsusc.2014.03.156.
- [217] J. Tong, H. Suda, K. Haraya, Y. Matsumura, A novel method for the preparation of thin dense Pd membrane on macroporous stainless steel tube filter, *J. Memb. Sci.* 260 (2005) 10–18. doi:10.1016/j.memsci.2005.03.016.
- [218] J. Tong, L. Su, K. Haraya, H. Suda, Thin Pd membrane on α -Al₂O₃ hollow fiber substrate without any interlayer by electroless plating combined with embedding Pd catalyst in polymer template, *J. Memb. Sci.* 310 (2008) 93–101. doi:10.1016/j.memsci.2007.10.053.
- [219] X. Hu, W. Chen, Y. Huang, Fabrication of Pd/ceramic membranes for hydrogen separation based on low-cost macroporous ceramics with pencil coating, *Int. J. Hydrogen Energy.* 35 (2010) 7803–7808. doi:10.1016/j.ijhydene.2010.05.102.
- [220] H.-B. Zhao, K. Pflanz, J.-H. Gu, A.-W. Li, N. Stroh, H. Brunner, G.-X. Xiong, Preparation of palladium composite membranes by modified electroless plating procedure, *J. Memb. Sci.* 142 (1998) 147–157. doi:[http://dx.doi.org/10.1016/S0376-7388\(97\)00287-1](http://dx.doi.org/10.1016/S0376-7388(97)00287-1).
- [221] A. Bottino, M. Broglia, G. Capannelli, A. Comite, P. Pinacci, M. Scrinari, F. Azzurri, Sol-gel synthesis of thin alumina layers on porous stainless steel supports for high temperature palladium membranes, *Int. J. Hydrogen Energy.* 39 (2014) 4717–4724. doi:10.1016/j.ijhydene.2013.11.096.
- [222] S. Tosti, A. Basile, L. Bettinali, F. Borgognoni, F. Gallucci, C. Rizzello, Design and process study of Pd membrane reactors, *Int. J. Hydrogen Energy.* 33 (2008) 5098–5105. doi:10.1016/j.ijhydene.2008.05.031.

- [223] S.T. D. Alique, G. Bruni, R. Sanz, J.A. Calles, Ultra-Pure Hydrogen via Co-Valorization of Olive MillWastewater and Bioethanol in Pd-Membrane Reactors, *Processes*. 8 (2020) 219–235. doi:10.3390/pr8020219.
- [224] M. Nomura, Y. Nishi, T. Sakanishi, K. Utsumi, R. Nakamura, Preparation of thin Li₄SiO₄ membranes by using a CVD method, *Energy Procedia*. 37 (2013) 1012–1019. doi:10.1016/j.egypro.2013.05.197.
- [225] M.F. Ashby, D.R.H. Jones, *Engineering Materials: An Introduction to Microstructures, Processing and Design* (vol. 2), second edi, n.d.
- [226] N. Pal, M. Agarwal, K. Maheshwari, Y.S. Solanki, A review on types, fabrication and support material of hydrogen separation membrane, *Mater. Today Proc.* 28 (2020) 1386–1391. doi:10.1016/j.matpr.2020.04.806.
- [227] M. Amanipour, E. Ganji Babakhani, A. Safekordi, A. Zamaniyan, M. Heidari, Effect of CVD parameters on hydrogen permeation properties in a nano-composite SiO₂-Al₂O₃ membrane, *J. Memb. Sci.* 423–424 (2012) 530–535. doi:10.1016/j.memsci.2012.09.007.
- [228] R. Schelfhout, K. Strijckmans, D. Depla, Sputter yield measurements to evaluate the target state during reactive magnetron sputtering, *Surf. Coatings Technol.* 399 (2020) 126097. doi:10.1016/j.surcoat.2020.126097.
- [229] I. Bieloshapka, P. Jiricek, Y. Yakovlev, K. Hruska, E. Tomsik, Thermal and chemical activation methods applied to DFAFC anodes prepared by magnetron sputtering, *Int. J. Hydrogen Energy*. (2020) 1–12. doi:10.1016/j.ijhydene.2020.03.116.
- [230] J. O'Brien, R. Hughes, J. Hisek, Pd/Ag membranes on porous alumina substrates by unbalanced magnetron sputtering, *Surf. Coatings Technol.* 142–144 (2001) 253–259. doi:10.1016/S0257-8972(01)01198-7.
- [231] J.F. Shackelford, W. Alexander, *Materials Science and Engineering Handbook*, Third edit, 2001.
- [232] B. A., R. G., Nickel plating on steel by chemical reduction, *J. Res. Nat. Bur. Std.* 37 (1946) 31–34.
- [233] B. Zornoza, C. Casado, A. Navajas, Chapter 11 - Advances in Hydrogen Separation and Purification with Membrane Technology, in: L.M. Gandía, G. Arzamendi, P.M. Diéguez (Eds.), *Renew. Hydrot. Technol.*, Elsevier, Amsterdam, 2013: pp. 245–268. doi:<http://dx.doi.org/10.1016/B978-0-444-56352-1.00011-8>.
- [234] M. De Falco, G. Iaquaniello, E. Palo, B. Cucchiella, V. Palma, P. Ciambelli, 11 - Palladium-based membranes for hydrogen separation: preparation, economic analysis and coupling with a water gas shift reactor, in: A. Basile (Ed.), *Handb. Membr. React.*, Woodhead Publishing, 2013: pp. 456–486. doi:<http://dx.doi.org/10.1533/9780857097347.2.456>.
- [235] M.J. den Exter, 3 - The use of electroless plating as a deposition technology in the fabrication of palladium-based membranes, in: A. Doukelis, K. Panopoulos, A. Koumanakos, E. Kakaras (Eds.), *Palladium Membr. Technol. Hydrot. Prod. Carbon Capture Other Appl.*, Woodhead Publishing, 2015: pp. 43–67. doi:<http://dx.doi.org/10.1533/9781782422419.1.43>.
- [236] A. Basile, J. Tong, P. Millet, 2 - Inorganic membrane reactors for hydrogen production: an overview with particular emphasis on dense metallic membrane materials, in: A. Basile (Ed.), *Handb. Membr. React.*, Woodhead Publishing, 2013: pp. 42–148. doi:<http://dx.doi.org/10.1533/9780857097330.1.42>.

Bibliografía

- [237] Y.S. Cheng, K.L. Yeung, Effects of electroless plating chemistry on the synthesis of palladium membranes, *J. Memb. Sci.* 182 (2001) 195–203. doi:[http://dx.doi.org/10.1016/S0376-7388\(00\)00563-9](http://dx.doi.org/10.1016/S0376-7388(00)00563-9).
- [238] M. Dogan, S. Kilicarslan, Effects of process parameters on the synthesis of palladium membranes, *Nucl. Instruments Methods Phys. Res. Sect. B Beam Interact. with Mater. Atoms.* 266 (2008) 3458–3466. doi:<https://doi.org/10.1016/j.nimb.2008.05.011>.
- [239] K.L. Yeung, S.C. Christiansen, A. Varma, Palladium composite membranes by electroless plating technique: Relationships between plating kinetics, film microstructure and membrane performance, *J. Memb. Sci.* 159 (1999) 107–122. doi:[https://doi.org/10.1016/S0376-7388\(99\)00041-1](https://doi.org/10.1016/S0376-7388(99)00041-1).
- [240] S.S. Djokić, Fundamentals of Electroless Deposition BT - Reference Module in Chemistry, Molecular Sciences and Chemical Engineering, in: Elsevier, 2016. doi:<https://doi.org/10.1016/B978-0-12-409547-2.11701-9>.
- [241] M. G.O., H. J.B., Electroless plating: fundamentals and applications, American Electroplaters and Surface Finishers Society, 1990.
- [242] J. Shu, B.P.A. Grandjean, E. Ghali, S. Kaliaguine, Simultaneous deposition of Pd and Ag on porous stainless steel by electroless plating, *J. Memb. Sci.* 77 (1993) 181–195. doi:[http://dx.doi.org/10.1016/0376-7388\(93\)85068-8](http://dx.doi.org/10.1016/0376-7388(93)85068-8).
- [243] K.S. Rothenberger, A. V Cugini, B.H. Howard, R.P. Killmeyer, M. V Ciocco, B.D. Morreale, R.M. Enick, F. Bustamante, I.P. Mardilovich, Y.H. Ma, High pressure hydrogen permeance of porous stainless steel coated with a thin palladium film via electroless plating, *J. Memb. Sci.* 244 (2004) 55–68. doi:<http://dx.doi.org/10.1016/j.memsci.2004.06.036>.
- [244] S.N. Paglieri, J.D. Way, INNOVATIONS IN PALLADIUM MEMBRANE RESEARCH, *Sep. Purif. Methods.* 31 (2002) 1–169. doi:<10.1081/SPM-120006115>.
- [245] L. Wei, J. Yu, X. Hu, R. Wang, Y. Huang, Effects of Sn residue on the high temperature stability of the H₂-permeable palladium membranes prepared by electroless plating on Al₂O₃ substrate after SnCl₂–PdCl₂ process: A case study, *Chinese J. Chem. Eng.* 24 (2016) 1154–1160. doi:<http://dx.doi.org/10.1016/j.cjche.2016.04.008>.
- [246] Y.-H. Chi, J.-Y. Uan, M.-C. Lin, Y.-L. Lin, J.-H. Huang, Preparation of a novel Pd/layered double hydroxide composite membrane for hydrogen filtration and characterization by thermal cycling, *Int. J. Hydrogen Energy.* 38 (2013) 13734–13741. doi:<10.1016/j.ijhydene.2013.08.052>.
- [247] M. Seshimo, M. Ozawa, M. Sone, M. Sakurai, H. Kameyama, Fabrication of a novel Pd/γ-alumina graded membrane by electroless plating on nanoporous γ-alumina, *J. Memb. Sci.* 324 (2008) 181–187. doi:<http://dx.doi.org/10.1016/j.memsci.2008.07.007>.
- [248] F. Touyeras, J.Y. Hihn, S. Delalande, R. Viennet, M.L. Doche, Ultrasound influence on the activation step before electroless coating, *Ultrason. Sonochem.* 10 (2003) 363–368. doi:[http://dx.doi.org/10.1016/S1350-4177\(03\)00098-1](http://dx.doi.org/10.1016/S1350-4177(03)00098-1).
- [249] S.N. Paglieri, K.Y. Foo, J.D. Way, J.P. Collins, D.L. Harper-Nixon, A New Preparation Technique for Pd/Alumina Membranes with Enhanced High-Temperature Stability, *Ind. Eng. Chem. Res.* 38 (1999) 1925–1936. doi:<10.1021/ie980199c>.
- [250] B. Zhu, C.H. Tang, H.Y. Xu, D.S. Su, J. Zhang, H. Li, Surface activation inspires

- high performance of ultra-thin Pd membrane for hydrogen separation, *J. Memb. Sci.* 526 (2017) 138–146. doi:<http://dx.doi.org/10.1016/j.memsci.2016.12.025>.
- [251] S. Uemiya, N. Sato, H. Ando, E. Kikuchi, The water gas shift reaction assisted by a palladium membrane reactor, *Ind. Eng. Chem. Res.* 30 (1991) 585–589. doi:[10.1021/ie00051a022](https://doi.org/10.1021/ie00051a022).
- [252] Z. Shi, S. Wu, J.A. Szpunar, M. Roshd, An observation of palladium membrane formation on a porous stainless steel substrate by electroless deposition, *J. Memb. Sci.* 280 (2006) 705–711. doi:<https://doi.org/10.1016/j.memsci.2006.02.026>.
- [253] X. Zhang, G. Xiong, W. Yang, A modified electroless plating technique for thin dense palladium composite membranes with enhanced stability, *J. Memb. Sci.* 314 (2008) 226–237. doi:<http://dx.doi.org/10.1016/j.memsci.2008.01.051>.
- [254] K.L. Yeung, J.M. Sebastian, A. Varma, Novel preparation of Pd/Vycor composite membranes, *Catal. Today.* 25 (1995) 231–236. doi:[http://dx.doi.org/10.1016/0920-5861\(95\)00077-S](http://dx.doi.org/10.1016/0920-5861(95)00077-S).
- [255] R.S. Souleimanova, A.S. Mukasyan, A. Varma, Effects of osmosis on microstructure of Pd-composite membranes synthesized by electroless plating technique, *J. Memb. Sci.* 166 (2000) 249–257. doi:[http://dx.doi.org/10.1016/S0376-7388\(99\)00268-9](http://dx.doi.org/10.1016/S0376-7388(99)00268-9).
- [256] A. Li, W. Liang, R. Hughes, Characterisation and permeation of palladium/stainless steel composite membranes, *J. Memb. Sci.* 149 (1998) 259–268. doi:[http://dx.doi.org/10.1016/S0376-7388\(98\)00192-6](http://dx.doi.org/10.1016/S0376-7388(98)00192-6).
- [257] D.A. Pacheco Tanaka, M.A. Llosa Tanco, T. Nagase, J. Okazaki, Y. Wakui, F. Mizukami, T.M. Suzuki, Fabrication of hydrogen-permeable composite membranes packed with palladium nanoparticles, *Adv. Mater.* 18 (2006) 630–632. doi:[10.1002/adma.200501900](https://doi.org/10.1002/adma.200501900).
- [258] C. Zhao, H. Xu, A. Goldbach, Duplex Pd/ceramic/Pd composite membrane for sweep gas-enhanced CO₂ capture, *J. Memb. Sci.* 563 (2018) 388–397. doi:[10.1016/J.MEMSCI.2018.05.057](https://doi.org/10.1016/J.MEMSCI.2018.05.057).
- [259] P.M. Thoen, F. Roa, J.D. Way, High flux palladium-copper composite membranes for hydrogen separations, *Desalination.* 193 (2006) 224–229. doi:[10.1016/j.desal.2005.09.025](https://doi.org/10.1016/j.desal.2005.09.025).
- [260] S.K. Gade, P.M. Thoen, J.D. Way, Unsupported palladium alloy foil membranes fabricated by electroless plating, *J. Memb. Sci.* 316 (2008) 112–118. doi:[10.1016/J.MEMSCI.2007.08.022](https://doi.org/10.1016/J.MEMSCI.2007.08.022).
- [261] Y.-H. Chi, J.-J. Lin, Y.-L. Lin, C.-C. Yang, J.-H. Huang, Influence of the rotation rate of porous stainless steel tubes on electroless palladium deposition, *J. Memb. Sci.* 475 (2015) 259–265. doi:<http://dx.doi.org/10.1016/j.memsci.2014.10.031>.
- [262] G. Zeng, A. Goldbach, H. Xu, Defect sealing in Pd membranes via point plating, *J. Memb. Sci.* 328 (2009) 6–10. doi:<http://dx.doi.org/10.1016/j.memsci.2008.11.053>.
- [263] R. Sanz, J.A. Calles, S. Ordóñez, P. Marín, D. Alique, L. Furones, Modelling and simulation of permeation behaviour on Pd/PSS composite membranes prepared by “pore-plating” method, *J. Memb. Sci.* 446 (2013) 410–421. doi:<http://dx.doi.org/10.1016/j.memsci.2013.06.060>.
- [264] Ø. Hatlevik, S.K. Gade, M.K. Keeling, P.M. Thoen, A.P. Davidson, J.D. Way, Palladium and palladium alloy membranes for hydrogen separation and production: History, fabrication strategies, and current performance, *Sep. Purif. Technol.* 73 (2010) 59–64. doi:[10.1016/j.seppur.2009.10.020](https://doi.org/10.1016/j.seppur.2009.10.020).

Bibliografía

- [265] H.W. Abu El Hawa, S.N. Paglieri, C.C. Morris, A. Harale, J. Douglas Way, Identification of thermally stable Pd-alloy composite membranes for high temperature applications, *J. Memb. Sci.* 466 (2014) 151–160. doi:10.1016/j.memsci.2014.04.029.
- [266] J.J. Conde, M. Maroño, J.M. Sánchez-Hervás, Pd-Based Membranes for Hydrogen Separation: Review of Alloying Elements and Their Influence on Membrane Properties, *Sep. Purif. Rev.* 46 (2017) 152–177. doi:10.1080/15422119.2016.1212379.
- [267] J. Shu, B. P. A. Grandjean, A. Van Neste, Catalytic Palladium-Based Membrane Reactors: A Review, 1991. doi:10.1002/cjce.5450690503.
- [268] W.H. Lin, H.F. Chang, Characterizations of Pd-Ag membrane prepared by sequential electroless deposition, *Surf. Coatings Technol.* 194 (2005) 157–166. doi:10.1016/j.surfcoat.2004.07.089.
- [269] A. Santucci, F. Borgognoni, M. Vadrucci, S. Tosti, Testing of dense Pd-Ag tubes: Effect of pressure and membrane thickness on the hydrogen permeability, *J. Memb. Sci.* 444 (2013) 378–383. doi:10.1016/j.memsci.2013.05.058.
- [270] J.A. Medrano, E. Fernandez, J. Melendez, M. Parco, D.A.P. Tanaka, M. van Sint Annaland, F. Gallucci, Pd-based metallic supported membranes: High-temperature stability and fluidized bed reactor testing, *Int. J. Hydrogen Energy.* 41 (2016) 8706–8718. doi:10.1016/J.IJHYDENE.2015.10.094.
- [271] H.W. Abu El Hawa, S.N. Paglieri, C.C. Morris, A. Harale, J. Douglas Way, Application of a Pd-Ru composite membrane to hydrogen production in a high temperature membrane reactor, *Sep. Purif. Technol.* 147 (2015) 388–397. doi:10.1016/j.seppur.2015.02.005.
- [272] H.W. Abu El Hawa, S.-T.B. Lundin, N.S. Patki, J. Douglas Way, Steam methane reforming in a PdAu membrane reactor: Long-term assessment, *Int. J. Hydrogen Energy.* 41 (2016) 10193–10201. doi:10.1016/j.ijhydene.2016.04.244.
- [273] N.S. Patki, S.T. Lundin, J.D. Way, Rapid annealing of sequentially plated Pd-Au composite membranes using high pressure hydrogen, *J. Memb. Sci.* 513 (2016) 197–205. doi:10.1016/j.memsci.2016.04.034.
- [274] B.D. Morreale, M. V Ciocco, B.H. Howard, R.P. Killmeyer, A. V Cugini, R.M. Enick, Effect of hydrogen-sulfide on the hydrogen permeance of palladium–copper alloys at elevated temperatures, 241 (2004) 219–224. doi:10.1016/j.memsci.2004.04.033.
- [275] H. Kurokawa, H. Yakabe, I. Yasuda, T. Peters, R. Bredesen, Inhibition effect of CO on hydrogen permeability of Pd-Ag membrane applied in a microchannel module configuration, *Int. J. Hydrogen Energy.* 39 (2014) 17201–17209. doi:10.1016/j.ijhydene.2014.08.056.
- [276] T.A. Peters, O. Liron, R. Tschentscher, M. Sheintuch, R. Bredesen, Investigation of Pd-based membranes in propane dehydrogenation (PDH) processes, *Chem. Eng. J.* 305 (2016) 191–200. doi:10.1016/j.cej.2015.09.068.
- [277] T.A. Peters, T. Kaleta, M. Stange, R. Bredesen, Hydrogen transport through a selection of thin Pd-alloy membranes: Membrane stability, H₂S inhibition, and flux recovery in hydrogen and simulated WGS mixtures, *Catal. Today.* 193 (2012) 8–19. doi:10.1016/j.cattod.2011.12.028.
- [278] A.M. Tarditi, C. Imhoff, F. Braun, J.B. Miller, A.J. Gellman, L. Cornaglia, PdCuAu ternary alloy membranes: Hydrogen permeation properties in the presence of H₂S,

- J. Memb. Sci. 479 (2015) 246–255. doi:10.1016/J.MEMSCI.2014.12.030.
- [279] F. Braun, A.M. Tarditi, J.B. Miller, L.M. Cornaglia, Pd-based binary and ternary alloy membranes: Morphological and perm-selective characterization in the presence of H₂S, J. Memb. Sci. 450 (2014) 299–307. doi:10.1016/j.memsci.2013.09.026.
- [280] M.L. Bosko, J.B. Miller, E.A. Lombardo, A.J. Gellman, L.M. Cornaglia, Surface characterization of Pd-Ag composite membranes after annealing at various temperatures, J. Memb. Sci. 369 (2011) 267–276. doi:10.1016/j.memsci.2010.12.006.
- [281] H. Gao, Y.S. Lin, Y. Li, B. Zhang, Chemical Stability and Its Improvement of Palladium-Based Metallic Membranes, Ind. Eng. Chem. Res. 43 (2004) 6920–6930. doi:10.1021/ie049722f.
- [282] J. Okazaki, T. Ikeda, D.A.P. Tanaka, K. Sato, T.M. Suzuki, F. Mizukami, An investigation of thermal stability of thin palladium-silver alloy membranes for high temperature hydrogen separation, J. Memb. Sci. 366 (2011) 212–219. doi:10.1016/j.memsci.2010.10.011.
- [283] K. Zhang, J.D. Way, Palladium-copper membranes for hydrogen separation, Sep. Purif. Technol. 186 (2017) 39–44. doi:10.1016/J.SEPPUR.2017.05.039.
- [284] S.K. Gade, E.A. Payzant, H.J. Park, P.M. Thoen, J.D. Way, The effects of fabrication and annealing on the structure and hydrogen permeation of Pd-Au binary alloy membranes, J. Memb. Sci. 340 (2009) 227–233. doi:10.1016/j.memsci.2009.05.034.
- [285] R.A. Bond, J. Evans, I.R. Harris, D.K. Ross, Hydrogen isotope separation using palladium alloy membranes, in: Fusion Technol. 1982, Elsevier, 1983: pp. 537–542. doi:10.1016/B978-1-4832-8374-6.50076-9.
- [286] J. Evans, I.R. Harris, D.K. Ross, A proposed method of hydrogen isotope separation using palladium alloy membranes, J. Less Common Met. 89 (1983) 407–414. doi:10.1016/0022-5088(83)90350-8.
- [287] P. Pérez, C.A. Cornaglia, A. Mendes, L.M. Madeira, S. Tosti, Surface effects and CO/CO₂ influence in the H₂ permeation through a Pd–Ag membrane: A comprehensive model, Int. J. Hydrogen Energy. 40 (2015) 6566–6572. doi:10.1016/j.ijhydene.2015.03.106.
- [288] E. Otero Huerta, Corrosión y degradación de materiales, 2^a edición, Madrid, 2012.
- [289] F. Roa, M.J. Block, J.D. Way, The influence of alloy composition on the H₂ flux of composite Pd-Cu membranes., Desalination. 147 (2002) 411–416.
- [290] F. Roa, J.D. Way, The effect of air exposure on palladium-copper composite membranes, Appl. Surf. Sci. 240 (2005) 85–104. doi:10.1016/j.apsusc.2004.06.023.
- [291] H. Lu, L. Zhu, W. Wang, W. Yang, J. Tong, Pd and Pd-Ni alloy composite membranes fabricated by electroless plating method on capillary α-Al₂O₃ substrates, Int. J. Hydrogen Energy. 40 (2015) 3548–3556. doi:10.1016/j.ijhydene.2014.09.121.
- [292] J.C. Reboredo, A. Ugolini, Quantile causality between gold commodity and gold stock prices, Resour. Policy. 53 (2017) 56–63. doi:10.1016/j.resourpol.2017.05.013.
- [293] H. Zhu, C. Peng, W. You, Quantile behaviour of cointegration between silver and gold prices, Financ. Res. Lett. 19 (2016) 119–125. doi:10.1016/j.frl.2016.07.002.
- [294] C. Liu, Z. Hu, Y. Li, S. Liu, Forecasting copper prices by decision tree learning, Resour. Policy. 52 (2017) 427–434. doi:10.1016/j.resourpol.2017.05.007.

Bibliografía

- [295] M. Balcilar, S. Hammoudeh, N.-A.F. Asaba, A regime-dependent assessment of the information transmission dynamics between oil prices, precious metal prices and exchange rates, *Int. Rev. Econ. Financ.* 40 (2015) 72–89. doi:10.1016/j.iref.2015.02.005.
- [296] S. Sumrunronnasak, S. Tantayanon, S. Kiatgamolchai, Influence of layer compositions and annealing conditions on complete formation of ternary PdAgCu alloys prepared by sequential electroless and electroplating methods, *Mater. Chem. Phys.* 185 (2017) 98–103. doi:10.1016/j.matchemphys.2016.10.010.
- [297] A.M. Tarditi, L.M. Cornaglia, Novel PdAgCu ternary alloy as promising materials for hydrogen separation membranes : Synthesis and characterization, *Surf. Sci.* 605 (2011) 62–71. doi:10.1016/j.susc.2010.10.001.
- [298] L. Furones, D. Alique, Interlayer Properties of In-Situ Oxidized Porous Stainless Steel for Preparation of Composite Pd Membranes, *ChemEngineering.* 2 (2017) 1. doi:10.3390/chemengineering2010001.
- [299] A. Brunetti, P.F. Zito, L. Giorno, E. Drioli, G. Barbieri, Membrane reactors for low temperature applications: An overview, *Chem. Eng. Process. Process Intensif.* 124 (2018) 282–307. doi:10.1016/j.cep.2017.05.002.
- [300] P.A. Ramachandran, T. Chompupun, C. Kanhari, T. Vatanatham, S. Limtrakul, Experiments, modeling and scaling-up of membrane reactors for hydrogen production via steam methane reforming, *Chem. Eng. Process. - Process Intensif.* 134 (2018) 124–140. doi:10.1016/j.cep.2018.10.007.
- [301] S.A. Wassie, S. Cloete, A. Zaabout, F. Gallucci, M. van Sint Annaland, S. Amini, Experimental investigation on the generic effects of gas permeation through flat vertical membranes, *Powder Technol.* 316 (2017) 207–217. doi:10.1016/j.powtec.2016.12.026.
- [302] M.A. Soria, D. Barros, L.M. Madeira, Hydrogen production through steam reforming of bio-oils derived from biomass pyrolysis: Thermodynamic analysis including in situ CO₂ and/or H₂ separation, *Fuel.* 244 (2019) 184–195. doi:10.1016/j.fuel.2019.01.156.

Índice de figuras

<i>Figura 1.1.1. Mecanismo de solución-difusión para la permeación de hidrógeno a través de una membrana metálica densa [29].....</i>	2
<i>Figura 1.1.2. Análisis de citas usando como palabras claves: paladio+ membrana+ hidrógeno (a,b) y paladio+ reactor de membrana+ hidrógeno (c,d). (fuente: Scopus).....</i>	3
<i>Figura 1.2.1. Visión del hidrógeno como vector energético.....</i>	6
<i>Figura 1.3.1. Capacidad de producción de hidrógeno en 2020 a nivel mundial (a) y a nivel europeo (b) [83].</i>	8
<i>Figura 1.3.2. Principales métodos de producción de hidrógeno basados en combustibles fósiles y fuentes de energía renovables.....</i>	8
<i>Figura 1.4.1. Clasificación de membranas según su estructura, régimen de separación y naturaleza.</i>	18
<i>Figura 1.4.2. Visión general de la permeabilidad y selectividad al H₂ para diversos tipos de membranas [136].....</i>	20
<i>Figura 1.5.1. Coeficientes de expansión térmicos de los principales materiales utilizados para la fabricación de membranas de base paladio selectivas al hidrógeno [29].</i>	28
<i>Figura 1.5.2. Valores de temperatura y espesor de la capa selectiva asociados a los principales procesos de fabricación utilizados.</i>	35
<i>Figura 1.5.3. Representación esquemática de la distancia mínima de difusión del H₂ y N₂ con una capa selectiva (a) y dos capas selectivas (b) [258].</i>	39
<i>Figura 1.5.4. Esquema del proceso de deposición de paladio no electrolítico mediante la alternativa ELP-PP.</i>	41
<i>Figura 1.5.5. Diferentes alternativas al proceso de deposición de aleaciones binarias mediante la deposición no electroquímica: codeposición (a), deposición secuencial consecutiva (b, c) y deposición secuencial alterna (d, e)[29].</i>	44
<i>Figura 1.5.6. Permeabilidad de H₂ en función de la composición de la aleación de Pd con Cu, Ag y Au a 350°C [284].</i>	46
<i>Figura 2.1.1 Esquema del proceso de deposición de la capa intermedia.....</i>	57
<i>Figura 2.1.2 Esquema del proceso de deposición de paladio no electrolítico mediante la alternativa ELP-PP.</i>	59
<i>Figura 2.2.1 Esquema de la instalación experimental para la permeación de gases.</i>	64
<i>Figura 2.2.2 Esquema de la celda de permeación de la instalación experimental describiendo los dos modos de operación posibles: modo in-out (a) y out-in (b)..</i>	65
<i>Figura 3.1.1 Imagen SEM de vista superior de soporte de PSS oxidado tras la incorporación de la capa intermedia de grafito.</i>	71

Índice de figuras

<i>Figura 3.1.2 Micrografía SEM del corte transversal de la membrana compuesta de Pd con capa intermedia de grafito a varios aumentos.....</i>	72
<i>Figura 3.1.3 Ensayos de permeación de hidrógeno de una membrana con capa intermedia de grafito después de la deposición de Pd por ELP-PP: a) ajustando a la ley de Sieverts mediante (0,0) y b) considerando la presencia de una resistencia adicional al proceso de permeación de H₂.</i>	73
<i>Figura 3.2.1 Coeficientes de expansión térmicos de los principales materiales utilizados para la fabricación de membranas de base paladio selectivas al hidrógeno H₂ [29].....</i>	75
<i>Figura 3.2.2 Morfología superficial obtenida mediante perfilometría óptica (x500) para el soporte PPS oxidado antes (a) y después de la incorporación de las capas intermedias de CeO₂ con distintos grados de retirada de exceso: OXI-CeO₂-01 (b), OXI-CeO₂-02 (c) y OXI- CeO₂-03 (d).</i>	77
<i>Figura 3.2.3 Flujo de N₂ de los soportes de PSS oxidados y modificados con CeO₂ a temperatura ambiente.</i>	78
<i>Figura 3.2.4 Imágenes SEM de la superficie externa para: (a) soporte PSS oxidado y (b) modificación seleccionada mediante la incorporación de una capa intermedia de CeO₂, OXI-CeO₂-02.</i>	80
<i>Figura 3.2.5 Imágenes SEM después de la deposición de Pd por ELP-PP sobre el soporte modificado OXI-CeO₂-02: a) vista superior (antes de los experimentos de permeación) y b) sección transversal (después de los experimentos de permeación).</i>	81
<i>Figura 3.2.6 Ensayos de permeación de la membrana OXI-CeO₂-02 después de la deposición de Pd por ELP-PP: a) ajustando a la ley de Sieverts mediante (0,0) y b) considerando la presencia de una resistencia adicional al proceso de permeación de H₂.</i>	83
<i>Figura 3.3.1 Morfología superficial obtenida mediante perfilometría óptica del soporte PSS calcinado antes (a) y después (b) de la incorporación de la capa intermedia.</i>	87
<i>Figura 3.3.2 Imagen SEM de la superficie externa del soporte de PSS calcinado después de la incorporación de partículas de CeO₂ dopadas como capa intermedia.</i>	88
<i>Figura 3.3.3 Imágenes SEM de la superficie de Pd incorporado por ELP-PP sobre un soporte modificado con CeO₂ dopado a un aumento: (a) x350 y (b) x1000.</i>	89
<i>Figura 3.3.4 Imágenes SEM del corte transversal de las membranas preparadas sobre soportes PSS modificados con capas intermedias formadas por: (a) CeO₂ comercial o (b) dopado con Pd.</i>	91
<i>Figura 3.3.5 Flujo de permeado de la membrana preparada con partículas de ceria dopada como capa intermedia, considerando la presencia de una resistencia adicional al proceso de permeación de H₂.</i>	92

<i>Figura 3.4.2 Micrografías SEM de la membrana compuesta de Pd preparada sobre un soporte de PSS con una capa intermedia de OMC: a) Superficie externa y b) Vista del corte transversal.</i>	95
<i>Figura 3.4.3 Flujo de permeado de la membrana preparada con partículas de ceria mesoporosa como capa intermedia, considerando la presencia de una resistencia adicional al proceso de permeación de H₂.</i>	95
<i>Figura 3.4.4 Esquema de la celda de permeación de la instalación experimental describiendo los dos modos de operación posibles: modo in-out (a) y out-in (b).</i> ..	96
<i>Figura 3.4.5 Vista esquemática de una membrana ELP-PP, distinguiendo la superficie externa (marcada en rojo, ●) y la interna (marcada en azul, ●) de la película de Pd generada sobre el soporte poroso.</i>	98
<i>Figura 3.4.6 Efecto de la dilución de la corriente de alimentación con mezclas binarias de H₂-N₂ a 400 °C para membranas con capas intermedias de CeO₂ comercial (triángulos) o dopado (círculos) y mesoporoso (cuadrados) para ambos modos de permeación: in-out (símbolos llenos) y out-in (símbolos vacíos).</i>	99
<i>Figura 3.4.7 Mecanismo de permeación alimentando una mezcla de hidrógeno y nitrógeno en el modo de operación a) in-out y b) out-in</i>	100
<i>Figura 3.4.8. Variación de la permeanza al alimentar mezclas binarias de H₂-N₂ en distintas proporciones a diferentes temperaturas y modos de operación: in-out (a) o out-in (b).</i>	101
<i>Figura 3.4.9 Comparación de los valores de espesores de la capa de paladio y permeanza para los distintos tipos de membranas desarrolladas.</i>	102
<i>Figura 3.5.1 Esquema de los distintos procesos de síntesis de membranas analizados.</i>	104
<i>Figura 3.5.2 Distribución de costes de los distintos procesos de fabricación.</i>	107
<i>Figura 3.6.1 Efecto de presión en experimentos de reformado con vapor de ácido acético ($T = 450\text{ }^{\circ}\text{C}$, GHSV = 4500 h⁻¹) en configuraciones PBR (negro, ●) y PBMR (rojo, ●): conversión de ácido acético (a), rendimiento de hidrógeno (b), selectividad de productos en PBR (c) y PBMR (d). Referencia de equilibrio termodinámico: ---.</i>	110

Índice de tablas

<i>Tabla 1.5.1 Soportes inorgánicos comerciales más comúnmente utilizados para la preparación de membranas de paladio.....</i>	24
<i>Tabla 1.5.2 Alternativas de modificación de soportes comerciales inorgánicos para la preparación de membranas de base Pd.</i>	32
<i>Tabla 1.5.3 Modificaciones al proceso de deposición ELP para la preparación de membranas base en Pd.</i>	42
<i>Tabla 2.1.1 Composición de las disoluciones utilizadas en la activación.</i>	58
<i>Tabla 2.1.2 Composición de las disoluciones utilizadas para la deposición.</i>	60
<i>Tabla 3.2.1 Propiedades de los soportes modificados con capas intermedias de CeO₂.</i>	79
<i>Tabla 3.3.1 Cargas de paladio obtenidas en las partículas de CeO₂ después de los procesos de dopado.....</i>	85
<i>Tabla 3.4.1 Resumen de las permeanzas obtenidas a 400°C con los diferentes tipos de membranas para ambos modos de operación.....</i>	97
<i>Tabla 3.5.1 Disoluciones utilizadas en la síntesis de los distintos tipos de membranas.....</i>	104
<i>Tabla 3.5.2 Costes de las distintas etapas para cada tipo de membrana.....</i>	106
<i>Tabla 3.5.3 Coste, permeanza y factor M de los distintos tipos de membranas..</i>	108

6

Anexos

Article

Effective H₂ Separation through Electroless Pore-Plated Pd Membranes Containing Graphite Lead Barriers

David Martínez-Díaz ¹, Raúl Sanz ², Alicia Carrero ¹, José Antonio Calles ¹ and David Alique ^{1,*}

¹ Department of Chemical, Energy and Mechanical Technology, Rey Juan Carlos University, C/ Tulipán s/n, 28933 Móstoles, Spain; david.martinez.diaz@urjc.es (D.M.-D.); alicia.carrero@urjc.es (A.C.); joseantonio.calles@urjc.es (J.A.C.)

² Department of Chemical and Environmental Technology, Rey Juan Carlos University, C/ Tulipán s/n, 28933 Móstoles, Spain; raul.sanz@urjc.es

* Correspondence: david.aliique@urjc.es; Tel.: +34-91-488-7603

Received: 27 October 2020; Accepted: 4 December 2020; Published: 10 December 2020



Abstract: Hydrogen promotion as a clean energy vector could provide an efficient strategy for realizing real decarbonization of the current energy system. Purification steps are usually required in most H₂-production processes, providing the use of Pd-based membranes, particularly those supported on porous stainless steel (PSS), important advantages against other alternatives. In this work, new composite membranes were prepared by modifying PSS supports with graphite, as an intermediate layer, before incorporating a palladium film by electroless pore-plating. Fully dense Pd layers were reached, with an estimated thickness of around 17 µm. Permeation measurements were carried out in two different modes: H₂ permeation from the inner to the outer side of the membrane (in-out) and in the opposite way (out-in). H₂ permeances between 3.24×10^{-4} and 4.33×10^{-4} mol m⁻² s⁻¹ Pa^{-0.5} with $\alpha_{H_2/N_2} \geq 10,000$ were reached at 350–450 °C when permeating from the outer to the inner surface. Despite a general linear trend between permeating H₂ fluxes and pressures, the predicted intercept in (0,0) by the Sieverts' law was missed due to the partial Pd infiltration inside the pores. H₂-permeances progressively decreased up to around 33% for binary H₂-N₂ mixtures containing 40 vol% N₂ due to concentration–polarization phenomena. Finally, the good performance of these membranes was maintained after reversing the direction of the permeate flux. This fact practically demonstrates an adequate mechanical resistance despite generating tensile stress on the Pd layer during operation, which is not accomplished in other Pd membranes.

Keywords: hydrogen; composite membrane; palladium; electroless plating; intermediate layer; graphite

1. Introduction

Human activities and lifestyles with a high industrialization level, excessive consumerism, and global mobility require large amounts of energy, mainly covered by fossil fuels that cause significant environmental problems [1,2]. The promotion of hydrogen as a clean energy vector could provide a very efficient strategy for realizing real decarbonization of the current energy system without compromising the continuous growth of the economy [3,4]. Moreover, hydrogen can be obtained from a wide variety of feedstock [5], including hydrocarbon molecules not only from fossil fuels but also from biomass [6] or waste materials [7], as well as ammonia [8] or water [9], among others. In this manner, the use of current mature technologies at the first stages may facilitate a progressive transition to real green hydrogen; meanwhile, other complementary technologies for its transport and storage

can be developed to an acceptable standard [10,11]. During this period, which probably will take some decades, pure hydrogen will not be directly produced but will be mixed with other gases such as carbon monoxide, carbon dioxide, nitrogen, or steam. Therefore, additional separation steps will be required to adjust its purity for each application. Among diverse technologies, the use of H₂-selective membranes provides substantial advantages against other options, such as simplicity, low energy requirements, flexible operation, and moderate cost [12,13]. Moreover, process intensification could be reached by combining both chemical reaction and separation in a unique device, a membrane reactor, where the membrane continuously extracts almost-pure hydrogen from the reactive area [14–16].

In this context, fully dense Pd membranes are especially suitable for these applications due to their ideal complete selectivity toward hydrogen, relatively high permeability, and the possibility to work at high temperatures as usually required for most of the reactions [17,18]. A key aspect for these membranes is to reduce as much as possible the thickness of the Pd film to save costs and increase the permeate flux [19,20]. One of the most frequent strategies is to consider a composite structure for the membrane, in which the palladium is deposited as a thin layer onto a porous substrate that provides the required mechanical resistance for the set [12,21]. However, more stacked layers can also be generated to modify the original properties of the porous support [22,23] or protect the H₂-selective film against certain molecules or particular operating conditions [24,25]. In those cases, the final mechanical properties of the system should be carefully addressed under operation because the possibility of a dramatic failure of the membrane noticeably increases with the number of stacked layers made of different materials.

Moreover, an eventual unacceptable cost for membranes with a certain number of layers or materials must also be considered for their industrial implementation in multiple processes. In this context, an extremely facile, low-cost, but effective technique for modifying porous alumina substrates with a graphite lead pencil was proposed for the first time by Hu et al. [26]. They achieved membranes with Pd thickness of around 5 μm by conventional electroless plating (ELP), permeate of 25 m³ m⁻² h⁻¹ (at 1 bar and 450 °C), and ideal H₂/N₂ separation factor of up to 3700. The same authors followed this strategy for obtaining bi-functional membranes in which the alumina support is doped with Ni particles to prevent the presence of residual amounts of carbon monoxide in the permeate stream [27]. Terra et al. [28] used a similar strategy for the generation of a graphite-based intermediate layer but manually spreading the powder obtained by the milling of a commercial 2B pencil onto the outer surface of alumina hollow fibers. This interlayer allows 25% thinner Pd films to be made with complete H₂-N₂ selectivity and a permeance of 1×10^{-6} mol m⁻² s⁻¹ Pa⁻¹ (at 450 °C). Wei et al. also applied a pencil coating to modify the original surface of macroporous stainless steel supports [29]. They detected some delamination problems but finally reached a Pd thickness of around 7 μm and H₂ permeance of 4.43 m³ m⁻² h⁻¹ kPa^{-0.5} (at 450 °C) after applying vacuum during the intermediate layer incorporation. However, these membranes also evidenced limited ideal H₂/N₂ separation factors below 150. It should be noted that all these membranes containing graphite as interlayer were always tested by applying the higher pressure on the outer surface of the membrane, where the Pd film is placed. Thus, all membranes work under the most favorable conditions, with only compression stress that eventually protects any delamination.

Besides the intrinsic material compatibility of stacked layers in any composite membrane, the technology applied for the deposition of the top Pd film could also noticeably improve the mechanical resistance of the overall system. In the last years, a modification of the traditional electroless plating alternative in which the main reactants are separated by the wall of the porous support during the entire deposition process has exhibited very promising results in terms of Pd-thickness reduction and mechanical stability [17,22,30]. This alternative, denoted as electroless pore-plating (ELP-PP), has been satisfactorily applied onto both raw ceramic and metallic porous substrates or modified ones with different intermediate layers such as mixed iron-chromium oxides [31], ceria [22], or SBA-15 [32].

The present study tries to combine, for the first time, an adequate porous stainless steel (PSS) substrate modification with graphite lead as an interlayer with the typical mechanical strength of

the Pd film provided by ELP-PP. In contrast to other materials used as intermediate layer when preparing previous ELP-PP membranes, graphite has a greater ductility, thermo-electrical conductivity, and extreme resistance against thermal shocks while presenting a relatively low-cost. Moreover, previous studies in which this intermediate layer based on graphite was deposited onto tubular PSS supports evidenced some limitations for reaching ultra-high H₂ selectivities, as previously mentioned. Therefore, we consider that this contribution could provide further insights and possibilities for this particular type of H₂-selective composite membrane. This manuscript addresses the membrane fabrication and also evaluates the membrane's permeation behavior under a wide variety of operating conditions, including contrary permeation flux directions. This point is especially interesting, since few studies have carried out permeation experiments at unfavorable conditions in terms of tensile stress generation, for example collecting the permeate flux from the outer side of tubular membranes where both intermediate layer and Pd film are placed on the external surface of the porous support.

2. Materials and Methods

2.1. Membrane Preparation

In this work, tubular porous stainless steel (PSS) tubes with 0.1 µm media grade and 1/2" outside diameter, purchased from Mott Metallurgical Corp. (Farmington, CT, USA), were used as support for the Pd composite membranes' preparation. The original tube of around 60 cm in length was cut into shorter pieces of 30 mm. After that, the general procedure followed for the preparation of the membranes consisted of five successive steps: (i) preliminary cleaning, (ii) support calcination (12 h at 600 °C), (iii) incorporation of graphite as an intermediate layer, (iv) seeding with homogeneously distributed Pd nuclei, and (v) deposition of a palladium film by electroless pore-plating (ELP-PP). Details about the first two general steps, in which the supports were cleaned and calcined, can be found in previous works [17,31].

The intermediate layer was generated by using a graphite lead taken from a 2B pencil according to the original procedure described by Hu et al. [26]. Specifically, the external surface of the PSS substrates was first directly painted with a commercial 2B pencil up to achieve a homogeneous dark gray color but with a significant amount of graphite that was weakly sticky. Then, the excess material was removed by dry brushing with a clean cloth, only leaving the graphite particles just placed inside the deepest pores of the raw support. Cleaning was complete when the textile did not get significantly dirty after this process. All supports modified in this way were then calcined at 500 °C for 5 h to ensure the complete removal of binders and waxes, thus guaranteeing better stability for later stages.

Finally, substrate activation with both Pd nuclei and Pd deposition was carried out based on the well-established electroless pore-plating alternative [12,17,33]. Accordingly, the solutions containing the Pd source and the reducing agent were fed from opposite sides of the support with the aim that they will be present and reactive just in the pores or surrounding areas [30,34,35].



Palladium chloride was always used as the metal source but highly diluted (0.1 g/L) into an acidic aqueous solution (HCl, 0.1 mL/L) for the activation step or moderately diluted (5.4 g/L) into a basic one containing ammonium hydroxide (390 mL/L) and ethylenediaminetetraacetic acid (70 g/L) for the deposition itself. On the contrary, a mixture of hydrazine (0.2 M) and ammonia (2.0 M) always formed the reducing solution. These solutions were used at room temperature or 50 °C for each case, i.e., activation or deposition step. However, it should be noted that activation is carried out only once for 2 h, but several recurrences for the Pd deposition are usually required. These ELP-PP cycles were performed until the membrane weight gain became negligible, thus suggesting that a fully dense membrane was reached, and the different solutions could not reach each other because of the blockages

of the pores with palladium. This fact was confirmed by gas tightness with helium when the membrane was immersed into ethanol and maintained at room temperature under 3 bar for at least 30 min.

2.2. Characterization

The morphology of all samples included here was characterized entirely with a scanning electron microscope Philips XL30 ESEM (Eindhoven, The Netherlands). The external membrane surface was observed before and after incorporating graphite and palladium layers to analyze the uniformity and eventual presence of defects. Furthermore, gravimetric analyses were also used to determine the deposited amount of each material in the membrane, graphite and palladium, by an electronic balance Kern and Sohn ABS-4 (Balingen, Germany) with a precision of 1.0×10^{-4} g. Thus, their average layer thicknesses were estimated from these data by assuming a homogeneous distribution on the external surface of the supports. The obtained values were compared with the real thickness obtained from the analysis of cross-sectional SEM images.

Besides the morphology of the membranes, their permeation capacities with pure gases (H_2 , N_2) and their mixtures (N_2 content in the range 5%–40%) were also measured using a homemade facility, depicted in Figure 1 and used in previous studies [22,35].

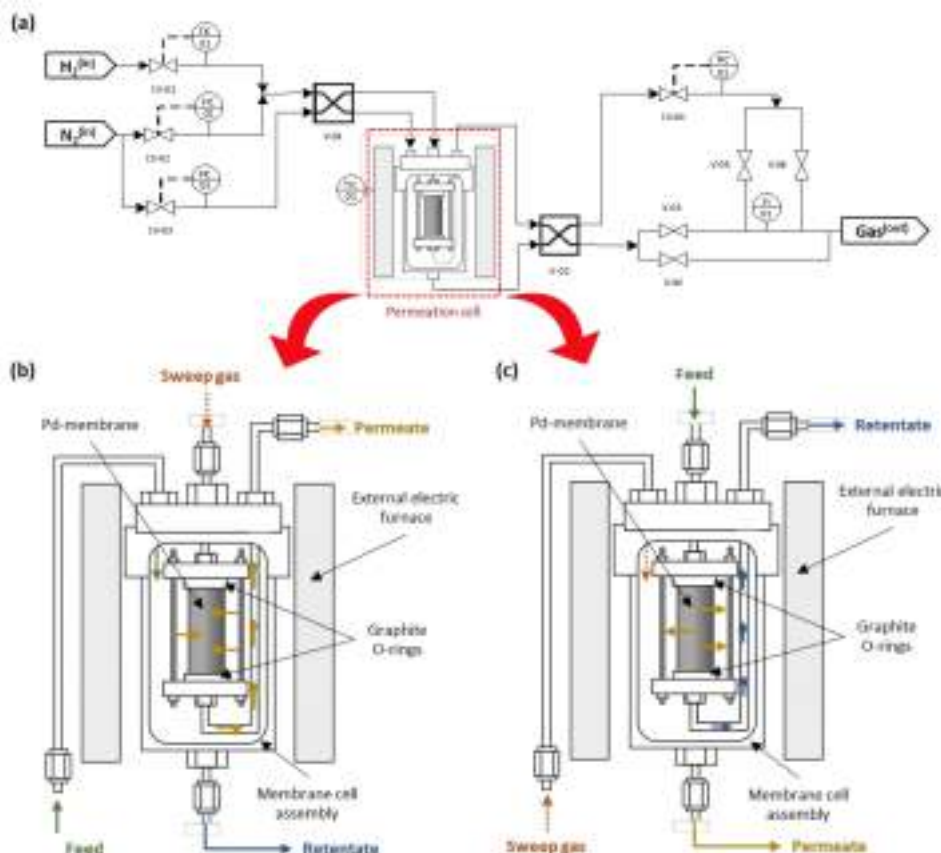


Figure 1. Basic scheme of the permeation setup (a) and possible configurations for permeation experiments: mode out-in (b) and mode in–out (c).

In essence, the membrane was placed inside a 316L SS vessel rounded by an electrical furnace to operate in the range 350–450 °C. Two graphite O-rings were used to ensure good sealing of the membrane, maintaining both permeate and retentate streams completely separated during the complete set of experiments. The feed stream could be properly adjusted by several Bronkhorst Hi-Tech mass-flow controllers (Ruurlo, The Netherlands) of maximum capacity 400 NmL min⁻¹ mounted in independent H₂ and N₂ inlet lines. These lines were joined in a unique inlet tube to feed the permeate cell. At this point, it should be noted that two different four-way valves (V-01 and V-02) were mounted in the system to direct the feed stream at the lumen or shell side of the membrane, as later will be explained in detail. On the other hand, permeate or retentate flow rates were measured using an additional Hi-Tech mass-flow meter of maximum capacity 200 NmL min⁻¹. In order to avoid any uncertainty while measuring very low fluxes for any retentate of the permeate streams, this equipment was replaced in those cases by a Ritter Mili-GasCounter able to detect volumetric flow-rates from 1.67×10^{-2} mL min⁻¹. Finally, the equipment counted on the help of a gas chromatograph (GC), Varian CP-4900, with a thermal conductivity detector (TCD) and two analytical columns (Molsieve 5 A° and PoraPLOT-Q) to analyze the composition of both permeate and retentate streams when testing gas mixtures. For the entire set of experiments carried out at pressure driving forces in the range 0.5–2.0 bar (controlled by a Bronkhorst High-Tech EL-PRESS back-pressure regulator—Ruurlo, The Netherlands), the permeate stream was always maintained at atmospheric conditions, and no sweep gas was used. At this point, it should be noted that two different operation modes were studied in which the function of the position of the aforementioned four-way valves indicated:

- (i) Mode out-in: The gas is fed to the shell side, thus meeting first the Pd film that extracts part of the gas into the lumen side of the membrane. In this configuration, the adherence of diverse layers is relatively ensured due to the compression stress caused by the higher feed pressure.
- (ii) Mode in-out: In this case, the feed is introduced to the inner membrane side, thus first passing through the porous support before meeting the Pd film and permeating to the shell side. At these conditions, an inevitable tensile stress is produced between support and the Pd layer, affecting the overall mechanical resistance and possibly causing a dramatic deterioration of the composite membrane by delamination.

3. Results and Discussion

3.1. Membrane Morphology

The morphology of the composite membranes prepared in this work was analyzed just after incorporating each stacked layer onto the raw PSS support. Figure 2 shows the top-view images of the stainless-steel support, before and after the graphite incorporation. These images were taken by using both secondary electron (Figure 2a,c) and backscattered electron detectors (Figure 2b,d) to analyze more clearly not only the external morphology of the samples but also their composition and material distribution along the surface, respectively.

As can be seen, the calcined supports (Figure 2a,b) present a relatively high roughness with a wide pore-size distribution, at least in their pore mouths. This morphology is very similar to commercial substrates despite generating oxide around the stainless-steel particles by the thermal treatment of calcination [31]. However, this morphology noticeably changes after incorporating the graphite lead (Figure 2c,d). Carbon particles remain preferentially inside the external pores, thus partially blocking the original biggest superficial pores of the substrate and generating a new porous structure with smaller average pore sizes. The starting hypothesis is that these smaller pores could be more easily closed by palladium than the original bigger ones, promoting a relatively thin film with high H₂ perm-selectivity. Moreover, the initial high roughness of calcined PSS supports was also partially smoothed after incorporating this new intermediate layer.

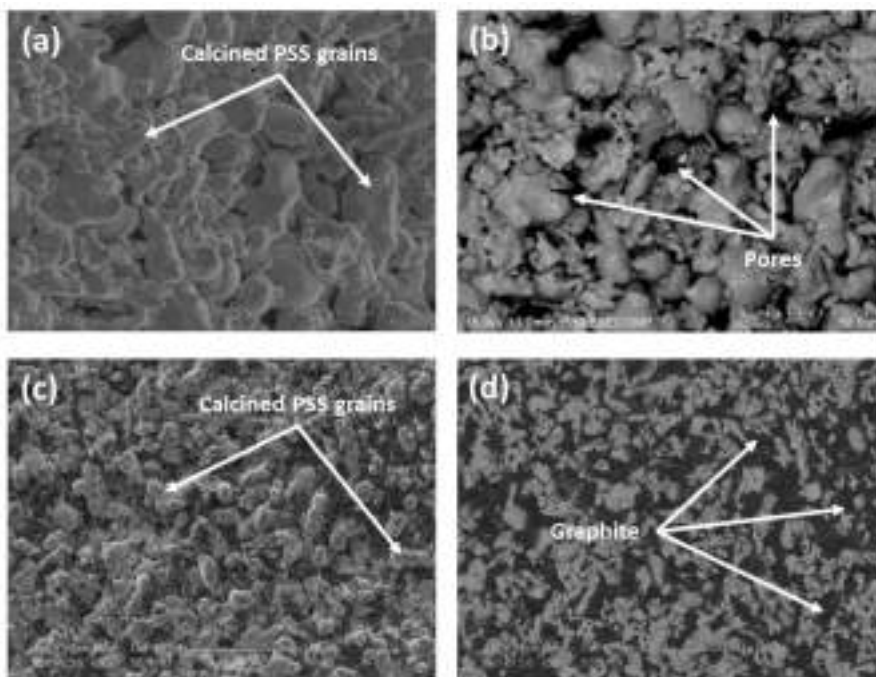
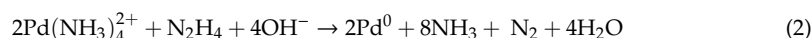


Figure 2. Top-view SEM images of commercial porous stainless steel (PSS) support after modification by calcination in air at 600 °C for 12 h (a,b) and incorporation of graphite lead particles (c,d).

Then, the morphology of the final composite membranes reached after the Pd incorporation by ELP-PP was also analyzed by SEM. The characteristic top-view images of this membrane type are collected in Figure 3. Despite the preferential incorporation of the palladium particles just inside the pores of the support or their surrounding areas when using the ELP-PP alternative, in this case, a continuous Pd film that covers the entire surface of the modified supports with graphite can be observed by both SE (secondary electrons) and BSE (back-scattering electrons) images. This morphology, with a spherical grain growth of palladium deposits (Figure 3a), is certainly similar to the ones reached for other ELP-PP membranes in which diverse ceramic intermediate layers were used [32,35]. It can be explained by the presence of a certain pore size distribution in the porous substrates due to the irregularity of the SS grains and the graphite particles. In this manner, the solutions containing the reducing agent (hydrazine) and the metal source (palladium) can probably meet through the smallest pores but not inside the biggest ones. In fact, the higher diffusion velocity of hydrazine toward the metal solution means that the reducing agent reaches the external surface in a relatively short time, where the following autocatalytic reaction initiates:



Additionally, Figure 3b denotes good compactness of the metal particles and homogeneity along with the entire top film with a palladium content over 95%, as evidenced by EDX analysis. Based on these results evidencing a homogeneous deposition of the palladium around the external surface of modified supports, the palladium thickness can be directly estimated as a uniform outer layer from gravimetric measurements. This value, denoted in the present work as t_{Pd}^e , was around 17 μm , which is close to other values obtained when using the ELP-PP procedure to synthesize Pd membranes with intermediate layers such as CeO_2 [35] or SBA-15 [32].

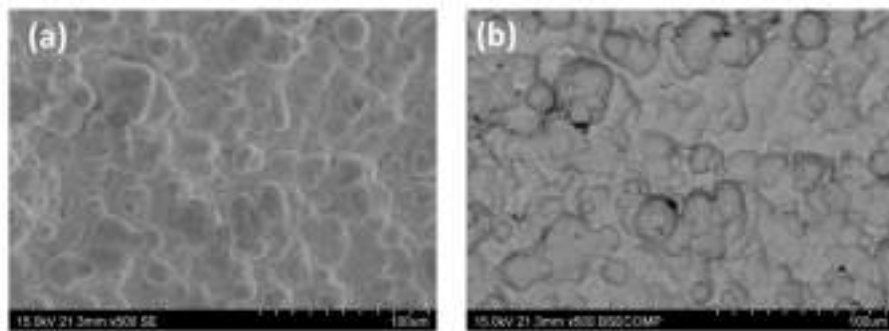


Figure 3. SEM images of the external surface after the palladium incorporation by electroless pore-plating (ELP-PP): (a) SE and (b) BSE.

More interesting is the analysis of typical cross-sectional views for the new ELP-PP membranes presented in this study with an intermediate graphite layer (Figure 4). The real Pd thickness (t_{Pd}^t) can be determined more accurately in these images and the particular distribution of the stacked layers can be analyzed. First, the good continuity of the external Pd film is evident as previously found when analyzing the SEM top-views. However, specific insights can be extracted from the analysis of the image taken at higher magnification. Each material that forms the final composite membrane can be distinguished. The thicker layer, placed on the bottom area of the SEM image, corresponds to the bulk stainless steel support; it indicates the porous stainless steel. Close to the external surface of this support, a very thin dark gray layer with an average thickness below 0.5 μm can also be observed. This layer is made of Fe–Cr oxides generated during the air calcination step at 600 °C for 12 h. It should be noted that these oxides are present not only on the external surface of the support but also inside most of the pores between SS grains. However, due to the low thickness of this first intermediate layer, only the average size of the smallest pores was noticeably reduced. The biggest ones could be modified after incorporating graphite, which can be observed in the figures as dark gray non-spherical particles with a large size distribution. These particles were preferentially placed just inside the mouth of the biggest pores of the calcined support, thus reducing their average size.

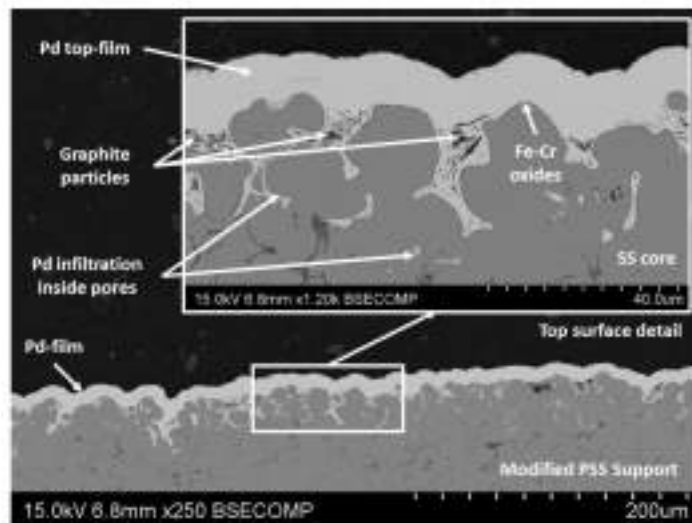


Figure 4. Cross-section of the Pd composite membrane at various magnifications.

A deeper discussion is needed for the top Pd film observed as a light gray layer on the cross-sectional views. This layer presents a true external thickness in the range of around 8–12 μm if it is measured from the crests of the modified support. However, palladium also penetrates some of the pores up to around 35 μm in depth. This is caused by the intrinsic characteristics of the ELP-PP process used for its incorporation, where the chemical reaction between palladium ions and hydrazine (Equation (2)) starts just inside most of the pores, especially in the case of their size becoming limited. This particular distribution of the palladium justifies the differences previously estimated by gravimetric analysis and SEM.

Moreover, it should be noted that the above-mentioned Pd infiltration into most of the external pores of the support could help to improve the adherence of this layer. Consequently, the mechanical resistance of the composite membrane against unfavorable operating conditions, i.e., permeation tests from the inner to the outer side of the membrane in which tensile stress is generated, can also be improved. This potential benefit will be furtherly discussed later while analyzing the permeation behavior of these membranes.

3.2. Permeation Behavior

As mentioned before, while describing the experimental procedure to prepare the membranes, preliminary gas bubble tests with helium at room temperature were carried out to ensure enough gas tightness up to 3 bar and to validate the quality of the palladium film. However, it is widely known that additional experiments at different operating conditions closer to the expected ones in real industrial independent separators or membrane reactors are also required. In this context, the present section analyzes in detail the results obtained after performing various permeation tests with pure gases and binary mixtures for a wide variety of experimental conditions, including pressure, temperature, and permeate flux direction (operating mode).

3.2.1. Pure Gases: N₂ and H₂

First of all, pressure and temperature effects on the permeation capacity of these membranes were evaluated throughout a series of permeation experiments with pure gases, N₂ and H₂, according to the out-in operation mode. These results have been collected in Figure 5. The H₂ permeate flux is represented against the pressure driving force ($P_{H_2,ret}^{0.5} - P_{H_2,perm}^{0.5}$) for temperatures in the range 350–450 °C (Figure 5a) and calculated H₂ permeances are correlated with the inverse of the temperature to determine the activation energy of the membrane (Figure 5b). It should be noted that, in all cases, a complete gas tightness against nitrogen was observed at these conditions, thus suggesting an almost ideal complete selectivity to hydrogen according to the available detection limit of the experimental setup (1.67×10^{-2} mL min⁻¹).

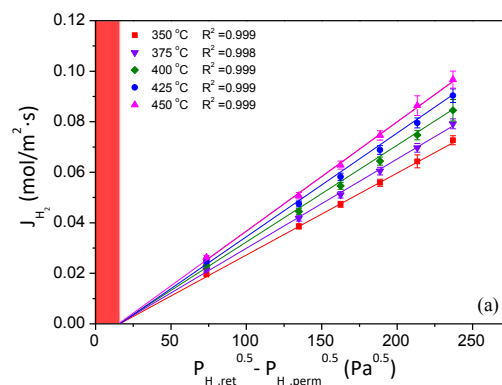


Figure 5. Cont.

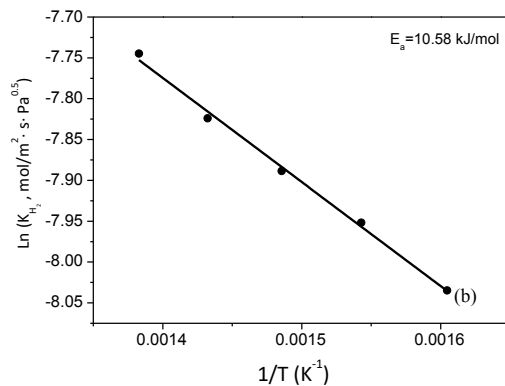


Figure 5. Permeation behavior for out-in operating mode: (a) Overall pressure and temperature effects on H_2 permeate fluxes (deviation from origin interception marked as a red vertical band) and (b) determination of the activation energy.

Moreover, it is also important to address that both reproducibility and thermal stability of membranes were previously ensured by several permeation tests before considering further experiments. Particularly, three different membranes were prepared following an analogous experimental procedure, and they were tested under diverse thermal cycles. Each membrane was first heated up to 400 °C under inert atmosphere, measuring the permeate flux after feeding independent single gases, N_2 and H_2 , at pressures ranged from 0.5 to 2.5 bar before cooling down again up to room temperature under inert conditions. This process was repeated at least five times to ensure adequate membrane resistance and the reliability of permeate fluxes. Further details about the results reached in these experiments can be found in Supplementary Figure S1 as supplementary information. In general, only slight deviations in permeation data were obtained for the entire set of experiments and were assumed as reasonably acceptable. Deviations below 5% were found between each data point taken at similar experimental conditions. In this manner, it is possible to state an adequate reproducibility of permeate values and enough mechanical resistance of the composite membranes against the experimental conditions. Consequently, the membrane GRAPH#01 was selected as reference to continue the analysis of its permeation behavior. In this context, while analyzing in detail the general relationship between H_2 fluxes and pressure driving forces (shown in Figure 5a), a clear linear trend was observed for the entire range of temperatures. This fact, together with the absence of nitrogen detected in the permeate side during previous experiments carried out with this gas at analogous conditions, confirms the absence of defects in the palladium layer under those conditions. Thus, H_2 diffusion through the bulk Pd can be considered as the rate-determining step, as described by Sieverts' law and typically occurs in most Pd composite membranes [19]. At these conditions, the diffusion rate is proportional to the concentration of hydrogen atoms on opposite sides of the metal surface and the hydrogen concentration is proportional to the square root of the hydrogen pressure. On the contrary, the presence of defects and pinholes usually favors other permeation mechanisms different from solution diffusion (i.e., Knudsen diffusion or Poiseuille mechanism) and the pressure exponent should be replaced by other values ranged from 0.5 to 1.0 in order to maintain a good linear fitting. Particularly, n-values of greater than 0.5 when working with Pd films thicker than 5 μm can be attributed to a noticeable permeation of hydrogen through small pore-like defects or pinholes without the necessity of being dissociated, dissolved, and diffused through the bulk metal.

However, it is also relevant to mention that the linear trends do not intercept the origin, as usual in multiple Pd composite membranes prepared by electroless plating. This particular behavior is characteristic of most ELP-PP membranes reported up to now, and it has been widely discussed in our previous manuscripts [17,30,36]. This effect can be explained by the partial infiltration of palladium into the pores of the support. This particular morphology of the Pd film causes both external and internal surfaces of the layer become noticeably different. The outer surface (as previously shown in Figure 3) is certainly smooth and maintains good contact with the gas phase, thus making the pressure values in the bulk gas phase and the surface of the membrane almost identical. However, the internal one is much more tortuous, and the assumptions of negligible differences between both sides of the Pd film and accuracy of the pressure value for that side are not clear. At these conditions, the calculated pressure driving force from retentate and permeate bulk gas phases can be imprecise, and apparent additional resistances to the permeation process appear. In previous studies, it was demonstrated that this deviation is strongly affected by Pd infiltration into the porous substrate [17,36].

On the other hand, the temperature effect on the H₂ permeate fluxes is also evident for all performed experiments. Independently of the considered temperature for the range 350–450 °C, the above-mentioned linear trend without a clear intercept within the origin is maintained, but reaching higher fluxes as the temperature increases (Figure 5a). In this manner, H₂ permeance values increase from 3.24×10^{-4} to 4.33×10^{-4} mol m⁻² s⁻¹ Pa^{-0.5} when working at the lowest or the highest temperature, 350 or 450 °C, respectively. Figure 5b shows the relationship between all these H₂ permeance values and the temperature at which they were calculated. As can be seen, really good linearity is obtained as predicted by a typical Arrhenius-type dependence. At these conditions, activation energy around 10.6 kJ/mol was obtained within the standard range of other composite Pd-based membranes reported in the literature [17,37,38].

3.2.2. N₂–H₂ Binary Mixtures

After analyzing the permeation behavior when feeding pure H₂, additional tests with binary H₂–N₂ mixtures were also performed to investigate more realistic permeation conditions in which deviation from the theoretical behavior (i.e., concentration–polarization effects) could appear. All these experiments were carried out at a constant temperature of 400 °C while maintaining the out-in configuration for extracting high-purity H₂ in the permeate side. In this context, Figure 6 collects the experimental results obtained when feeding mixtures in which H₂ is diluted with different N₂ concentrations from 0 to 40 vol%. These results are depicted as the relative variation between the permeance values reached for each particular condition and the reference one, 3.75×10^{-4} mol m⁻² s⁻¹ Pa^{-0.5}, considered when feeding pure H₂.

First, it should be noted that membrane integrity was maintained during all these experiments since no N₂ was detected by gas chromatography on the permeate side. However, a clear effect on the H₂ permeance values appears when increasing the feed dilution with nitrogen. In fact, H₂ permeances progressively decreased up to around 33% at worst conditions, as the N₂ content in the feed stream increased from 0 to 40 vol%. This fact cannot be explained by the inherent dilution of the mixture and associated reduction of H₂ partial pressure. This reduction provokes a consequent decrease of the real pressure driving force, but it was formally considered for data calculation. Then, a certain concentration–polarization effect should be occurring despite the strongly inert character of nitrogen but not at a constant rate for all the analyzed dilutions. First, a significant H₂ permeance drop of around 28% was obtained when the N₂ content increases from 0 to 20 vol% in the feed stream. However, dilution up to 30 vol% in N₂ only generates an additional 5% H₂ permeance drop concerning the previously given one. This situation appeared to be stabilized for different conditions in which further dilutions were considered.

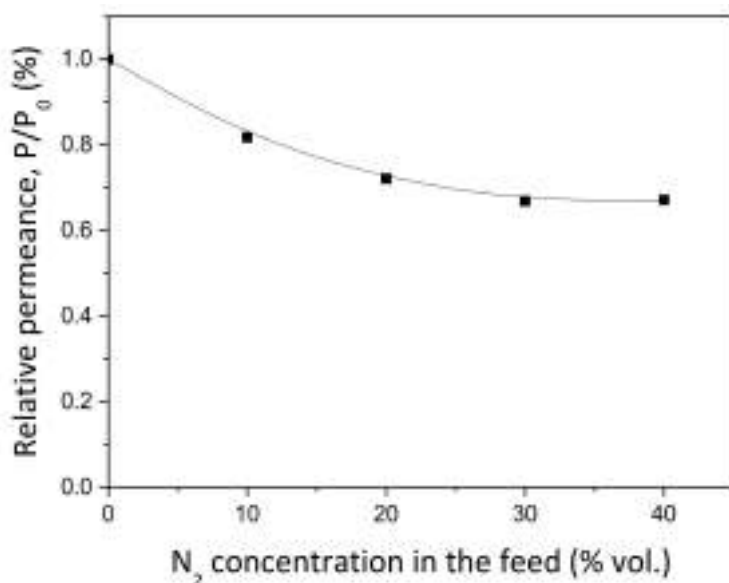


Figure 6. Effect of feed stream dilution with binary H_2-N_2 mixtures (out-in operating mode, $400\text{ }^\circ\text{C}$).

3.2.3. Effect of the Permeate Flux Direction

The effect of the permeate flux direction in Pd composite membranes prepared by ELP-PP onto modified tubular PSS supports with an intermediate graphite barrier was also analyzed in this work. In all previous tests, the gas was fed to the shell side of the permeation cell, while collecting the permeate from the inner side. This operation mode (out-in) generates compressive stress on the palladium layer and protects the system against possible delamination. Usually, most of the Pd-based membranes from literature are characterized following similar tests, in which permeate flux goes from the outer to the inner side of the membrane [39,40]. However, it could be highly interesting to analyze the results reached in other configurations in which H_2 permeates in the contrary direction, from the inner to the outer side of the composite membrane. This operating mode, denoted as in-out in the present study, generates certain tensile stress on the top palladium film due to the pressure difference between both system sides. Therefore, these operating conditions could be used as an indirect measurement of the tensile strength of the membrane and, as a consequence, its mechanical resistance. Moreover, it could also be interesting to demonstrate an adequate resistance of the membranes against these operating conditions for their use in membrane reactors, where it would be convenient to place a solid catalyst in the membrane lumen for certain applications in which direct contact between palladium and diverse chemicals should be avoided.

In this context, Figure 7 collects the H_2 permeate fluxes reached at $400\text{ }^\circ\text{C}$ in case of working under both operating modes, out-in and in-out.

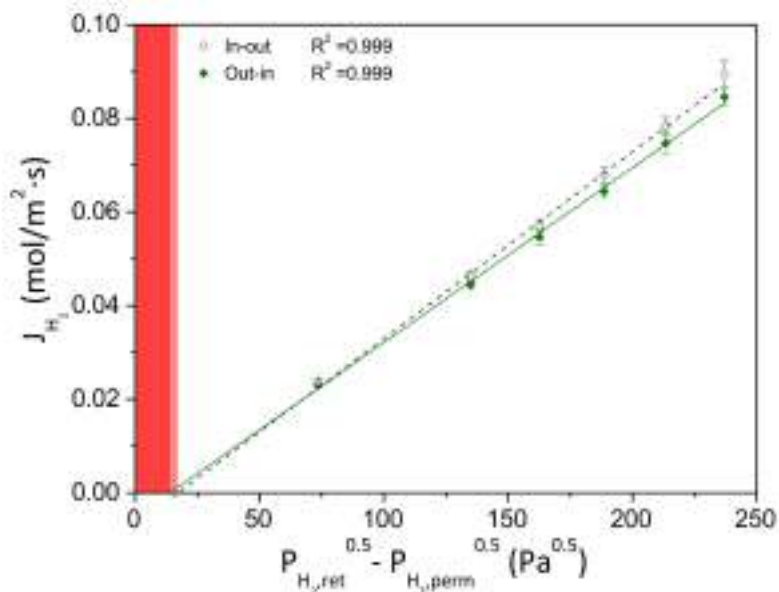


Figure 7. Permeation behavior working at diverse operating modes: out-in (colored symbols) and in-out (hollow symbols). Deviation from origin interception marked as a red vertical band for each case.

First, it should be mentioned that no nitrogen was detected for the entire range of pressures despite the new configuration. Thus, an adequate mechanical resistance of the Pd layer and, consequently, of the whole membrane, can be deduced. Moreover, as can be seen, very similar behavior can be observed independently of the followed operating mode. A clear linear relationship between the H_2 permeate flux and pressure driving forces appears, although with a certain deviation from the origin as previously addressed. This deviation slightly increases in the case of permeating from the inner to the outer side of the membrane (mode in-out). The presence of the porous support on the retentate side, where the highest pressure is applied, can explain this fact. In this manner, the permeate has to pass through the intrinsic porosity of the modified graphite-PSS support and its tortuosity. Moreover, it is possible to find a certain amount of palladium inside the pores, before reaching the fully dense Pd film that is placed on the contrary side. It provokes a certain resistance to the mass transfer and, consequently, a deviation between the measured feed/retentate pressure and the exact value just close to the palladium layer. This particular behavior was widely explained in some previous studies for other ELP-PP membranes [36,41].

As a consequence of the above-mentioned behavior, H_2 permeance slightly increases for this operating mode (in-out) up to $3.75 \times 10^{-4} \text{ mol m}^{-2} \text{ s}^{-1} \text{ Pa}^{-0.5}$ from the value $4.01 \times 10^{-4} \text{ mol m}^{-2} \text{ s}^{-1} \text{ Pa}^{-0.5}$ reached with contrary permeate flux direction (out-in).

3.2.4. Literature Setting for Permeation Behavior

Finally, Table 1 includes a literature survey about some representative achievements reached for other composite Pd-based membranes to be compared with the results presented in this study. The comparison consists of membranes fabricated by electroless plating or related techniques onto supports made of different materials or various geometries. The wide variety of information about membrane composition, structure, morphology, and permeation experimental details, among others, clearly increases the complexity of a rigorous comparison.

Table 1. Comparison of main characteristics and performance for relevant membranes in literature.

Support	Intermediate Layer	H ₂ -Selective Layer		Membrane Performance at ΔP = 1 bar					Ref.
		Incorporation Technique	Composition	t _{Pd} (μm)	Operating Mode	T (K)	Permeate Flux (m ³ m ⁻² h ⁻¹)	α _{H2/N2}	
- ⁽¹⁾	-	Cold-rolling	PdAg	50	in-out	573	1.1 × 10 ⁻²	-	[42]
PSS ⁽¹⁾	Fe ₂ O ₃ –Cr ₂ O ₃	ELP	Pure Pd	20	out-in	623	3.4	500	[43]
PSS ⁽¹⁾	Fe ₂ O ₃ –Cr ₂ O ₃	ELP-PP	Pure Pd	11–20	in-out	623–723	1.1–2.2	∞	[30]
PSS ⁽¹⁾	Al ₂ O ₃	ELP	Pure Pd	5	out-in	673	3.3	500	[44]
PSS ⁽¹⁾	CeO ₂	ELP	Pure Pd	13	out-in	773–823	10.2–22.2	∞	[45]
PSS ⁽²⁾	CeO ₂	ELP	PdCu	8	-	723	5.9	2369	[46]
PSS ⁽¹⁾	ZrO ₂	ELP	PdAu	14–27	out-in	673–773	3.8–7.8	4000	[47]
Al ₂ O ₃ ⁽¹⁾	-	ELP-duplex	Pure Pd	2.8/2.5	out-in	773	17.7	14,429	[40]
PSS ⁽¹⁾	Fe ₂ O ₃ –Cr ₂ O ₃ /CeO ₂	ELP-PP	Pure Pd	15.4	out-in	673	4.6	≥10,000	[22]
PSS ⁽¹⁾	Fe ₂ O ₃ –Cr ₂ O ₃ /CeO ₂	ELP-PP	Pure Pd	15.4	in-out	673	4.8	≥10,000	[22]
PSS ⁽¹⁾	Fe ₂ O ₃ –Cr ₂ O ₃ /Pd-doped CeO ₂	ELP-PP	Pure Pd	9.1	out-in	673	5.1	≥10,000	[35]
PSS ⁽¹⁾	Fe ₂ O ₃ –Cr ₂ O ₃ /Pd-doped CeO ₂	ELP-PP	Pure Pd	9.1	in-out	673	5.3	≥10,000	[35]
Al ₂ O ₃ ⁽¹⁾	Graphite	ELP	Pure Pd	5	out-in	673	22.7	3100	[26]
NiO/Al ₂ O ₃ ⁽¹⁾	Graphite	ELP	Pure Pd	5	out-in	623–723	16–20	500–750	[27]
Al ₂ O ₃ ⁽¹⁾	Graphite	ELP	Pure Pd	5	out-in	623–723	14–18	5500–7500	[27]
Al ₂ O ₃ ⁽¹⁾	Nontronite-15A	ELP	Pure Pd	5	out-in	623–723	11.3–16.9	2000–3700	[48]
Al ₂ O ₃ ⁽³⁾	Graphite	ELP	Pure Pd	1.81	out-in	573–723	0.8–8.9	∞	[28]
PSS ⁽¹⁾	Graphite	ELP	Pure Pd	7	out-in	623–723	12–18	60–120	[29]
PSS ⁽¹⁾	Fe ₂ O ₃ –Cr ₂ O ₃ /Graphite	ELP-PP	Pure Pd	17	out-in	623–723	3.7–4.8	≥10,000	This work
PSS ⁽¹⁾	Fe ₂ O ₃ –Cr ₂ O ₃ /Graphite	ELP-PP	Pure Pd	17	in-out	673	4.4	≥10,000	This work

Membrane geometry: ⁽¹⁾ tubular, ⁽²⁾ disc, and ⁽³⁾ hollow fiber.

In general, the thinnest selective films have the highest hydrogen permeation, although it is also common to find a limited H₂ permeation in these cases. In this work, an ideal H₂/N₂ separation factor higher than 10,000 was obtained for the entire set of experiments, independently of the operating mode, out-in or in-out. This fact remarks on the excellent mechanical resistance of the ELP-PP membranes with an intermediate layer made of graphite presented in this work. Similar demonstrations for other Pd membranes reported in the literature are certainly scarce. However, the membranes shown here maintained their integrity against diverse permeation flux directions for the entire set of experiments carried out under compressive or tensile strengths generated by the pressure difference between both retentate and permeate sides, thus opening new possibilities for use in a wide variety of reactor configurations. At these conditions, the permeate fluxes reached at ΔP = 1 bar were maintained in the range 3.7–4.8 m³ m⁻² h⁻¹.

These values are within the typical ones reached for other completely H₂-selective membranes prepared by ELP-PP but containing various intermediate layers. However, they seem to be slightly lower than those of other membranes prepared by conventional ELP, mostly onto alumina supports. The initial high surface quality of these supports, in terms of roughness and average pore sizes, makes the incorporation of a thin Pd film easier and, in general, they present a lower Pd thickness and higher permeate fluxes. On the contrary, it should be noted that H₂ selectivity is usually compromised.

4. Conclusions

Previously calcined porous stainless-steel supports with an initial media grade of 0.1 μm were satisfactorily modified by incorporating graphite particles from a lead pencil as an intermediate layer to improve the following incorporation of palladium by electroless pore-plating. The carbon particles remained preferentially inside the external pores of the supports, thus partially blocking the original biggest superficial pore mouths and generating a new porous structure with smaller average pore sizes and lower roughness. After this modification, completely dense Pd layers with an estimated gravimetric thickness of around 17 μm were obtained. However, cross-sectional SEM images revealed a slightly thinner true external thickness in the range 8–12 μm with a certain infiltration of the palladium inside the pores up to around 35 μm in depth. This particular incorporation of the palladium is caused by the intrinsic characteristics of the ELP-PP process, where the chemical reaction between palladium ions and hydrazine initiates inside the pores.

These new membranes exhibit H₂ permeances in the range 3.24×10^{-4} to 4.33×10^{-4} mol m⁻² s⁻¹ Pa^{-0.5} when permeating from the outer to the inner side (mode out-in) at temperatures ranging from 350 to 450 °C, respectively. Moreover, an ideal H₂/N₂ perm-selectivity ≥10,000 was maintained for the entire set of experiments. Going into detail about the permeation behavior of these membranes, a general linear trend between permeate H₂ fluxes and pressure-driving forces can be found but without a clear intercept in (0,0) as predicted by the Sieverts' law. The Pd partial infiltration inside the pore structure of the support during the ELP-PP process explains this deviation, as typically occurs for other similar membranes in which both external and internal Pd surfaces become noticeably different. The outer surface is certainly smooth, with the measured pressure values into the bulk gas phase and the surface of the membrane being almost identical. However, the internal one is much more tortuous, and the assumptions of negligible differences between both sides are not clear. At these conditions, the calculated pressure-driving force from retentate and permeate bulk gas phases can be imprecise, and apparent additional resistances to the permeation process appear. The temperature effect on the H₂ permeate fluxes, according to an Arrhenius-type dependence, was also evident for all performed experiments with activation energy around 10.6 kJ/mol, very close to that of multiple Pd composite membranes.

In the case of testing binary H₂–N₂ mixtures, increasing the N₂ content in the feed stream from 0 to 40 vol%, H₂ permeances progressively decreased up to around 33% in the worst conditions. A certain contribution of the well-known concentration–polarization effect, despite the strongly inert character

of nitrogen, could explain this fact. This effect is not constant for any concentration of the mixture, being more marked for lower dilutions.

Finally, some additional experiments were also performed after reversing the direction of the permeate flux. Certainly, similar results were reached in terms of permeate fluxes and H₂ selectivity. Therefore, adequate mechanical resistance was practically demonstrated despite operating at the most unfavorable conditions (mode in-out) in which certain tensile stress is generated on the Pd layer.

Supplementary Materials: The following are available online at <http://www.mdpi.com/2077-0375/10/12/410/s1>, Figure S1: Validation of permeation measurements by testing three different membranes prepared at analogous conditions (PSS/GRAPH/Pd) under consecutive thermal cycles.

Author Contributions: Conceptualization, D.A. and D.M.-D.; methodology, D.M.-D. and D.A.; formal analysis, D.A., J.A.C., R.S. and A.C.; investigation, D.M.-D.; resources, D.A.; writing—original draft preparation, D.A. and D.M.-D.; writing—review and editing, D.A., J.A.C., R.S. and A.C.; supervision, D.A., J.A.C., R.S. and A.C.; funding acquisition, J.A.C. and A.C. All authors have read and agreed to the published version of the manuscript.

Funding: This research was funded by the Spanish Ministry of Economy and Competitiveness through grant number ENE2017-83696-R.

Acknowledgments: The authors sincerely express their gratitude to the Spanish Ministry of Economy and Competitiveness for the financial support previously indicated and the Material Science and Engineering area of Rey Juan Carlos University for supporting the characterization of samples by scanning electron microscopy.

Conflicts of Interest: The authors declare no conflict of interest.

References

- Yue, X.-L.; Gao, Q.-X.; Xi-Liu, Y.; Qing-Xian, G. Contributions of natural systems and human activity to greenhouse gas emissions. *Adv. Clim. Chang. Res.* **2018**, *9*, 243–252. [[CrossRef](#)]
- Szulejko, J.E.; Kumar, P.; Deep, A.; Tsang, D.C.W. Global warming projections to 2100 using simple CO₂ greenhouse gas modeling and comments on CO₂ climate sensitivity factor. *Atmos. Pollut. Res.* **2017**, *8*, 136–140. [[CrossRef](#)]
- Abdin, Z.; Zafaranloo, A.; Rafiee, A.; Mérida, W.; Lipiński, W.; Khalilpour, K.R. Hydrogen as an energy vector. *Renew. Sustain. Energy Rev.* **2020**, *120*, 109620. [[CrossRef](#)]
- Iulianelli, A.; Liguori, S.; De Vita, A.; Italiano, C.; Fabiano, C.; Huang, Y.; Basile, A. The oncoming energy vector: Hydrogen produced in Pd-composite membrane reactor via bioethanol reforming over Ni/CeO₂ catalyst. *Catal. Today* **2016**, *259*, 368–375. [[CrossRef](#)]
- Baykara, S.Z. Hydrogen: A brief overview on its sources, production and environmental impact. *Int. J. Hydrot. Energy* **2018**, *43*, 10605–10614. [[CrossRef](#)]
- Sołowski, G.; Shalaby, M.S.; Abdallah, H.A.M.; Shaban, A.; Cerian, A. Production of hydrogen from biomass and its separation using membrane technology. *Renew. Sustain. Energy Rev.* **2018**, *82*, 3152–3167. [[CrossRef](#)]
- Matsakas, L.; Gao, Q.; Jansson, S.; Rova, U.; Christakopoulos, P. Green conversion of municipal solid wastes into fuels and chemicals. *Electron. J. Biotechnol.* **2017**, *26*, 69–83. [[CrossRef](#)]
- Itoh, N.; Kikuchi, Y.; Furusawa, T.; Sato, T. Tube-wall catalytic membrane reactor for hydrogen production by low-temperature ammonia decomposition. *Int. J. Hydrot. Energy* **2020**. [[CrossRef](#)]
- Ahmad, H.; Kamarudin, S.; Minggu, L.J.; Kassim, M.B. Hydrogen from photo-catalytic water splitting process: A review. *Renew. Sustain. Energy Rev.* **2015**, *43*, 599–610. [[CrossRef](#)]
- Abdalla, A.M.; Hossain, S.; Nisfindy, O.B.; Azad, A.T.; Dawood, M.; Azad, A.K. Hydrogen production, storage, transportation and key challenges with applications: A review. *Energy Convers. Manag.* **2018**, *165*, 602–627. [[CrossRef](#)]
- Quarton, C.J.; Samsatli, S. Power-to-gas for injection into the gas grid: What can we learn from real-life projects, economic assessments and systems modelling? *Renew. Sustain. Energy Rev.* **2018**, *98*, 302–316. [[CrossRef](#)]
- Alique, D.; Zhang, J.; Jung, Y.-G. (Eds.) Processing and Characterization of Coating and Thin Film Materials in. *Adv. Ceram. Met. Coat. Thin Film Mater. Energy Environ. Appl.* **2018**. [[CrossRef](#)]
- Bernardo, G.; Araújo, T.; Lopes, T.D.S.; Sousa, J.; Mendes, A. Recent advances in membrane technologies for hydrogen purification. *Int. J. Hydrot. Energy* **2020**, *45*, 7313–7338. [[CrossRef](#)]

14. Gao, Y.; Jiang, J.; Meng, Y.; Yan, F.; Aihemaiti, A. A review of recent developments in hydrogen production via biogas dry reforming. *Energy Convers. Manag.* **2018**, *171*, 133–155. [[CrossRef](#)]
15. Brunetti, A.; Caravella, A.; Drioli, E.; Barbieri, G. CHAPTER 1: Membrane Reactors for Hydrogen Production. In *Membrane Engineering for the Treatment of Gases: Gas-separation Issues Combined with Membrane Reactors*; Royal Society of Chemistry: London, UK, 2017; Volume 2, pp. 1–29. [[CrossRef](#)]
16. Di Marcoberardino, G.; Binotti, M.; Manzolini, G.; Viviente, J.L.; Arratibel Plazaola, A.; Roses, L.; Gallucci, F. Achievements of European projects on membrane reactor for hydrogen production. *J. Clean. Prod.* **2017**, *161*, 1442–1450. [[CrossRef](#)]
17. Alique, D.; Sanz, R.; Calles, J. Pd membranes by electroless pore-plating. *Curr. Trends Future Dev. (Bio-) Membr.* **2020**, *31*–62. [[CrossRef](#)]
18. Peters, T.; Rørvik, P.; Sunde, T.; Stange, M.; Roness, F.; Reinertsen, T.; Ræder, J.; Larring, Y.; Bredesen, R. Palladium (Pd) Membranes as Key Enabling Technology for Pre-combustion CO₂ Capture and Hydrogen Production. *Energy Procedia* **2017**, *114*, 37–45. [[CrossRef](#)]
19. Yun, S.; Oyama, S.T. Correlations in palladium membranes for hydrogen separation: A review. *J. Membr. Sci.* **2011**, *375*, 28–45. [[CrossRef](#)]
20. Melendez, J.; Fernandez, E.; Gallucci, F.; Annaland, M.V.S.; Arias, P.L.; Tanaka, D.A.P. Preparation and characterization of ceramic supported ultra-thin (~1 μm) Pd-Ag membranes. *J. Membr. Sci.* **2017**, *528*, 12–23. [[CrossRef](#)]
21. Li, H.; Caravella, A.; Xu, H.Y. Recent progress in Pd-based composite membranes. *J. Mater. Chem. A* **2016**, *4*, 14069–14094. [[CrossRef](#)]
22. Martinez-Diaz, D.; Sanz, R.; Calles, J.A.; Alique, D. H₂ permeation increase of electroless pore-plated Pd/PSS membranes with CeO₂ intermediate barriers. *Sep. Purif. Technol.* **2019**, *216*, 16–24. [[CrossRef](#)]
23. Lee, C.-B.; Lee, S.-W.; Park, J.-S.; Ryi, S.-K.; Lee, D.-W.; Hwang, K.-R.; Kim, S.-H. Ceramics used as intermetallic diffusion barriers in Pd-based composite membranes sputtered on porous nickel supports. *J. Alloy. Compd.* **2013**, *578*, 425–430. [[CrossRef](#)]
24. Arratibel, A.; Medrano, J.A.; Melendez, J.; Tanaka, D.A.P.; Annaland, M.V.S.; Gallucci, F. Attrition-resistant membranes for fluidized-bed membrane reactors: Double-skin membranes. *J. Membr. Sci.* **2018**, *563*, 419–426. [[CrossRef](#)]
25. Arratibel, A.; Tanaka, A.P.; Laso, I.; Annaland, M.V.S.; Gallucci, F. Development of Pd-based double-skinned membranes for hydrogen production in fluidized bed membrane reactors. *J. Membr. Sci.* **2018**, *550*, 536–544. [[CrossRef](#)]
26. Hu, X.; Chen, W.; Huang, Y. Fabrication of Pd/ceramic membranes for hydrogen separation based on low-cost macroporous ceramics with pencil coating. *Int. J. Hydrol. Energy* **2010**, *35*, 7803–7808. [[CrossRef](#)]
27. Hu, X.; Yan, W.; Ding, W.; Yu, J.; Huang, Y. Bifunctional palladium composite membrane for hydrogen separation and catalytic CO methanation. *Chin. J. Catal.* **2013**, *34*, 1720–1729. [[CrossRef](#)]
28. Terra, N.M.; Bessa, L.P.; Cardoso, V.L.; Reis, M.H.M. Graphite coating on alumina substrate for the fabrication of hydrogen selective membranes. *Int. J. Hydrol. Energy* **2018**, *43*, 1534–1544. [[CrossRef](#)]
29. Wei, L.; Yu, J.; Hu, X.; Huang, Y. Facile surface modification of porous stainless steel substrate with TiO₂ intermediate layer for fabrication of H₂-permeable composite palladium membranes. *Sep. Sci. Technol.* **2016**, *51*, 998–1006. [[CrossRef](#)]
30. Sanz, R.; Calles, J.A.; Alique, D.; Furones, L. New synthesis method of Pd membranes over tubular PSS supports via “pore-plating” for hydrogen separation processes. *Int. J. Hydrol. Energy* **2012**, *37*, 18476–18485. [[CrossRef](#)]
31. Furones, L.; Alique, D. Interlayer Properties of In-Situ Oxidized Porous Stainless Steel for Preparation of Composite Pd Membranes. *Chem. Eng.* **2017**, *2*, 1. [[CrossRef](#)]
32. Sanz-Villanueva, D.; Alique, D.; Vizcaíno, A.; Sanz, R.; Calles, J. Pre-activation of SBA-15 intermediate barriers with Pd nuclei to increase thermal and mechanical resistances of pore-plated Pd-membranes. *Int. J. Hydrol. Energy* **2020**. [[CrossRef](#)]
33. Alique, D.; Martinez-Diaz, D.; Sanz, R.; Calles, J. Review of Supported Pd-Based Membranes Preparation by Electroless Plating for Ultra-Pure Hydrogen Production. *Membranes* **2018**, *8*, 5. [[CrossRef](#)]
34. Alique, D.; Imperatore, M.; Sanz, R.; Calles, J.A.; Baschetti, M.G. Hydrogen permeation in composite Pd-membranes prepared by conventional electroless plating and electroless pore-plating alternatives over ceramic and metallic supports. *Int. J. Hydrol. Energy* **2016**, *41*, 19430–19438. [[CrossRef](#)]

35. Martinez-Diaz, D.; Alique, D.; Calles, J.; Sanz, R. Pd-thickness reduction in electroless pore-plated membranes by using doped-ceria as interlayer. *Int. J. Hydrol. Energy* **2020**, *45*, 7278–7289. [[CrossRef](#)]
36. Calles, J.A.; Sanz, R.; Alique, D.; Furones, L.; Marín, P.; Ordóñez, S. Influence of the selective layer morphology on the permeation properties for Pd-PSS composite membranes prepared by electroless pore-plating: Experimental and modeling study. *Sep. Purif. Technol.* **2018**, *194*, 10–18. [[CrossRef](#)]
37. Conde, J.J.; Maroño, M.; Sánchez-Hervás, J.M. Pd-Based Membranes for Hydrogen Separation: Review of Alloying Elements and Their Influence on Membrane Properties. *Sep. Purif. Rev.* **2017**, *46*, 152–177. [[CrossRef](#)]
38. Al-Mufachi, N.; Rees, N.; Steinberger-Wilkins, R. Hydrogen selective membranes: A review of palladium-based dense metal membranes. *Renew. Sustain. Energy Rev.* **2015**, *47*, 540–551. [[CrossRef](#)]
39. Fernandez, E.; Medrano, J.A.; Melendez, J.; Parco, M.; Viviente, J.L.; Annaland, M.V.S.; Gallucci, F.; Tanaka, D.A.P. Preparation and characterization of metallic supported thin Pd–Ag membranes for hydrogen separation. *Chem. Eng. J.* **2016**, *305*, 182–190. [[CrossRef](#)]
40. Zhao, C.; Xu, H.; Goldbach, A. Duplex Pd/ceramic/Pd composite membrane for sweep gas-enhanced CO₂ capture. *J. Membr. Sci.* **2018**, *563*, 388–397. [[CrossRef](#)]
41. Sanz, R.; Calles, J.; Ordóñez, S.; Marín, P.; Alique, D.; Furones, L. Modelling and simulation of permeation behaviour on Pd/PSS composite membranes prepared by “pore-plating” method. *J. Membr. Sci.* **2013**, *446*, 410–421. [[CrossRef](#)]
42. Miguel, C.; Mendes, A.; Tosti, S.; Madeira, L.M. Effect of CO and CO₂ on H₂ permeation through finger-like Pd–Ag membranes. *Int. J. Hydrol. Energy* **2012**, *37*, 12680–12687. [[CrossRef](#)]
43. Mardilovich, P.P.; She, Y.; Ma, Y.H.; Rei, M.-H. Defect-free palladium membranes on porous stainless-steel support. *AIChE J.* **1998**, *44*, 310–322. [[CrossRef](#)]
44. Gade, S.K.; Thoen, P.M.; Way, J.D. Unsupported palladium alloy foil membranes fabricated by electroless plating. *J. Membr. Sci.* **2008**, *316*, 112–118. [[CrossRef](#)]
45. Tong, J.; Matsumura, Y.; Suda, H.; Haraya, K. Thin and dense Pd/CeO₂/MPSS composite membrane for hydrogen separation and steam reforming of methane. *Sep. Purif. Technol.* **2005**, *46*, 1–10. [[CrossRef](#)]
46. Qiao, A.; Zhang, K.; Tian, Y.; Xie, L.; Luo, H.; Lin, J.Y.; Li, Y. Hydrogen separation through palladium-copper membranes on porous stainless steel with sol-gel derived ceria as diffusion barrier. *Fuel* **2010**, *89*, 1274–1279. [[CrossRef](#)]
47. Contardi, I.; Cornaglia, L.; Tarditi, A.M. Effect of the porous stainless steel substrate shape on the ZrO₂ deposition by vacuum assisted dip-coating. *Int. J. Hydrol. Energy* **2017**, *42*, 7986–7996. [[CrossRef](#)]
48. Huang, Y.; Liu, Q.; Jin, X.; Ding, W.; Hu, X.; Li, H. Coating the porous Al₂O₃ substrate with a natural mineral of Nontronite-15A for fabrication of hydrogen-permeable palladium membranes. *Int. J. Hydrol. Energy* **2020**, *45*, 7412–7422. [[CrossRef](#)]

Publisher's Note: MDPI stays neutral with regard to jurisdictional claims in published maps and institutional affiliations.



© 2020 by the authors. Licensee MDPI, Basel, Switzerland. This article is an open access article distributed under the terms and conditions of the Creative Commons Attribution (CC BY) license (<http://creativecommons.org/licenses/by/4.0/>).



H₂ permeation increase of electroless pore-plated Pd/PSS membranes with CeO₂ intermediate barriers

D. Martinez-Díaz, R. Sanz, J.A. Calles, D. Alique*

Dep. of Chemical, Energy and Mechanical Technology, Rey Juan Carlos University, C/Tulipán s/n, 28933 Móstoles, Spain



ARTICLE INFO

Keywords:
 Supported-membrane
 Porous stainless steel
 Surface modification
 Ceria
 Palladium
 Electroless plating
 Hydrogen

ABSTRACT

This work presents the improvement of hydrogen permeance on electroless pore-plated Pd-composite membranes by the incorporation of ceria as intermediate barrier. This modification, in case of preparing a thick barrier, reduces both average pore size and external roughness of an oxidized Porous Stainless Steel (PSS) tube used as support. However, it also provokes a marked reduction of its permeance, turning more difficult the pass of the hydrazine through the modified support and, therefore, the palladium incorporation by electroless pore-plating. An optimization of this process leads to a Pd/CeO₂/PSS composite membrane in which the initial roughness is halved, achieving a stable and selective Pd layer of around 15 μm. This composite membrane exhibits a hydrogen permeance of $5.37 \cdot 10^{-4} \text{ mol m}^{-2} \text{ s}^{-1} \text{ Pa}^{-0.5}$ at 400 °C, an ideal H₂/N₂ perm-selectivity $\geq 10,000$ and an activation energy of 8.9 kJ mol⁻¹. Moreover, the hydrogen flux increases around 400% with regard to previous results, in which no ceria was used as intermediate layer (measured range: 0.03–0.12 mol m⁻² s⁻¹ versus 0.01–0.03 mol m⁻² s⁻¹). This increase is derived from a high reduction, of around 30%, in the resistance to the permeation process when using electroless pore-plated membranes due to a lower penetration grade of the Pd external film into the support. In addition, it has been confirmed the successfully stability of the Pd membrane under thermal cycles and different operating conditions, including the variation of permeate flux direction from the inner to the outer of the membrane, where the Pd-layer is placed, or *vice versa*.

1. Introduction

Future perspectives foreseen an increase of the worldwide energy demand, mainly as a result of the continuous growth of emerging countries [1,2]. Maintaining the current energy system, based on the massive use of fossil fuels, the global warming produced by anthropogenic carbon dioxide emissions will get worse [3] and therefore, different strategies have been considered to mitigate this problem. A progressive transition to renewable energies has been initiated, principally promoted by Europe and Japan, with very ambitious policies and important investments to develop new technologies [4,5]. Moreover, improvements in energy efficiency and reductions in energy demand are expected to contribute more than half of the reduction in global carbon emissions in the next few decades. The use of process intensification strategies in most of current industrial processes is one of the most challenge alternatives [6,7]. Moreover, the hydrogen economy could also play a very important role to realize these transitions [8].

Despite hydrogen can be produced by multiple resources, nowadays thermal processes based on hydrocarbons represent the most important

contribution in terms of production and it is certainly the first alternative to be considered in order to facilitate the mentioned transition for a sustainable energy scenario in the future [8]. However, it is important to point out that hydrogen obtained by thermal processes is always accompanied by other sub-products, in this manner additional separation and purification steps are key aspects to obtain hydrogen at required purity and reasonable cost for each particular application [9]. The use of selective palladium-based dense membranes is as a very attractive alternative for hydrogen purification. In an ideal case, this technology allows a complete H₂ selectivity by a solution-diffusion permeation mechanism while maintaining adequate integrity and permeate fluxes at high temperatures, as it is typically required for most of the industrial processes [10,11]. The permeability of these membranes is mainly influenced by the membrane composition (distinguishing pure palladium and multiple palladium-based alloys) [12], the metal thickness (being inversely proportional to the permeate flux, as described the Sieverts' law) [13] and the operating conditions (pressure difference between retentate and permeate sides, temperature and feed composition) [14,15]. In this context, most researchers suggest the use

* Corresponding author.

E-mail address: david.aliique@urjc.es (D. Alique).

of composite membranes, in which a porous substrate provides enough mechanical resistance to the membrane allowing to reduce the Pd-based selective film thickness up to a few microns [16,17]. This selective film is deposited onto an appropriate support controlling and minimizing the presence of defects in the composite system [16].

Ceramic supports (mainly made of alumina) provides a smooth surface with proper accuracy for pore size distribution. Thus, they make possible to achieve high porosity with really narrow pore sizes that makes the preparation of the palladium film easier [18,19]. However, the important difference of thermal expansion coefficients between both materials and difficulties to achieve proper sealing with common industrial devices (usually made of stainless steel) are the main disadvantages of this alternative. On the other side, porous metals (mainly stainless steel, SS) overcome these problems at the expense of presenting a rough surface with a wide pore size distribution that compromises the generation of a thin palladium film [20,21]. Additionally, in the case of operating at high temperatures for long times, metal inter-diffusion between support and selective layer might occurs, worsening dramatically the membrane performance [22]. In order to overcome this phenomenon and avoid direct contact between these two, metal support and H₂-selective palladium film, the use of intermediate layers has been widely proposed [22,23]. Moreover, the incorporation of other materials as intermediate layer can also improve the external surface of the support reducing both roughness, pore mouth sizes and, consequently, the minimum palladium thickness required to prepare a totally defect-free H₂-selective layer [24]. At this point, the material selection for this intermediate layer is a key of interest, being possible to find multiple options in literature, i.e. Fe₂O₃ [25,26], Cr₂O₃ [27], SiO₂ [28], Al₂O₃ [22,29], ZrO₂ [30], YSZ [31,32], TiO₂ [33] or CeO₂ [34], among others [24,35,36]. Recently, it has been published a review including an interesting representation of thermal expansion coefficients of most common technical ceramics used as intermediate layers for membrane preparation over porous metal supports, also covering the values for support, palladium and other alloying metals [16]. In this review, the authors affirm that the ideal situation to ensure a proper mechanical performance of the composite membrane implies the selection of a technical ceramic with a thermal expansion coefficient in the region between those H₂-selection layer and metal support constituents, as occurs in case of considering CeO₂ [16].

After selecting both support and intermediate layer (in case of being considered), the incorporation of the palladium layer can be carried out by several techniques. Among them, electroless plating (ELP) is one of the preferred ones due to the low energy requirements, the equipment simplicity and the possibility to cover complex geometries [37]. Usually, both palladium source (typically containing Pd²⁺) and reducing agent are fed together from the same side of the support (inner or outer) to obtain a Pd⁰ layer. The Pd deposition progress increases its thickness until the reactants are spent or the membrane is removed from the solution. However, a modification of this bare method, denoted as electroless pore-plating (ELP-PP), has been presented as a good alternative to ensure correct anchoring between both support and palladium film while the presence of defects during the preparation process is minimized [15,38,39]. Basically, the method consists of feeding both solutions (Pd source and reducing agent) from opposite sides of the support until the pores get completely sealed. The final membrane contains an external palladium film as well as a certain grade of palladium infiltration inside the pores in function of the experimental conditions used for the membrane preparation [38,40]. After optimizing these experimental conditions for raw and oxidized porous stainless steel (PSS) supports, membranes with good performance (high H₂-selectivity and mechanical resistance for both permeation and reaction tests) were obtained, although the mentioned palladium distribution in the support provokes the generation of an additional resistance to the overall permeation process [40,41].

The present work includes for the first time the preparation of an electroless pore-plated membrane over a PSS support modified by the

incorporation of a CeO₂ intermediate layer. This ceramic material presents a thermal expansion coefficient of 11.8–13.2 $\mu\text{strain}/^\circ\text{C}$, which is fairly close to that of both palladium and AISI 316L SS (10.6–12.6 and 15.0–18.0, respectively). This fact theoretically ensures a good mechanical resistance of the composite membrane. Furthermore, the surface modification derived from the incorporation of this intermediate layer expects to improve the permeation behavior of previously obtained electroless pore-plated membranes.

2. Experimental procedure

2.1. Membrane preparation

Tubular AISI 316L PSS supports purchased from Mott Metallurgical Corp. with 0.1 μm grade and symmetric structure were used for this work. The original support with $1/2"$ OD was cut into shorter pieces of 30 mm. The general procedure for the membrane preparation consists of five successive steps: (i) initial cleaning, (ii) support calcination, (iii) CeO₂ intermediate layer incorporation, (iv) activation and (v) palladium deposition by ELP-PP. Details about the first two general steps in which the supports were cleaned and calcined can be found in previous works [26,42].

The main novelty of this work is based on the incorporation of a CeO₂ intermediate layer in order to reduce the inter-metallic diffusion and modify both pore mouth size and external surface roughness prior to generate the palladium layer. In this context, the calcined supports were modified with CeO₂ by means of a vacuum-assisted method. A suspension of commercial CeO₂ particles (Alfa-Aesar, 100 nm average particle size) in water and polyvinyl alcohol (2 wt.%) was prepared for a CeO₂ concentration of around 20 wt.% and the material was incorporated to the external surface of the support by dip-coating. After sealing the inner side of the calcined support, it was introduced into the suspension twice applying vacuum at the last minutes of the second cycle in order to guarantee the particles deposition into the pores of the support, leading to a really thick and wet CeO₂ layer on the external surface. In this work, the possible influence of this layer thickness has been also considered, evaluating the facility to be permeable for different gases and the reactants of the ELP-PP process. Thus, samples with different CeO₂ thicknesses were prepared by removing in different grade the excess of ceria incorporated onto the external surface of the support. This process was carried out by successive rinsing steps in distilled water. After adjusting the optimal thickness for the CeO₂ intermediate layer, all modified supports were calcined at 500 °C for 5 h in order to ensure their stability. Finally, the palladium deposition was carried out by ELP-PP following the experimental procedure detailed elsewhere [38–40] with a hydrazine concentration of 0.2 M as reducing agent. Diverse cycles were performed up to the membrane weight gain became negligible, indicative to a good sealing of pores with palladium.

2.2. Membrane characterization

The morphology of all samples here included were completely characterized with a scanning electron microscope (Philips XL30 ESEM) equipped with an energy dispersive analytical system (EDAS) for microprobe analysis. The external surface was observed before and after the incorporation of CeO₂ intermediate layers and the ELP-PP Pd film to analyze the uniformity and possible presence of defects. Additionally, some final composite membranes were also cut in order to observe the membrane conformation in radial direction. The external roughness of the samples after each experimental step, defined as the arithmetic mean height of the external surface from its ideally smooth form, were also determined with an optical profiler (Zeta-20 Optical Profiler). Furthermore, gravimetric analyses were also used to measure the material incorporation to the membrane (for both CeO₂ and Pd layers) and estimate the average layer thickness through the membrane weight gain after each process.

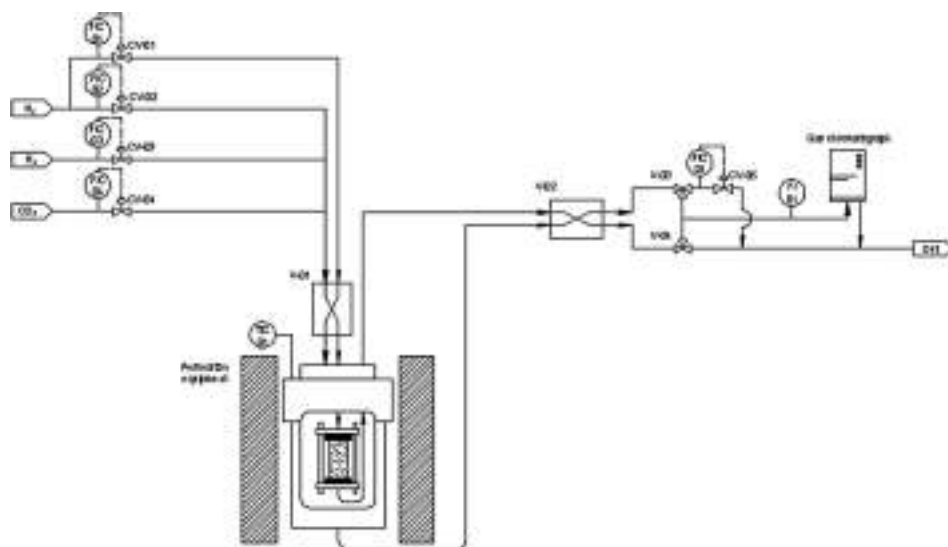


Fig. 1. Basic scheme of the permeation setup.

2.3. Permeation measurements

First, some preliminary leak tests at room temperature were performed to ensure good properties of the membranes and absence of defects, mainly in the palladium layer. After that, the permeation behavior of membranes at high temperature was analyzed in a previously reported home-made setup [41], including here a basic scheme (Fig. 1). Basically, the setup consisted in a stainless steel cell that contains the Pd-membrane placed between two graphite O-rings to ensure the seal between retentate and permeate sides. This assembly is placed into an electrical furnace to achieve the desired temperature for each experiment. Several permeation experiments with pure gases (nitrogen and hydrogen) and pressure differences between retentate and permeate sides from 0.5 to 2.0 bar have been carried out to determine the membrane permeability and ideal hydrogen selectivity of the prepared samples. In these experiments the permeate stream is always maintained at atmospheric conditions without help of sweep gas. Taking into account the use of pure palladium for the preparation of the composite membranes here included, all experiments were performed at temperatures ranged from 350 to 475 °C to avoid the possible hydrogen embrittlement of the palladium film. The influence of permeation flux direction was also studied. In this way, the palladium layer is always placed onto the external support surface and two different experiments were performed by introducing the feed stream: a) in the inner side of the tubular membrane while the permeate stream is collected in the shell side and b) vice versa, permeating from the outer to the inner side. In the first set of experiments, the membrane is working at the most unfavorable conditions for mechanical resistance and tensile stress.

3. Results and discussion

The most relevant results here presented have been organized in three different sections: the modification of oxidized PSS support by incorporation of CeO₂ intermediate layers, the palladium deposition by ELP-PP over the new modified supports and the permeation properties of the materials obtained with pure gases. Finally, a comparison of the reached permeation behavior with the previously published ones in case of omitting the use of a ceramic intermediate barrier has been included as well.

3.1. Support modification: preparation of CeO₂ intermediate layers

Oxidized PSS supports by calcination in air at high temperature have been previously reported as suitable alternative to prepare composite Pd-membranes by ELP-PP method [15,40]. This treatment generates mixed Fe-Cr oxides on the external surface for each SS particle of the supports, obtaining a mass variation per unit length of $\Delta m/L = 5.8000 \pm 0.2500 \text{ g/m}$ at 600 °C and 12 h. The oxidized PSS supports maintain a permeability greater than the suggested one by DOE target values, while the external surface is just slightly modified. In this section, the modification of original surface properties for these supports is presented by incorporating an intermediate layer formed by CeO₂ particles onto the previously oxidized PSS supports. As it has been detailed in the experimental section, this intermediate layer was generated by vacuum-assisted dip-coating with a suspension containing a 20 wt.% in ceria, which yields an initial thick ceramic layer to ensure good homogeneity and reproducibility. However, this great thickness could represent an important drawback for the mechanical stability of the membrane due to the limited adhesion strength of the ceramic particles with the oxidized PSS support. This problem could be also especially relevant for permeation experiments, in which tensile stresses are generated by the permeation direction (from the inner to the outer side of the tubular composite membranes). In this context, a small amount of incorporated ceria was later partially removed, analyzing the most suitable option for the subsequent Pd deposition by ELP-PP and permeability of the composite membrane. Three different membranes were prepared by rinsing in distilled water the initial modified supports, and therefore, obtaining CeO₂ intermediate layers with different thicknesses to determine the optimal removal grade for the excess of ceria. Some differences can be observed after analyzing the external surface of these samples, detecting that the greater amount of ceria is removed, the lower original surface modification is obtained. Fig. 2 collects original and modified oxidized PSS support surfaces observed with an optical profiler after partially removing a certain amount of ceria, previously incorporated by dip-coating. As it can be seen, the calcined support, denoted as OXI, presents a very rough surface (Fig. 2a, $R_a = 4.579 \pm 0.3 \mu\text{m}$) in which the original morphology of a typical PSS support is maintained, as was reported elsewhere [26,41]. The first sample containing a ceria intermediate layer, OXI-CeO₂-01, has been prepared with the lower ceria removal grade after

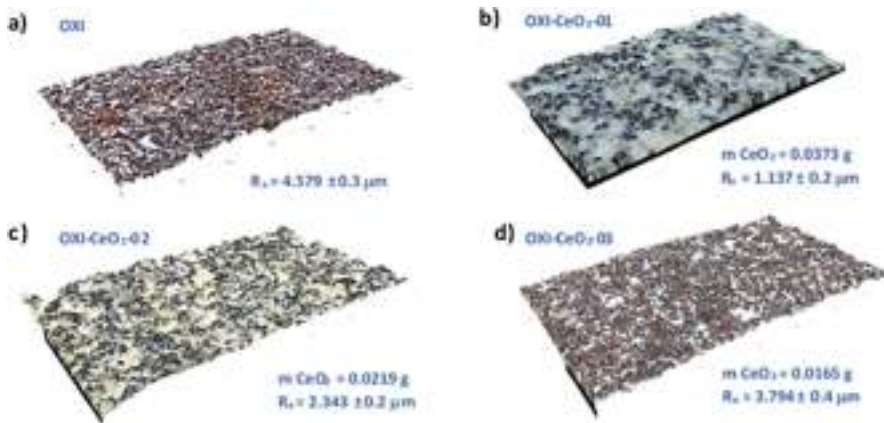


Fig. 2. Surface morphology obtained by an optical profiler (x500) for oxidized PSS support before (a) and after incorporating CeO₂ intermediate layers with diverse excess removal grades: OXI-CeO₂-01 (b), OXI-CeO₂-02 (c) and OXI-CeO₂-03 (d).

the dip-coating step reaching a weight increase of 0.0373 g for the oxidized support (Fig. 2b), which will be considered as reference to analyze the other removal grades. At these conditions, the remained ceria covers completely the surface of the oxidized support, hiding all the original pores. Consequently, the lowest surface roughness was obtained with a value of $R_a = 1.137 \pm 0.2 \mu\text{m}$. The second alternative, OXI-CeO₂-02, considers a higher removal grade, maintaining 0.0219 g of CeO₂ as intermediate layer (Fig. 2c). In this case, part of the oxidized particles of the support arises due to the ceria particles that are mostly placed inside the pores, increasing the average roughness from the previous situation up to $2.343 \pm 0.2 \mu\text{m}$. The last modification involves a deep removal of ceria from the modified support, OXI-CeO₂-03, mainly remaining the ceramic particles placed inside the pores with strong adhesion. The total weight of remaining ceria was around 0.0165 g, reaching a high roughness value so close to the oxidized PSS support, $R_a = 3.794 \pm 0.4 \mu\text{m}$ (Fig. 2d).

It is well known that support modifications by the incorporation of ceramic intermediate layers makes the deposition of free-defect thin Pd film easier, but it can also affect to the mechanical resistance and permeation of the original substrate, compromising the future permeability of the composite membrane [22,43]. As explained in the introduction section, the mechanical resistance of composite membranes prepared with ceria intermediate layers is guaranteed due to the similar thermal expansion coefficient of this material if it compared with palladium or PSS support coefficients [16]. Then, the permeation of the modified supports needs to be analyzed in order to select the most appropriate strategy to prepare the H₂-selective composite membranes. Fig. 3 shows the permeation fluxes measured in these experiments. Pure nitrogen gas and pressure differences in the range 0.5–1.0 bar at room temperature were measured. The oxidized support, taken as a reference for this study, presents flux in the range of 0.551–1.233 mol m⁻² s⁻¹ for the analyzed pressure driving forces.

As it can be clearly seen, this permeate flow-rate progressively decreases as the ceria amount of the intermediate layer increases. Thus, the modified support by incorporating the greatest amount of ceria (sample OXI-CeO₂-01) exhibits the lowest flow-rate for both evaluated pressures, obtaining 0.059 and 0.137 mol m⁻² s⁻¹ for 0.5 and 1.0 bar, respectively. This fact is explained by the partial block of the support original pores with dense CeO₂ particles, reducing the original open porosity. Additionally, the use of vacuum during the membrane preparation together with the high thickness of the intermediate layer provokes a high compaction grade of the ceramic particles and, consequently, a marked decrease in the permeation of the substrate. Accordingly, a permeation flux 30% lower than the oxidized support

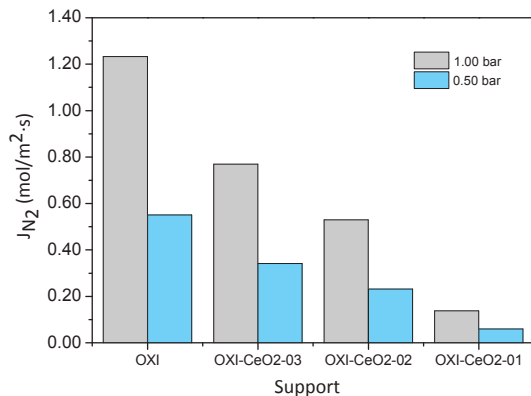


Fig. 3. N₂ flux of oxidized and CeO₂-modified PSS supports at room temperature.

(0.341 and 0.769 mol m⁻² s⁻¹ for 0.5 and 1.0 bar, respectively) has reached in case of considering the highest CeO₂ removal grade (OXI-CeO₂-03). This result evidences the limited modification of the oxidized support surface achieved following this experimental procedure, as previously discussed in terms of external roughness. Finally, an intermediate situation was also considered (OXI-CeO₂-02), partially removing the excess of CeO₂ particles but maintaining a good coverage of the most of the pores and ensuring a suitable modification of the support in order to facilitate the later incorporation of the palladium film. At these conditions, congruent permeation data were observed between both samples (0.231 and 0.529 mol m⁻² s⁻¹ for 0.5 and 1.0 bar, respectively). It means the lower ceria amount in the intermediate layer, the higher flux through the modified support. All these values, except the first ones obtained for the sample OXI-CeO₂-01, ensure to avoid any limitation in the modified supports to reach the DOE target values at 400 °C and similar pressure differences (0.300 and 0.420 mol m⁻² s⁻¹ for 0.5 and 1.0 bar, respectively) suggested for the viable implementation of a Pd-membrane in the industry.

In summary, the incorporation of a CeO₂ intermediate layer on an oxidized PSS support significantly affects to the resulting surface morphology and permeation properties (Table 1), being also foreseen a certain influence on the palladium deposition by ELP-PP. In fact, the ELP-PP method is based on the reaction of hydrazine and amino-

Table 1Summary of support modifications with CeO₂ intermediate layers.

Intermediate layer	m _{CeO₂} (g)	R _a (μm)	J _{N2} (mol/m ² ·s)	
			ΔP = 0.50 bar	ΔP = 1.00 bar
OXI	–	4.579 ± 0.3	0.550	1.233
OXI-CeO ₂ -01	0.0373	1.137 ± 0.2	0.059	0.137
OXI-CeO ₂ -02	0.0219	2.343 ± 0.2	0.231	0.529
OXI-CeO ₂ -03	0.0165	3.794 ± 0.4	0.341	0.769

palladium complex preferentially into the pores, after passing through the support. Thus, any modification of the support can affect to the Pd deposition method. In order to elucidate this hypothesis, some preliminary experiments were carried out to deposit the Pd film at the optimal experimental conditions determined in previous works [40]. During these experiments the hydrazine solution (with a concentration 0.2 M) encountered serious resistance to pass through the support OXI-CeO₂-01, modified with the greater amount of CeO₂ particles, due to the collapse of most of the pores with the ceramic particles. This problem was avoided by increasing the reducing agent concentration up to the ELP-PP reaction takes place and, as it has been previously reported elsewhere [40], high concentration levels of hydrazine reach to thicker Pd-membranes. On the other hand, a modified support with lower amount of CeO₂ (OXI-CeO₂-03), in which most of original external pore sizes of the supports are only slightly reduced, makes very difficult the generation of a total dense palladium layer with a limited thickness. In fact, Mardilovich et al. suggested that the thickness of a palladium film to achieve a complete defect-free composite membrane can be related to the biggest pore sizes of the support, being this value three times the limiting pore size [44]. In this context, it is recommendable to use an intermediate situation that simultaneously makes possible the reduction of the support surface roughness and the pore-mouth sizes, but maintains a great number of interconnected pores with enough diameter to facilitate the diffusion of hydrazine through the modified support from the inner to the outer side. Under these premises, the sample OXI-CeO₂-02 has been selected in this work as the most adequate for the preparation of a composite membrane by ELP-PP. For this intermediate layer, the original roughness of the oxidized support has been approximately halved, while enough permeation fluxes have been maintained. The reproducibility of this process was confirmed by the preparation of 10 ceria modified supports in analogous experimental conditions. In all cases, the incorporated amount of ceria was maintained around 0.0201 ± 0.0020 g.

The external surface obtained for the selected sample (OXI-CeO₂-02) has been additionally analyzed by scanning electron microscopy. Fig. 4 shows the SEM images, including the oxidized support (OXI) for comparison. As it can be seen, a very rough surface with wide distribution of pore mouth diameters can be observed for the calcined support (Fig. 4a), while many of these big pores are covered by CeO₂ particles after incorporating the intermediate layer (Fig. 4b). As it can be clearly drawn in the zoom image, these ceramic particles remain preferentially inside the external pores after removing the excess of material but maintaining a porous structure with smaller pore-mouth sizes. These smaller pores are supposed to be more easily closed by palladium than the original ones, promoting the generation of a thin selective film with high H₂ perm-selectivity. At this point, it should be noted that a complete prevention for the diffusion of some components from the SS support to the palladium layer cannot be ensured, although the presence of CeO₂ particles always will have a beneficial effect. The ceria particles reduce the contact area between the support and the palladium film, consequently decreasing the possible intermetallic diffusion. Moreover, the additional generation of mixed Fe-Cr oxides before incorporating the ceria intermediate layer could also contribute to reduce this possible effect.

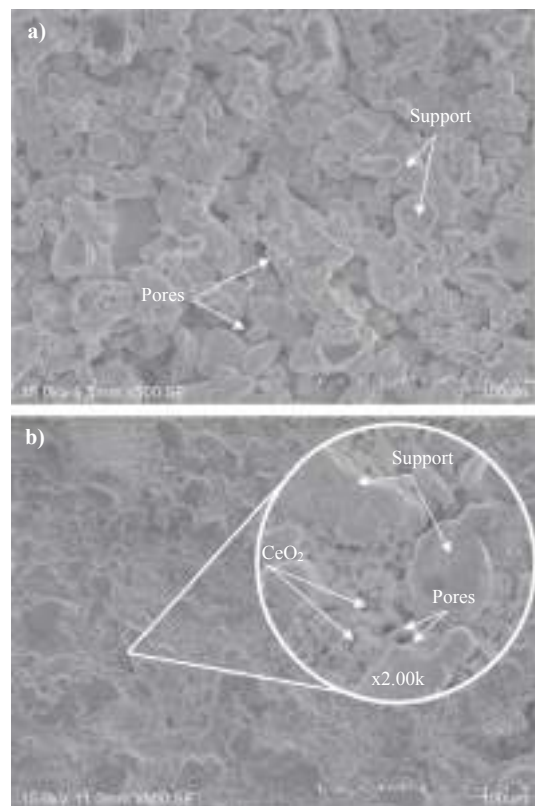


Fig. 4. SEM images of the external surface for: (a) oxidized PSS support and (b) selected modification by incorporation of a CeO₂ intermediate layer, OXI-CeO₂-02.

3.2. Palladium deposition: electroless pore-plating

In this section, the morphology and main characteristics of the palladium film achieved by ELP-PP on the selected support OXI-CeO₂-02 are discussed. The average thickness of this selective layer, estimated from gravimetric analyses, was 15 μm. Fig. 5 shows the SEM images of the composite membrane obtained after depositing the external palladium layer, including the external surface (Fig. 5a) as well as the cross-section view (Fig. 5b).

As it can be seen in Fig. 5a, the external surface of the palladium layer deposited by ELP-PP presents a relative smooth surface with a cavernous morphology that appears in some punctures. However, these pores cannot be found in the cross-section view (Fig. 5b), thus, it was established that these surface pores are not interconnected due to the palladium incorporation inside the pores. Taking into account the nature and characteristics of the palladium pore-plating alternative used in this work, the presence of external pores does not imply a low quality (in terms of H₂ perm-selectivity) of the membrane. In fact, the palladium particles can be ideally deposited only inside the pores of the supports, achieving a material totally impermeable to nitrogen, helium or other gases different of hydrogen. In this particular case, a preliminary leak test at room temperature was carried out, not detecting helium in the permeate side for the entire range of pressure differences (up to 3 bar). Analyzing in detail the cross-section view (Fig. 5b), both ceria particles and palladium film can be easily distinguished from the bulk PSS support. The first ones were incorporated partially covering the biggest pore mouths of the porous stainless-steel support, while the

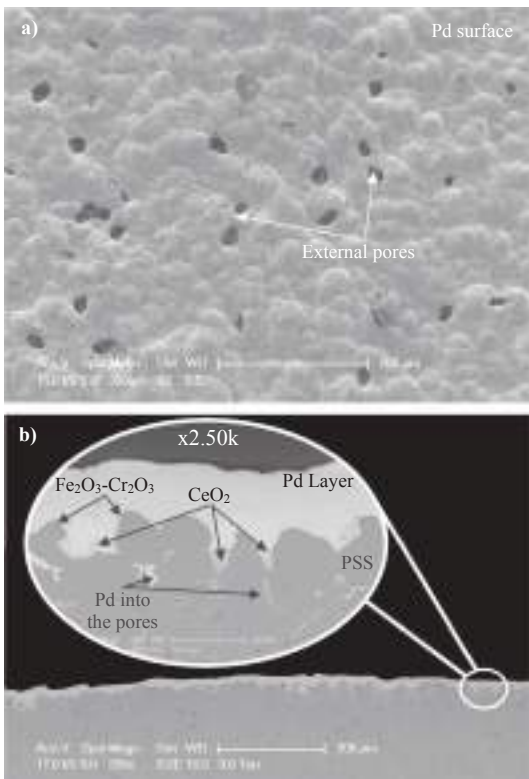


Fig. 5. SEM images after Pd deposition by ELP-PP over the modified OXI-CeO₂-O₂ support: (a) top view (before permeation experiments) and (b) cross-section (after permeation experiments).

palladium was deposited simultaneously into the pores and in the external surface due to the hydrazine pass through the larger pores, only partially covered. This particular morphology, inherent to the ELP-PP process if the support presents a certain pore size distribution, was extensively explained in previous works [38–40,45]. In this context, the deposition of palladium inside the pores expects to provide good anchoring for the H₂-selective layer and, consequently, increase the mechanical resistance of the composite membrane. In this case, it has been evidenced that the mentioned effect was maintained in case of incorporating a CeO₂ intermediate layer. Finally, attending to the real thickness for the external palladium layer, it can be concluded that a very close value (around 15 µm) to the estimated one from gravimetric analyses was observed in the SEM image.

3.3. Permeation behavior

As it has been detailed in the experimental section, permeation experiments with pure gases (nitrogen and hydrogen) have been performed to determine the composite membrane properties at high temperatures, ranged from 350 to 475 °C, to avoid the possible hydrogen embrittlement of the palladium film. In this context, two configurations for the permeation experiments were considered: (a) introducing the feed stream from the inner side of the membrane (tensile stress, mode in-out) or (b) vice versa, permeating from the outer to the inner side (compressive stress, mode out-in). For the entire set of performed experiments, it should be point out that no nitrogen was detected in the permeate side, and therefore, the quality of the membrane was demonstrated. In this context, an ideal H₂/N₂ selectivity ≥10,000 can be

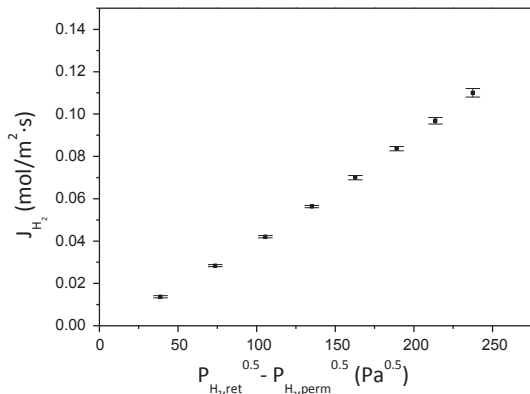


Fig. 6. Permeation results for stability to thermal cycles: pure H₂ and T = 400 °C (average values and error bars after 5 cycles).

ensured, taking into account the detection limit of the gas flow-meter used in these experiments (1 N mL/h).

After permeation tests with pure nitrogen, multiple thermal cycles with pure hydrogen were performed in the out-in operation mode to analyze the stability of the membrane and permeate measurements (Fig. 6). For each cycle the membrane cell was heated up to 400 °C in nitrogen atmosphere and the gas feed was changed to pure hydrogen to determine the permeation flux after a stabilization period of around 2 h. Finally, the system was cooled down to return until room temperature. Following this procedure, five thermal cycles were sequentially performed with an average operation time of around 5 h per cycle. Fig. 6 shows the hydrogen fluxes for these experiments. As it can be seen, a linear trend was observed as increasing the applied pressure driving force. This general trend will be further discussed after studying the effect provoked by the permeation operation mode (out-in or in-out). In general, it can be emphasized that the fluxes obtained for each thermal cycle slightly vary with a deviation ranged from 1 to 2% respect to the average value determined from all the experiments. Thus, the permeation behavior of this membrane, formed by an oxidized PSS support, a ceria intermediate layer and a final H₂-selective palladium film, can be considered stable.

After these preliminary thermal stability tests, the effect of operation mode was analyzed varying the direction of the hydrogen flux (out-in and in-out modes) at temperatures and trans-membrane pressure differences in the range 350–450 °C and 0.5–2.0 bar, respectively. These results are shown in Fig. 7, evidencing that all experimental data fit fairly well for a linear trend in which the hydrogen flux increases as the pressure driving force or temperature does. As it can be seen, the H₂ flux obtained when using the in-out operating mode is slightly higher than the values reached in case of permeating by using the opposite mode, permeating from the outer to the inner side (out-in mode). This variation is maintained in the range 2–5% and this could be due to a deviation from the real pressure on both sides of the palladium layer and the measured values from each bulk gas phase. In this manner, it can be concluded that the permeation operation mode does not affect to the H₂ flux in a significant grade. However, it can be pointed out the high mechanical stability of the prepared membrane, mainly for the in-out mode in which the pressure driving forces generate tensile stress making possible the delamination of the palladium layer (in-out mode). Since this fact is not produced, it demonstrates a good anchoring of the selective layer to the support due to the partial palladium deposition inside the pores provided by ELP-PP deposition method.

At this point, as it has been previously anticipated, different experiments were carried out at several temperatures (350–475 °C) and trans-membrane pressure driving forces (0.5–2.0 bar) to analyze in

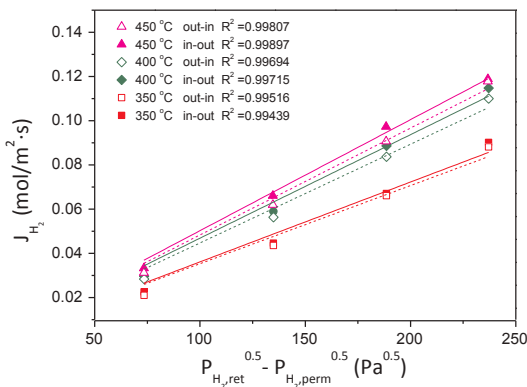


Fig. 7. Comparison of feed direction effect in the permeation properties for different temperatures: feeding from the inner side (●) and feeding from the shell side (○).

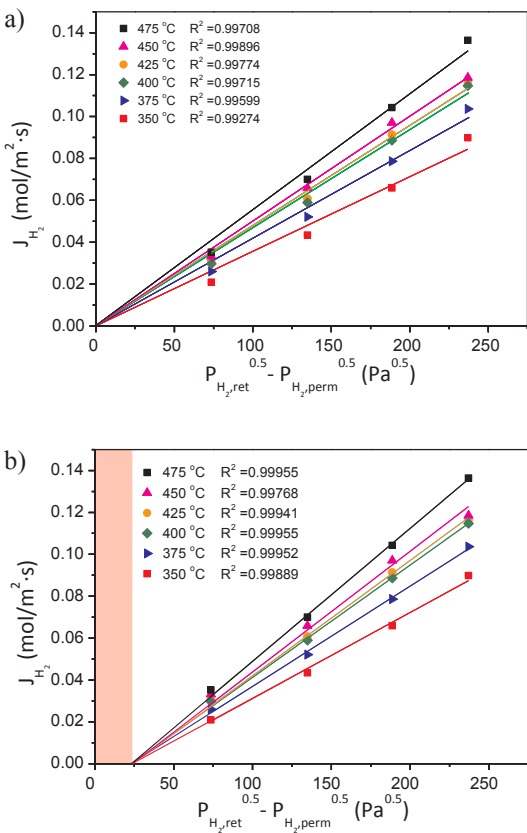


Fig. 8. Permeation behavior of OXI-CeO₂-02 after Pd deposition by ELP-PP: (a) fitting to Sieverts' law through (0,0) and (b) considering the presence of an additional resistance to the H₂ permeation process.

detailed the effect of each operating conditions. For all these experiments, the in-out permeation mode was considered to compare the obtained results with the previously reported for other pore-plated membranes in which a ceria intermediate layer was not incorporated [26,39–42,45].

All these results are summarized in Fig. 8, where the H₂ permeation flux with pressure is shown at different temperatures. Fig. 8a shows the mathematical adjust of collected data, evidencing a linear trend between flux and pressure driving force that is maintained independently of the experimental temperature. Although an increase of pressure provokes a consequent rise of the flux, as suggested the Sieverts' law, the intercept with the origin (that implies no permeation is reached when no pressure driving force is applied) is not clear. This linear fit can be significantly improved by considering the presence of an additional resistance to the permeation process (Fig. 8b), as it was suggested in previous works, in which composite membranes prepared by electroless pore-plating were analyzed [39,40]. This additional resistance is explained by the presence of a minimum pressure value below which the hydrogen permeation through the palladium membrane does not occur. The contribution of the support to this effect was negligible, as it was demonstrated elsewhere [39,40]. However, it is necessary to point out that the additional resistance to the hydrogen permeation determined for the membrane prepared in this work is significantly lower, around 30%, from the value previously determined for a similar membrane, also prepared by ELP-PP, but without including the CeO₂ intermediate layer [16,39,40]. This new behavior could be derived from the reduction of larger pores of the PSS support by the incorporation of the ceria particles, being also partially reduced the thickness of the Pd external layer and its penetration into the pores of the support. Consequently, an increase of the hydrogen flux around four times was reached, obtaining a permeance in the range $4.74 \cdot 10^{-4}$ – $6.35 \cdot 10^{-4}$ mol m⁻² s⁻¹ Pa^{-0.5} (respect to the values $1.00 \cdot 10^{-4}$ – $2.00 \cdot 10^{-4}$ mol m⁻² s⁻¹ Pa^{-0.5} obtained for a similar ELP-PP membrane without the ceria intermediate barrier [38]), while a complete ideal hydrogen perm-selectivity was maintained. Moreover, an activation energy of 8.9 kJ mol^{-1} was calculated, within the range of other palladium membranes reported in the literature [32]. As final insight, it also necessary to mention that the membrane exhibited a really good performance and stability for prolonged times (> 400 h) at high temperature (≥ 350 °C) and the most unfavorable permeation mode in terms of mechanical resistance, in-out permeation mode.

Finally, Table 2 compares the results obtained in this work with other experimental data reported in the literature. This comparison has been limited to composite membranes prepared by electroless-plating onto porous stainless steel supports, but including different materials as intermediate layer. It has to be pointed out that a rigorous comparison between permeation properties for all these Pd membranes is not easy due to the wide variety of parameters involved in the permeation process. In most of the cases, the permeation properties are intimately related to both reached metal thickness and composition of the selective layer, pure Pd or alloys. In general, the thinnest membranes present higher hydrogen permeances, but their selectivity is far away of the ideal value. On the contrary, thicker membranes usually present higher selectivity at the expense of lower hydrogen permeances. In this work, a complete H₂/N₂ selectivity ($\geq 10,000$, detection limit of 1 NmL/h) was obtained for the entire set of experiments. Moreover, a hydrogen permeance in the range 4.74 – $6.35 \cdot 10^{-4}$ mol m⁻² s⁻¹ Pa^{-0.5} was obtained when feeding pure gases. These permeance values are inside the typical range of the presented ones by other researchers for pure Pd-membranes, but providing a really high separation factor at ideal conditions. On the other hand, this value is maintained below other referenced membranes formed by Pd alloys. Furthermore, here it is important to point out that a significant increase of the permeance has been obtained in comparison with similar ELP-PP membranes, but prepared without incorporating the ceria intermediate layer, as it has been previously discussed in detail [38].

4. Conclusions

Three ceria intermediate layers were prepared onto oxidized 0.1 μm media grade porous stainless-steel supports to improve the performance

Table 2
Composite Pd-based membranes on PSS supports.

Membrane type	Deposition method	t_{Pd} (μm)	Permeation conditions		Permeation	H_2/N_2 separation factor	Ref.
			T (°C)	ΔP (kPa)			
-/Pd	ELP	20.0	350	100	$3.11 \cdot 10^{-4(a)}$	500	[44]
NaA zeolite/Pd	ELP	19.0–26.0	400–450	20–150	$\leq 1.12 \cdot 10^{-3(a)}$	20–608	[46]
SiO ₂ /Pd	ELP	5.0	500	50	0.14 ^(b)	300–450	[47]
Al ₂ O ₃ /Pd	ELP	5.0	400	100	$3.05 \cdot 10^{-3(a)}$	500	[48]
Al ₂ O ₃ –SiO ₂ /Pd	ELP	n.a.	350	42	$0.60\text{--}2.30 \cdot 10^{-8(c)}$	30–115	[49]
YSZ/Pd	ELP	27.7	350–450	30–400	$4.50 \cdot 10^{-4(a)}$	∞	[32]
CeO ₂ /Pd	ELP	13.0	500–550	100–200	0.127–0.275 ^(b)	∞	[50]
CeO ₂ /PdCu	ELP	8.0	450	100	0.074 ^(b)	2369	[51]
ZrO ₂ /PdAu	ELP	14.0–27.0	400–500	10–100	$3.48\text{--}7.14 \cdot 10^{-4(a)}$	4000	[52]
YSZ/PdAu	ELP	15.0	400	50	$1.8 \cdot 10^{-2(a)}$	> 10000	[53]
YSZ/PdAuAg	ELP	13.0–15.0	400	50	$2.5 \cdot 10^{-2(a)}$	> 10000	[53]
YSZ/Pd	ELP	4.9	600	82	$2.40 \cdot 10^{-3(a)}$	200–2000	[54]
ZrO ₂ /PdAuCu	ELP	14.0	400	50	$1.36 \cdot 10^{-4(a)}$	n.a.	[55]
OXI/Pd	ELP	19.0	n.a.	n.a.	n.a.	n.a.	[25]
OXI/Pd	ELP-PP	11.0–20.0	350–450	100–250	$1.00\text{--}2.00 \cdot 10^{-4(a)}$	∞	[38]
OXI-CeO ₂ /Pd	ELP-PP	15.4	350–450	100–200	$4.74\text{--}6.35 \cdot 10^{-4(a)}$	> 10,000	This work

Permeation: ^(a) permeance ($\text{mol m}^{-2} \text{s}^{-1} \text{Pa}^{-0.5}$), ^(b) permeation flux ($\text{mol m}^{-2} \text{s}^{-1}$) and ^(c) permeance ($\text{mol m}^{-2} \text{s}^{-1} \text{Pa}^{-1}$).

of composite Pd-membranes prepared by electroless pore-plating. The amount of ceria incorporated on the external surface of the support determines surface roughness and porosity as well, thus influencing the permeation properties of the modified substrates. Despite the increase of the incorporated amount of ceria reduces both, external roughness and average pore size, the resulting porosity makes difficult the hydrazine pass through the modified support. Moreover, the great amount of ceramic particles provokes a marked reduction of the permeation properties of the support, compromising its capability to reach adequate permeate fluxes as DOE targets suggest. On the contrary, scarce amounts of ceria make the generation of a thin free-defects palladium layer difficult. Thus, it is necessary to use an intermediate situation as achieved with the sample OXI-CeO₂-02, halved the roughness value of the starting oxidized PSS support but ensuring good permeability. After this modification, a completely dense Pd layer was reached by Electroless Pore-Plating with an average thickness of $t_{Pd} = 15 \mu\text{m}$. This composite membrane exhibits a H_2 -permeance of $5.37 \cdot 10^{-4} \text{ mol m}^{-2} \text{s}^{-1} \text{Pa}^{-0.5}$ at 400°C and ideal H_2/N_2 perm-selectivity $\geq 10,000$. These values represent an increase of around 400% with respect to that of previously reported without using a ceria intermediate layer ($1.50 \cdot 10^{-4} \text{ mol m}^{-2} \text{s}^{-1} \text{Pa}^{-0.5}$) while a high hydrogen selectivity was maintained. This fact could be derived from a high reduction, of around 30%, in the resistance to the permeation process when using electroless pore-plated membranes due to a lower penetration grade of the Pd external film into the support. Besides, experiments varying the direction of the permeate flux were also performed, obtaining similar results and evidencing the mechanical resistance of the prepared membrane despite operating at most unfavorable conditions (mode in-out with tensile stress for the Pd-layer). Analyzing in detail the permeation fluxes, a general behavior accordingly to the Sieverts' law was observed, increasing linearly as pressure driving force does. An increase of the operating temperature also promoted the H_2 permeate fluxes following an Arrhenius type dependence with an activation energy of 8.9 kJ mol^{-1} . However, as previously discussed for ELP-PP, an additional resistance to the permeation was also observed due to the driving force for the permeation process was insufficient to overcome the material resistance at lower pressures. Nevertheless, the incorporation of the ceria intermediate layer for the preparation of the Pd composite membrane on oxidized PSS supports reduces this additional resistance in 30% increasing the permeance of the membrane to obtain more than 400% of hydrogen flux respect to other previously ELP-PP reported membranes.

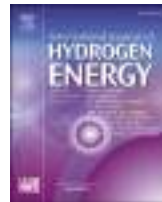
Acknowledgements

The authors of the present contribution thank to the organizers of the 15th International Conference on Inorganic Membranes (ICIM-18) the invitation to participate in this special issue. They also recognize the financial support achieved from the Spanish government through the competitive projects COT2013-44447-R and ENE2017-83696-R to develop this research and the contract of the researcher David Martínez-Díaz through the Young Employment Initiative program of the European Commission. Finally, the authors express their gratitude to prof. María Victoria Bonache Bezares and Nuria Pulido González for supporting the characterization of samples by optical profilometry and scanning electron microscopy, respectively.

References

- [1] S. Adams, E.K.M. Klobodu, A. Apio, Renewable and non-renewable energy, regime type and economic growth, Renew. Energy 125 (2018) 755–767, <https://doi.org/10.1016/j.renene.2018.02.135>.
- [2] M. Shahbaz, M. Zakaria, S.J.H. Shahzad, M.K. Mahalik, The energy consumption and economic growth nexus in top ten energy-consuming countries: fresh evidence from using the quantile-on-quantile approach, Energy Econ. 71 (2018) 282–301, <https://doi.org/10.1016/j.eneco.2018.02.023>.
- [3] N. Muradov, Low to near-zero CO₂ production of hydrogen from fossil fuels: status and perspectives, Int. J. Hydrogen Energy 42 (2017) 14058–14088, <https://doi.org/10.1016/j.ijhydene.2017.04.101>.
- [4] F.J. Vivas, A. De las Heras, F. Segura, J.M. Andújar, A review of energy management strategies for renewable hybrid energy systems with hydrogen backup, Renew. Sustain. Energy Rev. 82 (2018) 126–155, <https://doi.org/10.1016/j.rser.2017.09.014>.
- [5] C. Furlan, C. Mortarino, Forecasting the impact of renewable energies in competition with non-renewable sources, Renew. Sustain. Energy Rev. 81 (2018) 1879–1886, <https://doi.org/10.1016/j.rser.2017.05.284>.
- [6] F.W. Geels, T. Schwanen, S. Sorrell, K. Jenkins, B.K. Sovacool, Reducing energy demand through low carbon innovation: a sociotechnical transitions perspective and thirteen research debates, Energy Res. Soc. Sci. 40 (2018) 23–35, <https://doi.org/10.1016/j.jerss.2017.11.003>.
- [7] M.R. Rahimpour, F. Samimi, A. Babapoor, T. Tohidian, S. Mohebi, Palladium membranes applications in reaction systems for hydrogen separation and purification: a review, Chem. Eng. Process. Process Intensif. 121 (2017) 24–49, <https://doi.org/10.1016/j.cep.2017.07.021>.
- [8] T. da Silva Veras, T.S. Mozer, D. da Costa Rubim Messeder dos Santos, A. da Silva César, Hydrogen: trends, production and characterization of the main process worldwide, Int. J. Hydrogen Energy 42 (2017) 2018–2033, <https://doi.org/10.1016/j.ijhydene.2016.08.219>.
- [9] B. Zornoza, C. Casado, A. Navajas, Chapter 11 - Advances in hydrogen separation and purification with membrane technology, in: L.M. Gandía, G. Arzamendi, P.M. Diéguez (Eds.), Renew. Hydrog. Technol., Elsevier, Amsterdam, 2013, pp. 245–268, <https://doi.org/10.1016/B978-0-444-56352-1.00011-8>.
- [10] J.J. Conde, M. Maroño, J.M. Sánchez-Hervás, Pd-based membranes for hydrogen separation: review of alloying elements and their influence on membrane properties, Sep. Purif. Rev. 46 (2017) 152–177, <https://doi.org/10.1080/15422119.2016.1212379>.

- [11] B.D. Adams, A. Chen, The role of palladium in a hydrogen economy, *Mater. Today* 14 (2011) 282–289, [https://doi.org/10.1016/S1369-7021\(11\)70143-2](https://doi.org/10.1016/S1369-7021(11)70143-2).
- [12] A.M. Tarditi, M.L. Bosko, L.M. Cornaglia, *Electroless Plating of Pd Binary and Ternary Alloys and Surface Characteristics for Application in Hydrogen Separation*, Elsevier, Oxford, 2017, pp. 1–24 <https://doi.org/10.1016/B978-0-12-803581-8.09166-9>.
- [13] S. Yun, S. Ted Oyama, S.T. Oyama, Correlations in palladium membranes for hydrogen separation: a review, *J. Memb. Sci.* 375 (2011) 28–45, <https://doi.org/10.1016/j.memsci.2011.03.057>.
- [14] F. Gallucci, M. De Falco, S. Tosti, L. Marrelli, A. Basile, The effect of the hydrogen flux pressure and temperature dependence factors on the membrane reactor performances, *Int. J. Hydrogen Energy* 32 (2007) 4052–4058, <https://doi.org/10.1016/j.ijhydene.2007.03.039>.
- [15] J.A. Calles, R. Sanz, D. Alique, L. Furones, Thermal stability and effect of typical water gas shift reactant composition on H₂ permeability through a Pd-YSZ-PSS composite membrane, *Int. J. Hydrogen Energy* 39 (2014) 1398–1409, <https://doi.org/10.1016/j.ijhydene.2013.10.168>.
- [16] D. Alique, M. Martinez-Diaz, R. Sanz, J.A. Calles, Review of supported pd-based membranes preparation by electroless plating for ultra-pure hydrogen production, 2018. doi:10.3390/membranes8010005.
- [17] S. Tosti, Supported and laminated Pd-based metallic membranes, *Int. J. Hydrogen Energy* 28 (2003) 1445–1454, [https://doi.org/10.1016/S0360-3199\(03\)00028-4](https://doi.org/10.1016/S0360-3199(03)00028-4).
- [18] C. Zhao, H. Xu, A. Goldbach, Duplex Pd/ceramic/Pd composite membrane for sweep gas-enhanced CO₂ capture, *J. Memb. Sci.* 563 (2018) 388–397, <https://doi.org/10.1016/j.memsci.2018.05.057>.
- [19] J. Melendez, E. Fernandez, F. Gallucci, M. van Sint Annaland, P.L. Arias, D.A.P. Tanaka, Preparation and characterization of ceramic supported ultra-thin (~1 μm) Pd-Ag membranes, *J. Memb. Sci.* 528 (2017) 12–23, <https://doi.org/10.1016/j.memsci.2017.01.011>.
- [20] K.-R. Hwang, D.-K. Oh, S.-W. Lee, J.-S. Park, M.-H. Song, W.-H. Rhee, Porous stainless steel support for hydrogen separation Pd membrane: fabrication by metal injection molding and simple surface modification, *Int. J. Hydrogen Energy* 42 (2017) 14583–14592, <https://doi.org/10.1016/j.ijhydene.2017.04.032>.
- [21] E. Fernandez, J.A. Medrano, J. Melendez, M. Parco, J.L. Viviente, M. van Sint Annaland, D.A. Pacheco Tanaka, Preparation and characterization of metallic supported thin Pd-Ag membranes for hydrogen separation, *Chem. Eng. J.* 305 (2016) 182–190, <https://doi.org/10.1016/j.cej.2015.09.119>.
- [22] C.-B. Lee, S.-W. Lee, J.-S. Park, S.-K. Ryi, D.-W. Lee, K.-R. Hwang, S.-H. Kim, Ceramics used as intermetallic diffusion barriers in Pd-based composite membranes sputtered on porous nickel supports, *J. Alloys Compd.* 578 (2013) 425–430, <https://doi.org/10.1016/j.jallcom.2013.06.007>.
- [23] S.-E. Nam, K.-H. Lee, Hydrogen separation by Pd alloy composite membranes: introduction of diffusion barrier, *J. Memb. Sci.* 192 (2001) 177–185, [https://doi.org/10.1016/S0376-7388\(01\)00499-9](https://doi.org/10.1016/S0376-7388(01)00499-9).
- [24] J.A. Calles, R. Sanz, D. Alique, Influence of the type of siliceous material used as intermediate layer in the preparation of hydrogen selective palladium composite membranes over a porous stainless steel support, *Int. J. Hydrogen Energy* 37 (2012) 6030–6042, <https://doi.org/10.1016/j.ijhydene.2011.12.164>.
- [25] C. Mateos-Pedrero, M.A. Soria, I. Rodríguez-Ramos, A. Guerrero-Ruiz, Modifications of porous stainless steel previous to the synthesis of Pd membranes, *Stud. Surf. Sci. Catal.* (2010) 779–783, [https://doi.org/10.1016/S0167-2991\(10\)75159-4](https://doi.org/10.1016/S0167-2991(10)75159-4).
- [26] L. Furones, D. Alique, Interlayer properties of in-situ oxidized porous stainless steel for preparation of composite Pd membranes, *Chem. En. 2* (2017) 1, <https://doi.org/10.3390/chemengineering2010001>.
- [27] S. Samingprai, S. Tantayanon, Y.H. Ma, Chromium oxide intermetallic diffusion barrier for palladium membrane supported on porous stainless steel, *J. Memb. Sci.* 347 (2010) 8–16, <https://doi.org/10.1016/j.memsci.2009.09.058>.
- [28] T. Van Gestel, F. Hauler, M. Bram, W.A. Meulenberg, H.P. Buchkremer, T. Van Gestel, F. Hauler, M. Bram, W.A. Meulenberg, H.P. Buchkremer, Synthesis and characterization of hydrogen-selective sol-gel SiO₂ membranes supported on ceramic and stainless steel supports, *Sep. Purif. Technol.* 121 (2014) 20–29, <https://doi.org/10.1016/j.seppur.2013.10.035>.
- [29] Y.-H. Chi, P.-S. Yen, M.-S. Jeng, S.-T. Ko, T.-C. Lee, Preparation of thin Pd membrane on porous stainless steel tubes modified by a two-step method, *Int. J. Hydrogen Energy* 35 (2010) 6303–6310, <https://doi.org/10.1016/j.ijhydene.2010.03.066>.
- [30] A. Tarditi, C. Gerboni, L. Cornaglia, PdAu membranes supported on top of vacuum-assisted ZrO₂-modified porous stainless steel substrates, *J. Memb. Sci.* 428 (2013) 1–10, <https://doi.org/10.1016/j.memsci.2012.10.029>.
- [31] H.W. Abu El Hawa, S.-T.B. Lundin, N.S. Patki, J. Douglas Way, Steam methane reforming in a PdAu membrane reactor: long-term assessment, *Int. J. Hydrogen Energy* 41 (2016) 10193–10201, <https://doi.org/10.1016/j.ijhydene.2016.04.244>.
- [32] R. Sanz, J.A. Calles, D. Alique, L. Furones, S. Ordóñez, P. Marín, P. Corengia, E. Fernandez, Preparation, testing and modelling of a hydrogen selective Pd/YSZ/SS composite membrane, *Int. J. Hydrogen Energy* 36 (2011) 15783–15793, <https://doi.org/10.1016/j.ijhydene.2011.08.102>.
- [33] M. Dehghani Mobarake, P. Jafari, M. Irani, Preparation of Pd-based membranes on Pd/TiO₂ modified NaX/PSS substrate for hydrogen separation: design and optimization, *Microp. Mesop. Mater.* 226 (2016) 369–377, <https://doi.org/10.1016/j.micromes.2016.02.022>.
- [34] S.K. Ryi, H.S. Ahn, J.S. Park, D.W. Kim, Pd-Cu alloy membrane deposited on CeO₂ modified porous nickel support for hydrogen separation, *Int. J. Hydrogen Energy* 39 (2014) 4698–4703, <https://doi.org/10.1016/j.ijhydene.2013.11.031>.
- [35] X. Wang, X. Tan, B. Meng, X. Zhang, Q. Liang, H. Pan, S. Liu, TS-1 zeolite as an effective diffusion barrier for highly stable Pd membrane supported on macro-porous [smal alpha]-Al₂O₃ tube, *RSC Adv.* 3 (2013) 4821–4834, <https://doi.org/10.1039/C3RA23086D>.
- [36] D. Alique, Processing and characterization of coating and thin film materials, in: J. Zhang, Y. Jung (Eds.), *Adv. Ceram. Met. Coat. Thin Film Mater. Energy Environ.*, 2018, doi:10.1007/978-3-319-59906-9.
- [37] D.A. Pacheco Tanaka, J. Okazaki, M.A. Llosa Tanco, T.M. Suzuki, 5 - Fabrication of supported palladium alloy membranes using electroless plating techniques BT - Palladium Membrane Technology for Hydrogen Production, Carbon Capture and Other Applications, in: Woodhead Publ. Ser. Energy, Woodhead Publishing, 2015, pp. 83–99, <https://doi.org/10.1533/9781782424191.1.83>.
- [38] R. Sanz, J.A. Calles, D. Alique, L. Furones, New synthesis method of Pd membranes over tubular PSS supports via “pore-plating” for hydrogen separation processes, *Int. J. Hydrogen Energy* 37 (2012) 18476–18485, <https://doi.org/10.1016/j.ijhydene.2012.09.084>.
- [39] D. Alique, M. Imperatore, R. Sanz, J.A. Calles, M.G. Baschetti, Hydrogen permeation in composite Pd-membranes prepared by conventional electroless plating and electroless pore-plating alternatives over ceramic and metallic supports, *Int. J. Hydrogen Energy* 41 (2016) 19430–19438, <https://doi.org/10.1016/j.ijhydene.2016.06.128>.
- [40] J.A. Calles, R. Sanz, D. Alique, L. Furones, P. Marin, S. Ordoñez, Influence of the selective layer morphology on the permeation properties for Pd-PSS composite membranes prepared by electroless pore-plating: Experimental and modeling study, *Sep. Purif. Technol.* 194 (2018) 10–18, <https://doi.org/10.1016/j.seppur.2017.11.014>.
- [41] R. Sanz, J.A. Calles, S. Ordóñez, P. Marín, L. Furones, Modelling and simulation of permeation behaviour on Pd/PSS composite membranes prepared by “pore-plating” method, *J. Memb. Sci.* 446 (2013) 410–421, <https://doi.org/10.1016/j.memsci.2013.06.060>.
- [42] R. Sanz, J.A. Calles, D. Alique, L. Furones, S. Ordóñez, P. Marín, Hydrogen production in a Pore-Plated Pd-membrane reactor: experimental analysis and model validation for the Water Gas Shift reaction, *Int. J. Hydrogen Energy* 40 (2015) 3472–3484, <https://doi.org/10.1016/j.ijhydene.2014.11.120>.
- [43] D. Yepes, L.M. Cornaglia, S. Irusta, E.A. Lombardo, Different oxides used as diffusion barrier in composite hydrogen permeable membranes, *J. Memb. Sci.* 274 (2006) 92–101, <https://doi.org/10.1016/j.memsci.2005.08.003>.
- [44] P.P. Mardilovich, Y. She, Y.H. Ma, M.-H. Rei, Defect-free palladium membranes on porous stainless-steel support, *AIChE J.* 44 (1998) 310–322, <https://doi.org/10.1002/aic.690440209>.
- [45] R. Sanz, J.A. Calles, D. Alique, L. Furones, H₂ production via water gas shift in a composite Pd membrane reactor prepared by the pore-plating method, *Int. J. Hydrogen Energy* 39 (2014) 4739–4748, <https://doi.org/10.1016/j.ijhydene.2013.12.145>.
- [46] M.L. Bosko, F. Ojeda, E.A. Lombardo, L.M. Cornaglia, NaA zeolite as an effective diffusion barrier in composite Pd/PSS membranes, *J. Memb. Sci.* 331 (2009) 57–65, <https://doi.org/10.1016/j.memsci.2009.01.005>.
- [47] Y. Matsumura, T. Yazawa, S. Caili, Tetsuro Jin, Koji Kuraoka, Thin palladium film supported on SiO₂-modified porous stainless steel for a high-hydrogen-flux membrane, *Ind. Eng. Chem. Res.* 44 (2005) 3053–3058.
- [48] S.K. Gade, P.M. Thoen, J.D. Way, Unsupported palladium alloy foil membranes fabricated by electroless plating, *J. Memb. Sci.* 316 (2008) 112–118, <https://doi.org/10.1016/j.memsci.2007.08.022>.
- [49] D. Lee, C. Yu, K. Lee, Synthesis of Pd particle-deposited microporous silica membranes via a vacuum-impregnation method and their gas permeation behavior, *J. Colloid Interface Sci.* 325 (2008) 447–452, <https://doi.org/10.1016/j.jcis.2008.06.021>.
- [50] J. Tong, Y. Matsumura, H. Suda, K. Haraya, Thin and dense Pd/CeO₂/MPSS composite membrane for hydrogen separation and steam reforming of methane, *Sep. Purif. Technol.* 46 (2005) 1–10, <https://doi.org/10.1016/j.seppur.2005.03.011>.
- [51] A. Qiao, K. Zhang, Y. Tian, L. Xie, H. Luo, Y.S. Lin, Y. Li, Hydrogen separation through palladium-copper membranes on porous stainless steel with sol-gel derived ceria as diffusion barrier, *Fuel.* 89 (2010) 1274–1279, <https://doi.org/10.1016/j.fuel.2009.12.006>.
- [52] I. Contardi, L. Cornaglia, A.M. Tarditi, ScienceDirect Effect of the porous stainless steel substrate shape on the ZrO₂ deposition by vacuum assisted dip-coating, *Int. J. Hydrogen Energy* 42 (2017) 7986–7996, <https://doi.org/10.1016/j.ijhydene.2017.01.024>.
- [53] A.D. Fontana, N. Sirini, L.M. Cornaglia, A.M. Tarditi, Hydrogen permeation and surface properties of PdAu and PdAgAu membranes in the presence of CO, CO₂ and H₂S, *J. Memb. Sci.* 563 (2018) 351–359, <https://doi.org/10.1016/j.memsci.2018.06.001>.
- [54] H.W.A. El Hawa, S.-T.B. Lundin, S.N. Paglieri, A. Harale, J.D. Way, The influence of heat treatment on the thermal stability of Pd composite membranes, *J. Memb. Sci.* 494 (2015) 113–120, <https://doi.org/10.1016/j.memsci.2015.07.021>.
- [55] A.M. Tarditi, C. Imhoff, F. Braun, J.B. Miller, A.J. Gellman, L. Cornaglia, PdCuAu ternary alloy membranes: hydrogen permeation properties in the presence of H₂S, *J. Memb. Sci.* 479 (2015) 246–255, <https://doi.org/10.1016/j.memsci.2014.12.030>.



Pd-thickness reduction in electroless pore-plated membranes by using doped-ceria as interlayer

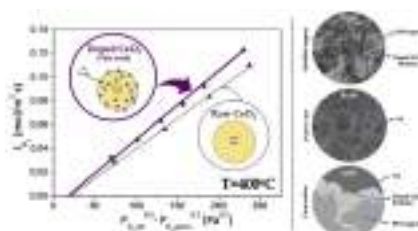
D. Martinez-Díaz, D. Alique*, J.A. Calles, R. Sanz

Chemical and Environmental Engineering Group, Rey Juan Carlos University, C/ Tulipán S/n, 28933, Móstoles, Spain

HIGHLIGHTS

- Pd-doped CeO_2 as intermediate barrier reduces metal thickness in ELP-PP membranes.
- Pd film below 10 μm was obtained, saving around 40% metal compared to raw CeO_2 .
- H_2 permeance $6.26 \cdot 10^{-4} \text{ mol/s m}^2 \text{ Pa}^{0.5}$, $\alpha_{\text{H}_2/\text{N}_2} \geq 10,000$ and $E_a = 13.1 \text{ kJ mol}^{-1}$ were reached.
- Excellent mechanical stability for long-term permeation tests (850 h at 400 °C).

GRAPHICAL ABSTRACT



ARTICLE INFO

Article history:

Received 28 June 2019

Received in revised form

27 September 2019

Accepted 10 October 2019

Available online 26 November 2019

Keywords:

Supported-membrane
Surface modification
Ceria
Palladium
Electroless plating
Hydrogen

ABSTRACT

This work presents the use of doped CeO_2 particles with palladium as intermediate barrier for the preparation of fully dense Pd films by Electroless Pore-Plating. The use of doped ceria particles instead of non-doped ones clearly helps to reduce the final palladium thickness required to prepare a fully dense membrane over porous stainless steel supports from 15 to 9 μm (average values by gravimetric analyses), thus saving around 40% of total palladium required in the process. Pure hydrogen permeation tests reveal a consequent increase in the H_2 flux in the range 15–30%, depending on the operation mode. Thus, a H_2 permeance of $6.26 \cdot 10^{-4} \text{ mol m}^{-2} \text{ s}^{-1} \text{ Pa}^{-0.5}$ at 400 °C and $\Delta P = 1 \text{ bar}$ is reached, maintaining a really high H_2/N_2 ideal separation factor ($\geq 10,000$) and an activation energy within the typical range for these type of membranes, $E_a = 13.1 \text{ kJ mol}^{-1}$. Permeation of binary H_2/N_2 gas mixtures and the effect of feeding the mixture from the inner or the outer side of the membrane have been also studied. A significant concentration-polarization effect was observed, being higher when the gas is fed from the inner to the outer side of the membrane. This effect becomes more relevant for the membrane prepared with doped CeO_2 , instead of raw CeO_2 , due to its lower Pd thickness and higher relative influence of the surface processes. However, it should be emphasized that higher H_2 permeance values were obtained for the entire set of experiments when using the Pd-membranes containing

* Corresponding author.

E-mail address: david.aliique@urjc.es (D. Alique).
<https://doi.org/10.1016/j.ijhydene.2019.10.140>

doped ceria. Finally, long-term permeation tests for more than 850 h with pure gases at $T = 400^\circ\text{C}$ and $\Delta P = 1$ bar were also carried out, demonstrating a suitable mechanical stability of membranes at these operating conditions.

© 2019 Hydrogen Energy Publications LLC. Published by Elsevier Ltd. All rights reserved.

Introduction

The emission of anthropogenic carbon dioxide, mainly generated by the use of fossil fuels, is the principal responsible of the global warming and progressive deterioration of the environment, [1–5]. In this context, the promotion of using clean renewable energies as well as the adoption of efficient energy strategies to reduce CO₂ emissions are critical issues [6]. The use of hydrogen as a clean energy vector is one of the most promising alternatives to facilitate a progressive transition towards this situation [7–9], since it could be produced by diverse techniques from a wide variety of feedstock [10]. However, in most cases it is not produced with the required purity, being necessary a separation step from other sub-products such as nitrogen, steam or carbon oxides, among others [11,12]. This purification process can be carried out downstream as an independent separation step with membranes modules [13,14] or coupled to the chemical reactions in a membrane reactor [15,16].

Membranes can be fabricated by using different types of materials [12], although pure palladium and Pd-based alloys offer clear advantages versus others in terms of mechanical and thermal resistances, H₂ selectivity and permeance [17–19]. However, the high cost of this noble metal, the reproducibility of the Pd-deposition process and the stability for long time operation at real conditions are the main bottle necks to introduce this technology in the industry [17,20].

Great efforts are being carried out during last years to develop new membrane formulations and fabrication strategies to overcome these limitations. In this context, it seems to be widely approved the use of a porous support to reduce the thickness of the selective Pd layer and, hence, save costs at the same time that the permeation is increased [21,22]. Porous ceramic materials provide excellent surface properties for this purpose, i.e. low roughness, adequate porosity, and narrow pore size distribution with small pore mouths [23,24]. However, porous metallic supports offer a better fitting in most of current industrial devices, usually made of Hastelloy or stainless steel (SS), as well as ensuring a suitable thermal resistance due to the similar thermal expansion coefficient to that of palladium [24,25]. In practice, many researchers combine both alternatives by using porous stainless steel (PSS) supports modified with diverse ceramic intermediate layers to improve the quality of the original PSS surface, while simultaneously preventing any possible metallic interdiffusion between SS and Pd layer [26–28].

A detailed analysis of the selected material to be used as intermediate layer is of key importance in order to ensure an adequate behavior of the composite structure [19]. Thus, the main properties of this material should be suitable adherence

onto the porous support, enough mechanical resistance and chemical stability for the operating conditions and thermal expansion coefficient between those Pd layer and metal support. CeO₂ has demonstrated to be an excellent candidate for this purpose, especially in case of using PSS supports [19]. In this context, Tong et al. [29] modified PSS tubes by the incorporation of dispersed ceria hydroxide particles with help of vacuum. Qiao et al. [30] used a similar strategy with a sol-gel procedure to incorporate CeO₂ particles onto PSS 316L disks. Additionally, ceramic particles or, in general, any intermediate layer can be also doped with palladium in order to facilitate later activation steps for the incorporation of the H₂ selective layer. This strategy was considered, for example, by Gao et al. [31] for ZrO₂ modified PSS disks and Botino et al. [32] for incorporating an alumina Pd-modified boehmite sol on PSS supports. However, detailed characterization for these doped intermediate layers were not presented, as well as the real quantification of benefits reached after these strategies in comparison with raw ceramic materials.

Different alternatives can be also considered to incorporate the Pd layer onto the support, although the electroless plating (ELP) is one of the most frequently used because of low energy requirements, equipment simplicity and possibility to cover complex geometries with good reproducibility [19,25,33]. ELP process, based on the chemical reaction between a reducing agent (typically hydrazine) and a metal solution containing Pd²⁺ ions, together with complexing and stabilizing agents (such as ammonia and EDTA), has been deeply investigated, and thus interesting proposals have been recently developed. Goldbach et al. published in 2018 a novelty Pd-membrane configuration in which the Pd is located in two different layers on each side of the porous support [34]. These membranes, denoted as duplex-membranes, avoid the necessity of reach a fully dense Pd film but increase in practice the H₂ selectivity of the composite material due to the low probability of other gases to find the correct path between two defects belonging to each Pd layer. Pacheco-Tanaka et al. proposed the use of double-skinned and pore-filled membranes to improve both H₂ permeance and attrition resistance of the membrane in fluidized-bed systems [23,27,35,36]. This last type of configuration, on the contrary to the previously described, contains the Pd-based film between two different ceramic layers that protect it against certain pollutants or catalyst blows in fluidization conditions. Other interesting membranes are prepared by electroless pore-plating (ELP-PP), where the incorporation of palladium inside the pores of the support is aimed by feeding both metal source and reducing agent from opposite sides of the porous support. In this case, an external layer is also obtained [24,37] and the Pd incorporation between this external Pd layer and pores depends on

the ELP-PP conditions [38]. In fact, it was reported that Pd location inside the PSS pores could be the responsible of additional permeation resistances [38,39]. The average Pd thickness in ELP-PP membranes, as occurs in any Pd composite membrane, can be reduced by the incorporation of diverse intermediate layers, as previously detailed. In this context, a significant improvement of the H₂ permeance on ELP-PP membranes was achieved after modifying PSS supports with raw CeO₂ particles [40], increasing the hydrogen flux around 400% when comparing to other previous results for ELP-PP membranes in which no ceria was used as intermediate layer [38]. Following the above-mentioned study, the present work analyzes the use of CeO₂ particles doped with Pd nuclei, instead of pure CeO₂, to prepare the intermediate layer onto a PSS support. The use of ceria homogeneously doped with Pd nuclei could facilitate the reaction just inside the pores between Pd source and hydrazine baths during the plating step, thus affecting positively both final layer thickness and H₂ permeation through the composite membrane. In this context, the morphology of the new prepared membranes and their permeation behavior with pure gases and mixtures have been properly addressed, including some long-term permeation tests for around 850 h to verify their stability. These results undoubtedly provide a significant insight for the continuous improvement of ELP-PP membranes.

Experimental procedure

Membrane preparation

All composite membranes used in this study were prepared onto PSS supports provided by Mott Metallurgical with 0.1 μm media grade and symmetric structure. The commercial supports, with tubular geometry and ½" OD, were cut to achieve a final dimension of 3 cm in length. The general procedure for the synthesis of the membranes consists of four successive steps: (i) initial cleaning of PSS support, (ii) support calcination, (iii) incorporation of a CeO₂ intermediate layer doped with Pd nuclei and (iv) palladium deposition by electroless pore-plating, ELP-PP. First steps, including initial cleaning and PSS calcination in air at 600 °C for 12 h, have been widely described in previous works [37,41].

The main novelty of this study is based on the preparation of the CeO₂ intermediate layer, modified with regard to a previous publication in which the preparation of ELP-PP membranes over PSS supports including a CeO₂ barrier is addressed [40]. Raw commercial CeO₂ (from Alfa-Aesar), with an average particle size around 100 nm, was doped with palladium nuclei before being incorporated onto the support by vacuum-assisted dip-coating (VA-DC) [40]. For the doping procedure, raw CeO₂ particles were vigorously stirred into a solution containing the metal source (0.1 g/L PdCl₂) at room temperature, adding hydrazine 0.2 M to reduce the palladium ions into metal nuclei. The composition of these solutions was taken from previous studies in which they were used for the activation steps of raw and modified PSS supports [24,28]. In contrast to other investigations, in which the sensitization-activation process of the PSS support is carried out with successive immersions in solutions containing tin and palladium

precursors, the procedure here proposed do not use any tin solution. Several ratios between CeO₂ particles amount and Pd precursor were considered from 1:6 to 1:36 (vol.). The doping step was extended for 120 min, and then the CeO₂ particles were filtered and dried overnight at 110 °C.

After doping the CeO₂ particles with palladium nuclei (denoted as doped CeO₂ from here on out), a suspension of 20 wt% of these particles in water with a small amount of polyvinyl alcohol (2 wt%), to ensure good adherence, were used for the preparation of the intermediate layer by VA-DC process [40]. Next, the calcined PSS support was introduced into the doped CeO₂ suspension for 5 min at room conditions, sealing by both extremes with Teflon tapes. This process was repeated twice to ensure good homogeneity and reproducibility during the intermediate layer incorporation. The final thickness of the intermediate layer was adjusted by successive rinsing in distilled water just after the VA-DC process, thus partially removing some ceria particles, as it was widely discussed in a previous work [40]. Finally, the modified PSS supports with doped CeO₂ were calcined at 500 °C for 5 h to ensure a complete removal of the organic linker (PVA) and a good mechanical stability of the intermediate layer. As usual for preparation of these membranes, diverse ELP-PP cycles were required up to the weight gain became negligible, thus suggesting a complete blockage of pores with palladium and, consequently, a fully dense palladium membrane [37,42].

Materials characterization

First, Pd content incorporated into the doped CeO₂ particles was analyzed by using an inductively coupled plasma atomic emission spectroscope (ICP-AES, Varian 720-ES with λ = 342 nm). Doped CeO₂ particles were previously dissolved by acidic digestion with HNO₃ and H₂O₂. Gravimetric analyses were used to determine the weight gain of the PSS support after the initial calcination, the incorporation of Pd doped CeO₂ particles as intermediate layer and the Pd deposition by ELP-PP. The equipment used was a Kern electronic balance type ABS 220-4 (accuracy of 0.1 mg). After that, all composite membranes were completely characterized before and after the palladium plating with a scanning electron microscope (Hitachi S-2100N) equipped with an energy dispersive analytical system (EDAS) for microprobe analysis and an optical profiler (Zeta-20 Optical Profiler). The uniformity of both doped CeO₂ and Pd layers as well as the possible presence of defects were analyzed in both axial and radial directions. Additionally, the membranes were also cut after permeation experiments in order to study the membrane conformation in radial direction and, thus, determine the real thickness of the Pd top layer.

Permeation measurements

Preliminary He-bubble membrane leak tests in distilled water were performed to ensure the complete absence of defects in the Pd layer at room temperature. Then, permeation experiments with pure gases (hydrogen and nitrogen) and mixtures were carried out at temperatures in the range 350–450 °C and pressure driving forces from 0.5 to 2.0 bar. In this manner, both permeance and ideal H₂/N₂ separation

factor are determined for each sample. These permeation data were collected in the homemade experimental setup previously reported [40]. It is equipped with a backpressure regulator and several mass-flow controllers from Bronkhorst High-Tech B.V. Additionally, in case of permeate fluxes below 5 NmL min^{-1} , a bubble-gas flow meter with a detection limit of 1 mL h^{-1} was used to refine all these measurements, as well as to ensure the absence of data for particular experimental conditions (i.e. 0 NmL min^{-1}). Here, it is important to note that no sweep gas was used for the entire set of experiments and the permeate side was always maintained at atmospheric pressure. Gas chromatography was also used to analyze the composition of the permeate stream in case of feeding $\text{H}_2\text{-N}_2$ mixtures (Varian CP-4900 equipped with TCD and two different channels, molecular sieve 5 \AA and Pora-PLOT Q columns).

The operation mode of the permeation setup was also addressed by changing the flux direction throughout the composite membrane. In this way, considering that the palladium top layer was always placed onto the external side of the tubular membrane, two different experiments were performed. First, gases were fed into the lumen side of the membrane, where they meet the porous media (PSS support and intermediate layers) before the Pd layer (mode in-out). In this manner, the composite structure of the membrane is working at the most unfavorable conditions in terms of mechanical resistance, generating tensile stress between different layers. Moreover, the opposite configuration was also analyzed, forcing to pass the permeate from the shell-side to the inner side of the membrane and thus meeting the Pd layer before the porous media (mode out-in).

Results and discussion

Modification of raw CeO_2 particles with Pd nuclei

Ceramic materials, such as CeO_2 , are commonly used as intermediate layers for preparing composite membranes onto porous metals, in order to avoid the possible inter-metallic diffusion between the metallic support and the palladium layer [42,43]. Furthermore, this intermediate layer can also reduce both average pore size and surface roughness of raw supports, and consequently turning the preparation of thin palladium layers easier [44,45]. This fact is especially interesting for membranes prepared by ELP-PP, in which both palladium source and reducing agent are fed from opposite sides of the porous support. In this context, as mentioned before, a recent study highlights the clear benefits of incorporating CeO_2 as intermediate layer in ELP-PP membranes, obtaining a good membrane performance with adequate mechanical resistance, complete hydrogen ideal separation factor and a significant increase of H_2 permeance [40]. Following this work, the present study includes a modification of the CeO_2 particles used for the preparation of the intermediate layer with the aim to improve even more the membrane properties. In this context, raw CeO_2 particles were doped with palladium nuclei before being incorporated to the support. Thus, the typical activation step required to prepare any Pd-based membrane by ELP or related techniques is

noticeably varied, since it is usually carried out after incorporating the intermediate barrier [46,47]. In the experimental procedure here proposed, the doping step of CeO_2 particles with Pd nuclei, before their incorporation by VA-DC in the calcined PSS support, avoids the necessity of the traditional activation step. Different doped CeO_2 particles were prepared by varying the ratio between the solutions containing the CeO_2 particles and Pd precursor from 1:6 to 1:36 (vol.). It has to be point out that the relation between the reducing agent and the plating solution volume was kept constant for all experiments. Table 1 collects the Pd load reached on the CeO_2 particles after the doping step performed at the different experimental conditions used as well as the efficiency of the process (η_{doping}), expressed as the ratio between the Pd nuclei deposited on the CeO_2 particles and the available metal amount into the doping solution.

A lower ratio between CeO_2 particles and the plating solution implies a greater amount of palladium available for the generation of Pd nuclei during the doping process. In fact, increasing Pd load on doped CeO_2 particles is reached when using a greater volume of Pd plating solution. A similar trend is achieved when analyzing the efficiency of the doping process, leading to a maximum doping yield (η_{doping}) around 52%.

Moreover, all samples exhibit a good distribution of Pd nuclei around the ceria particles, independently of the reached Pd load, although a progressive darker grey color can be observed as loaded Pd becomes higher. Thus, the original yellow color of raw CeO_2 particles is progressively turned into a dark grey when a greater amount of palladium is available in the medium.

Finally, in order to evaluate the efficiency of the doped CeO_2 particles for the later palladium deposition by ELP-PP, all samples summarized in Table 1 were used to prepare Pd-composite membranes. As a result, doped particles with a relation equal or lower than 1:18 (vol.) provokes a Pd weight gain on the membrane after the first ELP-PP cycle similar to that of the obtained one in case of using an activation process after incorporating the intermediate layer onto the PSS support ($\Delta m_{\text{pd}} \approx 10.2 \pm 0.5 \text{ mg cm}^{-2}$). So, under this premise and considering that the efficiency of the doping process seems to be slightly higher in case of using a particles/solution ratio of 1:18 (vol.), doped CeO_2 prepared at these conditions were selected as the most adequate ones for continuing the study.

Incorporation of doped ceria as intermediate layer

As previously described in detail, raw PSS supports were initially calcined in air at 600°C for 12 h and then a layer of doped CeO_2 particles with Pd nuclei was incorporated as intermediate layer by VA-DC. The raw PSS support maintains

Table 1 – Palladium load reached on CeO_2 particles after the doping process.

$\text{CeO}_2/\text{plating solution ratio (vol.)}$	Pd load (ppm)	$\eta_{\text{doping}} (\%)$
1:6	92.31	26.21
1:9	186.30	34.91
1:18	569.36	52.40
1:36	1077.95	52.00

the external morphology after the calcination process, presenting a relative rough surface ($R_a = 4.579 \pm 0.3 \mu\text{m}$), very close to the value obtained for raw PSS supports ($R_a = 5.082 \pm 0.4 \mu\text{m}$) [41,48]. This external roughness was reduced in a half after the incorporation of doped CeO_2 particles, reaching an average value of $R_a = 2.726 \pm 0.4 \mu\text{m}$. Fig. 1 shows the external morphology obtained by optical profilometry of calcined supports before (Fig. 1a) and after incorporating the doped CeO_2 particles (Fig. 1b). As it can be seen, doped CeO_2 (white colored) were preferentially placed around the deepest areas so covering the biggest pores of the calcined PSS support (brown-grey). It should be noted that some differences in calcined PSS grains between Fig. 1a and b are caused by profiler lighting adjustment due to the presence of ceramic particles. Here, it is important to emphasize that this behavior is almost identical to that obtained when raw CeO_2 were used to prepare the intermediate layer [40].

In order to analyze the morphology variation of the external surface of the support, SEM images before and after the incorporation of doped CeO_2 were also acquired (Fig. 2a and b). SEM image of calcined PSS support reveals a rough surface with a wide variety of pore mouth diameters up to a few microns (Fig. 2a). This morphology noticeably changes after the incorporation of doped CeO_2 particles (Fig. 2b). As it can be seen, the doped ceria particles were mostly placed inside the biggest pores of the external surface of the calcined PSS support, as it was previously observed by optical profiler at lower magnification. Additionally, new pores are generated between the ceramic particles of the intermediate barrier with a significantly smaller mouth sizes than original pores of the

support. Apparently, this new surface is quite similar to the obtained one when raw CeO_2 particles are used as intermediate layer. In fact, 0.0184 g of doped CeO_2 were incorporated onto the calcined support, thus obtaining a variation below an 8% respect to the average weight gain obtained when using directly raw CeO_2 particles [40].

The similar surface modification of supports despite doping the CeO_2 particles with Pd nuclei was also evidenced in permeation tests. Thus, N_2 fluxes through the modified supports with doped CeO_2 of 0.299 and 0.784 $\text{mol m}^{-2} \text{s}^{-1}$ were obtained at room temperature and pressure driving forces of 0.5 and 1.0 bar, respectively, really close to that of the obtained ones when using raw CeO_2 particles. At this point, it is necessary to point out that around 0.02 g of both doped and raw CeO_2 provide an optimal modification of the calcined PSS support. The average pore size diameter as well as the external roughness are noticeably reduced while a suitable permeability is maintained [40]. Moreover, the new porous media does not hinder the hydrazine pass through the pores during the ELP-PP deposition process, as described for certain cases in previous studies [40].

Palladium deposition by electroless pore-plating

To the best of our knowledge, this is the first study in which the combination of ELP-PP technique with a doped CeO_2 intermediate layer is investigated. In this context, Fig. 3 collects some micrographs of the external surface obtained after Pd incorporation by ELP-PP onto modified PSS support containing an intermediate layer formed by doped CeO_2 particles. As it

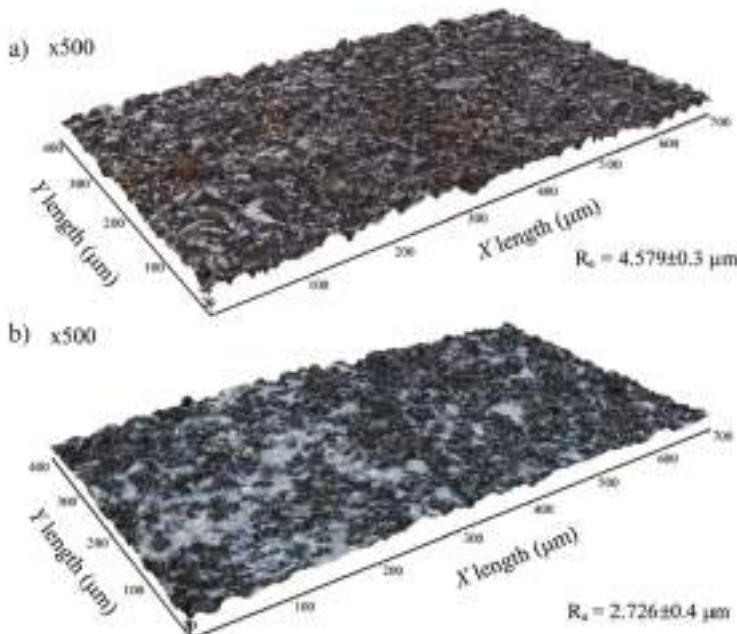


Fig. 1 – Surface morphology obtained by an optical profiler for calcined PSS support before (a) and after (b) the incorporation of doped CeO_2 particles as intermediate layer.

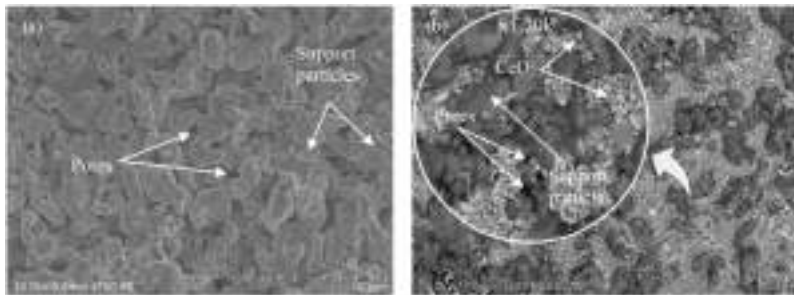


Fig. 2 – SEM images of the external surface of calcined PSS support before (a) and after (b) the incorporation of doped CeO₂ particles as intermediate layer.

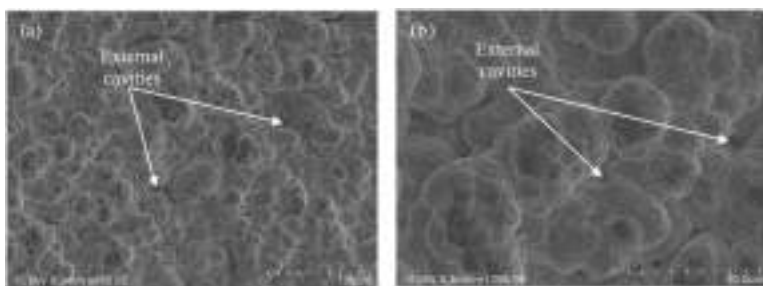


Fig. 3 – SEM micrographs of top Pd incorporated by ELP-PP onto a modified support with doped CeO₂ at magnification: (a) $\times 350$ and (b) $\times 1000$.

can be clearly seen, an apparent homogeneous and continuous palladium top layer was formed. It provides a noticeably smoother surface with only some residual cavities, as usual for most pore-plated membranes. However, the presence of these cavities on the superficial Pd layer does not imply a low H₂ selectivity, as it was suggested in previous works [38,40,49]. This fact was confirmed by He bubble-leak tests at room temperature, which evidences a good sealing for all the pores of the support with palladium. However, an important reduction of the estimated Pd thickness of around 40% is reached when replacing the use of raw CeO₂ particles by doped ones as intermediate layer. In this manner, an average

Pd layer with just 9 μm thickness, estimated by gravimetric analysis, is achieved when using doped CeO₂ as intermediate layer, in contrast to the 15 μm thick Pd layer reported when the intermediate layer is formed by raw CeO₂ [40].

Fig. 4 shows the cross-sectional view for membranes prepared by using raw (Fig. 4a) and Pd doped CeO₂ particles (Fig. 4b). In both cases, most external pores of the modified supports are filled with palladium, as usual for other ELP-PP membranes [37–39]. This fact can be explained by taking into account the nature of the ELP-PP process, in which both Pd source and reducing agent are fed from opposite sides of the support. The presence of Pd inside the pores is expected

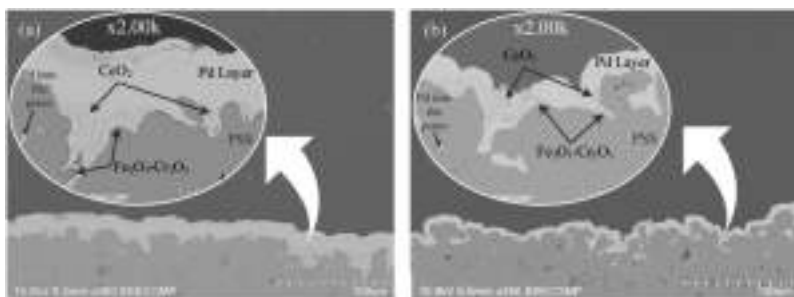


Fig. 4 – SEM cross-sectional views of ELP-PP membranes prepared onto modified supports with intermediate layers formed by: (a) raw or (b) doped CeO₂.

due to reactants meet just inside the pores, while a higher diffusion velocity of hydrazine from the inner to the outer side of the substrate can explain the preferential blockage of the nearest pores to the external surface of the support. Additionally, the pore distribution of the modified PSS support makes this process certainly heterogeneous, so hydrazine can reach the external surface through the biggest pores, thus making also possible the formation of a top Pd film. However, significant differences can be appreciated for this external Pd layer in case of using raw or doped CeO₂ particles. Pd membranes containing an intermediate barrier formed by raw CeO₂ (Fig. 4a) present a real external Pd thickness very close to the estimated one by gravimetric analysis, in the range 13–17 μm. This Pd layer covers almost completely the original morphology of the calcined PSS support, providing a very flat external surface. On the contrary, the use of an intermediate layer formed by Pd doped CeO₂ particles derives in a remarkably thinner external Pd film (Fig. 4b) with around 5 μm, despite the above-mentioned estimation from gravimetric analysis of 9 μm. This external and thin Pd layer replicates in a better way the original surface morphology of the PSS support.

This reduction in the Pd thickness after using doped CeO₂ represents to save around 40% of the noble metal during the membrane preparation and, consequently, to improve the overall cost of the process. This goal can be explained by a different distribution of Pd seeds throughout the porous modified supports in case of using raw or doped CeO₂ particles as intermediate layer, thus affecting the Pd film growth. In case of doping the CeO₂ particles before VA-DC step, the Pd nuclei are randomly distributed on the external surface of each ceramic particle, therefore providing an elevated number of active sites for starting the ELP-PP process. Probably, the new distribution of Pd seeds in doped CeO₂ particles facilitates the completion of ELP-PP process inside the pores in a better way, thus helping to obtain a fully dense membrane with lower Pd requirements. In fact, a 5 μm real external thickness was obtained by SEM (Fig. 4b), being significantly lower than the estimated one by gravimetric analyses ($t_{e,Pd} = 9 \mu m$). This discrepancy, not observed in case of using raw CeO₂ particles, can be due to the greater influence of an homogeneous Pd infiltration inside the pores of the substrate with respect to the total amount of Pd incorporated to the membrane. It has to be noted that both membranes, prepared with raw or doped CeO₂ particles, were obtained following identical experimental procedures for the incorporation of both intermediate layer and Pd film by VA-DC and ELP-PP, respectively. Therefore, it can be concluded that the new experimental procedure here proposed seems to be certainly attractive in terms of reducing the Pd requirements and, consequently, the Pd thickness. Additionally, it is expected that all membranes prepared by this method exhibit good mechanical properties due to the Pd infiltration inside the pores and the consequent good anchoring of the Pd layer.

Permeation behavior

As it has been detailed in the experimental section, permeation experiments with pure gases (N₂ and H₂) and mixtures have been performed at several temperatures. In this context,

two different configurations for the permeation tests were considered: a) mode in-out, introducing the feed stream to the lumen of the tubular membrane (tensile stress on the Pd layer) or b) vice versa, mode out-in, in which the permeate flux is produced from the outer to the inner side (compressive stress on the Pd layer). Previously to perform these experiments, preliminary He leak tests at room temperature were carried out to ensure the continuity of the Pd layer. Moreover, no N₂ was detected in the permeate stream for any higher temperature, taking into account that the minimum detection limit of the used gas flow-meter is 1 NmL h⁻¹. At this point, different experiments with pure H₂ were carried out at temperatures and trans-membrane pressures within the range of 350–450 °C and 0.5–2.0 bar, respectively. Moreover, it should be noted that 5 sequential thermal cycles were performed with an average operation time of around 5 h per cycle before considering stable permeate data. For each thermal cycle, the membrane was heated up to 400 °C in N₂, the gas feed was switched to H₂ to determinate the permeation flux after a minimum stabilization period of around 2 h and, finally, the membrane was cooled down again to room temperature in N₂. Results obtained by using the out-in operation mode are summarized in Fig. 5, where the H₂ flux is plotted against pressure at different temperatures. These results evidencing that permeate increases as the same time as doing pressure driving force or temperature. A linear trend between flux and pressure driving force was obtained, independently of the operating temperature. However, it is clear that this trend does not intercept in (0,0), in contrast to the expected behavior for Pd-based membranes according to the Sieverts' law ($n = 0.5$). This particular behavior has been previously addressed by considering the presence of an additional resistance to the permeation process when ELP-PP method is used. This effect was explained by the Pd penetration inside the pores of the porous media [38,40,49]. This additional resistance implies the presence of a minimum pressure value in the gas bulk phase below of which the H₂ permeation through the Pd layer does not occur. The additional resistance obtained in this work for the membrane prepared by using

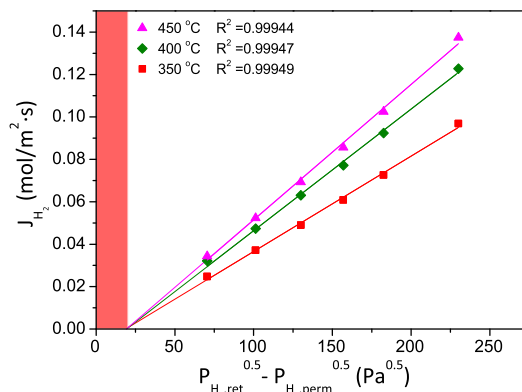


Fig. 5 – Permeation behavior of doped ceria as intermediate layer membrane, considering the presence of an additional resistance to the H₂ permeation process.

doped CeO_2 as intermediate layer is very close to the value obtained when using raw CeO_2 particles [40]. Thus, the calculated resistance is maintained around 35% below the value previously determined for an ELP-PP membrane without any ceramic intermediate layer but identical conditions for the palladium plating [38,49]. Taking into account this particular behavior, permeances values ranged from $4.50 \cdot 10^{-4}$ to $6.39 \cdot 10^{-4} \text{ mol m}^{-2} \text{ s}^{-1} \text{ Pa}^{-0.5}$ were reached at temperatures between 350 and 450 °C (out-in permeation mode). These values represent an increase of around 30% respect to using raw ceria as intermediate layer. In this manner, maintaining the out-in operation mode for the permeation experiments, the H_2 permeance has been increased from $4.46 \cdot 10^{-4}$ to $5.73 \cdot 10^{-4} \text{ mol m}^{-2} \text{ s}^{-1} \text{ Pa}^{-0.5}$ at 400 °C [40]. This improvement is mainly caused by saving around 40% of Pd thickness as well as the new morphology of the H_2 selective film reached after doping the CeO_2 , as previously discussed in Fig. 4. The effect of temperature on the permeance is determined by considering an Arrhenius-type dependence, thus obtaining an activation energy of 13.1 kJ mol^{-1} , within the typical range of other Pd-based membranes reported in literature [19,50].

Additionally, experiments with pure H_2 were completed with binary $\text{H}_2\text{-N}_2$ mixtures in order to investigate the influence of using non-pure feed streams and possible concentration-polarization effects. The results obtained for these experiments, performed at 400 °C in both possible operation modes (out-in and in-out), are depicted in Fig. 6.

Two different ELP-PP membranes containing CeO_2 intermediate layers with doped or raw particles have been analyzed. In general, the presence of N_2 in the feed stream always promotes a reduction in the permeance, independently of the intermediate layer and the N_2 concentration, thus suggesting possible concentration-polarization effects on the Pd layer. However, relevant differences can be appreciated for each membrane or permeation mode. Thus, permeance decrease in case of working according to the out-in operation method is significantly lower than the effect

obtained on the contrary operation mode. This effect, maintained for both membranes independently of using raw or doped CeO_2 particles as intermediate layer, can be explained by the position of the Pd layer. For in-out permeation experiments, the gas mixture is fed to the lumen of the membrane and H_2 needs to pass through the porous media before reaching the Pd layer. Most of H_2 in contact with the Pd layer is dissociated on the surface, diffusing through the bulk metal to be collected on the contrary side. However, in case of testing $\text{H}_2\text{-N}_2$ mixtures, nitrogen cannot pass through the Pd layer and it remains inside the pores of the supports some time, turning difficult the transport of hydrogen towards the Pd film in this area. This effect, known as concentration-polarization effect, becomes more relevant as increasing the dilution of the feed stream, thus explaining the reduction in permeance observed when testing gas mixtures.

The concentration-polarization effect has been reported by many researchers, being widely addressed in specialized literature [51–53]. However, in this work some differences arise for the analyzed membranes, obtaining a higher drop in permeance when using doped ceria instead of raw particles. In case of using the in-out operation mode, a maximum permeance drop of 20% and 36% was obtained with raw or doped CeO_2 as intermediate layer, respectively. This behavior can be explained by the final Pd thickness reached for each membrane. The ELP-PP membrane prepared with doped CeO_2 presents the thinnest Pd layer ($t_{\text{e,pd}} = 9 \mu\text{m}$) and, as consequence, provides the highest H_2 permeance with pure gases ($k = 6.26 \cdot 10^{-4} \text{ mol m}^{-2} \text{ s}^{-1} \text{ Pa}^{-0.5}$ at 400 °C). In this manner, a similar concentration-polarization effect, derived from the porosity of the support, will affect in a more important grade the permeance drop of the membrane with a higher initial permeation. Here, it is important to point out that a similar morphology of the intermediate layer was achieved after its incorporation, independently of using doped or raw CeO_2 particles, so the effect of the porous support on the gas transport should be certainly similar for both cases.

However, in case of using the out-in operation mode for the permeation tests with mixtures, a lower permeance decrease has been also obtained despite the feed gases reach now first the Pd layer, avoiding the above-mentioned effect on the porous support. Particularly, a permeance decrease of 10 and 19% when increasing the N_2 content from 0 to 10% was obtained in case of using raw or doped CeO_2 , respectively. This effect becomes more important for increasing the N_2 content up to 30%, although the permeance seem to be stabilized for greater dilution grades. Anyway, the observed permeance drop is always higher in case of testing the ELP-PP membrane prepared with doped CeO_2 . Differences on the external surface morphology of the Pd layer reached in this membrane (Fig. 4b) and the obtained one with raw CeO_2 particles (Fig. 4a) could explain this effect. The new membrane presented in this work, prepared with doped CeO_2 particles, contains small cavities on the external Pd layer surface. Thus, a higher roughness is obtained in comparison to the top Pd layer reached in case of using raw CeO_2 as intermediate layer, significantly flatter. The presence of these cavities and higher roughness can provoke a certain concentration-polarization effect, although less relevant to that of the previously discussed one in case of working in mode in-out. This makes

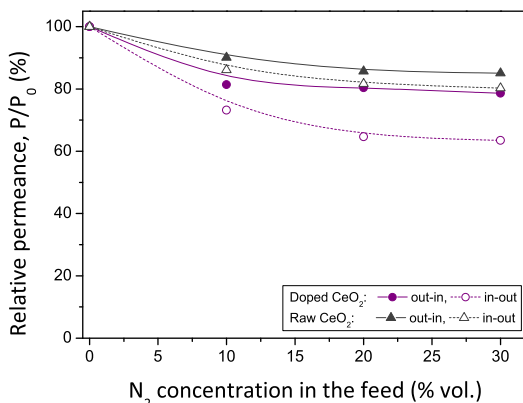


Fig. 6 – Effect of feed stream dilution with binary $\text{H}_2\text{-N}_2$ mixtures for ELP-PP membranes containing raw (triangles) or doped CeO_2 (circles) intermediate layers at diverse permeation modes: out-in (filled symbols) and in-out (empty symbols).

Table 2 – Literature survey about composite Pd-based membranes.

Membrane layers	Type	t_{Pd} (μm)	Permeation conditions		Permeation	H_2/N_2	Ref.
			T (°C)	ΔP (kPa)			
PSS-/Pd	Conventional	20.0	350	100	$3.11 \cdot 10^{-4a}$	500	[56]
PSS/OXI/Pd	ELP-PP	11.0–20.0	350–450	100–250	$1.00 \cdot 2.00 \cdot 10^{-4a}$	∞	[37]
PSS/Al ₂ O ₃ /Pd	Conventional	5.0	400	100	$3.05 \cdot 10^{-3a}$	500	[57]
PSS/CeO ₂ /Pd	Conventional	13.0	500–550	100–200	$0.127 \cdot 0.275^b$	∞	[29]
PSS/CeO ₂ /PdCu	Conventional	8.0	450	100	0.074^b	2369	[30]
YSZ/PdAu	Conventional	5.0	500	60	$1.80 \cdot 10^{-3a}$	4300	[54]
PSS/ZrO ₂ /PdAu	Conventional	14.0–27.0	400–500	10–100	$3.48 \cdot 7.14 \cdot 10^{-4a}$	4000	[55]
Pd/Al ₂ O ₃ /Pd	Duplex	3.8/2.5	500	100	$10.1 \cdot 10^{-3d}$	14429	[34]
Al ₂ O ₃ /PdAg/YSZ-Al ₂ O ₃	Double-skin	1.0	400	100	$4.60 \cdot 10^{-6c}$	25938	[23]
ZrO ₂ /TiO ₂ -Pd, ZrO ₂ -Pd/YSZ	Pore-filled	n.a.	400	100	$1.64 \cdot 10^{-7c}$	850	[36]
PSS/OXI-CeO ₂ /Pd	ELP-PP	15.4	350–475	100–200	$4.74 \cdot 6.35 \cdot 10^{-4a}$	>10000	[40]
PSS/OXI-doped CeO ₂ /Pd	ELP-PP	9.1	350–450	100–200	$4.46 \cdot 6.39 \cdot 10^{-4a}$	>10000	This work

^a Permeance ($\text{mol m}^{-2} \text{s}^{-1} \text{Pa}^{-0.5}$).^b Permeation flux ($\text{mol m}^{-2} \text{s}^{-1}$).^c Permeance ($\text{mol m}^{-2} \text{s}^{-1} \text{Pa}^{-1}$) and.^d Permeability ($\text{mol m}^{-1} \text{s}^{-1} \text{Pa}^{-0.5}$).

sense if tortuosity and pore size in the supports are compared with cavities detected on the top Pd layer. It is clear that occlusion of N₂ inside the pores of the support is easier than in external cavities, hence making the H₂ transport in this area more difficult.

To sum up the effect of binary H₂-N₂ mixtures on ELP-PP membranes containing CeO₂ as intermediate layer, it can be stated that thinner Pd layers are more affected by the concentration-polarization produced with diluted feeds, independently of permeating from the inner to the outer side or vice versa (in-out or out-in, respectively). This effect is mainly caused by meeting the support pores before the Pd layer in the first operating mode, or the presence of cavities on the Pd top film if the configuration out-in is used. Therefore, the new membrane presented in this work, with a 9 μm thick Pd top layer and higher permeance with pure gases than a similar membrane in which CeO₂ is not doped with palladium nuclei, suffers a more relevant concentration-polarization effect with N₂-H₂ mixtures, despite always reaching higher absolute permeance values.

After all these experiments at high temperatures, carried out for more than 120 h, the membrane exhibited a complete mechanical integrity. This mechanical strength was confirmed in a long-term stability test with pure H₂ at 400 °C and $\Delta P = 1$ bar, recovering the initial H₂ flux and maintaining a stable perm-selectivity despite extending the membrane operation for additional 720 h. As a result, the composite membrane was working for more than 30 days (approximately 850 h) without any mechanical problem. Here, it should be noted that this is especially interesting if considering the membrane resistance against the in-out operation mode in which pressure provoke tensile stress on the Pd film, making possible its delamination. Since this fact is not produced, a good anchoring of the Pd layer can be guaranteed when using ELP-PP on a modified support with doped CeO₂ intermediate layer at similar operating conditions.

Finally, Table 2 compares the results obtained in this work with other experimental data reported in literature. It should

be noted that this comparison has been limited to composite membranes prepared by ELP, but including a wide variety of materials used as supports, intermediate and selective layers, and some membrane configurations recently published, such as pore-filled [36], double-skin [23] or duplex membranes [34]. The large variety of configurations joint to the diverse equipment design for permeation tests and operating conditions increase the complexity for a rigorous comparison. In general, as it is well known, the thinnest selective films the biggest hydrogen fluxes. On the contrary, very high hydrogen fluxes usually involve limited H₂ selectivity. In most cases, the permeation properties are intimately related to both metal thickness and composition of the selective layer, pure Pd or Pd-based alloys. As previously detailed, a complete H₂/N₂ selectivity ($\geq 10,000$, detection limit of 1 NmL/h) was obtained for the membrane collected in this study during the entire set of experiments. Moreover, a H₂ permeance in the range $4.46 \cdot 6.39 \cdot 10^{-4}$ mol m⁻² s⁻¹ Pa^{-0.5} was reached at 350–450 °C when feeding pure H₂. As it can be seen in Table 2, these permeance values are within the typical range to that of the presented ones by other researchers for pure Pd-membranes, but achieving a really high H₂/N₂ separation factor at ideal conditions. On the other hand, it is also observed a lower H₂ permeance than the reached one by other membranes prepared by allowing the Pd with other metals, mainly Ag [23], Cu [30] and Au [54,55].

Conclusions

The use of doped CeO₂ particles with Pd nuclei to prepare intermediate layers and, hence, facilitate the consecutive formation of a fully dense Pd film by ELP-PP is reported in this study for the first time. The new intermediate layer provokes an increase of the support weight of 0.02 g, while the surface roughness is reduced up to 2.726 ± 0.4 μm. These values are quite similar to the obtained ones when using directly raw CeO₂ particles to prepare the intermediate layer, so the

reproducibility of the VA-DC experimental procedure is demonstrated with the doped particles. Additionally, the new intermediate layer makes possible to reduce the Pd thickness around 40% without affecting the complete H₂ selectivity of the membrane. Thus, an estimated value from gravimetric analysis of 9 μm was reached. Additionally, cross-sectional views of the membrane reveal the formation of an external top Pd layer with just 5 μm thickness, significantly lower than the previous estimated value. This behavior was not observed in case of using raw CeO₂ particles as intermediate layer, being both values in good agreement around 15 μm. It means that palladium has been preferentially incorporated around doped CeO₂ particles. In this manner, the replacement of raw CeO₂ particles by Pd doped ones in the intermediate layer significantly saves palladium for ELP-PP. In addition, a H₂ flux increase of around 15–30% was obtained for the different operation modes. Thus, a H₂ permeance of $6.26 \cdot 10^{-4}$ mol m⁻² s⁻¹ Pa^{-0.5} at 400 °C and ΔP = 1 bar is reached, without affecting the H₂/N₂ ideal separation factor (≥ 10000). The effect of feeding binary H₂-N₂ mixtures was also evaluated, obtaining a significant concentration-polarization effect. This effect is caused by the presence of cavities in the external side of the Pd layer (affecting the permeation mode out-in) and, more important, the tortuosity and pore sizes of the modified support (strongly affecting the permeation mode in-out). This effect becomes more relevant for membranes with thinner Pd layers. However, it should be noted that the new membrane prepared with doped CeO₂ always provides higher absolute H₂ permeance values at the entire range of experiments in comparison to a similar membrane with an intermediate layer formed by raw CeO₂ particles. Finally, long-term permeation tests up to 30 days with pure gases at T = 400 °C and ΔP = 1 bar were carried out to demonstrate the mechanical stability of the membrane, obtaining an almost steady H₂ flux and H₂/N₂ ideal separation factor really close to the values measured before analyzing the effect of feeding gas mixtures.

Acknowledgements

The authors acknowledge the financial support achieved from Economy, Industry and Competitiveness Ministry of the Spanish Government through the competitive project ENE2017-83696-R.

REFERENCES

- [1] Valente A, Iribarren D, Dufour J. Harmonised life-cycle global warming impact of renewable hydrogen. *J Clean Prod* 2017;149:762–72. <https://doi.org/10.1016/j.jclepro.2017.02.163>.
- [2] Szulejko JE, Kumar P, Deep A, Kim K-H. Global warming projections to 2100 using simple CO₂ greenhouse gas modeling and comments on CO₂ climate sensitivity factor. *Atmos Pollut Res* 2017;8:136–40. <https://doi.org/10.1016/J.APR.2016.08.002>.
- [3] Jiang J, Ye B, Liu J. Research on the peak of CO₂ emissions in the developing world: current progress and future prospect. *Appl Energy* 2019;235:186–203. <https://doi.org/10.1016/J.APENERGY.2018.10.089>.
- [4] Bai Y, Deng X, Gibson J, Zhao Z, Xu H. How does urbanization affect residential CO₂ emissions? An analysis on urban agglomerations of China. *J Clean Prod* 2019;209:876–85. <https://doi.org/10.1016/J.JCLEPRO.2018.10.248>.
- [5] Chen P-Y, Chen S-T, Hsu C-S, Chen C-C. Modeling the global relationships among economic growth, energy consumption and CO₂ emissions. *Renew Sustain Energy Rev* 2016;65:420–31. <https://doi.org/10.1016/J.RSER.2016.06.074>.
- [6] Cai Y, Sam CY, Chang T. Nexus between clean energy consumption, economic growth and CO₂ emissions. *J Clean Prod* 2018;182:1001–11. <https://doi.org/10.1016/J.JCLEPRO.2018.02.035>.
- [7] da Silva Veras T, Mozer TS, da Costa Rubim Messeder dos Santos D, da Silva César A. Hydrogen: trends, production and characterization of the main process worldwide. *Int J Hydrogen Energy* 2017. <https://doi.org/10.1016/j.ijhydene.2016.08.219>.
- [8] Parra D, Valverde L, Pino FJ, Patel MK. A review on the role, cost and value of hydrogen energy systems for deep decarbonisation. *Renew Sustain Energy Rev* 2019;101:279–94. <https://doi.org/10.1016/J.RSER.2018.11.010>.
- [9] Fonseca JD, Camargo M, Commengé J-M, Falk L, Gil ID. Trends in design of distributed energy systems using hydrogen as energy vector: a systematic literature review. *Int J Hydrogen Energy* 2018. <https://doi.org/10.1016/J.IJHYDENE.2018.09.177>.
- [10] Baykara SZ. Hydrogen: a brief overview on its sources, production and environmental impact. *Int J Hydrogen Energy* 2018;43:10605–14. <https://doi.org/10.1016/j.ijhydene.2018.02.022>.
- [11] Adhikari S, Fernando S. Hydrogen membrane separation techniques. *Ind Eng Chem Res* 2006;45:875–81. <https://doi.org/10.1021/ie0506441>.
- [12] Zornoza B, Casado C, Navajas A. Chapter 11 - advances in hydrogen separation and purification with membrane technology. In: Gandia LM, Arzamendi G, Diéguez PM, editors. *Renew. Hydrop. Technol.* Amsterdam: Elsevier; 2013. p. 245–68. <https://doi.org/10.1016/B978-0-444-56352-1.00011-8>.
- [13] (Balu) Balachandran U, Lee TH, Park CY, Emerson JE, Piccioli JJ, Dorris SE. Dense cermet membranes for hydrogen separation. *Separ Purif Technol* 2014;121:54–9. <https://doi.org/10.1016/j.seppur.2013.10.001>.
- [14] Dunbar ZW. Hydrogen purification of synthetic water gas shift gases using microstructured palladium membranes. *J Power Sources* 2015;297:525–33. <https://doi.org/10.1016/j.jpowsour.2015.08.015>.
- [15] Tosti S, Basile A, Bettinelli L, Borgognoni F, Gallucci F, Rizzello C. Design and process study of Pd membrane reactors. *Int J Hydrogen Energy* 2008;33:5098–105. <https://doi.org/10.1016/j.ijhydene.2008.05.031>.
- [16] De Falco M, Iaquaniello G, Palo E, Cucchiella B, Palma V, Ciambelli P. 11 - palladium-based membranes for hydrogen separation: preparation, economic analysis and coupling with a water gas shift reactor. In: Basile A, editor. *Handb. Membr. React.* Woodhead Publishing; 2013. p. 456–86. <https://doi.org/10.1533/9780857097347.2.456>.
- [17] Conde JJ, Maroño M, Sánchez-Hervás JM. Pd-based membranes for hydrogen separation: review of alloying elements and their influence on membrane properties. *Separ Purif Rev* 2017;46:152–77. <https://doi.org/10.1080/15422119.2016.1212379>.
- [18] Arratibel Plazaola A, Pacheco Tanaka D, Van Sint Annaland M, Gallucci F. Recent advances in Pd-based membranes for membrane reactors. *Molecules* 2017;22:51. <https://doi.org/10.3390/molecules22010051>.

- [19] Alique D, Martinez-Diaz D, Sanz R, Calles JA. Review of supported pd-based membranes preparation by electroless plating for ultra-pure hydrogen production. 2018. <https://doi.org/10.3390/membranes8010005>.
- [20] Alique D. Processing and characterization of coating and thin film materials. In: Zhang J, Jung Y, editors. *Adv. Ceram. Met. Coat. Thin film mater. Energy environ.*; 2018. <https://doi.org/10.1007/978-3-319-59906-9>.
- [21] Yun S, Ted Oyama S. Correlations in palladium membranes for hydrogen separation: a review. *J Membr Sci* 2011;375:28–45. <https://doi.org/10.1016/j.memsci.2011.03.057>.
- [22] Melendez J, Fernandez E, Gallucci F, van Sint Annaland M, Arias PL, Pacheco Tanaka DA. Preparation and characterization of ceramic supported ultra-thin (~1 µm) Pd-Ag membranes. *J Membr Sci* 2017;528:12–23. <https://doi.org/10.1016/j.memsci.2017.01.011>.
- [23] Arratibel A, Pacheco Tanaka A, Laso I, van Sint Annaland M, Gallucci F. Development of Pd-based double-skinned membranes for hydrogen production in fluidized bed membrane reactors. *J Membr Sci* 2018;550:536–44. <https://doi.org/10.1016/j.MEMSCI.2017.10.064>.
- [24] Alique D, Imperatore M, Sanz R, Calles JA, Giacinti Baschetti M. Hydrogen permeation in composite Pd-membranes prepared by conventional electroless plating and electroless pore-plating alternatives over ceramic and metallic supports. *Int J Hydrogen Energy* 2016;41:19430–8. <https://doi.org/10.1016/j.ijhydene.2016.06.128>.
- [25] Kiadehi AD, Taghizadeh M. Fabrication, characterization, and application of palladium composite membrane on porous stainless steel substrate with NaY zeolite as an intermediate layer for hydrogen purification. *Int J Hydrogen Energy* 2019;44:2889–904. <https://doi.org/10.1016/j.ijHYDENE.2018.12.058>.
- [26] Han J-Y, Kim C-H, Lim H, Lee K-Y, Ryi S-K. Diffusion barrier coating using a newly developed blowing coating method for a thermally stable Pd membrane deposited on porous stainless-steel support. *Int J Hydrogen Energy* 2017;42:12310–9. <https://doi.org/10.1016/j.ijhydene.2017.03.053>.
- [27] Arratibel A, Medrano JA, Melendez J, Pacheco Tanaka DA, van Sint Annaland M, Gallucci F. Attrition-resistant membranes for fluidized-bed membrane reactors: double-skin membranes. *J Membr Sci* 2018;563:419–26. <https://doi.org/10.1016/j.memsci.2018.06.012>.
- [28] Calles JA, Sanz R, Alique D. Influence of the type of siliceous material used as intermediate layer in the preparation of hydrogen selective palladium composite membranes over a porous stainless steel support. *Int J Hydrogen Energy* 2012;37:6030–42. <https://doi.org/10.1016/j.ijhydene.2011.12.164>.
- [29] Tong J, Matsumura Y, Suda H, Haraya K. Thin and dense Pd/CeO₂/MPSS composite membrane for hydrogen separation and steam reforming of methane. *Separ Purif Technol* 2005;46:1–10. <https://doi.org/10.1016/j.seppur.2005.03.011>.
- [30] Qiao A, Zhang K, Tian Y, Xie L, Luo H, Lin YS, Li Y. Hydrogen separation through palladium-copper membranes on porous stainless steel with sol-gel derived ceria as diffusion barrier. *Fuel* 2010;89:1274–9. <https://doi.org/10.1016/j.fuel.2009.12.006>.
- [31] Gao H, Lin JYS, Li Y, Zhang B. Electroless plating synthesis, characterization and permeation properties of Pd–Cu membranes supported on ZrO₂ modified porous stainless steel. *J Membr Sci* 2005;265:142–52. <https://doi.org/10.1016/j.memsci.2005.04.050>.
- [32] Bottino A, Broglia M, Capannelli G, Comite A, Pinacci P, Scignari M, Azzurri F. Sol–gel synthesis of thin alumina layers on porous stainless steel supports for high temperature palladium membranes. *Int J Hydrogen Energy* 2014;39:4717–24. <https://doi.org/10.1016/j.ijhydene.2013.11.096>.
- [33] Yun S, Ted Oyama S, Oyama ST. Correlations in palladium membranes for hydrogen separation: a review. *J Membr Sci* 2011;375:28–45. <https://doi.org/10.1016/j.memsci.2011.03.057>.
- [34] Zhao C, Xu H, Goldbach A. Duplex Pd/ceramic/Pd composite membrane for sweep gas-enhanced CO₂capture. *J Membr Sci* 2018;563:388–97. <https://doi.org/10.1016/j.memsci.2018.05.057>.
- [35] Tanaka DAP, Tanco MAL, Okazaki J, Wakui Y, Mizukami F, Suzuki TM. Preparation of “pore-fill” type Pd–YSZ–γ-Al₂O₃ composite membrane supported on α-Al₂O₃ tube for hydrogen separation. *J Membr Sci* 2008;320:436–41. <https://doi.org/10.1016/j.memsci.2008.04.044>.
- [36] Arratibel A, Pacheco Tanaka DA, Slater TJA, Burnett TL, van Sint Annaland M, Gallucci F. Unravelling the transport mechanism of pore-filled membranes for hydrogen separation. *Separ Purif Technol* 2018;203:41–7. <https://doi.org/10.1016/j.seppur.2018.04.016>.
- [37] Sanz R, Calles JA, Alique D, Furones L. New synthesis method of Pd membranes over tubular [PSS] supports via “pore-plating” for hydrogen separation processes. *Int J Hydrogen Energy* 2012;37:18476–85. <https://doi.org/10.1016/j.ijhydene.2012.09.084>.
- [38] Calles JA, Sanz R, Alique D, Furones L, Marín P, Ordoñez S. Influence of the selective layer morphology on the permeation properties for Pd-PSS composite membranes prepared by electroless pore-plating: experimental and modeling study. *Separ Purif Technol* 2018;194:10–8. <https://doi.org/10.1016/j.seppur.2017.11.014>.
- [39] Sanz R, Calles JA, Ordóñez S, Marín P, Alique D, Furones L. Modelling and simulation of permeation behaviour on Pd/PSS composite membranes prepared by “pore-plating” method. *J Membr Sci* 2013;446:410–21. <https://doi.org/10.1016/j.memsci.2013.06.060>.
- [40] Martinez-Diaz D, Sanz R, Calles JA, Alique D. H₂ permeation increase of electroless pore-plated Pd/PSS membranes with CeO₂ intermediate barriers. *Separ Purif Technol* 2019;216:16–24. <https://doi.org/10.1016/j.SEPPUR.2019.01.076>.
- [41] Furones L, Alique D. Interlayer properties of in-situ oxidized porous stainless steel for preparation of composite Pd membranes. *ChemEngineering* 2017;2:1. <https://doi.org/10.3390/chemengineering2010001>.
- [42] Yepes D, Cornaglia LM, Irusta S, Lombardo EA. Different oxides used as diffusion barriers in composite hydrogen permeable membranes. *J Membr Sci* 2006;274:92–101. <https://doi.org/10.1016/j.memsci.2005.08.003>.
- [43] Plazaola AA, Tanaka DAP, Annaland MVS, Gallucci F. Recent advances in pd-based membranes for membrane reactors. *Molecules* 2017;22:1–53. <https://doi.org/10.3390/molecules22010051>.
- [44] Zheng L, Li H, Xu H. “Defect-free” interlayer with a smooth surface and controlled pore-mouth size for thin and thermally stable Pd composite membranes. *Int J Hydrogen Energy* 2016;41:1002–9. <https://doi.org/10.1016/j.ijhydene.2015.09.024>.
- [45] Mateos-Pedrero C, Soria MA, Rodríguez-Ramos I, Guerrero-Ruiz A. Modifications of porous stainless steel previous to the synthesis of Pd membranes. In: *Stud. Surf. Sci. Catal.*; 2010. p. 779–83. [https://doi.org/10.1016/S0167-2991\(10\)75159-4](https://doi.org/10.1016/S0167-2991(10)75159-4).
- [46] Ayturk ME, Mardilovich IP, Engwall EE, Ma YH. Synthesis of composite Pd-porous stainless steel (PSS) membranes with Pd/Ag intermetallic diffusion barrier. *J Membr Sci* 2006;285:385–94. <https://doi.org/10.1016/j.memsci.2006.09.008>.

- [47] Zhu B, Tang CH, Xu HY, Su DS, Zhang J, Li H. Surface activation inspires high performance of ultra-thin Pd membrane for hydrogen separation. *J Membr Sci* 2017;526:138–46. <https://doi.org/10.1016/j.memsci.2016.12.025>.
- [48] Calles JA, Sanz R, Alique D, Furones L. Thermal stability and effect of typical water gas shift reactant composition on H₂ permeability through a Pd-YSZ-PSS composite membrane. *Int J Hydrogen Energy* 2014;39:1398–409. <https://doi.org/10.1016/j.ijhydene.2013.10.168>.
- [49] Alique D, Imperatore M, Sanz R, Calles JA, Baschetti MG. Hydrogen permeation in composite Pd-membranes prepared by conventional electroless plating and electroless pore-plating alternatives over ceramic and metallic supports. *Int J Hydrogen Energy* 2016;41:19430–8. <https://doi.org/10.1016/j.ijhydene.2016.06.128>.
- [50] Sanz R, Calles JA, Alique D, Furones L, Ordóñez S, Marín P, Corengia P, Fernandez E. Preparation, testing and modelling of a hydrogen selective Pd/YSZ/SS composite membrane. *Int J Hydrogen Energy* 2011;36:15783–93. <https://doi.org/10.1016/j.ijhydene.2011.08.102>.
- [51] Catalano J, Giacinti Baschetti M, Sarti GC. Influence of the gas phase resistance on hydrogen flux through thin palladium–silver membranes. *J Membr Sci* 2009;339:57–67. <https://doi.org/10.1016/j.memsci.2009.04.032>.
- [52] Nakajima T, Kume T, Ikeda Y, Shiraki M, Kurokawa H, Iseki T, Kajitani M, Tanaka H, Hikosaka H, Takagi Y, Ito M. Effect of concentration polarization on hydrogen production performance of ceramic-supported Pd membrane module. *Int J Hydrogen Energy* 2015;40:11451–6. <https://doi.org/10.1016/j.ijhydene.2015.03.088>.
- [53] Steil MC, Fouletier J, Geffroy PM. Surface exchange polarization vs. gas concentration polarization in permeation through mixed ionic-electronic membranes. *J Membr Sci* 2017;541:457–64. <https://doi.org/10.1016/j.memsci.2017.07.028>.
- [54] Patki NS, Lundin S-TB, Way JD. Apparent activation energy for hydrogen permeation and its relation to the composition of homogeneous PdAu alloy thin-film membranes. *Separ Purif Technol* 2018;191:370–4. <https://doi.org/10.1016/j.seppur.2017.09.047>.
- [55] Contardi I, Cornaglia L, Tarditi AM. ScienceDirect Effect of the porous stainless steel substrate shape on the ZrO₂ deposition by vacuum assisted dip-coating. *Int J Hydrogen Energy* 2017;42:7986–96. <https://doi.org/10.1016/j.ijhydene.2017.01.024>.
- [56] Mardilovich PP, She Y, Ma YH, Rei M-H. Defect-free palladium membranes on porous stainless-steel support. *AIChE J* 1998;44:310–22. <https://doi.org/10.1002/aic.690440209>.
- [57] Gade SK, Thoen PM, Way JD. Unsupported palladium alloy foil membranes fabricated by electroless plating. *J Membr Sci* 2008;316:112–8. <https://doi.org/10.1016/j.memsci.2007.08.022>.



Comprehensive permeation analysis and mechanical resistance of electroless pore-plated Pd-membranes with ordered mesoporous ceria as intermediate layer

D. Martínez-Díaz^a, D. Martínez del Monte^a, E. García-Rojas^b, D. Alique^a, J.A. Calles^a, R. Sanz^{b,*}

^a Department of Chemical, Energy and Mechanical Technology, Rey Juan Carlos University, C/ Tulipán s/n, 28933 Móstoles, Spain

^b Department of Chemical and Environmental Technology, Rey Juan Carlos University, C/ Tulipán s/n, 28933 Móstoles, Spain

ARTICLE INFO

Keywords:
 Membrane
 Porous stainless steel
 Intermediate layer
 Mesoporous ceria
 Palladium
 Electroless plating
 Hydrogen

ABSTRACT

H₂-selective composite membranes, particularly those based on palladium films deposited onto porous stainless-steel supports, represent a promising technology to be practically included in both independent devices and membrane reactors. To reach thin H₂-selective films and hence high permeance values, the use of a wide variety of intermediate layers is usually adopted in the literature. However, an agreement about the best solution is not found up to now. In this context, the current study presents the use of Ordered Mesoporous Ceria (OMC) particles as intermediate layer for the improvement of permeation properties of Electroless Pore-Plated (ELP-PP) Pd-composite membranes. OMC was obtained by nanocasting from SBA-15 as temporary template and cerium nitrate (III) hexahydrate as metal precursor. Resultant OMC particles have around 100 nm spherical diameter, an average pore-size diameter of 10–12 nm, and a total BET surface of around 134 m²/g. This material was next deposited onto the external surface of tubular Porous Stainless-Steel (PSS) supports by vacuum-assisted dip-coating (VA-DC) to form an intermediate layer that makes the preparation of a defect-free and thin Pd-film easier. This procedure allows the preparation of Pd composite membranes (OMC-Pd) with Pd thicknesses around 10 μm, H₂ permeances of 1.03·10⁻³ mol m⁻² s⁻¹ Pa^{-0.5} at 400 °C, and high ideal selectivity $\alpha_{H_2/N_2} \geq 24,000$. It should be noted that H₂ permeance has been increased up to 6 times in comparison with other ELP-PP membranes without any intermediate layer and 2 times in contrast to membranes containing dense CeO₂ particles instead of the mesoporous ones for the intermediate layer. Moreover, Pd-membranes so prepared (OMC-Pd) have shown excellent mechanical resistance in a wide variety of operating conditions such as temperature, pressure, and permeate flux direction, maintaining a high H₂-selectivity without delamination or peeling. These properties were also maintained in case of feeding different H₂/N₂ mixtures, where the concentration-polarization effect seems to stabilize for lower H₂ concentration values in the feed stream, not being noticeably influenced by temperature.

1. Introduction

Nowadays it is widely accepted the direct connection between climate change and increase of greenhouse gas emissions in the atmosphere, mainly carbon dioxide, due to multiple anthropogenic factors [1]. Among them, it can be emphasized activities for electricity and heat generation, industrial manufacturing, production of chemicals, and transport, with an overall contribution to the worldwide CO₂ emissions of around 80% [2,3]. The promotion of renewable energies and

hydrogen expects to modify the current situation by decarbonizing the energy system without compromising future economic development [4]. Additionally, actions directed to improve the energy efficiency of processes in the industry are also receiving great attention as an attractive alternative to save energy and CO₂ emissions [5]. In this context, a recent study conducted by Sholl and Lively demonstrates that around 50% of the current energy demand in industrial processes are caused by separation and purification operations, thus suggesting the enhancement of these technologies as a great opportunity to achieve most of the

* Corresponding author.

E-mail address: raul.sanz@urjc.es (R. Sanz).

previously described goals [6]. The use of H₂-selective membranes offers high potential in this field for both independent purifiers and the so-called membrane reactors, in which these membranes are combined with catalyzed assisted chemical reactions in a unique device [7,8]. Particularly, dense Pd-based membranes exhibit excellent properties in terms of permeability, H₂ selectivity, and thermal resistance to be used in high-temperature applications [9]. However, some problems related to the cost of the membranes, their reproducibility and stability at real conditions, and large scales need to be overcome before being introduced at industrial scale [10]. The stability of a membrane can be mainly affected by its mechanical resistance against the operating conditions and deactivation/poisoning processes caused by chemical compounds such as steam, carbon monoxide, hydrocarbon molecules, or sulfur compounds [11]. These critical parameters are noticeably relevant in the case of using membrane reactors due to the complexity of coupling the experimental conditions for both catalysts and membranes.

Most researchers stand up for preparing composite membranes in which a thin Pd or Pd-alloy film is stacked onto porous supports [12], usually formed by agglomeration and sintering of alumina or stainless steel (SS) particles [13]. The support choice determines the final properties of the H₂-selective Pd films in terms of morphology, homogeneity, adherence, and thickness [14]. In general, ceramic supports make the preparation of ultrathin Pd layers easier due to their lower external roughness and high-controlled pore distribution with sizes up to a few nanometers. However, these supports show important concerns related to their resistance against thermal cycles and to be fitted in a membrane reactor device [13]. On the contrary, the similar thermal expansion coefficient between Pd and SS guarantees a suitable membrane performance and sealing in most of the typical industrial devices. However, the high surface roughness of these supports, with noticeably large pores, turns the preparation of ultra-thin H₂ selective films really difficult [15]. Therefore, many authors propose the modification of raw porous stainless steel (PSS) supports by the incorporation of porous ceramic intermediate layers between both support and Pd film [16]. A wide variety of materials have been used with this purpose, including Al₂O₃ [17], SiO₂ [18], TiO₂ [19], ZrO₂ [20], Y₂O₃ [21] or CeO₂ [22,23], among others. In all cases, it was reduced the final Pd thickness of the membrane due to the modification of original surface properties of the PSS supports, at the same time that possible membrane deterioration by the intermetallic diffusion of SS components into the Pd film at high temperature was also prevented [24]. However, the use of any of these metal oxides for the generation of intermediate layers could considerably reduce the permeation of the final composite membranes. Therefore, it could be interesting the use of porous particles for the preparation of these intermediate layers, increasing their H₂ permeation due to the presence of both intra- and inter-particle porosity, avoiding the particle agglomeration and protecting the Pd film. Moreover, additional functionalities could be subsequently provided for particular applications, especially in the case they would be placed in a membrane reactor. This strategy could protect the Pd film against certain compounds by molecular sieving and even provide certain or additional catalytic activity. Despite these important potential benefits, only a few studies in which this strategy is applied can be found in the literature, being most of them based on zeolites and related materials.

In this context, Bosko et al. reported the use of NaA zeolite as an effective diffusion barrier in composite Pd/PSS membranes, reaching Pd thickness in the range 19–26 μm [25]. The NaA intermediate layer was prepared by dip-coating and hydrothermal synthesis, penetrating the pore system of the PSS support up to 40 μm. This membrane was also applied in a membrane reactor for dry reforming of methane without modification of the original crystalline structure nor morphological features [26]. Calles et al. followed a similar strategy for modifying raw PSS supports before the Pd incorporation, but in this case comparing the modification achieved with two different porous materials based on silica, silicalite-1, and hexagonal mesoporous silica (HMS). They reached a completely defect-free Pd film of around 5 μm with hydrogen

permeance of 1.423·10⁻⁴ mol m⁻² s⁻¹ Pa^{-0.5} in case of using the silicalite-1 intermediate barrier [18]. A similar intermediate layer formed by silicalite-1 particles was also presented by Guo et al. [12,27] in tubular macro-porous alumina supports, demonstrating certain stability of the membrane for about 15 days while operating at 400 °C. NaX nano-zeolites was also applied to modify the pore size of PSS supports and improve the hydrogen permeability of the membranes with ca. 20 μm Pd thickness [28,29]. Kiadehi and Taghizadeh coated planar PSS supports with NaY zeolite particles by initial seeding and secondary growth method, obtaining a Pd thickness of about 7 μm, hydrogen permeance of 6.2·10⁻⁴ mol m⁻² s⁻¹ Pa^{-0.5} and ideal H₂/N₂ selectivity of 736 [30]. The same authors also reported the preparation of other composite membranes with SAPO-34 intermediate layers, slightly improving the ideal H₂/N₂ selectivity up to 866. This new intermediate layer with a pore opening diameter of 0.38 nm is presented as a suitable candidate for multiple applications such as gas purification, support in hydrogen generation processes, catalyst for diverse chemical reactions, and sorption, especially relevant for removal of water from gas mixtures [31]. In most of these works, the materials' growth was directly carried out onto the surface of supports to control the orientation of crystals and, hence, the pores. However, these synthesis procedures usually involve multiple steps with a certain complexity, thus increasing both the cost and the possibilities of an increasing number of rejected membranes in an expected production scale-up. Problems for a suitable reproducibility could be also an important issue to take into account. In this framework, the evaluation of more simple preparation methods, i.e. the well-known dip-coating, could provide noticeably advantages for industrialization of the membrane preparation processes. Anyway, despite the above-mentioned advances when using zeolites as intermediate layer for the preparation of composite Pd-based membranes, it is evident the scarce number of studies and lack of information about particular benefits reached in real membrane reactor conditions. Moreover, the convenience of using other materials with better thermal expansion properties, i.e. ceria [14,22], needs to be carefully addressed. This ceramic material presents a thermal expansion coefficient of 11.8–13.2 μstrain/°C, which is fairly close to that of both palladium and AISI 316L SS (10.6–12.6 and 15.0–18.0 μstrain/°C, respectively). Experimental procedures for preparing a wide variety of ordered porous metal oxides are well known, being possible to report protocols for adjusting the porosity of these materials by nanocasting [32–34]. These materials provide a really high surface area with very homogeneous pores and controlled particle size distribution similar to zeolite structures. However, until our best knowledge, most of them are only considered for the fabrication of advanced catalysts instead of the preparation of a new generation of versatile membranes. Therefore, the present study aims to cover this gap, presenting for the first time the use of ordered-mesoporous ceria to modify commercial tubular PSS supports before the incorporation of a Pd continuous layer for H₂ permeation. These novel intermediate layers have been combined with Electroless Pore-Plating (ELP-PP) for the incorporation of Pd-films, analyzing in detail both morphology and permeation behavior of the new membranes so obtained.

2. Experimental procedure

2.1. Ordered mesoporous ceria (OMC) preparation

The ordered mesoporous ceria (OMC) used as intermediate layer was obtained by one of the most widely studied hard-templating methods, the nanocasting [32,33,35]. In this method, a porous template is filled with another material, afterward removing the initial template. In this particular case, cerium nitrate (III) hexahydrate (Aldrich, 99% purity), used as metal precursor, was impregnated onto the mesoporous silica-based material SBA-15 used as hard temporary template. SBA-15 was synthesized according to the procedure described by Zhao et al [36]. First, 4.85 g of Ce(NO₃)₃·6H₂O was dissolved in 50 mL of ethanol. Then, 6 g of SBA-15 was added stepwise to the alcoholic solution to achieve a

very homogeneous suspension and to avoid the formation of agglomerates in the mixture. The solution was subsequently stirred overnight at 300 rpm and room temperature up to the complete evaporation of the solvent. After that, SBA-15 particles in which all pores are filled with the cerium precursor were calcined at 600 °C for 6 h (heating ramp of 1 °C/min). During the calcination step, the precursor embedded inside the SBA-15 pores was transformed into the metal oxide, CeO₂. Both procedures were repeated multiple cycles to ensure a complete impregnation of each pore of the SBA-15 material, thus preparing high-quality nanocasted material. Finally, the complete removal of the SBA-15 used as hard-template was carried out by washing with an aqueous 2 M NaOH solution. The liquid-solid mixture was stirred at 300 rpm and 60 °C for 4 h and then it was left overnight at static conditions and room temperature to sediment the OMC particles. These particles were finally separated from the liquid phase by filtration. The washing procedure was repeated twice to ensure complete removal of SBA-15 material. Finally, OMC particles were successively rinsed with distilled water, ethanol, and acetone several times and dried overnight at 120 °C.

2.2. Membrane preparation

Tubular porous stainless steel supports provided by Mott Metallurgical Corporation were used for the preparation of all composite-membranes addressed in this work. The commercial supports present a symmetric structure with a porous media grade of 0.1 µm. This raw support can reject 95% of particles with size greater than the specified grade, although real pores in the range 2–5 µm can be typically found on its surface. The original tubes with ½ inch OD were cut into shorter pieces of around 30 mm in length to prepare the composite membranes. The general preparation procedure consists of five successive steps: (i) initial cleaning, (ii) raw PSS support calcination (600 °C for 12 h in air atmosphere), (iii) OMC intermediate layer incorporation, (iv) surface activation with Pd nuclei and (v) Pd layer formation by ELP-PP.

The initial cleaning consists of consecutive washing steps in NaOH (0.1 M), HCl (0.1 M), and ethanol (96 vol%) at 60 °C in an ultrasonic bath. After that, the supports were oxidized in air for 12 h at 600 °C with heating and cooling rates of 2.0 °C/min, according to the procedure described elsewhere [37].

The surface quality of the supports (average pore size and roughness) were tailored in the third step by the incorporation of ordered mesoporous ceria (OMC) intermediate layer following a vacuum-assisted dip-coating method (VA-DC). A suspension of OMC particles (10 wt%) in water with a certain amount of PVA (2 wt%), to improve the adherence of the layer, was used for the preparation of the intermediate layer. After that, the PSS support was sealed by both extremes with Teflon tapes and it was introduced twice into the suspension for 5 min at room conditions to generate the new layer on the external surface of the porous support. This step was repeated one more time applying vacuum from the lumen side of the support, at the last minutes of the second cycle as detailed in a previous work for other intermediate layers based on dense CeO₂ particles [22]. A very homogeneous but relatively thick intermediate layer is formed at this point, being necessary to remove part of this material by soft washing in distillate water. Finally, a calcination step of the modified support in air (500 °C, 6 h) is required to remove the used PVA during VA-DC.

Once the intermediate layer is incorporated, the modified support is activated with homogeneously distributed Pd nuclei by direct reduction of diluted PdCl₂ (0.1 g/L) with a mixture of N₂H₄ (0.2 M)–NH₃ (2.0 M). Later, the H₂-selective Pd-film is deposited by Electroless Pore-Plating feeding both Pd source and reducing agent from opposite sides of the support as detailed elsewhere [38–40]. Diverse recurrences of the ELP-PP process at 60 °C were performed up to the membrane weight gain became negligible, thus ensuring a good sealing of the modified support porosity with palladium [41].

2.3. Materials characterization

Textural properties of synthesized OMC particles were measured by N₂ adsorption/desorption analysis with a Quantachrome Nova 4000 Analyzer, thus obtaining BET surface area, pore volume, and average pore diameter of these particles. For that, OMC particles were previously degassed at 480 °C, performing the analyses at 77 K and 10⁻⁶ Pa vacuum level. X-ray diffraction measurements (Philips X-Pert MPD/MRD equipped with an X'Celerator detector) by using CuKα radiation source and transmission electron microscopy (JEM 2100 microscope working at 200 kV) were used to check the mesoscopic order in the OMC particles. OMC metal composition was determined by X-ray fluorescence (XRF) in a Philips Magix spectrometer. The average size of OMC particles was also analyzed by using a Mastersizer 200 laser diffraction analyzer.

The Pd-thickness for composite-membranes ($t_{Pd,c}$) was estimated from gravimetric analyses with a Kern electronic balance type ABS 220-4 (accuracy of ±0.001 g), measuring the weight gain of the membrane during the ELP-PP process and assuming homogeneous incorporation of the metal around the modified PSS support. Additionally, a scanning electron microscope Hitachi S-2100N was used to analyze both surface morphology and the cross-sectional view of the palladium composite-membranes. Thus, the real Pd-thickness ($t_{Pd,r}$) could be determined and compared with the estimated ones by gravimetric measurements.

2.4. Permeation measurements

Permeation measurements of the membranes here presented were carried out by using a home-made device designed by our research group. The apparatus and a basic process diagram of the permeation equipment are shown in Fig. 1. The permeation cell is basically formed by a cylindrical 316L stainless steel cell in which the membrane is placed between two graphite O-rings to ensure proper sealing between both retentate and the permeate sides. An electric furnace allows achieving the desired temperature of the cell during the experiments. A Bronkhorst EL-PRESS back-pressure regulator (PC-01, capacity 0–10 bar) maintains the requested retentate pressure, and hence the driving force of the permeation process due to the permeate side is always kept at atmospheric pressure. The feed stream mass flow and composition can be adjusted by diverse Bronkhorst EL-FLOW mass flow controllers (FIC-01 and FIC-02, max. capacity 400 NmL·min⁻¹), being possible to test the permeation of individual gases (N₂, H₂) or binary mixtures with variable composition. Additionally, N₂ as sweep gas can be also fed into the system with other Bronkhorst EL-FLOW mass flow controllers (FIC-03, max. capacity 400 NmL·min⁻¹). Both permeate and retentate streams can be also analyzed with a Bronkhorst EL-FLOW mass flow meter (FI-01, max. capacity 200 NmL·min⁻¹).

A basic process diagram of the permeation equipment is represented in Fig. 1a. Permeation experiments can be carried out with two different operation modes depending on the position of valves V-01 and V-02: i) mode in-out or ii) mode out-in. Fig. 1b represents the permeation process when using the first operation mode, denoted as in-out. In this configuration, the feed stream is sent to the inner side of the membrane, thus collecting the permeate flux in the shell side of the permeation cell. In this way, due to the membrane structure, H₂ passes first through the porous media before meeting the internal surface of the Pd film during the permeation process. On the contrary, the feed stream is introduced from the shell side when the permeation test is carried out considering the out-in operation mode, thus collecting the permeate in the lumen side of the membrane (Fig. 1c). Then, H₂ coming from the feed stream meets first the external surface of Pd film and then, after permeating through this fully dense layer, needs to be transported through the porous media.

Independently of the considered operation mode, the general procedure for the permeation experiments consists of the following steps: i) heat the system up to 400 °C in an inert atmosphere (N₂ from feed and

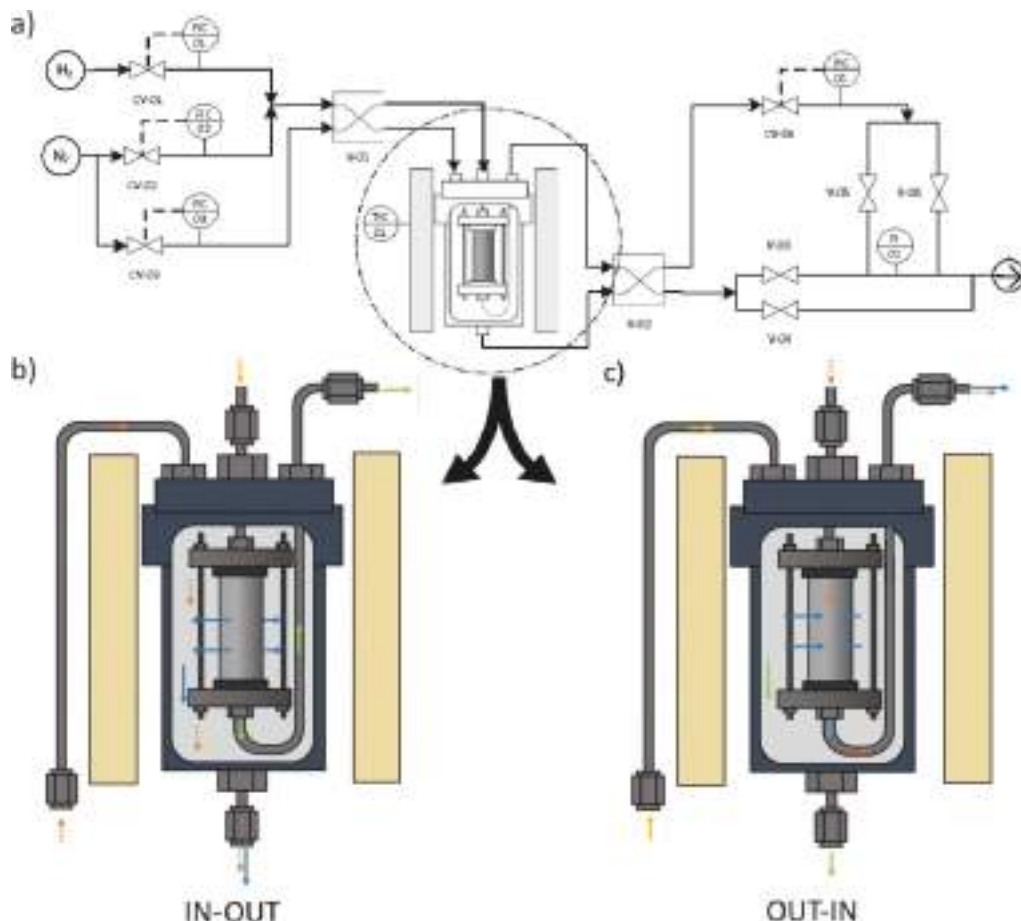


Fig. 1. Process diagram for the permeation system (a) and details of the permeation cell for different operation modes: in-out (b) and out-in (c). ● Feed, ● Permeate, ● Sweep gas, ● Retentate.

sweep gas streams), ii) cut off the sweep gas and determine the possible N₂ permeation through the membrane for relative retentate pressures in the range 0.2–2.0 bar (above the atmospheric value), iii) replace N₂ by H₂ and repeat the permeation measurements after waiting for around 2 h up to complete stabilization of the permeate flux, iv) repeat the steps (ii) and (iii) for other temperatures in the range 350–450 °C and/or different feed mixtures (H₂/N₂), v) flush both retentate and permeate sides with N₂ for at least 1 h and cold down the system up to room temperature. It should be noted that five sequential thermal cycles were performed with an average operation time of around 5 h per cycle before considering stable permeate data. For each thermal cycle, the membranes were heated up to 400 °C in N₂, the gas feed was switched to H₂ to determine the permeate flux after its stabilization and, finally, the membranes were cooled down again to room temperature in N₂.

Moreover, before permeation tests at high temperature, preliminary leak tests with He at room temperature and $\beta P = 2$ bar were always performed. For these tests, membranes are submerged in ethanol while He is fed into the lumen side at a controlled pressure while the possible formation of bubbles is observed. The presence of bubbles on the outer surface of the membrane can be associated with defects in the palladium layer through which the gas could pass, thus indicating the necessity of additional ELP-PP cycles to finish the membrane preparation process.

3. Results and discussion

3.1. Ordered mesoporous ceria (OMC): Synthesis and characterization

First, the characterization of the synthesized OMC particles was carried out to ensure adequate morphology and structure of the material before being incorporated onto the PSS supports. In this context, the textural properties of the material were determined by N₂ adsorption/desorption analysis, and a BET surface area of 135 m²/g was obtained, in consonance with other values typically found in the literature for different ordered mesoporous metal oxides [42–44]. Fig. 2 shows the N₂ adsorption-desorption isotherm which exhibits H1 hysteresis cycle, being possible to be classified as an IUPAC isotherm type IV [45]. This hysteresis is typical of mesoporous materials with different pore sizes. The figure also includes the pore size distribution for the prepared OMC material. As can be seen, the average pore size is around 10–12 nm, although some smaller and greater pores in the range of 2–50 nm can be also detected. Due to the synthesis procedure of OMC material, these pores should correspond to the thickness of SBA-15 used as a hard template during nanocasting, typically ranged from 3.1 to 6.4 nm [46]. However, the obtained values are noticeably higher than these. As described in other studies [47], this fact can be caused by the inter-connectivity of the SBA-15 pores.

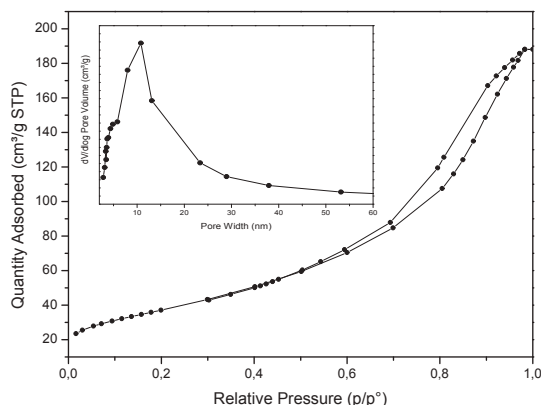


Fig. 2. N₂ adsorption isotherm and pore size distribution for OMC material.

Additionally, XRD analysis for 2θ range from 10 to 80° was also carried out to identify all crystalline phases present in the OMC material (Fig. 3). The resulting signals were compared with a standard pattern included in ICDD files for crystalline ceria (#00-034-0394). As it can be clearly seen, several diffraction peaks have been obtained at 28.66°, 33.03°, 47.56°, 56.39°, 59.05°, 69.34°, 76.61°, and 79.27°. All these signals can be assigned to ceria crystalline planes (111), (200), (220), (311), (222), (400), (331), and (420), respectively. OMC average crystallite size calculated from the Debye-Scherrer equation (using the full-width at half maximum at 28.66°) is around 8.5 nm. Additionally, the characteristic broad signal of amorphous silica around 20 angles of 5° and 25° has not been detected [48,49]. Thus, no silica derived from the SBA-15 temporary template could be detected by this technique after the generation of the OMC material. However, these results cannot ensure its complete removal if considering the detection limit of the equipment and multiple sites in which rests of silica could remain. In this manner, TEM analyses were also performed with the aim to study the morphology of OMC particles and to confirm the complete removal of SBA-15 template material.

Fig. 4 collects three TEM images of the material taken at different magnification. The OMC sample clearly shows an ordered porous structure in which multiple nanorods are formed. Thus, the OMC particles have an average spherical diameter of around 100 nm, as reflected by Mastersizer 2000 laser diffraction analyzer. At this point, it is

appropriate to clarify that OMC particles, used for the later generation of the ceramic intermediate layer onto PSS supports, are formed by the agglomeration of the above-mentioned nanorod structures. These nanorods are formed, in turn, by aggregated smaller CeO₂ nanoparticles, which replicate the unidirectional channels of SBA-15 used as a template during nanocasting synthesis. TEM analysis shows that these small ceria nanoparticles have an average diameter of around 7–12 nm, in good agreement with typical SBA-15 pore sizes used as template material. Here, it should be noted that this result is coherent with the previous value calculated for the crystallite size from XRD analysis by using the Debye-Scherrer equation. It should be noted that each nanorod is separated from their neighbors by a similar distance, first corresponding to the SBA-15 wall thickness and now to the pores of the new material. In this context, it is well-known the influence of SBA-15 loading during the synthesis procedure on the formation of the metal oxide nanorods and interconnectivity between future pores [47]. On the other hand, it is also possible to observe some certainly non-ordered regions, especially at the edges of OMC particles. It can be explained by structural collapse during the template removal, an incomplete filling of SBA-15 micropores with the ceria precursor during nanocasting, or ceria crystallization out of the template pores. Moreover, it should be marked that Si content detected by XRF in OMC particles is maintained always below 1 wt% (accordingly to the previous results extracted from XRD analyses). Thus, from all mention above, it can be concluded that the template was almost completely removed.

3.2. Intermediate layer generation

As previously described in the experimental procedure, Ordered Mesoporous Ceria (OMC) particles were incorporated as an intermediate layer onto previously calcined PSS supports by VA-DC, reaching a weight gain per membrane area of around 51.4 g m⁻². To determine the surface modification of calcined PSS supports with these OMC intermediate layers, SEM images before and after their incorporation were randomly acquired from diverse points of the external surface of each membrane. Due to no significant differences were appreciate between the analyzed points in diverse membranes, Fig. 5 collects some representative images of the achieved results in comparison to the original surface of the support.

As it was addressed in previous studies, the external surface of the calcined PSS support (Fig. 5a) reveals a wide pore size distribution despite the average pore size given in the specification by the manufacturer (0.1 μm). The presence of big pore mouths on the external surface of supports provokes the necessity of incorporating an intermediate layer, OMC in this work, to make possible the generation of a thin and continuous Pd film [17–24]. In this context, Fig. 5b shows a representative SEM image of the surface reached after the incorporation of OMC material as intermediate layer for the first time in literature. Taking into account that a BSE detector was used in this case, color differences clearly indicate the presence of diverse materials on the new surface. EDS analysis evidenced that light grey areas contain a noticeably amount of cerium and oxygen, in contrast to dark grey areas where the presence of both elements is negligible. Moreover, the modified surface presents a flatter surface with lower average pore-sizes in comparison to the surface of the calcined PSS used as support due to the filling of its largest pore mouths with OMC particles. As a consequence, a lower macro-porosity was reached in the external surface of PSS-OMC samples, more adequate for Pd deposition by ELP-PP [22]. The smaller pores, mainly coming from the space left between OMC and SS particles, should be more easily closed by palladium than the original ones between only SS particles, then being foreseeable a reduction of the final Pd thickness [15,24]. However, it is also expected that additional porosity coming from the internal pores in OMC particles could improve the properties of the final composite membrane, making possible a future functionalization/doping for particular applications, especially in the case of being used in membrane reactors.

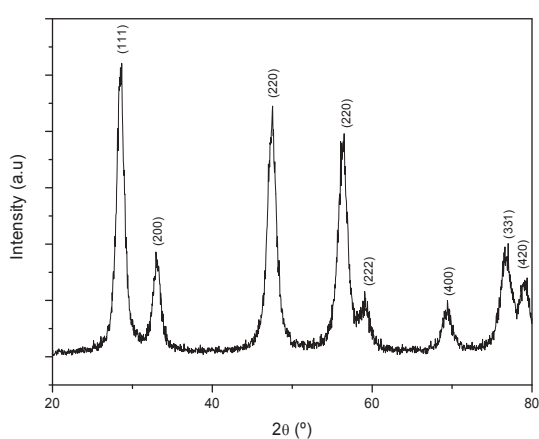


Fig. 3. XRD analysis for OMC material.

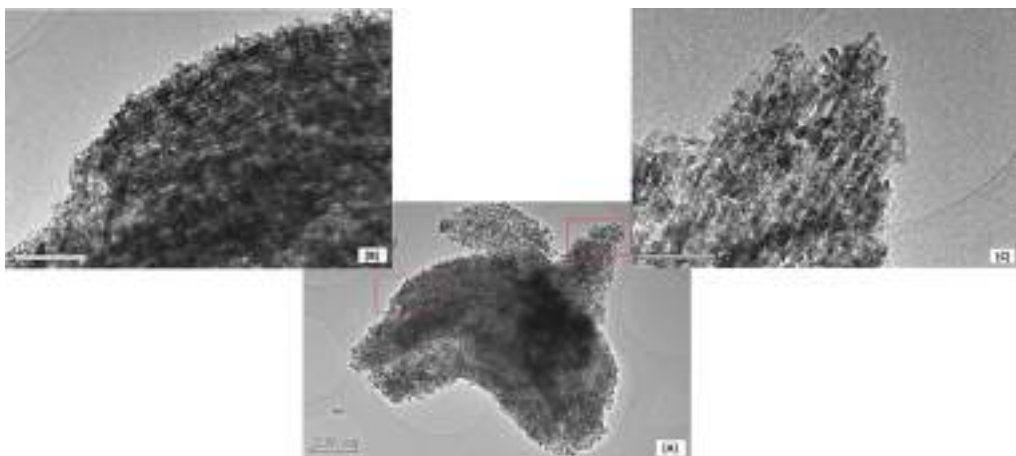


Fig. 4. TEM micrographs for OMC particles at diverse magnification.

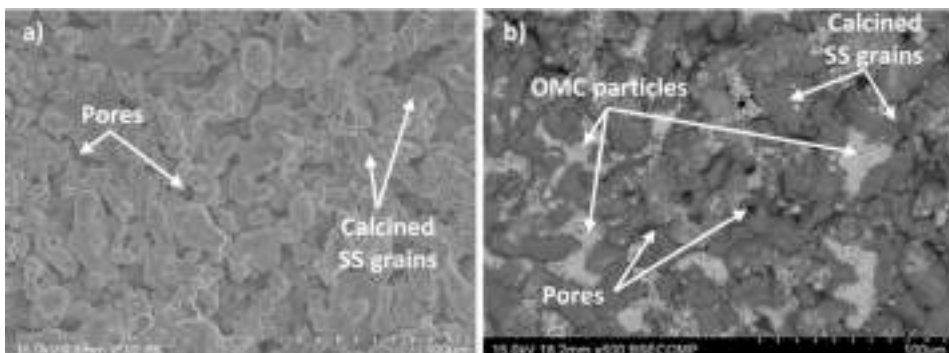


Fig. 5. External surface micrographs of (a) calcined PSS support (OXI) before and (b) after deposition of OMC particles.

The permeability of modified supports is also an important parameter to take into account for selecting the best possible intermediate layer since this value could significantly affect the Pd incorporation by ELP-PP but also the permeability reached in the final composite membrane and possible mass transfer resistances. The calcined PSS supports, before the deposition of any mesoporous ceria intermediate layer, present N_2 permeation values of $1.233 \text{ mol m}^{-2} \text{ s}^{-1}$ at room temperature and $\beta P = 1.0 \text{ bar}$. After the incorporation of OMC particles onto the support, this N_2 flux decreases around 30%. This effect can be explained by the partial blockage of original PSS pores with the ceramic particles that form the intermediate layer, despite they present a certain internal porosity. In fact, this reduction is noticeably lower than the value obtained after using commercial dense ceria (CDC) particles as intermediate layers, when permeation capacity was reduced in a half (52%) [22]. Various factors could explain the reduction in N_2 flux when ceria particles are employed as intermediate layer. To avoid some of them, similar experimental conditions during the VA-DC procedure were used, trying to get similar average diameters of CeO_2 particles, independently of being dense or porous. In fact, average diameters around 100 nm were reached in both cases. Moreover, the thickness of the OMC layer at this stage was controlled by the membrane weight gain after VA-DC, reaching a value of around 51.4 g m^{-2} , similar to that obtained when using dense CeO_2 particles [22]. However, a relevant increase in the permeation capacity of modified supports was observed when using the

OMC particles due to a possible different morphology of ceria particles, not directly related to their average size, affecting their compaction, and the benefit provoked by the mesoporosity of OMC particles. Consequently, it can be concluded that the initial average porosity of PSS supports was certainly reduced, although in a minor grade that after using dense ceramic particles for the preparation of the intermediate layers even despite considering a very cheap experimental procedure as VA-DC without any accurate control about the porosity orientation.

3.3. Final composite-membranes morphology

A representative area of the surface morphology of the composite membranes used in the present study is shown in Fig. 6. The external surface of the membranes, prepared by ELP-PP after the incorporation of an OMC intermediate layer onto the calcined tubular PSS supports, as previously described, exhibits a dendritic growth of the palladium film (Fig. 6a). Despite the technique used for the deposition of the H_2 -selective film, ELP-PP, in which the reduction of Pd^{2+} ion to Pd^0 is mainly produced inside the pores of the support, an external layer has been also formed. This behavior can be explained due to the facility of hydrazine to meet the external surface of the support [38,40,41]. It is caused by the higher diffusion velocity of hydrazine towards the Pd solution. In this manner, the reaction preferentially takes place inside the smaller pores but hydrazine can pass through the biggest ones, thus meeting the

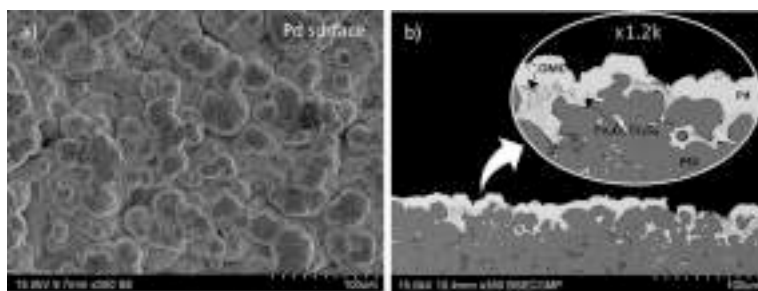


Fig. 6. Micrographs of the Pd-composite membrane prepared onto a PSS support with an OMC intermediate layer: a) External surface and b) Cross-sectional view.

palladium ions on the external surface of the support and generating the external film. However, the external film sometimes seems to be discontinuous or with a cavernous structure due to the complete blockage of all the pores before the complete formation of the external film.

Some cross-sectional views are also collected in Fig. 6b. Each sample was firstly examined at relatively low magnification ($350\times$) to evaluate both homogeneity and continuity of the external film. As can be seen, the external Pd layer presents a good continuity with a real thickness ($t_{\text{Pd},r}$) in the range $7\text{--}12 \mu\text{m}$. This value reasonably agrees with the average one estimated from gravimetric analyses, $t_{\text{Pd},e} \approx 9 \mu\text{m}$, despite being possible to observe the presence of palladium inside the neighbor pores to the external surface of the membrane. As previously addresses in other studies, this palladium infiltration into the pores of the support provides a better anchoring of the layer, thus noticeably improving the mechanical resistance of the composite Pd-membranes so obtained [38,40,41]. Moreover, the cross-sectional view has been also observed at higher magnification ($1.2k\times$) to analyze in detail the deep areas, i.e. pore mouths and throats. An almost continuous dark thin layer can be observed around the SS grains of the porous supports, coming from its initial calcination in air. This layer is mainly formed by a mixture of iron and chrome oxides, ensuring to avoid direct contact between palladium and SS. OMC particles can be also observed, preferentially deposited into the biggest pores of the porous support because of the vacuum applied during dip-coating and subsequent washing step of the external surface. These particles, with an average spherical diameter of around 100 nm , present pore sizes in the range $10\text{--}12 \text{ nm}$ that provide a total BET surface area of $135 \text{ m}^2/\text{g}$, as previously detailed. These values agree with the typical ones found in the literature for different ordered mesoporous metal oxides generated from SBA-15 as template material [32–34]. The presence of these OMC particles reduces the external roughness of the support and modifies the original porosity, generating smaller pores by the partial blockage of the original ones promoting the generation of thin selective film. This effect may be beneficial as suggested by Mardilovich et al. [50] when denoting that the required Pd thickness to obtain a fully dense membrane is around three times the biggest pore mouth diameter.

3.4. Permeation behavior with pure gases: effect of pressure and temperature

After describing the morphologic properties of the OMC-Pd membranes, permeation properties have been analyzed at diverse operating conditions. In this section, tests performed with pure gases (N_2 , H_2) are used to obtain both permeance (k) and ideal selectivity ($\alpha_{\text{H}_2/\text{N}_2}$) for diverse pressure and temperature conditions. These gases were fed to the shell side, while the permeate was collected from the membrane lumen, thus working according to the operation mode denoted as out-in. Moreover, it should be noted that the possible presence of defects on the membranes was previously evaluated by He bubble leak tests in

ethanol at room temperature. During these experiments, no He flux was detected at pressures driving forces up to $\rho P \Delta t$ bar, thus suggesting good preliminary quality of the membranes. Additionally, experiments at higher temperatures ($350\text{--}450^\circ\text{C}$) with pure N_2 were performed to confirm this fact. In this manner, Fig. 7 collects the results reached when feeding pure H_2 to the permeation cell at diverse operating conditions.

As can be seen, it is clear the linear relationship between permeate and pressure driving force for all considered temperatures ($R^2 \geq 0.999$ in all cases) [51–53]. However, these linear trends do not intercept with the origin, in contrast to the expected behavior for conventional palladium membranes that follow the Sieverts' law ($n = 0.5$). This peculiar effect has been exhibited by other ELP-PP membranes, being widely addressed in previous works [38,40,41]. Basically, it can be explained by considering the particular morphology of ELP-PP membranes, in which part of the deposited palladium is placed inside the pores of the support. In this manner, both surfaces of the Pd film (internal and external) become different, thus not meeting the assumption of identical surfaces considered in the Sieverts' law for most of the Pd-based membranes. As a result, additional resistance to the permeation process has been obtained for these membranes in comparison to other traditional Electroless Plated membranes with an almost ideal external Pd-film. This intrinsic characteristic of any ELP-PP membrane has been expressed as a deviation of the ideal intercept of experimental data into the origin along the x-axis, reaching a value near to $11.5 \text{ Pa}^{0.5}$ for this study. In this context, H_2 permeances ranged from $7.81 \cdot 10^{-4}$ to $9.91 \cdot 10^{-4} \text{ mol m}^{-2} \text{ s}^{-1} \text{ Pa}^{-0.5}$ were obtained for temperatures between 350 and 450°C , respectively, implying a really high ideal selectivity $\alpha_{\text{H}_2/\text{N}_2} \geq 24,000$, calculated from the minimum detection limit of the used gas flow-meter for the permeate stream (1 NmL h^{-1}).

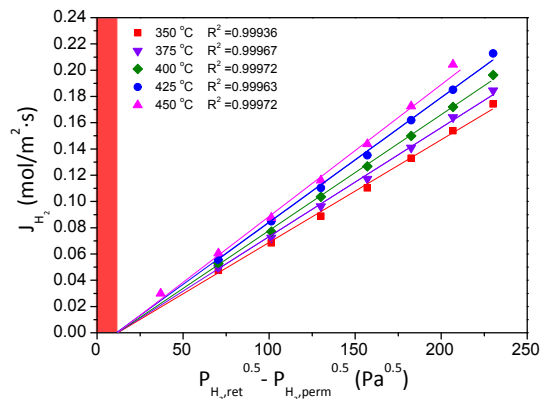


Fig. 7. Influence of pressure and temperature on H_2 permeation when feeding pure gases (out-in mode).

Finally, a short mention of the activation energy calculated for the process should be included. Considering an Arrhenius type-dependence of H₂ permeance values with temperature, activation energy of 8.91 kJ·mol⁻¹ is obtained, within the typical range published for other Pd membranes.

3.5. Permeation behavior with pure gases: effect of permeate flux direction

As previously detailed in the experimental section, the membrane permeation device can work with two different operation modes, denoted as out-in or in-out, intending to modify the permeate flux direction during permeation experiments and evaluate the mechanical resistance of the membranes. Fig. 8 shows the H₂ fluxes reached versus the applied driving force for the permeation process when operating in both alternative modes at 400 °C.

First, it is important to point out the good integrity of all the composite membranes, independently of the operation mode, due to nitrogen was not detected in the permeate side for the entire set of experiments, independently of the operation mode, thus maintaining an ideal hydrogen separation factor greater than 24,000. Then, it should be emphasized that a similar permeation behavior can be observed in any condition. It means that, in both cases, a linear trend of H₂ flux against pressure is obtained, although without a clear interception with the origin (0,0). However, 17% higher H₂ permeance is reached in case of using the in-out operation mode instead of the out-in previously addressed, although the initial resistance to the permeation process is also slightly increased (from 11.5 to 20.9 Pa^{0.5}). A hypothesis about this effect can be supported by the particular incorporation of palladium onto the porous substrate by ELP-PP, with partial infiltration of the noble metal into the closer pores to the external surface. This fact provokes that both internal and external surfaces of the Pd-films become significantly different and, hence, the processes involved in the global permeation of hydrogen through the membrane.

To understand this hypothesis in a better way, Fig. 9 represents a schematic view of a typical cross-section for a pore-plated membrane, marking in different colors both external and internal Pd film surfaces (red and blue, respectively). As can be seen, the outer surface of the palladium is relatively smoother in comparison with the internal one, which presents a greater tortuosity caused by the above-mentioned infiltration of palladium inside the pores of the support. In this manner, the palladium surface available for H₂ dissociation is significantly higher on the internal side than the external one. Thus, much more H₂ can be adsorbed onto the retentate side of the Pd-film when working flowing the in-out operation mode and, as a consequence,

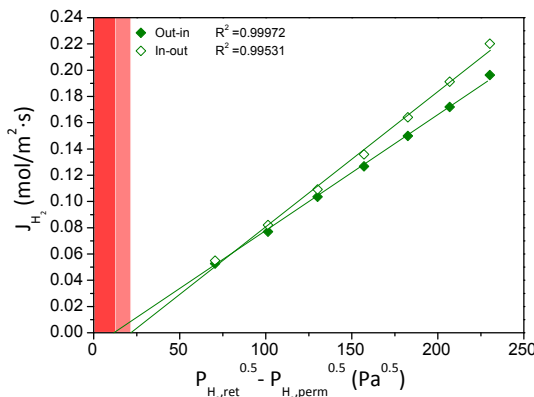


Fig. 8. Effect of permeate flux direction on the membrane performance (T = 400 °C).

higher permeance is reached.

3.6. Permeation behavior with binary gas mixtures

After the analysis of permeation with pure H₂, tests with binary H₂-N₂ mixtures were also performed to investigate more realistic permeation conditions. Five different H₂ concentrations (90, 80, 70, 60, and 50%) were analyzed at temperatures ranged from 350 to 450 °C in steps of 25 °C. For illustrating these results, as an example, Fig. 10 collects the H₂ permeation fluxes reached at 400 °C when diverse H₂-N₂ mixtures are fed accordingly to the out-in operation mode. As can be observed, in general, the higher nitrogen content in the feed stream the lower hydrogen flux on the permeate stream despite taking into account the dilution effect by considering hydrogen partial pressures for the calculation of the permeation driving forces. Thus, any concentration-polarization effect should be affecting the permeation process. However, this drop is not constant, affecting in a major grade at relatively low N₂ contents.

Taking into account all the experimental data reached when the feed stream contains N₂ concentrations ranged from 0 to 50 vol%, it is possible to calculate the corresponding H₂ permeances, representing in Fig. 11 their relative values by using the reached ones for pure H₂ as reference. Thus, the figure collects the effect of permeating binary H₂-N₂ mixtures at 400 °C for the above-mentioned two operation modes, out-in and in-out, where H₂ permeance values of 8.82·10⁻⁴ and 1.03·10⁻³ mol m⁻² s⁻¹ Pa^{-0.5}, respectively, were reached at the same conditions (T = 400 °C). At this point, it is important to point out that the integrity of the membranes was maintained during all these experiments since no N₂ was detected by gas chromatography on the permeate side, finding only the characteristic signal of hydrogen in the collected permeate stream.

In general, an increase of N₂ content in the feed stream always promotes a reduction in the H₂-permeance, independently of the permeation mode, and despite taking into account the inherent dilution effect in the mixture for data calculation, as previously addressed. This behavior suggests the influence of possible concentration-polarization effects on the Pd layer as the main responsible for the permeance loss. However, this effect is clearly more pronounced in the case of working with the in-out operation mode. Here, it should be remembered that H₂-permeance reached in this configuration (in-out) was higher than in the case of operating on the contrary direction (out-in), being maintained this trend for the entire set of experiments. However, despite these greater values, the relative permeance drop was more relevant for this configuration (in-out), as stated before. This particular result can be explained by the different pathways that H₂ needs to traverse through the composite membrane in case of using out-in or in-out operation modes. To elucidate this explanation more clearly, two simple schemes have been performed for the permeation process when feeding binary H₂-N₂ mixtures and operating in the above-mentioned modes (Fig. 12). As can be seen, when considering the out-in operation mode (Fig. 12a), H₂ can easily reach the external smooth surface of the Pd film, permeating through this layer by a typical solution-diffusion process while other different molecules are rejected (in this particular case, N₂). Although some polarization-concentration effect can be produced due to the contrary movements of new H₂ molecules trying to reach the Pd layer and the rejected N₂ molecules returning to the retentate bulk phase, the high velocity of the feed stream along the axial direction easily removes these molecules from the relatively smooth Pd surface. On the contrary, when considering the in-out operation mode, the feed stream needs to pass first through the porous media, formed by stacked layers of PSS support and OMC intermediate layer, before reaching the Pd film (Fig. 12b). Then, rejected N₂ molecules have some difficulties to leave the tortuous porous media, staying for some additional time and hence hindering the transport of new H₂ molecules towards the Pd film. As a result of these different pathways, a 10% higher relative permeance drop was obtained in case of operating as in-out mode.

Finally, the influence of feeding binary H₂-N₂ mixtures has been

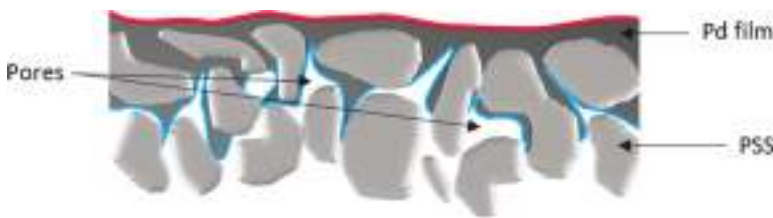


Fig. 9. Schematic drawing of a typical pore-plated membrane, distinguishing both external (marked in red, ●) and internal (marked in blue, ○) surface of the Pd-film generated onto the porous support. (For interpretation of the references to color in this figure legend, the reader is referred to the web version of this article.)

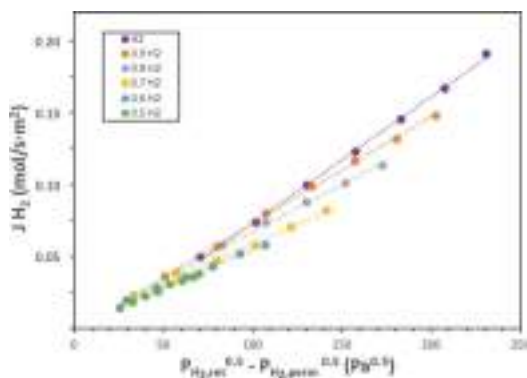


Fig. 10. Illustration of hydrogen permeation behavior for $\text{H}_2\text{-N}_2$ binary mixtures ($T = 400^\circ\text{C}$, out-in mode).

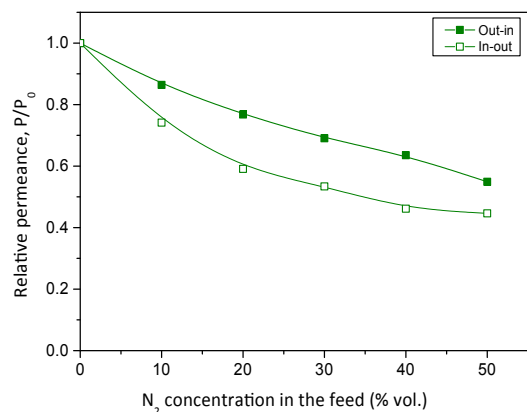


Fig. 11. Variation of H_2 -permeance when feeding binary $\text{H}_2\text{-N}_2$ mixtures of diverse composition at 400°C and different operation modes: in-out or out-in.

completed by analyzing the effect of operating temperature. These experimental results have been collected in Fig. 13, also representing the relative variation of the H_2 -permeance reached at each condition and operation mode.

It should be noted that permeance drops were similar for all tests performed at different temperatures and N_2 concentrations in the range of $350\text{-}450^\circ\text{C}$ and $0\text{-}50\text{ vol\%}$, respectively. Moreover, the influence of using the in-out or out-in operation modes was also maintained, obtaining a greater effect for the first configuration. For example, the relative permeance drop observed in the case of feeding the most diluted

mixture (50 vol\% of N_2) was around 40% for the out-in operation mode, while this fall dropped up to 50% with the in-out operation mode. Analyzing the entire set of experiments altogether, it can be appreciated that deviation between all experimental results was lower than 5% for each N_2 concentration in the mixture, independently of the operation mode, thus being possible to conclude that concentration-polarization effect was not noticeably affected by temperature in this case.

3.7. Comparison of the permeation behavior with the current state-of-the-art

First, we compare the results obtained with membranes containing an OMC intermediate layer with other membranes also prepared by ELP-PP but containing different intermediate barriers [22,38,54]. In terms of N_2 permeation of the modified PSS supports with these intermediate layers, it can be stated that calcined PSS supports presents a permeation of around $1.233 \text{ mol m}^{-2} \text{ s}^{-1}$ at room temperature and $\beta P = 1.0 \text{ bar}$. This permeation capacity always decreases after the incorporation of any intermediate layer and, as previously detailed, this effect can be explained by the partial blockage of original PSS pores. In fact, permeation was decreased in a half (52%) when commercial dense ceria (CDC) particles are used for the preparation of the intermediate layers [22]. However, in the case of replacing this material with ordered mesoporous ceria (OMC), lower permeate drops were observed, just 30%, despite the particle size of both materials (dense and mesoporous one) is quite similar with an average spherical diameter of around 100 nm and thus the inter-particular porosity generated throughout the intermediate layer should be also similar in consequence. In the case of using these OMC particles, N_2 can pass not only through the porosity generated between the CeO_2 particles but also through their particle's internal mesoporosity. At this point, it should be noted that a random orientation of OMC particles and, hence, intra-particle porosity was generated along with the intermediate layers during VA-DC, a very simple and cheap alternative for that purpose. Despite this fact, a clear improvement in the permeation capacity (22%) of modified supports has been obtained and no significant differences were detected in several samples prepared by this method (reproducibility with deviations always below 10%).

Fig. 14a collects the average Pd thickness estimated by gravimetric analyses for diverse ELP-PP Pd-composite membranes. All of them were prepared onto PSS supports modified with CeO_2 intermediate layers, dense and mesoporous (CDC-Pd and OMC-Pd, respectively), as well as directly onto a calcined PSS support without any additional intermediate layer (denoted as OXI-Pd) [22,38,54]. As can be observed, the incorporation of any CeO_2 intermediate layer implies a reduction of the Pd thickness required for reaching fully dense membranes via ELP-PP. In general, this effect is due to the thinner pore size distribution with smaller pore mouths generated in the PSS support after the incorporation of CeO_2 particles as an intermediate layer. However, it should be noted that some differences were observed between samples prepared by using different CeO_2 particles. Thus, it was possible to reduce the estimated final thickness initially reached without CeO_2 intermediate layer membranes from $30 \mu\text{m}$ (OXI-Pd) [22,38,54] to around $15 \mu\text{m}$ (reduction of 50%), in case of dense ceria (CDC-Pd) [22], and $10 \mu\text{m}$

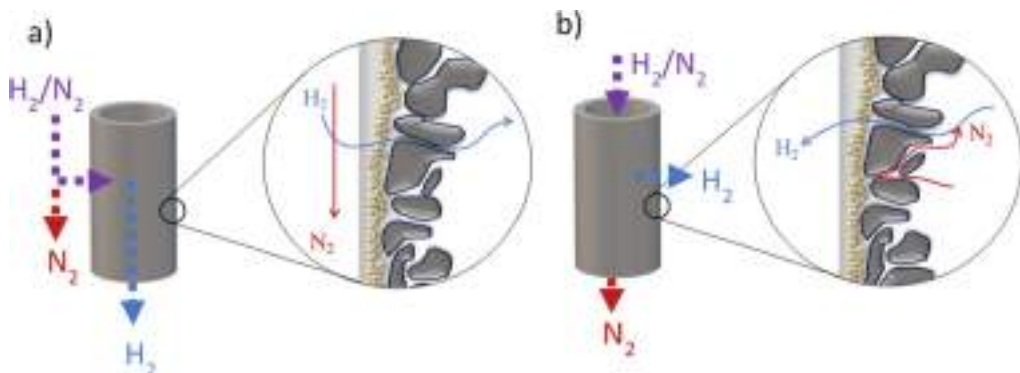


Fig. 12. Schematic representation of the permeation process in pore-plated membranes when feeding binary $\text{H}_2\text{-N}_2$ mixtures at different operation modes: a) out-in or b) in-out.

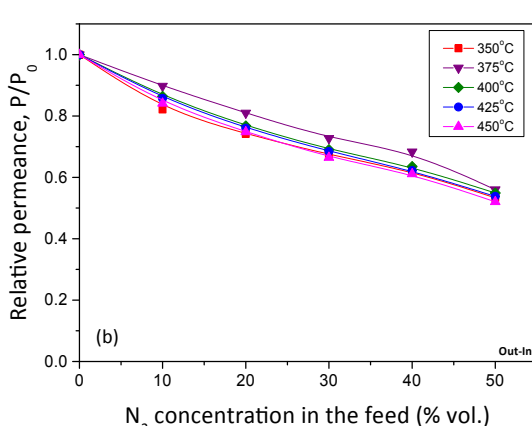
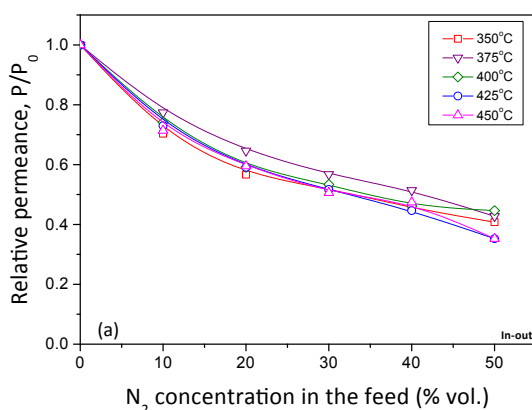


Fig. 13. Variation of H_2 -permeance when feeding binary $\text{H}_2\text{-N}_2$ mixtures of diverse composition at different temperatures and operation modes: a) out-in (a) or out-in (b).

(reduction of 66%) in case of using OMC particles (OMC-Pd). This new insight can be explained again by the morphology of the porous media, where the intra-particular mesoporosity, characteristic of OMC

particles, clearly makes possible their complete blockage with a lower amount of palladium. It could be due because of the better transport of reactants during the ELP-PP process. Therefore, the use of OMC particles allows us to reach the theoretical barrier of $10 \mu\text{m}$ for the Pd film, suggested in the literature as an adequate reference value to consider the cost of membranes so prepared potentially applicable to real industrial processes [55]. This fact could foreseeably prevail against the more expensive procedure required to achieve the OMC particles.

In terms of H_2 permeation capacity measured at the reference value of 400°C , the lower H_2 permeances were observed when calcined PSS supports are directly used for the membrane preparation without including any CeO_2 intermediate layer (OXI-Pd, $k = 1.34 \cdot 10^{-4} \text{ mol m}^{-2} \text{ s}^{-1} \text{ Pa}^{-0.5}$). Higher permeances were obtained in case of using CeO_2 additional intermediate layers, reaching values of $4.46 \cdot 10^{-4}$ and $8.82 \cdot 10^{-4} \text{ mol m}^{-2} \text{ s}^{-1} \text{ Pa}^{-0.5}$ for dense (CDC-Pd) and mesoporous (OMC-Pd) ceria, respectively. This last value represents a great permeance increase of 660% in comparison with other ELP-PP membranes developed without any ceria intermediate layer. In this context, Fig. 14b depicts the H_2 permeance values for each type of membrane on a relative scale for an easier comparison of the progressive improvements in ELP-PP membranes. As can be seen, a great enhancement of the permeation behavior has been reached with the use of ceria intermediate layers due to the modification of the original pore size distribution in PSS supports, reaching smaller pores and pore mouths on the external surface. This fact promotes the preparation of composite membranes with relatively thin Pd films. However, the noticeably advance of the new OMC-Pd membranes attracts great attention. This higher permeance could be justified by the lower estimated Pd thicknesses ($t_{\text{Pd,OMC-Pd}} = 10 \mu\text{m}$) than OXI-Pd and dense CeO_2 membranes, with 30 and $15 \mu\text{m}$, respectively. The higher H_2 permeation using OMC-Pd membranes should be caused by changes in the morphology of the Pd deposited not only in the available intraparticle porosity (as occur with dense CeO_2 particles) but also in the mesopores inside the new OMC particles. We suspect that lower pore sizes reached in intermediate layers formed by OMC particles facilitate its blockage by palladium during the ELP-PP process, thus reducing the final Pd-thickness. On the other hand, as mentioned before, the presence of mesopores in the particles opens new possibilities for the future functionalization/doping of the intermediate layer for particular applications, especially in membrane reactors.

Finally, Table 1 includes a comparison of the results presented in this study with other experimental data reported in available literature for a wide variety of composite Pd-membranes, most of them prepared by Electroless Plating and related techniques. The comparison includes different materials used as support and/or intermediate layers. The large information about membrane composition, structure, morphology, and permeation experimental details, among others, clearly increases the

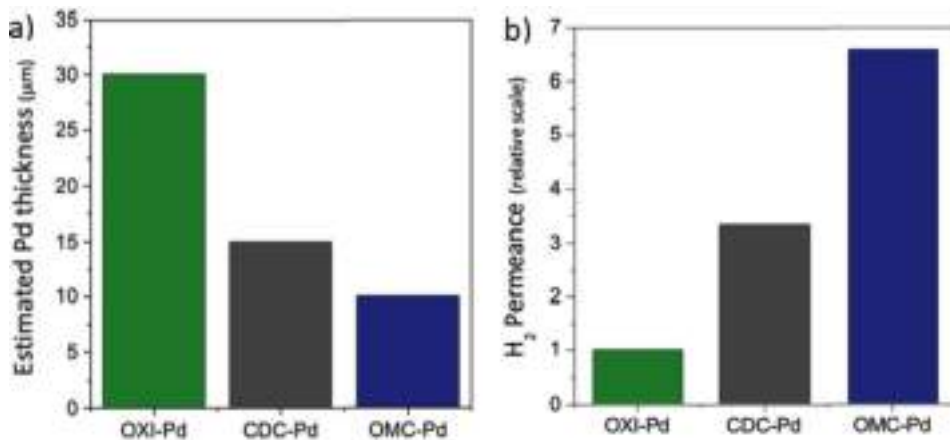


Fig. 14. Variation of the estimated Pd thickness (a) and H₂ permeance at 400 °C (b) for different ELP-PP membranes: without intermediate layer (OXI-Pd) and with dense (CDC-Pd) and mesoporous (OMC-Pd) ceria.

Table 1
State-of-the-art in permeation behavior of Pd-based membranes.

Membrane type	Operating mode	t _{Pd} (μm)	Permeation conditions		H ₂ -Permeance		H ₂ /N ₂	Ref.
			T (°C)	ΔP (kPa)	(mol m ⁻² s ⁻¹ Pa ^{-0.5})	(mol m ⁻² s ⁻¹ Pa ⁻¹)		
Pd ₇₇ Ag ₂₃	In-out	140	400	100–600	2.39·10 ⁻⁴ (*)	7.51·10 ⁻⁷ (*)	∞	[56]
Pd ₇₅ Ag ₂₅	In-out	50	300	100	4.09·10 ⁻⁵ (*)	1.29·10 ⁻⁷ (*)	–	[57]
PSS/Pd	Out-in	29	400	100–600	1.27·10 ⁻⁴ (*)	4.00·10 ⁻⁷	–	[58]
Al ₂ O ₃ /Pd	Out-in	6	500	100	7.58·10 ⁻⁴ (*)	2.38·10 ⁻⁶	956	[16]
PSS/Al ₂ O ₃ /Pd	Out-in	7	320	100–400	4.68·10 ⁻⁴ (*)	1.47·10 ⁻⁶	92	[59]
PSS/ZrO ₂ /Pd	Out-in	23	400	110	5.20·10 ⁻⁴	1.63·10 ⁻⁶ (*)	320	[60]
PSS/OXI/Pd	In-out	11.0–20.0	350–450	100–250	1.00–2.00·10 ⁻⁴	3.14–6.28·10 ⁻⁷ (*)	∞	[54]
PSS/CeO ₂ /Pd	Out-in	13.0	500–550	100–200	3.99–8.64·10 ⁻⁴ (*)	1.25–2.72·10 ⁻⁶ (*)	∞	[61]
PSS/NaY/Pd	–	7.0	450	100	6.20·10 ⁻⁴	1.95·10 ⁻⁶ (*)	736	[30]
PSS/NaA/Pd	Out-in	19.0	450	50	2.51·10 ⁻⁴ (*)	7.89·10 ⁻⁷ (*)	608	[25]
PSS/NaX/Pd	–	20.0	450	100	2.20·10 ⁻⁴ (*)	6.91·10 ⁻⁷ (*)	685	[29]
PSS/Pd ₇₇ Ag ₂₃	Out-in	2.2	400	2,630	6.40·10 ⁻³	2.01·10 ⁻⁵ (*)	1,400	[62]
Al ₂ O ₃ /Pd	Out-in	3.8	525	400–600	1.11·10 ⁻³ (*)	3.50·10 ⁻⁶ (*)	1,800	[63]
PSS/OXI-CeO ₂ /Pd	Out-in	15.4	400	100–200	4.96·10 ⁻⁴	1.56·10 ⁻⁶ (*)	>10,000	[22]
PSS/OXI-OMC/Pd	In-out	15.4	400	100–200	5.37·10 ⁻⁴	1.69·10 ⁻⁶ (*)	>10,000	[22]
	Out-in	10.0	400	100–200	8.82·10 ⁻⁴	2.77·10 ⁻⁶ (*)	>24,000	This work
	In-out	10.0	400	100–200	1.03·10 ⁻³	3.24·10 ⁻⁶ (*)	>24,000	This work

(*) Calculated values from original ones.

complexity of a rigorous comparison. To partially mitigate this problem, the membrane performance has been dually expressed as H₂ permeance in two different units, mol m⁻² s⁻¹ Pa⁻¹ and mol m⁻² s⁻¹ Pa^{-0.5}, independently of the reached selectivity of the membranes.

In general, the thinnest selective films the biggest hydrogen permeation. On the contrary, higher permeation usually involves a limited H₂ selectivity. In this work, an ideal H₂/N₂ separation factor higher than 24,000 (considering the minimum detection limit of the experimental, 1 NmL/h) was obtained for the entire set of experiments. The H₂ permeance was maintained around 1.03·10⁻³ mol m⁻² s⁻¹ Pa^{-0.5} for tests in pure H₂ at 400 °C. This value is relatively high compared to the overall presented ones by other researchers for pure Pd-membranes in which an almost ideal H₂/N₂ selectivity is reached. Finally, it has to point out that only cold-rolled membranes [56,57] and ELP-PP membranes [22,38,54] report an operation with in-out configuration. This fact remarks the excellent mechanical resistance of ELP-PP membranes against diverse permeation flux directions with compressive or tensile strengths generated by the pressure difference between both retentate and permeate sides, thus opening new possibilities for being used in a wide variety of reactor configurations. Additionally, it should be noted that this advantage, also provided by unsupported thick membranes, is

added to the intrinsic higher H₂ permeance derived from its lower Pd thickness.

4. Conclusions

The synthesis method for the preparation of Ordered Mesoporous Ceria (OMC) particles and their use as intermediate layer in Pd-composite membranes are presented for the first time in this work, denoting this new type of membranes as OMC-Pd. The OMC intermediate layer particles present a BET surface area of 135 m²/g with a narrow pore size distribution, around 10–12 nm. These mesoporous particles exhibit an average size of around 100 nm. In this manner, the deposition method carried out for the incorporation of these types of intermediate layers based on CeO₂ particles was not noticeably affected by the presence of mesoporous in the ceramic particles. The permeation behavior of Electroless Pore-Plated Pd-membranes prepared by modification of tubular PSS supports with ordered mesoporous ceria particles as intermediate layer has been carefully analyzed in the present study, reaching H₂ permeance of around 1.03·10⁻³ mol m⁻² s⁻¹ Pa^{-0.5} at 400 °C with really high ideal selectivity $\alpha_{H_2/N_2} \geq 24,000$ and only 10 μm in Pd thickness. This permeation capacity is affected by temperature

according to an Arrhenius-type dependence with an activation energy of 8.91 kJ·mol⁻¹, within the range typically published for other similar Pd-composite membranes. The mechanical resistance against diverse operating conditions has been demonstrated by the maintenance of the H₂-selectivity without any delamination or peeling but diverse permeation flux directions. These operation modes were carried out from the outer to the inner side of the tubular membrane (out-in mode) or vice versa (in-out mode), when compressive or tensile strengths are generated on the pore-plated Pd-film, respectively. Nevertheless, an outlined variation of permeance values has been obtained for each particular operation mode. In this manner, 17% higher H₂ permeances were reached in case of working with the in-out mode, in which the feed stream meets first the porous support (modified PSS with OMC particles as intermediate layer) and then the palladium top layer from its internal surface. Due to the nature of the ELP-PP, both internal and external surfaces of the Pd-film present clearly different morphologies. Thus, greater roughness and tortuosity are generated on the internal one because of the partial infiltration of Pd inside the pores of the support during the plating step, hence producing a slightly higher surface area. As a consequence, a higher deviation from the origin is observed when trying to fit the experimental data to the Sieverts' law. It also causes a different permeation behavior between both operating modes, in-out and out in, in the case of feeding H₂/N₂ mixtures instead of pure gases. In that case, it has been found that the concentration-polarization effect becomes more relevant when the mixture is fed into the lumen of the membrane (in-out mode). This behavior could be explained by the presence of both SS grains and OMC particles of the modified porous support between inlet H₂ molecules and the Pd film, where the presence of N₂ molecules turn the H₂ transport more difficult, thus decreasing the real hydrogen partial pressure reached on the retentate side of the film. This concentration-polarization effect seems to stabilize for lower H₂ concentration values in the feed stream, not being noticeably influenced by temperature in the range 350–450 °C since deviations ≤5% in the relative H₂ permeance drop were experimentally obtained.

CRediT authorship contribution statement

D. Martinez-Diaz: Conceptualization, Methodology, Validation, Investigation, Resources, Writing - original draft. **D. Martinez del Monte:** Conceptualization, Methodology, Validation, Investigation, Resources, Writing - original draft. **E. Garcia-Rojas:** Methodology, Investigation, Writing - original draft. **D. Alique:** Conceptualization, Validation, Formal analysis, Investigation, Resources, Writing - original draft, Supervision. **J.A. Calles:** Validation, Formal analysis, Writing - review & editing, Supervision. **R. Sanz:** Validation, Formal analysis, Writing - review & editing, Supervision.

Declaration of Competing Interest

The authors declare that they have no known competing financial interests or personal relationships that could have appeared to influence the work reported in this paper.

Acknowledgments

The authors sincerely express their gratitude to the Spanish government for the financial support provided through the competitive project ENE2017-83696-R. Additionally, David Alique acknowledges funds received from Young Researchers R&D Project Ref. M2182 - MEMRESPIP - financed by the Community of Madrid and Rey Juan Carlos University. Additionally, we want also to express our gratitude for the TEM analyses performed in the National Center of Electron Microscopy placed in Complutense University of Madrid (Spain), as well as the Material Science and Engineering area of Rey Juan Carlos University for supporting the characterization of samples by Scanning Electron Microscopy.

References

- [1] Sustainable Innovation Forum 2015, 2015. <http://www.cop21paris.org/>.
- [2] IPCC, in: Clim. Chang. 2013 Phys. Sci. Basis, Stockholm, 2013.
- [3] IPCC reports, (n.d.). <https://www.ipcc.ch/report/ar5/wg3>.
- [4] D. Parra, L. Valverde, F.J. Pino, M.K. Patel, A review on the role, cost and value of hydrogen energy systems for deep decarbonisation, Renew. Sustain. Energy Rev. 101 (2019) 279–294, <https://doi.org/10.1016/J.RSER.2018.11.010>.
- [5] F.W. Geels, T. Schwanen, S. Sorrell, K. Jenkins, B.K. Sovacool, Reducing energy demand through low carbon innovation: a sociotechnical transitions perspective and thirteen research debates, Energy Res. Soc. Sci. 40 (2018) 23–35, <https://doi.org/10.1016/j.erss.2017.11.003>.
- [6] R.P. Sholl, D.S.; Lively, Seven chemical separation to change the world, Nature. 532 (2016) 435–437.
- [7] P. Li, Z. Wang, Z. Qiao, Y. Liu, X. Cao, W. Li, J. Wang, S. Wang, Recent developments in membranes for efficient hydrogen purification, J. Memb. Sci. 495 (2015) 130–168, <https://doi.org/10.1016/j.memsci.2015.08.010>.
- [8] Y. Gao, J. Jiang, Y. Meng, F. Yan, A. Aihemaiti, A review of recent developments in hydrogen production via biogas dry reforming, Energy Convers. Manag. 171 (2018) 133–155, <https://doi.org/10.1016/j.enconman.2018.05.083>.
- [9] M. De Falco, G. Iaquaniello, E. Palo, B. Cucchiella, V. Palma, P. Ciambelli, 11 - Palladium-based membranes for hydrogen separation: preparation, economic analysis and coupling with a water gas shift reactor, in: A. Basile (Ed.), Handb. Membr. React., Woodhead Publishing, 2013: pp. 456–486. 10.1533/9780857097947.2.456.
- [10] D. Alique, Processing and Characterization of Coating and Thin Film Materials, in: J. Zhang, Y. Jung (Eds.), Adv. Ceram. Met. Coat. Thin Film Mater. Energy Environ., 2018. 10.1007/978-3-319-59906-9.
- [11] Z.W. Dumbar, I.C. Lee, Effects of elevated temperatures and contaminated hydrogen gas mixtures on novel ultrathin palladium composite membranes, Int. J. Hydrogen Energy. 42 (2017) 29310–29319, <https://doi.org/10.1016/j.ijhydene.2017.10.032>.
- [12] Y. Guo, Y.J. Jin, H.M. Wu, D.X. Li, L.D. Zhou, Q.Q. Chen, X.F. Zhang, Preparation of Pd Composite Membrane and its Surface Morphological Changes after Elevating Temperature in Different Atmosphere, in: Mater. Process. Technol. V, Trans Tech Publications, 2014: pp. 1602–1605. 10.4028/www.scientific.net/AMR.941-944.1602.
- [13] D. Alique, M. Imperatore, R. Sanz, J.A. Calles, M. Giacinti Baschetti, M. G. Baschetti, Hydrogen permeation in composite Pd-membranes prepared by conventional electroless plating and electroless pore-plating alternatives over ceramic and metallic supports, Int. J. Hydrogen Energy. 41 (2016) 19430–19438, <https://doi.org/10.1016/j.ijhydene.2016.06.128>.
- [14] D. Alique, D. Martinez-Diaz, R. Sanz, J.A. Calles, Review of supported pd-based membranes preparation by electroless plating for ultra-pure hydrogen production, 2018. 10.3390/membranes8010005.
- [15] I.P. Mardilovich, E. Engwall, Y.H. Ma, Dependence of hydrogen flux on the pore size and plating surface topology of asymmetric Pd-porous stainless steel membranes, Desalination 144 (2002) 85–89, [https://doi.org/10.1016/S0010-9164\(02\)00293-X](https://doi.org/10.1016/S0010-9164(02)00293-X).
- [16] Y. Guo, H. Wu, X. Fan, L. Zhou, Q. Chen, Palladium composite membrane fabricated on rough porous alumina tube without intermediate layer for hydrogen separation, Int. J. Hydrogen Energy 42 (2017) 9958–9965, <https://doi.org/10.1016/j.ijhydene.2017.01.226>.
- [17] D. Yépez, L.M. Cornaglia, S. Irusta, E.A. Lombardo, Different oxides used as diffusion barriers in composite hydrogen permeable membranes, J. Memb. Sci. 274 (2006) 92–101, <https://doi.org/10.1016/j.memsci.2005.08.003>.
- [18] J.A. Calles, R. Sanz, D. Alique, Influence of the type of siliceous material used as intermediate layer in the preparation of hydrogen selective palladium composite membranes over a porous stainless steel support, Int. J. Hydrogen Energy. 37 (2012) 6030–6042, <https://doi.org/10.1016/j.ijhydene.2011.12.164>.
- [19] D. Zhang, S. Zhou, Y. Fan, N. Xu, Y. He, Preparation of dense Pd composite membranes on porous Ti-Al alloy supports by electroless plating, J. Memb. Sci. 387–388 (2012) 24–29, <https://doi.org/10.1016/j.memsci.2011.10.004>.
- [20] C.-B. Lee, S.-W. Lee, J.-S. Park, S.-K. Ryi, D.-W. Lee, K.-R. Hwang, S.-H. Kim, Ceramics used as intermetallic diffusion barriers in Pd-based composite membranes sputtered on porous nickel supports, J. Alloys Compd. 578 (2013) 425–430, <https://doi.org/10.1016/j.jallcom.2013.06.007>.
- [21] Y. Yan, R. Bateni, J. Harris, O. Kesler, Fabrication of reactive element oxide coatings on porous ferritic stainless steel for use in metal-supported solid oxide fuel cells, Surf. Coatings Technol. 272 (2015) 415–427, <https://doi.org/10.1016/j.surfcoat.2015.03.041>.
- [22] D. Martinez-Diaz, R. Sanz, J.A. Calles, D. Alique, H₂ permeation increase of electroless pore-plated Pd/PSS membranes with CeO₂ intermediate barriers, Sep. Purif. Technol. 216 (2019) 16–24, <https://doi.org/10.1016/j.seppur.2019.01.076>.
- [23] S.-K. Ryi, H.-S. Ahn, J.-S. Park, D.-W. Kim, Pd–Cu alloy membrane deposited on CeO₂ modified porous nickel support for hydrogen separation, Int. J. Hydrogen Energy. 39 (2014) 4698–4703, <https://doi.org/10.1016/j.ijhydene.2013.11.031>.
- [24] Y. Huang, R. Dittmeyer, Preparation of thin palladium membranes on a porous support with rough surface, J. Memb. Sci. 302 (2007) 160–170, <https://doi.org/10.1016/j.memsci.2007.06.040>.
- [25] M.L. Bosko, F. Ojeda, E.A. Lombardo, L.M. Cornaglia, NaA zeolite as an effective diffusion barrier in composite Pd/PSS membranes, J. Memb. Sci. 331 (2009) 57–65, <https://doi.org/10.1016/j.memsci.2009.01.005>.
- [26] M.L. Bosko, J.F. Minera, E.A. Lombardo, L.M. Cornaglia, Dry reforming of methane in membrane reactors using Pd and Pd-Ag composite membranes on a

- NaA zeolite modified porous stainless steel support, *J. Memb. Sci.* 364 (2010) 17–26, <https://doi.org/10.1016/j.memsci.2010.07.039>.
- [27] Y. Guo, Y. Jin, H. Wu, L. Zhou, Q. Chen, X. Zhang, X. Li, Preparation of palladium membrane on Pd/silicalite-1 zeolite particles modified macroporous alumina substrate for hydrogen separation, *Int. J. Hydrogen Energy* 39 (2014) 21042–21052, <https://doi.org/10.1016/j.ijhydene.2014.10.089>.
- [28] M.D. Mobarake, L. Samiee, ScienceDirect Preparation of palladium/NaX/PSS membrane for hydrogen separation, *Int. J. Hydrogen Energy* 41 (2016) 79–86, <https://doi.org/10.1016/j.ijhydene.2015.10.009>.
- [29] M. Dehghani Mobarake, P. Jafari, M. Irani, Preparation of Pd-based membranes on Pd/TiO₂ modified NaX/PSS substrate for hydrogen separation: design and optimization, *Microporous Mesoporous Mater.* 226 (2016) 369–377, <https://doi.org/10.1016/j.micromeso.2016.06.022>.
- [30] A.D. Kiadehi, M. Taghizadeh, ScienceDirect Fabrication, characterization, and application of palladium composite membrane on porous stainless steel substrate with NaY zeolite as an intermediate layer for hydrogen purification, *Int. J. Hydrogen Energy* 44 (2018) 2889–2904, <https://doi.org/10.1016/j.ijhydene.2018.12.058>.
- [31] A.D. Kiadehi, M. Taghizadeh, M.D. Rami, Journal of Industrial and Engineering Chemistry Preparation of Pd/SAPO-34/PSS composite membranes for hydrogen separation: effect of crystallization time on the zeolitic growth on PSS support, *J. Ind. Eng. Chem.* (2019), <https://doi.org/10.1016/j.jiec.2019.09.010>.
- [32] C. Deeprasertkul, R. Longloilert, T. Chaisuwant, Impressive low reduction temperature of synthesized mesoporous ceria via nanocasting, *Mater. Lett.* 130 (2014) 218–222, <https://doi.org/10.1016/j.matlet.2014.05.124>.
- [33] X. Deng, K. Chen, Protocol for the Nanocasting Method: Preparation of Ordered Mesoporous Metal Oxides, (2017). [10.1021/acs.chemmater.6b02645](https://doi.org/10.1021/acs.chemmater.6b02645).
- [34] W. Xiao, S. Yang, P. Zhang, P. Li, P. Wu, M. Li, N. Chen, K. Jie, C. Huang, N. Zhang, S. Dai, Facile synthesis of highly porous metal oxides by mechanochemical nanocasting, *Chem. Mater.* 30 (2018) 2924–2929, <https://doi.org/10.1021/acs.chemmater.7b05405>.
- [35] C. Soc, Synthesis of non-siliceous mesoporous oxides, *Chem. Soc. Rev.* (2014) 313–344, <https://doi.org/10.1039/c3cs60155b>.
- [36] G.D. Zhao, D. Feng, J. Huo, Q. McElroy, N. Fredrickson, G.H. Chmelka, B.F. Stucky, Triblock copolymer syntheses of mesoporous, *Science* (80-.). 279 (1998) 548–552.
- [37] L. Furones, D. Alique, Interlayer properties of in-situ oxidized porous stainless steel for preparation of composite Pd membranes, *ChemEngineering* 2 (2017) 1, <https://doi.org/10.3390/chemengineering201001>.
- [38] D. Martinez-Diaz, D. Alique, J.A. Calles, R. Sanz, Pd-thickness reduction in electroless pore-plated membranes by using doped-ceria as interlayer, *Int. J. Hydrogen Energy* (2019), <https://doi.org/10.1016/j.ijhydene.2019.10.140>.
- [39] E. Tosto, D. Alique, D. Martinez-Diaz, R. Sanz, J.A.A. Calles, A. Caravella, J.A. Medrano, F. Gallucci, Stability of pore-plated membranes for hydrogen production in fluidized-bed membrane reactors, *Int. J. Hydrogen Energy* 45 (2020) 7374–7385, <https://doi.org/10.1016/j.ijhydene.2019.04.285>.
- [40] J.A. Calles, R. Sanz, D. Alique, L. Furones, P. Marín, S. Ordoñez, Influence of the selective layer morphology on the permeation properties for Pd-PSS composite membranes prepared by electroless pore-plating: experimental and modeling study, *Sep. Purif. Technol.* 194 (2018) 10–18, <https://doi.org/10.1016/j.seppur.2017.11.014>.
- [41] D. Alique, R. Sanz, J.A. Calles, Pd membranes by electroless pore-plating: synthesis and permeation behavior, *Curr. Trends Futur. Dev. Membr.* (2020) 31–62, <https://doi.org/10.1016/B978-0-12-818332-8.00002-8>.
- [42] C. Ahn, H. Mo, M. Jin, J. Man, T. Kim, Y. Suh, K. June, J. Wook, Microporous and Mesoporous Materials Catalyst deactivation by carbon formation during CO hydrogenation to hydrocarbons on mesoporous Co 3 O 4, *Microporous Mesoporous Mater.* 188 (2014) 196–202, <https://doi.org/10.1016/j.micromeso.2013.12.035>.
- [43] J.M. Cho, S.R. Lee, J. Sun, N. Tsubaki, E.J. Jang, J.W. Bae, Highly Ordered Mesoporous Fe 2 O 3 – ZrO 2 Bimetal Oxides for an Enhanced CO Hydrogenation Activity to Hydrocarbons with Their Structural Stability, (2017). [10.1021/acscata.17b01989](https://doi.org/10.1021/acscata.17b01989).
- [44] A. Lolli, R. Amadori, C. Lucarelli, M.G. Cutrufello, E. Rombi, F. Cavani, S. Albonetti, Microporous and Mesoporous Materials Hard-template preparation of Au/CeO 2 mesostructured catalysts and their activity for the selective oxidation of 5-hydroxymethylfurfural to 2, 5-furan dicarboxylic acid, *Microporous Mesoporous Mater.* 226 (2016) 466–475, <https://doi.org/10.1016/j.micromeso.2016.02.014>.
- [45] M. Thommes, K. Kaneko, A. V Neimark, J.P. Olivier, F. Rodriguez-reinoso, J. Rouquerol, K.S.W. Sing, Physisorption of gases , with special reference to the evaluation of surface area and pore size distribution (IUPAC Technical Report), 87 (2015) 1051–1069. [10.1515/pac-2014-1117](https://doi.org/10.1515/pac-2014-1117).
- [46] J.P. Thielemann, F. Girsdes, R. Schlägl, C. Hess, Pore structure and surface area of silica SBA-15 : influence of washing and scale-up, *Catal. Today* 123 (2011) 110–118. [10.3762/bjnano.2.13](https://doi.org/10.3762/bjnano.2.13).
- [47] A. Rumplecker, F. Kleitz, E. Salabas, F. Schu, V. La, Q. Gk, R. V May, V. Re, M. Reczi, V. September, Hard Templating Pathways for the Synthesis of Nanostructured Porous Co 3 O 4, (2007) 485–496. [10.1021/cm0610635](https://doi.org/10.1021/cm0610635).
- [48] Q. Zhang, C. Chen, M. Wang, J. Cai, J. Xu, C. Xia, Facile preparation of highly-dispersed cobalt- silicon mixed oxide nanosphere and its catalytic application in cyclohexane selective oxidation, (2011) 1–7.
- [49] J.V.G. Tinio, K.T. Simfros, A. Dea, M. P. Peguit, R.T.C. Jr, Influence of OH – Ion Concentration on the Surface Morphology of ZnO-SIO 2 Nanostructure, 2015 (2015).
- [50] P.P. Mardilovich, Y. She, Y.H. Ma, M.-H. Rei, Defect-free palladium membranes on porous stainless-steel support, *AIChE J.* 44 (1998) 310–322, <https://doi.org/10.1002/aic.690440209>.
- [51] J. Catalano, M. Giacinti Baschetti, G.C. Sarti, Influence of the gas phase resistance on hydrogen flux through thin palladium–silver membranes, *J. Memb. Sci.* 339 (2009) 57–67, <https://doi.org/10.1016/j.memsci.2009.04.032>.
- [52] M. Nordio, S. Soresi, G. Manzolini, J. Melendez, M. Van Sint Annaland, D.A. Pacheco Tanaka, F. Gallucci, Effect of sweep gas on hydrogen permeation of supported Pd membranes: Experimental and modeling, *Int. J. Hydrogen Energy*, (2019). <https://www.sciencedirect.com/science/article/pii/S0360319918341399> (accessed January 22, 2019).
- [53] N.D. Deveau, Y.H. Ma, R. Datta, Beyond Sieverts' law: A comprehensive microkinetic model of hydrogen permeation in dense metal membranes, *J. Memb. Sci.* 437 (2013) 298–311, <https://doi.org/10.1016/j.memsci.2013.02.047>.
- [54] R. Sanz, J.A. Calles, D. Alique, L. Furones, New synthesis method of Pd membranes over tubular PSS supports via “pore-plating” for hydrogen separation processes, *Int. J. Hydrogen Energy* 37 (2012) 18476–18485, <https://doi.org/10.1016/j.ijhydene.2012.09.084>.
- [55] S. Ligouri, K. Kian, N. Buggy, B.H. Anzelmo, J. Wilcox, Opportunities and challenges of low-carbon hydrogen via metallic membranes, *Prog. Energy Combust. Sci.* 80 (2020) 100851, <https://doi.org/10.1016/j.proe.2020.100851>.
- [56] S. Tosti, C. Cavezza, M. Fabbricino, L. Pontoni, V. Palma, C. Ruocco, Production of hydrogen in a Pd-membrane reactor via catalytic reforming of olive mill wastewater, *Chem. Eng. J.* 275 (2015) 366–373, <https://doi.org/10.1016/j.cej.2015.04.001>.
- [57] C.V. Miguel, A. Mendes, S. Tosti, L.M. Madeira, Effect of CO and CO₂ on H₂ permeation through finger-like Pd–Ag membranes, *Int. J. Hydrogen Energy* 37 (2012) 12680–12687, <https://doi.org/10.1016/j.ijhydene.2012.05.131>.
- [58] P. Pinacci, M. Broglia, C. Valli, G. Capannelli, A. Comite, Evaluation of the water gas shift reaction in a palladium membrane reactor, *Catal. Today* 156 (2010) 165–172, <https://doi.org/10.1016/J.CATTOD.2010.02.034>.
- [59] S.-W. Lin, C.-Y. Chen, Y.-H. Chi, Y.-L. Lin, Impact of vacuum operation on hydrogen permeation through a palladium membrane tube, *Int. J. Hydrogen Energy* 44 (2019) 14434–14444, <https://doi.org/10.1016/j.ijhydene.2019.02.103>.
- [60] F. Guazzone, E.E. Engwall, Y.H. Ma, Effects of surface activity, defects and mass transfer on hydrogen permeance and n-value in composite palladium–porous stainless steel membranes, *Catal. Today* 118 (2006) 24–31, <https://doi.org/10.1016/j.cattod.2005.12.010>.
- [61] J. Tong, Y. Matsumura, H. Suda, K. Haraya, Thin and dense Pd/CeO₂/MPSS composite membrane for hydrogen separation and steam reforming of methane, *Sep. Purif. Technol.* 46 (2005) 1–10, <https://doi.org/10.1016/j.seppur.2005.03.011>.
- [62] T.A. Peters, M. Stange, H. Klette, R. Bredesen, High pressure performance of thin Pd-23%Ag/stainless steel composite membranes in water gas shift gas mixtures; influence of dilution, mass transfer and surface effects on the hydrogen flux, *J. Memb. Sci.* 316 (2008) 119–127, <https://doi.org/10.1016/j.memsci.2007.08.056>.
- [63] M. Sarić, Y.C. Van Delft, R. Sumbharaju, D.F. Meyer, A. De Groot, Steam reforming of methane in a bench-scale membrane reactor at realistic working conditions, *Catal. Today* 193 (2012) 74–80, <https://doi.org/10.1016/j.cattod.2012.04.009>.

LIFE CYCLE ASSESSMENT OF H₂-SELECTIVE Pd MEMBRANES FABRICATED BY ELECTROLESS PORE-PLATING

D. Martínez-Díaz¹, P. Leo², A. Carrero¹, J.A. Calles¹, and D. Alique^{1,*}

¹ Department of Chemical, Energy and Mechanical Technology, Rey Juan Carlos University, Móstoles, Spain

² Department of Chemical and Environmental Technology, Rey Juan Carlos University, Móstoles, Spain

Abstract

The promotion of clean renewable energies, as well as the adoption of efficient energy strategies to reduce carbon dioxide emissions, are critical issues to mitigate global warming and progressive deterioration of the environment. Particularly, the use of hydrogen is one of the most promising alternatives to facilitate a progressive transition towards this situation, especially when considering its simultaneous production and purification through dense palladium membranes in membrane reactors. This strategy provides important competitive advantages compared to other traditional process schemes in which the separation unit is placed downstream after the main reactor. Despite the recent advances in the fabrication of composite membranes with thinner Pd films and higher permeation capacities, their commercialization and penetration in the industry are still scarce. It is caused by omitting economic or environmental aspects during the fabrication of the membranes. This work tries to cover partially this gap in the case of considering the fabrication of supported membranes by Electroless Pore-Plating (ELP-PP). Therefore, a LCA study focused on the membrane preparation, at a laboratory scale, has been performed for the first time. It has been carried out for two different types of supported ELP-PP Pd-membranes onto porous stainless steel supports, including or not the presence of a possible additional CeO₂ intermediate layer. Thereafter, environmental impacts were quantified through ReCiPe methodology by using the software Simapro 8.5. The LCA has demonstrated that, in general, the most impacting manufacturing step is the palladium deposition (Pd), not only due to the metal consumption, but also to the high-energy consumption required during the different required deposition cycles. Therefore, the electric production system of each country is key to reducing the impacts generated during the production of membranes. For this reason, European countries are the locations where the minor environmental impact would be generated, while China would rank as one of the most unfavorable from the environmental point of view. On the other hand, the incorporation of intermediate layers, i.e. CeO₂, before palladium deposition (MB#02) significantly reduces the amount of Pd, therefore being most environmentally friendly process.

Keywords: Membrane, palladium, electroless plating, hydrogen production, LCA, environmental impacts, sustainability.

*To whom the correspondence should be addressed

Tel: +34 91 488 76 03

e-mail: david.alique@urjc.es

1. Introduction

The current energy system is mainly supported by fossil fuels, responsible for most anthropogenic CO₂ and NOx emissions that provoke serious environmental concerns [1,2]. The continuous population and economic growth have been made this situation progressively worse during the last decades [3,4]. Only external factors and the natural economic cycles have been slightly modified the velocity of this general trend. For example, the recent world pandemic caused by COVID-19 negatively affects industrial and domestic energy demands, resulting in a marked decrease in atmospheric pollutant levels for many regions worldwide [5–8]. Moreover, the numerous international mobility restrictions also significantly influence the restrained energy demand for the transport sector [9]. However, it is foreseen this circumstantial situation changes in a few months/years, and the above-mentioned growth's footsteps will be recovered with all its associated environmental implications [9,10].

In this context, strong policies with a clear roadmap towards a new energy system are fundamental for promoting future sustainability. In fact, diverse regions such as Europe and Japan bet on a progressive transition to renewable energies with very ambitious policies and important investments to develop new technologies and increase their efficiency [11,12]. As a clean energy vector, hydrogen is one of the most promising alternatives to facilitate the above-mentioned progressive transition towards a net-zero carbon emissions system [13]. In this context, new ambitious policies try to promote this technology in Europe during next years [14,15], following the first steps recently taken by Japan [16,17]. Among other multiple reasons, the possibility to be produced from a wide variety of feedstock by diverse technologies, some of them very mature, could definitively promote its penetration in the industry with assumable risks [18]. In fact, most of the current hydrogen is produced by methane steam reforming [19–21], although many other hydrocarbons can also be considered with similar technologies. The use of biomass-derivate compounds and wastes to generate hydrogen could be especially attractive for a circular economy [18,22,23]. However, in all these processes involving traditional thermochemical routes, hydrogen is not directly obtained in its pure form but accompanied by other sub-products such as carbon monoxide, carbon dioxide, methane, or steam water, among others [18,24]. Therefore, down-stream additional purification steps are always required to adjust the hydrogen purity for each particular final application [25,26]. At this point, it is important to point out that the overall economy of the production processes is significantly affected by these purification steps, reaching up to 50% of the total cost in function of the selected technology and operating conditions [27]. Pressure swing adsorption (PSA) is currently the prevalent alternative for hydrogen purification in most industrial processes, despite its high energy consumption and limited profitability for small production-scale as suggested by a decentralized energy system [28–30]. Many researchers have also promoted the use of H₂-selective membranes for this purpose during the last years [31]. This alternative provides the possibility to reach an ultra-high purity in a wide variety of operating conditions, including the combination of both production and separation steps in a unique device so-called membrane reactor [32,33]. The continuous separation of hydrogen throughout the membrane from the bulk reaction promotes its generation by an equilibrium displacement towards the products [34]. This technology simultaneously aims to facilitate the process intensification and increase their overall efficiency [35,36].

Among the various membranes used in the devices mentioned above, those dense ones made of pure palladium or its alloys provide clear advantages in terms of H₂ perm-selectivity and

mechanical resistance at high temperatures [37,38]. Hydrogen permeation through these metal dense-membranes is typically expressed by the Sieverts' law, defined as follows:

$$J_{H_2} = \frac{k'}{t_{Pd}} [P_{H_2,r}^{0.5} - P_{H_2,p}^{0.5}] = k [P_{H_2,r}^{0.5} - P_{H_2,p}^{0.5}] \quad (\text{Eq. 1})$$

where J_{H_2} is the permeate flux ($\text{mol m}^{-2} \text{s}^{-1}$), k' the H_2 permeability ($\text{mol m}^{-1} \text{s}^{-1} \text{Pa}^{-0.5}$), k the H_2 permeance ($\text{mol m}^{-2} \text{s}^{-1} \text{Pa}^{-0.5}$), t_{Pd} the thickness of the Pd-based layer (m^{-1}) and $P_{H_2,i}$ (Pa) the hydrogen partial pressure in both retentate (subscript $i=r$) and permeate (subscript $i=p$) sides.

In this manner, the hydrogen flux through a Pd-based membrane depends on some operating conditions and intrinsic membrane properties. The pressure difference between both retentate and permeate side is the first group's most relevant one together with the temperature, which affects the membrane permeability by an Arrhenius type dependence [39]. On the other side, the membrane composition and the metal thickness are the second group's most relevant ones [40,41]. They should be considered in any membrane fabrication strategy for their final commercialization. In this context, great efforts are being carried out during last years to reduce as much as possible the metal thickness of these membranes, reaching values below 15 μm by incorporating the Pd-film onto porous supports that provide the required mechanical resistance [42]. Electroless plating (ELP) and its variants have demonstrated a great potential to achieve these goals onto porous supports of diverse nature and geometry with contained expenses [43–45]. Particularly, the Electroless Pore-Plating (ELP-PP) alternative offers an excellent adherence of the Pd-film onto the porous support and, hence, a high mechanical resistance of resulting composite-membranes even in case of generating tensile stress during their operation [46,47]. It is reached thanks to a partial palladium infiltration into some pores after placing both Pd-source and hydrazine solution, the reducing agent, from opposite sides of the support [31,48].

Moreover, an intermediate layer between the porous support and the top Pd-film is frequently included to reduce both original roughness and average pore sizes and, consequently, make the generation of thin Pd layers easier [49–51]. A wide variety of materials have been proposed as interlayers, highlighting technical ceramics such as alumina [52], zirconia [53], yttria-stabilized zirconia [54–56], or ceria [57–59], among others. These materials have also been used as an additional fourth layer onto the H_2 -selective Pd-film for protection against the particular operating conditions of fluidized-bed reactors [60,61]. Most of these fabrication strategies are developed to improve the final performance of the membrane in terms of permeation capacity and mechanical stability. However, reports about economic or environmental implications are certainly scarce even though these implications are critical issues for commercializing the membranes and their penetration in the industry. In this sense, the use of Life Cycle Assessments (LCA) is extended as an accurate technique to quantify the environmental impacts generated by processes or products rigorously [62]. This methodology allows a systematic estimation of the environmental changes caused during the fabrication of a certain material or a process itself. Basically, it consists of examining all processes involved in the case under study, quantifying all material and energy inputs/outputs to determine their effects on both human health and the environment according to a standardized procedure described in ISO-14040 and ISO-14044 [63]. In this context, LCA has proved to be a useful tool for assessment of environmental impacts in the energy and fuel sector [64,65]. However, the studies focused on hydrogen production processes containing Pd-based membranes are scarce. Di Marcobernardino et al. analyzed the environmental and economic performances of an innovative micro-CHP system based on a membrane-reactor and a PEM fuel-

cell [66]. The results were compared with an analogous system in which the hydrogen is produced in a traditional steam reformer for diverse scenarios. They evidenced that the innovative system based on a membrane-reactor reduces or has similar impacts for the carbon footprint depending on the assumed scenarios. Simultaneously, water withdrawal and human health were positive or negative, depending on the case.

However, to the best of our knowledge, no available studies address the environmental implications of diverse fabrication strategies of Pd-based membranes. This work tries to cover this gap and includes a systematic environmental analysis throughout LCA to fabricate different composite-membranes containing dense Pd-based layers incorporated by Electroless Pore-Plating onto PSS supports. The influence of incorporating CeO_2 intermediate layers on the overall environmental impacts is also considered for this study.

2. Experimental section

2.1. Membrane preparation

All composite-membranes considered in this work were prepared onto commercial AISI 316L porous stainless-steel (PSS) supports with cylindrical geometry purchased from Mott Metallurgical corp. The original tubes present a symmetric structure with 0.1 μm porous media grade, an external diameter of 1.27 mm, and 0.20 mm wall thickness. These tubes were cut into smaller lengths of around 30 mm for preparing each composite-membrane at a laboratory scale.

Two different composite-structures containing various intermediate layers were considered for the analysis, as illustrated in Figure 1.

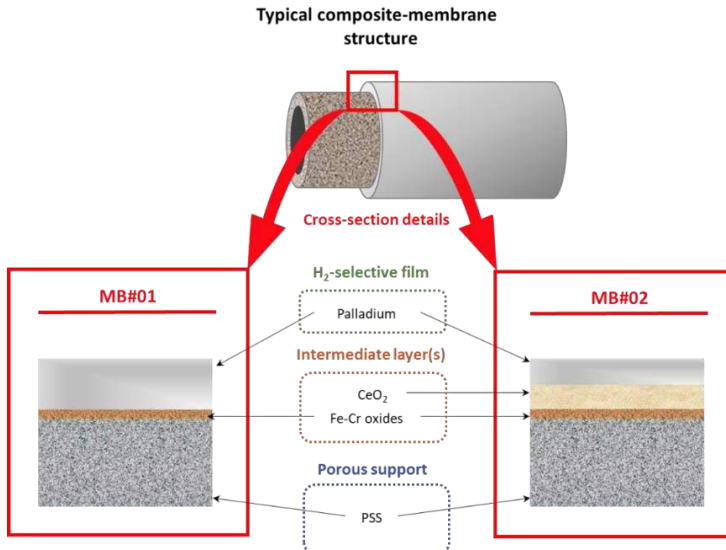


Figure 1. Schematic composite-structures of Pd-membranes considered in the present study.

In both cases, the raw PSS supports were first calcined in air to generate an initial thin intermediate layer made of Fe-Cr oxides according to a previous investigation [67,68]. One of these samples, denoted as MB#01, was directly used to incorporate the top H₂-selective film made of pure palladium by Electroless Pore-Plating (ELP-PP) following the procedure described elsewhere

[48,69]. On the other hand, an additional intermediate layer formed by dense cerium oxide particles was incorporated by vacuum-assisted dip-coating in the sample MB#02 before the top Pd-film [57].

Figure 2 summarizes a detailed scheme of the synthesis procedure followed for each membrane. Basically, all steps can be divided into two main groups: Support Modification (SM) and Palladium Deposition (PD). The first one, SM, consists of an initial cleaning of raw PSS supports to remove eventual dirty or grease from their manipulation (SM-1) and the incorporation of intermediate layers (Fe-Cr oxides and CeO₂) to modify the original surface supports (SM-2 to SM-4). The second one, PD, includes the activation of the modified surface with homogeneously distributed fine Pd-nuclei (PD-1), the incorporation of the fully dense Pd-film by ELP-PP (PD-2), and the required cleaning and drying steps after both steps (PD-3). At this point, it should be noted that the last steps were repeated several times up to reach complete gas tightness, thus evidencing a good continuity of the Pd-film and absence of detectable defects at room conditions.

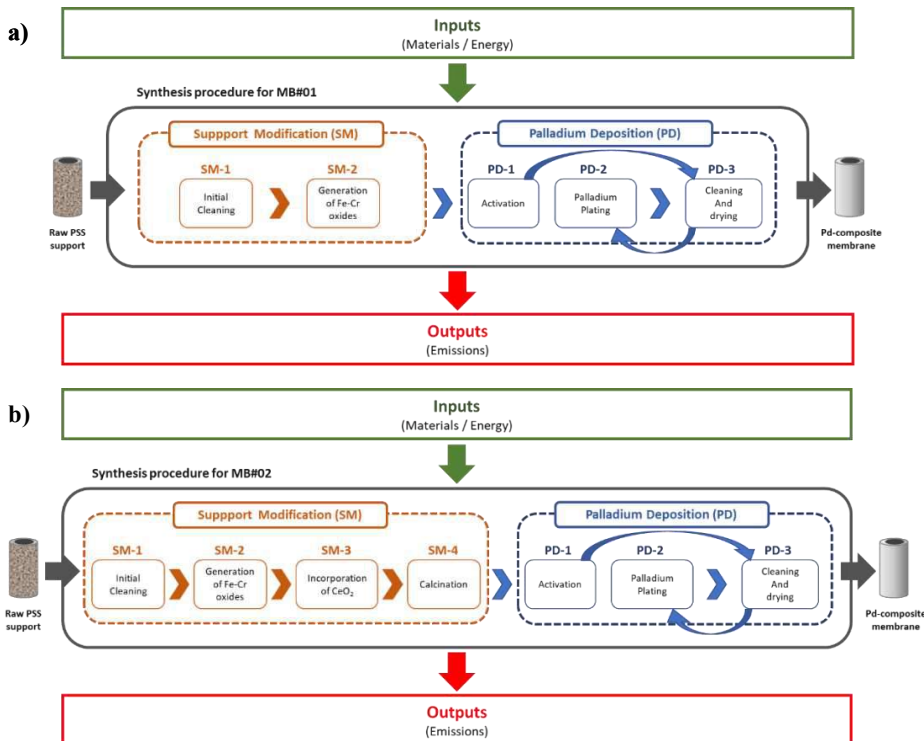


Figure 2. Detailed scheme of the synthesis procedure followed for: a) MB#01 and b) MB#02.

All these steps require particular inputs in form of materials and/or energy while generating some eventual output emissions. To a better understanding of these inputs and outputs during the synthesis process of each membrane included in the present work, some additional key information is included here. The first step always consists of cleaning the raw PSS supports by successive immersions in diverse solutions of sodium hydroxide 0.1 M (SM-1.1), hydrochloric acid 0.1M (SM-1.2), and ethanol 96 vol.% (SM-1.3) at 60 °C under ultrasonic stirring. Then, the clean supports were oxidized in air at 600 °C (heating and cooling rams of 1.8 °C/min) for 12 h in a tubular furnace to generate a primary intermediate layer formed by a thin Fe/Cr oxides layer. In previous studies, it was concluded that this thin film slightly reduces the roughness and average

pore size of the original PSS supports at the external surface, thus moderately promoting the subsequent incorporation of a Pd-film with reduced thickness by ELP-PP [67,68].

MB#01 has been prepared directly at these conditions, without considering further modifications of the porous substrate. The palladium deposition by ELP-PP always involves three successive main steps, repeating some of them several times up to achieve a fully dense membrane. Some nano-sized Pd-nuclei need to be finely distributed onto the surface of the pores before initiating the plating. This is to guarantee a homogeneous growth of the film, good adherence, and reasonable induction times to initiate spontaneously the chemical reactions involved in ELP-PP. In this step, denoted as activation, the extremes of the support are sealing with Teflon tapes to maintain separated both external and internal sides from where two different solutions are fed: 0.1 g/l acidic palladium chloride as metal source (PD-1.1) and 0.2 M N₂H₄ – 2.0 M NH₄OH mixture as reducing agent (PD-1.2), respectively. The immersion of the support in the solutions is maintained for 2 h at room temperature, preferentially meeting both PD-1.1 and PD-1.2 solutions just into the pores and initiating the generation of the first Pd-nuclei. After this time, the support is washed in distilled water and dried at 110 °C for at least 8 h before starting the ELP-PP strictly speaking. The Pd plating is then completing in similar conditions but increasing the temperature up to 60 °C and replacing both Pd source and reducing solutions with new ones: PD-2.1 and PD-2.2. The first one, PD-2.1, contains the Pd precursor (PdCl₂, 99 w.%) complexed and stabilized with NH₄OH (32 vol.%) and Na₂EDTA, while the second one, PD-2.2, includes diluted N₂H₄ in water (0.2 M) as reducing agent. Then, Pd²⁺ ions contained in PD-2.1 are reduced to Pd⁰ in a controlled autocatalytic chemical reaction for various cycles of 2-7 h. Intermediate washing in distilled water and dried at 110 °C for at least 8 h are performed between each cycle. This procedure is repeated up to the Pd weight gain of the membrane became negligible due to the complete blockage of pores and, consequently, the achievement of a fully dense Pd-membrane [31,46,70].

MB#02 has been prepared following a similar experimental procedure but incorporating an additional CeO₂ intermediate layer as described in a previous study [57]. It involves two new steps for the support modification: the incorporation of the material onto the support by vacuum-assisted dip-coating (VA-DC) and its calcination to ensure good stability of the new layer, respectively denoted as SM-3 and SM-4. In particular, commercial dense CeO₂ particles (Alfa-Aesar, 100 nm average particle size) are suspended in water containing 2 wt.% polyvinyl alcohol (PVA) to reach a CeO₂ concentration of around 20 wt.% (SM-3.1). After sealing the inner side of the support with appropriate Teflon tapes, VA-DC is repeated twice by applying vacuum only during the half-second cycle. The CeO₂ layer thickness is finally adjusted by rinsing in distilled water and then the composite-structure is calcined at 500 °C (heating and cooling ramp of 1.8 °C/min) for 5 h to ensure the complete removal of the organic linker (PVA) and good mechanical stability of the intermediate layer [57].

Table 1 summarizes all chemicals and materials used for the preparation of the above-mentioned SM and PD solutions. Besides all these chemicals and materials, the energy requirements of each step need to be also considered in the present study. At this point, it is important to emphasize the laboratory scale of the analyzed membrane synthesis procedures. Thus, the optimization of these issues should be taken into account for the next scale-up considerations. In this context, a different number of membranes can be managed at each particular preparation step. Four membranes can be simultaneously handled in steps SM-1, PD-1, PD-2, and PD-3, while two samples can be processed in steps SM-2 and SM-4 at the same time. Other steps (SM-3 and PD-1) are performed individually for each membrane.

Table 1. Summary of chemical and materials requirements for solutions used during the synthesis of the membranes.

SM: Surface Modification			PD: Palladium Deposition		
SM-1: Initial cleaning		SM-3: CeO ₂ barrier	PD-1: Activation		PD-2: ELP-PP
SM-1.1		SM-3.1	PD-1.1		PD-2.1
NaOH (g/l)	2	CeO ₂ (g/l)	PdCl ₂ (g/l)	0.1	PdCl ₂ (g/l)
SM-1.2		PVA (g/l)	HCl 35% (ml/l)	1	NH ₄ OH 32% (ml/l)
HCl 35% (ml/l)	2	PD-1.2		120	Na ₂ EDTA (g/l)
SM-1.3		NH ₄ OH 32% (ml/l)	N ₂ H ₄ (ml/l)	10	PD-2.2
Ethanol 96% (ml/l)	1000				N ₂ H ₄ (ml/l)
					10

2.2. LCA methodology

The LCA analysis presented in the present study was performed according to standards ISO-14040 and ISO-14044 to determine the effects of each material and energy input/output used in the previously described membranes manufacturing process on both human health and the environment.

2.2.1 LCA goal and scope

The present study is focused on the evaluation of all main environmental impacts and energy demand related to the fabrication of two different supported Pd-based membranes by ELP-PP at a laboratory scale (MB#01 and MB#02). A cradle to gate perspective was considered to perform the analysis and determine the corresponding inputs and outputs. It implies to contemplate all issues required from the acquisition of the raw materials to Pd deposition by ELP-PP, as previously represented in Figure 2. The functional unit selected to compare the environmental burdens was the synthesis of one Pd-membrane with 3 cm in length.

2.2.2 System boundaries and life cycle inventory

All inputs and outputs required for the fabrication of Pd-membranes, including both materials and energy, were considered within the system boundaries described in Figure 2. Their values were taken from the inventory database Ecoinvent 3.4 for each particular fabrication step. It should be noted that the original conditions available in the database were updated to diverse situations in the energy mix. In fact, specific conditions of five different countries were considered: Spain, Germany, China, Japan, and the United States of America. Table 2 collects the contribution of each primary source to the available energy mix in these countries.

Table 2. Energy mix 2019 available in different countries with a particular interest in the present study.

Source	Contribution to the energy mix (%)				
	Spain [71]	Germany [72]	China [73]	Japan [74]	USA [75]
Hard coal	4.3	6.4	65.6	32.7	23
Lignite	-	13.5	-	8.7	-
Hydro	10	3.4	17.7	7.9	6.6
Natural gas	32.7	16.1	3.1	39.5	38.8
Nuclear	22.6	11.3	4.8	3.1	20.7
Wind	21.5	26.8	5.5	2.3	7.3
Biomass	-	8.0	0.2	2.7	1.4
Solar	2.1	9.7	3.1	3.1	1.8
Others	6.8	4.8	-	-	0.4

2.2.3 Life cycle impact assessment (LCIA)

In this work, the software Simapro v8.5 was used to assess all environmental impact by using the inventory data above detailed. In this case, the recipe methodology [76] was used as a midpoint methodology, selecting the following environmental impact categories: climate change (CC), human toxicity (HT), acidification (AC), freshwater ecotoxicity (FWE), metal depletion (MD) and fossil fuel resources depletion (FD). Moreover, the total energy requirements of the process were also quantified through cumulative energy demand (CED) [77].

3. Results and discussion

3.1. Fundamental membrane characterization

The primary characterization of any composite-membrane always includes the analysis of the morphology variation during the synthesis procedure. As previously addressed, the two different ELP-PP membranes included in the present work were fabricated following a similar strategy with the unique variation of incorporating an additional intermediate layer formed by dense CeO_2 particles [46,57]. Figure 3 collects some relevant micrographs taken for each membrane to discuss briefly their main characteristics.

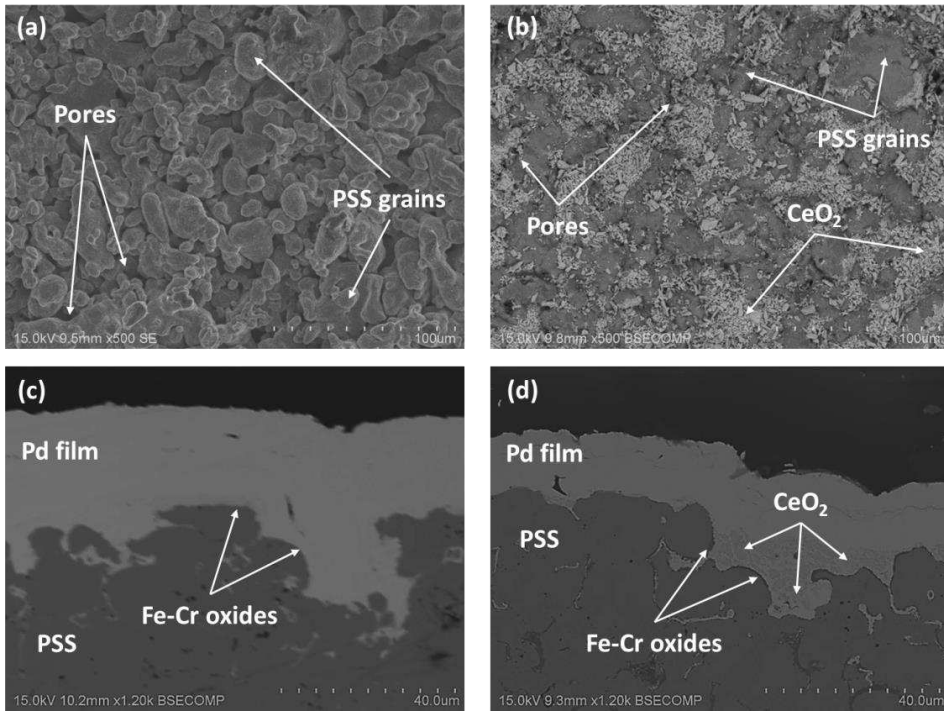


Figure 3. Morphology of MB#01 and MB#02 membranes before (a and b, respectively) and after incorporating the Pd-film by ELP-PP (c and d, respectively).

As can be seen, a very irregular external surface with a wide variety of pore sizes and high roughness appears in MB#01 despite being oxidized in air to generate a first intermediate layer of Fe-Cr oxides (Figure 3a). Only after the incorporation of CeO_2 particles in MB#02 was possible to smooth the external surface of supports, significantly reducing the average pore-mouth

diameter before the palladium plating (Figure 3a). The different morphologies reached for each case provokes an important effect on the Pd-film characteristics. In this manner, an estimated Pd-thickness from gravimetric analysis around 28 μm was required to obtain a gas-tightness membrane (MB#01), although it was reduced up to 15 μm in case of including the CeO₂ intermediate layer (MB#02). These values are fairly close to the real Pd-thicknesses directly measured onto the SEM cross-sectional images, as shown in Figures 3c and 3d for membranes MB#01 and MB#02, respectively. This relevant improvement can be explained by the generation of a new media grade with smaller pore sizes that can be more easily close by palladium particles during ELP-PP as widely discussed in previous works [46,57].

As a consequence of the different membrane properties, mainly the final Pd-thickness reached for each case, a marked effect on the membrane performance was observed in terms of permeation capacity. Figure 4 collects the H₂-permeate fluxes reached at 400 °C for pressures ranged from 0.25 to 2.50 bar when operating with MB#01 and MB#02. At this point, it is important to note that no nitrogen was detected in the permeate during the complete set of experiments (detection limit 1.67·10⁻² mL min⁻¹), and therefore, an ideal H₂/N₂ separation factor ($\alpha_{\text{H}_2/\text{N}_2}$) greater than 10,000 can be ensured for both samples.

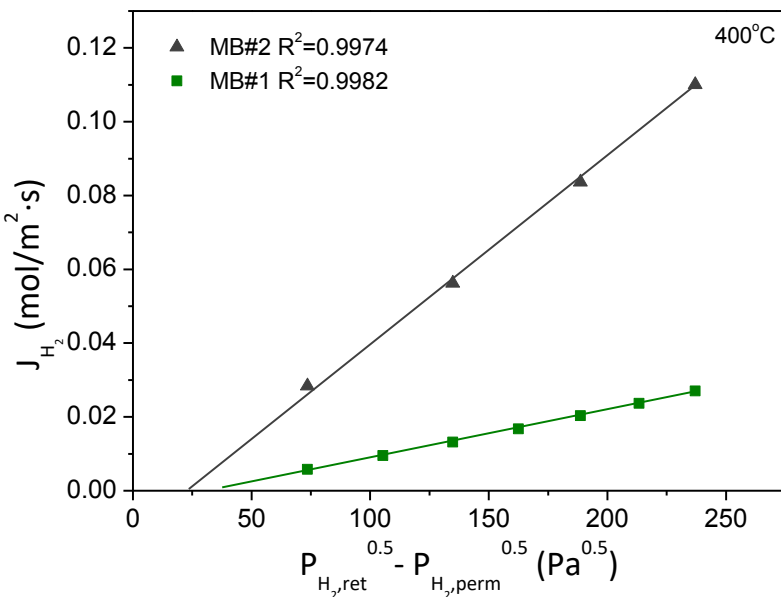


Figure 4. Permeation behavior of ELP-PP membranes MB#01 and MB#02 at 400 °C.

Analyzing in detail for each sample the relationship between H₂ fluxes and pressures raised to the power of 0.5, a clear linear trend is observed, as predicted by the well-known Sieverts' law (Eq.1) [40,78].

This fact together with the undetectable permeate fluxes in the case of feeding nitrogen confirms the absence of defects in the palladium film previously supposed after the membrane preparation. Thus, H₂-diffusion through the Pd-film can be considered as the rate-determining step, as typically occurs in most of the Pd-composite membranes [79,80].

However, it is also clear that the above-mentioned linear trends do not intercept the origin as common in other cases. This peculiar behavior is typical of most ELP-PP membranes reported up to now, being widely addressed in previous studies [31,46,70]. In essence, this deviation is justified by the partial infiltration of palladium into some pores of the support during the ELP-PP cycles due to feeding both metal source and the reducing agent from opposite sides of the porous substrate. This fact generates noticeably differences between both external and internal surfaces of the Pd-film that affect to the accurate calculation of the pressure driving force just onto the surfaces, as considered in the Sieverts' law [81]. Pressure values into the bulk gas phase and smooth surfaces are almost identical, thus being possible to precise them with minimal errors. On the contrary, in the case of presenting relevant tortuosity, as typically occurs for ELP-PP Pd-film surfaces in contact with porous supports, relevant pressure drops could appear between the measured pressure value into the bulk gas phase and just onto that palladium side. It can be quantified as an apparent additional resistance against the permeation process (R_i) as detailed in previous works [31,46,70]. Anyway, the benefits of using an additional CeO₂ intermediate layer in MB#02 becomes obvious in terms of its performance, reaching H₂ permeance of $5.37 \cdot 10^{-4}$ mol m⁻² s⁻¹ Pa^{-0.5} at 400 °C, in contrast to the lower value obtained in MB#01, $1.50 \cdot 10^{-4}$ mol m⁻² s⁻¹ Pa^{-0.5} at analogous conditions. Undeniably, this improvement of the permeation capacity in around 350% is caused by the reduction of the Pd-thickness required to achieve a fully dense membrane in case of using the additional CeO₂ barrier (from 28 to 15 µm, as previously discussed). Table 3 summarizes all these results for easier comparison.

Table 3. Summary of main properties for membranes included in the present study.

Sample	Membrane morphology			Permeation behavior		
	Intermediate layer(s)	Pd-thickness (µm)	Variation (%)	R_i (Pa ^{0.5})	k_{H_2} (mol m ⁻² s ⁻¹ Pa ^{-0.5})	Variation (%)
MB#01	Fe-Cr oxides	28	-	24	$1.50 \cdot 10^{-4}$	-
MB#02	Fe-Cr oxides / CeO ₂	15	- 46.4%	33	$5.37 \cdot 10^{-4}$	+ 358%

3.2. Materials inventory for membranes preparation

Up to now, it is clear the benefits provided by the strategy of using an additional ceramic intermediate layer for the preparation of ELP-PP membranes in terms of palladium savings and final performance. However, no considerations about the environmental impacts of all associate experimental steps have been taken into account. This lack of information is very common in most of the available researches despite it could generate important implications for the commercialization and spread of this technology. This work tries to fill in the gap in this field, providing complete and precise information about all materials required for the preparation of the membranes step by step, particularly those obtained by ELP-PP. At this point, it should be remembered that two different synthesis strategies have been considered for the preparation of these composite-membranes in the present study, including or not an intermediate ceramic barrier formed by CeO₂ particles. Since all the membranes were prepared onto the same tubular PSS supports, its contribution to the environmental impact has been omitted to point out exclusively the considerations of each synthesis procedure.

In this context, Tables 4 and 5 include a complete material inventory for each step carried out for the surface modification (SM) and palladium deposition (PD), respectively, during the preparation of two different types of ELP-PP membranes. At this point, it has to point out that 6 different membranes of each type (similar to MB#01 and MB#02) were fabricated to ensure good

reproducibility of the results here collected. The solutions required for modifying the original surface of raw PSS supports (SM) used to prepare the composite membranes accordingly to the procedures previously described are summarized in Table 4. Only the initial cleaning of the supports (SM-1), common for both membranes included in the present study, and the incorporation of the CeO₂ intermediate layer (SM-3), carried out just for MB#02, require the use of chemicals and solutions. However, it should be noted that after each of the above-mentioned cycles the membrane is always rinsed with distilled water, thus requiring an additional water consumption of around 40 mL besides the considered one for the preparation of the aqueous solutions. Moreover, it is important to emphasize that all these consumptions were identical for the preparation of all the membranes, reaching a very similar modification of the original surface with an identical number of cycles.

Table 4. Materials inventory for surface modification of PSS supports during membrane preparation (referred to the selected functional unit).

Sample	Solutions required for surface modification (SM)									
	SM-1				SM-2	SM-3		SM-4		
	SM-1.1		SM-1.2			SM-1.3				
	cycles	V (mL)	cycles	V (mL)		cycles	V (mL)			
MB#01	1	50	1	50	-	-	-	-		
MB#02	1	50	1	50	-	1	12.5	-		

A similar analysis has been presented in Table 5, where the solutions consumed for the palladium deposition (PD) are reported.

Table 5. Materials inventory for palladium deposition during membrane preparation (referred to the selected functional unit).

Sample	Solutions required for palladium deposition (PD)									
	PD-1				PD-2				PD-3	
	PD-1.1		PD-1.2		PD-2.1		PD-2.2			
	cycles	V (mL)	cycles	V (mL)	cycles	V (mL)	cycles	V (mL)		
MB#01	1	50	1	50	27±3	200±60	27±3	81±9	-	
MB#02	1	50	1	50	12±2	100±40	12±2	36±6	-	

The support activation with Pd-nuclei (PD-1) always requires a constant volume of solutions PD-1.1 and PD-1.2 due to a unique cycle of 2 h generates enough Pd-seeds for the subsequent ELP-PP step in both membranes. However, a slight variation in the consumption of PD-2.1 and PD-2.2 solutions was observed during the preparation of the set of membranes, with 6 analogous samples of each type: MB#01 and MB#02. It could be attributed to the certainly heterogeneous surface of original supports and the possibility of certain differences between various supports. In fact, the greater modification of the original PSS substrates achieved after the incorporation of a ceramic intermediate barrier in MB#02 implies a noticeable reduction of the total number of ELP-PP recurrences in comparison to MB#01 in which only a surface calcination of the original supports was carried out. In addition to this variation in the total number of ELP-PP recurrences due to the different surface properties of the supports, other causes can also provoke an increase in the spent volume of each solution. In fact, despite reusing the same solution for the entire set of recurrences in most cases, its degradation was also occasionally observed, thus turning in a dark orange-red color and being necessary its substitution by a fresh one. For this reason, errors collected in Table 5 could seem certainly high. This problem can be caused by diverse and unexpected operating issues, i.e. deviations in the control of temperature during the ELP-PP recurrences or direct contact between the solution and the metal assembling parts of the deposition

cell, normally covered by Teflon. Anyway, it should be noted that the probability of this occurrence is relatively low, avoiding taking into account these deviations for the present study. On the other hand, the final properties of all analogous composite-membranes were almost constant in terms of Pd-thickness, with an average deviation below 7%. Therefore, it can be assumed that the above-mentioned deviations do not affect the final quality of the membranes. Finally, as occurs during the surface modification, some washing and rinsing with distilled water were performed after both activation and ELP-PP recurrences, thus additionally consuming around $1,400 \pm 120$ and 650 ± 80 mL during the fabrication of MB#01 and MB#02, respectively. These deviations of consumptions are caused by the above-mentioned necessity of additional ELP-PP recurrences in some cases.

3.3. Environmental performance: LCA results

LCA analysis of MB#01 is summarized in Figure 5 as the relative contribution of each process stage in several environmental impacts. As can be clearly seen, the environmental impact is dominated by cleaning and drying step (PD-3), independently of the impact category selected. This result is directly related to the energy required to carry out the twenty-eight drying cycles (furnace at 110°C for at least 8 h, each cycle) necessary to obtain a complete gas tightness using this procedure. At this point, it is necessary to point out one more time the lab-scale nature of the membrane synthesis procedure considered for the present study. The use of a more favorable production scale should minimize this contribution, replacing the electricity requirements of the electrical furnace by other alternatives well established in the industry. The high-energy consumption is also the reason that the SM-2 stage contributes around 15% to all the impact categories evaluated. It must be noticed that the electricity used in the studied process is assumed to be supplied by the Spanish electricity mix, having about 60% contribution of non-renewable resources. The incorporation of the fully dense Pd-film (PD-2) generates environmental impacts in all the selected categories due to the consumption of chemical products for the preparation of the required solutions, as well as their agitation. On the other hand, both the SM-1 and the PD-1 produce minimal environmental impacts, since they do not require the use of equipment with high electrical consumption, but only chemical reagents are used.

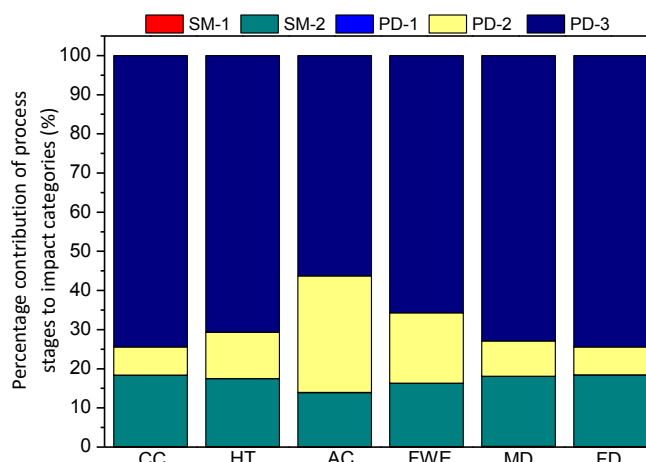


Figure 5. LCA results for MB#01: percentage contribution of process stages to the evaluated impacts categories (CC: Climate Change; HT: Human Toxicity; AC: Acidification; FWE: Freshwater Ecotoxicity; MD: Metal Depletion; FD: fossil fuels depletion)

These results indicate that the environmental impacts associated with the production of MB#01 could be considerably reduced, improving the palladium deposition process, since it accounts for 80% of the total environmental impact. For this reason, the second method of membrane preparation called MB#02 has also been analyzed, to check whether the generation of an intermediate layer of CeO₂ before the deposition of palladium, allows reducing the environmental impact. The results for MB#02 are shown in Figure 6.

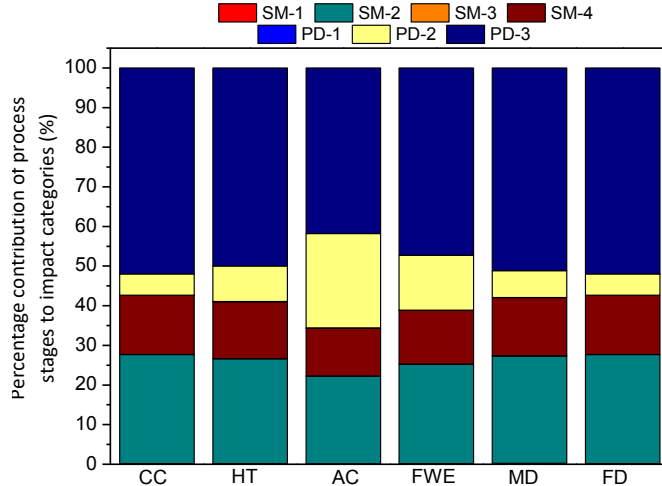


Figure 6. LCA results for MB#02: percentage contribution of process stages to the evaluated impacts categories (CC: Climate Change; HT: Human Toxicity; AC: Acidification; FWE: Freshwater Ecotoxicity; MD: Metal Depletion; FD: fossil fuels depletion).

Again, the stage with the greatest contribution to environmental impacts is PD-3, a stage in which the membrane is washed and dried before incorporating a new layer of palladium, although its impact has been reduced by an average of 20% in the selected categories regarding the MB#01 procedure. This is due to the lower number of cycles, thirteen in this procedure compared to twenty-eight in the MB#01. Therefore, the electrical consumption has been remarkably reduced. This method MB#02, also favors the reduction of the impacts associated with plating (PD-2), specifically in the acidification and freshwater ecotoxicity categories because the amount of chemical reagents necessary to carry out the deposition of palladium is less. The two additional stages of this method (SM-3 and SM-4) only contribute 15% to the environmental impact generated. This new impact generated is mainly due to the calcination of the support.

Table 6. Mid-point indicators of ReCiPe methodology of the different evaluated synthesis procedure (referred to the functional unit: one Pd-membrane with 3 cm in length)

	MB#01	MB#02
ReCiPe indicators	Climate change (kg CO _{2eq})	7467.8
	Human toxicity (kg 1,4-DB _{eq})	630.5
	Terrestrial acidification (kg SO _{2eq})	26.1
	Freshwater ecotoxicity (kg 1,4-DB _{eq})	9.4
	Metal depletion (kg Fe _{eq})	230.6
	Fossil depletion (kg Oil _{eq})	2761.8
		1835.4

Comparing the LCA of the analyzed membranes (Table 6), an average reduction in the environmental impact of around 35% can be observed in the categories evaluated of the MB#02 as compare to MB#01. It can be seen that MB#02, despite being a synthesis procedure with a greater number of stages, to generate an intermediate layer of CeO₂ before palladium deposition, reduces the total environmental impact. Likewise, it should be noted that MB#02 improved its permeation behavior by around 350% compared to MB#01, generating a synergistic effect from an environmental point of view.

Proven the great influence generated by electricity consumption on the environmental impact referred to the functional unit. The specific energy production of each country was taken into account for a comparative objective, due to their different energy sources (Table 2). Figure 7 shows LCA results for the MB#02 preparation process, at a laboratory scale for each country. In a general way, countries with a high contribution of renewable energies provide a more friendly manufacturing process of the functional unit. On the contrary, mix electricity production mainly based on fossil sources generate a higher environmental impact. Therefore, membrane preparation in countries with higher renewables sources can achieve a clean energy vector to a greater extent.

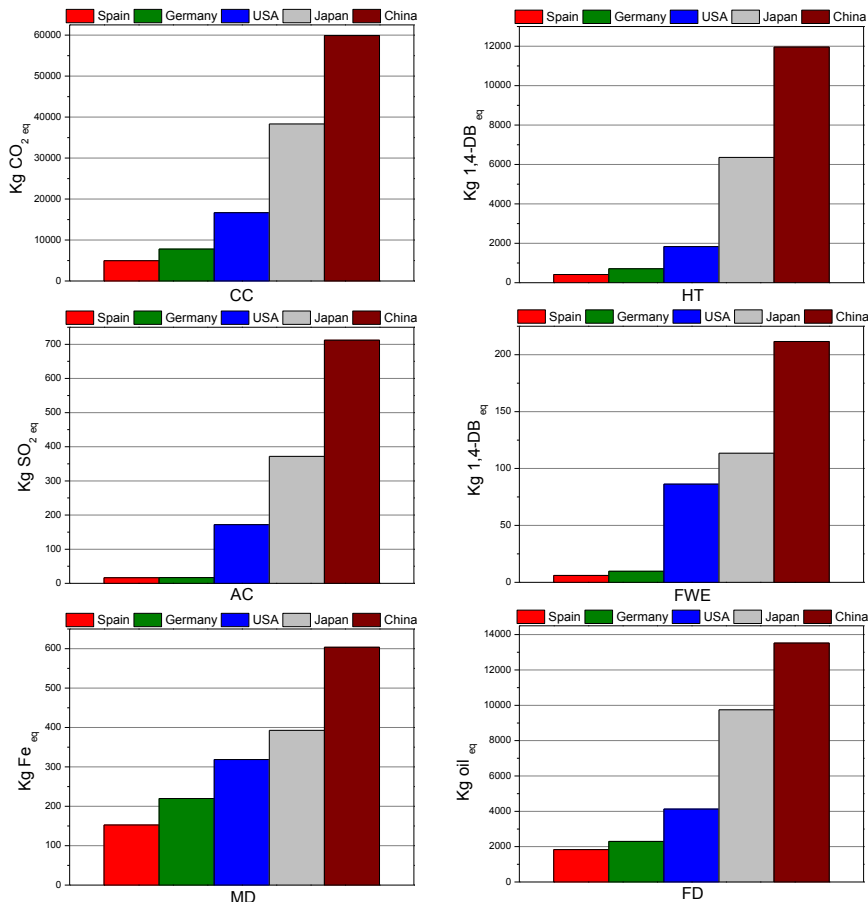


Figure 7. LCA results for the preparation process of membrane MB#02 at lab-scale for different countries. Evaluated environmental impacts: Climate Change (CC), Human Toxicity (HT), Acidification (AC), Freshwater Ecotoxicity (FWE), Metal Depletion (MD) and Fossil-fuels Depletion (FD).

4. Conclusions

This study focuses on the analysis of the environmental impacts generated during the preparation of diverse composite Pd-membranes onto porous stainless steel supports by Electroless Pore-Plating. Two different membrane structures in which the palladium film has been incorporated directly onto the PSS support or after including an additional CeO₂ intermediate layer have been considered. The use of this secondary ceramic barrier allows reducing the required palladium amount to reach a fully dense membrane by 50%, while 350% higher H₂ permeances were obtained. LCA analysis of both manufacturing processes have highlighted the main contributor to the environmental impacts. Specifically, data have shown that cleaning and drying step (PD-3), is the most harmful stage. Principally, due to the multiple cleaning and drying stages that are associated with each of the cycles necessary to achieve a completely dense layer of palladium and the energy consumption that entails. This drawback can get over by incorporation of CeO₂ intermediate layer, with fewer ELP-PP cycles being necessary. The ceria incorporation leads to a better environmental performance of the membrane, reduction in the environmental impact of 35% in the categories evaluated since energy requirements are considerably lower. These energy requirements make the location of the membrane production center to be crucial. Since a high percentage of the environmental impacts generated are associated with the electricity production system. This LCA study has proved that the CeO₂ intermediate layer is certainly an interesting option, not only for their lower environmental impacts but also as it has significantly higher H₂ permeance than MB#01, generating a synergistic effect from an environmental point of view.

Acknowledgments

The authors acknowledge the financial support achieved from the Spanish government through the competitive project ENE2017-83696-R and funds received from Young Researchers R&D Project Ref. M2182 - MEMRESPIP - financed by the Community of Madrid and Rey Juan Carlos University.

References

- [1] X.-L. YUE, Q.-X. GAO, Contributions of natural systems and human activity to greenhouse gas emissions, *Adv. Clim. Chang. Res.* 9 (2018) 243–252. doi:10.1016/J.ACCRE.2018.12.003.
- [2] N.Z. Muradov, T.N. Veziroğlu, “Green” path from fossil-based to hydrogen economy: An overview of carbon-neutral technologies, *Int. J. Hydrogen Energy.* 33 (2008) 6804–6839. doi:10.1016/j.ijhydene.2008.08.054.
- [3] Y. Cai, C.Y. Sam, T. Chang, Nexus between clean energy consumption, economic growth and CO₂ emissions, *J. Clean. Prod.* 182 (2018) 1001–1011. doi:10.1016/J.JCLEPRO.2018.02.035.
- [4] P.-Y. Chen, S.-T. Chen, C.-S. Hsu, C.-C. Chen, Modeling the global relationships among economic growth, energy consumption and CO₂ emissions, *Renew. Sustain. Energy Rev.* 65 (2016) 420–431. doi:10.1016/J.RSER.2016.06.074.
- [5] M.A. Aktar, M.M. Alam, A.Q. Al-Amin, Global economic crisis, energy use, CO₂ emissions, and policy roadmap amid COVID-19, *Sustain. Prod. Consum.* 26 (2021) 770–781. doi:10.1016/j.spc.2020.12.029.
- [6] P. Jiang, Y. Van Fan, J.J. Klemeš, Impacts of COVID-19 on energy demand and consumption: Challenges, lessons and emerging opportunities, *Appl. Energy.* 285 (2021). doi:10.1016/j.apenergy.2021.116441.
- [7] A. Abu-Rayash, I. Dincer, Analysis of the electricity demand trends amidst the COVID-19 coronavirus pandemic, *Energy Res. Soc. Sci.* 68 (2020) 101682. doi:10.1016/j.erss.2020.101682.

- [8] B.K. Sovacool, D. Furszyfer Del Rio, S. Griffiths, Contextualizing the Covid-19 pandemic for a carbon-constrained world: Insights for sustainability transitions, energy justice, and research methodology, *Energy Res. Soc. Sci.* 68 (2020) 101701. doi:10.1016/j.erss.2020.101701.
- [9] A.N. Corpus-Mendoza, H.S. Ruiz-Segoviano, S.F. Rodriguez-Contreras, D. Yañez-Dávila, A. Hernández-Granados, Decrease of mobility, electricity demand, and NO₂ emissions on COVID-19 times and their feedback on prevention measures, *Sci. Total Environ.* 760 (2021) 143382. doi:10.1016/j.scitotenv.2020.143382.
- [10] J.E. Szulejko, P. Kumar, A. Deep, K.-H. Kim, Global warming projections to 2100 using simple CO₂ greenhouse gas modeling and comments on CO₂ climate sensitivity factor, *Atmos. Pollut. Res.* 8 (2017) 136–140. doi:10.1016/J.APR.2016.08.002.
- [11] A. Saeedmanesh, M.A. Mac Kinnon, J. Brouwer, Hydrogen is essential for sustainability, *Curr. Opin. Electrochem.* 12 (2018) 166–181. doi:10.1016/j.colec.2018.11.009.
- [12] C. Furlan, C. Mortarino, Forecasting the impact of renewable energies in competition with non-renewable sources, *Renew. Sustain. Energy Rev.* 81 (2018) 1879–1886. doi:<https://doi.org/10.1016/j.rser.2017.05.284>.
- [13] D. Parra, L. Valverde, F.J. Pino, M.K. Patel, A review on the role, cost and value of hydrogen energy systems for deep decarbonisation, *Renew. Sustain. Energy Rev.* 101 (2019) 279–294. doi:10.1016/J.RSER.2018.11.010.
- [14] B. Lux, B. Pfluger, A supply curve of electricity-based hydrogen in a decarbonized European energy system in 2050, *Appl. Energy*. 269 (2020) 115011. doi:10.1016/j.apenergy.2020.115011.
- [15] G. Kakoulaki, I. Kougias, N. Taylor, F. Dolci, J. Moya, A. Jäger-Waldau, Green hydrogen in Europe – A regional assessment: Substituting existing production with electrolysis powered by renewables, *Energy Convers. Manag.* 228 (2021). doi:10.1016/j.enconman.2020.113649.
- [16] N.A. Pambugi, K. Itaoka, A. Kurosawa, N. Yamakawa, Impact of Hydrogen fuel for CO₂ Emission Reduction in Power Generation Sector in Japan, *Energy Procedia*. 105 (2017) 3075–3082. doi:10.1016/j.egypro.2017.03.642.
- [17] A. Ozawa, Y. Kudo, A. Murata, T. Honda, I. Saita, H. Takagi, Hydrogen in low-carbon energy systems in Japan by 2050: The uncertainties of technology development and implementation, *Int. J. Hydrogen Energy*. 43 (2018) 18083–18094. doi:10.1016/j.ijhydene.2018.08.098.
- [18] S.Z. Baykara, Hydrogen: A brief overview on its sources, production and environmental impact, *Int. J. Hydrogen Energy*. 43 (2018) 10605–10614. doi:10.1016/j.ijhydene.2018.02.022.
- [19] D.H. Choi, S.M. Chun, S.H. Ma, Y.C. Hong, Production of hydrogen-rich syngas from methane reforming by steam microwave plasma, *J. Ind. Eng. Chem.* 34 (2016) 286–291. doi:10.1016/j.jiec.2015.11.019.
- [20] C. Coutanceau, S. Baranton, T. Audichon, Chapter 2 - Hydrogen Production From Thermal Reforming BT - Hydrogen Electrochemical Production, in: *Hydrog. Energy Fuel Cells Prim.*, Academic Press, 2018: pp. 7–15. doi:<https://doi.org/10.1016/B978-0-12-811250-2.00002-9>.
- [21] C.-H. Kim, J.-Y. Han, H. Lim, K.-Y. Lee, S.-K. Ryi, Methane steam reforming using a membrane reactor equipped with a Pd-based composite membrane for effective hydrogen production, *Int. J. Hydrogen Energy*. (2017). doi:<https://doi.org/10.1016/j.ijhydene.2017.10.054>.
- [22] T. Detchusanand, K. Im-orb, P. Ponpesh, A. Arpornwichanop, Biomass gasification integrated with CO₂ capture processes for high-purity hydrogen production: Process performance and energy analysis, *Energy Convers. Manag.* 171 (2018) 1560–1572. doi:10.1016/j.enconman.2018.06.072.
- [23] H. Yin, A.C.K. Yip, A Review on the Production and Purification of Biomass-Derived Hydrogen Using Emerging Membrane Technologies, *Catal.* . 7 (2017). doi:10.3390/catal7100297.
- [24] P. Nikolaidis, A. Poulikkas, A comparative overview of hydrogen production processes, *Renew. Sustain. Energy Rev.* 67 (2017) 597–611. doi:10.1016/j.rser.2016.09.044.
- [25] B. Zornoza, C. Casado, A. Navajas, Chapter 11 - Advances in Hydrogen Separation and Purification with Membrane Technology, in: L.M. Gandía, G. Arzamendi, P.M. Diéguez (Eds.), *Renew. Hydrog. Technol.*, Elsevier, Amsterdam, 2013: pp. 245–268. doi:<http://dx.doi.org/10.1016/B978-0-444-56352-1.00011-8>.
- [26] G. Bernardo, T. Araújo, T. da Silva Lopes, J. Sousa, A. Mendes, Recent advances in membrane technologies for hydrogen purification, *Int. J. Hydrogen Energy*. (2020). doi:10.1016/j.ijhydene.2019.06.162.
- [27] R.P. Sholl, D.S.; Lively, Seven chemical separation to change the world, *Nature*. 532 (2016) 435–437.
- [28] and M.W. Wim Elseviers, Paula Flowers Hassett, Jean-Louis Navarre, 50 Years of PSA Technology for H₂ Purification, UOP. (2015). <https://www.uop.com/?document=psa-50-paper&download=1>.
- [29] A. Mivechian, M. Pakizeh, Performance Comparison of Different Separation Systems for H₂ Recovery from Catalytic Reforming Unit Off-Gas Streams, *Chem. Eng. Technol.* 36 (2013) 519–527. doi:10.1002/ceat.201200558.
- [30] C. Voss, Applications of pressure swing adsorption technology, *Adsorption*. 11 (2005) 527–529. doi:10.1007/s10450-005-5979-3.
- [31] D. Alique, D. Martinez-Diaz, R. Sanz, J.A. Calles, Review of supported pd-based membranes preparation by electroless plating for ultra-pure hydrogen production, 2018. doi:10.3390/membranes8010005.
- [32] A. Brunetti, A. Caravella, E. Drioli, G. Barbieri, CHAPTER 1. Membrane Reactors for Hydrogen Production, 2 (2017) 1–29. doi:10.1039/9781788010443-00001.
- [33] S. Liguori, K. Kian, N. Buggy, B.H. Anzelmo, J. Wilcox, Opportunities and Challenges of Low-Carbon Hydrogen via Metallic Membranes, *Prog. Energy Combust. Sci.* 80 (2020) 100851. doi:10.1016/j.pecs.2020.100851.
- [34] Z. Cao, H. Jiang, H. Luo, S. Baumann, W.A. Meulenberg, H. Voss, J. Caro, Simultaneous overcome of the equilibrium limitations in BSCF oxygen-permeable membrane reactors: Water splitting and methane coupling, *Catal. Today*. 193 (2012) 2–7. doi:10.1016/j.cattod.2011.12.018.
- [35] F. Gallucci, E. Fernandez, P. Corengia, M. van Sint Annaland, Recent advances on membranes and membrane reactors for hydrogen

- production, *Chem. Eng. Sci.* 92 (2013) 40–66. doi:<http://dx.doi.org/10.1016/j.ces.2013.01.008>.
- [36] S. Karagöz, T.T. Tsotsis, V.I. Manousiouthakis, Multi-scale model based design of membrane reactor/separator processes for intensified hydrogen production through the water gas shift reaction, *Int. J. Hydrogen Energy.* (2020). doi:10.1016/j.ijhydene.2019.05.118.
- [37] A. Arratibel Plazaola, D. Pacheco Tanaka, M. Van Sint Annaland, F. Gallucci, A.A. Plazaola, D.A.P. Tanaka, M.V.S. Annaland, F. Gallucci, Recent advances in pd-based membranes for membrane reactors, *Molecules.* 22 (2017) 1–53. doi:10.3390/molecules22010051.
- [38] J.J. Conde, M. Maroño, J.M. Sánchez-Hervás, Pd-Based Membranes for Hydrogen Separation: Review of Alloying Elements and Their Influence on Membrane Properties, *Sep. Purif. Rev.* 46 (2017) 152–177. doi:10.1080/15422119.2016.1212379.
- [39] J.A. Calles, R. Sanz, D. Alique, L. Furones, Thermal stability and effect of typical water gas shift reactant composition on {H₂} permeability through a Pd-YSZ-PSS composite membrane, *Int. J. Hydrogen Energy.* 39 (2014) 1398–1409. doi:<http://dx.doi.org/10.1016/j.ijhydene.2013.10.168>.
- [40] S. Yun, S. Ted Oyama, S.T. Oyama, Correlations in palladium membranes for hydrogen separation: A review, *J. Memb. Sci.* 375 (2011) 28–45. doi:<http://dx.doi.org/10.1016/j.memsci.2011.03.057>.
- [41] A.M. Tarditi, M.L. Bosko, L.M. Cornaglia, Electroless plating of Pd binary and ternary alloys and surface characteristics for application in hidrogen separation, in: Elsevier, Oxford, 2017; pp. 1–24. doi:<https://doi.org/10.1016/B978-0-12-803581-8.09166-9>.
- [42] J. Melendez, E. Fernandez, F. Gallucci, M. van Sint Annaland, P.L. Arias, D.A. Pacheco Tanaka, D.A.P. Tanaka, Preparation and characterization of ceramic supported ultra-thin (~1 μm) Pd-Ag membranes, *J. Memb. Sci.* 528 (2017) 12–23. doi:<http://dx.doi.org/10.1016/j.memsci.2017.01.011>.
- [43] M. Dogan, S. Kilicarslan, Effects of process parameters on the synthesis of palladium membranes, *Nucl. Instruments Methods Phys. Res. Sect. B Beam Interact. with Mater. Atoms.* 266 (2008) 3458–3466. doi:<https://doi.org/10.1016/j.nimb.2008.05.011>.
- [44] R.S. Souleimanova, A.S. Mukasyan, A. Varma, Effects of osmosis on microstructure of Pd-composite membranes synthesized by electroless plating technique, *J. Memb. Sci.* 166 (2000) 249–257. doi:[http://dx.doi.org/10.1016/S0376-7388\(99\)00268-9](http://dx.doi.org/10.1016/S0376-7388(99)00268-9).
- [45] M. G.O., H. J.B., Electroless plating: fundamentals and applications, American Electroplaters and Surface Finishers Society, 1990.
- [46] D. Alique, R. Sanz, J.A. Calles, Pd membranes by electroless pore-plating: synthesis and permeation behavior, *Curr. Trends Futur. Dev. Memb.* (2020) 31–62. doi:10.1016/B978-0-12-818332-8.00002-8.
- [47] E. Tosto, D. Alique, D. Martinez-Diaz, R. Sanz, J.A.A. Calles, A. Caravella, J.A.A. Medrano, F. Gallucci, Stability of pore-plated membranes for hydrogen production in fluidized-bed membrane reactors, *Int. J. Hydrogen Energy.* 45 (2020) 7374–7385. doi:10.1016/j.ijhydene.2019.04.285.
- [48] R. Sanz, J.A. Calles, D. Alique, L. Furones, New synthesis method of Pd membranes over tubular {PSS} supports via “pore-plating” for hydrogen separation processes, *Int. J. Hydrogen Energy.* 37 (2012) 18476–18485. doi:<http://dx.doi.org/10.1016/j.ijhydene.2012.09.084>.
- [49] D. Yépes, L.M. Cornaglia, S. Irusta, E.A. Lombardo, Different oxides used as diffusion barriers in composite hydrogen permeable membranes, *J. Memb. Sci.* 274 (2006) 92–101. doi:<http://dx.doi.org/10.1016/j.memsci.2005.08.003>.
- [50] C. Mateos-Pedrero, M.A. Soria, I. Rodriguez-Ramos, A. Guerrero-Ruiz, Modifications of porous stainless steel previous to the synthesis of Pd membranes, in: *Stud. Surf. Sci. Catal.*, 2010; pp. 779–783. doi:10.1016/S0167-2991(10)75159-4.
- [51] L. Zheng, H. Li, H. Xu, “Defect-free” interlayer with a smooth surface and controlled pore-mouth size for thin and thermally stable Pd composite membranes, *Int. J. Hydrogen Energy.* 41 (2016) 1002–1009. doi:10.1016/j.ijhydene.2015.09.024.
- [52] A. Bottino, M. Broglia, G. Capannelli, A. Comite, P. Pinacci, M. Scrinari, F. Azzurri, Sol–gel synthesis of thin alumina layers on porous stainless steel supports for high temperature palladium membranes, *Int. J. Hydrogen Energy.* 39 (2014) 4717–4724. doi:10.1016/j.ijhydene.2013.11.096.
- [53] Ø. Hatlevik, S.K. Gade, M.K. Keeling, P.M. Thoen, A.P.P. Davidson, J.D. Way, Palladium and palladium alloy membranes for hydrogen separation and production: History, fabrication strategies, and current performance, *Sep. Purif. Technol.* 73 (2010) 59–64. doi:<http://dx.doi.org/10.1016/j.seppur.2009.10.020>.
- [54] J.-Y. Han, C.-H. Kim, H. Lim, K.-Y. Lee, S.-K. Ryi, Diffusion barrier coating using a newly developed blowing coating method for a thermally stable Pd membrane deposited on porous stainless-steel support, *Int. J. Hydrogen Energy.* 42 (2017) 12310–12319. doi:<https://doi.org/10.1016/j.ijhydene.2017.03.053>.
- [55] Y. Huang, R. Dittmeyer, Preparation of thin palladium membranes on a porous support with rough surface, *J. Memb. Sci.* 302 (2007) 160–170. doi:10.1016/j.memsci.2007.06.040.
- [56] R. Sanz, J.A. Calles, D. Alique, L. Furones, S. Ordóñez, P. Marín, P. Corengia, E. Fernandez, Preparation, testing and modelling of a hydrogen selective Pd/YSZ/SS composite membrane, *Int. J. Hydrogen Energy.* 36 (2011) 15783–15793. doi:10.1016/j.ijhydene.2011.08.102.
- [57] D. Martinez-Diaz, R. Sanz, J.A. Calles, D. Alique, H₂ permeation increase of electroless pore-plated Pd/PSS membranes with CeO₂ intermediate barriers, *Sep. Purif. Technol.* 216 (2019) 16–24. doi:10.1016/J.SEPPUR.2019.01.076.
- [58] D. Martinez-Diaz, D. Alique, J.A.A. Calles, R. Sanz, Pd-thickness reduction in electroless pore-plated membranes by using doped-ceria as interlayer, *Int. J. Hydrogen Energy.* 45 (2020) 7278–7289. doi:10.1016/j.ijhydene.2019.10.140.
- [59] S.-K. Ryi, H.-S. Ahn, J.-S. Park, D.-W. Kim, Pd–Cu alloy membrane deposited on CeO₂ modified porous nickel support for hydrogen separation, *Int. J. Hydrogen Energy.* 39 (2014) 4698–4703. doi:<https://doi.org/10.1016/j.ijhydene.2013.11.031>.
- [60] A. Arratibel, J.A. Medrano, J. Melendez, D.A. Pacheco Tanaka, M. van Sint Annaland, F. Gallucci, Attrition-resistant membranes for fluidized-bed membrane reactors: Double-skin membranes, *J. Memb. Sci.* 563 (2018) 419–426. doi:10.1016/j.memsci.2018.06.012.
- [61] A. Arratibel, A. Pacheco Tanaka, I. Laso, M. van Sint Annaland, F. Gallucci, Development of Pd-based double-skinned membranes for hydrogen production in fluidized bed membrane reactors, *J. Memb. Sci.* 550 (2018) 536–544.

- doi:10.1016/J.MEMSCI.2017.10.064.
- [62] K. Simonen, Life cycle assessment, *Life Cycle Assess.* (2014) 1–159. doi:10.4324/9781315778730.
- [63] M. Finkbeiner, A. Inaba, R.B.H. Tan, K. Christiansen, H.-J. Klüppel, The New International Standards for Life Cycle Assessment, *Int. J. Life Cycle Assess.* 11 (2006) 80–85. doi:10.1065/lca2006.02.002.
- [64] R. Turconi, A. Boldrin, T. Astrup, Life cycle assessment (LCA) of electricity generation technologies: Overview, comparability and limitations, *Renew. Sustain. Energy Rev.* 28 (2013) 555–565. doi:10.1016/j.rser.2013.08.013.
- [65] E. Igos, B. Rugani, S. Rege, E. Benetto, L. Drouet, D.S. Zachary, Combination of equilibrium models and hybrid life cycle-input-output analysis to predict the environmental impacts of energy policy scenarios, *Appl. Energy.* 145 (2015) 234–245. doi:10.1016/j.apenergy.2015.02.007.
- [66] G. Di Marcoberardino, M. Binotti, G. Manzolini, J.L. Viviente, A. Arratibel, L. Roses, F. Gallucci, Achievements of European projects on membrane reactor for hydrogen production, *J. Clean. Prod.* 161 (2017) 1442–1450. doi:<https://doi.org/10.1016/j.jclepro.2017.05.122>.
- [67] L. Furones, D. Alique, Interlayer Properties of In-Situ Oxidized Porous Stainless Steel for Preparation of Composite Pd Membranes, *ChemEngineering.* 2 (2017) 1. doi:10.3390/chemengineering2010001.
- [68] M. Maroño, G. D'Alessandro, A. Morales, D. Martínez-Díaz, D. Alique, J.M. Sánchez, Influence of Si and Fe/Cr oxides as intermediate layers in the fabrication of supported Pd membranes, *Sep. Purif. Technol.* 234 (2020). doi:10.1016/j.seppur.2019.116091.
- [69] J.A. Calles, R. Sanz, D. Alique, L. Furones, P. Marin, S. Ordoñez, Influence of the selective layer morphology on the permeation properties for Pd-PSS composite membranes prepared by electroless pore-plating: Experimental and modeling study, *Sep. Purif. Technol.* 194 (2018) 10–18. doi:<https://doi.org/10.1016/j.seppur.2017.11.014>.
- [70] D. Alique, Processing and Characterization of Coating and Thin Film Materials, in: J. Zhang, Y. Jung (Eds.), *Adv. Ceram. Met. Coat. Thin Film Mater. Energy Environ.*, 2018. doi:10.1007/978-3-319-59906-9.
- [71] E.L. Sistema, Informe 2019 Red Electrica Española, (2019).
- [72] BDEW, Die Energiesversorgung 2020 – Jahresbericht, (2020). https://www.bdew.de/media/documents/Jahresbericht_2020_20201218.pdf.
- [73] US Energy Information Administration (EIA), Country Analysis Executive Summary: China, (2020) 9. https://www.eia.gov/international/content/analysis/countries_long/China/china.pdf.
- [74] A. Yanagisawa, R. Ikarii, S. Iwata, I.H. Hwang, K. Tomokawa, Y. Shibata, K. Ito, Economic and Energy Outlook of Japan for FY2015, (2014) 1–28. <http://eneken.ieej.or.jp/data/5903.pdf>.
- [75] EIA, Short-Term Energy Outlook (STEO) Forecast highlights, US EIA - Short-Term Energy Outlook. (2020) 1–53. <https://www.eia.gov/outlooks/steo/report/electricity.php>.
- [76] M.A.J. Huijbregts, Z.J.N. Steinmann, P.M.F. Elshout, G. Stam, F. Verones, M. Vieira, M. Zijp, A. Hollander, R. van Zelm, ReCiPe2016: a harmonised life cycle impact assessment method at midpoint and endpoint level, *Int. J. Life Cycle Assess.* 22 (2017) 138–147. doi:10.1007/s11367-016-1246-y.
- [77] M.A.J. Huijbregts, S. Hellweg, R. Frischknecht, H.W.M. Hendriks, K. Hungerbühler, A.J. Hendriks, Cumulative Energy Demand As Predictor for the Environmental Burden of Commodity Production, *Environ. Sci. Technol.* 44 (2010) 2189–2196. doi:10.1021/es902870s.
- [78] A. Caravella, S. Hara, E. Drioli, G. Barbieri, Sieverts law pressure exponent for hydrogen permeation through Pd-based membranes: Coupled influence of non-ideal diffusion and multicomponent external mass transfer, *Int. J. Hydrogen Energy.* 38 (2013) 16229–16244. doi:10.1016/j.ijhydene.2013.09.102.
- [79] M. Vadrucci, F. Borgognoni, A. Moriani, A. Santucci, S. Tosti, Hydrogen permeation through Pd–Ag membranes: Surface effects and Sieverts' law, *Int. J. Hydrogen Energy.* 38 (2013) 4144–4152. doi:<http://dx.doi.org/10.1016/j.ijhydene.2013.01.091>.
- [80] S. Bellini, G. Azzato, A. Caravella, Mass transport in hydrogen permeation through Pd-based membranes, *Curr. Trends Futur. Dev. Membr.* (2020) 63–90. doi:10.1016/B978-0-12-818332-8.00003-X.
- [81] D. Martínez-Díaz, D. Martínez del Monte, E. García-Rojas, D. Alique, J.A. Calles, R. Sanz, Comprehensive permeation analysis and mechanical resistance of electroless pore-plated Pd-membranes with ordered mesoporous ceria as intermediate layer, *Sep. Purif. Technol.* 258 (2021) 118066. doi:10.1016/j.seppur.2020.118066.



Stability of electroless pore-plated Pd-membranes in acetic acid steam membrane-reformers for ultra-pure hydrogen production

G. Adduci^{a,b}, D. Martínez-Díaz^b, D. Sanz-Villanueva^b, A. Caravella^a, J.A. Calles^b, R. Sanz^c, D. Alique^{b,*}

^a Department of Computer Engineering, Modelling, Electronics and Systems Engineering (DIMES), University of Calabria, Via P. Bucci, Cubo 44A, Rende, CS 87036, Italy

^b Department of Chemical, Energy and Mechanical Technology, Rey Juan Carlos University, C/ Tulipán s/n, 28933 Móstoles, Spain

^c Department of Chemical and Environmental Technology, Rey Juan Carlos University, C/ Tulipán s/n, 28933 Móstoles, Spain



ARTICLE INFO

Keywords:
Acetic acid
Steam reforming
Membrane
Palladium
Electroless plating
Hydrogen production

ABSTRACT

Electroless Pore-Plated (ELP-PP) membranes were successfully incorporated for the first time into a membrane reactor to produce hydrogen by acetic acid steam reforming (AASR), exhibiting adequate resistance against harsh operating conditions. Membranes were prepared onto tubular PSS supports modified with Pd/CeO₂ particles and scaled-up around four times in length with high reproducibility respect previous studies. H₂ permeances from 4.49 to 5.67·10⁻⁴ mol m⁻² s⁻¹ Pa^{0.5} were found for pure H₂ at 350–450 °C, decreasing for mixtures due to concentration-polarization at higher pressures but also certain inhibition caused by CO₂ at pressures below 50 Pa^{0.5}. The combination of membranes with Ni/SBA-15 catalysts in packed-bed membrane reactors (PBMR) evidenced the simultaneous improvement of acetic acid conversion and hydrogen yield respect to analogous experiments in traditional packed-bed reactors (PBR). A very similar product distribution was obtained for both configurations, PBR and PBMR, when using fresh catalysts, although marked deviations were found in case of regenerating the catalysts. Then, higher selectivity towards coke reached for PBMR, which lead to around 30% for the most elevated pressure under investigation. However, even at these harsh conditions, the mechanical integrity of ELP-PP membranes was maintained. Thus, the benefits of combining catalysts and ELP-PP membranes in a PBMR for AASR were demonstrated.

1. Introduction

The promotion of hydrogen for energy applications expects to replace the massive use of fossil fuels in the near-middle future, thus reducing the current high levels of anthropogenic carbon dioxide and other emissions, responsible for global warming and health problems in humans [1,2]. Among other alternatives, hydrogen could be obtained from a wide variety of feedstock and technologies, providing a tremendous competitive advantage for a progressive transition from traditional to renewable energy sources in both concentrated or decentralized centers [3,4]. Particularly, mature thermochemical routes such as steam reforming, pyrolysis, or gasification are mainly fed by fossil fuels in industry. However, all of them can be easily adapted for working with renewable, i.e. bio-ethanol, bio-gas or, in general, biomass [5–7], and residual feedstock, i.e. agricultural, industrial or municipal wastes [8,9].

In this context, a combination of thermochemical and biological processes, i.e. steam reforming of gaseous product streams from algae

liquefaction, has been proposed as an interesting alternative [10,11]. In practice, most of these studies optimize both catalyst design and operating conditions for some model compounds that simulate fairly well the behavior of real complex mixtures containing multiple molecules [12]. This is the particular case of acetic acid (AA), usually considered as an excellent model compound to prepare a synthetic aqueous fraction coming from bio-oil production [12–15]. However, even though steam reforming of light hydrocarbons has been widely investigated [16–19], particular conditions for using acetic acid or related aqueous phases containing this compound are still under investigation.

One of the first references appeared in 2004 when Takanabe et al. published the use of acetic acid as a model oxygenate for steam reforming of bio-oil with Pt/ZrO₂ catalysts [20]. They evidenced an almost complete acetic acid conversion and hydrogen yield close to thermodynamic equilibrium but noted a significant catalyst deactivation by forming of oligomers, which blocked active sites. Basagiannis and Verykios adopted a similar strategy with acetic acid as a model compound of a synthetic bio-oil to study its reaction network under

* Corresponding author.

E-mail address: david.alique@urjc.es (D. Alique).

steam reforming with a Ni-based catalyst [21]. They found that decomposition and ketonization became relevant together with the main steam reforming reactions, especially at intermediate temperatures. Moreover, despite the presence of Ni, the catalyst promoted steam reforming reactions while shifting its activity towards lower temperatures and retarding the coke deposition rate onto the catalyst surface. However, significant deactivation was observed at particularly low temperatures. Iwasa et al. compared the catalytic activity for these reactions in mesoporous materials containing various metals as active-phase, establishing a decreasing AA conversion for the series Pt > Pt/Ni > Ni, although maintaining comparable H₂ production levels for all the catalysts [22]. Thaicharoenutcharittham et al. analyzed in detail the catalytic activity of diverse Ni-based materials as a function of the metal loading, concluding a strong relationship between both factors [23]. An et al. performed a similar study at $T = 600\text{ }^{\circ}\text{C}$, $P = 1\text{ atm}$, $\text{H}_2\text{O}/\text{AA} = 4$, and $\text{WHSV} = 5.01\text{ g}_{\text{AA}}\text{ g}_{\text{catalyst}}^{-1}\text{ h}^{-1}$, evidencing again the above-mentioned influence of Ni loading on both catalytic activity and carbon formation [24]. Particularly, the amount of deposited carbide-like carbon decreased, and graphitic-like carbon increased with Ni loading from 9 to 15 wt%, thus selecting an intermediate content (12 wt %) as best conditions for the catalyst performance.

Other works also evaluated the hydrogen production by acid acetic steam reforming (AASR) at mild-temperatures in the presence of a wide variety of catalysts containing Ni as active metal but over diverse substrates, especially attending critical aspects such as conversion, hydrogen yield, and deactivation by coke formation [25–31]. In this context, Chen et al. aimed to gather together the results reached with different catalysts and published a critical review on the main catalysts used for AASR, including fabrication strategies, mechanic understanding, and most frequent catalyst deactivation processes [32]. Besides both AASR operating conditions and metal loading in catalysts, the intrinsic effect of the metal precursors on the final behavior of catalysts was also suggested [33]. Moreover, the addition of other metals as co-active phases in Ni-based catalysts shown a clear impact on both reaction performance and formation of reaction intermediates [34–37]. The research group headed by Calles has also published diverse works addressing the synthesis of multiple Ni-based catalysts supported over SBA-15 and their application for hydrogen production via steam reforming from ethanol [38,39], glycerol [40,41], or acetic acid [11,42,43].

All the above-mentioned studies were carried out in traditional packed-bed reactors, where a certain amount of catalyst was placed in the lumen, and produced hydrogen must be later purified in independent equipment [5,44,45]. The combination of both stages in a single membrane reactor, until our best knowledge, very scarce up to now. This fact contrasts other processes in which ultra-pure hydrogen is generated and separated in-situ in a new reactor configuration by selective permeation through the reactor wall acting as a membrane, usually made of pure palladium or Pd-based alloys [46,47]. Basile et al. studied the effect of the catalytic bed pattern in AASR in a membrane reactor by using two different commercial catalysts based on Ni and Ru as active metals from Engelhard and Johnson Matthey, respectively, and an unsupported thick Pd₇Ag₂₃ membrane with around 50 μm, demonstrating its experimental viability [48]. Iulianelli et al. expanded this preliminary study focusing on the influence of the different flow configurations inside the membrane reactor, as well as the sweep factor and the reaction itself [49]. They recently reported these results and most of the available literature about previous studies for AASR in traditional reactors instead of those carried out in membrane reactors [50].

However, it should be noted that noticeably advances in the development of new Pd-supported membranes are produced during the last years [51,52], mainly aimed to reduce their metal thickness and to increase both H₂ permeation and stability, thus being highly recommended their test in membrane reactor applications. Among others, Electroless Pore-Plated (ELP-PP) membranes have evidenced an

excellent performance for a wide variety of experimental conditions during permeation tests with metal thicknesses in the range 10–20 μm, also including contrary directions for the permeate flux, which could cause tensile stress and possible delamination of other traditional palladium top coatings and intermediate layers [53]. However, their evaluation should be completed with more complex gas mixtures, typical of common industrial applications, as well as in real membrane reactor conditions. In this context, the behavior of ELP-PP membranes has been recently evaluated in both fixed and fluidized bed membrane reactors for a relatively simple H₂ production process via water gas shift reaction (WGS), in which carbon monoxide reacts with steam water to be completely oxidized into carbon dioxide while generating additional hydrogen. This reaction, carried out at mild conditions ($T = 300\text{--}450\text{ }^{\circ}\text{C}$ and simple gas mixtures), typically appears after any reformer to adjust the composition of the syngas for each particular application. From the above-mentioned experiments, the mechanical stability of ELP-PP membranes was ensured in real conditions [54]. However, two important issues should be considered at this point. First, the analyzed membranes in the above-mentioned study lack any ceramic intermediate layer and, as a consequence, they were thicker than the most recent ones, all of them prepared onto modified porous stainless steel (PSS) supports with CeO₂ intermediate layers but still not tested into real membrane reactor devices [55,56]. Second, it should also be taken into account that the most interesting thermochemical reactions for hydrogen production, i.e. gasification or steam reforming, usually involve complex reaction schemes in which appear multiple compounds, not only H₂, CO, or CO₂ as occurring in the WGS. Therefore, combining these recent ELP-PP membranes with the above-mentioned processes could attract great interest for both researchers and industrial stakeholders.

Under these premises, the present study analyzes for the first time the combination of a heterogeneous Ni/SBA-15 catalyst with ELP-PP composite Pd-membranes prepared onto CeO₂/PSS supports in a tubular packed-bed membrane reactor for H₂ production via acetic acid steam reforming. First, the available characterization of this type of membranes is completed after scaling-up their length around four times, including their behavior against CO₂-rich gas mixtures. All main operating conditions for AASR (temperature, pressure, and gas hourly space velocity) are evaluated in both traditional and membrane reactor configurations, also considering catalysts deactivation by coke formation and their regeneration.

2. Experimental procedure

2.1. Membrane preparation

The composite Pd-based membranes applied for this study have been prepared using modified tubular AISI 316L porous stainless-steel (PSS) supports, purchased from Mott Metallurgical Corporation with 0.1 μm media grade pore size and symmetric structure. The supports were modified by adding an outer coat of dense CeO₂ particles as an intermediate layer and following by incorporating a top palladium film by Electroless Pore-Plating (ELP-PP). The original PSS supports were first cut into pieces of 70 mm in length, welding two dense stainless-steel tubes of 20 mm in length on each extreme (total length of tubes 110 mm) and cleaning the surface by successive immersions in sodium hydroxide (0.1 M, 5 min), hydrochloric acid (0.1 M, 5 min) and ethanol (96 vol%, 15 min) at 60 °C under ultrasonic stirring. After completely drying the supports (110 °C for at least 8 h), the composite membranes were prepared by following the general procedure described elsewhere [55,56], adapted to the new length of supports, around four times larger than previous ones. Briefly, the supports were calcined at 600 °C for 12 h in air atmosphere to generate a first thin top layer of Fe/Cr oxides [57] and then further modified with the incorporation of dense CeO₂ particles (average particle diameter of around 100 nm, Alfa-Caeser) by Vacuum-Assisted Dip-Coating (VA-DC) and calcination at

500 °C for 5 h [55]. These CeO₂ particles, doped with fine Pd-nuclei before to be incorporated onto the porous support, expect to reduce both pore mouth size and average external surface roughness before the palladium plating while preventing any possible metal interdiffusion between support and palladium [56]. Finally, the Pd topcoat was deposited by ELP-PP following the detailed procedure published elsewhere [53,55,56]. The Pd precursor, PdCl₂ from Sigma-Aldrich (99 w.% purity, with 60% palladium content), is complexed with NH₄OH (Scharlau, 32 vol%) and a certain amount of Na₂EDTA (Scharlau) as stabilizer, reacting with N₂H₄ (Scharlau, 99 w.% purity diluted up to 0.2 M) in a controlled autocatalytic chemical reaction to reduce Pd²⁺ ions into Pd⁰. It should be noted that both metal precursor and reducing solutions were added from opposite sides of the modified porous substrate to prevail the reaction just inside the pores or vicinities.

2.2. Membrane characterization: morphological analysis and permeation tests

The morphology of composite membranes included in this study was analyzed by scanning electron microscopy (Hitachi S-2100N, equipped with an energy dispersive analytical system for microprobe analysis) and optical profilometry (Zeta-20 Optical Profiler). Gravimetric analyses from a Kern electronic balance type ABS 220-4 (accuracy of ± 0.001 g) were also used to obtain the weight gain of the membrane after each preparation step. The reproducibility of the process and the estimated Pd-thickness by considering homogeneous incorporation around the external surface of supports were determined from these data. For this purpose, good reproducibility was assumed for similar membrane weight gains after calcination and incorporation of CeO₂ particles and Pd-film.

Moreover, a series of permeation tests were also carried out to evaluate the particular behavior of these membranes. Fig. 1 shows the experimental setup used for these tests, which was also employed to perform the reaction tests described later.

The apparatus is formed by a cylindrical 316L stainless steel cell where a tubular Pd-based membrane can be placed between two graphite O-rings to separate both retentate and permeate zones. This cell is housed inside an electric furnace with three independent heating resistances that accurately control the working temperature during experiments along the axial direction. The feed stream can be properly adjusted by several Bronkhorst Hi-Tech mass-flow controllers mounted in H₂, N₂, and CO₂ inlet lines. Permeate or retentate flow-rates were measured by using a drum-type gas flow-meter Ritter TG 05/5 with an accuracy of ± 0.5% (minimum detection limit of around 17 mL min⁻¹). In case of reaching very low fluxes for any retentate or permeate streams, this equipment was replaced by a Ritter Mili-GasCounter able to detecting volumetric flow-rates from 1.67·10⁻² mL min⁻¹. On the other hand, the operating pressure is controlled by a Bronkhorst Hi-Tech EL-PRESS back-pressure regulator (0–10 bar), whereas the permeate stream is always maintained at atmospheric conditions. Finally, the equipment is also equipped with a gas chromatograph (GC) Varian CP-4900 with a thermal conductivity detector (TCD) and two analytical Molsieve 5 Å and Poraplot-Q columns.

The standard procedure followed in permeation tests includes some preliminary bubble leak tests to ensure the absence of defects in the composite membranes before being placed inside the permeation cell. For that, each membrane is first sealed with appropriate O-rings and immersed into ethanol, where helium is fed to the lumen side up to reach at least 3 bar while maintaining the retentate stream completely closed. In this manner, helium molecules only can pass through eventual defects on the palladium film. Only membranes in which no bubbles are detected during this preliminary test and the selected pressure is maintained for at least 30 min are mounted in the previously described permeation setup for testing at higher temperatures.

After that, a series of single gas permeation experiments with both pure nitrogen and hydrogen were carried out at different temperatures

in the range 350–450 °C and pressure differences between retentate and permeate sides up to 2.0 bar. From these experimental data, both permeance and ideal hydrogen separation factor (α_{H_2/N_2}) can be determined. Additionally, it should be noted that five thermal cycles were also performed with the aim to ensure both mechanical and thermal resistance of the membrane against temperature cyclic variations and stability of permeate measurements. Moreover, a stabilization period of at least 2 h for each membrane was considered when hydrogen was fed for the first time. Later, binary mixtures containing 80 vol% of hydrogen balanced with nitrogen or carbon dioxide were also studied at a constant temperature (400 °C) to evaluate possible concentration-polarization or inhibition effects. In this way, the potential contribution of the concentration-polarization effect was evaluated when working with binary mixtures containing certainly inert species such as nitrogen, being possible to determine a general Concentration Polarization Coefficient (CPC) accordingly to the previous publication of Bellini et al. [58] and described here as Eq. (1). The combined contribution of both concentration-polarization and inhibition effects can be evaluated by permeation tests conducted with any other binary mixture containing species with a certain inhibition contribution. From these tests, the overall Permeation Reduction Coefficient (PRC) can be calculated by Eq. (2). Then, it could be possible to evaluate the Inhibition Coefficient (IC) caused by any molecule from its definition based on previous CPC and PRC coefficients, shown in Eq. (3), as previously also suggested by Bellini et al. [58]. At this point, it should be mentioned that the present study has been focused on the specific contribution of carbon dioxide on the above-mentioned parameters, with a great influence on the permeation capacity of other previously published ELP-PP membranes, most of them with a thicker Pd-film and diverse materials as an intermediate layer.

$$CPC = 1 - \frac{\text{Permeance}_{N_2\text{mixture}}}{\text{Permeance}_{\text{Clean membrane}}} \quad (1)$$

$$PRC = 1 - \frac{\text{Permeance}_{\text{Inhibited membrane}}}{\text{Permeance}_{\text{Clean membrane}}} \quad (2)$$

$$IC = 1 - \frac{(1 - PRC)}{(1 - CPC)} \quad (3)$$

2.3. Reaction tests

As previously addressed, both membrane permeation and reaction tests were performed by using the same experimental setup described in the previous section (Fig. 1). However, it is necessary to add some additional descriptions in this section to complete the given information. Beside the inlet gas-flow settled by the previously indicated Bronkhorst mass-flow controllers, also a liquid feed can be introduced into the system by a Gilson 307 HPLC pump. The liquid is pumped to a simple electrical furnace, where it is evaporated and mixed with other gases introduced to the setup. Particularly, this system was used to feed a mixture of reagents for the reaction tests performed in the present study, steam reforming, consisting of acetic acid (AA, Scharlau, ≥ 99.7%) diluted in distilled water ($n_{H_2O}/n_{AA} = 4$) that simulates a simplified synthetic stream coming from micro-algae liquefaction [10,11,42,43]. The evaporated liquid was always mixed with small amounts of nitrogen to facilitate the composition analysis of outlet streams and to ensure an accurate calculation of the mass-balance. Moreover, the experimental setup also contains a cold-trap on the outer retentate stream intending to condense any possible excess of the acetic acid solution in water and certain possible liquid sub-products such as alcohols or acetone. The composition of the condensate fraction collected in the cold-trap was later analyzed by high-performance liquid chromatography (Varian CP-3900 chromatograph equipped with a CP-WAX 52 CB column and flame ionization detector). For all these tests, around 1.0 g of a home-made Ni/SBA-15 catalyst containing

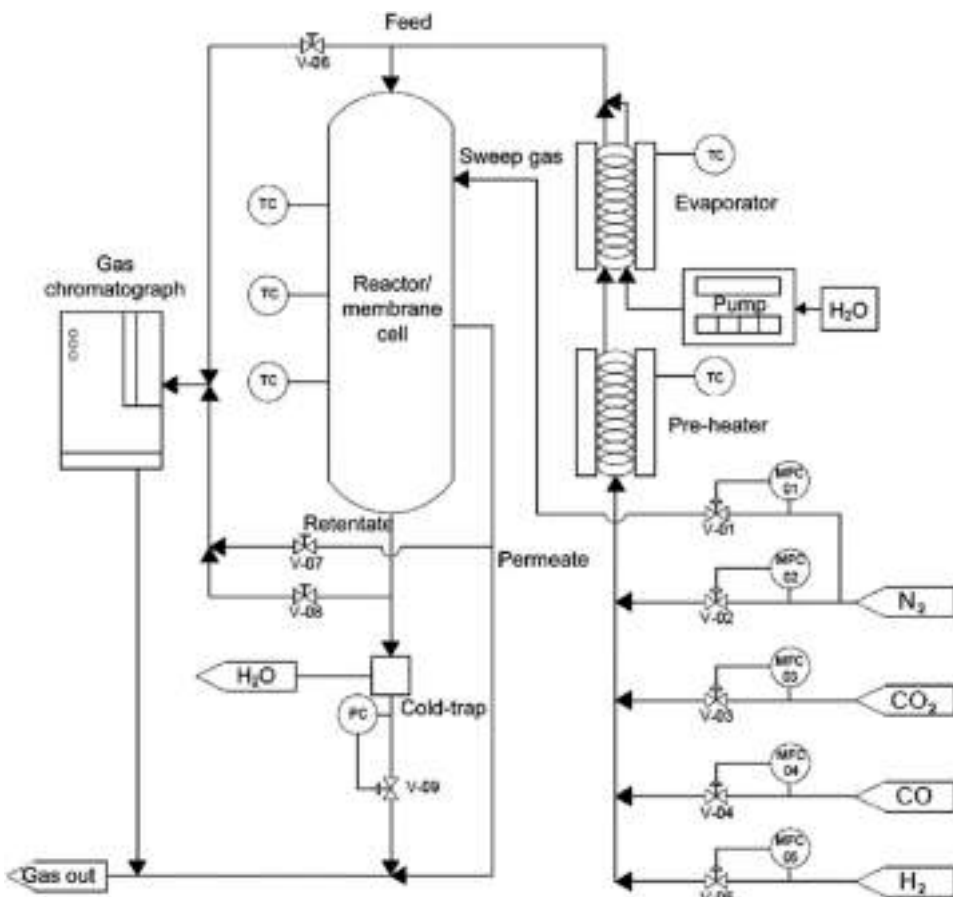


Fig. 1. Experimental setup used for permeation and reaction tests.

13.5 wt% of nickel was introduced into the lumen of the reactor. Complete details about its general synthesis procedure and performance in powder for different steam reforming reactions can be found in previous publications [11,43]. However, its total BET surface and pore volume of around 521 m² and 0.77 m³ g⁻¹, respectively, as well as average pore diameters in the range 8.3–10.6 nm, can be here emphasized as main physical properties. In this work, the catalyst was pelletized into small cylinders of around 2 × 5 mm containing a 70 wt % of Ni/SBA-15 material and 30 w.% clays, being mixed with quartz spheres in order to fill in the entire lumen space available into the reactor (around 5.5 cm³).

Two types of reaction experiments were performed, distinguishing those carried out in a conventional packed-bed reactor (PBR) with the catalyst inside a dense 316 L SS tube from tests in which the SS tube is replaced by the ELP-PP Pd-based membrane, thus working with a membrane reactor configuration (PBMR) as illustrating in Fig. 2. For the second option, in which a PBMR configuration is adopted, it should be noted that direct contact between palladium film and catalyst pellets is always avoided due to the presence of both wall of the PSS support and CeO₂ intermediate layer. Moreover, a possible contribution of the Pd-film to the overall catalytic activity of chemical reactions has been dismissed due to the negligible conversion reached in blank tests carried out in the absence of the catalyst.

Anyway, a similar procedure was adopted in both cases to study the influence of some important operating conditions such as temperature

($T = 400\text{--}450^\circ\text{C}$), gas hourly space velocity ($\text{GHSV} = 2500\text{--}4500 \text{ h}^{-1}$), or feed pressure ($P = 1\text{--}4 \text{ bar}$). First, heating-up and cooling-down steps were always performed in nitrogen atmosphere to avoid any possible oxidation of the catalyst or the membrane (in case of working as PBMR). However, it should be noted that fresh catalyst was always treated by flowing hydrogen ($Q_{\text{H}_2} = 50 \text{ NmL min}^{-1}$) at 450 °C for 2 h before to initiate any set of reactions to ensure a complete reduction of the nickel particles dispersed on the bulk SBA-15. Later, each operating condition was properly adjusted into the desired values, and the reaction test was extended for 60 min with continuous monitoring of gas composition in outlet streams to ensure reaching a steady-state. During this period, diverse samples were taken from both gas and liquid outer streams and analyzed by chromatography.

Here, it is important to highlight that not only fresh catalyst was used for all the above-mentioned experiments, and also its regeneration was considered. If assuming a possible catalyst deactivation and system blockage by coke formation, H₂ decrease in the product stream and a non-controlled pressure increase in the lumen side should be observed during experiments. For those cases, 100 NmL min⁻¹ of compressed air were flushed for at least 1 h into the reactor at 450 °C to enhance the coke gasification and the consequent recovery of catalytic activity. This fact has been noted in the present study by marking the catalyst as "fresh" or "regenerated". An identical procedure was followed to work as PBMR, but using 200 NmL min⁻¹ of nitrogen as sweep gas in the

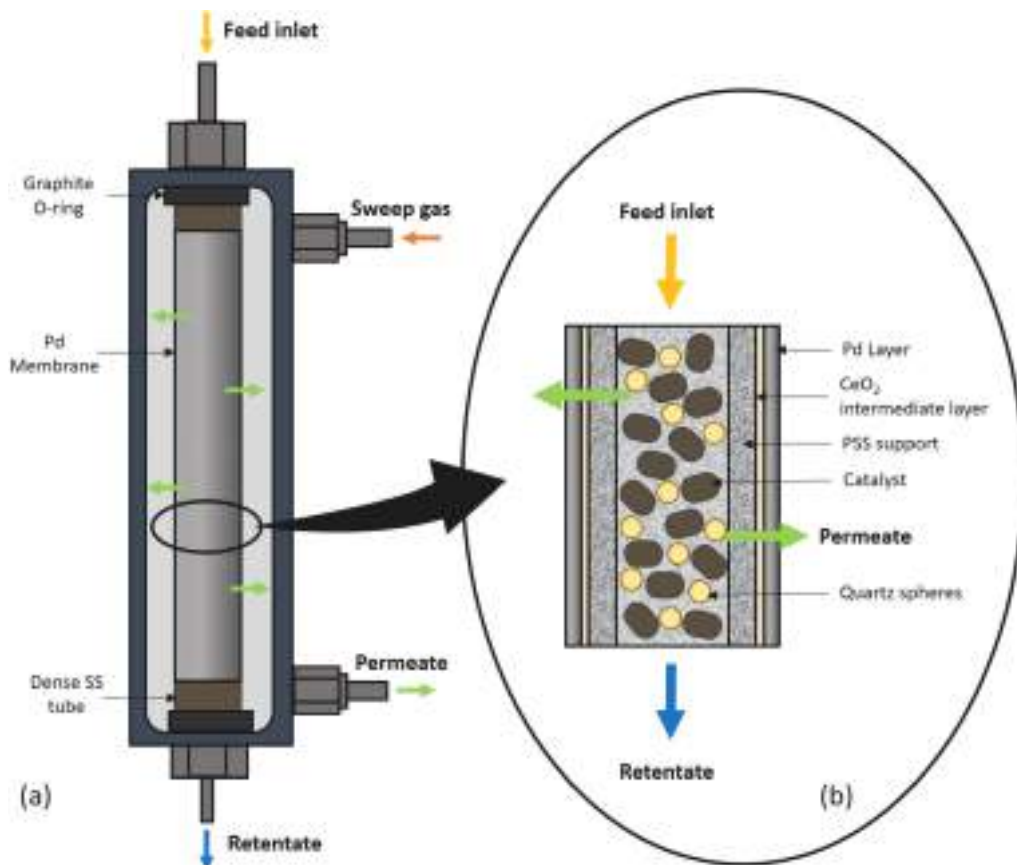


Fig. 2. Detail of membrane assembly and general layout of elements for PBMR experiments.

permeate stream to improve the overall pressure driving force for H₂ permeation through the membrane.

In both cases, PBR and PBMR, the progress of the acetic acid steam reforming was monitored by calculation of acetic acid conversion (x_{AA}), hydrogen yield (Y_{H_2}) and product selectivity (S_i) as follows:

$$x_{AA} = \frac{n_{AA,in} - n_{AA,out}}{n_{AA,in}} \quad (4)$$

$$Y_{H_2} = \frac{n_{H_2}}{4 \cdot n_{AA,in}} \quad (5)$$

$$S_i = \frac{n_i}{\sum_{j=1}^n n_j} \quad (6)$$

where $n_{AA,in}$ and $n_{AA,out}$ show the acetic acid molar flow-rate fed into the system or collected in the cold-trap, respectively, and n_{H_2} the hydrogen produced during the reaction. Subscripts i and j represent each generic product obtained throughout the experiment taking into account all species identified by chromatography analyses except reagents (acetic acid and water).

In the case of analyzing the results obtained in PBMR configuration, two additional parameters were also considered to determine the hydrogen recovered from the total produced in the reactor (Recovery Factor, RF) and the recovered one from the maximum amount that theoretically is possible to produce according to the stoichiometry of chemical reaction (Recovery Yield, RY). Both parameters are defined by expressions given in Eqs. (7) and (8) as follows:

$$RF = \frac{n_{H_2,p}}{n_{H_2,TOT}} = \frac{n_{H_2,p}}{n_{H_2,ret} + n_{H_2,p}} \quad (7)$$

$$RY = \frac{n_{H_2,p}}{n_{H_2}|_{theory}} = \frac{n_{H_2,p}}{4 \cdot n_{AA,in}} \quad (8)$$

In addition to all these experimental and calculated data, theoretical values about the thermodynamic chemical equilibrium were also determined by the minimization of the Gibbs free-energy with the help of ASPEN-HYSYS software. The property method used for the simulation was Redlich-Kwong-Soave (SRK), which provide suitable solutions for most gas mixtures, where the polarity of compounds is not noticeably strong.

3. Results and discussion

3.1. Membrane morphology

Fig. 3 shows the external morphology of one typical membrane reached after scaling-up the synthesis procedure published elsewhere [56], in which the palladium film was coated by ELP-PP onto a larger tubular PSS support (total length of 110 mm) modified with an intermediate layer formed by CeO₂ particles previously doped with Pd nuclei. The characteristic morphology of other ELP-PP membranes was reached despite the larger dimension of the supports. In fact, a continuous Pd top film with a certain cavernous structure can be observed

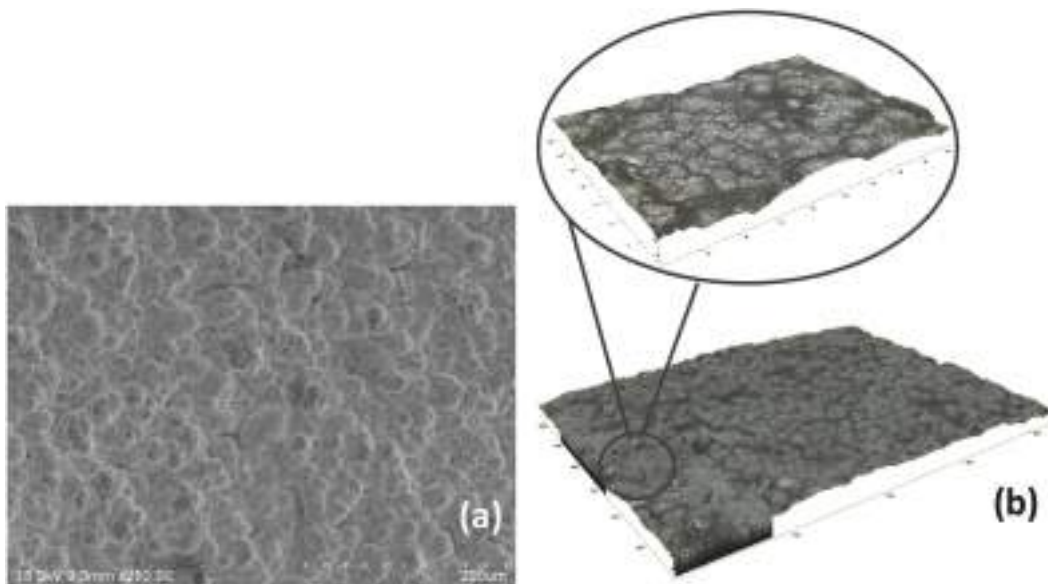


Fig. 3. Pd-Membrane morphology for the top surface: a) SEM image and b) topography analysis by optical profiler.

in the SEM image (Fig. 3a), not detecting significant differences in the axial direction. The average thickness for this Pd-film has been estimated into around 15 μm from gravimetric analyses, slightly thicker than the reached one for similar membranes prepared onto shorter supports up to 3 cm in length (8–12 μm) [56]. The average external roughness obtained from an optical profiler (Fig. 3b) also increased by around 15% respect to the previously published membrane, reaching a value of $R_a = 3.451 \pm 0.47 \mu\text{m}$. Nevertheless, this value is still noticeably smaller than the provided one by the raw PSS support, with a starting external roughness around $R_a = 5.082 \pm 0.40 \mu\text{m}$.

3.2. Permeation behavior with pure gases

As previously indicated in the experimental section, preliminary bubble-leak tests with helium in ethanol at room temperature were performed to guarantee the absence of defects in the Pd-film of the membranes collected in this work. After ensuring this fact, a series of single gas permeation experiments with both pure nitrogen and hydrogen was carried out at temperatures in the range 350–450 °C and pressure driving forces up to 2.0 bar, always avoiding the use of any sweep gas for collecting the permeate stream. First, it is important to highlight that the analyzed ELP-PP membrane was completely impermeable to nitrogen for the entire set of experiments, since no nitrogen flux was detected in the permeate side at any operating condition of temperature and pressure. Therefore, the initial quality of the Pd film was maintained at higher temperatures and an eventually complete ideal separation factor to hydrogen ($\alpha_{\text{H}_2/\text{N}_2}$) could be assumed for all the analyzed conditions.

Particular data reached for the entire set of permeation experiments carried out with pure H₂ are collected in Fig. 4, where the permeate flux (J_p) for each pressure driving force ($P_r^{0.5} - P_p^{0.5}$) is represented at diverse temperatures in the range 350–450 °C.

As can be seen, a higher permeate flux is reached for increasing values of pressure and temperature, as usually predicts the available literature [58–60]. A clear linear trend reasonably fitting into the origin between permeate fluxes and pressure driving forces for each series of experimental data was also observed for the entire range of temperatures, as predicted by the well-known Sieverts' law for H₂ permeation

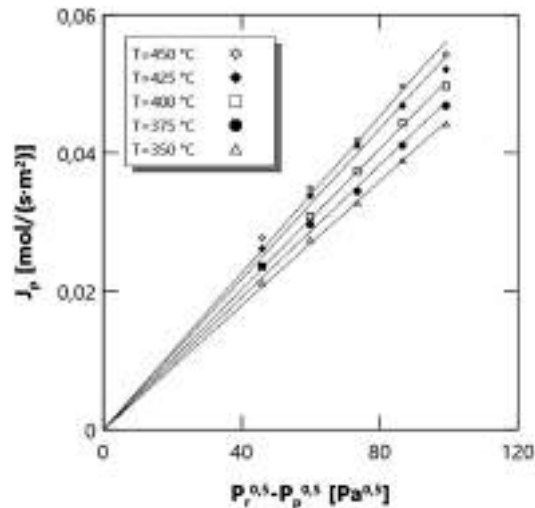


Fig. 4. Results for permeation experiments when feeding pure hydrogen.

through Pd-based membranes [61,62]. This fact implies H₂ permeances in the range of $4.49\text{--}5.67 \cdot 10^{-4} \text{ mol m}^{-2} \text{ s}^{-1} \text{ Pa}^{0.5}$ and activation energy of 8.59 kJ mol^{-1} , which agree with typical performances of other composite Pd-based membranes found in the literature [53,63]. These values and trends are consistent with the solution-diffusion model of permeation through a Pd-membrane when the rate-determining step is the H₂ diffusion throughout a dense and defect-free metallic film. However, it should be noted that the particular permeation behavior previously reported for many other ELP-PP membranes and widely discussed in previous works [53,56,64], in which the Sieverts' linear fit does not intercept in the origin, does not appear for this time. Although some experimental data taken at lower pressures slightly deviate for the general trend, the linearity maintains a really high correlation factor

($R \geq 0.999$), so the above-mentioned effect can be considered negligible. This fact could be explained by the larger axial dimension of the membrane respect to most of the previously reported ones [55–57,64], which requires a slight modification of the synthesis conditions in terms of volume ratio between Pd source and reducing agent solutions. This fact could affect the Pd penetration inside the pores of the supports, responsible for the above-mentioned deviation in shorter membranes.

All these previous results also suggest a good mechanical stability of the membrane after being tested at different pressures and temperatures, especially considering the used permeation mode in which the highest pressure always remains in the lumen and the lowest one on the shell side. It forces the permeation direction from the inner to the outer side of the tubular membrane, where the Pd film is placed, thus generating tensile stresses that could derive into delamination or cracks generation. However, five additional thermal cycles from room temperature up to 400 °C were also performed in order to reinforce this term about the stability of both membrane integrity and permeation measurements. It can be emphasized that only a slight variation below 2% in the permeate fluxes reached for each thermal cycle was obtained, thus demonstrating the good anchoring between support and palladium film and no generation of cracks or pinholes.

3.3. Permeation behavior with binary gas mixtures

It is well-known that working with gas mixtures in Pd-based membranes usually produces a noticeable decay in the hydrogen permeation capacity of these systems. Particularly, the presence of several molecules containing carbon atoms in the gas mixture, such as carbon monoxide, carbon dioxide, or light hydrocarbons, significantly decreases the permeate flux, as it is widely reported in the literature [58,65,66]. Despite a typical higher inhibition effect of carbon monoxide for most of the studies [67–70], ELP-PP membranes exhibited a peculiar behavior, mostly affected by carbon dioxide [63,71]. Due to this fact and the significant improvement on the quality of ELP-PP membranes during last years, especially taking into account those prepared onto modified PSS supports with CeO₂ intermediate layers [55,56], this section has been focused on the particular behavior of these membranes in the presence of mixtures containing nitrogen or carbon dioxide.

First, it should be noted that the quality of the tested membrane in terms of H₂ selectivity was maintained for the entire set of experiments collected in this section since neither nitrogen nor carbon dioxide was found in permeate streams through GC analyses. Thus, all permeate fluxes reached in the present section are composed only by pure hydrogen. Moreover, additional experiments with pure gases were also performed after operating with the gas mixtures, maintaining the good properties of the membrane addressed in the last section, especially those related to the almost complete H₂ selectivity up to the available detection limit of the equipment.

Fig. 5 collects the results about the permeation behavior of the membrane with binary mixtures containing 20 vol% of nitrogen or carbon dioxide balanced in hydrogen. All experiments were carried out at 400 °C and pressure differences between retentate and permeate sides in the range 0.4–2.0 bar.

Permeate fluxes reached at each particular condition are shown in Fig. 5a, obtaining a clear decrease of H₂ permeate flux in comparison to previous tests performed with pure H₂ at similar conditions, as well as a marked deviation from the linear relationship between permeate and pressure driving forces. Moreover, a more pronounced decrease was obtained for the permeate flux in case of feeding a mixture containing carbon dioxide instead of nitrogen. A certain dilution effect is always present when working with gas mixtures, thus decreasing the total pressure driving force for the permeation process with greater intensity as the hydrogen concentration in the feed stream decrease and, hence, the permeate flux through the membrane. This unavoidable fact has been taken into account in the calculation of the pressure driving force

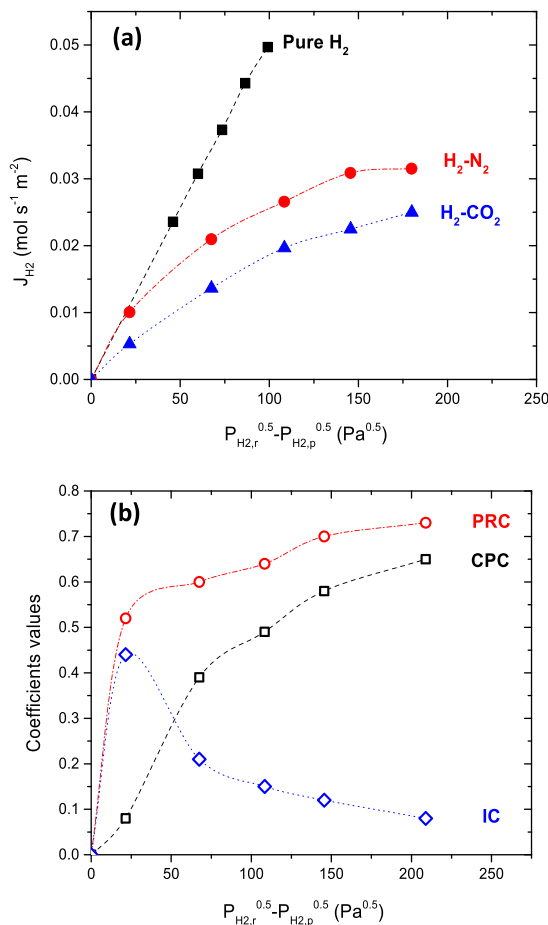


Fig. 5. H₂ permeation variation when feeding binary gas mixtures containing 20 vol% N₂ or CO₂ ($T = 400$ °C) (a) and detailed analysis of contributing effects: CPC, PRC, and IC (b).

by considering hydrogen partial pressures for both retentate and permeate sides, so the observed permeate flux decay should be caused by other different reasons. In this context, other authors explain similar behaviors by competitive adsorption between hydrogen and other molecules present in the feed mixture to reach the palladium surface (concentration-polarization effect) or deactivation of the membrane due to inhibition processes caused by particular compounds [58].

Fig. 5b tries to elucidate the particular contribution of these effects for experiments carried out in the present study by calculating and depicting separately CPC, PRC, and IC coefficients, previously described in the experimental section, at each particular pressure driving force. First, the concentration-polarization effect (CPC) caused by any totally inert molecule with no inhibition effect has been evaluated using experiments in which a binary mixture H₂-N₂ is fed to the membrane. As can be seen, CPC progressively increases in the range of 0.39–0.65 for pressure driving forces higher than 65 Pa^{0.5}. In fact, the higher the pressure, the higher the permeating flux and, hence, the lower the hydrogen concentration in the retentate outlet. Moreover, the diffusivity of molecules in the gas phase decreases for increasing pressure values. These issues clearly turn the external mass transfer of hydrogen molecules to the palladium surface more difficult, thus increasing the

value of the CPC [72,73]. However, a noticeably lower CPC value of only around 0.08 was obtained for $P_{H_2,r}^{0.5}$, $P_{H_2,p}^{0.5} = 21.6 \text{ Pa}^{0.5}$. This fact suggests that the above-mentioned increase of the concentration-polarization effect is greater for relatively low pressure values, while a progressive stabilization around a certain value seems to reach at higher pressures.

By replacing nitrogen by carbon dioxide in the feed mixture, it is possible to determine the overall permeation reduction coefficient, PRC, which involves both possible concentration-polarization and inhibition effects. Even though carbon dioxide is considered as a very inert molecule, the results evidence a certain inhibition effect because of PRC values, ranged from 0.52 to 0.73, always exceed the previously calculated CPC ones. Anyway, a similar global trend is observed for both CPC and PRC, increasing their values as the pressure does, but predicting a certain stabilization for the highest pressures. From these values, it is possible to quantify the inhibition effect of carbon dioxide for permeation through an ELP-PP membrane, reaching values for IC from 0.08 to 0.44. It should be noted that the inhibition coefficient follows a different trend to coefficients previously addressed, CPC and PRC, thus decreasing its contribution for higher pressures. In this manner, almost the total decay of H₂ permeability for the analyzed ELP-PP membrane at pressure driving forces below $P_{H_2,r}^{0.5}$, $P_{H_2,p}^{0.5} = 50 \text{ Pa}^{0.5}$ is caused by a marked inhibition effect of carbon dioxide, instead of the typical concentration-polarization effect reported for working with gas mixtures containing inert membranes. This insight is very useful for designin permeation devices that include ELP-PP membranes and selecting the best operating conditions to maximize their performance. At this point, it is necessary to remember the great influence of this compound for H₂ permeation through ELP-PP membranes described in our previous study [71]. It is provoked by the particular distribution of palladium between the external surface of the membrane and inside the pores of the support, thus generating a certain tortuosity that affects the mass transfer differently for diverse gas molecules. On the contrary, a decrease in H₂ permeation reached at higher pressures is mainly governed by the concentration-polarization effect.

3.4. Reaction tests: acetic acid steam reforming

An ELP-PP membrane containing an external Pd film with an estimated thickness around 15 μm, previously analyzed in terms of permeability, was also used to perform some reaction tests in a packed-bed membrane reactor to evaluate its resistance and potential benefits for the steam reforming of acetic acid. The feed used for the reaction consists of a mixture of acetic acid in water ($n_{H_2O}/n_{AA} = 4$), thus simulating a simplified synthetic stream coming from micro-algae liquefaction [10,11,42,43]. Even though steam reforming of light hydrocarbons such as methane or alcohols in both conventional packed-bed or membrane reactors has been widely investigated by many authors in last years [16–19], literature addressing the use of acetic acid or the aqueous phase coming from bio-oil production techniques is still under investigation, as discussed in the introduction section. However, it is widely accepted in all cases that the overall equilibrium for any steam reforming (SR) results from combining multiple reactions between all compounds involved in the process. Therefore, together with the main SR reaction, many other reactions, such as water gas shift (WGS), methanation (MTN), or thermal decomposition of compounds (TD), may also take place. Moreover, especially in case of using supported catalysts, ketonization reactions to form coke precursors (i.e. acetone) or directly coke by Boudouard reaction or reverse carbon gification (RCG) would also be possible.

In this context, Table 1 collects important information about all these possible chemical reactions involved in the steam reforming of acetic acid considered for the present study to facilitate the interpretation of the experimental results. This information includes a description of each chemical reaction, its enthalpy ($\Delta H, \text{ kJ mol}^{-1}$), and the variation in moles between products and reactants (Δn).

3.4.1. Influence of temperature

First, the temperature effect on AASR in a conventional PBR working with a fresh catalyst at $P = 1.0 \text{ bar}$ and $\text{GHSV} = 4500 \text{ h}^{-1}$ was analyzed for the range 400–450 °C. Both experimental and calculated thermodynamic equilibrium data by ASPEN-HYSYS for the conversion of acetic acid, hydrogen yield and product selectivity are collected in Fig. 6.

According to the thermodynamic predictions, AASR is entirely feasible from a thermodynamic point of view, and a complete conversion for acetic acid can be reached at the entire range of evaluated temperatures (Fig. 6a). However, a limited experimental conversion below the predicted data was obtained due to kinetic effects. Both conversion values, experimental and predicted ones, becomes progressively closer at higher temperatures because of the increasing kinetics constants by an Arrhenius-type dependence.

Similar behavior can be found in Fig. 6b while analyzing the hydrogen yield. Among the wide number of reactions involved into the process, as previously discussed in Table 1, Steam Reforming and Thermal Decomposition are probably affected in a greater grade by temperature due to their endothermic character and higher enthalpy, thus playing an important role for controlling both acetic acid conversion and hydrogen yield inside the reactor. Additionally, the selectivity to diverse products was also addressed in the present study, collecting the reached experimental data in Fig. 6c. In this context, it should be mentioned that thermodynamic equilibrium calculations from ASPEN-HYSYS software only reflect hydrogen, methane, carbon monoxide and carbon dioxide as products. However, the analysis of condensates during real experiments evidenced an incomplete conversion of acetic acid, and the formation of various by-products such as acetone and coke.

Due to the above-mentioned discrepancy and the interest in analyzing the real behavior inside a reactor containing a heterogeneous catalyst, thus affected by both thermodynamics and kinetics, only experimental data are collected in Fig. 6c. As can be seen, on the contrary of previous parameters, selectivity towards hydrogen remains almost constant within the entire range of temperatures under evaluation, being possible to explain by the synergy between AASR and WGS reactions. Higher temperatures increase H₂ production by AASR but affect WGS and vice-versa, thus maintaining a certainly stable amount of hydrogen in the outlet stream. At lower temperatures, carbon monoxide production is mainly controlled by WGS, as confirmed by the marked drop in its selectivity. However, CO production could also be favored by Thermal Decomposition (strongly endothermic) and Dehydration to form ketene and its further Steam Reforming. Selectivity to acetone does not appear to be significant even at higher temperatures, where the ketonization reaction (slightly endothermic) could become relevant. However, coke formation seems to play a decisive role in the reaction pathway. In fact, Boudouard and reverse carbon gasification, along with acetone polymerization, prevailed at lower temperatures, leading to a vast quantity of coke in terms of selectivity (around 14% at $T = 400 \text{ }^{\circ}\text{C}$). Furthermore, in compliance with exothermic Methanation reactions, a reasonable selectivity towards methane (nearly 7% at $T = 400 \text{ }^{\circ}\text{C}$) was found at these conditions of relatively low temperatures.

To minimize the formation of methane and particularly coke during further experiments, thus retarding a possible catalyst deactivation, membrane fouling, and blockage of the system, the highest temperature of 450 °C was selected to continue the present study.

3.4.2. Influence of space velocity

Later, similar analyses were performed to evaluate the effect of the gas hourly space velocity (GHSV) between 2500 and 4500 h⁻¹ on the system, showing the main reached results in Fig. 7. These experiments were also carried out in a conventional PBR working at fixed $T = 450 \text{ }^{\circ}\text{C}$ and $P = 1.0 \text{ bar}$ but including for the first time in this study the use of fresh and regenerated catalysts.

Table 1
Expected chemical reactions for steam reforming of acetic acid.

Reaction		ΔH [kJ/kmol]	Δn
Acetic Acid Steam Reforming (AASR)	$\text{CH}_3\text{COOH} + 2\text{H}_2\text{O} \leftrightarrow 4\text{H}_2 + 2\text{CO}_2$	131.4	+3
Water Gas Shift (WGS)	$\text{CO} + 2\text{H}_2\text{O} \leftrightarrow \text{CO}_2 + \text{H}_2$	-41.1	0
Thermal decomposition (TD)	$\text{CH}_3\text{COOH} \leftrightarrow 2\text{H}_2 + 2\text{CO}$	213.7	+3
Decarboxylation	$\text{CH}_3\text{COOH} \leftrightarrow \text{CH}_4 + \text{CO}_2$	-33.5	+1
Methanation (MTN)	$\text{CO} + 3\text{H}_2 \leftrightarrow \text{CH}_4 + \text{H}_2\text{O}$	-206.1	-2
	$\text{CO}_2 + 4\text{H}_2 \leftrightarrow \text{CH}_4 + 2\text{H}_2\text{O}$	-165.1	-2
Ketonization (KTZ)	$2\text{CH}_3\text{COOH} \leftrightarrow (\text{CH}_3)_2\text{CO} + \text{H}_2\text{O} + \text{CO}_2$	16.7	+1
Dehydration	$\text{CH}_3\text{COOH} \leftrightarrow \text{CH}_2\text{CO} + \text{H}_2\text{O}$	144.4	+1
Ketene steam reforming	$\text{CH}_2\text{CO} + \text{H}_2\text{O} \leftrightarrow 2\text{CO} + 2\text{H}_2$	ΔH > 0	+3
Acetone Oligomerization	$(\text{CH}_3)_2\text{CO} \rightarrow \text{oligomerization} \rightarrow \text{coke}$	ΔH < 0	Δn < 0
Boudouard reaction	$2\text{CO} \leftrightarrow \text{C} + \text{CO}_2$	-172.4	-1
Reverse carbon gasification	$\text{CO} + \text{H}_2 \leftrightarrow \text{C} + \text{H}_2\text{O}$	-131.3	-1

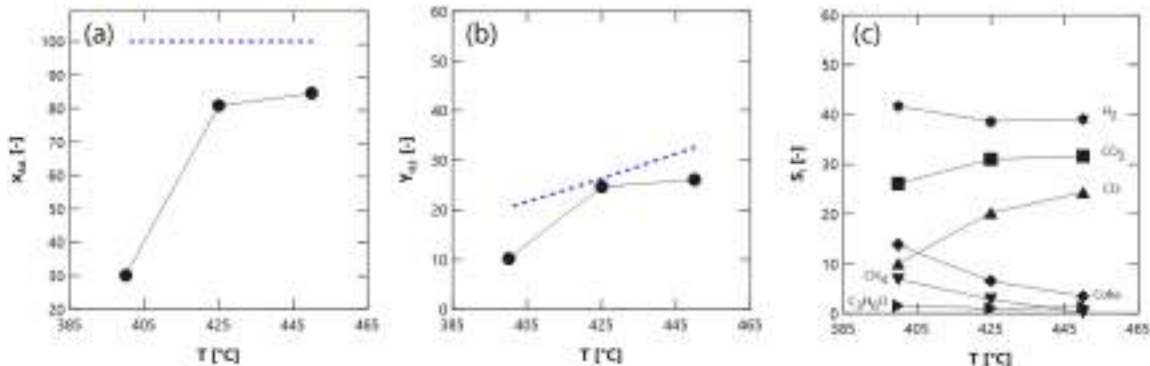


Fig. 6. Temperature effect in PBR-AASR experiments ($P = 1.0$ bar, $\text{GHSV} = 4500 \text{ h}^{-1}$) with fresh catalyst: acetic acid conversion (a), hydrogen yield (b), and product selectivity (c). Thermodynamic equilibrium reference: —.

As expected, a slight decrease in both experimental acetic acid conversion (Fig. 7a) and hydrogen yield (Fig. 7b) were obtained for increasing values of the gas hourly space velocity due to the shorter contact time between reactants and catalyst. This behavior is not obtained for simulated data because they only come from calculating the thermodynamic equilibrium. Attending to the products selectivity shown in Fig. 7c, the negative effect of increasing GHSV on hydrogen production is evident, even in a greater grade, being explained by a lower contribution to the WGS on the overall process, thus obtaining a considerable increasing amount of CO, also coming from reverse Methanation. In all these cases, better reaction performances were achieved for all tests carried out using a fresh catalyst instead of a regenerated one, although with differences below 10% for the entire set of experiments. In general, lower acetic acid conversion, hydrogen yield, and hydrogen selectivity can be found using a regenerated catalyst, while coke formation starts being slightly higher. The opposite trend between hydrogen and carbon monoxide appears to be fairly noticeable, especially when a new catalyst is employed. At this point, it is also necessary to note that the overall performance reached by the regenerated catalyst seems to be closer to the data collected with a fresh catalyst for increasing values of GHSV. For this reason, a $\text{GHSV} = 4500 \text{ h}^{-1}$ has been selected to proceed with the study and evaluate the pressure effect in both PBR and PBMR configurations, where a continuous replacement of the catalyst by a fresh one for each new experiments becomes unpractical for any potential industrial application.

3.4.3. Influence of pressure

Fig. 8 compares all results for reactions reached at constant operating conditions of $T = 450^\circ\text{C}$ and $\text{GHSV} = 4500 \text{ h}^{-1}$ by using a

different catalyst status (fresh or regenerated) and pressures in the range 1.0–3.0 bar for the two different reactor setups: PBR and PBMR containing the ELP-PP Pd-composite membrane. A quite evident decrease in the reaction extent occurs as the reaction pressure increases in PBR configuration, without any H_2 separation, since lower acetic acid conversion and hydrogen yield were found, as depicted in Fig. 8a and b, respectively. In fact, Steam Reforming and Thermal Decomposition reactions are the most affected ones by the pressure due to the biggest increase in moles between products and reactants ($\Delta n = +3$). Comparing the results reached in both PBR and PBMR configurations, it is clear the equilibrium displacement reached by the in-situ permeation of hydrogen through the membrane with an increase up to 15% in the acetic acid conversion (Fig. 8a). In fact, it is well-known that the direct reaction rate could be promoted by selectively removing a product from the reaction system, thus reducing, as a consequence, the reaction rate of the reverse reaction at the same operating conditions [47,74]. This is one of the main advantages of working with membrane reactors together with the extraction of hydrogen with an ultra-high purity in a unique operation [14,46,75]. Thus, a higher conversion might be reached while maintaining a constant operating temperature, just as occurring in the present case. However, the permeation effect could not totally overcome the thermodynamic restrictions in the experimental conditions used. In this manner, their negative impact over the thermodynamic of the overall AASR process, as previously addressed in PBR experiments, prevails against the membrane effect despite higher pressures clearly promote increasing hydrogen permeation flow-rates.

The membrane shift effect over the process is also evidenced in Fig. 8b, where a significant improvement on the hydrogen yield can be observed replacing the conventional PBR configuration by the PBMR, even overcoming the predicted values by the equilibrium for some

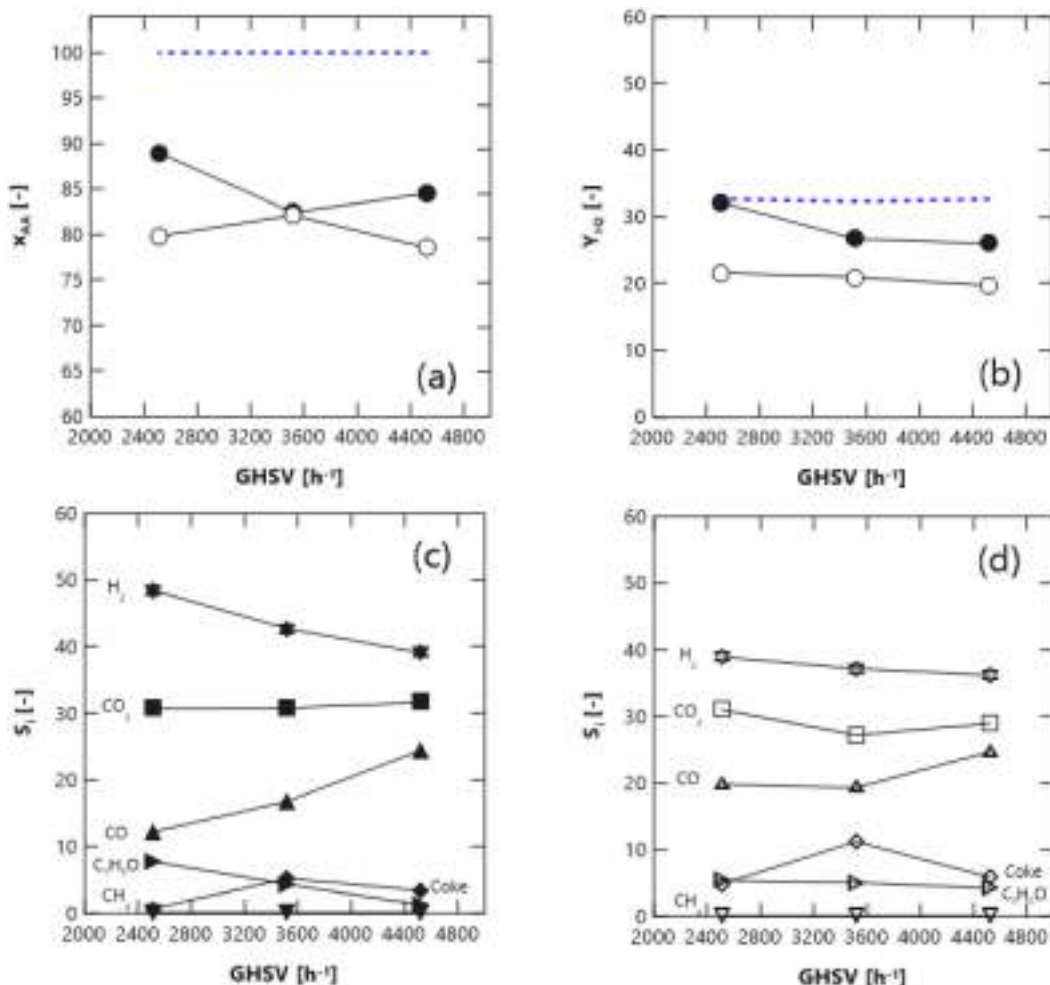


Fig. 7. GHSV effect in PBR-AASR experiments ($P = 1.0$ bar, $T = 450$ °C) with fresh (shadow symbols) and regenerated (hollow symbols) catalyst: acetic acid conversion (a), hydrogen yield (b), and product selectivity obtained with fresh (c) or regenerated catalyst (d). Thermodynamic equilibrium reference: —.

particular conditions. This fact suggests that marked differences in product selectivity are generated when a continuous extraction of hydrogen through a highly-selective membrane is combined with a catalyst in a PBMR, as later will be discussed. Once again, it is important to emphasize that slightly lower performances were always reached when employing a regenerated catalyst. However, this difference is not so clear in the case of operating in PBMR.

A more detailed analysis is required to explain the results reached in product selectivity for both PBR and PBMR systems when operating with fresh and regenerated catalysts at diverse pressures. These experimental data are shown from Fig. 8c to f. In this context, a marked selectivity towards hydrogen was reached for all cases, although appreciable amounts of coke were also detected. In fact, hydrogen was the main product of chemical reactions involved in catalytic AASR in terms of selectivity, with values ranged from 35 to 45%, being followed by carbon dioxide. The impact of reaction pressure over coke formation becomes clear in good agreement with Boudouard reaction and reverse carbon gasification. Thus, this effect becomes fairly evident as increasing the pressure on the reaction side. In fact, excluding the presence of a solid phase due to the coke formation, both chemical

reactions involve a reduction in the total number of moles, and then higher pressures push the thermodynamic equilibrium forward. Nevertheless, it should be taken into account that, besides Boudouard and RCG reactions, coke formation is the result of a complicated network of side-reactions involved in the general AASR scheme. Acetic acid is particularly favorable towards self- and intra-molecular ketonization. In general, catalytic supports with marked acidity might be harmful to the steam reforming reaction, since acidic sites would prone certain dehydration process, throughout acetone could be formed. This compound usually acts as a coke precursor via ketonization instead of being converted into hydrogen via steam reforming, causing additional catalyst deactivation [32]. However, some recent studies [76] have demonstrated that materials with marked basicity, just as occurring with supported catalyst onto SBA-15, could also favor ketonization processes. In this manner, AA ketonization to form acetone may initiate a series of transformations that would cause the formation of oligomers and, eventually, coke. This route can only be minimized by working at temperatures above 600 °C, where the reforming reactions are dominant, although the use of these operating conditions in a PBMR could negatively affect the integrity of the Pd-based membrane [51].

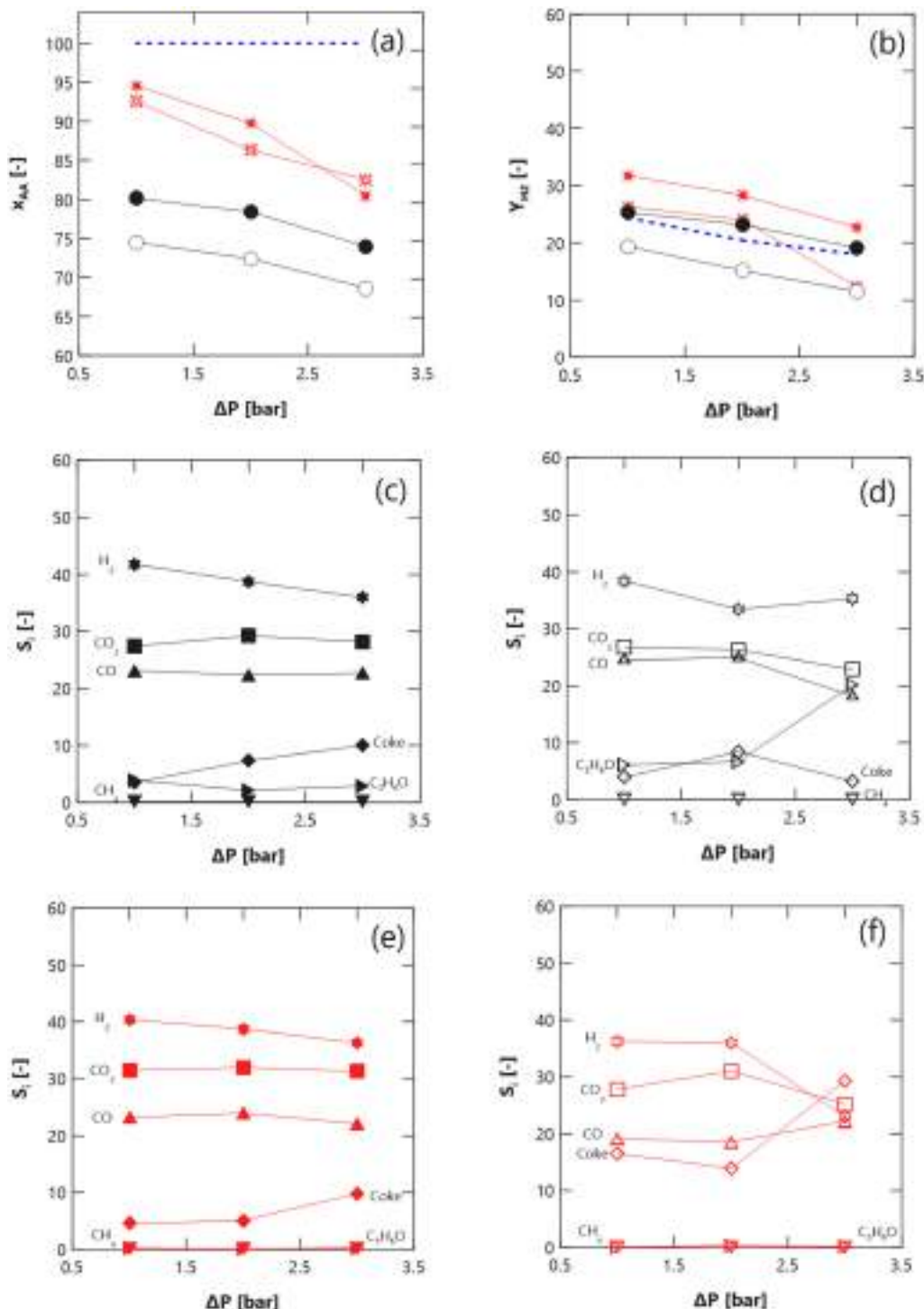


Fig. 8. Pressure effect in AASR experiments ($T = 450^\circ\text{C}$, GHSV = 4500 h^{-1}) with fresh (shadow symbols) and regenerated (hollow symbols) catalyst in both PBR (black color, ●) and PBMR (red color, ○) configurations: acetic acid conversion (a), hydrogen yield (b), product selectivity in PBR with fresh (c) or regenerated catalyst (d), and products selectivity in PBMR with fresh (e) or regenerated catalyst (f). Thermodynamic equilibrium reference: —. (For interpretation of the references to color in this figure legend, the reader is referred to the web version of this article.)

However, despite the above-mentioned trend, experiments carried out in PBR with regenerated catalysts (Fig. 8d) exhibit strange behavior, obtaining an unusual presence of acetone for the highest pressure conditions. The minimum amount of methane reached during these experiments could be caused by the mitigation of both methanation, expected up to 600 °C, and decarboxylation processes. On the other hand, it is well-known that interactions between nickel (employed as active metal into the catalyst used in the present study) and its support (in this case, SBA-15) could limit methanation reactions while increasing the selectivity towards hydrogen [76], thus justifying the observed general behavior of the entire set of experiments.

Analyzing in-depth the results reached in a PBMR, a certainly similar behavior to the above-mentioned ones reached for PBR working with fresh catalysts is observed, as it can be noticed by comparing Fig. 8c and e. However, in case of considering the use of a regenerated catalyst (Fig. 8d and f), a higher selectivity towards coke was obtained for PBMR configuration, which leads to around 30% for the most elevated pressure under investigation. In this context, the presence of acetone, generated via AA ketonization, and its equilibrium with incoming oligomerization and further polymerization, plays an important role in developing the reaction with a progressively stronger impact at higher pressures. Thus, the clear decrease in selectivity towards both hydrogen and carbon dioxide, which can be appreciably seen at high pressures, might thereby suggest the strong action of competitive ketonization at the expense of acetic acid steam reforming and thermal decomposition.

Finally, Recovery Factor (RF) and Recovery Yield (RY) for the membrane used in all the above-mentioned PBMR-AASR experiments are shown in Fig. 9 as a function of reaction pressure and catalyst status. A pronounced decrease of RF from 0.25 to 0.09 was reached for increasing pressures in case of using a fresh catalyst (Fig. 9a), while quite similar results but decreasing in the range 0.06–0.01 were also reached in case of evaluating RY at identical conditions (Fig. 9b). This trend seems to be contrary to conventional membrane performances, in which higher pressures usually provoke an increase of the permeate flow-rate. However, here it should also be taken into account all the previous results of this study, where the higher the pressure, the lower the hydrogen yield and, thus, the available hydrogen amount to be permeated through the membrane. Therefore, the kinetic effect appears to be predominant against the thermodynamic equilibrium displacement potentially reached by the membrane shift effect at evaluated conditions.

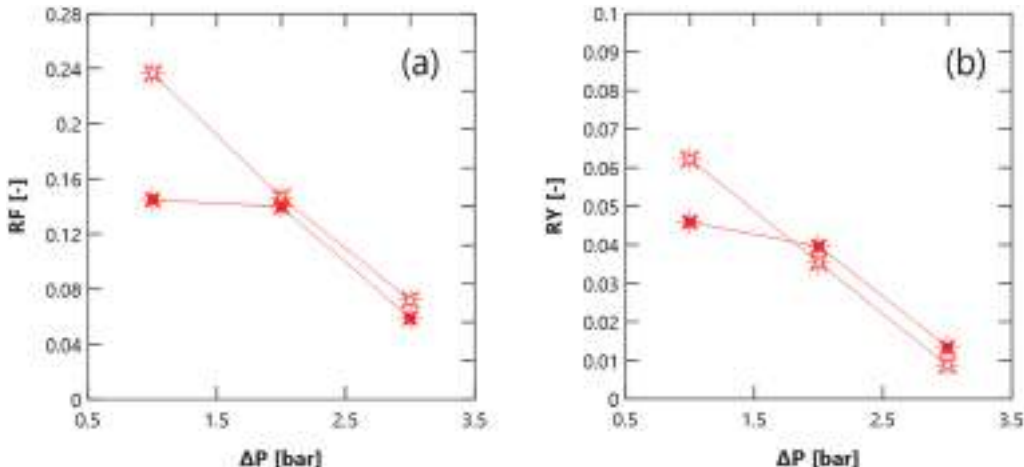


Fig. 9. Membrane Recovery Factor (a) and Recovery Yield (b) behavior with pressure in PBMR experiments with both fresh (shadow symbols) and regenerated (hollow symbols) catalysts ($T = 450$ °C, GHSV = 4500 h⁻¹).

4. Conclusions

New composite Pd-membranes onto PSS, including an intermediate layer of CeO₂ particles doped with Pd nuclei, were successfully obtained after scaling-up the total length of tubular supports up to 110 mm. No marked differences along the axial direction were found on the top Pd film, with an estimated thickness of around 15 μm and average roughness of 3.451 ± 0.47 μm. H₂ permeances in the range of $4.49\text{--}5.67 \cdot 10^{-4}$ mol m⁻² s⁻¹ Pa^{0.5} with an activation energy of 8.59 kJ mol⁻¹ were reached in permeation experiments with pure H₂ at temperatures between 350 and 450 °C. The use of gas binary mixtures with N₂ or CO₂ in these tests revealed a noticeable decrease of permeate flux, mainly caused by concentration-polarization at higher pressure driving forces. However, a significant contribution of inhibition caused by CO₂ has also been found for pressure driving forces below 50 Pa^{0.5}.

These membranes were subsequently combined with pelletized Ni/SBA-15 catalysts in a membrane reactor to produce hydrogen by acetic acid steam reforming. This particular feedstock was selected as a model component of a synthetic aqueous fraction generated in most hydrothermal liquefaction of microalgae to produce bio-oil. Temperature and GHSV were evaluated in a traditional PBR with both fresh and regenerated catalysts, to select the most appropriate conditions for the operation with the membrane. Later, a comparison between the theoretical equilibrium and the experimental data reached at PBMR configurations was established for multiple tests carried out with both fresh and regenerated catalysts, but pressures ranged from 1 to 3 bar. In all cases, both overall conversion of acetic acid and hydrogen yield were increased in a similar grade due to the shift effect on equilibrium reactions caused by hydrogen permeation through the membrane contained in the MR in comparison to the PBR configuration. A very similar product distribution was obtained for each case when working with fresh catalysts, but marked deviations were found in case of regenerating the catalysts. At these conditions, higher selectivity towards coke was obtained for PBMR configuration, which leads to around 30% for the most elevated pressure under investigation. Here, it should be emphasized that the mechanical integrity of the ELP-PP membrane resisted in a good grade during all the experiments, thus demonstrating its strength to be used in real MR applications. Finally, additional experiments are suggested to complete the present study and to optimize the MR operating conditions to reach higher RF and RY.

CRediT authorship contribution statement

Conceptualization (D. Alique, R. Sanz, J.A. Calles), Methodology (D. Alique, D. Martinez-Diaz, D. Sanz, G. Adduci), Validation (D. Alique, A. Caravella, D. Martinez-Diaz, D. Sanz, G. Adduci), Formal analysis (D. Alique, A. Caravella), Investigation (G. Adduci, D. Sanz, D. Martinez-Diaz, D. Alique), Resources (D. Alique, D. Martinez-Diaz, D. Sanz), Writing -original draft- (G. Adduci, D. Martinez-Diaz, D. Alique), Writing -review and editing- (D. Alique, J.A. Calles, A. Caravella), Visualization (D. Alique, D. Martinez-Diaz, G. Adduci), Supervision (D. Alique, A. Caravella, J.A. Calles, R. Sanz), Funding acquisition (J.A. Calles, D. Alique).

Declaration of competing interest

The authors declare that they have no known competing financial interests or personal relationships that could have appeared to influence the work reported in this paper.

Acknowledgements

The authors acknowledge the financial support achieved from the Spanish Ministry of Economy and Competitiveness through the project ENE2017-83696-R.

References

- [1] F. Dawood, M. Anda, G.M. Shaifullah, Hydrogen production for energy: an overview, *Int. J. Hydrol. Energy* (2020), <https://doi.org/10.1016/j.ijhydene.2019.12.059>.
- [2] E.S. Hanley, J.P. Deane, B.P.Ó. Gallachóir, The Role of Hydrogen in Low Carbon Energy Futures-a Review of Existing Perspectives, *Renew. Sustain. Energy Rev.* 2017, <https://doi.org/10.1016/j.rser.2017.10.034>.
- [3] N.Z. Muradov, T.N. Veziroğlu, "Green" path from fossil-based to hydrogen economy: an overview of carbon-neutral technologies, *Int. J. Hydrol. Energy* 33 (2008) 6804–6839, <https://doi.org/10.1016/j.ijhydene.2008.05.04>.
- [4] T.S. Uyar, D. Be?ikci, Integration of hydrogen energy systems into renewable energy systems for better design of 100% renewable energy communities, *Int. J. Hydrogen Energy* 42 (2017) 2453–2456, <https://doi.org/10.1016/j.ijhydene.2016.09.086>.
- [5] A. Iulianelli, V. Palma, G. Bagnato, C. Ruocco, Y. Huang, N.T. Veziroğlu, A. Basile, From bioethanol exploitation to high grade hydrogen generation: Steam reforming promoted by a Co-Pt catalyst in a Pd-based membrane reactor, *Renew. Energy* 119 (2018) 834–843, <https://doi.org/10.1016/j.renene.2017.10.050>.
- [6] G. Di Marcoberardino, S. Foresti, M. Binotti, G. Manzolini, Potentiality of a biogas membrane reformer for decentralized hydrogen production, *Chem. Eng. Process. - Process Intensif.* 129 (2018) 131–141, <https://doi.org/10.1016/j.cep.2018.04.023>.
- [7] A.A. Ahmad, N.A. Zawawi, F.H. Kasim, A. Inayat, A. Khasri, Assessing the gasification performance of biomass: a review on biomass gasification process conditions, optimization and economic evaluation, *Renew. Sust. Energ. Rev.* 53 (2016) 1333–1347, <https://doi.org/10.1016/j.rser.2015.09.030>.
- [8] V. Singh Yadav, V. R, D. Yadav, Biohydrogen production from waste materials: a review, *MATEC Web Conf.* 192 (2018) 02020, <https://doi.org/10.1051/matecconf/201819202020>.
- [9] P. Xu, Y. Jin, Y. Cheng, Thermodynamic Analysis of the Gasification of Municipal Solid Waste-NC-ND license (<http://creativecommons.org/licenses/by-nc-nd/4.0/>), *Engineering.* 3 (2017) 416–422, <https://doi.org/10.1016/J.ENG.2017.03.004>.
- [10] A. DemirbaÅ, Biomass resource facilities and biomass conversion processing for fuels and chemicals, *Energy Convers. Manag.* 42 (2001) 1357–1378, [https://doi.org/10.1016/S0196-8904\(00\)00137-0](https://doi.org/10.1016/S0196-8904(00)00137-0).
- [11] J.A. Calles, A. Carrero, A.J. Vizcaíno, L. García-Moreno, P.J. Megía, Steam reforming of model bio-oil aqueous fraction using Ni-(Cu, Co, Cr)/SBA-15 catalysts, *Int. J. Mol. Sci.* 20 (2019), <https://doi.org/10.3390/ijms20030512>.
- [12] S. Wang, Q. Cai, F. Zhang, X. Li, L. Zhang, Z. Luo, Hydrogen production via catalytic reforming of the bio-oil model compounds: Acetic acid, phenol and hydroxyacetone, *Int. J. Hydrol. Energy* 39 (2014) 18675–18687, <https://doi.org/10.1016/j.ijhydene.2014.01.142>.
- [13] W. Nabgan, T.A. Tuan Abdullah, R. Mat, W. Nabgan, Y. Gambo, M. Ibrahim, A. Ahmad, A.A. Jalil, S. Triwahyono, I. Saeh, Renewable hydrogen production from bio-oil derivative via catalytic steam reforming: an overview, *Renew. Sust. Energ. Rev.* 79 (2017) 347–357, <https://doi.org/10.1016/j.rser.2017.05.069>.
- [14] M.A. Soria, D. Barros, L.M. Madeira, Hydrogen production through steam reforming of bio-oils derived from biomass pyrolysis: thermodynamic analysis including in situ CO2 and/or H2 separation, *Fuel* 244 (2019) 184–195, <https://doi.org/10.1016/j.fuel.2019.01.156>.
- [15] L. Zhang, X. Hu, K. Hu, C. Hu, Z. Zhang, Q. Liu, S. Hu, J. Xiang, Y. Wang, S. Zhang, Progress in the reforming of bio-oil derived carboxylic acids for hydrogen generation, *J. Power Sources* 403 (2018) 137–156, <https://doi.org/10.1016/j.jpowsour.2018.09.097>.
- [16] T. Sato, T. Suzuki, M. Aketa, Y. Ishiyama, K. Mimura, N. Itoh, Steam reforming of biogas mixtures with a palladium membrane reactor system, *Chem. Eng. Sci.* 65 (2010) 451–457, <https://doi.org/10.1016/j.ces.2009.04.013>.
- [17] M. Saidi, Application of catalytic membrane reactor for pure hydrogen production by flare gas recovery as a novel approach, *Int. J. Hydrol. Energy* 43 (2018) 14834–14847, <https://doi.org/10.1016/j.ijhydene.2018.05.156>.
- [18] C. Coutanceau, S. Baranton, T. Audichon, Chapter 2 - Hydrogen Production From Thermal Reforming BT - Hydrogen Electrochemical Production, in: *Hydrog.*, Academic Press, Energy Fuel Cells Prim, 2018, pp. 7–15, <https://doi.org/10.1016/B978-0-12-811250-2.00002-9>.
- [19] D.N. Muraviev, N.V. Orehkova, E.Y. Mironova, A.B. Yaroslavtsev, M.M. Ermilova, Production of high purity hydrogen by ethanol steam reforming in membrane reactor, *Catal. Today* 236 (2014) 64–69, <https://doi.org/10.1016/j.cattod.2014.01.014>.
- [20] K. Takanabe, K.I. Aika, K. Seshan, L. Lefferts, Sustainable hydrogen from bio-oil - Steam reforming of acetic acid as a model oxygenate, *J. Catal.* 227 (2004) 101–108, <https://doi.org/10.1016/j.jcat.2004.07.002>.
- [21] A.C. Basagiannis, X.E. Verykios, Reforming reactions of acetic acid on nickel catalysts over a wide temperature range, *Appl. Catal. A Gen.* 308 (2006) 182–193, <https://doi.org/10.1016/j.apcata.2006.04.024>.
- [22] N. Iwasa, T. Yamane, M. Takei, I. ichi Ozaki, M. Arai, Hydrogen production by steam reforming of acetic acid: comparison of conventional supported metal catalysts and metal-incorporated mesoporous smectite-like catalysts, *Int. J. Hydrogen Energy* 35 (2010) 110–117, <https://doi.org/10.1016/j.ijhydene.2009.10.053>.
- [23] S. Thaicharoenutscharitham, V. Meeyoo, B. Kitiyanan, P. Rangsuvigit, T. Rirkosbom, Hydrogen production by steam reforming of acetic acid over Ni-based catalysts, *Catal. Today* 164 (2011) 257–261, <https://doi.org/10.1016/j.cattod.2010.10.054>.
- [24] L. An, C. Dong, Y. Yang, J. Zhang, L. He, The influence of Ni loading on coke formation in steam reforming of acetic acid, *Renew. Energy* 36 (2011) 930–935, <https://doi.org/10.1016/j.renene.2010.08.029>.
- [25] Z. Li, X. Hu, L. Zhang, G. Lu, Renewable hydrogen production by a mild-temperature steam reforming of the model compound acetic acid derived from bio-oil, *J. Mol. Catal. A Chem.* 355 (2012) 123–133, <https://doi.org/10.1016/j.molcata.2011.12.006>.
- [26] R.R. Hu, C.F. Yan, X.X. Zheng, H. Liu, Z.Y. Zhou, Carbon deposition on Ni/ZrO2-CeO2 catalyst during steam reforming of acetic acid, *Int. J. Hydrol. Energy* 38 (2013) 6033–6038, <https://doi.org/10.1016/j.ijhydene.2012.12.141>.
- [27] F.G.E. Nogueira, P.G.M. Assaf, H.W.P. Carvalho, E.M. Assaf, Catalytic steam reforming of acetic acid as a model compound of bio-oil, *Appl. Catal. B Environ.* 160–161 (2014) 188–199, <https://doi.org/10.1016/j.apcatab.2014.05.024>.
- [28] S. Goicoechea, E. Kraleva, S. Sokolov, M. Schneider, M.M. Pohl, N. Kockmann, H. Ehrlich, Support effect on structure and performance of Co and Ni catalysts for steam reforming of acetic acid, *Appl. Catal. A Gen.* 514 (2016) 182–191, <https://doi.org/10.1016/j.apcata.2015.12.025>.
- [29] M.V. Gil, J. Fermo, C. Pevida, D. Chen, F. Rubiera, Production of fuel-cell grade H2 by sorption enhanced steam reforming of acetic acid as a model compound of biomass-derived bio-oil, *Appl. Catal. B Environ.* 184 (2016) 64–76, <https://doi.org/10.1016/j.apcata.2015.11.028>.
- [30] G. Esteban-Díez, M.V. Gil, C. Pevida, D. Chen, F. Rubiera, Effect of operating conditions on the sorption enhanced steam reforming of blends of acetic acid and acetone as bio-oil model compounds, *Appl. Energy* 177 (2016) 579–590, <https://doi.org/10.1016/j.apenergy.2016.05.149>.
- [31] R.B.S. Junior, R.C. Rabeno-Neto, R.S. Gomes, F.B. Noronha, R. Fréty, S.T. Brandão, Steam reforming of acetic acid over Ni-based catalysts derived from La1-xCaxNiO3 perovskite type oxides, *Fuel* 254 (2019) 115714, <https://doi.org/10.1016/j.fuel.2019.115714>.
- [32] G. Chen, J. Tao, C. Liu, B. Yan, W. Li, X. Li, Hydrogen production via acetic acid steam reforming: a critical review on catalysts, *Renew. Sust. Energ. Rev.* 79 (2017) 1091–1098, <https://doi.org/10.1016/j.rser.2017.05.107>.
- [33] Z. Yu, X. Hu, P. Jia, Z. Zhang, D. Gong, D. Hu, S. Hu, Y. Wang, J. Xiang, Steam reforming of acetic acid over nickel-based catalysts: the intrinsic effects of nickel precursors on behaviors of nickel catalysts, *Appl. Catal. B Environ.* 237 (2018) 538–553, <https://doi.org/10.1016/j.apcatab.2018.06.020>.
- [34] Z. Zhang, Y. Wang, K. Sun, Y. Shao, L. Zhang, S. Zhang, X. Zhang, Q. Liu, Z. Chen, X. Hu, Steam reforming of acetic acid over Ni-Ba/Al2O3 catalysts: impacts of barium addition on coking behaviors and formation of reaction intermediates, *J. Energy Chem.* 43 (2020) 208–219, <https://doi.org/10.1016/j.jecchem.2019.08.023>.
- [35] Z. Yu, L. Zhang, C. Zhang, G. Gao, Z. Ye, S. Zhang, Q. Liu, G. Hu, X. Hu, Steam reforming of acetic acid over nickel catalysts: Impacts of fourteen additives on the catalytic behaviors, *J. Energy Inst.* 93 (2020) 1000–1019, <https://doi.org/10.1016/j.joei.2019.09.002>.
- [36] A. Kumar, R. Singh, A.S.K. Sinha, Catalyst modification strategies to enhance the catalyst activity and stability during steam reforming of acetic acid for hydrogen production, *Int. J. Hydrol. Energy* 44 (2019) 12983–13010, <https://doi.org/10.1016/j.ijhydene.2019.03.136>.
- [37] I.H. Choi, K.R. Hwang, K.Y. Lee, I.G. Lee, Catalytic steam reforming of biomass-derived acetic acid over modified Ni/T-Al2O3 for sustainable hydrogen production, *Int. J. Hydrol. Energy* 44 (2019) 180–190, <https://doi.org/10.1016/j.ijhydene.2018.04.192>.
- [38] M. Lindo, A.J. Vizcaíno, J.A. Calles, A. Carrero, Ethanol steam reforming on Ni/Al-SBA-15 catalysts: effect of the aluminium content, *Int. J. Hydrol. Energy* 35 (2010) 5895–5901, <https://doi.org/10.1016/j.ijhydene.2009.12.120>.
- [39] A.J. Vizcaíno, A. Carrero, J.A. Calles, Comparison of ethanol steam reforming using

- Co and Ni catalysts supported on SBA-15 modified by Ca and Mg, *Fuel Process. Technol.* 146 (2016) 99–109, <https://doi.org/10.1016/j.fuproc.2016.02.020>.
- [40] J.A. Calles, A. Carrero, A.J. Vizcaíno, L. García-Moreno, Hydrogen production by glycerol steam reforming over SBA-15-supported nickel catalysts: effect of alkaline earth promoters on activity and stability, *Catal. Today* 227 (2014) 198–206, <https://doi.org/10.1016/j.cattod.2013.11.006>.
- [41] A. Carrero, J.A. Calles, L. García-Moreno, A.J. Vizcaíno, Production of renewable hydrogen from glycerol steam reforming over bimetallic Ni-(Cu,Co,Cr) catalysts supported on SBA-15 silica, *Catalysts* 7 (2017), <https://doi.org/10.3390/catal7020055>.
- [42] J.A. Calles, A. Carrero, A.J. Vizcaíno, P.J. Megía, Agglomerated Co-Cr/SBA-15 catalysts for hydrogen production through acetic acid steam reforming, *Int. J. Hydrog. Energy* (2019) 1–10, <https://doi.org/10.1016/j.ijhydene.2019.05.237>.
- [43] A.J. Megía, J. Pedro, Alicia Carrero, José A. Calles, vizcaíno, Hydrogen production from steam reforming of acetic acid as a model compound of the aqueous fraction of microalgae HTL using Co-M/SBA-15 (M: Cu, Ag, Ce, Cr) catalysts, *Catalysts* 9 (2019) 1013–1032, <https://doi.org/10.3390/catal9101013>.
- [44] M. De Falco, G. Iaquaniello, E. Palo, B. Cucchiella, V. Palma, P. Ciambelli, 11 - Palladium-based membranes for hydrogen separation: preparation, economic analysis and coupling with a water gas shift reactor, in: A. Basile (Ed.), *Handb. Membr. React.* Woodhead Publishing, 2013, pp. 456–486, , <https://doi.org/10.1533/9780857097347.2.456>.
- [45] P. Li, Z. Wang, Z. Qiao, Y. Liu, X. Cao, W. Li, J. Wang, S. Wang, Recent developments in membranes for efficient hydrogen purification, *J. Memb. Sci.* 495 (2015) 130–168, <https://doi.org/10.1016/j.memsci.2015.08.010>.
- [46] M.R. Rahimpour, F. Samimi, A. Babapoor, T. Tohidian, S. Mohebi, Palladium membranes applications in reaction systems for hydrogen separation and purification: a review, *Chem. Eng. Process. Process Intensif.* 121 (2017) 24–49, <https://doi.org/10.1016/j.cep.2017.07.021>.
- [47] A. Brunetti, P.F. Zito, L. Giorno, E. Drioli, G. Barbieri, Membrane Reactors for Low Temperature Applications: An Overview, *Chem. Eng. Process. Process Intensif.*, 2017, <https://doi.org/10.1016/j.cep.2017.05.002>.
- [48] A. Basile, F. Gallucci, A. Iulianelli, F. Borgognoni, S. Tosti, Acetic acid steam reforming in a Pd-Ag membrane reactor: the effect of the catalytic bed pattern, *J. Memb. Sci.* 311 (2008) 46–52, <https://doi.org/10.1016/j.memsci.2007.11.033>.
- [49] A. Iulianelli, T. Longo, A. Basile, CO-free hydrogen production by steam reforming of acetic acid carried out in a Pd-Ag membrane reactor: the effect of co-current and counter-current mode, *Int. J. Hydrog. Energy* 33 (2008) 4091–4096, <https://doi.org/10.1016/j.ijhydene.2008.05.061>.
- [50] 8 - Membrane reactors for steam reforming of glycerol and acetic acid to produce hydrogen, in: A. Iulianelli, F. Dalena, S. Liguori, V. Calabro, A. Basile, A. Basile, L. Di Paola, F.L. Hai, V.B.T.-M.R. for E.A., B.C.P. Piemonte (Eds.), *Woodhead Publ., Woodhead Publishing, Ser. Energy*, 2015, pp. 249–266, , <https://doi.org/10.1016/978-1-78242-223-5.00008-X>.
- [51] D. Alique, D. Martínez-Díaz, R. Sanz, J.A. Calles, Review of Supported Pd-based Membranes Preparation by Electroless Plating for Ultra-pure Hydrogen Production, (2018), <https://doi.org/10.3390/membranes8010005>.
- [52] A.A. Plazaola, D.A.P. Tanaka, M.V.S. Annaland, F. Gallucci, Recent advances in pd-based membranes for membrane reactors, *Molecules* 22 (2017) 1–53, <https://doi.org/10.3390/molecules22010051>.
- [53] D. Alique, R. Sanz, J.A. Calles, Pd membranes by electroless pore-plating: synthesis and permeation behavior, *Curr. Trends Futur. Dev. Membr.* (2020) 31–62, <https://doi.org/10.1016/B978-0-12-818332-8.00002-8>.
- [54] E. Tosto, D. Alique, D. Martínez-Díaz, R. Sanz, J.A. Calles, A. Caravella, J.A. Medrano, F. Gallucci, Stability of pore-plated membranes for hydrogen production in fluidized-bed membrane reactors, *Int. J. Hydrog. Energy* 45 (2020) 7374–7385, <https://doi.org/10.1016/j.ijhydene.2019.04.285>.
- [55] D. Martínez-Díaz, R. Sanz, J.A. Calles, D. Alique, H₂ permeation increase of electroless pore-plated Pd/PSS membranes with CeO₂ intermediate barriers, *Sep. Purif. Technol.* 216 (2019) 16–24, <https://doi.org/10.1016/J.SEPUR.2019.01.076>.
- [56] D. Martínez-Díaz, D. Alique, J.A. Calles, R. Sanz, Pd-thickness reduction in electroless pore-plated membranes by using doped-ceria as interlayer, *Int. J. Hydrog. Energy* 45 (2020) 7278–7289, <https://doi.org/10.1016/j.ijhydene.2019.10.140>.
- [57] L. Furones, D. Alique, Interlayer properties of in-situ oxidized porous stainless steel for preparation of composite Pd membranes, *ChemEngineering*. 2 (2017) 1, <https://doi.org/10.3390/chemengineering2010001>.
- [58] S. Bellini, G. Azzato, A. Caravella, Mass transport in hydrogen permeation through Pd-based membranes, *Curr. Trends Futur. Dev. Membr.* (2020) 63–90, <https://doi.org/10.1016/B978-0-12-818332-8.00003-X>.
- [59] S. Yun, S. Ted Oyama, S.T. Oyama, Correlations in palladium membranes for hydrogen separation: a review, *J. Memb. Sci.* 375 (2011) 28–45, <https://doi.org/10.1016/j.memsci.2011.03.057>.
- [60] F. Gallucci, M. De Falco, S. Tosti, L. Marrelli, A. Basile, The effect of the hydrogen flux pressure and temperature dependence factors on the membrane reactor performances, *Int. J. Hydrog. Energy* 32 (2007) 4052–4058, <https://doi.org/10.1016/j.ijhydene.2007.03.039>.
- [61] A. Santucci, F. Borgognoni, M. Vadrucci, S. Tosti, Testing of dense Pd–Ag tubes: effect of pressure and membrane thickness on the hydrogen permeability, *J. Memb. Sci.* 444 (2013) 378–383, <https://doi.org/10.1016/j.memsci.2013.05.058>.
- [62] M. Vadrucci, F. Borgognoni, A. Moriani, A. Santucci, S. Tosti, Hydrogen permeation through Pd–Ag membranes: Surface effects and Sieverts' law, *Int. J. Hydrog. Energy* 38 (10) (2013) 4144–4152, <https://doi.org/10.1016/j.ijhydene.2013.01.091>.
- [63] D. Alique, Processing and characterization of coating and thin film materials, in: J. Zhang, Y. Jung (Eds.), *Adv. Ceram. Met. Coat. Thin Film Mater. Energy Environ.*, 2018, <https://doi.org/10.1007/978-3-319-59906-9>.
- [64] J.A. Calles, R. Sanz, D. Alique, L. Furones, P. Marín, S. Ordoñez, Influence of the selective layer morphology on the permeation properties for Pd-PSS composite membranes prepared by electroless pore-plating: Experimental and modeling study, *Sep. Purif. Technol.* 194 (2018) 10–18, <https://doi.org/10.1016/j.seppur.2017.11.014>.
- [65] M.M. Barreiro, M. Maroño, J.M. Sánchez, Hydrogen permeation through a Pd-based membrane and RWGS conversion in H₂/CO₂, H₂/N₂/CO₂and H₂/H₂O/CO₂mixtures, *Int. J. Hydrog. Energy* 39 (2014) 4710–4716, <https://doi.org/10.1016/j.ijhydene.2013.11.089>.
- [66] M.M. Barreiro, M. Maroño, J.M. Sánchez, Hydrogen separation studies in a membrane reactor system: influence of feed gas flow rate, temperature and concentration of the feed gases on hydrogen permeation, *Appl. Therm. Eng.* 74 (2015) 186–193, <https://doi.org/10.1016/j.applthermaleng.2013.12.035>.
- [67] A.S. Augustine, Y.H. Ma, N.K. Kazantzis, High pressure palladium membrane reactor for the high temperature water-gas shift reaction, *Int. J. Hydrog. Energy* 36 (2011) 5350–5360, <https://doi.org/10.1016/j.ijhydene.2011.01.172>.
- [68] L. Cornaglia, J. Múnera, E. Lombardo, Recent advances in catalysts, palladium alloys and high temperature (WGS) membrane reactors: a review, *Int. J. Hydrog. Energy* 40 (2015) 3423–3437, <https://doi.org/10.1016/j.ijhydene.2014.10.091>.
- [69] A. Caravella, F. Scura, G. Barbieri, E. Drioli, Inhibition by CO and polarization in Pd-based membranes: a novel permeation reduction coefficient, *J. Phys. Chem. B* 114 (2010) 12264–12276, <https://doi.org/10.1021/jp104767q>.
- [70] H. Kurokawa, H. Yakabe, I. Yasuda, T. Peters, R. Bredesen, Inhibition effect of CO on hydrogen permeability of Pd-Ag membrane applied in a microchannel module configuration, *Int. J. Hydrog. Energy* 39 (2014) 17201–17209, <https://doi.org/10.1016/j.ijhydene.2014.08.056>.
- [71] J.A. Calles, R. Sanz, D. Alique, L. Furones, Thermal stability and effect of typical water gas shift reactant composition on H₂ permeability through a Pd-YSZ-PSS composite membrane, *Int. J. Hydrog. Energy* 39 (2014) 1398–1409, <https://doi.org/10.1016/j.ijhydene.2013.10.168>.
- [72] A. Caravella, G. Barbieri, E. Drioli, Concentration polarization analysis in self-supported Pd-based membranes, *Sep. Purif. Technol.* 66 (2009) 613–624, <https://doi.org/10.1016/j.seppur.2009.01.008>.
- [73] O. Nekhamkina, M. Sheintuch, Approximate models of concentration-polarization in Pd-membrane separators. Fast numerical analysis, *J. Memb. Sci.* 500 (2016) 136–150, <https://doi.org/10.1016/j.memsci.2015.11.027>.
- [74] P.A. Ramachandran, T. Chompupun, C. Kanharu, T. Vatanathan, S. Limtrakul, Experiments, modeling and scaling-up of membrane reactors for hydrogen production via steam methane reforming, *Chem. Eng. Process. - Process Intensif.* 134 (2018) 124–140, <https://doi.org/10.1016/j.cep.2018.10.007>.
- [75] S.A. Wassie, S. Cloete, A. Zaabout, F. Gallucci, M. van Sint Annaland, S. Amini, Experimental investigation on the generic effects of gas permeation through flat vertical membranes, *Powder Technol.* 316 (2017), <https://doi.org/10.1016/j.powtec.2016.12.026>.
- [76] F. Bossola, S. Recchia, V. Dal Santo, Catalytic steam reforming of acetic acid: latest advances in catalysts development and mechanism elucidation, *Curr. Catal.* 07 (2017), <https://doi.org/10.2174/221154470766171219162653>.